# CLEAN SYNTHESIS OF NOVEL GREEN SURFACTANTS




**Payal Arvindkumar Baheti**

Thesis submitted to the University of Nottingham for the degree of Doctor of Philosophy

**January 2019**









*Dedicated to*

*My Parents*

*Madhuri Baheti*

*&*

*Arvind Baheti*







SINCHEM – The European Joint Doctorate Programme Sustainable Industrial Chemistry funded this project.

Erasmus Mundus Action (framework agreement N°2013-037; specific grant agreement n°2015- 1600 / 001- 001- EMJD).

**Acknowledgements**

I would first like to express my deepest gratitude to both supervisors; Prof. Steve Howdle for selecting me for this project, for encouragement and giving research freedom, for being cool and calm guide, for sharing his 'cool' presentation skills, and Dr. Patrick Lacroix-Desmazes for looking after me through all ups and down as a strong support system especially when I was an 'Illegal Alien' and for his invaluable supervision which helped me to achieve this work. I must also thank my co-supervisor Dr Cécile Bouilhac for her guidance, advice and motivation and all French translation – Merci beaucoup. I am indebted to Dr Andrea Hufendiek for helping me with proofreading and presentation of data. Special thanks go to Dr Olinda Gimello for passing her pool of SEC- and MS- knowledge and to Céline Bonneaud for helping me achieve the coating project efficiently in a very short time. Thanks to Dr Christine Joly-Duhamel for her guidance in coating project. Thank you everyone for the quick feedback to all the interminable emails I sent in past three months.

Thanks also go to Helen Carson for organising everything for me during my stay in Nottingham, and I highly appreciate all help from Christine Euzet, Gaëlle Ammeloot and other IAM secretaries for understanding me, despite my average French.

Mark Guyler, Richard Wilson, Peter Fields, Clive Dixon and everyone at the workshops deserve big thanks for dealing with the inevitable technical problems and big thanks go to Mike, Ben, Shahz, Kev in taking the time to introduce me to the analytical techniques and always helping me with all the MS/NMR related questions. Thanks extend to NMRC people: Chris Parmenter, Rhys Lodge, Graham Rance, Denise, for training me and for their help with microscopy techniques.

I am also thankful to the collaborators, Dr Frederik Wurm (MPIP, Germany) for hosting and welcoming me to his group, to Timo Rheinberger and Thomas Wolf for sharing their monomer expertise with me and for all the fruitful discussion, to all student in the group for such a wonderful time. Big thanks also go to my industrial supervisor, Dr. Amy Goddard for organising my placement at Cowick and for all her advises in the project and to Mrs Adeline Coulson for passing invaluable knowledge and to everyone at Personal Care team for such a wonderful time.

My thanks also to everyone at Laboratory B10. I had a wonderful time in Nottingham and I would always cherish all the delicious cakes, crosswords, pub times and sports day, summer party. Thanks to all my lab mates at Montpellier for their support and enthusiasm, and to the big SIMCHEM family for being supportive throughout my PhD journey - although I could not meet you guys on many gathering but I have treasured all the sweet memories of the time spent together. Thanks to all my Indian friends in Nottingham and to Deepthee, Bijol, Dhirendra and Sachin Ji for all the good times and I will miss the delicious Indian food at parties.

As the saying goes in India, 'God doesn't come to help but send angels'. For all the tough time with administrative work when everything went wrong, thank you for supporting me and looking after me: Rishi Bhaiya – Anjali Bhabhi, Reeturaj Bhaiya – Jyoti Bhabhi.

Finally, I would like to thank all my family and relatives for always being there for me over all Skype and phone calls when I was in need. To my brother, Dr Varun Baheti for always guiding me, to my sweet sister and Maa - Papa for always encouraging me to achieve my goals and believing in me. I thank Almighty God for giving me various challenges in life and the courage to face them all and come up with fruitful results. This Thesis is one of them!

**Abstract**

Star polymers have attracted considerable attention because of their unique thermal and mechanical properties. At the same time, as sustainable chemistry is growing in impact at an unprecedented rate, we propose in this work to implement a greener pathway for the synthesis of star *D*-sorbitol-poly(ε-caprolactone) (star PCL-$OH_x$) using clean solvents (polymerisation in the bulk or in supercritical $CO_2$) and either FDA-approved $Sn(Oct)_2$ catalyst or enzyme catalyst (Novozym® 435). The influence of these parameters on the star architecture (number of arms, MW of arms etc.) was rigorously analysed and corroborated with various analytical techniques ($^1$H NMR, SEC-MALS, SEC-UC, phosphitylation quantitative $^{31}$P NMR approach). Linear monohydroxy PCL-OH and dihydroxy telechelic HO-PCL-OH samples were also prepared. The PCL materials obtained were used as hydrophobic macroinitiators for the polymerisation of cyclic hydrophilic ethylene ethyl phosphonate monomer for the synthesis of a range of different amphiphilic materials (i.e. star diblock, linear diblock and triblock copolymers). Self-assembly behaviour in aqueous solution of these copolymers was investigated by DLS, TEM and cryo-TEM. Triblock and star amphiphilic copolymers were revealed to be able to reduce the surface tension (γ) of water down to 45 mN $m^{-1}$. Finally, enzyme catalysed star PCL-$OH_x$ polymers were functionalised with carboxylic end-groups using maleic anhydride. Water-dispersible surface-active ionic star polymers were then obtained. These maleate-functionalised star polymers were then photopolymerised with a small amount of tri(ethylene glycol) divinyl ether (~9wt% of total composition). The UV-cured crosslinked star PCL films produced were then analysed by FTIR, DSC and TGA.

**Résumé**

Les polymères en étoile connaissent un intérêt accru en raison de leurs propriétés thermiques et mécaniques inimitables. Partant du constat qu'en parallèle la chimie durable se développe à un rythme sans précédent, nous proposons dans cette thèse de développer une stratégie plus « verte » pour la synthèse de polymères en étoile de type *D*-sorbitol-poly(ε-caprolactone) (star PCL-$OH_x$). Ces derniers seront synthétisés sans solvant (en masse) ou dans des solvants « propres » ($CO_2$ supercritique) et en présence du catalyseur métallique $Sn(Oct)_2$ (qui a été approuvé par la FDA) ou d'un catalyseur enzymatique (Novozym® 435). L'influence de ces paramètres sur l'architecture des étoiles (nombre de bras, masse molaire des bras…) a été rigoureusement analysée et confirmée par différentes techniques d'analyse (RMN $^{1}H$, SEC-MALS, SEC-UC, analyse RMN $^{31}P$ quantitative *via* la méthode de phosphitylation). Des polymères linéaires monohydroxy (PCL-OH) et téléchéliques dihydroxy (OH-PCL-OH) ont également été synthétisés en parallèle. Ces différentes PCL ont été utilisées comme macro-amorceurs hydrophobes pour la polymérisation du monomère cyclique hydrophile éthylphosphonate d'éthylène. Une large gamme de copolymères amphiphiles a ainsi pu être développée (i.e. des copolymères diblocs en étoile ou des copolymères diblocs et triblocs linéaires). Le comportement d'auto-assemblage en solution de ces copolymères a été étudié par DLS ainsi que par TEM et cryo-TEM. Nous avons également montré que les copolymères amphiphiles triblocs et en étoile sont capables de diminuer la tension de surface (γ) de l'eau en dessous de 45 mN $m^{-1}$. Enfin, les étoiles PCL-$OH_x$ synthétisées en présence d'enzyme ont été fonctionnalisées par réaction avec l'anhydride maléique. Des polymères en étoile, ioniques, tensio-actifs et directement dispersables dans l'eau ont ainsi pu être obtenus. Dans un second temps, ces mêmes polymères ont été photopolymérisés en présence d'une faible quantité de tri(éthylène glycol) divinyl éther (~ 9% par rapport à la masse totale). Les films afférents à ces copolymères en étoile réticulés sous UV ont été analysés par IRTF, DSC et ATG.

## List of Contents

Acknowledgements ..... I
Abstract ..... III
Résumé ..... IV
List of Contents ..... V
List of Abbreviations ..... X
**Chapter 1 General Introduction ..... 1**
1.1 Motivation for the Choice of Various Material Systems ..... 1
1.2 Thesis Structure ..... 4
1.3 References ..... 7
**Chapter 2 State of the Art ..... 9**
2.1 Surfactants ..... 9
2.1.1 Biobased Building Blocks and Green Surfactants ..... 12
2.1.1.1 Renewable Hydrophiles ..... 12
2.1.1.2 Renewable Hydrophobes ..... 14
2.1.1.3 Commercial Biobased Surfactants ..... 16
2.1.2 Biosurfactants ..... 18
2.1.3 Structure-Property Relationship of Surfactants ..... 19
2.1.3.1 Surface Tension ..... 19
2.1.3.2 Surfactant Bulk Aggregation ..... 21
2.2 Self-Assembly of Surface-Active Polymers ..... 23
2.3 Biobased and Biodegradable Polymers ..... 29
2.3.1 Biobased Polyesters ..... 30
2.3.2 Synthesis of Aliphatic Polyesters ..... 30
2.3.2.1 Ring-Opening Polymerisation ..... 31
2.3.2.2 Metal Catalyst for Polyester Synthesis ..... 32
2.3.2.3 Organocatalyst for Polyester Synthesis ..... 34
2.3.2.4 Bio-Catalysed Enzymatic Ring-Opening Polymerisation (eROP) ..... 35
2.4 Supercritical Fluids ..... 39
2.4.1 Supercritical Carbon Dioxide ..... 40
2.4.2 Supercritical Fluid Extraction ..... 41
2.4.3 Polymerisation in Supercritical Carbon Dioxide ..... 42
2.5 Conclusions ..... 44
2.6 References ..... **Error! Bookmark not defined.**
**Chapter 3 Experimental and Characterisation Techniques ..... 55**
3.1 High-Pressure Equipment ..... 55
3.1.1 MKIII Clamp-Sealed Autoclave ..... 56

3.1.1.1 Standard operating procedure of MKIII Autoclave ..... 59
3.1.2 View Cell Studies Set-up ..... 61
3.2 Characterisation Techniques ..... 62
3.2.1 Nuclear Magnetic Resonance Spectroscopy (NMR) ..... 62
3.2.2 Size Exclusion Chromatography-Multi-Angle Light Scattering (SEC-MALS) ..... 62
3.2.3 SEC using Universal Calibration ($SEC^{UC}$) for Arms Evaluation ..... 63
3.2.4 Conventional Size Exclusion Chromatography Technique ..... 67
3.2.5 $^{31}P$ NMR Phosphitylation ..... 68
3.2.2.1 Quantification by Phosphitylation Method ..... 69
3.2.6 Matrix Assisted Laser Desorption and Ionisation-Time of Flight Mass Spectrometry .. 76
3.2.7 Electrospray Ionisation Mass Spectrometry (ESI MS) ..... 77
3.2.8 Differential Scanning Calorimetry (DSC) ..... 77
3.2.9 Dynamic Light Scattering (DLS) ..... 77
3.2.10 Transmission Electron Microscopy (TEM) ..... 78
3.2.11 Cryogenic Transmission Electron Microscopy (Cryo-TEM) ..... 79
3.2.12 Tensiometry ..... 79
3.2.12.1. Static: Krüss Tensiometer ..... 79
3.2.12.2. Dynamic: Bubble Pressure Tensiometer ..... 79
3.2.12.3 Critical Aggregation Concentration by Krüss Tensiometer ..... 80
3.2.13 Thermogravimetric Analysis (TGA) ..... 80
3.2.14 Real-Time Fourier-Transform Infrared Spectroscopy (FTIR) ..... 80
3.3 References ..... 81
**Chapter 4 Biobased Star Poly(ε-Caprolactone) Hydrophobe ..... 83**
4.1 Abstract ..... 83
4.2 Introduction ..... 84
4.3 Experimental Section ..... 88
4.3.1 Materials ..... 88
4.3.2 Synthesis of Polyol-PCL from Sugar Alcohols in the Bulk using $Sn(Oct)_2$ ..... 88
4.3.3 Synthesis of Star PCL from *D*-Sorbitol in the Bulk using Novozym 435 ..... 89
4.3.4 Synthesis of Star PCL from *D*-Sorbitol using $Sn(Oct)_2$ in Supercritical $CO_2$ ..... 89
4.3.5 Synthesis of Star PCL from *D*-Sorbitol using Novozym 435 in Supercritical $CO_2$ ..... 90
4.4 Results and Discussion ..... 91
4.4.1 Synthesis of Polyol-PCL in the Bulk or in $ScCO_2$: using $Sn(Oct)_2$ ..... 91
4.4.2 Star *D*-Sorbitol-PCL in the Bulk or in $ScCO_2$: using $Sn(Oct)_2$ ..... 94
4.4.3 Star *D*-Sorbitol-PCL by eROP in the Bulk or in $ScCO_2$: using Novozym 435 ..... 99
4.4.4 Assessing MW of Arms of Star *D*-Sorbitol-PCL by $^1H$ NMR ..... 104
4.4.5 Assessing the Structure of Star *D*-Sorbitol-PCL by MALDI-TOF MS ..... 107

4.4.6 Quantifying Number of Arms by a Phosphitylation/$^{31}$P NMR Method ..... 109
4.4.7 Mark-Houwink Plot for Structure of Star-Branched PCL ..... 116
4.4.8. Determining Arms by SEC-UC-MH Conformation Plots ..... 118
4.4.9 Thermal Analysis of Star Polyol-PCL by DSC ..... 122
4.5 Conclusions ..... 124
4.6 References ..... 125
**Chapter 5 Poly(ε-Caprolactone) – *Block* – Poly(Ethyl Phosphonate) Copolymers ... 129**
5.1 Abstract ..... 129
5.2 Introduction ..... 130
5.3 Experimental Section ..... 137
5.3.1 Materials ..... 137
5.3.2 Synthesis of ethyl phosphonate (EP) monomer ..... 137
5.3.3 Polymerisation of ethyl phosphonate by AROP using DBU ..... 138
5.3.4 Synthesis of PCL-*b*-PEP diblock and triblock copolymer in the bulk ..... 139
5.3.5 Synthesis of Star PCL-*b*-PEP Diblock Copolymers in DCM ..... 140
5.3.6 View-Cell Study of Ethyl Phosphonate using $scCO_2$ ..... 141
5.3.7 Purification of Polymers ..... 141
5.4 Results and Discussion ..... 142
5.4.1 Ethyl Phosphonate (EP) Monomer Synthesis ..... 142
5.4.2 Linear Homo PEP by AROP in DCM, in the Bulk and in $scCO_2$ ..... 143
5.4.2.1 Poly(Ethyl Phosphonate) Synthesis in DCM and in the Bulk ..... 143
5.4.2.2 View-cell to Assess Solubility of Ethyl Phosphonate in $scCO_2$ ..... 146
5.4.2.3 Poly(Ethyl Phosphonate) Synthesis in $ScCO_2$ ..... 148
5.4.2.4 Purification of PEP Homopolymer using $scCO_2$ ..... 151
5.4.3 Linear PCL-*b*-PEP Diblock and PEP-*b*-PCL-*b*-PEP Triblock Copolymers ..... 152
5.4.3.1 Purification of Triblock Copolymers using SCFE ..... 159
5.4.4 Star-Shaped PCL-*b*-PEP Diblock Copolymer ..... 163
5.4.4.1 High MW Star PCL-PEP Diblock Copolymer (DCM vs. Bulk) ..... 163
5.4.4.2 Quantifying Number of Arms by a Phosphitylation/$^{31}$P NMR Method ..... 169
5.4.4.3 Bulk ROP of Low MW Star PCL and Star PCL-PEP Compounds ..... 172
5.4.5 MALDI-TOF of PEP-*b*-PCL-*b*-PEP Triblock Copolymer ..... 176
5.4.6 Self-Assembly of PCL-*b*-PEP Amphiphilic Block Copolymers ..... 179
5.4.6.1 Low MW Triblock and Star Compounds: Direct Dissolution Method ..... 180
5.4.6.1.1 Critical Aggregation Concentration of Triblock Amphiphile ..... 180
5.4.6.1.2 Low MW Triblock Amphiphile Size Investigation by DLS ..... 181
5.4.6.1.3 Critical Aggregation Concentration of Star Amphiphile ..... 183
5.4.6.1.4 Low MW Star Diblock Amphiphile Size Investigation by DLS ..... 186

5.4.6.2 Intermediate MW Linear vs. Star Size Investigation: Direct Dissolution Method.... 187
5.4.6.3 High MW Star PCL-*b*-PEP Copolymers: Direct Dissolution Method ..... 190
5.4.6.4 High MW Star PCL-*b*-PEP Diblock Copolymers: Nanoprecipitation Method..... 190
5.4.6.5 TEM and Cryo-TEM of Star *D*-sorbitol[PCL-*b*-PEP] Copolymer..... 195
5.5 Conclusions ..... 199
5.6 References ..... 202
**Chapter 6 Applications of Star Polymers ..... 207**
6.1 Abstract ..... 207
6.2 Introduction ..... 209
6.3 Experimental (Surfactants)..... 221
6.3.1 Materials and Methods ..... 221
6.3.2 Surface Active Properties and Applications..... 221
6.3.2.1 Solubilisation of Fragrance..... 221
6.3.2.2 Emulsion Studies..... 222
6.3.3 Biobased Star *D*-sorbitol-$PCL_nOH_x$ Functionalisation with Maleic Anhydride (Surfactants and Coatings) ..... 222
6.4 Result and Discussion (Surfactants)..... 223
6.4.1 Surface Activity of $PCL_n$-$PEP_m$ Block Copolymers..... 223
6.4.1.1 Surface Tension: Static and Equilibrium..... 226
6.4.1.2 Dynamic Surface Tension ..... 229
6.4.1.3 Solubilisation of Fragrances ..... 232
6.4.1.4 Emulsion Studies using Star *D*-sorbitol[PCL-*b*-PEP] ..... 234
6.4.2 Biobased Star PCL Surfactants ..... 237
6.4.2.1 Star *D*-Sorbitol[$PCL_nOH_x$] Functionalisation (Surfactants and Coatings) ..... 237
6.4.2.2 Dispersion of Star *D*-sorbitol[$PCL_n$-MA-$COOH_{3x}$]$OH_3$ in Water (Surfactants)..... 240
6.4.2.3 Surface Tension of Functionalised S-PCL-MA-$COONEt_3OH_3$ ..... 243
6.5 Conclusions (Surfactants)..... 244
6.6 Experimental (Coatings)..... 245
6.6.1 Materials and Methods ..... 245
6.6.2 Biobased Star PCL (Coatings)..... 245
6.6.2.1 Functionalisation of Star *D*-sorbitol-$PCL_nOH_x$ (Surfactants and Coatings)..... 245
6.6.2.2 Photo-curable Formulation of Star *D*-Sorbitol[$PCL_n$-$MAc_x$] ..... 245
6.6.2.3 Films of Star *D*-Sorbitol[$PCL_n$-$MAc_x$] and UV-curing Procedure..... 245
6.7 Results and Discussion (Coatings) ..... 246
6.7.1 Functionalisation of Biobased Star *D*-Sorbitol[$PCL_nOH_x$] ..... 246
6.7.2 Star PCL Film Preparation and Characterisation. ..... 246
6.7.3 Kinetic Analysis of Star *D*-Sorbitol [PCL-$MAc_x$] Polymerisation with DVE ..... 247

6.7.4 UV-Cured Network of Star Poly[CL-Maleate-*alt*-Vinyl Ether] Films..... 250
6.7.5 DSC Studies ..... 254
6.7.6 TGA Studies..... 255
6.8 Conclusions (Coatings) ..... 256
6.9 References ..... 257
**Chapter 7 Conclusions and Future Work ..... 261**
7.1 Conclusions ..... 261
7.2 Future Work ..... 269
7.4 References ..... 271
Appendix A (Related to Chapter 3)..... 272
Appendix B (Related to Chapter 4)..... 274
Appendix C (Related to Chapter 5)..... 280
Appendix D (Related to Chapter 6)..... 286
Appendix E (Résumé Étendu)..... 289

## List of Abbreviations

| | |
|---|---|
| APG | Alkyl polyglucoside |
| AROP | Anionic ring-opening polymerisation |
| ε-CL | ε-Caprolactone |
| CaLB | *Candida antarctica* Lipase B |
| Cl-TMDP | 2-chloro-4,4,5,5-tetramethyl-1,3,2-dioxaphospholane |
| $Cr(acac)_3$ | Chromium (III) acetylacetonate |
| CAC | Critical aggregation concentration |
| CMC | Critical micellization concentration |
| $T_C$ | Critical temperature |
| $T_c$ | Crystallisation temperature |
| Cryo-TEM | Cryogenic-transmission electron microscopy |
| %Conv. | %monomer conversion |
| $D_{cryo\text{-}TEM}$ | Diameter by cryo-TEM |
| DBU | 1,8-diazabicyclo[5.4.0]undec-7-ene |
| DCTB | Trans-2-[3-(4-tert-butylphenyl)-2-methyl-2-propenylidene]malononitrile |
| $DP^{NMR}$ / $DP_n^{NMR}$ | Degree of polymerisation by NMR |
| $DP_n^{targ}$ | Degree of polymerisation targeted |
| $DP_n^{theo}$ | Degree of polymerisation theoretical |
| dRI | Differential refractive index detector |
| DSC | Differential scanning calorimetry |
| DMF | Dimethylformamide |
| DMSO | Dimethyl sulfoxide |
| $Đ$ | Dispersity |
| DLS | Dynamic light scattering |
| ESI MS | Electrospray ionisation mass spectrometry |
| eROP | Enzymatic ring-opening polymerisation |
| EP | Ethyl phosphonate |
| EO | Ethylene oxide |
| EPDM | Ethylene propylene diene monomer |
| FDA | Food and Drug Administration |
| FTIR | Fourier-transform infrared |
| $T_g$ | Glass transaction temperature |
| g | Radius of gyration contraction factor |
| g' | Intrinsic viscosity contraction factor |

| | |
|---|---|
| $D_H$ | Hydrodynamic diameter |
| $D_{H,\ DLS}$ | Hydrodynamic diameter by DLS |
| $D_{H,\ DLS\ (IWD)}$ | Hydrodynamic diameter by DLS (intensity weight distribution) |
| $D_{H,\ DLS\ (IWD)}$ | Hydrodynamic diameter by DLS (number weight distribution) |
| HLB | Hydrophilic-lipophilic balance |
| HEMA | Hydroxylethyl methacrylate |
| HMF | 5-(hydroxymethyl)furfural |
| IS | Internal standard |
| η | Intrinsic viscosity |
| MAH | Maleic anhydride |
| MH | Mark-Houwink |
| MS | Mass spectrometry |
| m/z | Mass-to-charge ratio |
| MALDI-TOF | Matrix assisted laser desorption and ionisation-time of flight |
| $T_m$ | Melting temperature |
| SEC-E | SEC-DMF (at ENSCM) |
| SEC-G | SEC-DMF (at Germany) |
| SEC-N | SEC-DMF (at Nottingham) |
| SEC-U | SEC-DMF (at University of Montpellier) |
| MW/ M | Molecular weight |
| MWCO | Molecular weight cut-off |
| MALS | Multi-angle light scattering |
| NIST | National institute of standards and technology |
| NRV | Non-return valves |
| NMR | Nuclear magnetic resonance spectroscopy |
| PI | Photoinitiator |
| PFDA | Poly(1,1,2,2- tetrahydroperfluorodecyl acrylate) |
| PAA | Poly(acrylic acid) |
| PAMAM | Poly(amidoamine) |
| PEG | Poly(ethylene glycol) |
| PEO | Poly(ethylene oxide) |
| PEP | Poly(ethyl phosphonate) |
| PGA | Poly(glycolic acid) |
| PLA | Poly(lactic acid) |
| PLGA | Poly(lactic-*co*-glycolic acid) |
| PLMA | poly(lauryl methacrylate) |

| | |
|---|---|
| PMMA | Poly(methyl methacrylate) |
| POEGMA | Poly(oligo(ethylene glycol) methacrylate) |
| PPE | Poly(phosphoester) |
| S-PCL | *D*-sorbitol-poly(ε-caprolactone)/*D*-sorbitol-PCL |
| S-PCL-MAc | *D*-sorbitol-PCL functionalised hemi-ester of maleic acid |
| S-PCL-MAc-*C*-DVE | *D*-sorbitol-PCL-MAc-*crosslinked*-DVE |
| PPO | Poly(propylene oxide) |
| PCL | Poly(ε-caprolactone) |
| PDMAEMA | Poly[2-(dimethylamino)ethyl methacrylate] |
| HBPO | Poly[3-ethyl-3-(hydroxymethyl)oxetane] |
| PCL-*b*-PEP | Poly(ε-caprolactone)-block-poly(ethyl phosphonate) |
| PS | Polystyrene |
| PTFE | Polytetrafluorethylene |
| psi | Pound per square inch |
| PO | Propylene oxide |
| $R_g$ | Radius of gyration |
| RI | Refractive index |
| dn/dc | Refractive index increment |
| REACH | Registration, Evaluation and Authorisation of Chemicals |
| ROP | Ring-opening polymerisation |
| rpm | Revolutions per minute |
| RT | Room temperature |
| $scCO_2$ | Supercritical carbon dioxide |
| SCFE | Supercritical carbon dioxide fluid extraction |
| SCF | Supercritical fluid |
| SEC-UC | SEC using Universal Calibration |
| SEC-MALS | Size exclusion chromatography-multi-angle light scattering |
| $M_n^{\text{NMR}}/M_n^{\text{H-NMR}}$ | Number average molecular weight by $^1$H NMR |
| $M_n^{\text{P-NMR}}$ | Number average molecular weight by $^{31}$P NMR |
| $M_n^{\text{SEC}}$ | Number average molecular weight by SEC |
| $M_n^{\text{SEC-MALS}}$ | Number average molecular weight by SEC-MALS |
| $M_n^{\text{Copoly}}$ | Number average molecular weight of block copolymer |
| $N_{arms}$ | Number of arms |
| $N_{arms}^{\text{SEC-MALS/NMR}}$ | Number of arms from SEC-MALS and NMR |
| $N_{arms}$ ($^{31}$P) | Number of arms by $^{31}$P |
| $M_w$ | Weight average molecular weight |

| | |
|---|---|
| THF | Tetrahydrofuran |
| TEA | Triethylamine |
| TGA | Thermogravimetric analysis |
| $T_d$ | Thermal degradation temperature |
| $Sn(Oct)_2$ | Tin octanoate |
| TEM | Transmission electron microscopy |
| $D_{TEM}$ | Diameter by TEM |
| TBD | 1,5,7-triazabicyclo[4.4.0]dec-5-ene |
| DVE | Triethylene glycol (divinyl ether) |
| VOC | Volatile organic compound |
| $\gamma$ | Surface tension |
| $\gamma_{CAC}$ | Surface tension at CAC |
| wt% | weight/weight percentage |
| Pluronic | Ethylene oxide and propylene oxide block copolymers |
| Tweens | Ethoxylated sorbitan esters / Polysorbate surfactants |
| $\Gamma_{max}$ | Surfactant surface excess concentration |
| $A_{min}$ | Surface area occupied by a surfactant molecule |

# Chapter 1
# General Introduction

## 1.1 Motivation for the Choice of Various Material Systems

Polymers are an indispensable ingredient of human life. Numerous materials utilised in day-to-day life are made from polymers, such as shampoo bottles, washing liquids, food packaging, clothing of synthetic fibres, plastic bags, polymer-based paints the list is endless. A significant advantage can be gained if the polymeric materials are synthesised from biodegradable components that can be broken down by microorganisms and recycled in the environment after they have served their function.

Surfactants are based on short polymer chains and are found in every household cleaner and detergent to help remove dirt as washing-active substances, these are also found in numerous industrial applications including cosmeceutical, personal care, crop protection, elastomers, oilfield chemicals, food and beverages, etc. Personal care is one of the major end-users of surfactants.[1] In 2017, a worldwide turnover of about USD 36 Billion was achieved from surfactant market alone and is expected to reach around USD 45 Billion by 2022 at a compound annual growth rate (CAGR) of 5.41 %.[2]

Surfactants can be broadly divided into Synthetic Surfactants and Natural Surfactants[2] and the latter can further break down into two categories: chemically made Biobased Surfactants and Biosurfactants (Figure 1.1).

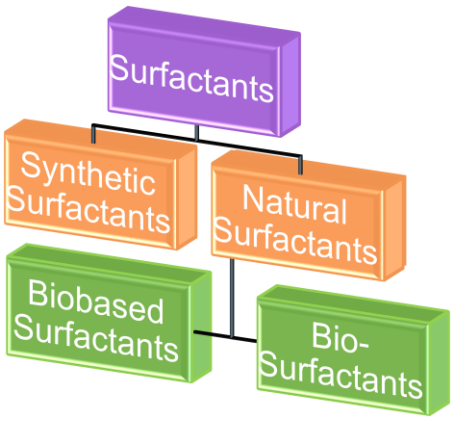



Figure 1.1. General classification of Surfactants.

Synthetic surfactants are tailor-made from feedstocks derived from fossil fuel refining i.e. from petroleum resources. When the raw material for surfactants is from non-

petrochemical resources/biodiversity, they are called natural surfactants.[4] When natural surfactants are chemically derived from eco-friendlier raw materials (plants or animals oil etc.) they are referred to as biobased surfactants.[3] Only, a thin line distinguishes biobased surfactants from biosurfactants.

In fact, biosurfactants are "*microbial amphiphilic compounds produced in living species or excreted extracellular hydrophobic and hydrophilic moieties that confer on the organism the ability to accumulate between fluid phases thus reducing surface and interfacial tension.*"[4]

Indeed, the commercial surfactants are made from both petrochemical feedstock and biobased resources, but the majority of them are still from the fossil origin.[5] The rapid price hike of petrochemical products and a diminishing supply of crude oil are driving the current market towards environment-friendly alternatives and have boosted a demand for bio-based surfactants.[1] Not only is the supply exhausting, but also fossil feedstocks negatively impact our environment (escalating greenhouse $CO_2$ emission) and often these materials are not biodegradable.[5] The global natural surfactants market (biobased surfactants) alone accounted for USD 13 Billion in 2016 and is projected to touch USD 17 Billion by 2022.[6]

Stringent environmental regulations and legal-political frameworks may be the factors triggering a paradigm shift towards the production of sustainable biobased surfactants in the industry. At the same time, rising environmental concerns among consumers are driving a demand for green, eco-friendly and biodegradable products.[7]

The European Committee of Organic Surfactants and their Intermediate (CESIO) is also actively contributing towards the development of standards for the classification of biobased surfactants:[8] For instance, when judging the sustainability of a material, all the influences and impacts of a furnished product from the cradle to grave are emphasised. For example, a question is posed "*can it always and automatically be claimed that a surfactant is more sustainable just because the raw material source is renewable?*" The increasing market pressure for sustainable products and an urge to stop damaging our ecosystem, are fuelling the demand for the industrial development of new detergents utilising natural, renewable feedstocks that are then biodegradable.[9] Not only the market pressure but also the concept of sustainable detergents have already

been put forward into various action plans by the European Policies. For example, a set of rules by European Commission[1]* (EC 648/2004) and its implementation guidelines and the REACH (Registration, Evaluation and Authorisation of Chemicals) initiatives for detergent systems are driving industrially to limit the use of conventional fossil-based systems and move towards biobased alternatives with a particular emphasis on the biodegradability of surfactants.

The 12 principles of green chemistry[10] include:

1) prevention; 2) atom economy; 3) less hazardous chemical syntheses; 4) designing safer chemicals; 5) safer solvents and auxiliaries; 6) design for energy efficiency 7) use of renewable feedstocks; 8) reduce derivatives; 9) catalysis; 10) design for degradation; 11) real-time analysis of pollution prevention; 12) inherently safer chemistry for accident prevention.

In combination with the **biobased raw materials**, the **reaction solvent** and the **catalytic system** are other essential pillars of the 12 principles playing an important role to mitigate the environmental problems in the context of maintaining a sustainable society.[10] These are accompanied by 12 principles of green engineering[11] which emphasise 'prevention instead of treatment' i.e. 'it is better to avoid waste production rather than clean up after it is formed.' Indeed, the steps of separation and purification are costly, time-consuming and in fact, these steps are responsible for the generation of a large part of the effluents.

Effective utilisation of green solvents, such as water, supercritical fluids (SCFs), ionic liquids, liquid polymers or switchable solvents is another pillar of green chemistry.[12] $CO_2$, among all, is a gas under ambient temperature and pressure, its use facilitates the effective separation and purification steps. The utilisation of supercritical carbon dioxide ($scCO_2$) has attracted great interest in industrial processes, such as low energy consumption during operation, replacing the environmentally damaging conventional organic solvents and higher-yield of products. Health and safety benefits are especially evident in the use of $scCO_2$ (and also in supercritical water).[13] Supercritical fluid extraction (SCFE) using $scCO_2$ is gaining momentum in applications designed to

[1]* European Commission Regulation (EC) No 907/2006 of 20 June 2006 amending Regulation (EC) No 648/2004 of the European Parliament and of the Council on detergents, Official Journal of the European Union).

extract flavours and aromas, such as in food and beverages, pharmaceuticals, fragrances and cosmetics industries.[14]

Among all the polymerisation methods, catalytic approaches appear to be the most likely to answer the current challenges and needs of society. The history of catalysis dates back to the 1920s when the basic and acid catalysts were used.[15] Then in the 1950s, the transition metal-based catalysts (Ziegler-Natta catalysts) were employed and more recently the works of Grubbs and Schrock (rare-earth based catalysts) have proven to be attractive. In the 1990s, organic catalysts gained popularity and in the 1980s the enzymatic catalysis became prominent.

Industrial and household catalysis are becoming more and more dependent on enzymes. Enzymes are a very well established product in biotechnology and a global sale ascribes to 31% for food and beverage enzymes, 6% for feed enzymes and the remaining for technical enzymes (e.g. in the leather market).[16] The global industrial enzymes market is forecast to reach USD 7 Billion by 2023 from USD 5.5 Billion in 2018 at a CAGR of 4.9% for the period 2018-2023.[17] Proteases constitute the largest product segment in the global industrial enzymes market whereas Lipases represent the other major product segment with high growth potential.[17]

The strategy of this research project is to investigate whether the utilisation of biobased feedstock, a biocatalyst in comparison to the conventional catalyst and a clean solvent-route can create green materials that have surface active properties.

## 1.2 Thesis Structure

As discussed earlier, research is emerging towards the investigation of more environmentally friendly raw materials and alternative greener synthetic procedures. A major challenge in such a process can be employing all biobased feedstock following a green pathway and creating a well-defined advanced architecture.

Research in this Thesis is conducted based on previous studies of biobased star *D*-sorbitol-poly(lactic acid) (star S-PLA) polymers and linear *D*-sorbitol-PLA surfactant.[18] One of the perspectives in the Thesis of Goddard[19] was the utilisation of another more hydrophobic biobased ε-caprolactone (ε-CL) monomer, to investigate if

the same approach of using US-FDA approved $Sn(Oct)_2$ and $scCO_2$ could yield a branched poly(ε-caprolactone) (PCL).

Moreover, an interest in finding greener replacements for the traditional catalyst and designing novel synthetic approaches is becoming crucial. Such a method might allow the synthesis to be performed in an eco-friendly manner, avoiding harsh reaction conditions and decreasing (or eliminating) the utilisation of volatile organic compounds (VOCs). Thus, enhancing the green credential of the synthesised biopolymer.

With this aim, this Thesis is divided into the following Chapters:

Chapter 2 provides an essential state of the art of the topics discussed.

Chapter 3 provides a brief description of the high-pressure autoclave, key analytical techniques and all of the experimental methods used to characterise the polymers.

Chapter 4 reports the synthesis of hydrophobic polyol-PCL from renewable sugars with different numbers of hydroxy-terminated PCL arms growing and depending on the type of catalyst and the nature of the initiating core. The topology of the materials (particularly star architecture) was investigated using size exclusion chromatography (SEC) and nuclear magnetic resonance (NMR). Based on the quantitative $^{31}$P-NMR titration methodology described for the determination of the number average of arms given by Goddard *et al.*,[18] attempts were made for the development of this technique to quantify the molecular weight of samples and are corroborated with the SEC and $^{1}$H-NMR. Attempts were made to estimate the average number of arms by SEC-Universal Calibration approach.

Chapter 5 exploits the preparation of amphiphilic linear diblock and triblock copolymers as well as star diblock copolymers from the polyol-PCL samples developed in Chapter 4. The influence of modifying $M_n$ (amphiphilicity), architecture (linear vs. star copolymers) and branching (number of arms) on the self-assembly properties were investigated using dynamic light scattering (DLS) as well as by transmission electron microscopy (TEM) and cryogenic-TEM (Cryo-TEM).

Chapter 6 examines the equilibrium and dynamic surface tension of the water-soluble triblock surfactants against commercial standards. Further derivatisation of the non-

water-soluble biobased star PCL prepared in Chapter 4 by enzymatic catalysis were exploited, with the aim of preparing water-soluble biobased star PCL samples that are surface active. Additionally, a preliminary investigation of the utilisation of the functionalised (maleic) star PCL polymers was conducted to prepare biobased star PCL crosslinked films through photopolymerisation with vinyl ether(s).

Chapter 7 gives a general conclusion highlighting the main findings of this research. Furthermore, some perspectives are discussed for the valorisation of the biobased star polymers.

The research in this Thesis has been carried out in collaboration with four laboratories with partners from the UK, France and Germany.

**In France:**

- Dr Habil. Patrick Lacroix-Desmazes and Dr. Cécile Bouilhac - Institut Charles Gerhardt Montpellier, Ingénierie et Architectures Macromoléculaires, Montpellier.

**In England:**

- Prof Steve Howdle at the University of Nottingham, Nottingham.
- Mrs Adeline Coulson and Dr Amy Goddard, Croda Europe.

**In Germany:**

- Dr Habil. Frederik Wurm, Max Planck Institute for Polymer Research, Mainz.

The European Commission within the European framework of the Sustainable Industrial Chemistry Doctoral Programme (SINCHEM) (http://www.sinchem.eu/) financed the PhD grant of Payal BAHETI.

## 1.3 References


1. Surfactants Market - Segmented by origin, type, Application, and Geography - Growth, Trends and Forecasts (2018 - 2023). *Modor Intelligence* (2018). Available at: https://www.mordorintelligence.com/industry-reports/global-market-for-surfactants-industry. (Accessed: 4th September 2018)
2. Global Surfactants Market 2018 - Segmented by Origin, Type, Application, Geography-Growth, Trends and Forecasts to 2023. *Reuters* (2018). Available at: https://www.reuters.com/brandfeatures/venture-capital/article?id=28431. (Accessed: 4th September 2018)
3. Douglas Hayes, Dai Kitamoto, Daniel Solaiman, R. A. *Biobased Surfactants and Detergents: Synthesis, Properties, and Applications*. (AOCS, 2010).
4. Md, F. Biosurfactant: Production and Application. *J. Pet. Environ. Biotechnol.* **3,** 124 (2012).
5. Market Study: Surfactants (3rd edition). *Ceresana Market Research* (2018). Available at: https://www.ceresana.com/en/market-studies/chemicals/surfactants/. (Accessed: 18th August 2018)
6. Natural Surfactants Market - Global Forecast to 2022. *MarketAndMarkets* (2018). Available at: https://www.marketsandmarkets.com/Market-Reports/natural-surfactant-market-25221394.html. (Accessed: 4th September 2018)
7. Future of Green Surfactants with Novel Materials. *Ecovia Intelligence* Available at: http://www.ecoviaint.com. (Accessed: 18th August 2018)
8. Surfactants and sustainability. *CESIO, Surfactants Europe* Available at: http://www.cesio.eu/index.php/about-surfactants/contribution-to-surfactants-and-sustainability. (Accessed: 16th August 2018)
9. Patel, M. Surfactants Based on Renewable Raw Materials. *J. Ind. Ecol.* **7,** 47–62 (2003).
10. Anastas P. T. & Warner J. C. *Green Chemistry: Theory and Practice*. (Oxford University Press, New York, USA, 1998).
11. Anastas, P. T. & Zimmerman, J. B. Peer Reviewed: Design Through the 12 Principles of Green Engineering. *Environ. Sci. Technol.* **37,** 94A–101A (2003).
12. Ceballos, A. M., Hernandez, G., Moreno, G. E., Portillo, O. & Gutierrez, R. Green synthesis of new chiral halogenated imines derived from Benzo[b]thiophene-2-carboxaldehyde. *Trends Green Chem.* **03,** 9889 (2017).
13. Knez, Ž. *et al.* Industrial applications of supercritical fluids: A review. *Energy* **77,** 235–243 (2014).
14. Method of Choice: Supercritical Fluid Extraction. *Evonik Power To Create* Available at: https://extraction.evonik.com/product/extraction/en/about/. (Accessed: 5th September 2018)
15. Wisniak, J. The History of Catalysis. From the Beginning to Nobel Prizes. *Educ. Química* **21,** 60–69 (2010).
16. Binod, P. *et al.* Industrial enzymes - Present status and future perspectives for India. *J. Sci. Ind. Res. (India).* **72,** 271–286 (2013).
17. Research, B. Global Markets for Enzymes in Industrial Applications. *In Report BIO030K* (2018). Available at: https://www.bccresearch.com/market-research/biotechnology/global-markets-for-enzymes-in-industrial-applications-bio030k.html. (Accessed: 5th September 2018)
18. Goddard, A. R. *et al.* Controlled polymerisation and purification of branched poly(lactic acid) surfactants in supercritical carbon dioxide. *Green Chem.* **18,** 4772–4786 (2016).
19. Goddard, A. R. Sustainable Synthesis of Renewable Surfactants. *Thesis* (University of Nottingham, 2016).

# Chapter 2
# State of the Art

The aim of this Chapter is to provide essential background for this Thesis. The chapter introduces biobased building blocks, renewable surfactants and biosurfactants. It also emphasises the fundamental properties of surfactants and their aggregation behaviour based on topology. The emphasis will be placed on green polymer chemistry and more specifically biodegradable polyesters, which will be the key focus of the research undertaken. The Chapter also introduces the use of supercritical carbon dioxide as a clean alternative to conventional solvents in polymer synthesis and purification. Finally, conclusions will be drawn leading to the research strategy followed on this PhD work will be outlined.

## 2.1 Surfactants

Surface-active agent (abbreviated surfactant) literally means active at the surface. Surfactants are organic compounds that constitute two portions having different polarities, the lyophilic (hydrophilic when in water) and a lyophobic (hydrophobic when in water), therefore they are also called amphiphiles. Hydrophilic and hydrophobic moieties of the surfactant are commonly called head and tails, respectively. They are used as ingredients in a variety of products as foaming agents, dispersants, emulsifiers, solubilising agents, cleansers, and conditioners, among others. In a classical surfactant, the hydrophobic part is generally a linear or branched hydrocarbon group (with various degrees of unsaturation sometimes). Other common hydrophobic tails include fluorinated or siloxane chain but for brevity, the research in this Thesis focuses mainly on hydrocarbon groups. The hydrophobic region is generally lipophilic (oil soluble), so it tends to disrupt the water molecule network hence, its presence in bulk water is not favoured energetically. The hydrophilic region is generally water-soluble (but not-lipophobic, some degree of oil solubility is possible) and different degrees of hydration can be observed.

Synthetic surfactants are classified according to the nature of the head group, i.e. electrical charges in water as ionic (anionic, cationic), amphoteric (zwitterionic), and non-ionic (Figure 2.1).[1] In recent decades, a new class of surface active substance has been introduced, so-called ‘polymeric surfactants’ or ‘surface active polymers’, due to the association of one or more macromolecular structures exhibiting hydrophilic and

lipophilic moieties, either as separated blocks or as grafts.[2] The majority (> ~90%) of the surfactant market are covered by anionic and non-ionic surfactants.[1] Although polymeric surfactants are not often accounted in such statistics they constitute a small portion (~10%) of the market share.[1]

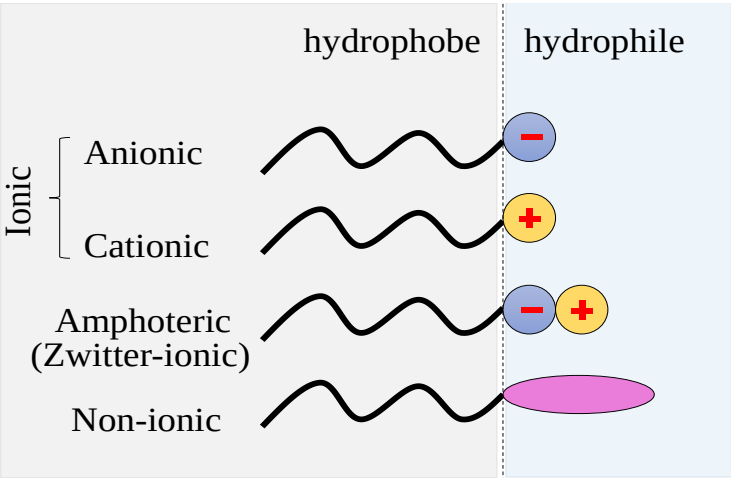



Figure 2.1. General classification of surfactants based on the type of the head group as anionic, cationic, amphoteric (zwitterionic), and non-ionic.

Ionic surfactants carry a net negative (anionic) or positive (cationic) permanent charge on the head group (the counter ion being free in water). The most common anionic surfactants are sulphates, sulphonates and phosphates (used extensively as a cleanser in detergents). However, it should be noted that the presence of the charge depends on the pH of the solution.[1] Cationic surfactants mostly consist of amines such as quaternary ammonium cation and can be charged or neutral depending on the pH.

Zwitterionic (also amphoteric) surfactants carry covalently linked opposite charges, for example, betaines which consist of an ammonium cation (basic amine) and a carboxylate (carboxylic acid).[1,2]

Non-ionic surfactants possess no charge and do not dissociate when dissolved in water. The most common examples are alkyl ethoxylates [based on poly(ethylene oxide), (PEO)] with varied structure of both the head and tail groups. They have the broadest range of properties depending upon the ratio of hydrophilic-lipophilic balance (HLB).[3] Actually, Griffin's HLB numbering system is also a measure of the percentage of ethoxylation present in a surfactant.

The HLB is a numerical system (the Griffin scale ranges from 1 to 20, given by HLB = 20 × $M_{\text{hydrophilic part}}/M_{\text{whole surfactant}}$) used to describe the relationship between the water-soluble and oil-soluble parts of a non-ionic surfactant (hydrocarbon portion for

polymeric surfactants).[4,5] Where $M_{hydrophilic\ part}$ is the molecular mass of the hydrophilic portion of the molecule, and $M_{whole\ surfactant}$ is the molecular mass of the whole molecule, giving a result on a scale of 0 to 20. An HLB value of 0 corresponds to a completely lipophilic/hydrophobic molecule, and a value of 20 corresponds to a completely hydrophilic/lipophobic molecule. For instance, a surfactant with an HLB of 1 will tend to be oil soluble (HLB <10), while a surfactant with an HLB of 15 will tend to be water-soluble (HLB >10). It helps to suggest, for instance, if a surfactant has an HLB >15, i.e. hydrophilic surfactant means they could be employed for solubilisation, detergency, and for products that will dilute readily with water, while those that have HLB between 13 - 15 have detergency properties (Figure 2.2).[4,5] According to the Bancroft empirical rule, the continuous phase of an oil-water emulsion will be the phase where the surfactant is the most soluble. Therefore, if the surfactant prefers water, it will tend to form a direct oil-in-water (O/W) emulsion (and vice-versa, if the surfactant prefers oil, it will tend to form an inverse water-in-oil (W/O) emulsion.[6,7] Thus, surfactants with HLB between 3 - 6 acts as water-in-oil (W/O) emulsifier while 8 to 16 acts as O/W emulsifier. Surfactants in the HLB range 1 to 3 tend to be anti-foaming agent while 7 to 9 acts as a wetting and spreading agent (Figure 2.2).[5]

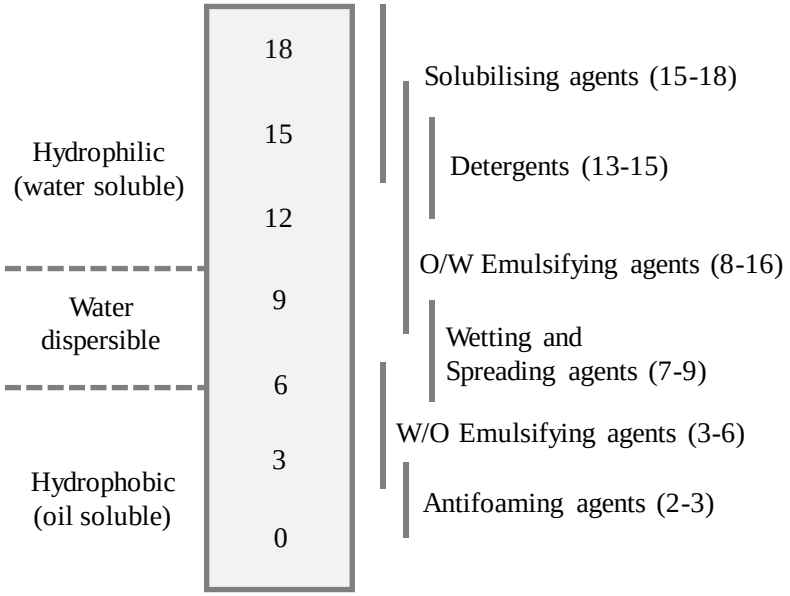



Figure 2.2. HLB scale showing classification of surfactant function.[5]

This HLB system will be employed for polymeric surfactants in Chapters 5 and 6.

### 2.1.1 Biobased Building Blocks and Green Surfactants

Bio-based materials are those made from renewable plant or animal feedstocks and thus the terms "biobased," "renewable" and "biotic" are often interchangeable.[8,9]

#### 2.1.1.1 Renewable Hydrophiles

The most important feedstocks for renewable hydrophile production include vegetable oils and cellulose (for glycerol), sugar cane and sugar beets (for sucrose), and starch-producing crops such as maize, wheat, potato and cassava (for glucose).[2,10,11] While glycerol, sucrose, and glucose are all used directly in surfactant production, glucose also serves as a common precursor to a variety of downstream chemicals that can also be used as hydrophiles.

Sustainability of the production of chemicals from naturally occurring biomass, however, is debated as critical concerns are raised about the current production of chemicals and fuels that relies on edible starch and sugar crops. Thus a limited supply of edible crops can lead to competition with food production.[12]

Lignocellulose is the most abundant inedible biomass that has important advantages over other biomass as they do not interfere with food supplies.[13,14] Lignocellulosic biomass is projected as an abundant carbon-neutral renewable source, which could decrease fossil-$CO_2$ emissions and atmospheric pollution.[15] Such biomasses for the production of value-added chemicals including renewable hydrophiles and hydrophobes are increasingly gaining attention.[11,14]

Lignocellulose consists of cellulose, hemicellulose and lignin (Figure 2.3, top schematic), in which the sugar polymers account for a large portion.[11] Cellulose is a water-insoluble polymer composed of glucose units linked by β-1,4-glycosidic bonds, whereas hemicellulose includes various pentoses and hexoses connected by several forms of glycosidic bonds. Lignin is a three-dimensional polymer based on phenylpropane units.[11] Sugars derived from lignocellulose would be the first platform chemicals in the next-generation bio-refinery.

Lignocellulosic biomass could become a major feedstock for sugar-containing polymers by providing $C_5$ (xylose, arabinose) and $C_6$ (glucose, mannose, galactose, rhamnose), monosaccharides and their many useful linear derivatives. For example, alditols (isosorbide, erythritol, mannitol, sorbitol, xylitol), aldonic acids (such as

gluconic acid), 1,4-diacids (succinic acid, fumaric acid, malic acid), 2-hydroxymethylfurfural (HMF), glycerol (Figure 2.3, bottom schematic)[11] and the list continues for other useful bio-based chemicals that can offer outstanding advantages for the preparation of bio-based polymers.[11,16]

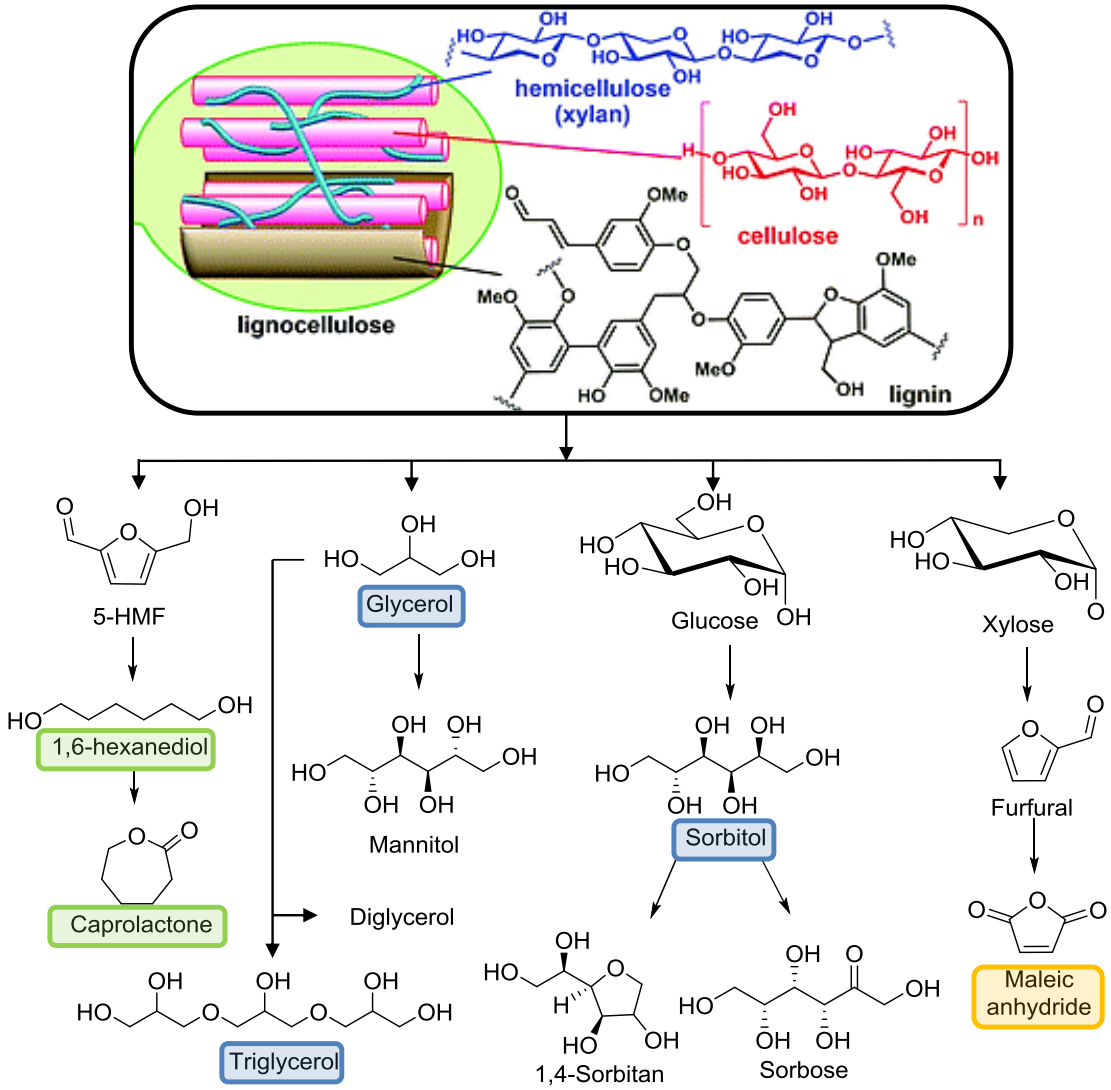



Figure 2.3. Structure of lignocellulosic biomass (top)[14] and representative one-pot conversion of cellulose to sugar-related compounds such as glucose, sorbitol, 5-HMF, glycerol, xylose.[11,14] Compounds discussed in this thesis are highlighted in green for hydrophobic, in blue for water-soluble moieties and in orange for chain-end functionalisation.

It is noteworthy that poly(ethylene oxide) (PEO) is the most used non-ionic hydrophile in the surfactants field. There are many PEO based surfactants in the market, which have gained regulatory approval from the US and/or the EU. Some well-established versatile surfactants are made from the oxyethylene family. Such as Spans (sorbitan esters), Tweens® (polyethoxylated sorbitan ester), Pluronic® (triblock copolymer of

ethylene oxide with propylene oxide, EO–PO) and Poloxamines (Tetronics®, X-shaped structure made of an ethylenediamine central group bonded to four chains of PEO–PPO blocks).[2,17–19] Some Pluronics and Tweens is utilised along with chemically synthesised biobased surfactants (discussed in Chapter 6).

But the oxidative degradation of PEO and unwanted toxic side-product formation have raised some serious concerns lately.[20] Thus, alternatives to PEO such as poly(2-oxazoline)s, polypeptoids, polyphosphoesters, as well as linear and hyperbranched poly(glycerol) have attracted attention (Figure 2.4).[20–22]

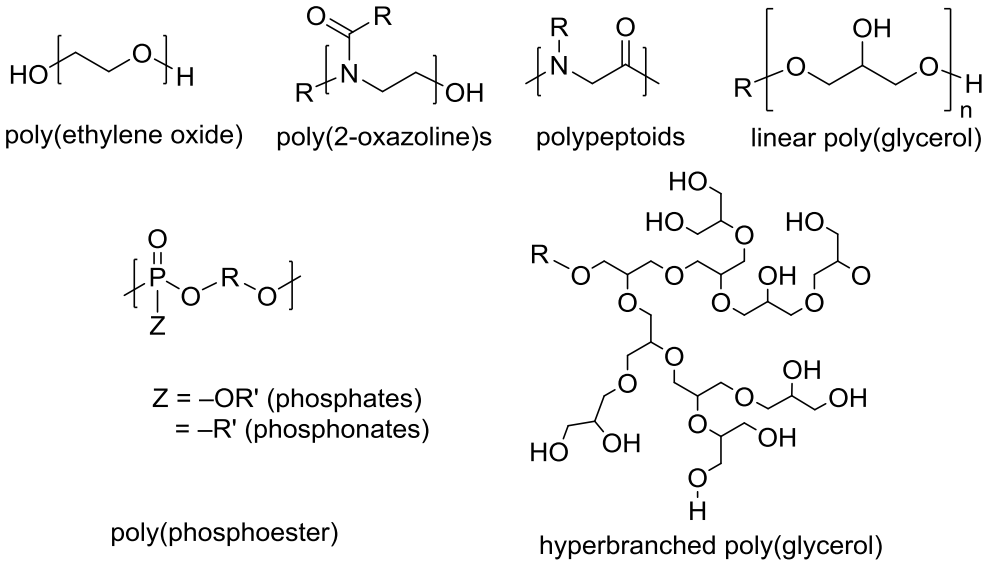



Figure 2.4. Chemical structures of water-soluble biomaterials that are currently gaining attention as alternatives to PEO.[20–22]

Polyphosphoesters (PPEs) can be biodegradable, biocompatible and have structural similarity to naturally occurring nucleic acids and thus have been investigated as biomaterials for tissue engineering, drug and gene delivery. One example is the poly(lactide-*co*-ethyl phosphate) copolymer[23] that is used as a drug carrier for paclitaxel in preclinical and clinical studies.[22]

This Thesis focuses on the polymerisation of cyclic phosphoesters (more precisely cyclic phosphonates) as a hydrophilic block in Chapter 5.

### 2.1.1.2 Renewable Hydrophobes

Most of the feedstock produced from biomass is employed as a hydrophobic moiety for surfactant production and the process is established industrially.

The fats and oils from plant or animal tallow triglycerides (TG) are hydrolysed to glycerol and fatty acids (FAs) (Figure 2.5), and FAs are the most common among the hydrophobes.[10] About 80% of the global oil and fat production was vegetable oils and only 20%, with declining tendency, were of animal origin.

Coconut oil and palm kernel oil contains a high share (~70%) of FAs containing a short or medium chain length with $C_{8\text{-}18}$ carbon atoms saturated FAs (such as caprylic, capric, lauric, myristic, palmitic and stearic chains).[10,24,25]

Palm, soybean, rapeseed, and sunflower oil, as well as animal fats such as tallow, contain mainly long-chain fatty acids such as $C_{18}$ unsaturated FAs such as oleic acid, linoleic acid, linolenic acid, erucic acid and ricinoleic acid.[24,25] Such unsaturated bonds in fatty acids are important for chemical modification to obtain bulkiness in the hydrophobic moiety of the surfactant and to tune surface active properties.[26]




Fatty acid Fatty alcohol

Figure 2.5. Most common renewable hydrophobes used in surfactant design. Fatty acids and fatty alcohols are generally between $C_6$-$C_{18}$ in length.[10]

Fatty alcohols (FOHs) (Figure 2.5, b) are also very important for surfactant production, with approximately 50% of those coming from renewable feedstocks.[10] At least two important classes of renewable surfactants are derived directly from FOHs; alkyl polyglucosides (APGs) and fatty alcohol sulfates (FASs).[10] Factors such as cost, availability and chemical composition can all limit the implementation of FAs and FOHs fatty alcohol feedstocks.

Another biobased hydrophobe from other natural oils include the alkylphenol derivatives that are isolated from the waste of cashew nut shells and contains anacardic acid, a mixture of saturated and unsaturated variants of 6-pentadecyl salicylic acid. The phenol can be glycosylated and the resulting glycolipids have interesting self-assembly properties in water.[24]

Hydrophobes from biobased dicarboxylic acids (e.g. succinic acid and adipic acid) are also interesting diacids which are produced by fermentation using various types of microorganisms and natural substrates.[11] Such dicarboxylic acids are important hydrophobes when linked with FOHs. For examples, a biobased azelaic acid condensed

with 1,6-hexanediol was employed as a hydrophobic block for surfactants and PEO was used as hydrophile.[27]

Biobased cyclic esters (Figure 2.6) can also be used to synthesise hydrophobic polyesters, such as poly(ε-caprolactone) (PCL), poly(γ-butyrolactone), poly(γ-valerolactone) and poly(δ-valerolactone). PCL is a biodegradable polymer and through polymerisation techniques, discussed in Chapter 4, the tuning of MW and the synthesis of well-defined architectures are possible. These polyesters are generally hydrophobic and copolymers with PEO are prepared to increase hydrophilicity.

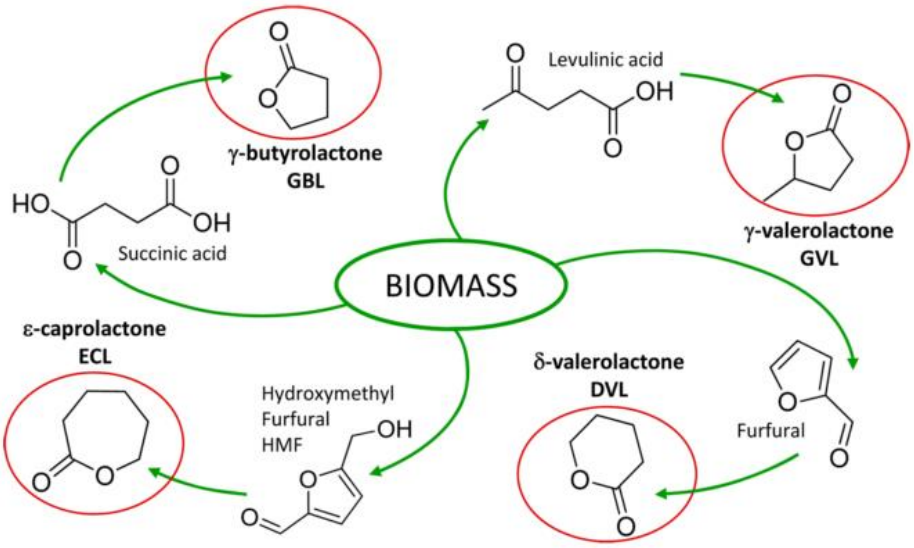



Figure 2.6. Cyclic lactones obtained from biobased resources.[28]

In addition, linear or star-shaped block copolymers of PCL as hydrophobe and poly(ethyl ethylene phosphate) as hydrophilic have been synthesised and used as drug carriers for Doxorubicin or Paclitaxel delivery.[29] The potential of poly(phosphoester)s as a hydrophilic block is discussed in Chapter 5.

### 2.1.1.3 Commercial Biobased Surfactants

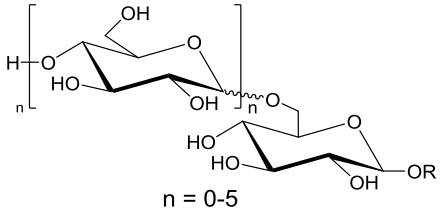
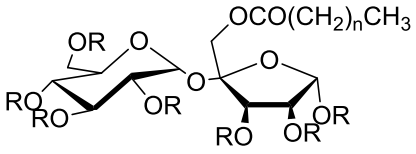
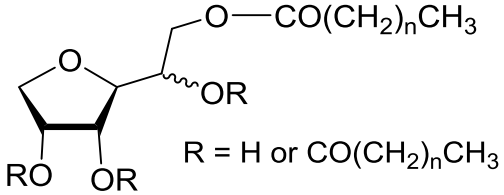
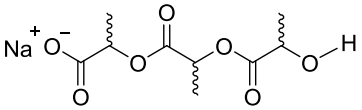
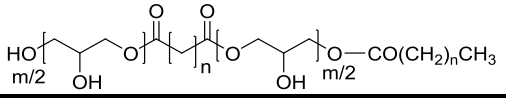
Among the nonionic surfactants, carbohydrate-based surfactants have gained a lot of attention due to their renewable profile, with non-toxic and biodegradable nature. However, only a small number have found their place in commercial products due to competitive price, purity and availability. Additionally, covalently linking the numerous hydroxyl groups of these hydrophiles with hydrophobic fatty acyl groups is rather challenging.[2,10,26] Consequently, only a few of them are commercialised such as sucrose esters, alkyl polyglucosides (APGs), sorbitan esters [2,26,30] from sucrose,

glucose, *D*-sorbitol respectively and also from derivative of glycerol as polyglycerol esters or from lactic acid as lactyl lactate ester (Table 2.1).[2,11,31]

The hydrophobic (or lipophilic) hydrocarbon chain of alkyl polyglycosides is formed by a fatty alcohol (dodecanol/tetradecanol) obtained from palm kernel oil or coconut oil. The hydrophilic part of the molecule is based on glucose (dextrose) obtained from starch (Table 2.1).[24]

Sorbitan fatty acid esters dominate the market under their trademark Span® and its polyethoxylated derivatives as Tween®. Spans generally have a high proportion of hydrophobic moieties which also includes mono-, di-, and triesters (HLB ≤ 9) (Table 2.1).[3] However, the synthesis of water-soluble surfactants with a high hydrophilic moiety (HLB > 9) is rather challenging as multiple hydrophilic building blocks are necessary.[2,26]

Table 2.1. Representation of some commercial biobased surfactants: APG, sucrose ester, sorbitan ester, lactyl lactate and polyglycerol diacid ester. [2,10,11,26,30,31]

| | Source | Surfactant Name | Surfactants Chemical Structure | HLB |
|---|---|---|---|---|
| Carbo-hydrates | Glucose | Alkyl polyglucoside (APG) |  n = 0-5 R = alkyl chain ($C_8$-$C_{16}$) | >10 |
| | Sucrose | Sucrose Esters |  (about 255 possible isomers) R = H or $C_{14}$-$C_{18}$ fatty acyl chain or $CO(CH_2)_nCH_3$ | 1-18 |
| | Sorbitan [a] | Sorbitan Esters |  R = H or $CO(CH_2)_nCH_3$ | ≤ 9 |
| Organic acid | Lactic acid/ Lactide | Lactyl lactate Esters |  | <12 |
| Biomass | Glycerol [b] | Polyglycerol Diacid Esters |  | ~10 |

[a] From dehydration of *D*-sorbitol. [b] obtained as a side-product during manufacturing of biodiesel fuel by transesterification of seed oils with methanol.

In commercial hydrophilic blocks (polyglycerol and polyglucosides), the number of repeat units is rather limited to oligoglycerols (<10) that restrict the versatility compared to PEO. This is because at higher extents of polymerisation the content of branched and cyclic structures predominates.[12] Thus the major drawback of such acid/base catalysed homopolymerisation is primarily missing selectivity at the high molecular weight but mainly the occurrence of side-reactions (dehydration, oxidation) that deteriorates the product quality by colouration.[32–34] Darkening of product colour makes them unfit for personal care applications. Several downstream processing steps including multiple bleaching and derivatisation with phosphate and carboxylate functionalities become essential in improving product colour, odour and cosmetic acceptability.[35]

The utilisation of sugar-based moieties for preparing linear polymer structures typically give enhanced hydrophilicity. The –OH and –COOH rich functionality of the linear carbohydrates make them particularly useful in polycondensation reactions to make surfactants.[11] Alditol-polyester has also been reported in surfactant design by using hydrophilic sugars with dicarboxylic acids as building blocks. For example, polyglycerol diacid esters (Table 2.1, last row), and it has numerous applications as biodegradable and biocompatible surfactants in foods, cosmetics and pharmaceuticals.[10] They are more prone to be non-toxic and biodegradable than petrochemical-based polycondensates.

Such polyol-polyesters of both linear and star architecture PCL utilising renewable sugars (*D*-sorbitol, glycerol and triglycerol) and renewable diol (1,6-hexanediol) is discussed in Chapter 4.

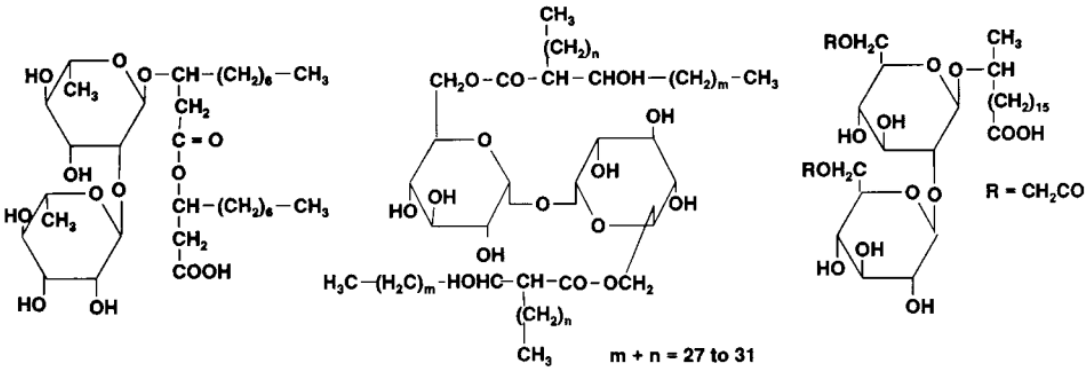
### 2.1.2 Biosurfactants

Another important type of natural surfactant are biosurfactants. They are amphiphilic chemicals produced by bacteria, yeasts, and fungi (biorefinery) and offer biodegradability, biocompatibility and digestibility over their chemically synthesised counterparts.[36,37] The hydrophilic moiety of biosurfactants typically consists of a carbohydrate source (i.e. glycolipids) or amino acids (i.e. lipopeptides), while the hydrophobic moiety is an unsaturated or saturated fatty acid.

Potential advantages over synthetic analogues include the use of waste products as fermentation substrates as well as desirable biodegradability and toxicity profiles.[10]

The microbial origin, chemical production and the potential application of various biosurfactants have been extensively discussed.[37–40]

Most known biosurfactants are glycolipids. Among the glycolipids, Rhamnolipid and Sophorolipid are the most discussed.[26,39,41] Rhamnolipid is obtained from *Pseudomonas aeruginosa* in which two-rhamnose subunits are linked to two β-hydroxydecanoic acids (Figure 2.7, a).




(a) Rhamnolipid (b) Trehalolipid (c) Sophorolipid

Figure 2.7. Chemical structure of some common glycolipid biosurfactants.[42]

Trehalose lipid is obtained from *Rhodococcus erythropolis*, in which disaccharide trehalose is linked to two long-chain α-branched β-hydroxy fatty acids (Figure 2.7, b) and Sophorolipid from *Torulopsis bombicola* in which dimeric sophorose is linked to a long-chain ($C_{18}$) hydroxy fatty acid (Figure 2.7, c).[42] Such renewable feedstocks are abundant and usually low-priced, but their complicated processing procedures lower the yields and raise the downstream costs of purification compared to pure substrates.[42] Better purification techniques and yields at economical costs seem to be key for the commercial success of biosurfactants.

### 2.1.3 Structure-Property Relationship of Surfactants

#### 2.1.3.1 Surface Tension

The amphiphilic characteristics of surfactant molecules are associated with two key features: adsorption at surfaces or interfaces and self-assembly in the bulk solution.

Amphiphiles adsorb or accumulate at interfaces between polar and non-polar media so that the hydrophilic portion is solvated in the polar medium and the lipophilic portion

in the non-polar medium. Examples of such surfaces are between those of water and air or the interface between water and oil.

The driving force to adsorb at an interface is to lower the free energy of that phase boundary. For example, if oil is mixed in water with a supply of mechanical energy, the formed droplets of oil in the water will be quite large. The droplets eventually begin to coalesce into bigger droplets to minimise the interfacial energy, and oil will be pushed upon the surface (lower density of oil). If a surfactant is, however, present in the system then it adsorbs between the interface of oil and water and lowers its surface energy. So that the droplets of the dispersed phase will be much smaller (larger interfacial areas) and an emulsion is formed (direct oil-in-water emulsion or an inverse water-in-oil emulsion, depending on the surfactant affinity for the continuous phase; cf. Bancroft rule). An interface between hydrophobic and hydrophilic media is always energetically unfavourable and a system is always trying to minimise this interfacial area, thus minimising the energy of the system.[43,44]

A molecule in the bulk of water (interior of the liquid) experiences attractive (cohesive) forces equally in every direction by neighbouring molecules (thus the resulting force is zero). Nonetheless, a molecule on the surface of a liquid lacks some neighbouring molecules and thus, experiences an imbalance of forces.[45] Attractive forces of a molecule to its remaining neighbours are stronger on the surface of the liquid; as a result, a force develops that directs at the interior of the medium. Force (F) against the intermolecular forces has to be performed to increase the surface area of a liquid or to move something through this.[45]

Surface tension ($\gamma$) is therefore defined as 'the amount of force (Nm) necessary to expand the surface ($m^2$) of a liquid by one unit'[45] and measured in milliNewton per meter ($mN\ m^{-1}$). As a result, the molecules at the surface have greater free potential energies than those in the bulk liquid. Surface tension ($\gamma$) can thus be defined as the excess free energy per unit area at the surface of a liquid compared to the bulk.[31]

The surface tension of a liquid can be measured using several static and dynamic methods. Static surface tension characterises the surface tension of the liquid in equilibrium and the commonly used measurement methods are Du Noüy ring and Wilhelmy plate.[31] Whereas dynamic surface tension is the time trajectory of surface tension before equilibrium is reached and the bubble pressure method is the most common method used for its determination.[31] It is an important property relevant to many practical, non-equilibrium processes such as emulsification and foaming. It is a

measure of how fast surfactants reduce the surface tension from the value of pure water (from 72 mN $m^{-1}$) to values in the range of ~30-40 mN $m^{-1}$.[31]

These methods have been used in Chapter 6 to determine whether the synthesised compounds display surface-active properties. According to the definition of REACH, any compound that could reduce the surface tension of water (~ 72 mN $m^{-1}$ at 25 °C) down to 45 mN $m^{-1}$ or below is classified as a surfactant. To have consistency and for comparison of surfactants with previous work by Goddard,[46] in the Thesis any compounds that can reduce this tension to <60 mN $m^{-1}$ will be considered surface active.

### 2.1.3.2 Surfactant Bulk Aggregation

As discussed above, one characteristic feature of surfactants is their tendency to adsorb at interfaces. Another fundamental property of surface-active agents is that unimers (free un-associated surfactant molecules) in bulk liquid tend to form aggregates above a certain concentration. The concentration at which further addition of surfactants molecules to liquid makes them go into finite-sized aggregates (so-called micelles) is referred as CAC (Critical Aggregation Concentration) or CMC (Critical Micellization Concentration).[43,44]

Water-soluble surfactants stay as unimers when they are solubilised in water at a very low concentration (Figure 2.8, a). The hydrocarbon chain (non-polar part) interacts weakly with the water molecules in an aqueous medium whereas the hydrophilic (polar) part interacts strongly with water molecules *via* dipole-dipole interactions. This strong interaction of hydrophile with the water molecules renders them soluble in water.

Because of the strong hydrogen bonding between water molecules, it tends to squeeze the hydrophobic moieties out of water leading to an increase in the free energy of the system. Thus, surfactants tend to minimise the contact between the hydrophobic group and water molecules and are first expelled to the air/water interface with their hydrophobic groups oriented on the opposite side of the water, towards air (Figure 2.8, b). Thus, an oriented monolayer is formed at the interface that contributes to the decrease of the surface tension.

Upon further addition of more surfactants when both the air/water interface and the bulk liquid becomes saturated, at this point (the CAC), aggregates begin to form in the bulk phase. And all additional surfactant added above this concentration goes into the

aggregates. Below the CAC, the increase in amphiphile concentration leads to the decrease of the surface tension, while in principle, above the CAC the surface tension remains constant, at increasing concentrations of surfactant leading to the saturation of air/liquid with surfactants and formation of aggregates in the bulk (Figure 2.8, b).

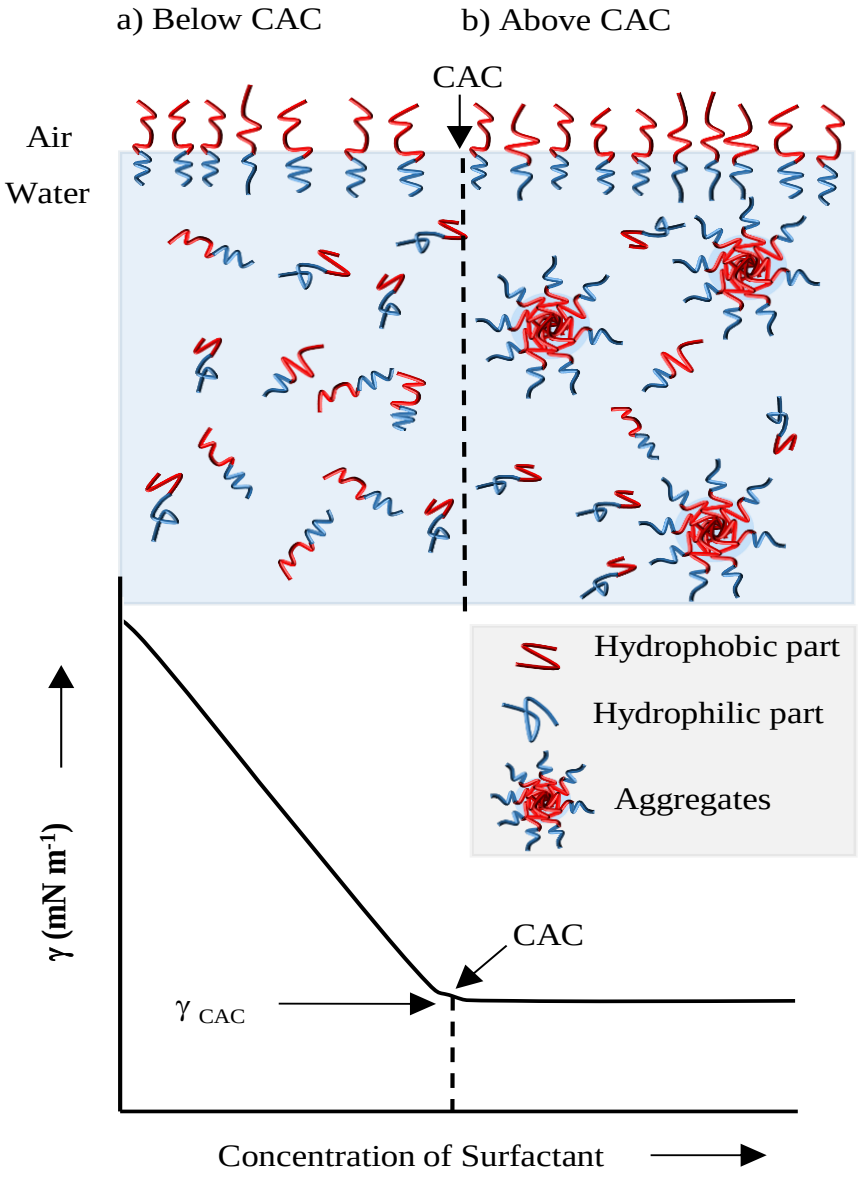



Figure 2.8. Surfactant self-assembly (a) at concentrations below the CAC compounds exist as unassociated unimer, which can align at the air/water interface to form a uniform monolayer that effects a drop-in surface tension; (b) at higher concentrations and above the CAC, surfactants form aggregates. A representative surface tension vs. concentration graph is shown below to aid interpretation of the CAC.

The mechanism of this aggregation is caused by the hydrophobic effect.[44] By which, the interaction between the hydrocarbon chains tries to minimise the contact with water molecules, in a way that surfactant hydrocarbon chains are attracted together in the hydrophobic interior of the aggregates while the hydrophilic part forms an outer

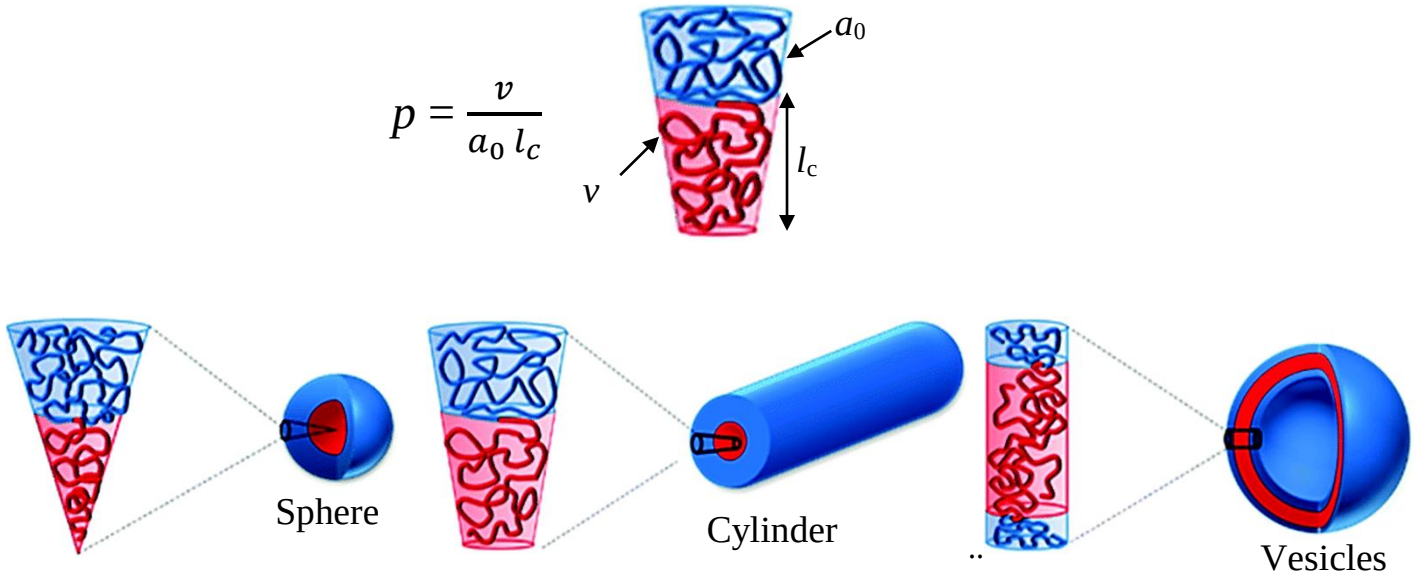
hydrophilic layer towards the water phase. Surfactant molecules are therefore able to self-associate in a given solvent thus forming different types of aggregates and structures of colloidal dimensions (Figure 2.8, b).[44]

## 2.2 Self-Assembly of Surface-Active Polymers

Surface active polymers, or polymeric surfactants, are employed in various applications the majority being for stabilisation of dispersions or as rheology controllers.[44]

If a polymeric surfactant consists of two chemically distinct regions (AB type block copolymer) that are immiscible blocks, it can form colloidal stable aggregates in an aqueous medium. For example, the interior region consists of hydrophobic blocks (the core region) and an outer region of well-solvated hydrophilic blocks (the corona or shell region).[47]

The morphologies of such aggregates depend on the structure and the size of the hydrophilic and hydrophobic group of surfactant molecular structure and can be described with the packing parameter, $p$, as $p = \frac{v}{a_0\, l_c}$, where $v$ is the volume of the hydrophobic segment, $a_o$ is the head group area of the hydrophilic and $l_c$ is the length of the hydrophobic segment.[48,49] Altering these parameters leads to a molecule possessing different interfacial curvature and therefore a different morphology. Spherical micelles are formed when $p \leq ⅓$ (single chain surfactants with large head group areas such as anionic surfactants) is high. The spherical aggregates are very small and their radius is roughly equal to the maximum stretched out the length of the surfactant molecule.[50] When the interfacial curvature is medium, $p$ is between ⅓ and ½, cylindrical aggregates (worm-like micelles) are formed and when $½ < p \leq 1$, vesicles are formed (Figure 2.9).[50]




| ***P* range** | $P < 1/3$ | $1/3 < P < 1/2$ | $½ < P < 1$ |
|---|---|---|---|
| **Extend of curvature** | High | Medium | Low |

Figure 2.9. Schematic illustration of different possible morphologies of aggregates formed from a linear amphiphilic diblock copolymer changing the volume fraction f of the B block from the sphere (a) to the cylinder (b) and to vesicles (lamella) (c) up to 50 %. The dashed curve in each morphology represents the curvature of the interface between A and B domains (adapted from Dencome *et al*[50]).

Amphiphilic block copolymers also consist of covalently bonded blocks forming a variety of architectures (e.g. linear diblock and triblock copolymers, star block copolymers, and miktoarm star copolymers).[47] The self-assembly and some surface-active properties of the above topologies are discussed in Chapter 5 and 6.

The formation of aggregates from diblock, graft and triblock copolymers in solution is represented (Figure 2.10). Diblock copolymer that shows a Gaussian chain in solution (unassociated or 'unimer' state) assembles into a spherical micelle having a 'core' consisting of the water-insoluble (hydrophobic) block and a 'corona' composed of solvated segments of the water-soluble blocks (Figure 2.10, a).[51]

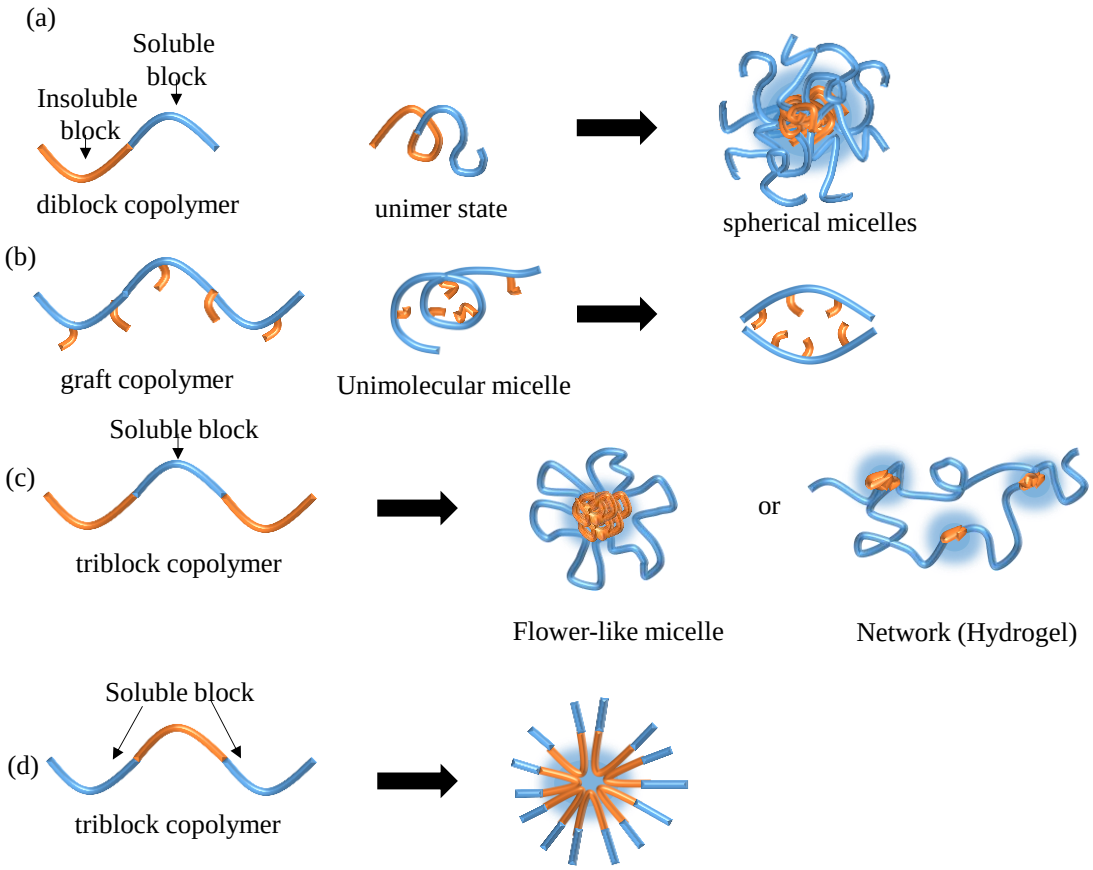



Figure 2.10. Formation of aggregates from the different architectures of amphiphilic copolymers in dilute aqueous solutions. The various states of association depicted here are thermodynamically stable and are attained spontaneously by the amphiphilic copolymers under appropriate conditions.[51,52]

In triblock copolymers, both termini of a hydrophilic (A) or a hydrophobic block (B) may be coupled with the second component to give B–A–B and A–B–A copolymers. A very usual combination is PEO block(s) (hydrophilic block) with PPO block(s) (thermo-responsive: it becomes hydrophobic upon heating) (Pluronic).[53,54] For the

B–A–B copolymer when the solvent is selective (good solvent) for the middle block, there is a possibility for loop formation if both end blocks are incorporated into the same micelle: this gives a flower-like micelle by loosely associated polymers with hydrophobic end-caps. It can also form a network (hydrogel) by the association of the hydrophobic parts of end-capped triblock copolymers (Figure 2.10, c).[51] When water-soluble blocks are the end blocks, spherical micelles are formed (Figure 2.10, d). Although, as discussed earlier, the morphology (phase diagram) of the micelles depends on the composition as well as the concentration of the copolymers (spheres to cylinders to vesicles).

In grafted copolymers, multiple chains are distributed along the main chain composed of hydrophilic units. It forms 'monomolecular micelle' by collapsed hydrophobically grafted polymers and aggregation of the graft copolymers (Figure 2.10, b).[51] It is important to note that the aggregates from randomly modified grafted copolymers are usually smaller in size than micelles formed by end-modified block copolymers since graft polymer can form aggregates within one polymeric chain leading to micelles with smaller aggregation number.[52,55] On the other hand, randomly modified grafted copolymers can form aggregates where some of the hydrophobic fragments may be in close contact with water, such particles can additionally aggregate into larger particles too.[52]

Indeed, the examples above are some of the simplest examples of self-assembly of linear block copolymer directly added to water. Self-organisation of block copolymers in the bulk (without solvent) has been studied extensively. However, the introduction of a solvent to induce the association increases the complexity for self-assembly in solution due to the kind of interactions taking place in the medium. These interactions are described by $\chi$-parameter (Flory-Huggins parameter).[56] A common preparation method to induce self-assembly uses a solvent and a co-solvent to force the assembly of an A-B block copolymer (polystyrene-*b*-poly(acrylic acid) in dioxane–water) that involves up to six $\chi$-parameters. Some polymers can form diverse morphologies of aggregates depending on the preparation, the so-called crew-cut aggregates. Mai and Eisenberg (2012)[56] observed more than 20 morphologies, some are thermodynamically induced, while others are kinetically controlled. These include spherical micelles, rods, bicontinuous structures, lamellae, vesicles, large compound micelles (LCMs), large compound vesicles (LCVs), tubules, ‘onions’, ‘eggshells’, ‘baroclinic tubules’,

'pincushions', *etc.* Polystyrene-*block*-poly(acrylic acid) ($PS_m$-*b*-$PAA_n$) block copolymers can form crew-cut aggregates depending on the block length ratio between PS and PAA (Figure 2.11).[56]

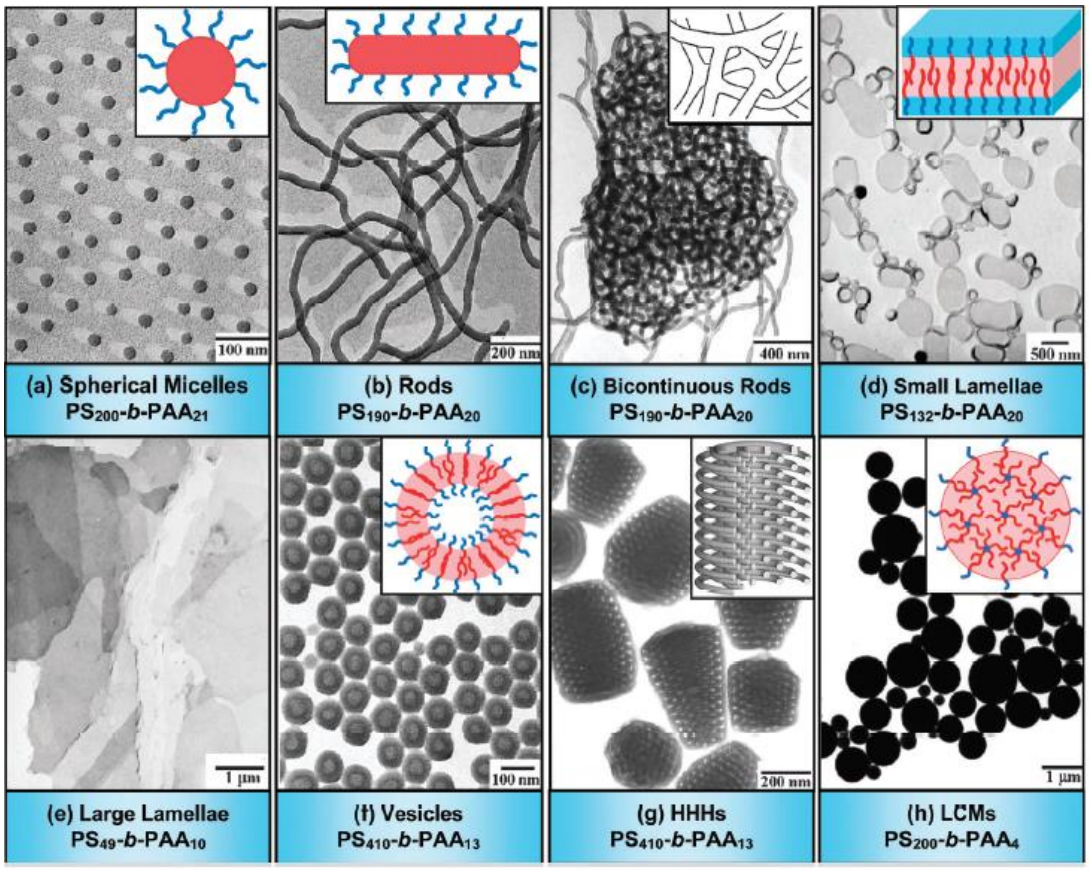



Figure 2.11. Transmission electron microscopy images and corresponding schematic diagrams (in inset) of various morphologies formed from amphiphilic $PS_m$-*b*-$PAA_n$ copolymers. In the schematic diagrams, red represents hydrophobic PS parts, while blue denotes hydrophilic PAA segments. HHHs: hexagonally packed hollow hoops; LCMs: large compound micelles, in which inverse micelles consist of a PAA core surrounded by PS coronal chains. Usually, the hydrophilic segments (e.g. coronas) of the crew-cut aggregates cannot be seen in TEM images if they are not stained.[56]

So far, the focus of the theoretical developments on the aggregation (micellization) has been postulated for linear architecture copolymers in selective solvents.[57] Another parameter that can strongly influence the micellization behaviour of block copolymers in solution is the architecture of polymer. Unfortunately, not much theoretical knowledge is available in this area.[57]

It is well-known that other architectures (i.e. star, graft, cyclic, hyperbranched, dendritic, etc.) significantly impact the physical material properties such as solubility, rheology, and thermal properties etc.[58] The effects of the non-linear topologies

(hyperbranched, dendrimers, star and cyclic) of amphiphilic polymers have already been extensively reviewed for their application in drug delivery.[59]

The hydrophobic part of a surfactant may be linear or branched. Architecture can also be designed to afford aggregate equilibrium stability. Indeed, although linear amphiphiles self-assemble only above a threshold CAC[60] highly branched amphiphilic polymers can exist as "unimolecular micelles" instead.[61] By itself, unimolecular micelle dendrimers by Hawker *et al*.[62] retain the ability to encapsulate guests even at very low concentrations. Moreover, Grayson and coworkers[63] explored the effect of branching in star block copolymers consisting of poly(oligo(ethylene glycol) methacrylate)-*block*-poly(lauryl methacrylate) (POEGMA-*b*-PLMA) arms. They showed that increasing the number of arms (e.g. from 6 to 12) lowered the CMC (when compared to the linear counterpart) and improved the encapsulation capacity of rhodamine B (polar guest) the resultant reverse aggregates in non-polar media (squalane solvent). However, from the UV and light scattering data, they proposed that aggregates of stars with a relatively small number of arms (6 or 12) had the size that might be expected for loosely packed stars. They proposed that the POEGMA-*b*-PLMA amphiphilic stars do not act as "unimolecular" micelles, but they do form smaller, more stable aggregates when compared with self-assembled "1-arm" linear block copolymer analogues.

Another study from this group (Kosakowska *et al*.[64]) on a series of branched polymers, consisting of a PEG core (fixed MW) and lipophilic peripheral lauric acid (LA) groups (fixed MW) as dendrons (Figure 2.12).

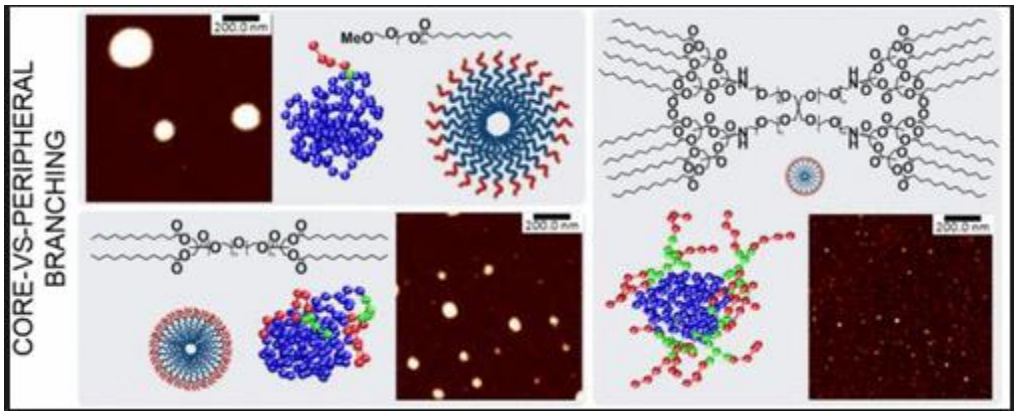



Figure 2.12. The chemical structure of three PEG-*b*-LA branched polymers, a schematic representation of aggregates and the atomic force microscopy data show that approximately half the size of aggregates is observed when doubling of the lauryl end groups.[64]

They showed that the number of branching i.e., the lauryl groups, rather than the position of the branches (core vs. periphery), appears to be the dominating factor in determining self-assembly behaviour i.e. the aggregate diameter by dynamic light scattering (DLS). In their study, the bis-laurylated amphiphiles exhibit a diameter of about 120 nm range, tetra-laurylated of ~70 nm, the octa-laurylated amphiphile of ~30 nm while the most branched amphiphile (with 16 lauryl chains) exhibits a diameter of ~18 nm.

To provide an accurate correlation between these structural parameters and the properties of 'polymer aggregates', it is paramount to have information about different compositions of blocks, molecular weights of arms and architectures (number of arms, and positions of the arms on the core, et)c. Thus, in this Thesis, the star architecture hydrophobic polymer core was comprehensively characterised (in Chapter 4) and then self-assembly properties of star amphiphilic (co)polymers were described for star-PCL-PEP (discussed in Chapter 5) and star PCL-maleic acid/triethylammonium (discussed in Chapter 6).

An increasing environmental concern of our society demands scientists to explore the materials from renewable resources for reducing the use of fossil resources as well as the processes using non-toxic substances. Biobased and biodegradable polymers can be an attractive route toward this goal.

## 2.3 Biobased and Biodegradable Polymers

The terms "bio-based polymer" and "renewably sourced (or renewable) polymer" have the same meaning and these materials could be considered to reduce the global dependence on petrochemical resources, minimise toxicity, and inhibit $CO_2$ emissions.[65,66]

Bio-based polymers may be referred to materials in which at least a portion of the polymers is produced from renewable raw materials.[67] So, some of the carbon must originate from renewable natural sources (e.g. plants, trees, algae etc.). Materials might be classified as renewably sourced when they contain a minimum of 20% by weight of plant-sourced ingredients verified by $^{14}C$ dating.[65,67] So, the rest of the portion of the polymers may be from fossil fuel-based carbon. [67,68] Since bio-based polymers (or biopolymers) are derived from the natural feedstock, they usually tend to be

biodegradable. They typically contain O and/or N atoms in their backbone, which are responsible for their biodegradability.[2]

The biobased polymers can be further divided into two subgroups: natural biopolymers and synthetic biopolymers.[2] Natural biopolymers include bio-based polymers found directly in nature, such as lignin, proteins, bacterial polyesters like poly(hydroxyalkanoate)s (PHAs), and carbohydrates (e.g. cellulose, starch, chitin, etc).[2]

On the other side, synthetic biopolymers are those that are produced by exploiting precursors that are abundant in nature (e.g. lignocellulosic biomass, carbohydrates).[2,66] The most noteworthy examples of this group of biopolymers are poly(lactic acid) (PLA), poly(glycolic acid) (PGA) and their copolymer poly(lactic-*co*-glycolic acid) (PLGA), or poly(ε-caprolactone) (PCL) (refer to section 2.1.1.1, Figure 2.3).

### 2.3.1 Biobased Polyesters

The most common class of polymer that is gaining attention in biomedical and pharmaceutical applications is aliphatic polyesters. One reason for the growing interest in this type of degradable polymer is that their physical and chemical properties can be tuned over a wide range by, e.g. copolymerisation and by advanced macromolecular architectures. The synthesis of novel polymer structures through ring-opening polymerisation has been studied for a number of years.[69]

### 2.3.2 Synthesis of Aliphatic Polyesters

In this Thesis, the synthesis of polyesters and polyphosphoesters from cyclic monomers will be discussed. Therefore, a detailed description of the mechanisms involved in their syntheses is presented in this section.

Polyesters can be synthesised by two different methods, by polycondensation between bifunctional monomers (Figure 2.13 (a)) or by ring-opening polymerisation (ROP) of cyclic esters (Figure 2.13 (b)).

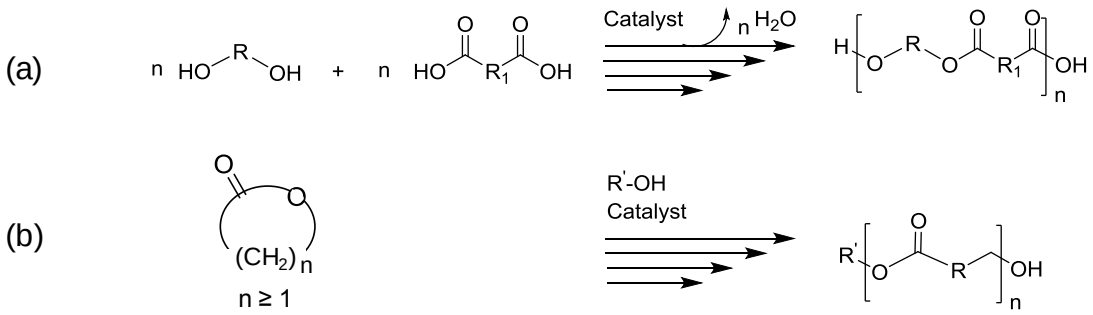



Figure 2.13. General representation of methods for the synthesis of polyesters where (a) polycondensation between bifunctional reactants and (b) ROP of cyclic esters initiated by an alcohol.

The condensation polymerisation follows the step-growth method. In this approach, bifunctional monomers react stepwise; to procedure dimer, trimer, tetramer, oligomer etc. and a small condensate (often a small molecule such as water or ethanol) is liberated in each step. A high molecular weight polymer is obtained only at higher monomer conversions.[70] One drawback of polycondensation reactions is the broadening of the molecular weight distribution because the number of polymer chains varies.[71]

The ROP follows a different approach, the chain-growth pathway, where the monomer molecules add sequentially to elongate the length of the growing polymer chains.[70] The most remarkable feature of ROP is the possibility to obtain nearly monodisperse polymers even at the high molecular weight, which is attributed to the successive addition of monomer to the fixed number of propagating chains as theoretically illustrated by Flory.[72]

The following sections provide detail of the ROP mechanisms, with an emphasis on different catalytic systems, conventional catalysts, organocatalyst and bio-catalysed ROP since these polymerisation methods were employed in Chapter 4 and Chapter 5.

#### 2.3.2.1 Ring-Opening Polymerisation

Ring-opening polymerisation (ROP) is an industrially important method applied to produce a wide range of valuable polyesters.[70,73] ROP can be performed either in the bulk, in solution, emulsion or dispersion.[74] ROP of lactones follows four main mechanisms, depending on the initiators: anionic, cationic, monomer-activated and coordination-insertion ROP.[75] With the development in the area of catalysis, polyesters can also be prepared using enzymes, so classified as enzymatic ring-opening polymerisation.[74,76]

This thesis discusses the ROP of lactones with two different catalytic systems, the metal-based and enzymatic catalyst to tailor the architecture of polyesters with catalyst and the ROP of the cyclic phosphonate with organocatalyst.

### 2.3.2.2 Metal Catalyst for Polyester Synthesis

Tin octanoate [tin(II) 2-ethylhexanoate, $Sn(Oct)_2$, Figure 2.14] is the most common and commercially available catalyst used for ROP of lactones and has approval from Food and Drug Administration (FDA).[74,77]

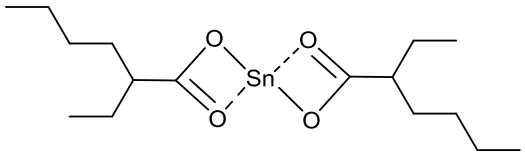



Figure 2.14. Tin octanoate, $Sn(Oct)_2$, used as a catalyst for ROP of lactones.[78]

ROP by $Sn(Oct)_2$ is a pseudo-anionic ROP method that is often referred as "coordination-insertion" ROP. In the coordination-insertion mechanism, a nucleophilic species (typically an alcohol, ROH, initiator) coordinates with the metal centre and releases 2-ethyl hexanoic acid to form a tin alkoxide species (RO-Sn-OR) (Figure 2.15).[78–80]

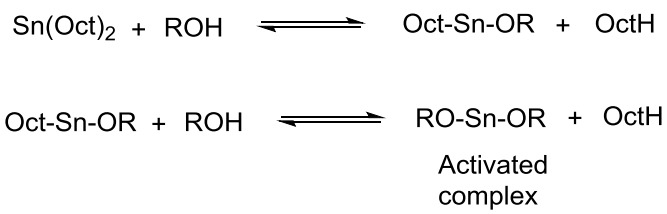



Figure 2.15. Activated tin alkoxide (RO-Sn-OR) complex formed from the coordination of the tin catalyst with an alcohol initiator (ROH), and 2-ethyl hexanoic acid (OctH) is liberated.[78,79,81]

The tin alkoxide (activated complex) species then coordinates to the carbonyl group of ε-caprolactone (ε-CL) monomer and initiates the ring-opening process (Figure 2.16, a).[79] The ring-opened monomeric species may either undergo further propagation by adding to another monomer (Figure 2.16, c) or may be deactivated *via* intermolecular exchange with the alkoxide moiety (Figure 2.16, b).[74,82] Due to this interchange, a dynamic equilibrium is established between activated and deactivated chain ends (Figure 2.16, b).[82] Propagation occurs by addition of ε-CL to the active centre of the catalyst until all the monomer is consumed (Figure 2.16, c).[74,82,83] A competing reaction is also thought to occur due to the stronger interaction of protic species (such as $H_2O$)

with the SnO moiety (of catalyst) on the propagating chain end which shifts the equilibrium from active polymerising chain end to dormant chain end.[82]

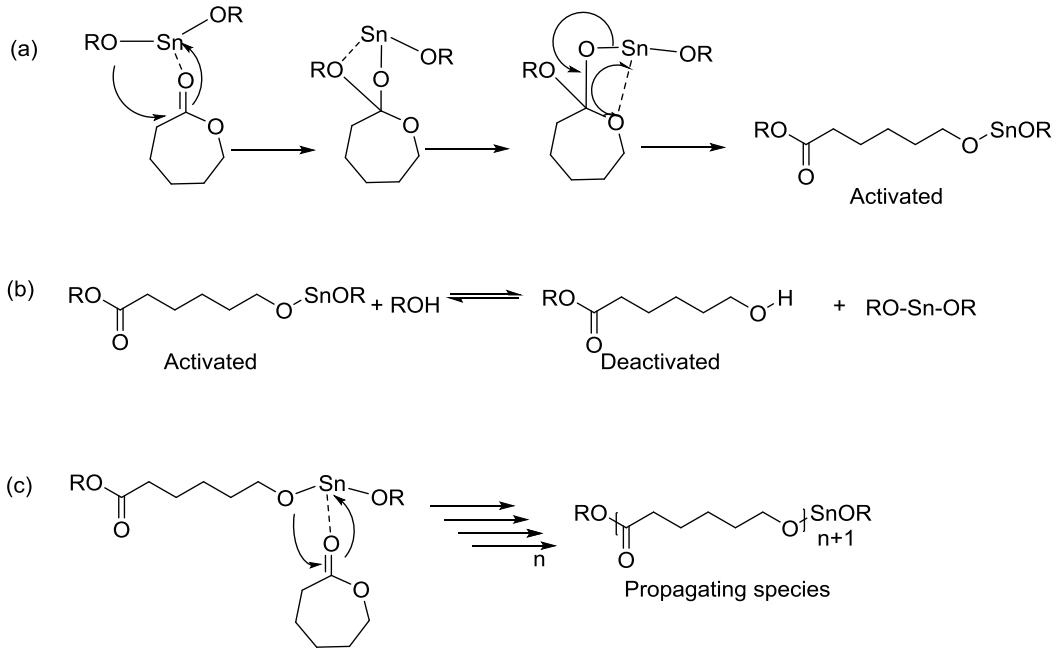



Figure 2.16. Schematic showing coordination-insertion polymerisation of ε-caprolactone with tin alkoxide complex, where (a) initiation, (b) dynamic equilibrium, (c) propagation step. It should be noted that tin is bound to the end of propagating polymer chains and OctH is thought to react with this catalyst, reforming $Sn(Oct)_2$, and yielding deactivated PCL chains with hydroxy end-groups.[78,79,82,84]

In the mechanism postulated by Penczek and coworkers,[78] it was stressed that one intact $Sn(Oct)_2$, is reformed either in "free" state or complexed, due to the interconversion reactions occurring throughout the polymerisation process (Figure 2.15).[78]

It is known that ROP ring-opening polymerisation of lactones under harsher reaction conditions (elevated temperatures or long reaction times) may cause secondary reactions (transesterification reactions).[84] These reactions are also thought to occur at high conversions resulting in the broadening of molecular weight distribution.[84,85] Intermolecular transesterification modifies the sequence of the repeating unit in the polymer chains while intramolecular transesterification reactions (back-biting) cause degradation of the polymer chain and the formation of cyclic oligomers (Figure 2.17).[86,83]

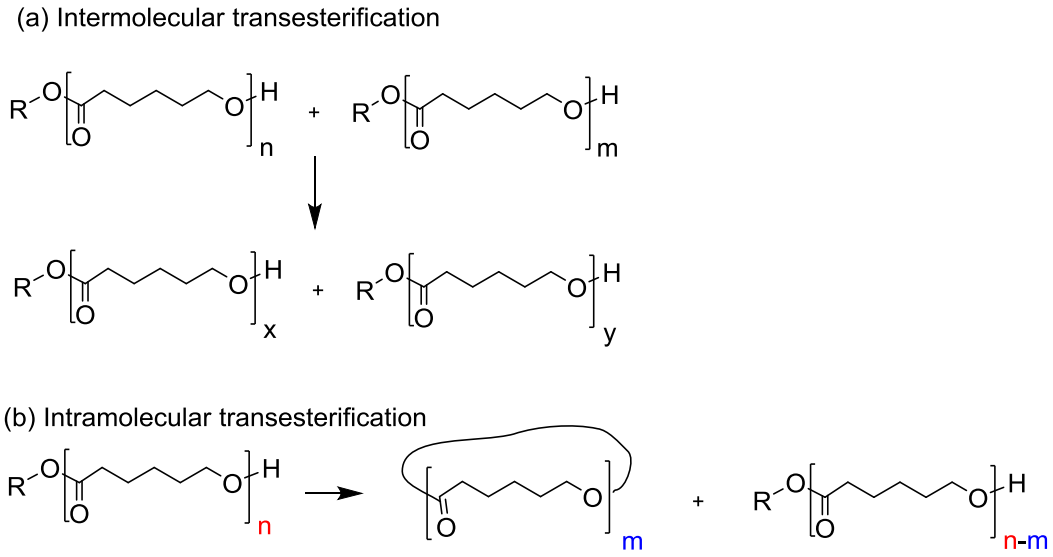



Figure 2.17. Side reactions occurring during ROP of ε-CL where (a) intermolecular transesterification and (b) intramolecular transesterification to produce cyclic macromolecules of poly(ε-caprolactone).[86,84]

Nevertheless, the presence of the heavy metal impurities from the residual catalyst can have detrimental effects on the performance of the final polymers, especially in the biomedical application.[87] Thus, organocatalysts avoiding metals have been developed to face this issue.

### 2.3.2.3 Organocatalyst for Polyester Synthesis

Anionic ring-opening polymerisation (AROP) of cyclic carbonate using 1,8-diazabicyclo[5.4.0]undec-7-ene (DBU) was reported by Murayama *et al.*[88] The use of the organocatalyst (metal-free catalyst), DBU and another strong guanidine base such as 1,5,7-triazabicyclo[4.4.0]dec-5-ene (TBD) (Figure 2.18)[84,89] for the synthesis of polyesters were reported by Lohmeijer and co-workers (2006).[90] There has been great interest since then on the synthesis of polyesters and polycarbonates using organocatalysts and the use of thiourea (as a co-catalyst) in the bulk[71] and in solution.[71,84,89,91–93]




Figure 2.18. Chemical structures of most commonly employed organocatalyst for ROP.[71,94]

Water-soluble linear poly(phosphonate) (bearing methyl[95] and ethyl[96] side chains and ethylene in the backbone) can also be polymerised by AROP using DBU catalyst acting as a base catalyst to activate benzyl alcohol for the nucleophilic attack on the ethyl phosphonate (EP) (Figure 2.19).[95]

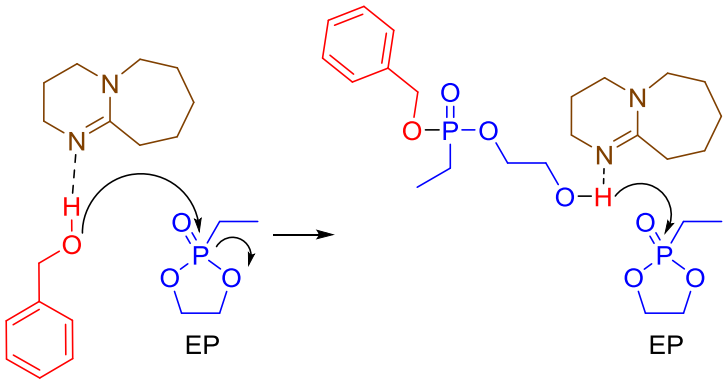



Figure 2.19. The mechanism for the AROP by DBU illustrated for 2-ethyl-2-oxo-1,3,2-dioxaphospholane (EP) with benzyl alcohol as initiator and DBU as a catalyst.[95]

The AROP of cyclic monomers from star PCL hydrophobic macroinitiators is reported in Chapter 5.

#### 2.3.2.4 Bio-Catalysed Enzymatic Ring-Opening Polymerisation (eROP)

Enzymes are proteins that catalyse specific biological reactions in living organisms. In recent decades, there has been tremendous interest in enzyme-catalysed polymerisation ('enzymatic polymerisation') as an alternative to metal-based catalyst.[41,97–101]

Enzymes are divided into six main classes:[102]

(1) Oxidoreductases (enzymes that catalyse oxidoreduction reactions and the substrate that is oxidised is regarded as a hydrogen donor);

(2) Transferases (enzymes that transfer a group, e.g. a methyl group or a glycosyl group, from one compound (generally regarded as a donor) to another compound (generally regarded as acceptor);

(3) Hydrolases (enzymes that catalyse the hydrolytic cleavage of C–O, C–N, C–C and some other bonds, including phosphoric anhydride bonds);

(4) Lyases (enzymes that cleave C–C, C–O, C–N, and other bonds by elimination, leaving double bonds or rings, or conversely that adds groups to double bonds);

(5) Isomerases (enzymes that catalyse geometric or structural changes within one molecule);

(6) Ligases (enzymes that catalyse the linking of two molecules along with the hydrolysis of a diphosphate bond in adenosine triphosphate or a similar triphosphate).[102]

Enzymes that are responsible for bond-cleavage reactions by hydrolysis fall under the class referred as hydrolases.[97] For example, esterases,[98] cutinases[103,104] and lipases,[98] are all known hydrolases for the breaking of the fatty ester bond *in vivo*. This reaction also occurs in the reverse direction resulting in the formation of ester or transesterification by working in non-aqueous media.[98,105]

Among all the hydrolases, lipases, by far, are the enzymes that have been widely investigated for polymerisation: to catalyse both polycondensation and ROP reactions in the bulk and in organic media.[106] Novozym 435 (an immobilised *Candida antarctica* lipase B, CaLB) is the benchmark enzyme among all lipases.[101,106,107]

From the yeast *Candida antarctica*, two different lipases are identified, lipase A and B. CaLA is considered not selective towards specific substrates,[108,109] whereas CaLB is characterised by its regio-, chemo-, and enantioselectivity, and hence it is the most accredited lipase for bio-catalysis.[110] The CaLB structure was resolved in 1994 by Uppenberg *et al*. according to which, 317 amino acids are involved in its crystal structure.[110] The active centre has a catalytic triad, serine (Ser105)-histidine (His224)-aspartic acid (Asp187),[105,110] that is approximately 10 Å × 4 Å wide and 12 Å deep.[111] The Ser-His-Asp triad is located at the bottom of a large funnel-like aperture/pocket with hydrophobic wall and a medium-sized pocket below.[105,110] It is considered that in the catalysis pathway the acyl moiety of the substrate lies in the large pocket, while the nucleophilic moiety lies in the medium pocket.[4,111] It should be noted that such a catalytic triad of an aspartate or glutamate, a histidine, and a nucleophilic serine residue is common to all serine hydrolases (lipases, esterases, etc).[107]

CaLB retains its activity in organic solvents of low dielectric constant but highly polar solvent like dimethyl sulfoxide or methanol dramatically decreases the catalytic activity.[111,112] It is established that the enzymes contain two types of water: (i) the hydration water and (ii) the structural water.[113,114] The hydration water is non-essential water present in the enzyme that promotes side-reactions and can be significantly removed before reactions by drying processes (such as freeze-drying).[115] By contrast, structural water is the enzyme-bound water essential for the enzyme to maintain its protein structure.[111] Indeed only hydration water needs to be effectively removed from

enzymes because an enzyme will show denaturation in a fully dry enzymes state or in environments with high amounts of water.[116]

A generally accepted catalytic mechanism of hydrolysis and trans-esterification by the catalytic-triad (Ser–His–Asp) is presented (Figure 2.20). The catalyst site is the $–CH_2OH$ group of Ser residue.[105] In the acylation step, the imidazole group of His residue on the free enzyme acts as a general base to pull the proton from $–CH_2OH$.[105,107] This enhances the nucleophilicity of the oxygen atom ($–CH_2\mathit{O}H$) and renders the carbonyl carbon of the substrate (R'*C*(=O)–OR) more prone to nucleophilic attack.[105,107] The substrate acts as the acyl donor and the first tetrahedral intermediate (THI-1) is formed. The negative charge in THI-1 is stabilised by three hydrogen bonds (dashed lines) within the oxyanion hole (a pocket in the active site formed by two amino acids that can stabilise negative charges). Whereas the positive charge on His224 is stabilised by interaction with Asp187.[107]

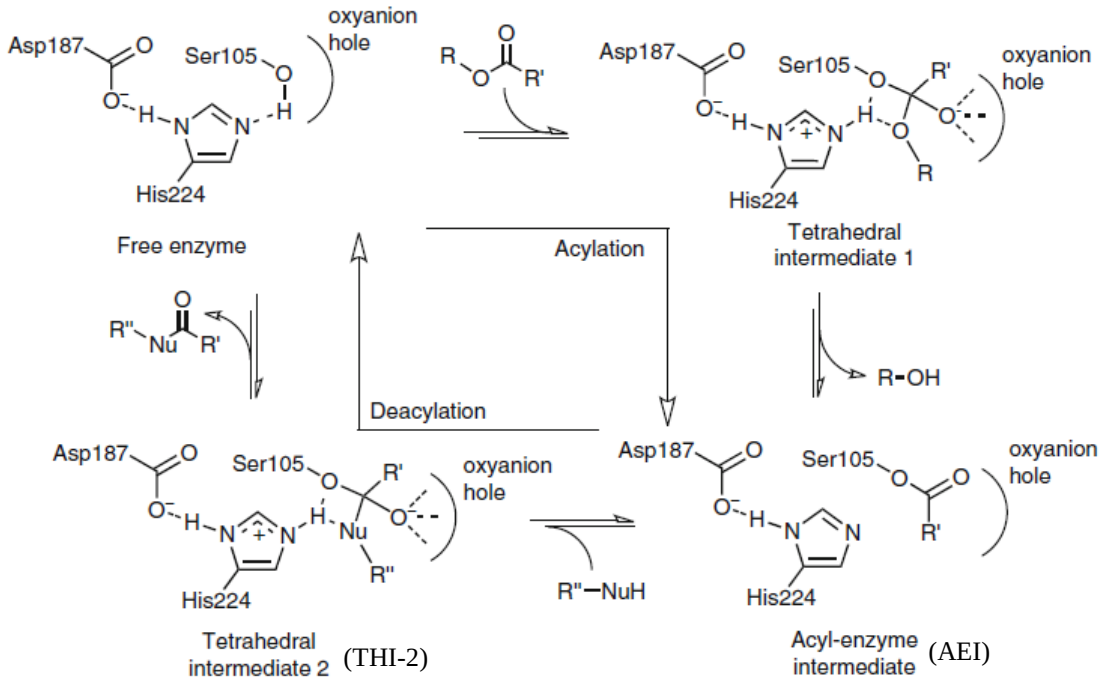



Figure 2.20. The catalytic mechanism of CaLB showing an acylation and deacylation step and the formation of a covalently bound acyl-enzyme intermediate.[107]

Simultaneously, the carboxylate group of Asp187 helps the imidazole group to pull the proton, and a covalently bound acyl-enzyme intermediate (AEI) is formed with liberating R–OH (acylation step).[105] Afterwards, initiation occurs by an incoming nucleophile (R"–NuH) (i.e. water or an alcohol) that attacks the AEI and a proton is transferred to the His224 residue to form a second tetrahedral intermediate. The THI-2

is again stabilised by hydrogen-bond interactions between the imidazole and carboxylate groups with the oxyanion hole (deacylation step) and a deacylated RC(=O)–NuR" is released.[114]

Propagation, on the other hand, occurs by deacylation of the acyl-enzyme intermediate by the terminal hydroxyl group of the growing polymer chain to produce a polymer chain that is elongated by one monomer unit.[114] Additionally, it is noteworthy that the ester bonds within the polymer can also undergo nucleophilic attack by the Ser105 residue of the lipase, resulting in the breaking of the polymer chains.[114] Indeed, the adventitious impurities such as water present in the reaction can also act as nucleophiles; for this reason, it is imperative to have the feedstock dried.

For synthesis purposes, CaLB is generally immobilised (adsorbed)[41] on an inert and insoluble material such as cross-linked acrylic resin beads [i.e. poly(methyl methacrylate-co-divinylbenzene)] which is commercially recognised as Novozym 435 (10% by weight of CaLB). It offers several benefits, in particular, immobilised enzymes usually have increased thermal and pH stability, improved activity and can be easily separated from the products, enabling recycling of the catalyst.[101,106] Novozym 435 is considered to have optimum reactivity between 30 °C-60 °C temperature range (declared by the supplier);[117] but, this immobilised lipase has been reported to be catalytically active up to 100 °C.[106] Nonetheless, harsh environments (for example, 24 h in toluene at 70 °C) has shown to dramatically decrease its activity (~35%) due to leaching of the enzyme.[118] Nevertheless, the immobilised (supported) enzymes are considered highly active compared to the "free enzyme".[119,120] In this research, Novozym 435 is employed for polymer synthesis.

It is noteworthy that enzymatic polymerisation offers several advantages over organometallic catalysis such as mild reaction conditions, high control of regio-, chemo, and enantioselectivity, clean process (product free of toxic metal residues), and relatively high catalytic activity toward macrocyclic lactones compared to chemical catalysis.[101,114,121] Thus, to sum up, enzymatic ROP for producing polymeric material is a good illustration of 'green polymer chemistry'.

## 2.4 Supercritical Fluids

Together with the choice of feedstock, the route of synthesis is also an important consideration for a fully sustainable pathway when synthesising bio-based materials.

A supercritical fluid (SCF) is any substance, the temperature and pressure of which are higher than their critical values i.e. above its critical temperature and critical pressure (Figure 2.21).[122,123]

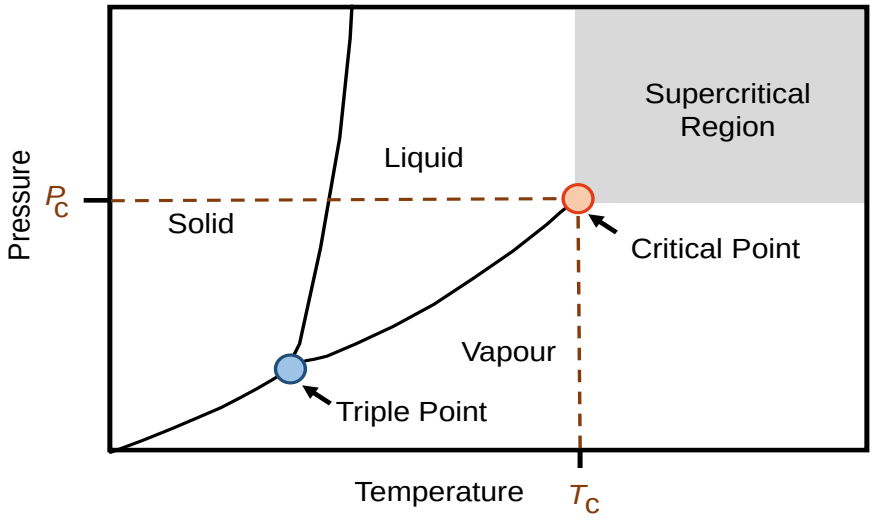



Figure 2.21. Phase-diagram representing the pressure *vs* temperature relationship for a pure substance. The triple point and the critical point are marked. The solid lines indicate the boundaries, at which phase transitions occur.[122]

At the triple point of any substance, the three phases (solid, liquid and vapour) coexist and are in equilibrium. When a liquid is heated above its critical point, the phase boundary between the liquid and vapour phase no longer exists and the substance is in a single phase in the supercritical region, where it possesses the combined properties of both liquid and gas.[124]

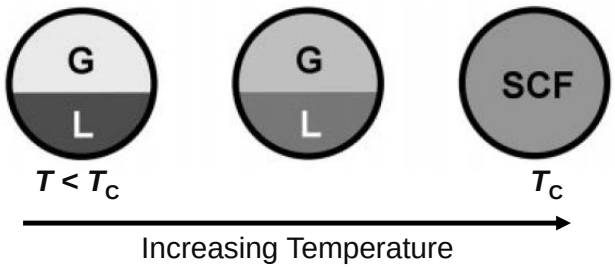



Figure 2.22. Schematic illustration of the change from gas-liquid (G-L) equilibrium ($T < T_C$) to SCF ($T \geq T_C$) conditions as a substance is heated at a pressure in excess of $P_c$.[124]

The physicochemical properties (the density, viscosity and diffusivity) of SCF are in between those of liquids and gases (Table 2.2).

Table 2.2. A comparison of the physical properties of fluids.[125] SCF has properties between those expected for classical gases and liquids.

| Property | Gas | SCF | Liquid |
|---|---|---|---|
| Density (g $cm^{-3}$) | $10^{-3}$ | 0.2 – 0.9 | 0.8 – 1.0 |
| Viscosity (Pa s) | $0.5 – 3.5 \times 10^{-5}$ | $0.2\text{-}1.0 \times 10^{-4}$ | $0.3\text{-}2.4 \times 10^{-3}$ |
| Diffusivity ($cm^2$ $s^{-1}$) | $10^{-2} – 1$ | $0.1\text{-}3.3 \times 10^{-4}$ | $0.5\text{-}2.0 \times 10^{-5}$ |

By far, the most promising and widely used SCF of interest to polymer scientists is supercritical carbon dioxide.

### 2.4.1 Supercritical Carbon Dioxide

Supercritical $CO_2$ ($scCO_2$) has emerged as the most extensively studied SCF and is attracting attention as an environmentally benign solvent as a potential replacement to volatile organic solvents (VOCs).[126,127]

Additionally, $CO_2$ obeys several principles from the 12 pillars of green chemistry and thus its use in chemical processes enhances the overall sustainability.[126] $CO_2$ is an abundant and renewable gas. Industrially, obtained as a waste product (such as obtained as a by-product during production of ammonia), $CO_2$ can be thus recycled to prevent pollution. It is also an inexpensive, non-toxic, non-corrosive, non-flammable gas and widely used as a clean solvent for polymerisation.[123,126,127]

The relatively mild critical temperature and critical point (73.8 bar and 31.1 °C) of $scCO_2$ and its tuneable properties; high diffusivity, gas-like viscosities to accelerate the chemical reaction kinetics and a liquid-like density render it as a most promising substitute to VOCs for a wide variety of applications from polymer synthesis to purification.[128–130]

Ease of separation of $CO_2$ from the product by simple decompression at the end of the process to afford a dry-product, creates this supercritical technology highly commercially sustainable and viable, as currently employed for $CO_2$-assisted extraction processes.[125] The most popular example of a $CO_2$-assisted extraction process is the industrial use of $scCO_2$ in the decaffeination of caffeine from coffee beans.[126,131]

### 2.4.2 Supercritical Fluid Extraction

Together with employing $scCO_2$ for polymerisations, supercritical fluid extraction (SFE) technology is also gaining attention in the purification of polymers and extraction of impurities.[126,132] The density of $scCO_2$ can be easily modified by adjusting applied pressure and/or temperature (Figure 2.23).

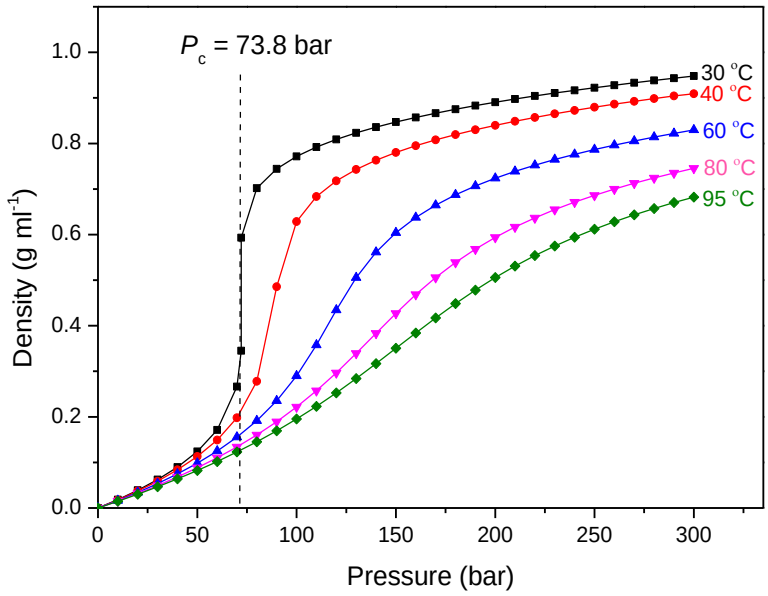



Figure 2.23. Isothermal change in density (g $mL^{-1}$) with pressure for $CO_2$ temperatures ranging from 30 – 95 °C. The largest deviations in density occur around the $P_c$ (73.8 bar) and the maximum density is obtained at the lowest temperature while as temperature increases the density decreases at constant pressure. Values are taken from the NIST webbook.[133]

This tunability of the solvent density can influence the solvation power of pressurised $CO_2$, which makes $scCO_2$ a 'selective-solvent' to selectively dissolve and extract a component.[122,128,134] To afford such solvent properties of $CO_2$, it is compressed to obtain the dense $CO_2$ (liquid or $scCO_2$ state).[135] As explained earlier, in the supercritical domain, the density of $CO_2$ varies over a wide range of values depending on the pressure and temperature. This is reflected in particular by a continuous variation of the solvent power with the pressure (P) and temperature (T). This concept of solvent power can be correlated with the Hildebrand solubility parameter ($\delta_{(T, P)}$) which is proportional to the density of the supercritical fluid ($\rho_{SCF\ (T,\ P)}$) according to the following relationship (Eq. 2.1).[135]

$$\delta_{(T, P)} = 1.25 \times (P_c.)^{1/2} \times (\rho_{SCF\ (T, P)}/2.66) \qquad \text{Eq. 2.1}$$

Thus, without any necessity of high temperatures or toxic solvents (that are usually required in conventional extraction processes), supercritical $CO_2$ fluid extraction (SCFE) acts as a benign route towards purification of products.[122,126,128,134]

### 2.4.3 Polymerisation in Supercritical Carbon Dioxide

$ScCO_2$ is a non-polar solvent (low dielectric constant) though it possesses 'polar' properties (Lewis acidity, strong quadrupole moment, polar C=O bond) that allows dissolution of a variety of materials (such as fluorinated, hydroxylated, carbonylated compounds) in it.[126, 136] Hence, it would be accurate to say that it has poor solvating power and cannot solubilise many polar chemicals and high molecular weight materials (including most polymers) with rare exceptions being some fluoropolymers, silicones and few vinyl ester polymers and copolymers.[137,138] Nonetheless, $CO_2$ is very effective at permeating and dissolving within a polymeric matrix, and efficiently plasticising (liquefying) many polymers at temperatures well below their normal ambient glass transition ($T_g$) and melting point ($T_m$).[124,129,139,140]

Even poorly $CO_2$-soluble polymers can significantly swell and expand (foam) in $scCO_2$, upon sorption or diffusion of $CO_2$ into the polymer chains to form a polymer/gas binary mixture (or solution). This results in bubble nucleation and growth upon depressurisation (which is the common pathway) or an increase in temperature (if the sorption occurred at relatively low temperatures). The foaming phenomenon continues until the mass transport stops upon crystallisation of the polymer.[130,140–142]

$scCO_2$ is suitable to perform free-radical reactions as it has low reactivity towards radicals and hence chain transfer to solvent is very unlikely.[126]

It can be said that the main downside of $CO_2$ is its poor ability to dissolve polar compounds, which implies that many reactions in the $scCO_2$ medium, including polymerisations, are often heterogeneous.

Surfactants allow hydrophilic compounds to be partly solubilised in $scCO_2$.[143] In this case, the hydrophobic part is usually a long lipophilic or fluorocarbon chain that has much higher affinity with $CO_2$ molecules than the polar moiety of the surfactant and thus is also referred as "$CO_2$-philic" part.[143] Similar to the self-assembly phenomenon of surfactant compounds in apolar solvents, they also spontaneously assemble in $scCO_2$ to form reverse micelles to reduce the free energy of the system.[143] Usually surfactants are employed for dispersion polymerisation processes in $scCO_2$.

Fluoropolymers[144] and siloxanes[145] are the usual choice of steric stabiliser for dispersion in $scCO_2$. The fluorinated compounds exhibit a higher solubility in $scCO_2$ in comparison to their homologous hydrocarbon surfactants. Thus, several fluorinated block copolymers as macromolecular surfactants have been exploited for $CO_2$ applications most readily using the reversible addition-fragmentation chain transfer polymerisation techniques.[146,147] Fluorinated hydrophilic/$CO_2$-philic block copolymers such as poly(ethylene oxide)-*b*-poly(1,1,2,2- tetrahydroperfluorodecyl acrylate) (PEO-*b*-PFDA) can stabilise polar monomers, such as 2-hydroxylethyl methacrylate (HEMA) in $scCO_2$ (at 370 bar 65 °C).[148] Such PEO-*b*-PFDA surfactants ensure steric stabilisation to give well-defined spherical nanoparticles (200–400 nm diameter) of poly(HEMA) and a narrow particle size distribution (~1.1) (Figure 2.24).[148]

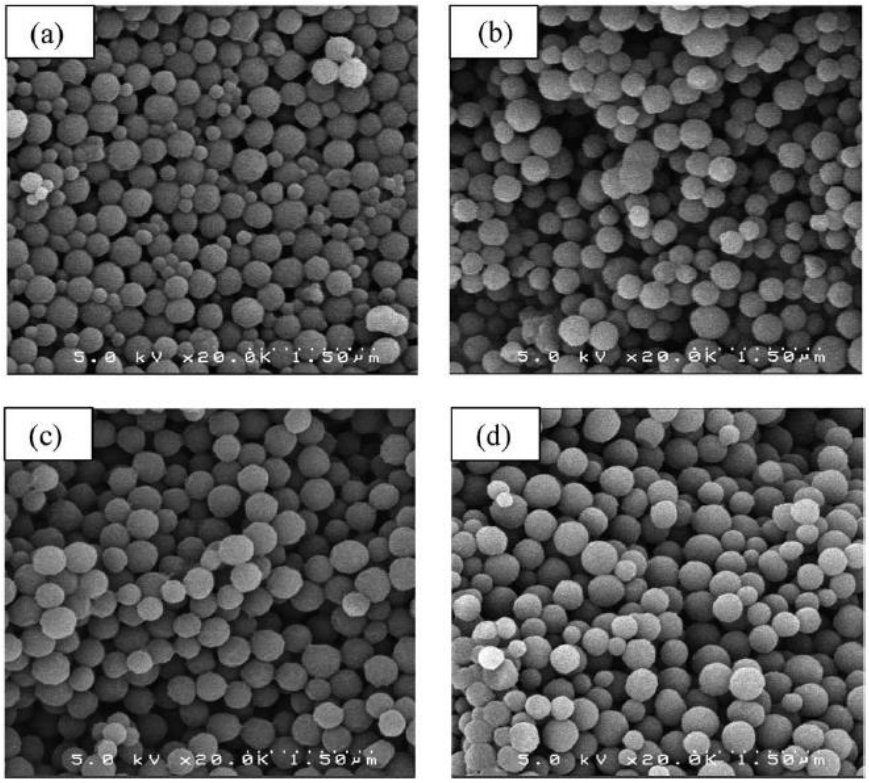



Figure 2.24. Scanning electron microscopy of poly(HEMA) particles synthesized with: different wt% of PEO-*b*-PFDA stabiliser: (a) 20%, (b) 10%, (c), 6.0%, (d) 3.5% in $scCO_2$ by dispersion polymerisation method.[148]

This Thesis focuses on ROP using $scCO_2$. It has been shown that polymerisation in $scCO_2$ has added benefit compared to solvent-free reactions. For example, for the ROP of *D*, *L*-lactide from *D*-sorbitol it has been shown that the use of supercritical $CO_2$ significantly reduces reaction temperature from 140 °C (when conducted in the bulk).to 80 °C using $scCO_2$.[46] Such reduction in temperature is particularly attractive

industrially when temperature-sensitive polyol based reactions are conducted at high temperatures and can lead to degradation of sugars.[46]

In this Thesis, both the bulk polymerisation method and $scCO_2$ will be employed in parallel for polymerisation discussed in Chapter 4 and Chapter 5, and low-energy pathway, SCFE technology will be utilised for purification of the synthesised product along with conventional methods in Chapter 4 and 5.

## 2.5 Conclusions

This Chapter has outlined the general background upon which the work in this thesis is based. As highlighted in the introduction, use of renewable feedstock, catalyst and reaction solvent are at the forefront of green polymer chemistry and offer immense potential to address the current and future challenges that industries are facing. Sustainable products can be designed effectively if some of the raw materials (20 wt% of the product is from plant-sourced ingredients as verified by $^{14}C$ dating)[65] are derived from 'waste biomasses' and eco-friendly solvents are employed for processing of materials. As discussed earlier and in Chapter 1, most surfactants that are employed today are petrochemical and there is a growing demand for research and development of green surfactants and green material. Thus, a choice of specific natural resources provides a significant opportunity for development of novel biobased surfactants that may be biodegraded (follows the 'cradle to grave' rule).

In recent work (2016) an exciting class of linear and star architecture poly(lactides) were reported.[46] This is a stepping-stone towards the development of the next generation of green surfactants and biopolymers using renewable building blocks (*D*-sorbitol and *D, L*-Lactide), at the same time, low energy $scCO_2$ processing pathways were presented.[46] For polymerisation of *D,L*-lactide an FDA approved $Sn(Oct)_2$ catalyst for polymerisation both in the bulk and in $scCO_2$.[46] The initial strategy for the choice of catalyst and solvents can be related to this work,[46] and to some of the perspective outlined in the Thesis by Goddard.[35]

At present, enzymatic catalysis illustrates a great potential to substitute metal-based catalysts to avoid the toxicity of metal contaminants in the final product and are in perfect agreement with the concepts of green chemistry and sustainable synthesis. Enzymatic ROP of lactones can be dated back to 1993,[149] and the eROP of ε-CL has

shown great promise. Thus, ε-CL being as a biomass-derived monomer offers great potential as a hydrophobic block for a surfactant.

The literature has explored the use of linear alcohols and ε-CL as building blocks for linear PCL synthesis in $scCO_2$.[150,151] However, there has not been any demonstration of the impact of using multifunctional alcohol, for this reason, Chapter 4 is focused on the preparation and characterisation of linear, telechelic dihydroxy and star architecture PCL hydrophobic blocks developed using both $Sn(Oct)_2$ and enzyme catalysts in the bulk or in $scCO_2$.

The current most popular approach to introduce hydrophilicity in polymers is the use of poly(ethylene glycol), which is petroleum-based non-biodegradable hydrophile. Cyclic phosphonates offer an alternative. They are a novel class of monomer that provides aliphatic water-soluble poly(phosphonate)s and research has proven both biodegradability and non-toxicity.[96,152] Such cyclic phosphonates offer great potential to undergo ROP from the hydroxy group of branched PCL to yield new attractive architectures. Considering the advantages offered by poly(phosphonate)s, Chapter 5 discusses the synthesis and characterisation of linear diblock, linear triblock and star diblock polymers of PCL-block-poly(phosphonates). The self-assembly behaviour of these block copolymers will also be discussed. Finally, surface-active properties and the application of these block copolymers with the different architectures will be exploited.

## 2.6 References


1. Salager, J.-L. *Surfactants Types and Uses*. (Mérida-Venezuela, 2002).
2. Gandini, Alessandro and Belgacem, M. N. *Monomers, Polymers and Composites from Renewable Resources*. (Elsevier Science, 2008).
3. Peltonen, L. J. & Yliruusi, J. Surface pressure, hysteresis, interfacial tension, and CMC of four sorbitan monoesters at water-air, water-hexane,and hexane-air interfaces. *J. Colloid Interface Sci.* **227,** 1–6 (2000).
4. Griffin, W. C. Calculation of HLB values of Nonionic Surfactants. *J. Soc. Cosmet. Chem.* **5,** 249–256 (1954).
5. Griffin, W. C. Classification of Surface-Active Agents by HLB. *J. Soc. Cosmet. Chem.* **1,** 311–326 (1949).
6. Bancroft, W. D. The Theory of Emulsification, VI. *J. Phys. Chem.* **19,** 275–309 (1914).
7. Bancroft, W. D. The Theory of Emulsification, V. *J. Phys. Chem.* **17,** 501–519 (1912).
8. Gendell, A. Biobased, Biodegradable, Compostable. *Sustainable Packaging Coalition* (2016). Available at: https://sustainablepackaging.org/101-biobased-biodegradable-compostable/. (Accessed: 19th August 2018)
9. Crenna, E., Sozzo, S. & Sala, S. Natural biotic resources in LCA: Towards an impact assessment model for sustainable supply chain management. *J. Clean. Prod.* **172,** 3669–3684 (2018).
10. Foley, P., Kermanshahi pour, A., Beach, E. S. & Zimmerman, J. B. Derivation and synthesis of renewable surfactants. *Chem. Soc. Rev.* **41,** 1499–1518 (2012).
11. Isikgor, F. H. & Becer, C. R. Lignocellulosic biomass: a sustainable platform for the production of bio-based chemicals and polymers. *Polym. Chem.* **6,** 4497–4559 (2015).
12. Cherubini, F. The biorefinery concept: Using biomass instead of oil for producing energy and chemicals. *Energy Convers. Manag.* **51,** 1412–1421 (2010).
13. Sun, Y. & Cheng, J. Hydrolysis of lignocellulosic materials for ethanol production: a review. *Bioresour. Technol.* **83,** 1–11 (2002).
14. Kobayashi, H. & Fukuoka, A. Synthesis and utilisation of sugar compounds derived from lignocellulosic biomass. *Green Chem.* **15,** 1740 (2013).
15. Haq, F. *et al.* Recent progress in bioethanol production from lignocellulosic materials: A review. *Int. J. Green Energy* **13,** 1413–1441 (2016).
16. Galbis, J. A., García-Martín, M. D. G., de Paz, M. V. & Galbis, E. Synthetic Polymers from Sugar-Based Monomers. *Chem. Rev.* **116,** 1600–1636 (2016).
17. Tadros, T. *Encyclopedia of Colloid and Interface Science*. (Springer, 2013).
18. Raffa, P., Wever, D. A. Z., Picchioni, F. & Broekhuis, A. A. Polymeric Surfactants: Synthesis, Properties, and Links to Applications. *Chem. Rev.* **115,** 8504–8563 (2015).
19. Vyas, B., Pillai, S. A., Bahadur, A. & Bahadur, P. A comparative study on micellar and solubilizing behavior of three EO-PO based star block copolymers varying in hydrophobicity and their application for the in vitro release of anticancer drugs. *Polymers (Basel).* **10,** (2018).
20. Knop, K., Hoogenboom, R., Fischer, D. & Schubert, U. S. Poly(ethylene glycol) in Drug Delivery: Pros and Cons as Well as Potential Alternatives. *Angew. Chemie Int. Ed.* **49,** 6288–6308 (2010).
21. Ulbricht, J., Jordan, R. & Luxenhofer, R. On the biodegradability of

polyethylene glycol, polypeptoids and poly(2-oxazoline)s. *Biomaterials* **35,** 4848–4861 (2014).
22. Zhao, Z., Wang, J., Mao, H.-Q. & Leong, K. W. Polyphosphoesters in drug and gene delivery. *Adv. Drug Deliv. Rev.* **55,** 483–499 (2003).
23. Wen, J., Kim, G. J. A. & Leong, K. W. Poly(D,Llactide-co-ethyl ethylene phosphate)s as new drug carriers. *J. Control. Release* **92,** 39–48 (2003).
24. Hill, K. Fats and oils as oleochemical raw materials. *Pure Appl. Chem.* **72,** 1255–1264 (2000).
25. Metzger, J. O. & Bornscheuer, U. Lipids as renewable resources: current state of chemical and biotechnological conversion and diversification. *Appl. Microbiol. Biotechnol.* **71,** 13–22 (2006).
26. M. Kjellin and I. Johansson. *Surfactants from Renewable Resources*. *Wiley* (John Wiley & Sons, Ltd, 2010).
27. Curia, S. & Howdle, S. M. Towards sustainable polymeric nano-carriers and surfactants: facile low temperature enzymatic synthesis of bio-based amphiphilic copolymers in scCO2. *Polym. Chem.* **7,** 2130–2142 (2016).
28. Caretto, A., Noè, M., Selva, M. & Perosa, A. Upgrading of Biobased Lactones with Dialkylcarbonates. *ACS Sustain. Chem. Eng.* **2,** 2131–2141 (2014).
29. Shao, H., Zhang, M., He, J. & Ni, P. Synthesis and characterization of amphiphilic poly(caprolactone)-b- polyphosphoester diblock copolymers bearing multifunctional pendant groups. *Polym. (United Kingdom)* **53,** 2854–2863 (2012).
30. Gozlan, C. *et al.* Preparation of amphiphilic sorbitan monoethers through hydrogenolysis of sorbitan acetals and evaluation as bio-based surfactants. *Green Chem.* **18,** 1994–2004 (2016).
31. Farn, R. J. *Chemistry and Technology of Surfactants*. *Chemistry and Technology of Surfactants* (Blackwell Publishing Ltd, 2006).
32. Martin, A. & Richter, M. Oligomerization of glycerol - a critical review. *Eur. J. Lipid Sci. Technol.* **113,** 100–117 (2011).
33. Salehpour, S. & Dubé, M. A. Towards the sustainable production of higher-molecular-weight polyglycerol. *Macromol. Chem. Phys.* **212,** 1284–1293 (2011).
34. Iaych, K., Dumarcay, S., Gérardin, C. & Gérardin, P. Polyglycerol cyclic carbonate synthesis and application to preparation of surfactant molecules. *J. Mater. Environ. Sci.* **6,** 178–183 (2015).
35. Goddard, A. R. Sustainable Synthesis of Renewable Surfactants. *Thesis* (2016).
36. Hayes, D. G. *Biobased Surfactants and Detergents: Synthesis, Properties and Applications*. (AOCS Press, 2009).
37. Mulligan, C. N. & Gibbs, B. F. Types, production and application of biosurfactants. *Proc. Indian Nat. Sci. Acad.* **B70,** 31–55 (2004).
38. Vijayakuma, S. & Saravanan, V. Biosurfactants-Types, Sources and Applications. *Res. J. Microbiol.* **10,** 181–192 (2015).
39. Lang, S. Biological amphiphiles (microbial biosurfactants). *Curr. Opin. Colloid Interface Sci.* **7,** 12–20 (2002).
40. Marchant, R. & Banat, I. M. Biosurfactants: a sustainable replacement for chemical surfactants? *Biotechnol. Lett.* **34,** 1597–1605 (2012).
41. Gross, R. A, Kumar, A. & Kalra, B. Polymer synthesis by in vitro enzyme catalysis. *Chem. Rev.* **101,** 2097–2124 (2001).
42. Desai, J. D. & Banat, I. M. Microbial production of surfactants and their commercial potential. *Fuel Energy Abstr.* **38,** 221 (1997).

43. Shosa, J. D. & Schramm, L. L. Surfactants: Fundamentals and Applications in the Petroleum Industry. *Palaios* **16,** 614 (2001).
44. Holmberg, K., Bo, J. & Kronberg, B. *Surfactants and Polymers in Aqueous Solution*. (John Wiley & Sons, Ltd, 2002).
45. Solutions, S. P. Bubble pressure method for measuring the dynamic surface tension. Available at: https://www.sita-process.com/information-service/process-parameter-surface-tension/overview/. (Accessed: 28th September 2018)
46. Goddard, A. R. *et al.* Controlled polymerisation and purification of branched poly(lactic acid) surfactants in supercritical carbon dioxide. *Green Chem.* **18,** 4772–4786 (2016).
47. Riess, G. Micellization of block copolymers. *Prog. Polym. Sci.* **28,** 1107–1170 (2003).
48. Israelachvili, J. N. *Intermolecular and Surface Forces*. (Elsevier Inc., 2011). doi:10.1016/C2009-0-21560-1
49. Israelachvili, J. N., Mitchell, D. J. & Ninham, B. W. Theory of self-assembly of lipid bilayers and vesicles. *BBA - Biomembr.* **470,** 185–201 (1977).
50. Doncom, K. E. B., Blackman, L. D., Wright, D. B., Gibson, M. I. & O'Reilly, R. K. Dispersity effects in polymer self-assemblies: A matter of hierarchical control. *Chem. Soc. Rev.* **46,** 4119–4134 (2017).
51. Alexandridis, P. Amphiphilic copolymers and their applications. *Curr. Opin. Colloid Interface Sci.* **1,** 490–501 (1996).
52. Torchilin, V. P. Structure and design of polymeric surfactant -based drug delivery systems. *J. Control. Release* **73,** 137–172 (2001).
53. Mao, G., Sukumaran, S., Beaucage, G., Saboungi, M. L. & Thiyagarajan, P. PEO-PPO-PEO block copolymer micelles in aqueous electrolyte solutions: Effect of carbonate anions and temperature on the micellar structure and interaction. *Macromolecules* **34,** 552–558 (2001).
54. Zhang, W. *et al.* Synthesis, surface and aggregation properties of a series of amphiphilic dendritic copolymers. *Colloids Surfaces A Physicochem. Eng. Asp.* **348,** 45–48 (2009).
55. Winnik, F. M., Davidson, A. R., Hamer, G. K. & Kitano, H. Amphiphilic Poly(N-isopropylacrylamides) Prepared by Using a Lipophilic Radical Initiator: Synthesis and Solution Properties in Water. *Macromolecules* **25,** 1876–1880 (1992).
56. Mai, Y. & Eisenberg, A. Self-assembly of block copolymers. *Chem. Soc. Rev.* **41,** 5969–5985 (2012).
57. Hadjichristidis, N., Pispas, S. & Floudas, G. Block Copolymer Morphology. *Block Copolym. Synth. Strateg. Phys. Prop. Appl.* 346–361 (2003).
58. Wooley, K. L., Fréchet, J. M. J. & Hawker, C. J. Influence of shape on the reactivity and properties of dendritic, hyperbranched and linear aromatic polyesters. *Polymer (Guildf).* **35,** 4489–4495 (1994).
59. Wang, Y. & Grayson, S. M. Approaches for the preparation of non-linear amphiphilic polymers and their applications to drug delivery. *Adv. Drug Deliv. Rev.* **64,** 852–865 (2012).
60. Owen, S. C., Chan, D. P. Y. & Shoichet, M. S. Polymeric micelle stability. *Nano Today* **7,** 53–65 (2012).
61. Hawker, C., Wooley, K. & Fréchet, J. Unimolecular micelles. *J. Chem. Soc.* **1,** 1178–1180 (1993).
62. Hawker, C. J., Wooley, K. L. & Fréchet, J. M. J. Unimolecular micelles and

globular amphiphiles: dendritic macromolecules as novel recyclable solubilization agents. *J. Chem. Soc., Perkin Trans. 1* 1287–1297 (1993). doi:10.1039/P19930001287

63. Poree, D. E., Giles, M. D., Lawson, L. B., He, J. & Grayson, S. M. Synthesis of amphiphilic star block copolymers and their evaluation as transdermal carriers. *Biomacromolecules* **12,** 898–906 (2011).
64. Kosakowska, K. A. *et al.* Synthesis and Self-Assembly of Amphiphilic Star/Linear–Dendritic Polymers: Effect of Core versus Peripheral Branching on Reverse Micelle Aggregation. *Biomacromolecules* **19,** acs.biomac.8b00679 (2018).
65. Renewable biobased polymers. Available at: http://www.dupont.com/products-and-services/plastics-polymers-resins/bio-based-polymers.html. (Accessed: 19th August 2018)
66. Holmberg, A. L., Reno, K. H., Wool, R. P. & Epps, T. H. Biobased building blocks for the rational design of renewable block polymers. *Soft Matter* **10,** 7405–7424 (2014).
67. Chandrasekaran, C. *Anticorrosive Rubber Lining*. (Elsevier Inc., 2017).
68. Bio-Based Polymers. *IHS Market* Available at: https://ihsmarkit.com/products/chemical-technology-pep-bio-based-polymers-2013.html. (Accessed: 19th August 2018)
69. Jiang, Y. & Loos, K. Enzymatic Synthesis of Biobased Polyesters and Polyamides. *Polymer (Guildf).* **8,** 243 (2016).
70. Odian, G. *Principles of Polymerization*. *Reservoir Engineering Handbook* (John Wiley & Sons, Inc., 2004).
71. Kamber, N. E. *et al.* Organocatalytic Ring-Opening Polymerization. *Chem. Rev.* **107,** 5813–5840 (2007).
72. Flory, J. Molecular Size Distribution. *J. Am. Chem. Soc.* **62,** 1561–1565 (1940).
73. Nuyken, O. & Pask, S. D. Ring-opening polymerization-An introductory review. *Polymers (Basel).* **5,** 361–403 (2013).
74. Albertsson, A.-C. & Varma, I. K. Recent Developments in Ring Opening Polymerization of Lactones for Biomedical Applications. *Biomacromolecules* **4,** 1466–1486 (2003).
75. Dubois, P., Coulembier, O. & Raquez, J.-M. *Handbook of Ring-Opening Polymerization*. (Wiley-VCH Verlag GmbH & Co. KGaA, 2009).
76. Kobayashi, S. & Uyama, H. *Enzymatic Polymerization to Polyesters*. *Biopolymers Online* (Wiley-VCH Verlag GmbH & Co. KGaA, 2005).
77. Jerome, C. & Lecomte, P. Recent advances in the synthesis of aliphatic polyesters by ring-opening polymerization. *Adv. Drug Deliv. Rev.* **60,** 1056–1076 (2008).
78. Kowalski, A., Duda, A. & Penczek, S. Kinetics and Mechanism of Cyclic Esters Polymerization Initiated with Tin(II) Octoate. 3. Polymerization of L,L-Dilactide. *Macromolecules* **33,** 7359–7370 (2000).
79. Kricheldorf, H. R., Kreiser-Saunders, I. & Stricker, A. Polylactones 48. SnOct 2 -Initiated Polymerizations of Lactide: A Mechanistic Study. *Macromolecules* **33,** 702–709 (2000).
80. Dechy-Cabaret, O., Martin-Vaca, B. & Bourissou, D. Controlled Ring-Opening Polymerization of Lactide and Glycolide. *Chem. Rev.* **104,** 6147–6176 (2004).
81. Kowalski, A. *et al.* Kinetics and Mechanism of Cyclic Esters Polymerization Initiated with Tin(II) Octoate. Polymerization of ε-Caprolactone and L,L-Lactide Co-initiated with Primary Amines. *Macromolecules* **38,** 8170–8176

(2005).
82. Storey, R. F. & Sherman, J. W. Kinetics and Mechanism of the Stannous Octoate-Catalyzed Bulk Polymerization of ε-Caprolactone. *Macromolecules* **35,** 1504–1512 (2002).
83. Kowalski, A., Duda, A. & Penczek, S. Mechanism of Cyclic Ester Polymerization Initiated with Tin(II) Octoate. 2. Macromolecules Fitted with Tin(II) Alkoxide Species Observed Directly in MALDI−TOF Spectra. *Macromolecules* **33,** 689–695 (2000).
84. Labet, M. & Thielemans, W. Synthesis of polycaprolactone: a review. *Chem. Soc. Rev.* **38,** 3484 (2009).
85. Baimark, Y. & Molloy, R. Synthesis and Characterization of Poly(L-lactide-co-ε-caprolactone) Copolymers: Effects of Stannous Octoate Initiator and Diethylene Glycol Coinitiator Concentrations. *Sci. Asia* **30,** 327–334 (2004).
86. Stridsberg, K. M., Ryner, M. & Albertsson, A.-C. Controlled Ring-Opening Polymerization: Polymers with designed Macromolecular Architecture. *Degrad. Aliphatic Polyesters* **157,** 41–65 (2002).
87. Chen, H.-Y., Zhang, J., Lin, C.-C., Reibenspies, J. H. & Miller, S. A. Efficient and controlled polymerization of lactide under mild conditions with a sodium-based catalyst. *Green Chem.* **9,** 1038 (2007).
88. Murayama, M;Sanda, F;Endo, T. Anionic Ring-Opening Polymerization of a Structure with Amine Initiators. *Macromolecules* **31,** 919–923 (1998).
89. Sherck, N. J., Kim, H. C. & Won, Y.-Y. Elucidating a Unified Mechanistic Scheme for the DBU-Catalyzed Ring-Opening Polymerization of Lactide to Poly(lactic acid). *Macromolecules* **49,** 4699–4713 (2016).
90. Lohmeijer, B. G. G. *et al.* Guanidine and Amidine Organocatalysts for Ring-Opening Polymerization of Cyclic Esters. *Macromolecules* **39,** 8574–8583 (2006).
91. Pratt, R. C., Lohmeijer, B. G. G., Long, D. A., Waymouth, R. M. & Hedrick, J. L. Triazabicyclodecene : A Simple Bifunctional Organocatalyst for Acyl Transfer and Ring-Opening Polymerization of Cyclic Esters. *J. Am. Chem. Soc.* **128,** 4556–4557 (2006).
92. Nederberg, F. *et al.* Organocatalytic Ring Opening Polymerization of Trimethylene Carbonate. *Biomacromolecules* **8,** 153–160 (2007).
93. Leibfarth, F. a *et al.* Organocatalytic Ring Opening Polymerization of Cyclic Monomers: Mechanistic and Synthetic Studies. *Biomacromolecules* **48,** 984–985 (2007).
94. Suriano, F., Coulembier, O., Hedrick, J. L. & Dubois, P. Functionalized cyclic carbonates: From synthesis and metal-free catalyzed ring-opening polymerization to applications. *Polym. Chem.* **2,** 528–533 (2011).
95. Steinbach, T., Ritz, S. & Wurm, F. R. Water-Soluble Poly(phosphonate)s via Living Ring-Opening Polymerization. *ACS Macro Lett.* **3,** 244–248 (2014).
96. Wolf, T., Steinbach, T. & Wurm, F. R. A Library of Well-Defined and Water-Soluble Poly(alkyl phosphonate)s with Adjustable Hydrolysis. *Macromolecules* **48,** 3853–3863 (2015).
97. Kobayashi, S. & Uyama, H. in *Biopolymers Online* (eds. Doi, Y. & Steinbüchel, A.) 373–379 (Wiley-VCH Verlag GmbH & Co. KGaA, 2005).
98. Yang, Y. *et al.* Lipase/esterase-catalyzed ring-opening polymerization: A green polyester synthesis technique. *Process Biochem.* **46,** 1900–1908 (2011).
99. Matsumura, S. *Enzyme-catalyzed synthesis of polymers*. *Adv Polym Sci* **194,** (Springer Berlin Heidelberg, 2006).

100. Sen, S. & Puskas, J. E. Green polymer chemistry: Enzyme catalysis for polymer functionalization. *Molecules* **20,** 9358–9379 (2015).
101. Zhang, J. *et al.* Recent developments in lipase-catalyzed synthesis of polymeric materials. *Process Biochem.* **49,** 797–806 (2014).
102. Shoda, S., Uyama, H., Kadokawa, J., Kimura, S. & Kobayashi, S. Enzymes as Green Catalysts for Precision Macromolecular Synthesis. *Chem. Rev.* **116,** 2307–2413 (2016).
103. Ferrario, V., Pellis, A., Cespugli, M., Guebitz, G. & Gardossi, L. Nature Inspired Solutions for Polymers: Will Cutinase Enzymes Make Polyesters and Polyamides Greener? *Catalysts* **6,** 205 (2016).
104. Heredia, A. Biophysical and biochemical characteristics of cutin, a plant barrier biopolymer. *Biochim. Biophys. Acta - Gen. Subj.* **1620,** 1–7 (2003).
105. Kobayashi, S. Lipase-catalyzed polyester synthesis – A green polymer chemistry. *Proc. Japan Acad. Ser. B* **86,** 338–365 (2010).
106. Semlitsch, S., Torron, S., Johansson, M. & Martinelle, M. Enzymatic catalysis as a versatile tool for the synthesis of multifunctional, bio-based oligoester resins. *Green Chem.* **18,** 1923–1929 (2016).
107. Palmans, A. R. A. & Heise, A. *Enzymatic Polymerisation*. (Springer Berlin Heidelberg, 2010).
108. Verho, O. & Bäckvall, J. E. Chemoenzymatic dynamic kinetic resolution: A powerful tool for the preparation of enantiomerically pure alcohols and amines. *J. Am. Chem. Soc.* **137,** 3996–4009 (2015).
109. Kirk, O. & Christensen, M. W. Lipases from Candida antarctica: Unique biocatalysts from a unique origin. *Org. Process Res. Dev.* **6,** 446–451 (2002).
110. Uppenberg, J., Hansen, M. T., Patkar, S. & Jones, T. A. The sequence, crystal structure determination and refinement of two crystal forms of lipase B from Candida antarctica. *Structure* **2,** 293–308 (1994).
111. Trodler, P. & Pleiss, J. Modeling structure and flexibility of Candida antarctica lipase B in organic solvents. *BMC Struct. Biol.* **8,** 9 (2008).
112. Kulschewski, T., Sasso, F., Secundo, F., Lotti, M. & Pleiss, J. Molecular mechanism of deactivation of C. antarctica lipase B by methanol. *J. Biotechnol.* **168,** 462–469 (2013).
113. Johnson, P. M., Kundu, S. & Beers, K. L. Modeling enzymatic kinetic pathways for ring-opening lactone polymerization. *Biomacromolecules* **12,** 3337–3343 (2011).
114. Van Buijtenen, J. *et al.* Switching from S - to R- Selectivity in the Candida antarctica Lipase B-Catalyzed Ring-Opening of ω-Methylated Lactones: Tuning Polymerizations by Ring Size. *J. Am. Chem. Soc.* **129,** 7393–7398 (2007).
115. Duchiron, S. W., Pollet, E., Givry, S. & Avérous, L. Mixed systems to assist enzymatic ring opening polymerization of lactide stereoisomers. *RSC Adv.* **5,** 84627–84635 (2015).
116. Zaks, A. & Klibanov, A. M. The effect of water on enzyme action in organic media. *J. Biol. Chem.* **263,** 8017–8021 (1988).
117. Novozymes Biopharma DK A/S. *Enzymes for biocatalysis for smarter chemical synthesis: Immobilized Lipases*. (2014).
118. Poojari, Y. & Clarson, S. J. Thermal stability of Candida antarctica lipase B immobilized on macroporous acrylic resin particles in organic media. *Biocatal. Agric. Biotechnol.* **2,** 7–11 (2013).
119. Plurolite & c-LEcta. *CalB immo Plus Immobilized Enzyme*. (2018).
120. Kulshrestha, A. S., Gao, W. & Gross, R. A. Glycerol copolyesters: Control of

branching and molecular weight using a lipase catalyst. *Macromolecules* **38,** 3193–3204 (2005).
121. Kadokawa, J. ichi & Kobayashi, S. Polymer synthesis by enzymatic catalysis. *Current Opinion in Chemical Biology* **14,** 145–153 (2010).
122. Darr, J. A. & Poliakoff, M. New Directions in Inorganic and Metal-Organic Coordination Chemistry in Supercritical Fluids. *Chem. Rev.* **99,** 495–541 (1999).
123. Kendall, J. L., Canelas, D. A., Young, J. L. & DeSimone, J. M. Polymerizations in Supercritical Carbon Dioxide. *Chem. Rev.* **99,** 543–564 (1999).
124. Cooper, A. I. Polymer synthesis and processing using supercritical carbon dioxide. *J. Mater. Chem.* **10,** 207–234 (2000).
125. Goodship, Vannessa and Ogur, E. O. *Polymer Processing with Supercritical Fluids*. *Polymer processing with supercritical fluids. Rapra review reports* **15,** (Rapra Technology Ltd, 2004).
126. Beckman, E. J. Supercritical and near-critical CO2 in green chemical synthesis and processing. *J. Supercrit. Fluids* **28,** 121–191 (2004).
127. Kelly, C. A., Naylor, A., Illum, L., Shakesheff, K. M. & Howdle, S. M. Supercritical CO2: A Clean and Low Temperature Approach to Blending PDLLA and PEG. *Adv. Funct. Mater.* **22,** 1684–1691 (2012).
128. Leitner, W. Designed to dissolve. *Nature* **405,** 129–30 (2000).
129. Kiran, E. Supercritical fluids and polymers - The year in review - 2014. *J. Supercrit. Fluids* **110,** 126–153 (2016).
130. Aionicesei, E., Škerget, M. & Knez, Ž. Solubility and Diffusivity of Supercritical CO2 in Bioresorbable Polymers : Measurements, Calculations and Potential Applications in Polymer Foaming. *12th Eur. Meet. Supercrit. Fluids* 1–10 (2010).
131. De Marco, I., Riemma, S. & Iannone, R. Life cycle assessment of supercritical CO2extraction of caffeine from coffee beans. *J. Supercrit. Fluids* **133,** 393–400 (2018).
132. Grignard, B., Stassin, F., Calberg, C., Jérôme, R. & Jérôme, C. Synthesis of biodegradable poly-epsilon-caprolactone microspheres by dispersion ring-opening polymerization in supercritical carbon dioxide. *Biomacromolecules* **9,** 3141–9 (2008).
133. National Institute of Standards and Technology (NIST), Chemistry WebBook-Thermophysical Properties Systems, of Fluid. Available at: http://webbook.nist.gov/chemistry/fluid/. (Accessed: 17th September 2018)
134. Patil, P. D., Dandamudi, K. P. R., Wang, J., Deng, Q. & Deng, S. Extraction of bio-oils from algae with supercritical carbon dioxide and co-solvents. *J. Supercrit. Fluids* **135,** 60–68 (2018).
135. Lacroix-Desmazes, P. Polymères et CO2 supercritique. *Polymères et éco-conception* 76–82 (2017).
136. Zhang, X., Heinonen, S. & Levänen, E. Applications of supercritical carbon dioxide in materials processing and synthesis. *RSC Adv.* **4,** 61137–61152 (2014).
137. Picchioni, F. Supercritical carbon dioxide and polymers: An interplay of science and technology. *Polym. Int.* **63,** 1394–1399 (2014).
138. Du, L., Kelly, J. Y., Roberts, G. W. & DeSimone, J. M. Fluoropolymer synthesis in supercritical carbon dioxide. *J. Supercrit. Fluids* **47,** 447–457 (2009).
139. Handa, Y. P., Zhang, Z. & Wong, B. Effect of Compressed CO2 on Phase Transitions and Polymorphism in Syndiotactic Polystyrene. *SocietyMacromolecules* **30,** 8499–8504 (1997).
140. Bos, A., Pünt, I. G. M., Wessling, M. & Strathmann, H. CO2-induced

plasticization phenomena in glassy polymers. *J. Memb. Sci.* **155,** 67–78 (1999).
141. Di Maio, E. & Kiran, E. Foaming of Polymers with Supercritical Fluids and Perspectives on the Current Knowledge Gaps and Challenges. *J. Supercrit. Fluids* **134,** 157–166 (2017).
142. Nalawade, S. P., Picchioni, F. & Janssen, L. P. B. M. Supercritical carbon dioxide as a green solvent for processing polymer melts: Processing aspects and applications. *Prog. Polym. Sci.* **31,** 19–43 (2006).
143. Galy, J. *et al.* Decontamination of solid substrates using supercritical carbon dioxide-Application with trade hydrocarbonated surfactants. *J. Supercrit. Fluids* **42,** 69–79 (2007).
144. DeSimone, J. M. *et al.* Dispersion Polymerizations in Supercritical Carbon Dioxide. *Science (80-. ).* **265,** 356–359 (1994).
145. Hussain, Y. A., Liu, T. & Roberts, G. W. Synthesis of cross-linked, partially neutralized poly(acrylic acid) by suspension polymerization in supercritical carbon dioxide. *Ind. Eng. Chem. Res.* **51,** 11401–11408 (2012).
146. Lacroix-Desmazes, P., Andre, P., Desimone, J. M., Ruzette, A. V. & Boutevin, B. Macromolecular surfactants for supercritical carbon dioxide applications: Synthesis and characterization of fluorinated block copolymers prepared by nitroxide-mediated radical polymerization. *J. Polym. Sci. Part A Polym. Chem.* **42,** 3537–3552 (2004).
147. André, P., Lacroix-Desmazes, P., Taylor, D. K. & Boutevin, B. Solubility of fluorinated homopolymer and block copolymer in compressed CO2. *J. Supercrit. Fluids* **37,** 263–270 (2006).
148. Ma, Z. & Lacroix-Desmazes, P. Dispersion polymerization of 2-hydroxyethyl methacrylate stabilized by a hydrophilic/CO2-philic poly(ethylene oxide)-b-poly(1,1,2,2- tetrahydroperfluorodecyl acrylate) (PEO-b-PFDA) diblock copolymer in supercritical carbon dioxide. *Polymer (Guildf).* **45,** 6789–6797 (2004).
149. Uyama, H., Takeya, K. & Kobayashi, S. Synthesis of Polyesters by Enzymatic Ring-Opening Copolymerization Using Lipase Catalyst. *Proc. Japan Acad. Ser. B Phys. Biol. Sci.* **69,** 203–207 (1993).
150. Bratton, D., Brown, M. & Howdle, S. M. Tin(II) Ethyl Hexanoate Catalyzed Precipitation Polymerization of ε-Caprolactone in Supercritical Carbon Dioxide. *Macromolecules* **38,** 1190–1195 (2005).
151. Thurecht, K. J. *et al.* Kinetics of Enzymatic Ring-Opening Polymerization of ε-Caprolactone in Supercritical Carbon Dioxide. *Macromolecules* **39,** 7967–7972 (2006).
152. Steinbach, T., Ritz, S. & Wurm, F. R. Water-Soluble Poly(phosphonate)s via Living Ring-Opening Polymerization. 244–248 (2014).

# Chapter 3
# Experimental and Characterisation Techniques

Reactions in $scCO_2$ require special equipment to produce and withstand high pressures. The first section outlines the high-pressure set-up, stainless steel autoclave and the view-cell employed in the thesis. Experimental practises are then summarised covering the standard operating procedures for all equipment used. Further details related to specific reactions can be found in the individual Chapters.

The second section focuses on the analytical techniques used to characterise and analyse the products synthesised in this Thesis.

## 3.1 High-Pressure Equipment

As a general description, the high-pressure systems consist of a mode of generating the pressure to the systems (i.e. a pump), high-pressure tubing and fittings, a stainless-steel vessel and appliances to monitor continuously the pressure and temperature of the system.

For polymerisations and purifications, an in-house built clamp-sealed reactor (autoclave), made from stainless steel 316, attached to the Pickle pump *via* a series of high-pressure stainless-steel Swagelok® pipes and fittings, was utilised. To study the behaviour of samples in $CO_2$, an in-house built stainless steel view cell equipped with sapphire windows was employed. For all the high-pressure equipment used in this work, $CO_2$ (BOC, 99.99%) was delivered from the cylinder through a PM-101 SFE Pickle pump (New Ways of Analytics, Germany).

The pump consists of a gas input, a refrigerated condenser unit for gas liquefaction and an outlet. The $CO_2$ is introduced from a cylinder at a pressure of 55 bar through a refrigerated condenser to ensure liquid phase $CO_2$ fills the pump. Compressed air at ~ 3-5 bar (supplied by an external compressor) is needed to compress the liquid $CO_2$ and reach the desired output pressure (typically up to 260-270 bar in this Thesis).

A series of T-pieces, tubing (both Swagelok®, SS316, 1/8" and 1/16"), brass nuts and ferrules (Autoclave Engineers) and valves (High-Pressure Equipment, HIP) fittings connect the main $CO_2$ line to each autoclave. Manual HIP valves (High-Pressure Equipment Company, USA) were used to control the $CO_2$ inlet and outlet flow when filling the autoclaves and at the end of the reactions to vent the system. Non-return

valves (NRV) were also placed before each autoclave, to prevent the backflow and hence avoid reagents flowing back into the pump (Figure 3.1).

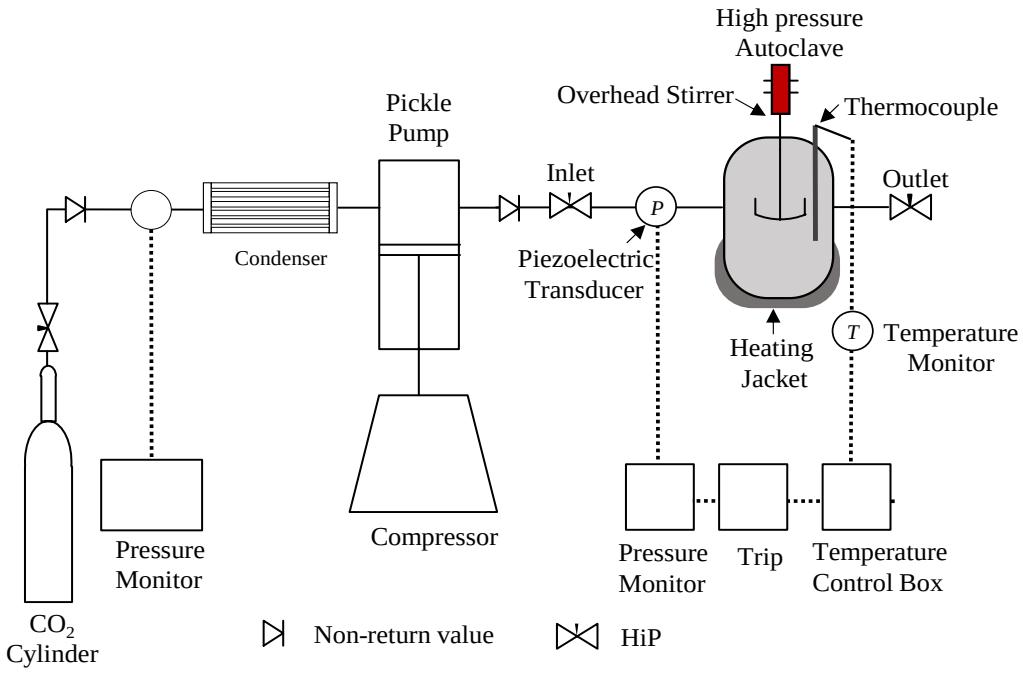



Figure 3.1. A general high-pressure setup is represented. Non-return valves (NRV) are placed before and after the Pickel pump to prevent backflows.

### 3.1.1 MKIII Clamp-Sealed Autoclave

High-pressure autoclaves developed in-house at the University of Nottingham, were used for polymerisations in $scCO_2$. A schematic of a 60 mL autoclave (Figure 3.2) and images of a 20 mL autoclave are shown (Figure 3.3).

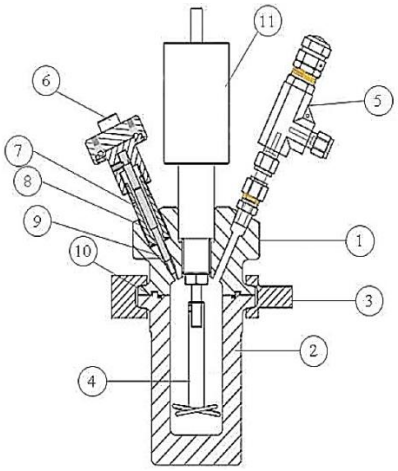



Figure 3.2. Schematic diagram of a 60 mL MKIII autoclave. (1) Head, (2) cell body, (3) clamp, (4) stirrer, (5) spring-loaded pressure release valve, (6) knob, (7) screw insert, (8) vent hole, (9) safety needle, (10) EPDM O-ring, and (11) overhead stirrer coupling.

The autoclave consists of two parts, the head (Figure 3.2, (1)) and the body (Figure 3.2, (2)). The autoclave head is equipped with ports suitable for flow of $CO_2$ (an inlet and outlet high-pressure pipes), an internal thermocouple, a spring-loaded pressure-relief valve and linked to temperature (*T*) and pressure (*P*) monitoring devices. (Figure 3.3, head).

The two parts are sealed by an O- ring (typically ethylene propylene diene monomer, EPDM rubber) (Figure 3.2, (10)) placed in between the head and the body. The use of EPDM rubber O-rings limits the conditions for safe operation to temperatures between $T$ = –50 to 150 °C and a maximum pressure of $P$ =300 bar, although typically a maximum $T$ of 130 °C is used in case of overheating. The maximum working limit pressure of this stainless steel vessel with the use of O-ring is 150 °C and 300 bar.

A stainless steel clamp holds the two parts together, secured by a screw mechanism, tightened with a unique key. The key is composed of a safety needle and a knob (Figure 3.3, bottom). The safety needle creates a final seal when inserted in the autoclave head before pressurising.

Two safety measures result from this key-clamp assembly. Firstly, the clamp can only be unfastened if autoclave does not have any residual pressure since it can only be opened by the unique key which thus needs to be removed first. This guarantees that it is not possible to open the autoclave whilst the system is under pressure. Secondly, in the event of a valve blockage, during the venting process, the safety needle can be loosened slowly to release the residual pressure *via* the vent hole (Figure 3.2, (8)).

The pressure is monitored through a quartz piezoelectric transducer (RDP Electronics) that is connected before the inlet high-pressure valve in each autoclave (Figure 3.1). The transducer makes use of the piezoelectric mechanism to emit an electrical current when the quartz crystal experiences strain under pressure. This strain is read out in pounds-per-square-inch (psi, 1 bar = 14.7 psi) by an in-house manufactured pressure monitor.

A spring-loaded pressure relief valve (SS-4R3A Swagelok, maximum pressure 300 bar) is incorporated, on the head of the autoclave, to protect from over-pressure (Figure 3.2, (8)). During a standard reaction, a disk seals this valve held tightly by a spring of pre-set tension. The main principle of the safety valve is the protection of the system and the surrounding in case of overpressure incident. If the pressure of the system exceeds

the set value (300 bar), the safety valve opens to release the pressure. It recloses and prevents the further release of fluids after safe operating conditions have been attained.

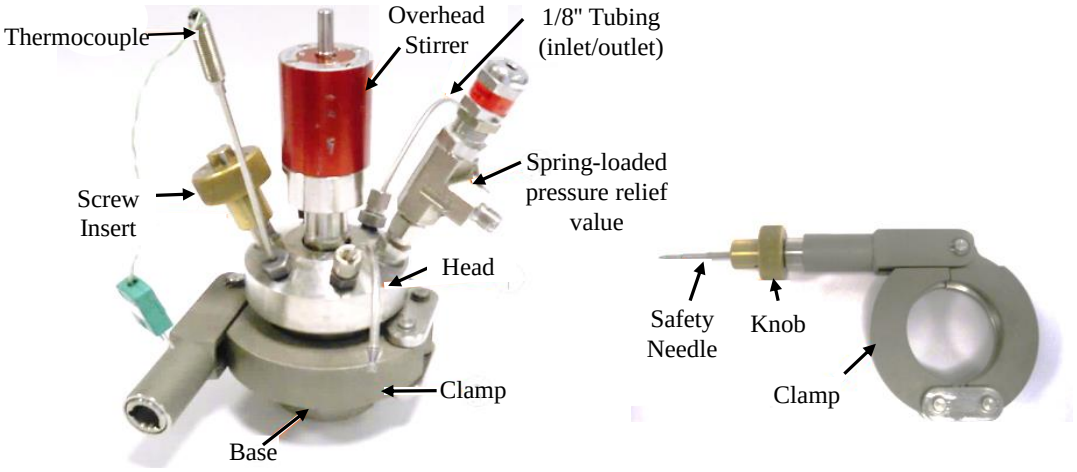



Figure 3.3. MKIII clamp-seal stainless steel autoclave equipped with a 20 mL base (left) and the safety key and clamp to seal the autoclave (right).

A trip box is connected in the setup. Both the pressure controller and digital temperature controller are connected to a trip box. An external stainless steel heating jacket (Watlow, UK) and an internal K-type thermocouple (chromel-alumel) (RS Components), are also connected to the temperature controller. In case of overpressure (> 300 bar), it receives a signal from the pressure box an electrical trip cuts the power supply to the heating jacket, and the pressure will decrease as a consequence of the temperature drop.

Reactions were mixed through a mechanically coupled overhead stirrer (Figure 3.2, (11)) that is connected to a motor (IKA Eurostar Germany) typically set at 250 revolutions per minute (rpm).

For small-scale polymerisations, a standard 20 mL MKIII high-pressure was modified in order to have a total capacity of 0.5 mL (made in-house at Nottingham).

To have an autoclave with 0.5 mL volume, firstly, the head of the 20 mL autoclave was modified. The mechanically coupled stirrer and the shaft were removed from the 20 mL head (Figure 3.5, b), and a different stainless body where a PTFE (polytetrafluorethylene) was inserted in the base to create smaller volume (of 0.5 mL) (Figure 3.5, c). A schematic of modified MKIII high-pressure autoclave is shown (Figure 3.4).

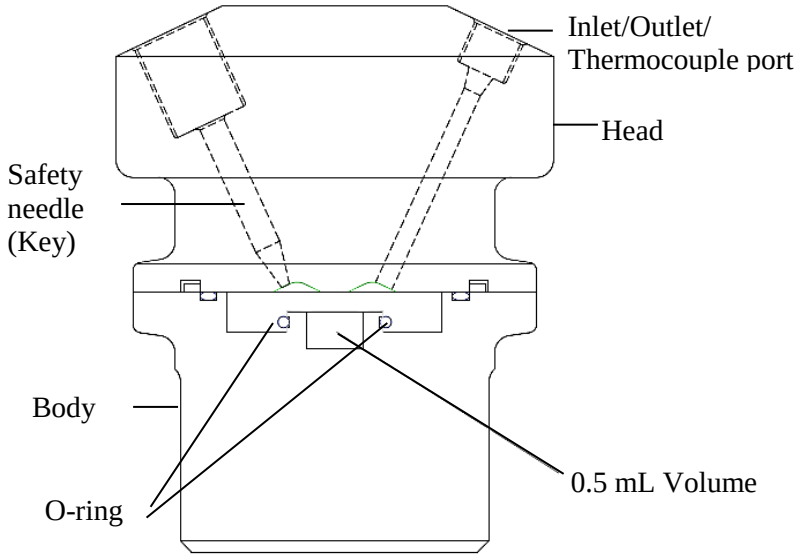



Figure 3.4. Schematic representation of a modified MKIII head and the base to decrease the volume capacity from 20 mL to a 0.5 mL for small-scale polymerisations.

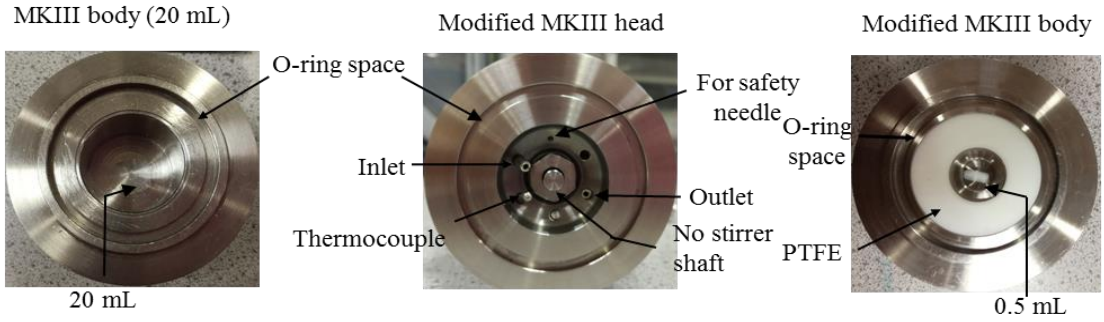



Figure 3.5. A standard MKIII stainless steel base with a volume capacity of 20 mL (left), the modified MKIII head where the stirring shaft is removed (middle) and the modified body with a total capacity of 0.5 mL equipped with a magnetic stirrer bar (right).

### 3.1.1.1 Standard operating procedure of MKIII Autoclave

To minimise risks and increase the safety of the high-pressure polymerisations a standard operating procedure was followed for each reaction:

1. An EPDM o-ring was placed in the autoclave body and then the head was clamped together with the body. The clamp was securely tightened using the safety key. The inlet and outlet pipes were connected and all the Swagelok® fittings were tightened then the heating jacket was secured around the body.

2. The thermocouple was connected to the control box to monitor the internal autoclave temperature.

3. The setup was pressurising to ~55 bar at room temperature in order to leak test all the fittings with 'snoop' (the liquid used to detect leaks).

4. If required, the autoclave was vented to ambient pressure through the outlet HIP tap and any leaking fittings adjusted. Fittings were never tightened when the autoclave is under pressure.

5. Steps 3 and 4 were repeated after adjusting the fitting and until no leaks remained.

6. Residual pressure from the leak test was vented until the autoclave was at atmospheric pressure. The key-clamp assembly was undone and the necessary amount of reactive was added to the base of the autoclave.

7. The autoclave was once again clamped together and purged with a flow of $CO_2$ (at 2 bar) to flush out residual air from the system (keeping the safety key unscrewed) for about 5 min.

8. After this, the safety key was hand-tightened into the head to seal the vessel.

9. The vessel pressurised to around 55 bar $CO_2$ and the mechanical stirrer was switched on (250 rpm).

10. The internal thermocouple was plugged in; the heating jacket was connected to the control box and the temperature set to the desired value while monitoring the pressure throughout this process.

11. The autoclave was allowed to reach its final temperature and the pressure was increased to ~275 bar by slow addition of $CO_2$.

12. After the desired reaction time, the reactions were stopped by switching off the heating and unplugging the connection to the temperature controller. The autoclave was allowed to cool to room temperature while monitoring the temperature.

13. After the autoclave had cooled to ambient temperature (~20 bar), the heating jacket was removed from the body and the $CO_2$ was vented into the fume hood by opening the outlet HIP tap (slowly). Typically, the release of the residual pressure took 20- 30 min.

14. Once at ambient temperature and pressure, the safety key was removed and the Swagelok® fittings were undone.

15. Finally, the clamp was disconnected to open the autoclave and the product was collected.

### 3.1.2 View Cell Studies Set-up

A fixed volume (100 mL) view cell was utilised to study the behaviour of the material under high-pressure $CO_2$ (discussed in Chapter 4 and Chapter 5).

The basic design of the view cell (also designed at the University of Nottingham) and working principle is very similar to the stainless steel MKIII high-pressure autoclave (Figure 3.3). The main difference is the cylindrical stainless steel body, oriented horizontally, featuring two sapphire windows that fit into the front and rear and are sealed to the body using the same key-clamp assembly. The heating elements (cylindrical rods) sit within in the walls of the horizontally oriented body. This set-up required an increased wall thickness than MKIII autoclave. Therefore, two thermocouples are included to monitor potential temperature gradients. The external thermocouple sits in the body wall (connected to the trip) whereas the internal one is located in the $scCO_2$ phase (used to monitor the temperature).

A mechanical stirrer is located in the body of the view-cell but was not used during any view-cell studies (Figure 3.6).

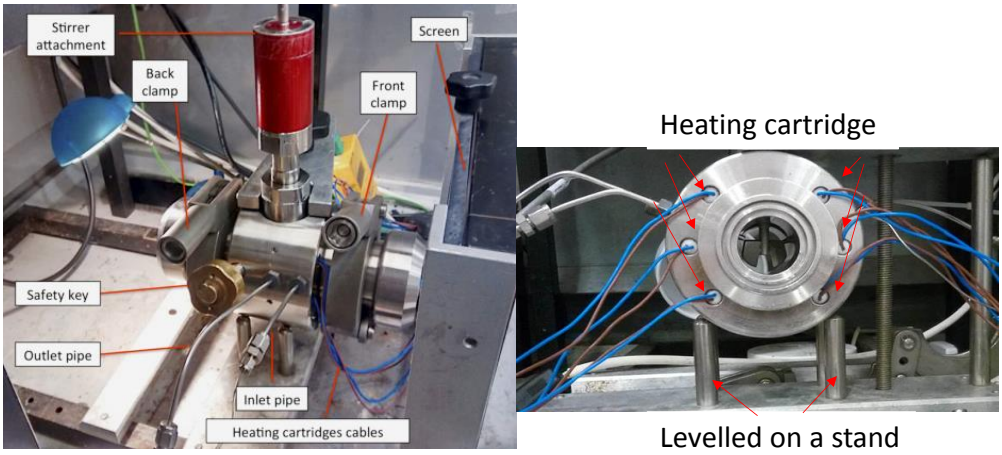



Figure 3.6. Side view of the high-pressure view cell (fully assembled) (left) and a front view showing the heating elements (right).

**Standard operating procedure.** After placing a glass vial with the sample under investigation in the body, steps 1-6 and 8 of section 3.1.1.1 were followed. The pressure (*P*) and temperature (*T*) were set to the desired value starting from ambient conditions by step-wise increasing *P* and *T* by 10 bar and 5 °C after each observation. The system was allowed to equilibrate for 1 h after any phase change was observed. The maximum working conditions of this view cell are 100 °C and 300 bar. Note: *To improve visibility*

*inside the view cell an external lamp can be utilised near the rear window when pictures are taken from the front window.*

Once the assessment was complete, the autoclave was cooled by switching off the heating power supply. After cooling to ambient temperature and obtaining a low $CO_2$ pressure (~50 bar) the system was vented slowly (~1 psi/sec).
The characterisation techniques for polymers used in this thesis are described below. For clarity of the set-ups used characterisation techniques are abbreviated according to the place where the analyses were performed. This is especially the case for SEC-DMF set-up employed discussed below and employed in Chapter 4 and Chapter 5.

## 3.2 Characterisation Techniques

The polymers were characterised by analytical techniques including $^{1}$H NMR, $^{31}$P-NMR after phosphitylation of OH-groups, SEC-MALS, SEC-UC, MALDI-TOF, ESI-MS, DSC, DLS, TEM, Cryo-TEM, Tensiometer, FTIR and TGA.

### 3.2.1 Nuclear Magnetic Resonance Spectroscopy (NMR)

Nuclear Magnetic Resonance Spectroscopy (NMR) spectra were typically recorded on a Bruker Avance spectrometer operating at 300 MHz or 400 MHz with chemical shifts in parts per million (ppm) referenced relative to the deuterated solvent; DMSO-$d_6$, or $CDCl_3$.
$^{1}$H NMR was performed to evaluate conversions of the performed polymerisations (% conv.) and analyse the number average molecular weights ($M_n$) of the synthesised polymers.

### 3.2.2 Size Exclusion Chromatography-Multi-Angle Light Scattering (SEC-MALS)

A light scattering detector provides absolute molecular weights irrespective of a column calibration. Size Exclusion Chromatography-Multi-Angle Light Scattering Characterisation (SEC-MALS, Nottingham) was performed to determine the number average molecular weight ($M_{\mathrm{n}}^{\text{SEC-MALS}}$) and the dispersity ($Đ$) of the polymers discussed in Chapter 4.
SEC measurements were performed on a Agilent 1260 Infinity triple detection SEC set-up comprising a Wyatt Optilab multi-angle light scattering (MALS) detector, and an

Agilent differential refractometer. Separation was achieved using 2 PLgel mixed D columns (7.5 mm × 50 mm). The eluent was tetrahydrofuran (THF) at room temperature at a flow rate of 1 mL $min^{-1}$. The refractive index increment (dn/dc) of star *D*-sorbitol PCL was determined using a representative sample, star *D*-sorbitol-$[(PCL)_{9.7}\text{-}OH]_{5.1}$ (Table 4.2, Entry 3, Chapter 4). Five different concentrations of star *D*-sorbitol-$[(PCL)_{9.7}\text{-}OH]_{5.1}$ in THF were injected and the resulting RI signals were plotted as a function of concentration. The dn/dc value of 0.074 ± 0.04 mL $g^{-1}$ was obtained as the gradient of a linear fit using the ASTRA software, which is in good agreement with the dn/dc value from the literature for linear PCL in THF at 25 °C (dn/dc = 0.072 mL $g^{-1}$).[1] Therefore, this value (dn/dc = 0.072 mL $g^{-1}$) was used for MALS analysis of all samples in this work.

The refractive index increment (dn/dc) is the degree by which the refractive index of a solution varies as the concentration of solute changes. In light scattering, the intensity of scattered light is directly proportional to the square of dn/dc (also refer differential refractive index detector section 3.2.3).

It is noteworthy that the average molecular weight of each arm in a star structure can be approximated by dividing the molecular weight of the star by the functionality of the initiator. However, this procedure assumes that all the multifunctional groups have completely reacted which is not necessarily true.

Thus, different methods are employed to obtain more information on the length and the number of arms.

### 3.2.3 SEC using Universal Calibration ($SEC^{UC}$) for Arms Evaluation

SEC using Universal Calibration ($SEC^{UC}$, Univ. Montpellier) was performed employing differential refractometer and an online-viscometer detector on a 390-MSD Agilent system. The eluent was THF at 30°C with a flow rate of 1 mL $min^{-1}$. Separation was achieved using 2 PLgel mixed D columns (5 µm, 300 × 7.5 mm) connected in series. The Universal Calibration approach was used to calculate the molecular weight average for the linear PCL and star-branched PCL polymers using linear polystyrene (PS) standards (EasiCal PS standards, 9-point calibration based on the $M_p$ of the samples in the range: 1440 – 354000 g/mol, Agilent Technologies). The cirrus software was used to analyse SEC traces and calculate intrinsic viscosity and molecular weight (MW) data.

Using $SEC^{UC}$ and a Mark-Houwink (MH) plot approach enabled the determination of functionality and branching of the polymers discussed in Chapter 4.

**Differential Refractive Index Detector (DRI).** The DRI detector measures the change in refractive index (RI) of the eluate with respect to the pure solvent.[2] The RI changes when the polymer fraction reaches the detector. For most polymers, the RI value is expected to differ from the RI value of the solvent. This method cannot be employed if a polymer and the solvent have similar RI values. The SEC traces using the DRI are produced by plotting the signal intensity as a function of elution time, which is proportional to the elution volume, which depends on the hydrodynamic volume of the analyte. For polymers, the hydrodynamic volume is related to and increases with the molecular weight.

Since SEC separates, the polymer fraction based on polymer size the determination of polymer MW by SEC is a relative method and requires calibration. The calibration involves the analysis of a series of narrowly dispersed PS standards of known MW. Using these data, a calibration curve of Log MW vs. elution time is determined. The MW of the unknown sample with respect to PS can be determined from this curve based on its elution time.[3]

Since the polymers of interest in this Thesis are PCL and polymers with a star architecture, a calibration using linear PS standards is erroneous. Thus, to obtain absolute values a Universal Calibration based on the Mark-Houwink-Sakurada equation is employed (discussed later in this section).

**Online Viscometer Theory.** When a polymer (solute) dissolves in a liquid (solvent), the interaction between the two components results in an increase in polymer dimensions as compared to that of the unsolvated state. The vast difference in size between solvent and solute considerably alters the friction of the solvent in the mixture and an increase in viscosity occurs which depends on the size and shape of the solute, even in dilute solutions. In other words, the dissolved polymer coils disturb the linear flow of the solvent, resulting in a resistance to flow and an increase in viscosity (see Figure 3.7 (Top)).[3]

A viscometer can be employed to measure the specific viscosity though this resistance to flow. The specific viscosity is a measure of the thickening effect of the polymer solution as compared to the pure solvent.[4]

The intrinsic viscosity, [η] is obtained from the specific viscosity when the concentration of the polymer solution approaches zero, i.e. at very low concentrations (Eq. 3.1).[3]

$$[\eta] = \lim_{c \to 0} \left( \frac{\eta_{sp}}{c} \right) \qquad \text{Eq. 3.1}$$

This parameter is a characteristic of isolated polymer chains in solution and can be considered proportional to the density of the polymer coil.[3]

The concentrations used in system are low enough for the equation to be valid over a typical chromatogram, and thus an extrapolation to the true intrinsic viscosity is not required, since the concentration is close enough to the limiting concentration.[3] Cirrus™ Multi-Detector software can be used to calculate molecular weight and intrinsic viscosity using algorithms for Universal Calibration. Information on branching can also be obtained by the Cirrus software using a regular star-branched model. It can also be determined manually from the intrinsic viscosity (calculated in Chapter 4 manually) as discussed in the following sections.[3]

**Universal Calibration.** Benoit (1967)[5] showed that polymers of the different structure show the same calibration curve if the intrinsic viscosity is included as a calibration parameter. Universal Calibration (UC) plot is based on the principle that the product of the intrinsic viscosity and the molecular weight [η][M] is related on the hydrodynamic volume of the molecules in solution regardless of its shape.[3] A series of hydrodynamic volume values for a variety of narrow standards results in a singular calibration curve.[5] Once this "Universal" calibration has been established by calibrating the system with polymer standards, any random unknown polymer coil can be run in the appropriate solvent and still, an accurate molecular weight can be determined based on the Universal calibration curve.[3]

For a given polymer and solvent system at a specified temperature, intrinsic viscosity can be related to molecular weight through the Kuhn-Mark-Houwink-Sakurada equation, which is frequently referred as Mark- Houwink (MH) equation (Eq. 3.2)

$$[\eta] = K M^{\alpha} \qquad \text{Eq. 3.2}$$

The plot of log[η] against log M is also known as the viscosity law plot where the intercept is log K and α is the MH slope. These can be determined by calibrating with

polymer standards of known molecular weights (in this study PS standards were employed).

The MH plot is an important tool for polymer structure characterisation because intrinsic viscosity is very sensitive to structural differences. For example, in this work, MH data and Zimm-Stockmayer theory allowed the calculation of the number of arms of a star polymer (applied in Chapter 4).

In comparison with a linear polymer of the same molecular weight, polymers with long chain branches (such as a star- and comb-branched) have smaller $R_g$ (Radius of Gyration) and thus the hydrodynamic radius will be smaller. Thus, with the same molecular weight, the density of the star or branched polymer will be higher resulting into a lower intrinsic viscosity (Figure 3.7, top).

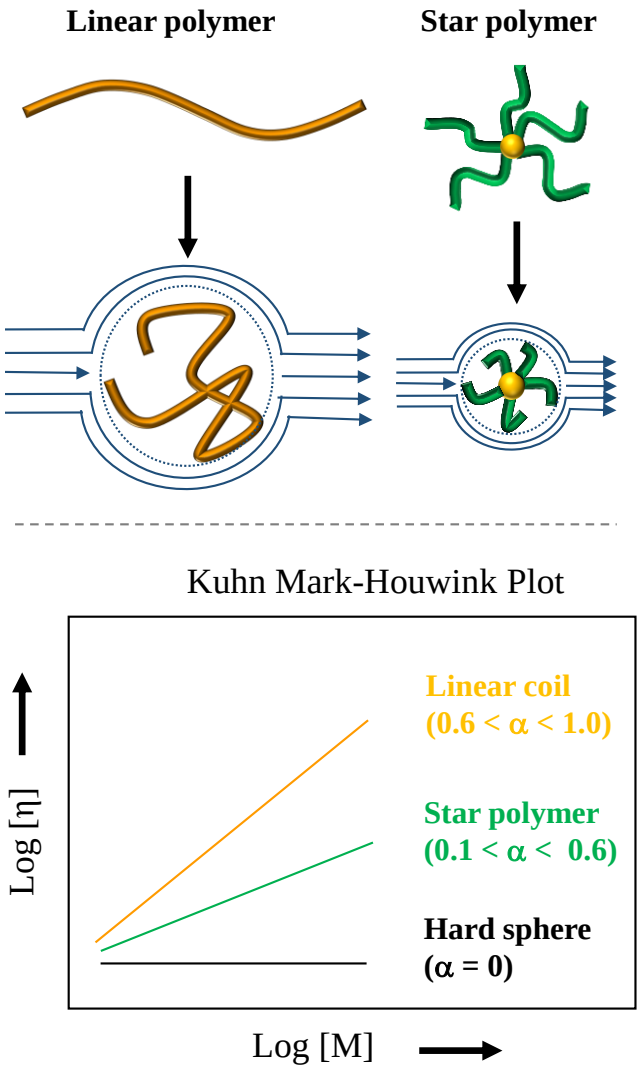



Figure 3.7. Schematic illustrating the impact of architecture (linear vs. star) on the size of polymer coil when dissolved in a solvent (Top) and a correlation of branching and the intrinsic viscosity [η] as a function of molecular weight [M] (bottom).[6]

A use of SEC with a viscometer coupled with the Universal Calibration calculation can indeed provide structural information related to the size and shape of the polymer molecules in solution from Mark-Houwink plots as represented (Figure 3.7, top).
The degree of branching can be estimated by following Eq 3.3 - 3.5.
The root-mean-square radius of a branched polymer is smaller than that of a linear polymer of the same molecular weight. The contraction factor (g) from a radius of gyration can thus be defined as the ratio of the $R_g$ square of the branched polymer to that of a linear polymer of same molecular weight by the following expression.[7,8]

$$g = (R_g{}^2{}_{branched})/(R_g{}^2{}_{linear}) \quad \text{Eq 3.3}$$

The contraction factor from intrinsic viscosity, g', is determined from the intrinsic viscosity of the branched polymer ($[\eta]_{branched}$) and a linear equivalent ($[\eta]_{linear}$) using the following relationship (Eq 3.4) from the MH plot.[7]

$$g' = \frac{[\eta]_{branched}}{[\eta]_{linear}} \quad \text{Eq 3.4}$$

g and g' are related by a power law and the exponent $1/\varepsilon$, where $\varepsilon$ is the so-called structure factor and for star polymers, $\varepsilon$ is 0.5. [8]

$$g = g'^{1/\varepsilon} \quad \text{Eq 3.5}$$

So the ratio of the intrinsic viscosity of star-branched polymers to that of linear polymers of the same molecular weight is approximately equal to $g^{1/2}$.[8]
The number of arms from $SEC^{UC}$ was calculated using the Zimm-Stockmayer equation[7] where the radius of gyration contraction factor (g) is given by:

$$g = (3f - 2)/f^2 \quad \text{Eq 3.6}$$

where $f$ is the functionality i.e. the number of arms and it can be obtained from the second-degree equation: $g f^2 - 3 f + 2 = 0$ (applied on star polymer in Chapter 4)

### 3.2.4 Conventional Size Exclusion Chromatography Technique

A conventional SEC analysis provides molecular weight relative to a column calibration. For the molecular weight analysis by conventional column calibration of water-soluble and amphiphilic polymers, four different SEC methods were employed in Chapter 5.

**(SEC-N, Nottingham) SEC-N** was carried out using a PL50 Polymer Laboratories system equipped with a refractive index detector, employing 2 mixed D columns at 50 °C, using DMF + 0.1wt% LiCl as the mobile phase at a flow rate of 1 mL $min^{-1}$. Poly(methyl methacrylate) (PMMA) standards ($M_n$ range: 505 to 1 810 000 g $mol^{-1}$) were used to calibrate the SEC.

**(SEC-G, Germany)**. **SEC-G** measurements were performed in DMF (containing 0.25 g $L^{-1}$ of lithium bromide as an additive) at 50 °C and a flow rate of 1 mL $min^{-1}$ with an Agilent 1100 Series integrated instrument, including a PSS HEMA column ($10^6/10^5/10^4$ g $mol^{-1}$) and a refractive index (RI) detector. Calibration was carried out using poly(ethylene glycol) (PEG) standards provided by Polymer Standards Service.

**(SEC-U, Univ. Montpellier). SEC-U** measurements were conducted on a system composed of a Varian 390-LC Multidetector suite fitted with a differential refractive index, double angle light scattering, and viscosimeter detector equipped with a guard column (Agilent PolarGel L 8 μM, 50 × 7.5 mm) and two PolarGel L columns (Agilent 5μM, 300 × 7.5 mm). The mobile phase was dimethylformamide (DMF) with 0.1wt% LiCl at 40 °C, at a flow rate of 0.8 mL $min^{-1}$. The results were calibrated against poly(methyl methacrylate) (PMMA) standards (1010-68000 g $mol^{-1}$) using Cirrus v3.3 software.

**(SEC-E, ENSCM). SEC-E** was performed on a Varian ProStar Model 210 equipped with a refractive index detector. Two PLgel 5 μm Resipore columns were used at 70 °C with a 0.8 mL $min^{-1}$ flow rate of DMF with 0.1wt% of LiBr, calibrated using PMMA standards. The injection volume was 20 μL at a sample concentration of 10 mg $mL^{-1}$.

### 3.2.5 $^{31}$P NMR Phosphitylation

Analysis of branched polyesters possessing multiple chemically similar functional group (e.g. various type of alcohols) can be challenging. Having that said, the $^{31}$P NMR spectroscopy has served as an extremely valuable tool for the structural elucidation of complex naturally occurring (macro)molecules such as lipids,[9] lignocellulose,[10–13]olive oil,[14] tannins,[15] etc. Quantification of hydroxy groups by a phosphitylation method in combination with $^{31}$P NMR spectroscopy has been successfully employed as a means to accurately determine the molecular weights of polyesters.[9,16,17]

Compared to standard potentiometric titrations and quantitative $^{13}C$ NMR measurements the $^{31}P$ NMR is highly attractive for several reasons: (1) low amount of sample is required for analysis (milligrams instead of grams), (2) the quantification of carboxylic acid and hydroxy groups is possible in the same measurement and (3) the time required for each measurement is significantly reduced. Moreover, the ability to differentiate between primary and secondary hydroxy groups is powerful.

The quantification approach includes selectively tagging the labile proton present in the sample with the phosphorus-tagging reagent followed by subsequent $^{31}P$ NMR spectroscopy analysis.

Appreciating the wide chemical shifts range of $^{31}P$ compounds,[18] this Thesis is mainly focused on phosphitylated products with a carboxylic acid or hydroxy functional groups. The most common reagent for *in situ* derivatisations of aliphatic alcohols, phenols, and carboxylic groups containing moieties present in the sample is 2-chloro-4,4,5,5-tetramethyl-1,3,2-dioxaphospholane (Cl-TMDP) (Figure 3.8).[1-16]

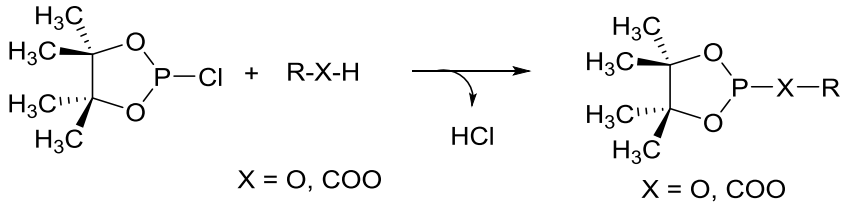



Figure 3.8. Scheme of alcohol and carboxylic acid derivatisation using 2-chloro-4,4,5,5-tetramethyl-1,3,2-dioxaphospholane (Cl-TMDP) for $^{31}P$-NMR analyses.

Besides, 2-chloro-1,3,2-dioxaphospholane[12,13,19,20] is also an excellent tagging reagent of labile protons present in the samples. But for comparative results with our previous work[21], Cl-TMDP was employed as a phosphitylating reagent.

### 3.2.2.1 Quantification by Phosphitylation Method

The most common internal standard for quantification is cyclohexanol and it has been used to quantify the amount of hydroxy and carboxy moieties present in polyol-polyester samples by Goddard *et al.*[21] and Gustini *et al.*[22]

**Stock Solution Preparation.** The analysis was performed following a similar procedure to Spyros *et al.*[17] The number, length and molecular weight of the arms of star *D*-sorbitol-PCL were quantified by $^{31}P$ NMR spectroscopy after phosphitylation of the terminal hydroxy and carboxy groups. A stock solution was typically prepared by dissolving Chromium (III) acetylacetonate [$Cr(acac)_3$] (11.9 mM, 25 mg) and

cyclohexanol (17.7 mM, 10.6 mg, internal standard) in 6 ml pyridine:$CDCl_3$ (3:1 volume ratio). Known amounts of samples were dissolved in the stock solution (600 µl), thus including 10.62 µmoles of internal standard ($n_{IS}$) in each polymer sample. The samples were vortexed until a clear purple solution was obtained. Subsequently, the phosphitylation reagent 2-chloro-4,4,5,5-tetramethyl-1,3,2-dioxaphospholane (Cl-TMDP) (60 µl) was added dropwise, and the samples were left to react on a mechanical shaker at ambient temperature for 60 min.

Similarly, for polyols model samples the amount of cyclohexanol was adjusted based on the mass (mg) of the alcohol/polyols under analysis (discussed in Table 3.1).

**Acquisition of $^{31}$P NMR Spectra.** Inverse gated decoupled $^{1}$H-$^{31}$P NMR spectra were recorded on a Bruker Avance III at 162 MHz for $^{31}$P using $CDCl_3$ as a locking solvent at room temperature. Usually, $^{31}$P NMR spectra are acquired in the presence of another radio frequency source (decoupler) in order to avoid the multiplet signals, that are due to the coupling between phosphorus and neighbouring hydrogen, $J\{^{31}P- ^{1}H\}$, nuclei. This process is called 'decoupling'. A typical phosphorus-decoupled NMR spectrum has singlet peaks for a phosphorus nucleus. In the inverse gated decoupling pulse sequence method, an elongated acquisition time (60 min), a 90° pulse angle, 30 s delay time, and 128 scans were employed.

To distinguish the type of functional groups in samples, $^{31}$P-$^{1}$H coupled spectra were recorded alongside. Multiplicity aids in interpreting the type of alcohols (e.g. triplet for primary (1°) and doublet for secondary (2°) hydroxy groups). The chemical shifts were referenced to $\delta$ = 132.20 ppm ($H_2O$ + Cl-TMDP adduct).

The overall chemistry of phosphorus derivatisation along with $^{31}$P NMR chemical shifts of the phosphitylated aryl/alkyl hydroxy, carboxy groups and water with Cl-TMDP are summarised (Figure 3.9).[23]

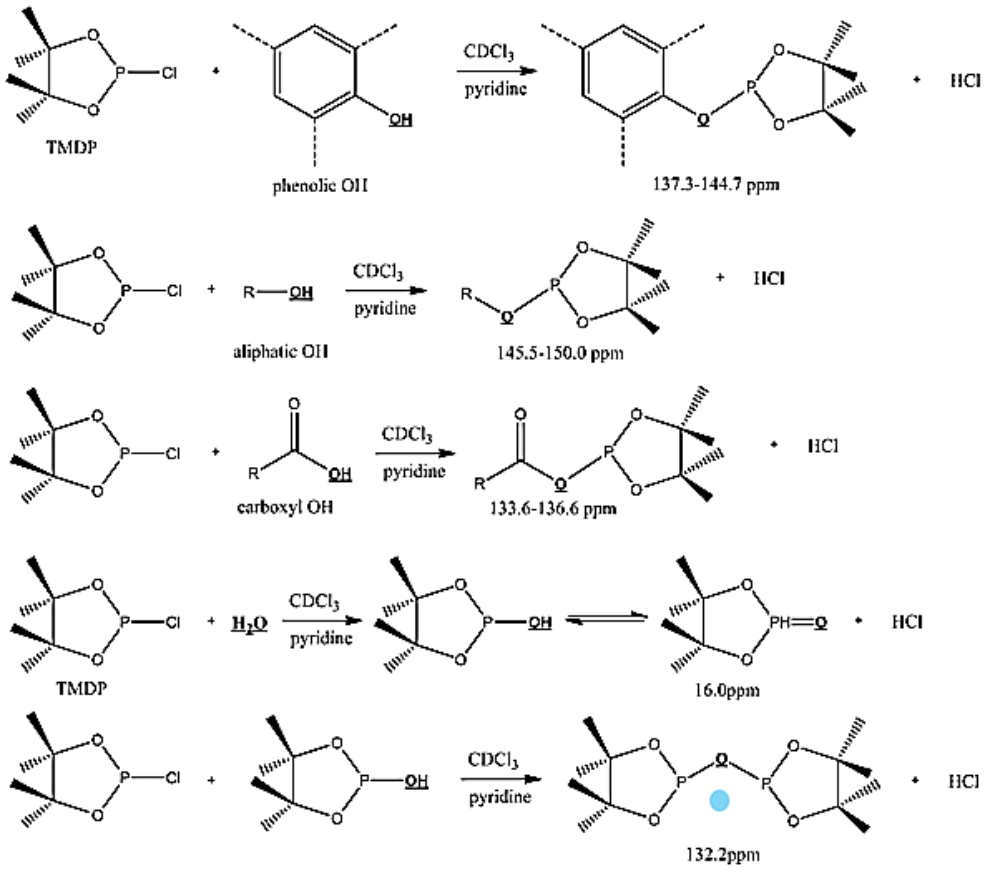



Figure 3.9. Reactions of the phosphorus reagent (Cl-TMDP) with various hydroxy functional groups and the $^{31}$P NMR shifts of the phosphitylated compounds. The signal at $\delta$ 132.20 ppm (●) was used as a reference for the chemical shifts of the other compounds.[23]

The proton-coupled $^{31}$P NMR spectra recorded on model compounds (benzyl alcohol, 1,6-hexanediol, glycerol, and pentaerythritol, *D*-sorbitol, *D*-mannitol) of known molecular weight aided the identification of primary (1°, ● triplet) and secondary (2°, ● doublet) hydroxy groups (refer to Appendix B); and for *D*-sorbitol spectrum (refer to Figure 3.11, (a)).

The use of a known quantity of cyclohexanol as an internal standard (●, $\delta$ 145.2 ppm) in the inverse-gated proton-decoupled $^{31}$P NMR spectra of the model compounds (Figure 3.10) facilitates the quantification of OH group. The analytical results revealing the molecular weight evaluated by phosphitylation of these model samples ($M_n$ $^{\text{P-NMR}}$ (sample)) are presented (Table 3.1).

Up to 98-99% accuracy in hydroxy group derivatisation of the hydroxy group of benzyl alcohol, 1-6 hexanediol, and glycerol was confirmed by comparing the estimated $M_n$ $^{\text{P NMR}}$ (sample) and the theoretical molar mass of model compounds following Eq. 3.9 (Table 3.1). For all these tested compounds, benzyl alcohol, 1,6-hexanediol,

glycerol, HO-PCL-OH, the $M_n$ $^{P\ NMR}$ is very close to theoretical molar mass leading to % of phosphitylation = 100% ± 2%.

The deviation in $M_n$ $^{P\ NMR}$ (sample) molar mass occurs for *D*-sorbitol (114% phosphitylation) > pentaerythritol (112% phosphitylation, although it is only 1° positions) > mannitol (94% phosphitylation). Indeed, for glycerol, very little minor extra peaks are visible (the premise of what becomes more visible with pentaerythritol and *D*-sorbitol). The presence of unreacted Cl-TMDP ensures there is an excess amount of phospholane reagent present to drive the derivatisation to full conversion. Nonetheless, the repeatability for signals and % of phosphitylation for *D*-sorbitol was tested in triplicates.

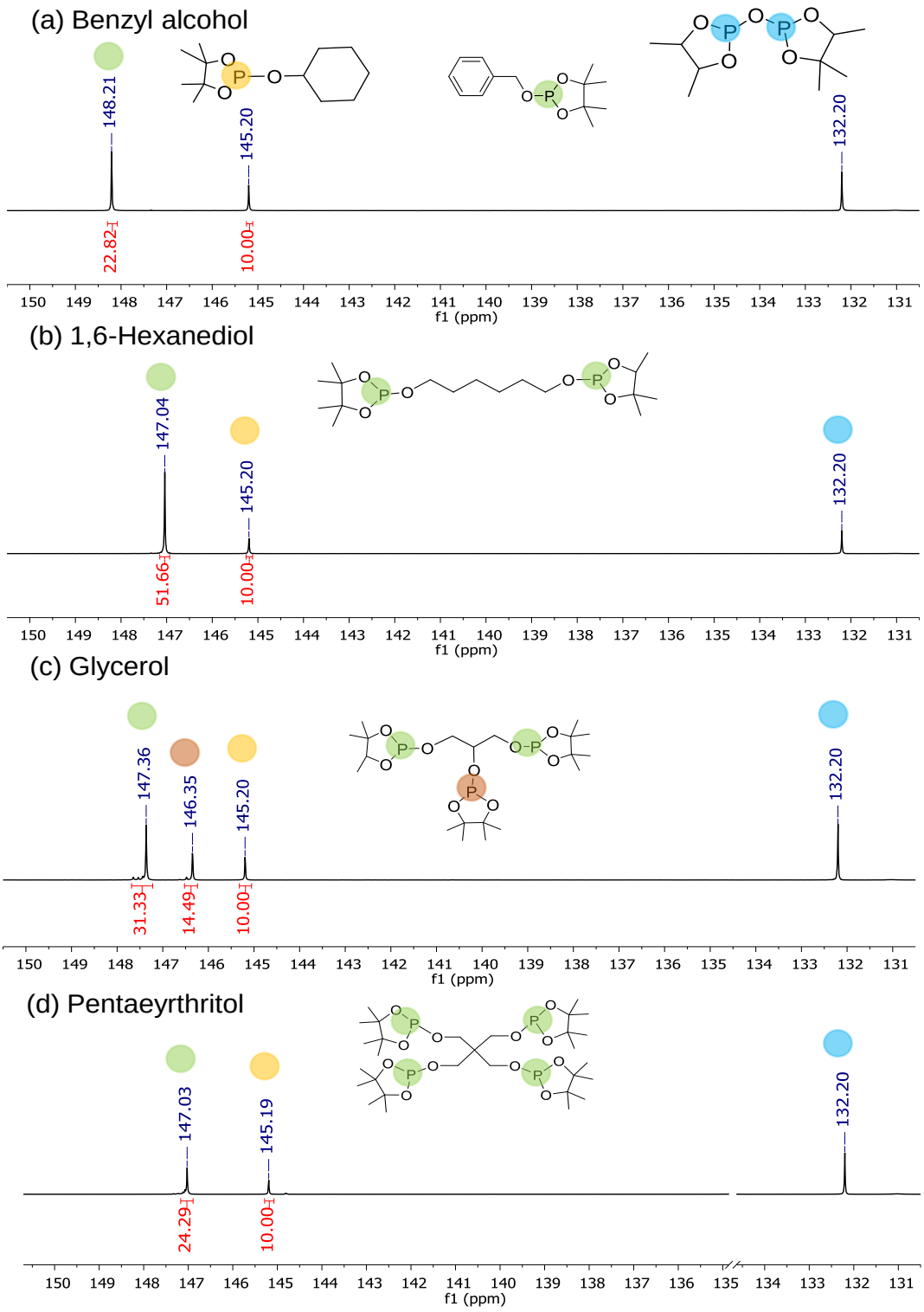



Figure 3.10. Inverse gated decoupled $^{31}$P NMR spectra of alcohols derivatised by 2-chloro-4,4,5,5-tetramethyl-1,3,2-dioxaphospholane. (a) benzyl alcohol, (b) 1,6-hexanediol, (c) glycerol, and (d) pentaerythritol where the phospholane ester of the primary (1°) and secondary (2°) hydroxy group show triplet ( )and doublet ( ) resonances, respectively. IS: Internal standard (cyclohexanol, ).

Table 3.1. Analytical results for the quantification of molecular weights of polyols by phosphitylation.

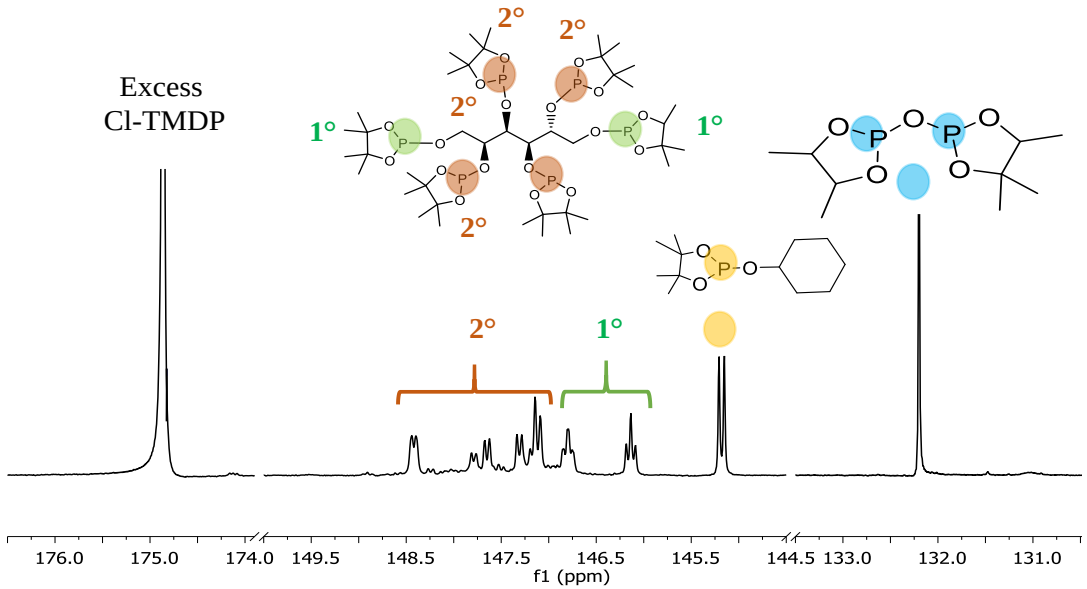
| Model Samples (S) | $^{31}$P NMR Spectrum | | | $N_{(OH)}$ (S) | $^{31}$P NMR calculation | | | Molar mass (theo.) ($g mol^{-1}$) | Phosphitylation (%) [g] |
|---|---|---|---|---|---|---|---|---|---|
| | $m_S$ [a] (mg) | $\int_{IS}$ [b] | $\int_S$ [c] | | $n_{S\ phosphitylated}$ [d] (μ mol) | $M_n^{P\text{-}NMR}$ (OH) [e] ($g mol^{-1}$) | $M_n^{P\text{-}NMR}$ (S) [f] ($g mol^{-1}$) | | |
| Benzyl alcohol | 4.55 | 10 | 22.8 | 1 | 42.4 | 107.2 | 107.2 | 108.14 | 100% |
| 1,6-Hexanediol | 5.64 | 10 | 51.7 | 2 | 97.0 | 58.1 | 116.2 | 118.18 | 101% |
| Glycerol | 2.57 | 10 | 45.8 | 3 | 85.3 | 30.1 | 90.37 | 92.09 | 101% |
| Pentaerythritol | 1.37 | 10 | 24.3 | 4 | 45.2 | 30.3 | 121.2 | 136.15 | 112% |
| *D*-Sorbitol | 4.87 | 10 | 98.6 | 6 | 183.7 | 26.5 | 159.1 | 182.17 | 114% |
| *D*-Mannitol | 0.88 | 10 | 27.2 | 6 | 27.3 | 32.3 | 193.9 | 182.17 | 114% |
| *OH-PCL-OH | 10.2 | 10 | 0.93 | 2 | 1.73 | 5900 | 11800 | 12000 | 101% |

[a] Mass of the sample ($m_s$) used for derivatisation with Cl-TMDP and subsequent NMR analysis. [b] Integral corresponding to the resonance of internal standard ($\delta$ = 147.04 ppm). [c] Integral of the hydroxy group in the sample relative to the IS. [d] Moles of the phosphitylated hydroxy group of the sample determined by following Eq. (3.7). [e] Number average molecular weight per hydroxy group determined by following Eq. (3.8). [f] Molecular weight of samples determined by following Eq. (3.9). * Commercial dihydroxy PCL.
[g] Following Eq. (3.10).

**Equations.**

| | | |
|---|---|---|
| $n_{S\ phosphitylated}$ (μ mol) | $= (n_{IS} \times \int_S) / \int_{IS}$ ; where $n_{IS}$ in each sample is 18.62 μmol | (Eq 3.7) |
| $M_n^{P\text{-}NMR}$ (OH) ($g mol^{-1}$) | $= [m_S / n_S] \times 1000$ | (Eq 3.8) |
| $M_n^{P\text{-}NMR}$ (sample) ($g mol^{-1}$) | $= M_n^{P\text{-}NMR}$ (OH) $\times N_{(OH)}$ (sample) | (Eq 3.9) |
| %Phosphitylation | $= n_{S\ phosphitylated} / n_{S\ total}$<br>$= [\text{Molar mass (theo.)} \times n_{S\ phoshpitylated}] / [m_S \times 1000 \times N_{(OH)}]$<br>$= [\text{Molar mass (theo.)} / M_n^{P\text{-}NMR}\text{(total)}] \times 100$ | (Eq 3.10) |

(a) *D*-Sorbitol + Cl-TMDP (coupled)




(b) *D*-Sorbitol + Cl-TMDP (decoupled)

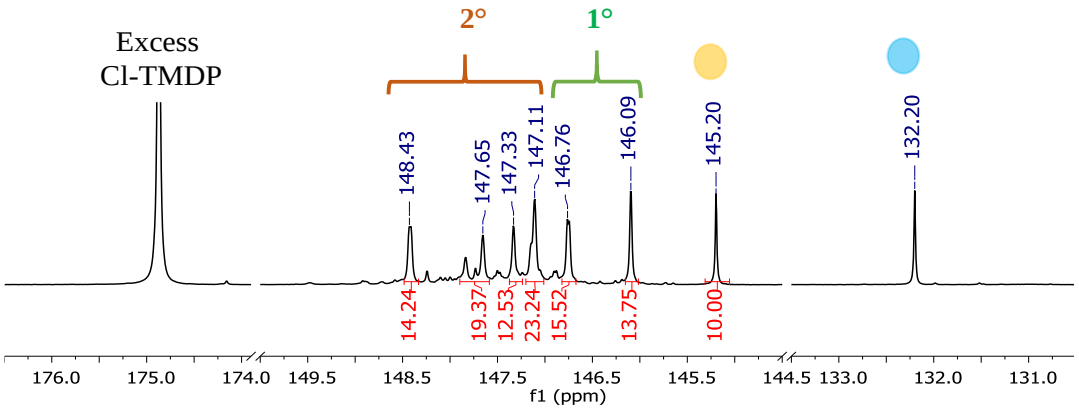



Figure 3.11. $^{31}$P NMR spectra of *D*-sorbitol derivatised by 2- chloro-4,4,5,5-tetramethyl-1,3,2-dioxaphospholane. (A) $^{31}$P NMR spectrum without decoupling, where the phospholane ester of the primary (1°) and secondary (2°) hydroxy group show triplet (●) and doublet (●) resonances, respectively. (B) The corresponding inverse gated decoupled $^{31}$P NMR spectrum used for quantification. IS: Internal standard (cyclohexanol, ●).

Applying the phosphitylation method for quantification on a commercial dihydroxy PCL (Aldrich, 12000 g mol$^{-1}$), results in about ~100% phosphitylation of hydroxy end-group) was noted. The values of molar mass were also in good agreement with those expected from the commercial PCL (measured by SEC-MALS).

Altogether, this method enables to distinguish the end-group hydroxy group from the hydroxy on the initiator. For example, the method enables to distinguish the hydroxy group of the initiator (1,6-hexanediol, $\delta$ 147.32 ppm), from the terminal hydroxy end-

group of PCLs (PCL-OP, $\delta$ 147.01 ppm) (Figure 3.12). A distinguishable chemical shift results from the carboxy-terminated PCL chain-ends (at $\delta$ 137.74 ppm). Quantification of the carboxy group-terminated polymers present in the sample, as well as the determination of molecular weight, number of arms etc. discussed in detail in Chapter 4 on star PCL and in part in Chapter 5 on star diblock copolymers.

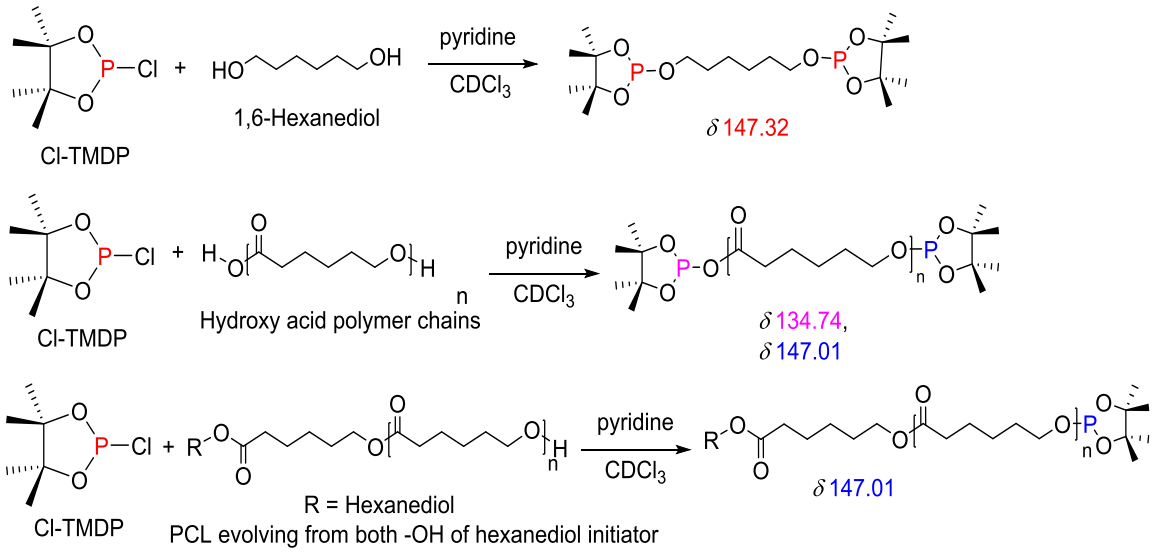



Figure 3.12. Reactions of 1,6-hexanediol, HO(C=O)-PCL-OH and HO-PCL-OH with Cl-TMDP and the chemical shift of the corresponding phospholane ester product in $^{31}$P NMR.

### 3.2.6 Matrix Assisted Laser Desorption and Ionisation-Time of Flight Mass Spectrometry

Matrix Assisted Laser Desorption and Ionisation-Time of Flight Mass Spectrometry (MALDI-TOF MS, Univ. Montpellier) data were recorded on a Bruker RapiFlex spectrometer operating at the following conditions: Nitrogen laser (337 nm), accelerating potential (20 kV) in positive linear ion or reflection mode. In delayed extraction mode, the delay time was ~300 ns optimised based on the mass range of the polymer distributions. External calibration was performed using PEG polymer standards. Trans-2-[3-(4-*tert*-butylphenyl)-2-methyl-2-propenylidene]malononitrile (DCTB) was employed as the matrix. An analyte solution and matrix solution with a concentration of 10 g L$^{-1}$ in THF (1:4 v/v analyte-to-matrix solution) were mixed with 1 µL of potassium trifluoroacetate (10 g L$^{-1}$) (Employed in Chapter 4).

A higher concentration of analyte was employed in Chapter 5. An analyte solution (at 40 g L$^{-1}$ in THF) and matrix solution with a concentration of 10 g L$^{-1}$ in THF (1:4 v/v

analyte-to-matrix solution) were mixed with 1 μL of potassium trifluoroacetate (10 g $L^{-1}$) ($K^+$ ionisation) (employed in Chapter 5).
1 μL of the resulting mixture was spotted on the MALDI plate for MS analysis. Data were analysed and normalised using the FlexAnalysis version 3.0 (Bruker) software.

### 3.2.7 Electrospray Ionisation Mass Spectrometry (ESI MS)

High-resolution Electrospray Ionisation Mass Spectrometry (ESI MS, Nottingham) analyses were performed on a Bruker microTOF II mass spectrometer (Bruker Daltonik, Bremen, Germany), connected to an Agilent 1200 HPLC set-up (Agilent Technologies, Santa Clara, USA). Samples were prepared in water as the solvent at 0.01 mg $mL^{-1}$. For analysis by Flow Injection, 1 μL of the solution was injected into the ion source of the instrument along with a flow of 0.2 mL $min^{-1}$ of the 70% methanol/water eluent. The mass spectrometer was operated in electrospray ionisation (ESI) mode at a typical resolving power of 8000. Control of the analysis was performed through Bruker's Compass Open Access QC automated data acquisition and reporting software (v1.3; Bruker Daltonik, Bremen, Germany).

### 3.2.8 Differential Scanning Calorimetry (DSC)

Differential Scanning Calorimetry (DSC, Nottingham) was employed to determine thermal properties of the polymers synthesised throughout this Thesis.
DSC analyses were performed on a Q2000 TA instrument calibrated with an indium standard under $N_2$ flow. In a standard experiment, the sample (2 – 5 mg) was placed in an aluminium pan with a blank reference pan in the instrument. DSC measurements were performed in a temperature range from -80 to 100 $^oC$ at a heating/cooling rate of 10 °C $min^{-1}$. The crystallisation temperature ($T_c$) and the melting temperature ($T_m$) were taken from the second cycle.

### 3.2.9 Dynamic Light Scattering (DLS)

Dynamic light scattering (DLS, Nottingham and Univ. Montpellier) measurements were performed on a Malvern Zetasizer Nano-ZS to determine the hydrodynamic diameter of the polymeric particles in water. The samples were placed in a polystyrene disposable cuvettes and analyses were performed at 25 °C on a 1 mL sample in Milli Q water as a solvent collecting the scattered light at a detection angle of 173° using the

CONTIN method for analysis. Data analysis was performed using the Zetasizer software version 7.12 and mean values obtained from three independent measurements were reported. The hydrodynamic diameter ($D_H$) was calculated from the Stokes-Einstein relation as follows: $D_H = \frac{k_B T}{3\pi\eta D}$

where $k_B$ is the Boltzmann constant, $T$ is the temperature, and $\eta$ is the viscosity of the medium (0.087 cP), and $D$ is the apparent diffusion coefficient.[24]

**(i) Direct suspension method.** The copolymers were directly dissolved in Milli-Q water at a concentration of 1 mg $mL^{-1}$ (0.1 wt%) and 5 mg $mL^{-1}$ (0.5 wt%) magnetically stirred at 500 rpm overnight at ambient temperature and allowed to equilibrate in a disposable cuvette for 1 h, at ambient temperature prior to analysis.

**(ii) Nanoprecipitation.** Nanoprecipitation method was adapted from Kakde *et al*.[25] The self-assembled nanoparticles of the star diblock copolymers were prepared by dissolving the copolymers (20 mg) in acetone (10 mL) and adding this solution into Milli- Q water (20 mL) with a syringe pump operating at a fixed rate of 0.5 mL $min^{-1}$ while stirring (1000 rpm). The final solvent to anti-solvent (acetone to water) composition was fixed at a 1:2 v/v ratio. The suspension was stirred for 4 h at ambient temperature and acetone was evaporated under vacuum. Similarly, lower concentrations (0.875, 0.75, 0.625, 0.5, 0.375, 0.25, 0.125 and 0.0125 mg $mL^{-1}$) were prepared directly by dissolving copolymer in acetone and adding the resulting solution into water, following the same procedure. The suspensions at 1 mg $mL^{-1}$ concentration were slowly transferred to a polystyrene disposable cuvette prior to analysis.

### 3.2.10 Transmission Electron Microscopy (TEM)

Transmission electron microscopy (TEM, Nottingham) micrographs were obtained using a Tecnai G2 (FEI, Oregon, USA) microscope and discussed in Chapter 5.

The star *D*-sorbitol-$PCL_{57}$-*b*-$PEP_{36}$ copolymer suspension in Milli-Q water (1 mg $mL^{-1}$) obtained by the nanoprecipitation method was diluted 10- fold and one drop (~3 μL), was cast on a flip side of a graphene oxide coated holey carbon copper grid (EM Resolutions, UK) (held upside down), and suspended in air for 90 sec. For drying of the water, a gentle flow of argon was passed on the grid. Samples were then imaged at 100 kV using TIA imaging software, without staining, at a magnification of × 43 000 up to 300 000.

### 3.2.11 Cryogenic Transmission Electron Microscopy (Cryo-TEM)

The Cryogenic-Transmission Electron Microscopy (Cryo-TEM, Nottingham) samples were prepared utilising a custom-built chamber (often) referred as the controlled environment vitrification system (CEVS). About 3.5 μL of the star *D*-sorbitol-$PCL_{57}$-*b*-$PEP_{36}$ copolymer in Milli-Q water (1 mg $mL^{-1}$) was placed onto the glow-discharged holey carbon-coated copper grid for about 3 min. Excess of water was soaked by a filter paper in CEVS after a minimum of 30 sec detainment; the sample grid was flash-frozen (vitrified) by plunging it into liquid ethane. The grid with vitrified sample solution had been maintained at liquid nitrogen temperature before the analysis was performed. Cryo TEM was performed on a JEOL JEM-2100 Plus electron microscope instrument with an acceleration voltage of 200 kV at a magnification of × 200 000.

### 3.2.12 Tensiometry

#### 3.2.12.1. Static: Krüss Tensiometer

The surface tension measurements were performed at 0.5 wt% concentration (typically 60 mL) in ultrapure water with a resistivity of 18.2 MΩ $cm^{-1}$ (Milli-Q, Millipore®) at ambient temperature (25 ± 0.5 °C) and at natural pH on a Force Tensiometer (Krüss K100, Croda and ENSCM). The Wilhelmy platinum plate was flame cleaned on a Bunsen burner after each new series of measurement. Between runs, the glass vessel was cleaned with isopropyl alcohol (or ethanol) followed by rinsing several times with Milli-Q water. In all cases, 50 successive measurements were repeated until a standard deviation of ≤ 0.03 mN $m^{-1}$ (for static) or ≤ 0.0001 mN $m^{-1}$ (for equilibrium) was obtained. For precise measurements, Tensiometer was calibrated by measuring the surface tension of Milli- Q water before every reading (applied on amphiphilic samples in Chapter 6).

#### 3.2.12.2. Dynamic: Bubble Pressure Tensiometer

The dynamic surface tension of aqueous solutions typically containing 0.5 wt% star $PCL_n$-*b*-$PEP_m$ and triblock $PEP_n$-*b*-$PCL_m$-*b*-$PEP_n$ copolymers were determined using a SITA t100 Bubble Pressure tensiometer. The instrument can measure surface tensions ranging from 10- 100 mN $m^{-1}$ ± 0.1 mN $m^{-1}$ (working principle is discussed in Chapter 6).

### 3.2.12.3 Critical Aggregation Concentration by Krüss Tensiometer

For $PCL_n$-*b*-$PEP_m$ based block copolymers the **Critical Aggregation Concentration** (CAC) was determined by Wilhelmy plate method using a fully automated micro dispenser equipment on K100 (Croda), which enabled a high number of measuring points at a broad concentration range (0.1-10000 mg $L^{-1}$). Typically, a starting concentration of 0.5 wt% was prepared and the aqueous solution was diluted stepwise, measuring the surface tension at each point. This high number of measurements increases the accuracy of the CAC determination. Surface tension vs. concentration (in μM, log scale) was plotted and the CAC value was calculated at the intersection between the descending line and close to the horizontal line (as the surface tension will plateau above the CAC) (applied on amphiphilic samples in Chapter 5 and Chapter 6).

### 3.2.13 Thermogravimetric Analysis (TGA)

Thermogravimetric analyses of the UV-cured coatings were performed on TG209 F1 (Netzsch). The samples were heated from 25 °C to 600 °C at a heating rate of 10 °C $min^{-1}$ in the air (Air Liquid) at a constant purge rate of 40 mL $min^{-1}$ at the alumina pan.

### 3.2.14 Real-Time Fourier-Transform Infrared Spectroscopy (FTIR)

Real Time-FTIR was employed for measuring the photopolymerisation kinetics on a Thermo Scientific Nicolet 6700 FTIR and were analysed using an OMNIC 32 software. The crosslinking reaction proceeded under UV irradiation (OmniCure S2000 Spot UV curing system, 200 W, 250-450 nm, Mercury lamp) calibrated with OmniCure R2000 UV Radiometer). The real intensity imparted to the samples was 10 mW $cm^{-2}$ measured using radiometer (Solatell). One drop of the above mixture was deposited on the Attenuated Total Reflectance (ATR) unit of the infrared spectrometer where it was exposed to UV irradiation for 300 s for crosslinking. The kinetics was monitored by real-time FTIR, following the disappearance of the bands at 1615 and 1635 $cm^{-1}$ corresponding to the vinyl ether.

Kinetics of photopolymerisation was performed in the absence of air, by placing a polypropylene film (PP) above the formulation, to prevent atmospheric oxygen from diffusing into the sample.

## 3.3 References


1. Zhou, X. & Hong, L. Controlled ring-opening polymerization of cyclic esters with phosphoric acid as catalysts. *Colloid Polym. Sci.* **291,** 2155–2162 (2013).
2. Sperling, L. H. *Introduction to Physical Polymer Science*. (John Wiley & Sons, Inc., 2005). doi:10.1002/0471757128
3. Operation Manual Varian. *390-LC Multi Detector Suite*. **1,** (2010).
4. Holmberg, K., Bo, J. & Kronberg, B. *Surfactants and Polymers in Aqueous Solution*. (John Wiley & Sons, Ltd, 2002).
5. Grubisic, Z., Rempp, P. & Benoit, H. A universal calibration for gel permeation chromatography. *J. Polym. Sci. Part B Polym. Lett.* **5,** 753–759 (1967).
6. Döring, A., Schneider, M., Wycisk, A. & Kuckling, D. *Branching Analysis of Star Polymers by SEC; International Symposium on GPC/SEC and Related Techniques Frankfurt*. (2014).
7. Zimm, B. H. & Stockmayer, W. H. The Dimensions of Chain Molecules Containing Branches and Rings. *J. Chem. Phys.* **17,** 1301–1314 (1949).
8. Zimm, B. H. & Kilb, R. W. Dynamics of branched polymer molecules in dilute solution. *J. Polym. Sci.* **37,** 19–42 (1959).
9. Zoia, L., Tolppa, E.-L., Pirovano, L., Salanti, A. & Orlandi, M. 1H-NMR and 31P-NMR Characterization of the lipid fraction in archaelogical ointments. *Archaeometry* **54,** 1076–1099 (2012).
10. Chung, Y.-L. *et al.* A Renewable Lignin–Lactide Copolymer and Application in Biobased Composites. *ACS Sustain. Chem. Eng.* **1,** 1231–1238 (2013).
11. Archipov, Y., Argyropoulos, D. S., Bolker, H. I. & Heitner, C. 31P NMR Spectroscopy in Wood Chemistry. I. Model Compounds. *J. Wood Chem. Technol.* **11,** 137–157 (1991).
12. Argyropoulos, D. S. 31P NMR in wood chemistry: A review of recent progress. *Res. Chem. Intermed.* **21,** 373–395 (1995).
13. Argyropoulos, D. S. 31P NMR in wood chemistry: A review of recent progress. *Res. Chem. Intermed.* **21,** 373–395 (1995).
14. Dais, P. & Spyros, A. 31P NMR spectroscopy in the quality control and authentication of extra-virgin olive oil: A review of recent progress. *Magn. Reson. Chem.* **45,** 367–377 (2007).
15. Melone, F., Saladino, R., Lange, H. & Crestini, C. Tannin structural elucidation and quantitative 31P NMR analysis. 2. Hydrolyzable tannins and proanthocyanidins. *J. Agric. Food Chem.* **61,** 9316–9324 (2013).
16. Siotto, M. *et al.* Monitoring biodegradation of poly(butylene sebacate) by Gel Permeation Chromatography, 1H-NMR and 31P-NMR techniques. *J. Environ. Manage.* **116,** 27–35 (2013).
17. Spyros, A., Argyropoulos, D. & Marchessault, R. A study of poly (hydroxyalkanoate) s by quantitative 31P NMR spectroscopy: Molecular weight and chain cleavage. *Macromolecules* **30,** 327–329 (1997).
18. Quin, L. D. & Williams, A. J. *Practical interpretation of P-31 Nmr Spectra and Computer Assisted Structure Verification*. (Advance Chemistry Development Inc., 2004).
19. Jiang, Z., Argyropoulos, D. S. & Granata, A. Correlation analysis of31P NMR chemical shifts with substituent effects of phenols. *Magn. Reson. Chem.* **33,** 375–382 (1995).
20. Argyropoulos, D. S. P-31 Nmr in Wood Chemistry - a Review of Recent Progress. *Res. Chem. Intermed.* **21,** 373–395 (1995).

21. Goddard, A. R. *et al.* Controlled polymerisation and purification of branched poly(lactic acid) surfactants in supercritical carbon dioxide. *Green Chem.* **18,** 4772–4786 (2016).
22. Gustini, L., Noordover, B. A. J., Gehrels, C., Dietz, C. & Koning, C. E. Enzymatic synthesis and preliminary evaluation as coating of sorbitol-based, hydroxy-functional polyesters with controlled molecular weights. *Eur. Polym. J.* **67,** 459–475 (2015).
23. Ben, H. & Ragauskas, A. J. NMR characterization of pyrolysis oils from kraft lignin. *Energy and Fuels* **25,** 2322–2332 (2011).
24. Brown, W., Schillén, K., Almgren, M., Hvidt, S. & Bahadur, P. Micelle and gel formation in a poly(ethylene oxide)/poly(propylene oxide)/ poly(ethylene oxide) triblock copolymer in water solution. Dynamic and static light scattering and oscillatory shear measurements. *J. Phys. Chem.* **95,** 1850–1858 (1991).
25. Kakde, D. *et al.* Amphiphilic block copolymers from a renewable ε-decalactone monomer: prediction and characterization of micellar core effects on drug encapsulation and release. *J. Mater. Chem. B* **4,** 7119–7129 (2016).

# Chapter 4
# Biobased Star Poly(ε-Caprolactone) Hydrophobe

## 4.1 Abstract

Biobased building blocks and sustainable synthesis pathways were used to synthesise star-shaped polymers composed of a *D*-sorbitol core and poly(ε-caprolactone) arms by ring opening polymerisation. The use of volatile organic solvents was avoided and less energy intense reaction conditions were achieved by performing the ROP in the bulk or in a green solvent, supercritical $CO_2$. Two catalysts were tested: conventional $Sn(Oct)_2$ which is FDA approved metal catalyst and an enzyme, Novozym 435 (Lipase B from *Candida Antarctica* immobilised on a solid support). The influence of the reaction medium and of the nature of the catalyst on the molecular weight as well as the dispersity and the architecture of the PCL stars were investigated. The star polymers were characterised by $^{1}H$ and $^{31}P$ nuclear magnetic resonance ($^{1}H$ and $^{31}P$ NMR) spectroscopy, size exclusion chromatography-multi-angle light scattering (SEC-MALS), SEC-Universal Calibration – Mark Houwink ($SEC^{UC}$ MH) plots and matrix-assisted laser desorption and ionisation-time of flight (MALDI-TOF) mass spectrometry. The obtained samples were characterised by several methods to ensure reliable results for number-average and weight-average molar masses and the results of the chemical characterisation are discussed in detail.

The use of $scCO_2$ enabled the reduction of the reaction temperature of $Sn(Oct)_2$ catalysed star *D*-sorbitol-polycaprolactone (star *D*-sorbitol-PCL) polymerisations from 140 to 95 °C. In addition, star polymers were successfully synthesised by enzyme catalysis in the bulk or in $scCO_2$ at 60 °C; lower temperatures that could provide significant energy savings on a commercial scale. The catalyst was shown to have a pronounced influence on the architecture of the PCL stars. More regular star polymers were obtained in the presence of $Sn(Oct)_2$ whereas Novozym 435 gave access to miktoarm-type star PCL. Finally, the influence of the number and length of the arms on the thermal properties of the star polymers was investigated by DSC.

## 4.2 Introduction

The accumulation of non-biodegradable plastics on earth has resulted in an increasing need for biodegradable polymers, ideally produced by green technologies. In addition, the simultaneously occurring depletion of fossil resources has promoted the utilisation of naturally occurring building blocks.[1] At the same time, there has been tremendous development in the synthesis of complex macromolecular architectures in order to design polymers tailored to specific functions and applications. In particular, star polymers have attracted attention, because of their unique rheological properties, lower hydrodynamic volume than their linear analogues, and their very interesting thermal, topological, and biological properties that are inaccessible from their linear counterparts.[2–5] Star polymers are an important class of branched polymers that have at least three arms of often similar lengths, fused on a central point (core) and the core may be an atom, a small molecule, or a macromolecular structure itself.[2] Based on the nature and uniformity of their arms, they are classified into regular or miktoarm types (Figure 4.1).[3,6] The regular star includes polymers consisting of the same homopolymers or blocks copolymers arms (Figure 4.1, (a)) while the miktoarm star polymers further subdivide into four types according to the asymmetric architecture: it can have variable chemical structure, asymmetric topology, different molecular weight asymmetry, and functional group asymmetry (Figure 4.1, (b)).[6]

The special properties of such star-like structures result from the higher number of functional end groups and their highly branched nature, which causes, for example, a lower intrinsic viscosity, by reducing the number of chain entanglements compared to linear polymers of similar molecular weight, and can lead to a reduced melting point.[2–4,7,8] A prominent example of star polymers for commercial applications is Lubrizol's Asteric™ viscosity modifiers. In this case, star poly(alkyl methacrylates) with 9-13 arms are used as additives for lubricants to decrease viscosity at lower temperatures while at the same time ensuring a higher viscosity index, i.e. reducing the variation in viscosity with changing temperature.[2]

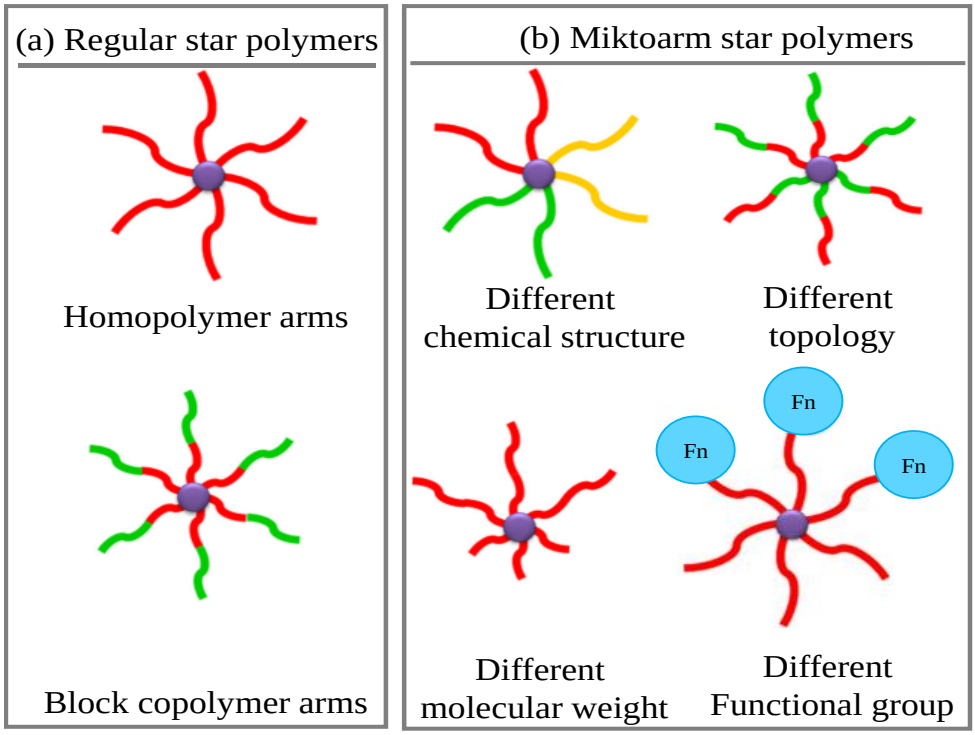



Figure 4.1. General classification of star polymers: (a) Regular star polymers and (b) Miktoarm star polymers, where ● indicates core of the star which can be an atom, small molecule, branched macromolecule, nanogel, nanoparticle, etc.[6]

Star polymers can be synthesised by an arm first approach, in which arms are synthesised and then attached to the core, or by a core first approach. In the core first approach, the arms are polymerised from multifunctional initiators using, for example, ring-opening polymerisation (ROP). Poly(ε-caprolactone) (PCL) is a particularly interesting polymer obtained by ROP since it is inexpensive, biocompatible and possesses a controlled degradability.[9] In the future, the monomer ε-caprolactone (ε-CL) could potentially be sourced from renewable resources.[10–12] For instance, ε-CL could be obtained from lignocellulosic biomass derived 5-hydroxymethylfurfural.[13,14] Additionally, ε-CL is an intermediate in the oxidation of cyclohexanol to adipic acid by an *Acinetobacter sp.* strain SE19 enzyme, resulting in a potential for biotechnological sourcing of ε-CL.[15] Typically, star PCL are synthesised from polyhydroxy alcohols (such as glycerol,[16,17] trimethylolpropane,[18–20] pentaerythritol,[16,17,19,20] di-trimethylolpropane,[18] *D*-sorbitol,[21] dipentaerythritol,[18] and maltitol[18]) as initiators, which constitute the core of the stars. Multifunctional polymeric macroinitiators such as star poly(ethylene glycol)[22] or hyperbranched polymers such as poly(2-hydroxyethyl methacrylate)[23] have also been employed to form star block copolymers with PCL. Sorbitol is of particular interest as a core for star PCL, since it is an inexpensive, highly

valuable polyol commercially derived from renewable feedstocks such as corn-starch, cellulose, cassava, wheat, etc.[24,25]

Tin(II) 2-ethyl hexanoate ($Sn(Oct)_2$) is commonly used as a catalyst[21,26] for the ROP of ε-CL. Although $Sn(Oct)_2$ is a well-known FDA approved metal catalyst, there are increasing concerns regarding the presence of toxic metal catalysts in the final products. This is of particular importance for polymers in skin care or cosmetic products. In previous work, we have shown that extraction using supercritical $CO_2$ ($scCO_2$) can be used to reduce the amount of catalyst residue in polymer products.[27] However, an alternative may be to avoid the use of a toxic metal catalyst and shift to more environmentally friendly alternatives such as enzymes.[28,29] Lipase is the most important class of biocatalyst for ROP because of its abundance in nature, high specificity, regio- and enantioselectivity and low environmental impact.[28] Uppenberg and co-workers discovered in 1994 that this selectivity was due to the 'open' conformation of the catalytic triad Ser-His-Asp in the active site of CaLB, which restricts the accessibility of the active site for certain substrates.[30] In particular, Novozym 435 (Lipase B from *Candida antarctica* (CaLB) immobilised on a macroporous acrylic resin) has shown extraordinary reactivity towards a wide range of cyclic monomers, high catalytic activity, good solvent resistance and has been broadly studied as a biocatalyst for polyester synthesis.[29]

Enzymatic ROP (eROP) of ε-CL by Novozym 435 has been studied extensively in the bulk and in various organic solvents to give linear PCL.[31,32] However, an obstacle in enzyme catalysis is the instability of the catalysts. At temperatures higher than 100 °C, which is typically employed in ROP of ε-CL in the bulk, denaturation of the protein structure occurs.[33] The optimum temperature for CaLB catalysis for enzymatic polyesters synthesis is thus between 60 and 70 °C.[34,35]Another challenge is the sensitivity of enzymes towards certain solvents, such as polar solvents, which interfere with the hydrogen bonding in the protein structure, thereby affecting the catalytic activity of the enzyme.[36] For example, Novozym 435 displays relatively high selectivity towards primary alcohols compared to secondary alcohols. However, the presence of a polar solvent affects the selectivity of Novozym 435. For instance, Xue *et al.* achieved three-arm star PCL polymers using glycerol as the initiator in presence of 1,4-dioxane at 70 °C confirming initiation from a secondary hydroxy group.[37] Other factors such as catalyst loading and the immobilisation process on the support can also influence the catalytic activity and regioselectivity.[38–40] Regarding the enantioselectivity of

Novozym 435, Gross and co-workers have investigated the incorporation of alditols such as *D*-sorbitol, *D*-galactitol, and *D*-mannitol into copolyesters with adipic acid and 1,8-octanediol by polycondensation.[41] They observed the highest molecular weights as well as the highest degree of branching for the polyesters with *D*-mannitol as the copolymer, indicating a preference of Novozym 435 towards all R-configuration of alditol. Accordingly, incorporation of *D*-sorbitol (SRRR) gave higher molecular weights and a higher degree of branching than the incorporation of *D*-galacitol.[41]

A potential alternative to the volatile organic solvents or reactions in the bulk at high temperatures is the use of non-toxic supercritical $CO_2$ ($scCO_2$).[42] The gas-like diffusivity of $scCO_2$ into polymer matrices provides a unique opportunity to liquefy polymers at temperatures below their glass transition temperature ($T_g$) and melting point ($T_m$). This not only lowers the viscosity of the reaction medium dramatically but also allows for a more sustainable low-temperature processing of polymers; both factors lead to significant process energy savings.[43,44] $ScCO_2$ is a well-established and versatile solvent for polymerisation,[45] polymer modification,[46,47] polymer blending,[44] purifications,[44] and extraction,[44] and has been successfully employed as a foaming agent,[48] and for polymer particle formation.[44,49] The liquefying ability of $scCO_2$ has previously been exploited for the synthesis of a range of polymeric materials with controlled molecular weights and narrow dispersities using enzyme catalyst at near ambient temperature, which ensures the stability of the biocatalysts.[50–53] For example, $scCO_2$ was previously employed as a solvent for the synthesis of linear PCL by ROP of ε-CL using $Sn(Oct)_2$ or Novozym 435 as a catalyst.[34,50,54,55]

In this work, several polyols were studied, including 1,6-hexanediol, glycerol, pentaerythritol and triglycerol, as initiators for the synthesis of star polyol-PCL by ring opening polymerisation. Eventually, we investigated the synthesis of complex star PCL architectures using a renewable polyol core, *D*-sorbitol, as the initiator, aiming at establishing an environmentally benign process to make biodegradable star *D*-sorbitol-PCL under mild conditions. A mild synthetic procedure is of particular importance when using temperature sensitive polyols such as *D*-sorbitol since it is well known to dehydrate into isosorbide at elevated temperatures.[56] Thus, we first investigated the use of $scCO_2$ as a solvent for the $Sn(Oct)_2$ catalysed star PCL synthesis at low temperatures (95 °C), taking advantage of the plasticization effects of $scCO_2$. The results were compared with the synthesis in the bulk at 140 °C. Moreover, we report on the synthesis of star PCL with a *D*-sorbitol core using Novozym 435 as the catalyst is reported for

the ROP in $scCO_2$ and in the bulk. Finally, the architecture of the PCL stars synthesised with both catalysts is compared. The effect of the number and the variable length of the arms of the star PCL on the thermal properties of the polymers was investigated.

## 4.3 Experimental Section

### 4.3.1 Materials

ε-Caprolactone (ε-CL, 97%), *D*-sorbitol (*D*-Sorb, >98%), pentaerythritol (PentE, 97%), triglycerol (TriG, 60%), glycerol (Gly, 99%), 1,6-hexanediol (HexD, 97%), benzyl alcohol (BzOH, 97%), tin (II) 2-ethyl hexanoate ($Sn(Oct)_2$, 98%) and 2-chloro-4,4,5,5-tetramethyl-1,3,2-dioxaphospholane (95%) (Cl-TMDP) were purchased from Sigma Aldrich (UK). ε-CL was dried over $CaH_2$ for 48 h followed by vacuum distillation and stored under an inert atmosphere. HexD, Gly, PentE, TriG and *D*-Sorb and $Sn(Oct)_2$ were stored in a desiccator and dried under vacuum at 25 °C overnight before use. Novozym 435 (10 wt% of *Candida antarctica* (CaLB) immobilised on cross-linked acrylic resin; enzyme activity is 5000 units/mg of protein) was kindly donated by Novozymes (Denmark), stored at 4 °C, dried overnight under vacuum (25 °C) and degassed for 30 min before use. All the solvents were of analytical grade or HPLC-grade and used as received. Supercritical Fluid Chromatography (SFC) grade carbon dioxide (minimum purity 99.9 %) was purchased from BOC gases (UK) and used as received.

### 4.3.2 Synthesis of Polyol-PCL from Sugar Alcohols in the Bulk using $Sn(Oct)_2$

A general procedure employed for the synthesis of multifunctional PCL using $Sn(Oct)_2$ in the bulk is as followed.

The glassware was flamed dried before use. For the synthesis of *D*-sorbitol-[$PCL_nOH_x$] with $M_n^{\ targ}$ of 6000 g $mol^{-1}$, ε-CL (5.15 g, 45.12 mmol), *D*-sorbitol (156 mg, 0.86 mmol) and 10 mol% of $Sn(Oct)_2$ (34 mg, 0.09 mmol) with respect to *D*-sorbitol were added to a 25 mL round-bottom flask equipped with a magnetic stirrer at 300 rpm. The reagents were degassed with argon for 30 min, subsequently heated to 95 °C for 7 days or to 140 °C for 10.5 h, respectively. The conversion was monitored by $^1H$ NMR by taking aliquots until 95-99% monomer conversion was reached. The resulting polymer was dissolved in THF, precipitated in cold diethyl ether and dried under vacuum (gravimetric yield: 96-97%).

SEC-MALS (THF): $M_n^{SEC\text{-}MALS}$ = 5600 g mol$^{-1}$, $Đ$ = 1.03.

The ROP of ε-CL from other alcohols, 1,6-hexanediol, glycerol, pentaerythritol and triglycerol was performed similarly for the reaction time specified in Table 4.1.

### 4.3.3 Synthesis of Star PCL from *D*-Sorbitol in the Bulk using Novozym 435

The glassware was flame dried before use. ε-CL (5.15 g, 45.12 mmol) was added into a three neck round bottom flask equipped with a mechanical stirrer, under inert conditions and heated in an oil-bath at 110 °C. *D*-Sorbitol (156 mg, 0.858 mmol) was then introduced under mechanical agitation at 300 rpm. Although the reaction mixture was initially biphasic, a homogeneous melt of *D*-sorbitol and ε-CL was observed within 30 min. Subsequently, the temperature was reduced to 60 °C and Novozym 435 beads (154 mg, 3 wt% or 515 mg, 10 wt% with respect to ε-CL) were introduced. The reaction was continued for 13 h (3 wt% Novozym 435, 85-87% conversion) or for 7 h (10 wt% Novozym 435, 89-91% conversion). After polymerisation, the reaction mixture was dissolved in THF and the enzyme beads were separated by filtration. Subsequently, the excess of solvent was evaporated, and the crude polymer was purified by precipitation into cold diethyl ether from THF and dried under vacuum. For both reactions using either 3 wt% or 10 wt% Novozym 435, the gravimetric yield after recycling the enzyme was 62-65%.

SEC-MALS (THF): $M_n^{SEC\text{-}MALS}$ (3 wt% Novozym 435) = 5650 g mol$^{-1}$, $Đ$ = 1.34.

SEC-MALS (THF): $M_n^{SEC\text{-}MALS}$ (10 wt% Novozym 435) = 7800 g mol$^{-1}$, $Đ$ = 1.36.

Similarly, the synthesis of star *D*-sorbitol PCL was also performed in the bulk at 95 °C and the analytical data are given in Table 4.3.

### 4.3.4 Synthesis of Star PCL from *D*-Sorbitol using Sn(Oct)$_2$ in Supercritical CO$_2$

A general procedure used to synthesis linear or polyol-PCL using Sn(Oct)$_2$ in scCO$_2$ is as followed.

The stainless steel high-pressure autoclave reactor (20 mL) used for the synthesis in scCO$_2$ has been described in Chapter 3.[51] Star *D*-sorbitol-PCL was synthesised in scCO$_2$ using Sn(Oct)$_2$ as the catalyst following a similar procedure as given above for the synthesis in the bulk but at 95 °C. *D*-sorbitol (93.8 mg, 0.52 mmol) and 10 mol% of Sn(Oct)$_2$ relative to *D*-sorbitol (20.8 mg, 0.05 mmol) were loaded into the base of the autoclave and degassed with CO$_2$ at 3 bar to ensure removal of air. ε-CL (3 ml,

27.07 mmol) was then added. The reactor was pressurised to 70 bar and gradually heated to 95 °C (10 °C $min^{-1}$). Subsequently, the pressure was increased to 240 bar by the addition of $CO_2$ and the reaction was allowed to stabilise at 95 °C and 240 bar for 10 min. Only after the desired reaction condition (95 °C and 240 bar) was attained, the reaction mixture was agitated using a mechanical stirrer at 300 rpm for 2.5 days. The gravimetric yield after polymerisation was 95-96% (polymer precipitated in cold ethanol from THF solution and dried under vacuum).

SEC-MALS (THF): $M_n^{\text{SEC-MALS}}$ = 6100 g $mol^{-1}$, $Đ$ = 1.11

Analogously, low molecular weight linear hydroxy terminated and dihydroxy telechelic PCL was synthesised using linear alcohols as initiators, BzOH and HexD, in $scCO_2$ (at 95 °C, 240 bar when using BzOH initiator and 80 °C, 240 bar for HexD). The summary of reactions is presented in Table 4.1.

### 4.3.5 Synthesis of Star PCL from *D*-Sorbitol using Novozym 435 in Supercritical $CO_2$

Before the reaction, the autoclave was dried by heating to 95 °C for 1 h, to avoid any contamination by water. *D*-sorbitol (156.3 mg, 0.858 mmol), and Novozym 435 (3 wt% or 10 wt% relative to monomer) were transferred to the base of the autoclave and degassed with $CO_2$ for 15 min at 3 bar pressure. ε-CL (5.15 g, 45.1 mmol) was then injected into the autoclave. The autoclave was pressurised with $CO_2$ to 70 bar and heated to 40 °C. The $CO_2$ was added to the autoclave up to 50 bar and the temperature was set to 60 °C. Subsequently, the pressure was raised up to 217 bar. After obtaining the desired reaction conditions (60 °C, 217 bar), the reaction was mechanically agitated at 300 rpm for 24 h (3 wt% Novozym 435) or for 7 h (10 wt% Novozym 435) to reach 96-99% monomer conversion. The reaction was stopped by cooling to ambient temperature, turning off the stirring, and venting the autoclave (at T<20 °C, P = 55-82 bar). The crude polymer was dissolved in THF and the enzyme beads were separated from the polymer by filtration. The polymer was then precipitated in cold diethyl ether from THF and dried under vacuum. The gravimetric yield after recycling the enzyme was 75-79%, regardless of the catalyst loading.

SEC-MALS (THF): $M_n^{\text{SEC-MALS}}$ (3 wt% Novozym 435) = 8800 g $mol^{-1}$, $Đ$ = 1.24

SEC-MALS (THF): $M_n^{\text{SEC-MALS}}$ (10 wt% Novozym 435) = 10100 g $mol^{-1}$, $Đ$ = 1.23.

Similarly, the synthesis of star *D*-sorbitol PCL was performed in $scCO_2$ at 95 °C and 220 bar and the analytical data are given in Table 4.3.

## 4.4 Results and Discussion

This Chapter focuses on the architecture of polymers of various molecular weights produced by bulk ROP or ROP in $scCO_2$ of ε-CL using a series of different alcohols (linear and polyols).

Two different catalytic systems are investigated, conventional metal-based catalyst $Sn(Oct)_2$, and an enzymatic catalyst, Novozym 435.

These reactions allow investigating the impact of changing initiator as well as the catalytic system on the topology of the product at the various molecular weights.

### 4.4.1 Synthesis of Polyol-PCL in the Bulk or in $ScCO_2$: using $Sn(Oct)_2$

Before investigating the star, PCL polymers initiated by *D*-sorbitol, less complex polymer architectures were synthesised from simpler alcohols such as 1,6-hexanediol (HexD), glycerol (Gly), pentaerythritol (PentE) and triglycerol (TriG) in the bulk (Figure 4.2).

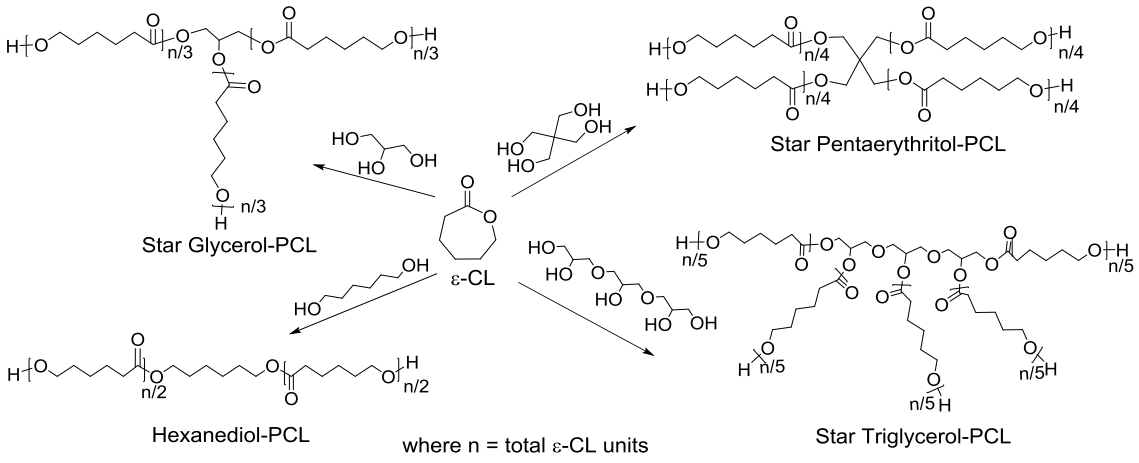



Figure 4.2. ROP of ε-caprolactone from polyols (1,6-hexanediol, glycerol, pentaerythritol, triglycerol) using $Sn(Oct)_2$ catalyst at 140 °C in the bulk to afford polyol-PCL with a variable number of PCL arms.

These syntheses provided the first overview of suitable polymerisation conditions and insights on how the structure of alcohol in combination with $Sn(Oct)_2$ as a catalyst and the temperature might influence the rate of polymerisation (Table 4.1).

At first, linear dihydroxy HexD was used as an initiator for the synthesis of PCL with a targeted molecular weight of 1000 g $mol^{-1}$ at 95 °C in the bulk. Full conversion was observed within 1 h (Table 4.1, Entry 1). However, when the amount of initiator was lowered to target a higher molecular weight of 6000 g $mol^{-1}$ the monomer consumption slowed down after 84% conversion, after 6.5 h (Table 4.1, Entry 2). At first, this phenomenon was attributed to lower mass transfer due to lower mobility of chains at higher viscosity. As the temperature was increased to 140 °C, higher monomer conversions of 97-99% were observed regardless of the initiator (Table 4.1, Entry 2 vs. Entries 3-6). Nevertheless, the polymerisation rate successively slowed down as the number of hydroxy groups on the initiator increased and the reaction time required to reach >98% conversion increased (Table 4.1, Entries 3-6).
This indicates that, despite the high temperature for polymerisation at 140 °C, the choice of initiator also influences the kinetics of $Sn(Oct)_2$ as a catalyst.

For the polymerisation in $scCO_2$, the synthesis of dihydroxy telechelic HO-$PCL_n$-OH samples for $M_n^{targ}$ of 480 g $mol^{-1}$ (HO-$PCL_4$-OH) and 1000 g $mol^{-1}$ (HO-$PCL_9$-OH) were performed (at 80 °C, 240 bar) using HexD as the initiator, which leads to quantitative monomer conversion of ~99% in ~0.5-1 h (Table 4.1, Entry 8 and 9, respectively). A mono-functional benzyl alcohol (BzOH) was utilised to target a slightly higher molecular weights ($M_n$) values in this case, i.e. $M_n^{targ}$ of 2500 g $mol^{-1}$ with BzOH to give a linear Bz-$PCL_{19}$OH that gave conversion of 90 % in 2 h in $scCO_2$ (95 °C, 240 bar) (Table 4.1, Entry 7). These low molecular weight PCL will be utilised as hydrophobic blocks for the synthesis of linear amphiphiles (discussed further in Chapter 5 and 6).

Table 4.1 The polymerisation of ε-CL using polyols as initiators and $Sn(Oct)_2$ as the catalyst in the bulk or in $scCO_2$.

| | Entry | I [a] | $[M]_0:[I]_0:[C]_0$ [b] | T (°C) | t (h) | Conv [c] (%) | $^1$H NMR $DP_n^{NMR}$ [d] (arm) | $^1$H NMR $M_n^{H\text{-}NMR}$ [d] (arm) (g mol$^{-1}$) | SEC-MALS $M_n^{SEC\text{-}MALS}$ (star polymer) [e] (g mol$^{-1}$) | SEC-MALS $Đ$ [e] | SEC-MALS/NMR $N_{arms}^{SEC\text{-}MALS/NMR}$ [f] |
|---|---|---|---|---|---|---|---|---|---|---|---|
| Bulk | 1 | HexD | 9:1:0.1 | 95 | 1 | 97 | 4.9 | 500 | 1100 | 1.04 | 2.0 |
| | 2 | HexD | 53:1:0.1 | 95 | 6.5 | 83 | 17.3 | 2000 | 3800 | 1.04 | 2.0 |
| | 3 | HexD | 53:1:0.1 | 140 | 1 | 98 | 23.6 | 2700 | 5900 | 1.07 | 2.0 |
| | 4 | Gly | 53:1:0.1 | 140 | 3 | 98 | 20.4 | 2300 | 5900 | 1.03 | ~ 2.5 |
| | 5 | PentE | 53:1:0.1 | 140 | 4 | 99 | 16.0 | 1800 | 5800 | 1.08 | ~ 3.2 |
| | 6 | TriG | 53:1:0.1 | 140 | 9 | 99 | 11.0 | 1250 | 5900 | 1.04 | ~ 4.0 |
| $scCO_2$ | 7 | BzOH | 22:1:0.1 | 95 | 2 | 90 | 19.0 | 2300 | 2400 | 1.03 | 1.0 |
| | 8 | HexD | 9:1:0.1 | 80 | 1 | 99 | 4.2 | 500 | 1200 | 1.26 | ~2.0 |
| | 9 | HexD | 4.2:1:0.1 | 80 | 0.5 | 99 | 2.0 | 250 | 800 | 1.26 | ~2.0 |

[a] I: initiator (benzyl alcohol (BzOH), 1,6-hexanediol (HexD), glycerol (Gly), pentaerythritol (PentE), triglycerol (TriG).
[b] Molar ratio of $[Monomer]_0:[Initiator]_0:[Catalyst]_0$ based on $DP_n^{targ} = [M]/[I]$; where M = ε-CL and C = $Sn(Oct)_2$ is 0.1 mole with respect to the initiator.
[c] Monomer conversion determined by $^1$H NMR.
[d] Degree of polymerisation of arms and average molecular weight of arms determined by following Eq. 4.1 and 4.2 respectively.
[e] Molecular weight and dispersity ($Đ$) determined by SEC-MALS using Eq. 4.3.
[f] Average number of arms estimated by SEC-MALS and $^1$H NMR following Eq. 4.4.

**Equations.**

| | | |
|---|---|---|
| $DP_n$ $^{NMR}$ (arm) | $= \int H_{a'+b'} / \int H_{f'}$ | Eq 4.1 |
| $M_n$ $^{H\text{-}NMR}$ (arm) | $= DP_n$ $^{NMR} \times M_{\varepsilon\text{-CL}}$ | Eq 4.2 |
| $M_n$ $^{SEC\text{-}MALS}$ (star polymer) | From SEC-MALS using dn/dc of 0.072 mL $g^{-1}$ | Eq 4.3 |
| $N_{arms}$ $^{SEC\text{-}MALS/NMR}$ | $= M_n$ $^{SEC\text{-}MALS}$ (star polymer) / $M_n$ $^{H\text{-}NMR}$ (arm) | Eq 4.4 |

where $M_{\varepsilon\text{-CL}}$ = molar mass of ε-CL (114.14 g $mol^{-1}$)

### 4.4.2 Star *D*-Sorbitol-PCL in the Bulk or in $ScCO_2$: using $Sn(Oct)_2$

It was discussed that the choice of initiator influences the rate of monomer conversion when using $Sn(Oct)_2$ as a catalyst (Table 4.1). To investigate how the temperature and the amount of catalyst affect the polymerisation of ε-CL when using *D*-sorbitol, bulk polymerisations were conducted at two temperatures of 95 and 140 °C.

ROP of ε-CL was carried out in the presence of *D*-sorbitol as the initiator and using two different catalytic systems (Figure 4.3): $Sn(Oct)_2$ and Novozym 435. The influence of both catalysts on the architecture of star *D*-sorbitol-PCL synthesised in the bulk or in $scCO_2$ was investigated, thereby avoiding organic solvents as the reaction medium.

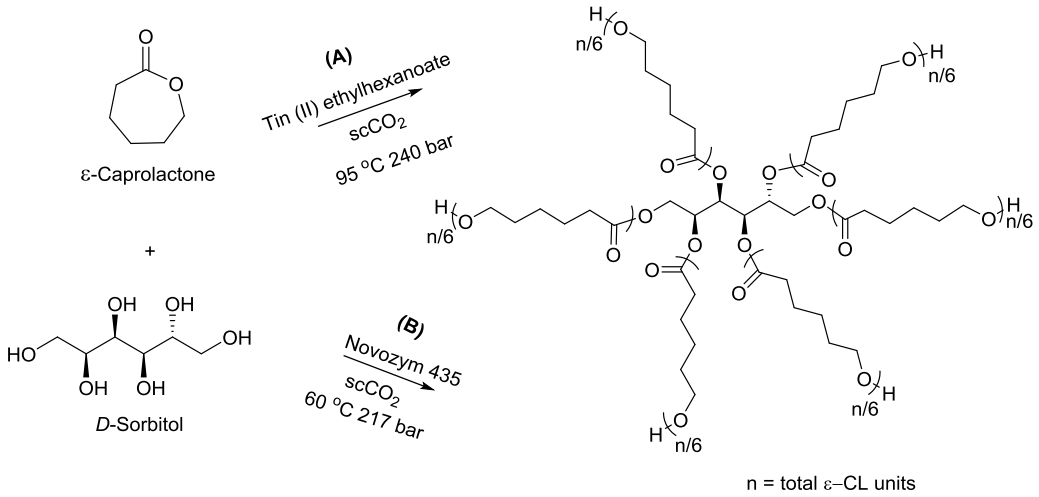



Figure 4.3. ROP of ε-caprolactone from *D*-sorbitol to afford a star *D*-sorbitol-PCL using (A) a conventional metal catalyst ($Sn(Oct)_2$); and (B) an enzyme (Novozym 435) in the bulk or using $scCO_2$.

Whatever the reaction medium, for star *D*-sorbitol-PCL polymerisations with $Sn(Oct)_2$ at 95 and 140 °C the evolution of $\ln([M]_0/[M]_t)$ with time is linear (Figure 4.4), indicating that rate of polymerisation is first order with respect to the monomer. However, when conducting the polymerisations at 95 °C in the bulk, an induction

period of approximately 65-70 h was observed, but this is common at lower temperatures. For example, Storey *et al*. observed an induction period of 40 h at 80 °C in the ROP of ε-CL using ethylene glycol as the initiator.[57] Slow heat transfer and the choice of initiator are factors that contribute to induction periods for $Sn(Oct)_2$ catalysed ROP of ε-CL.[58] By contrast, as the temperature is increased to 140 °C the rate of monomer consumption increases dramatically and $\ln([M]_0/[M]_t)$ increases linearly with time (Figure 4.4). A short induction period of up to 1-1.5 h was also observed at 140 °C, which can be attributed to the coordination-insertion of the $Sn(Oct)_2$ -*D*-sorbitol complex with ε-CL.

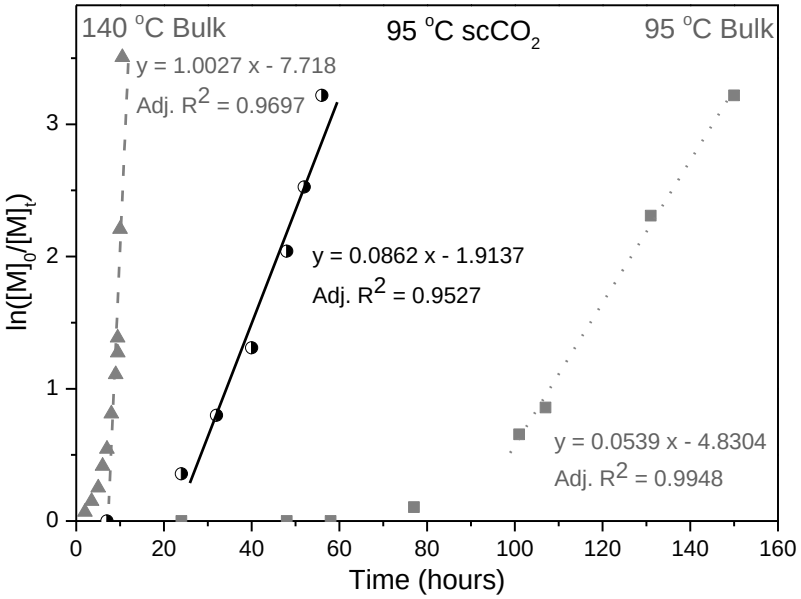



Figure 4.4. A plot of $\ln([M]_0/[M]_t)$ vs. polymerisation time for the synthesis of star *D*-sorbitol-PCL in the bulk at 95 and 140 °C and in $scCO_2$ at 95 °C.

A monomer conversion of 97-98% was achieved within 10.5 h at 140 °C whereas the same conversion was only obtained after 150 h at 95 °C (Table 4.2, Entry 1 vs. Entry 3) (Figure 4.4).

Furthermore, at a lower temperature (95 °C) a progressively faster rate of monomer consumption was witnessed as the concentration of $Sn(Oct)_2$ catalyst was raised 5 fold from 10 mol% (Table 4.2, Entry 1) to 50 mol% (Table 4.2, Entry 2). Although $Sn(Oct)_2$ is FDA approved, it is clear that producing polyesters uncontaminated with possible toxic metallic residues would be desirable for biomedical applications.[59,55] In addition, it is also difficult to completely remove the metal catalyst from the product even after several precipitations. Thus, increasing the catalyst content is highly undesirable.

The use of $scCO_2$ (95 °C, 240 bar) considerably reduced the induction period of the ROP compared to the bulk polymerisation from 70 h to less than 15 h (Figure 4.4). This induction period was followed by a linear trend for the evolution of $\ln([M]_0/[M]_t)$ during the propagation stage. Additionally, the use of $scCO_2$ also enhanced the propagation rate in comparison to the bulk reaction (Table 4.2, Entry 1 and Entry 2 vs. Entry 4) (Figure 4.4).

Table 4.2. Synthesis of *D*-Sorbitol-PCL by ROP in the bulk and in $scCO_2$ in the presence of $Sn(Oct)_2$.

| Entry | Solv. | [M]:[I]:[C] [a] | T (°C) | t (h) | $^1$H NMR | | | SEC-MALS | | SEC-MALS/ $^1$H NMR | SEC$^{UC}$ |
|---|---|---|---|---|---|---|---|---|---|---|---|
| | | | | | Conv.[b] (%) | $DP_n$ $^{NMR}$ [c] (arm) | $M_n$ $^{H\text{-}NMR}$ [c] (arm) (g mol$^{-1}$) | $M_n$ $^{SEC\text{-}MALS}$ (star polymer) [d] (g mol$^{-1}$) | $Đ$ [d] | $N_{arms}$ $^{SEC\text{-}MALS/NMR}$ [e] | MH (α) [f] |
| 1 | Bulk | 56:1:0.1 | 95 | 150 | 97 | 11.3 | 1290 | 5900 | 1.12 | 4.5 | 0.35 |
| 2 | | 56:1:0.5 | 95 | 20 | 99 | 11.0 | 1250 | 5500 | 1.38 | 4.4 | 0.35 |
| 3 | | 56:1:0.1 | 140 | 10.5 | 97 | 9.7 | 1100 | 5600 | 1.03 | 5.1 | 0.27 |
| 4 | $scCO_2$ | 56:1:0.1 | 95 | 56 | 96 | 11.0 | 1250 | 6100 | 1.11 | 4.9 | 0.39 |

[a] Molar ratio of $[Monomer]_0$:$[Initiator]_0$:$[Catalyst]_0$ based on $DP_n^{targ} = [M]/[I]$; where M = ε-CL and C = $Sn(Oct)_2$ with respect to the initiator.
[b] Monomer conversion determined by $^1$H NMR.
[c] Degree of polymerisation of arms and average molecular weight of arms determined by following Eq. 4.1 and 4.2 respectively.
[d] Molecular weight and dispersity (*Đ*) determined by SEC-MALS using Eq. 4.3.
[e] Average number of arms estimated by SEC-MALS and $^1$H NMR following Eq. 4.4.
[f] Mark-Houwink slope (α) determined by SEC$^{UC}$.

The monomer ε-CL is solubilised by $scCO_2$ (95 °C, 240 bar) and the resulting mixture plasticises *D*-sorbitol[60] (for the view-cell studies refer to Appendix B). Thus, the coordination-complexation between the tin catalyst and alkoxides of *D*-sorbitol and ε-CL can take place faster than in the bulk thereby reducing the induction period (Figure 4.5). The reduction of the induction period and the higher rate of propagation in $scCO_2$ as compared to the bulk at 95 °C can be attributed to the unique 'gas-like' mass transfer properties of $scCO_2$.[61]

Regardless of the reaction temperature or induction periods, the molecular weight of the star *D*-sorbitol-PCL increased linearly with monomer conversion both in the bulk and in $scCO_2$, indicating a well-controlled polymerisation (Figure 4.5).

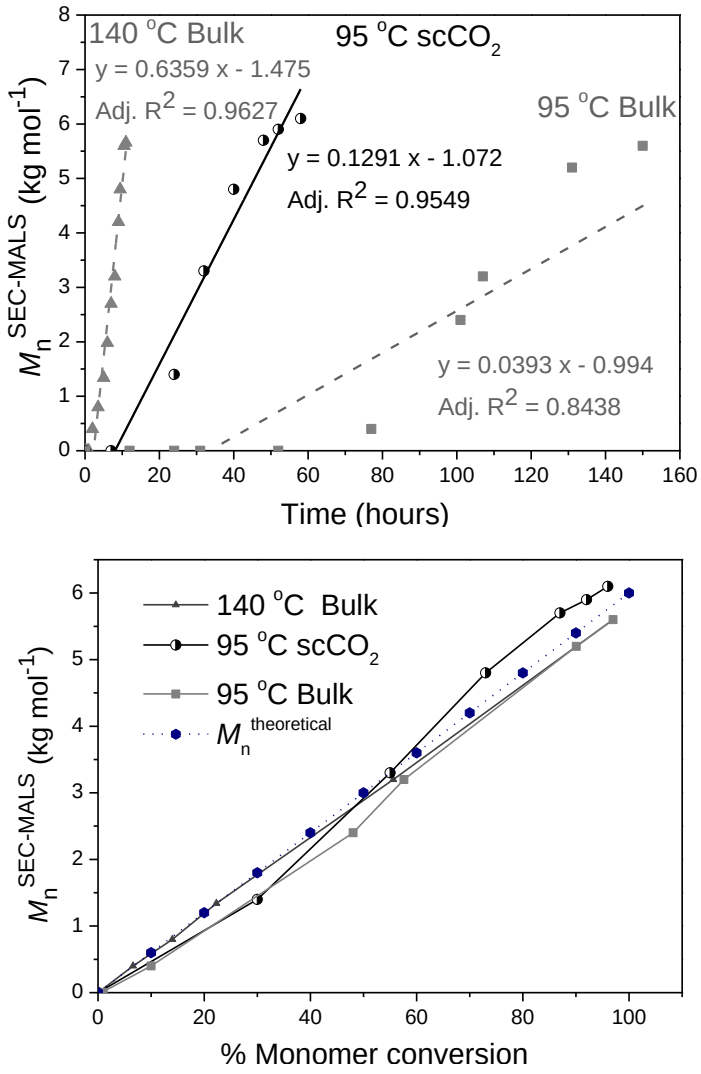



Figure 4.5. Evolution of $M_n$ $^{SEC\text{-}MALS}$ vs. time (top) and $M_n$ $^{SEC\text{-}MALS}$ with monomer conversion (bottom) for the synthesis of star *D*-sorbitol-PCL catalysed by $Sn(Oct)_2$ in $scCO_2$ (95 °C, round symbols) or in the bulk (95 °C, grey square symbols and 140 °C, grey triangle symbols). The theoretical molecular weight is included as well in the bottom figure for comparison.

The resulting star *D*-sorbitol-PCL polymers were analysed by SEC-MALS (Figure 4.6) using the dn/dc value of 0.072 mL $g^{-1}$.[41] The experimental molecular weights ($M_n^{SEC\text{-}MALS}$ (star polymer) = 5500 – 6100 g $mol^{-1}$) of star *D*-sorbitol-PCL synthesised using $Sn(Oct)_2$ were in good agreement with the targeted ($M_n^{targ}$ 6000 g $mol^{-1}$, Table 4.2). In addition, polymers with narrow dispersities ($Đ$ = 1.03 - 1.12) were obtained in both the bulk and $scCO_2$ (Table 4.2, Entry 1, Entry 3 and Entry 4) which is in good agreement with data on ROP of PCL from the literature.[58,59] An increase of dispersity ($Đ$ = 1.38 vs. 1.12) was observed for higher catalyst loading at 95 °C in the bulk (Table 4.2, Entry 2 vs. Entry 1) and this could be attributed to the inter- and intramolecular transesterification reactions, that predominate when a higher amount of $Sn(Oct)_2$ catalyst is present in the reaction mixture.

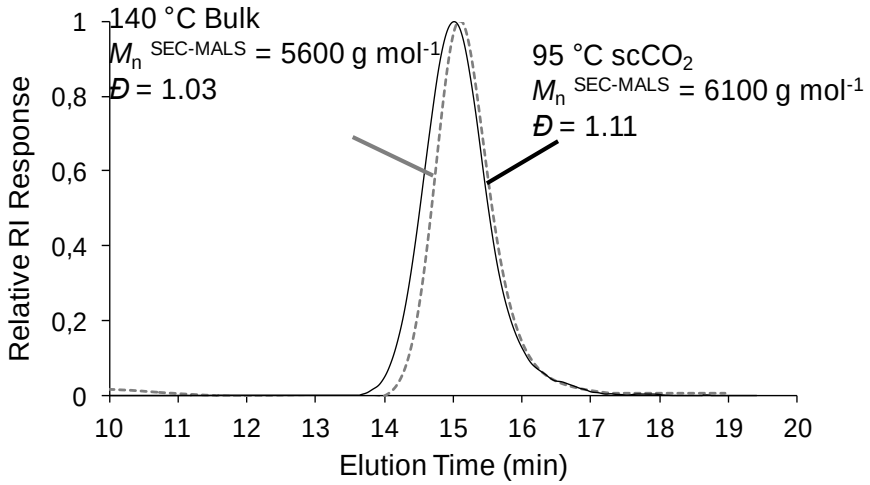



Figure 4.6. SEC-MALS traces overlay of star *D*-sorbitol-PCL catalysed by $Sn(Oct)_2$ in the bulk (140 °C) and in $scCO_2$ (95 °C, 240 bar) (Table 1, 3 vs. 4).

These data show that significantly lower temperatures can be utilised using $scCO_2$, although this does increase the reaction time. Most importantly, this opens up the opportunity to use temperature sensitive catalyst such as enzymes, which can catalyse ROP at lower temperatures than $Sn(Oct)_2$.[62]

### 4.4.3 Star *D*-Sorbitol-PCL by eROP in the Bulk or in $ScCO_2$: using Novozym 435

Lipases exhibit higher catalytic activity at lower temperatures.[63] Hence, enzymatic ring-opening polymerisations (eROP) of ε-CL initiated by *D*-sorbitol were initially conducted at 60 °C with varying enzyme concentrations (3 wt% and 10 wt% relative to monomer) to investigate the influence of the enzyme loading on the kinetics of the polymerisation, molecular weight and architecture of the polymers.

Since Novozym 435 contains 10 wt% of CaLB attached to a polymeric support, the actual weight ratio of CaLB to ε-CL used for this study was 0.3 and 1 wt% for 3 and 10 wt% Novozym 435, respectively. The analytical results of the eROP of ε-CL from *D*-sorbitol initiator (Table 4.3, Entries 1-4) and the kinetics of the eROP for $M_n^{targ}$ = 6000 g mol$^{-1}$ in the bulk and in $scCO_2$ are summarised (Figure 4.8 and Figure 4.7).

For the polymerisation in $scCO_2$, all the reactants were introduced in the reaction vessel before adding $CO_2$. By contrast, for polymerisations in the bulk, it was first necessary to thoroughly mix the *D*-sorbitol ($T_m$ = 98-99 °C) with ε-CL at 110 °C before introducing the Novozym 435 at a lower temperature of 60 °C.

Interestingly, the bulk eROP at a Novozym 435 loading of 10 wt% at 60 °C reached 91% conversion within 7 h (Table 4.3, Entry 4) whereas the ROP in the bulk catalysed by $Sn(Oct)_2$ reached only a slightly higher conversion of 97% within 10.5 h at a significantly higher temperature of 140 °C (Table 4.2, Entry 3). This effect is more pronounced in $scCO_2$ where comparable results to the bulk polymerisation are obtained for enzyme catalysis; i.e. a conversion of 96% after just 7 h at 60 °C (Table 4.3, Entry 4), whereas much longer reaction times (56 h) and higher temperatures (95 °C) are required with $Sn(Oct)_2$ as the catalyst (Table 4.2, Entry 4).

To study whether the higher dispersities and higher molecular weight than $M_n^{targ}$ observed when using enzyme catalysis, were resulting from the use of *D*-sorbitol or the innate nature of enzyme catalysis, different initiators were investigated. Star polyol-PCL based on different initiators, such as simpler polyols (HexD, Gly and PentE) were synthesised to assess whether enzyme catalysis influences the star polymer topology and the analytical data are summarised below (Table 4.3, Entries 5-7).

Table 4.3. Synthesis of star *D*-sorbitol-PCL by ROP in the presence of Novozym 435 in the bulk and in $scCO_2$.[a]

| Entry | Solv. | $M_n$ targ [a] (g mol$^{-1}$) | N 435 [b] (wt%) | t (h) | $^1$H NMR | | SEC-MALS | | | SEC-MALS/ $^1$H NMR) | SEC |
|---|---|---|---|---|---|---|---|---|---|---|---|
| | | | | | Conv. [c] (%) | $DP_n$ NMR [d] (arm) | $M_n$ H-NMR [d] (arm) (g mol$^{-1}$) | $M_n$ SEC-MALS (star polymer) [e] (g mol$^{-1}$) | $Đ$ [e] | $N_{arms}$ SEC-MALS/NMR [f] | Slope (α) [g] |
| 1 | Bulk | 6000 | 3 | 18 | 87% | 24 | 2700 | 5650 | 1.34 | 2.1 | 0.58 |
| 2 | | 6000 | 10 | 7 | 91% | 29 | 3300 | 7800 | 1.36 | 2.4 | 0.58 |
| 3 | $scCO_2$ | 6000 | 3 | 24 | 96% | 28 | 3200 | 8800 | 1.24 | 2.7 | 0.57 |
| 4 | | 6000 | 10 | 7 | 96% | 30 | 3400 | 10100 | 1.23 | 3.0 | 0.58 |

[a] [M]:[I] = 52.6:1 based on $M_n^{targ}$ = [M]:[I] × $M_{ε\text{-CL}}$ at 100 % monomer conversion = 6000 g mol$^{-1}$; I = *D*-sorbitol.
[b] N 435 = Novozym 435 given in wt% with respect to the weight of the monomer.
[c] Monomer conversion determined by $^1$H NMR.
[d] Degree of polymerisation of arms and average molecular weight of arms determined by following Eq. 4.1 and 4.2 respectively.
[e] Molecular weight and dispersity (*Đ*) determined by SEC-MALS using Eq. 4.3.
[f] Average number of arms estimated by SEC-MALS and $^1$H NMR following Eq. 4.4.
[g] Mark-Houwink slope (α) determined by $SEC^{UC}$.

Decreasing the supported enzyme loading from 10 to 3 wt% in $scCO_2$ resulted in a decrease in molecular weight and increase in reaction time to reach 96 % conversion (Table 4.3, Entry 4 vs. Entry 3, Figure 4.7 (top) vs. Figure 4.8 (top)). The same trend was observed in the bulk (Table 4.3, Entry 2 vs. Entry 1, Figure 4.7 (top) vs. Figure 4.8 (top)). However, for 3 wt% enzyme-loading in the bulk, the monomer to polymer conversion appeared to be incomplete (87%, Table 4.3, Entry 1) and plateaued between 13-18 h (Figure 4.8 (top)). By contrast, the use of $scCO_2$ with 3 wt% enzyme resulted in a higher molecular weight ($M_n$ $^{SEC\text{-}MALS}$ = 8800 g $mol^{-1}$ vs. $M_n$ $^{SEC\text{-}MALS}$ = 5650 g $mol^{-1}$) (Figure 4.7 (bottom) vs. Figure 4.8 (bottom)) and slightly higher conversion (96 %, 24 h vs. 87% 18 h) as compared to 10 wt% enzyme (Table 4.3, Entry 3 vs. Entry 1).

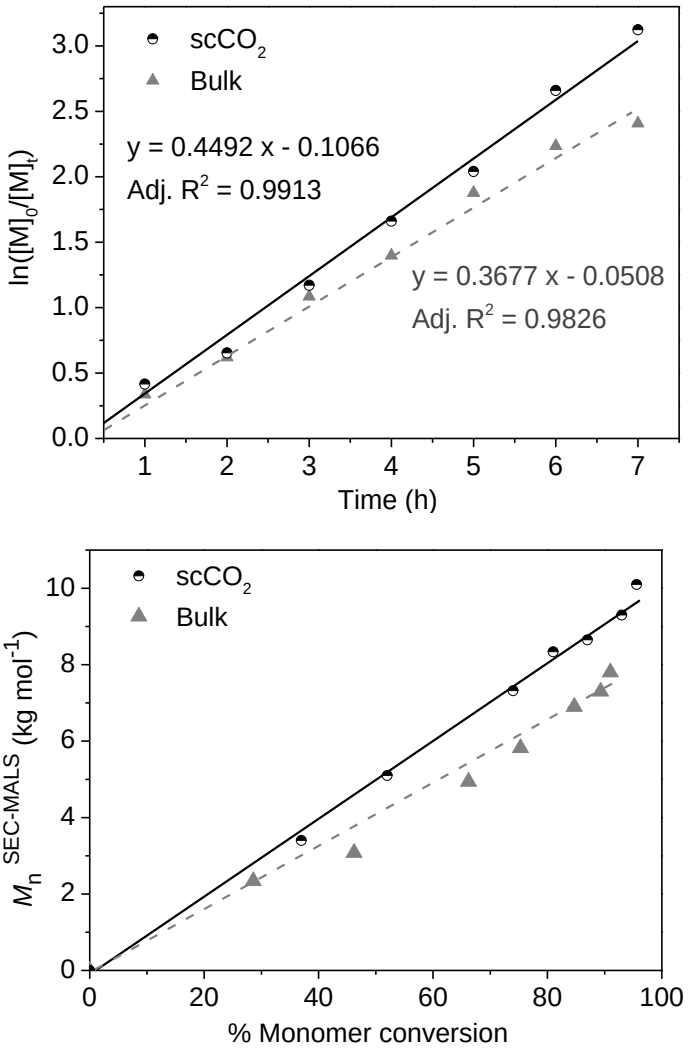



Figure 4.7. Evolution of $ln([M]_0/[M]_t)$ vs. time (top) and $M_n$ $^{SEC\text{-}MALS}$ (kg $mol^{-1}$) with increasing monomer conversion (bottom) for the synthesis of star *D*-sorbitol-PCL catalysed by 10 wt% Novozym 435 relative to ε-CL in the bulk (grey symbols) and in $scCO_2$ (black symbols) at 60 °C.

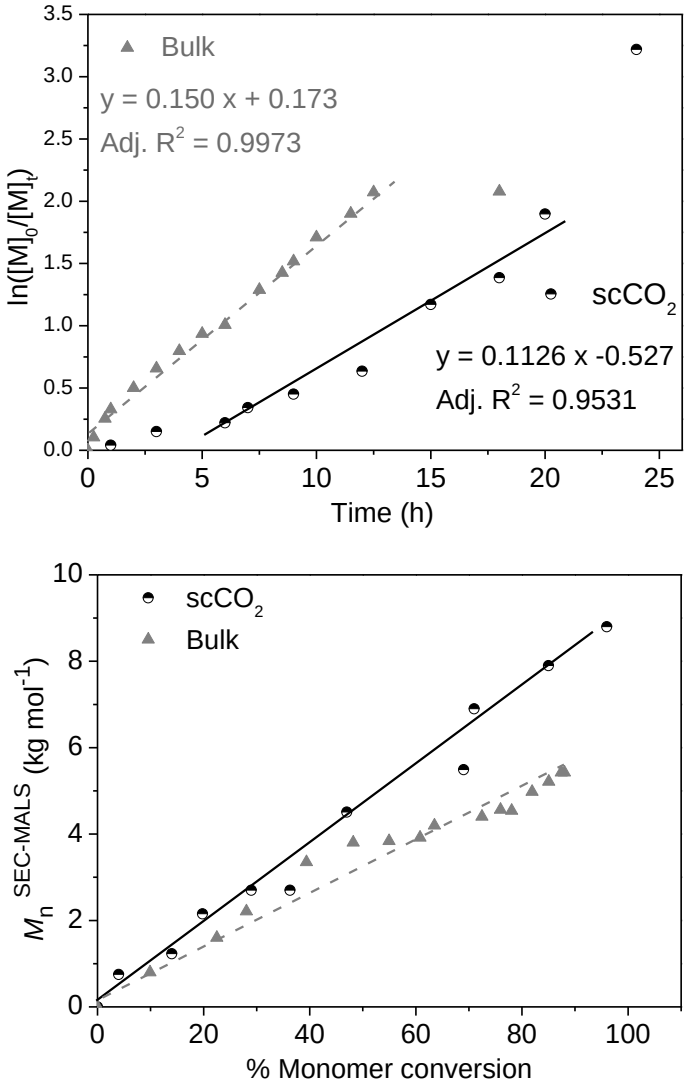



Figure 4.8. Evolution of $\ln([M]_0/[M]_t)$ vs. time (top) and $M_n$ $^{SEC\text{-}MALS}$ (kg $mol^{-1}$) with increasing monomer conversion (bottom) for the synthesis of star *D*-sorbitol-PCL catalysed by 3 wt% Novozym 435 relative to ε-CL in the bulk (grey symbols) and in $scCO_2$ (black symbols) at 60 °C.

The absolute number average molecular weight and dispersity of the star polymers obtained by enzymatic catalysis were determined by SEC-MALS (Figure 4.9).

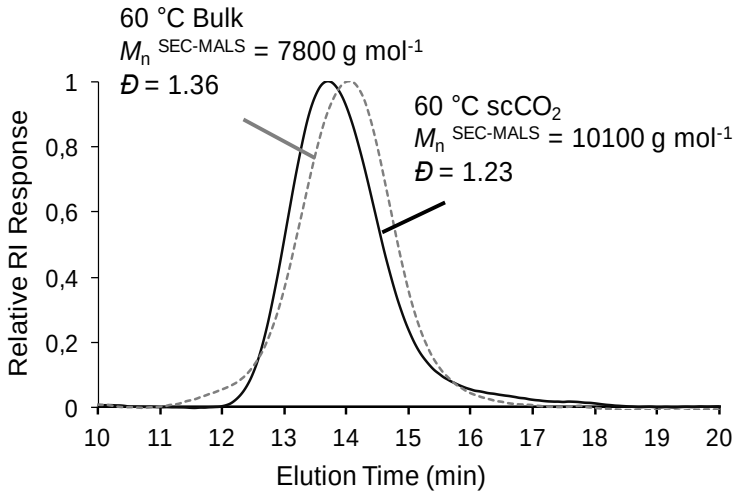



Figure 4.9. SEC-MALS traces overlay of star *D*-sorbitol-PCL catalysed by Novozym 435 (10 wt%) in the bulk and $scCO_2$ at 60 °C (Table 4.3, 2 vs. Entry 4).

For the polymerisation performed using $scCO_2$ and enzyme, the star *D*-sorbitol-PCL showed slightly lower dispersities (*Đ* = 1.23-1.24 *vs* 1.34-1.36) and higher molecular weights compared to reactions in the bulk (Table 4.3, Entry 3-4 vs. Entry 1-2). The narrow dispersity and higher molecular weight obtained in $scCO_2$ are in good agreement with reports on the synthesis of linear PCL by Novozym 435 in $scCO_2$.[51]
After optimising the polymerisation conditions, the star structures were characterised in detail by NMR ($^1$H and $^{31}$P), SEC (MALS and UC-Mark-Houwink plot), MALDI-TOF-MS and DSC. The notation star *D*-sorbitol$[(PCL)_nOH]_m$ will be used in the following discussion; n corresponds to the average amount of CL repeat units per arm of *D*-sorbitol ($DP_n$ (arms); values are given in Table 4.2 and Table 4.3) and m corresponds to the average number of arms.

### 4.4.4 Assessing MW of Arms of Star *D*-Sorbitol-PCL by $^1$H NMR

The influence of the catalyst and the reaction medium on the architecture of the star *D*-sorbitol-PCL polymers was studied by $^1$H NMR spectroscopy (Figure 4.10). In principle, star *D*-sorbitol-PCL can have up to 6 PCL arms emanating from the 6 hydroxy groups of *D*-sorbitol. The multiplets at δ 1.64 and δ 1.37 ppm correspond to the methylene protons of the PCL backbone (c' + c'' and d'). The triplet at δ 2.29 ppm corresponds to the methylene protons (a' + b') in α-position of the carbonyl group whereas the signal at δ 4.05 ppm corresponds to protons (e'). The methylene protons (f') in α-position to the hydroxy end-groups of the PCL chains are visible at δ 3.63 ppm (Figure 4.10 (A) and (B)). It is noteworthy that the signals corresponding to protons of

the esterified primary carbon atoms appear between $\delta$ = 4.0 - 4.4 ppm and in the range of $\delta$ 5.0 – 5.5 ppm for esterified secondary carbon atoms. Spectrum A corresponding to a sample synthesised in the bulk using $Sn(Oct)_2$ clearly shows the presence of protons adjacent to secondary esterified hydroxy groups (5 – 5.5 ppm).

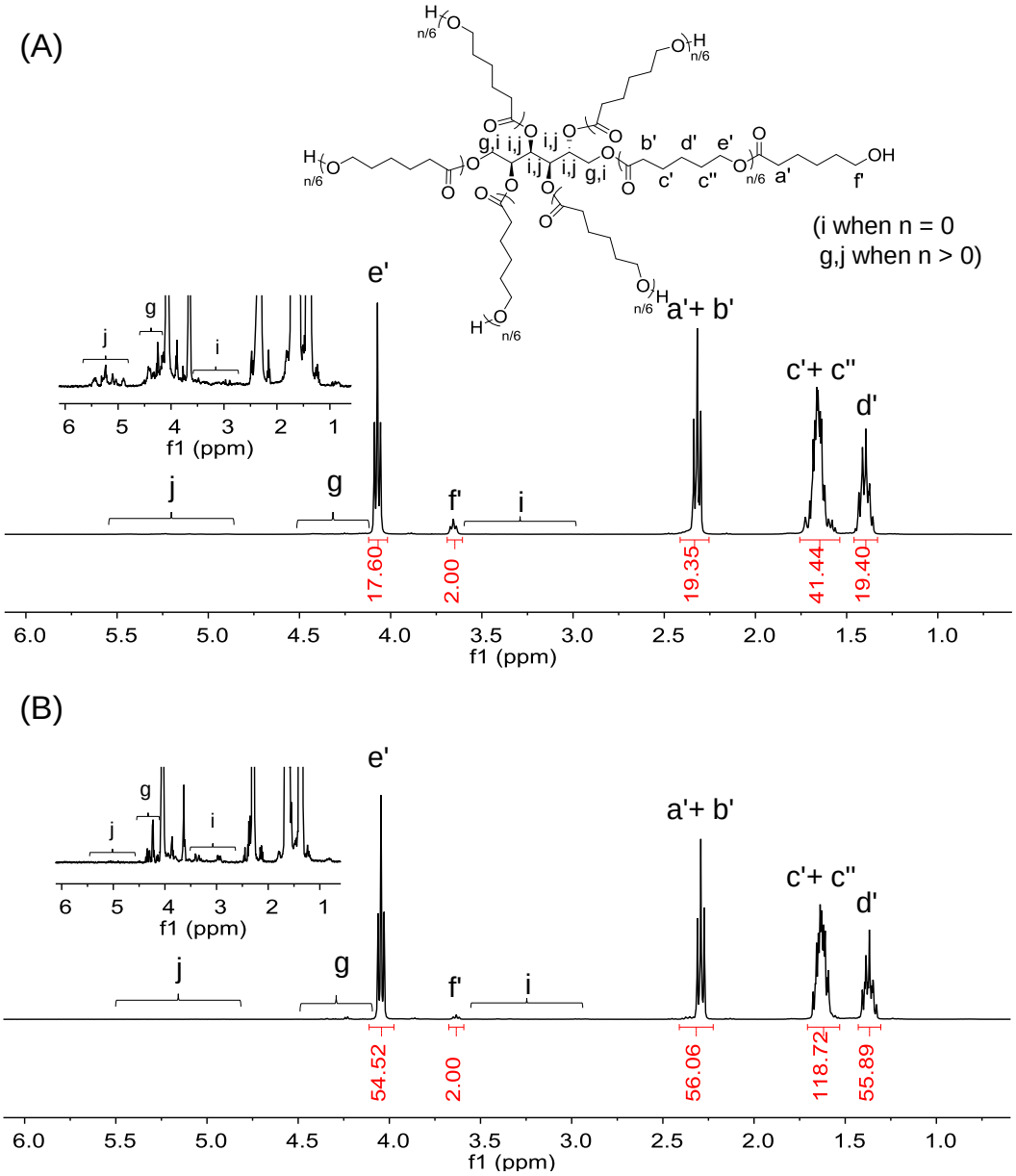



Figure 4.10. $^1$H NMR spectra ($CDCl_3$, 400 MHz) of (A) $Sn(Oct)_2$ catalysed *D*-sorbitol$[(PCL)_{9.7}OH]_m$ in the bulk (Table 4.2, Entry 3) and (B) Novozym 435 catalysed *D*-sorbitol$[(PCL)_{28}OH]_m$ in $scCO_2$ (Table 4.3, Entry 3). The inset shows the enlarged signals corresponding to the sorbitol core.

These resonances are not visible in spectrum B corresponding to a sample synthesised in $CO_2$ by enzyme catalysis, indicating a high degree of functionalisation of secondary hydroxy groups when using a metal catalyst, and a low degree of functionalisation of secondary hydroxy groups when using enzyme catalysis. The resonances of pendant

protons on the sorbitol core next to residual hydroxy groups are shifted to around 4 ppm and overlap with resonances from the polymer backbone. However, due to a poor signal to noise ratio for the resonances of the protons of *D*-sorbitol which are located at the core of the structure, quantification based on the sorbitol signals from $^{1}$H NMR is not-reliable (see Insets Figure 4.10).

The degree of polymerisation, $DP_n^{\text{NMR}}$ (arm) and number average molecular weight of each arm, $M_{n,}^{\text{H-NMR}}$ (arm), calculated using Eq. 4.1 and Eq. 4.2 for a representative sample star *D*-sorbitol[$(PCL)_{9.7}$-OH]$_m$ (Table 4.2, Entry 3 and Figure 4.10 (A)) are 9.7 and 1100 g mol$^{-1}$, respectively. In general, the $M_n^{\text{H-NMR}}$ (arm) of star *D*-sorbitol-PCL synthesised using $Sn(Oct)_2$ (1100-1290 g mol$^{-1}$, Table 4.2) were lower than those obtained with Novozym 435 (2700-3400 g mol$^{-1}$, Table 4.3).

Since SEC-MALS measurements give access to the absolute number average molecular mass of star *D*-sorbitol-PCL ($M_n^{\text{SEC-MALS}}$ (star polymer)), the average number of arms ($N_{\text{arms}}^{\text{SEC-MALS/NMR}}$) can be estimated by combining this information with the $M_n^{\text{H-NMR}}$ (arm) (as $N_{\text{arms}}^{\text{SEC-MALS/NMR}} = M_n^{\text{SEC-MALS}}$ (star polymer)/$M_n^{\text{H-NMR}}$ (arm)). Accordingly, the star *D*-sorbitol-PCL polymers synthesised using $Sn(Oct)_2$ exhibit $N_{\text{arms}}^{\text{SEC-MALS/NMR}}$ = 5.1 in the bulk and $N_{\text{arms}}^{\text{SEC-MALS/NMR}}$ = 4.9 in $scCO_2$ (Table 4.2, Entry 3 vs. Entry 4). Interestingly, polymerisations performed employing enzyme catalysis resulted into a lower number of arms, $N_{\text{arms}}^{\text{SEC-MALS/NMR}}$ = 2.4 and 3.0 (Table 4.3, Entry 2 and Entry 4) in the bulk and in $scCO_2$, respectively. A lower number of arms observed with eROP may be related to the regioselectivity of Novozym 435 since the eROP initiated from primary alcohols may be favoured in comparison to secondary alcohols.[64,65] Whatever the enzyme loading, a slightly higher $N_{\text{arms}}^{\text{SEC-MALS/NMR}}$ resulted for star PCL synthesised in $scCO_2$ compared to the analogues made in the bulk ($N_{\text{arms}}^{\text{SEC-MALS/NMR}}$ = 2.1 vs. 2.7 and 2.4 vs. 3.0, respectively (Table 4.3, Entry 1 vs. Entry 3 and Entry 2 vs. Entry 4).

For polymerisations in the presence of $Sn(Oct)_2$, all the star-PCL polymers exhibit narrow molecular weight distributions ($Đ$ = 1.03-1.12, Table 4.2) according to SEC-MALS analysis. Such low dispersities suggest a uniform sample of star-PCL, where the number of arms is the same. The length of the arms of one individual star polymer may be the same or of different length, but with a uniform architecture throughout the sample. Higher dispersities are, however, observed with Novozym 435 as the catalyst ($Đ$ = 1.23-1.36, Table 4.3).

These higher dispersities could be caused by transesterification side reactions occurring during eROP. Macrocycles formed by back-biting (intramolecular transesterification) or linear PCL initiated by water (mainly originating from the enzyme) can also be present in small amounts in the final star polymers.[50,66] In addition, since Novozym 435 is regioselective,[67] initiation from the primary hydroxy groups of *D*-sorbitol is expected to be faster than initiation from the secondary hydroxy groups, implying that there will be arms with different lengths (i.e. shorter arms from the secondary alcohols of *D*-sorbitol) and lead to star PCL with a miktoarm star architecture.

MALDI-TOF analyses were performed in order to further investigate the synthesised star polymers.

### 4.4.5 Assessing the Structure of Star *D*-Sorbitol-PCL by MALDI-TOF MS

A semi-quantitative investigation by MALDI-TOF-MS gave insights into the molecular structure of star *D*-sorbitol-PCL. The mass spectrum of star *D*-sorbitol-PCL synthesised using $Sn(Oct)_2$ regardless of the solvent medium showed one distribution where the signals were separated by 114.14 m/z corresponding to the mass of the ε-CL repeating units (Figure 4.11). All signals were assigned to PCL chains initiated by *D*-sorbitol with $K^+$ as the cation. These results confirm the formation of star *D*-sorbitol-PCL without side reactions. The inset (Figure 4.11) shows the signals at m/z = 5015.3, 5129.4 and 5243.6, which represent molecular masses of the $K^+$ adduct of *D*-sorbitol attached to 42, 43 and 44 ε-CL units, respectively.

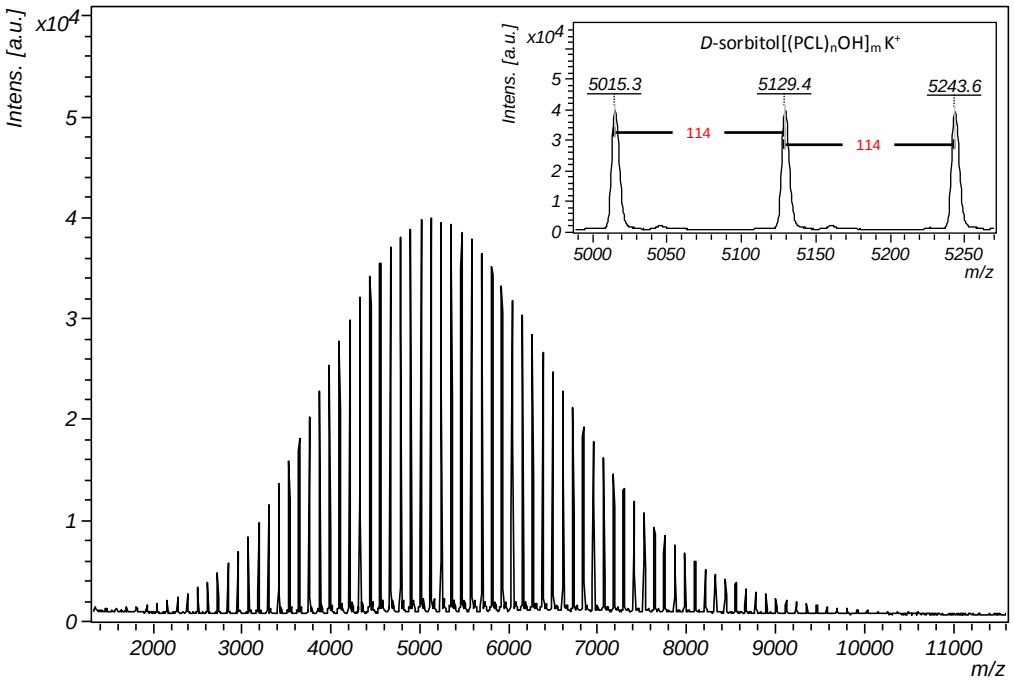



Figure 4.11. MALDI-TOF mass spectrum of *D*-sorbitol[$(PCL)_{9.7}OH]_m$ synthesised in the bulk in the presence of $Sn(Oct)_2$ (Table 4.2, Entry 3). The MALDI-TOF spectrum was acquired in linear mode.

All the signals in the mass spectrum of star *D*-sorbitol[$(PCL)_{28}OH_m$] (Table 4.3, Entry 3) catalysed by 3 wt% Novozym 435 in $scCO_2$ correspond to polymers with the ε-CL repeat unit as well (Figure 4.12). The main population (P1) is composed of $K^+$ adducts of *D*-sorbitol initiated PCL. For instance, the signal at m/z = 3074.9 in the inset corresponds to the $K^+$ adduct of *D*-sorbitol attached to 25 ε-CL units ([*D*-sorbitol$[(PCL)_{25}OH_m]+K]^+$). For both syntheses in the bulk and in $scCO_2$, three distributions were observed in the MALDI-TOF spectra of star *D*-sorbitol$[(PCL)_nOH]_m$ synthesised using Novozym 435. In addition to the main population (P1), a second population (P2) corresponding to PCL initiated by water (linear HOOC-PCL-OH) and a third population (P3) corresponding to PCL macrocycles formed by the back-biting side-reaction[68] were present in the low molecular mass region (m/z = 1000 – 3000, Figure 4.12, inset).

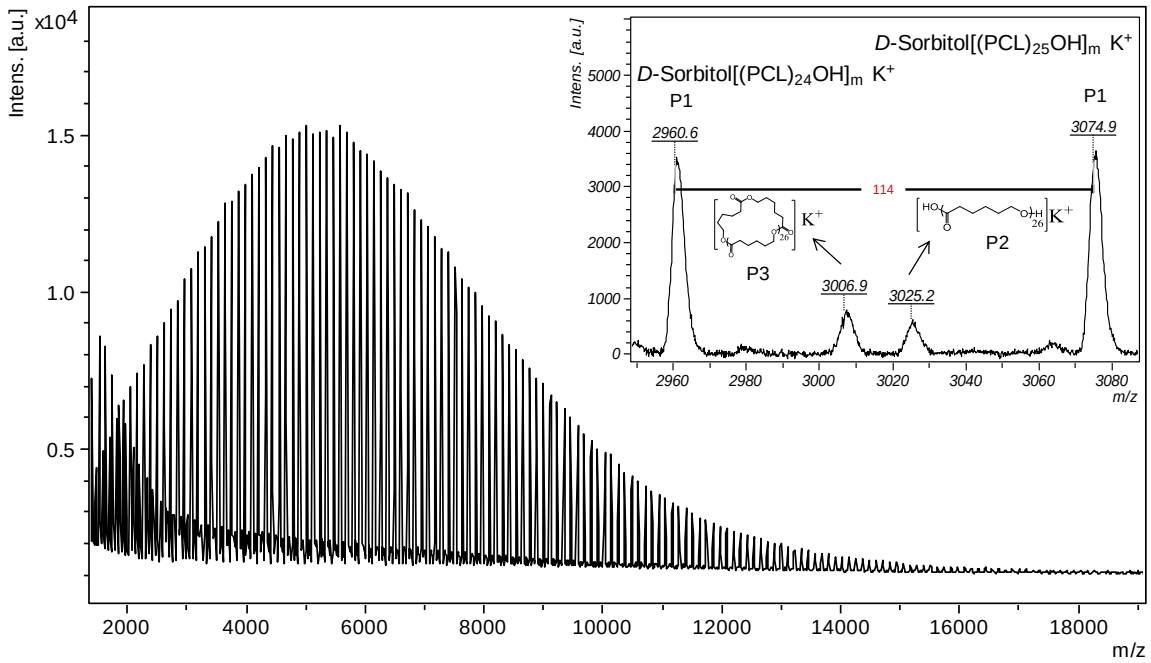



Figure 4.12. MALDI-TOF mass spectrum of *D*-sorbitol[$(PCL)_{28}OH]_m$ synthesised in presence of 3 wt% Novozym 435 using $scCO_2$ (Table 2, Entry 3). The m/z values given in the inset correspond to the main population *D*-sorbitol[$(PCL)_nOH]_m$ $K^+$. Additional populations (P2 and P3) observed in the low molecular weight region are assigned to side-products related to PCL initiated by water and macrocycles.

Thus, MALDI-TOF analysis revealed the formation of a mixture of structures for the star *D*-sorbitol-PCL synthesised using Novozym 435 as the catalyst (Figure 4.12) and therefore the ratio $M_n$ $^{SEC\text{-}MALS}$(star polymer)/$M_n$ $^{H\text{-}NMR}$(arm) is not a fully reliable estimation of the number of arms. In order to better understand the structure of star PCL, in particular, star PCL synthesised using Novozym 435 as the catalyst, the polymers were characterised by a phosphitylation/$^{31}$P NMR method.

### 4.4.6 Quantifying Number of Arms by a Phosphitylation/$^{31}$P NMR Method

The quantitative number of arms ($N_{arms}$($^{31}$P)), the number average molecular weight of the arms ($M_n$ $^{P\text{-}NMR}$(arm)), the molecular weight of the star polymer ($M_n$ $^{P\text{-}NMR}$(star polymer)) and the percentage of linear PCL chains present in star *D*-sorbitol-PCL were investigated by the phosphitylation method developed by Spyros *et al.* [69] (discussed in Chapter 3). This method utilises 2-chloro-4,4,5,5-tetramethyldioxaphospholane (Cl-TMDP) as a phospholane reagent and cyclohexanol as an internal standard for subsequent $^{31}$P NMR analysis.

The $^{31}$P NMR analysis of *D*-sorbitol was performed as a reference for the phospholane ester of *D*-sorbitol, the primary hydroxy groups (1°, triplet, -$CH_2O$**P**-, $\delta$ = 147.0-148.6 ppm) can be distinguished from the secondary hydroxy groups (2°, doublet, -CHO**P**- , $\delta$ = 145.5-147.0 ppm).[70] Moreover, the signal corresponding to the primary hydroxy groups of the PCL arm of star *D*-sorbitol-PCL polymer, exhibits a different chemical shift (1°, triplet, -PCL-O**P**, $\delta$ = ~147.02) than those originating from the *D*-sorbitol core (Figure 4.13 (A)-(C)). A downfield shift was also observed for any residual hydroxy group of the *D*-sorbitol core present in the star PCL for both catalytic systems (Figure 4.13 (B)-(C) vs. (A)). A phosphitylated carboxy acid group has a different chemical shift range (-COO**P-,** $\delta$= 133.0-136.6 ppm) than hydroxy groups.[70] Hence, it is possible to identify the end groups of the water initiated linear PCL.

The representative $^{31}$P NMR spectrum of the star *D*-sorbitol$[(PCL)_{9.7}OH]_m$ synthesised using $Sn(Oct)_2$ in the bulk (Table 4.2, Entry 3) shows no signal corresponding to -COO**P**- (Figure 4.13 (B)), which is in corroboration with MALDI-TOF MS data confirming the absence of water initiated linear PCL in the samples prepared using $Sn(Oct)_2$ as a catalyst. The corresponding inverse gated proton-decoupled $^{31}$P NMR spectra were recorded in the presence of an internal standard (cyclohexanol) for quantification (Figure 4.14).

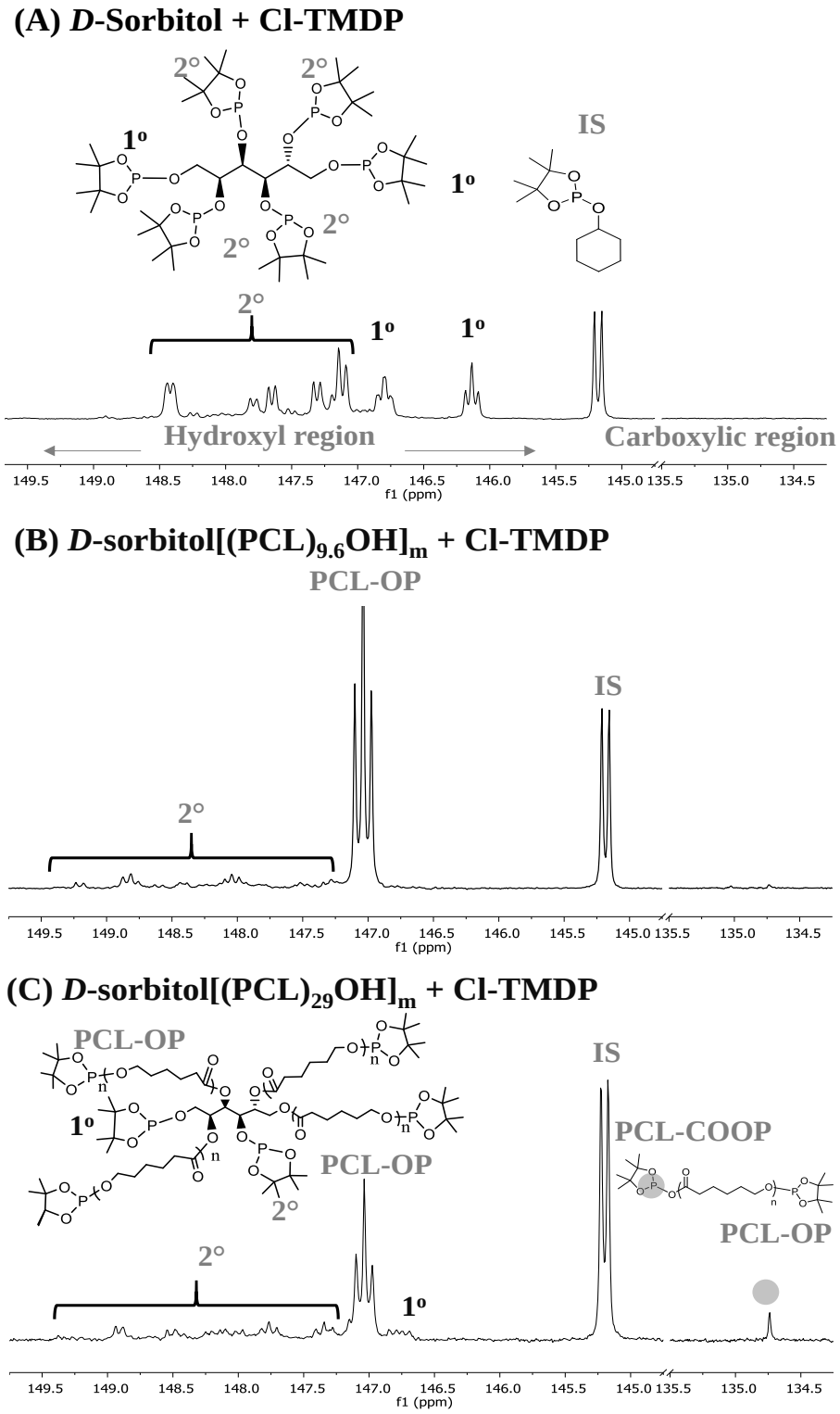



Figure 4.13. $^{31}$P NMR spectra without decoupling of phosphitylated (A) *D*-sorbitol, (B) star *D*-sorbitol$[(PCL)_{9.7}OH]_m$ (Table 4.2, Entry 3) showing residual secondary hydroxy groups on the *D*-sorbitol core and (C) star *D*-sorbitol$[(PCL)_{28}OH]_m$ (Table 4.3, Entry 3) showing residual primary and secondary hydroxy groups on *D*-sorbitol alongside linear PCL. IS: internal standard (cyclohexanol). It should be noted that from phospholane ester of *D*-sorbitol there are minor additional peaks that arise after the phosphitylation process and appear in the region of the 2° hydroxy.

The number of arms, $N_{arms}$ ($^{31}$P), of star *D*-sorbitol[(PCL)$_{9.7}$OH]$_m$ corresponds to the number of hydroxy groups of *D*-sorbitol that have effectively initiated the ROP of ε-CL. It was evaluated by comparing the number of phosphitylated PCL chain ends ($\int_{PCL\text{-}OP}$) with the total number of phosphitylated hydroxy groups in the sample (Eq. 4.5))[27]:

$$N_{arms}(^{31}P) = \frac{\int_{PCL-OP}}{\int_{(1^\circ + 2^\circ)} + \int_{PCL-OP}} \times 6 \qquad \text{Eq. 4.5}$$

The (1° + 2°) corresponds to the total number of residual phosphitylated hydroxy groups on the *D*-sorbitol core in the star polymer and (PCL-OP) corresponds to the phosphitylated hydroxy chain ends of the PCL arms, and 6 corresponds to the total amount of hydroxy groups of the initiator.

The absence of signals resulting from primary hydroxy groups of the core in star *D*-sorbitol[(PCL)$_{9.7}$OH]$_m$ implies that all primary hydroxy group initiate the ROP of ε-CL (two growing arms). In contrast, 23% of the secondary hydroxy of the core is still present in the star polymer indicating three growing arms from secondary hydroxy groups in average (Figure 4.14, (A)). This presence of residual secondary hydroxy groups could be explained by the steric hindrance resulting from adjacent PCL arms. An average of five arms was obtained for star *D*-sorbitol[(PCL)$_{9.7\text{-}11.3}$OH]$_5$ catalysed by Sn(Oct)$_2$ both in the bulk and in scCO$_2$ (Table 4.4).

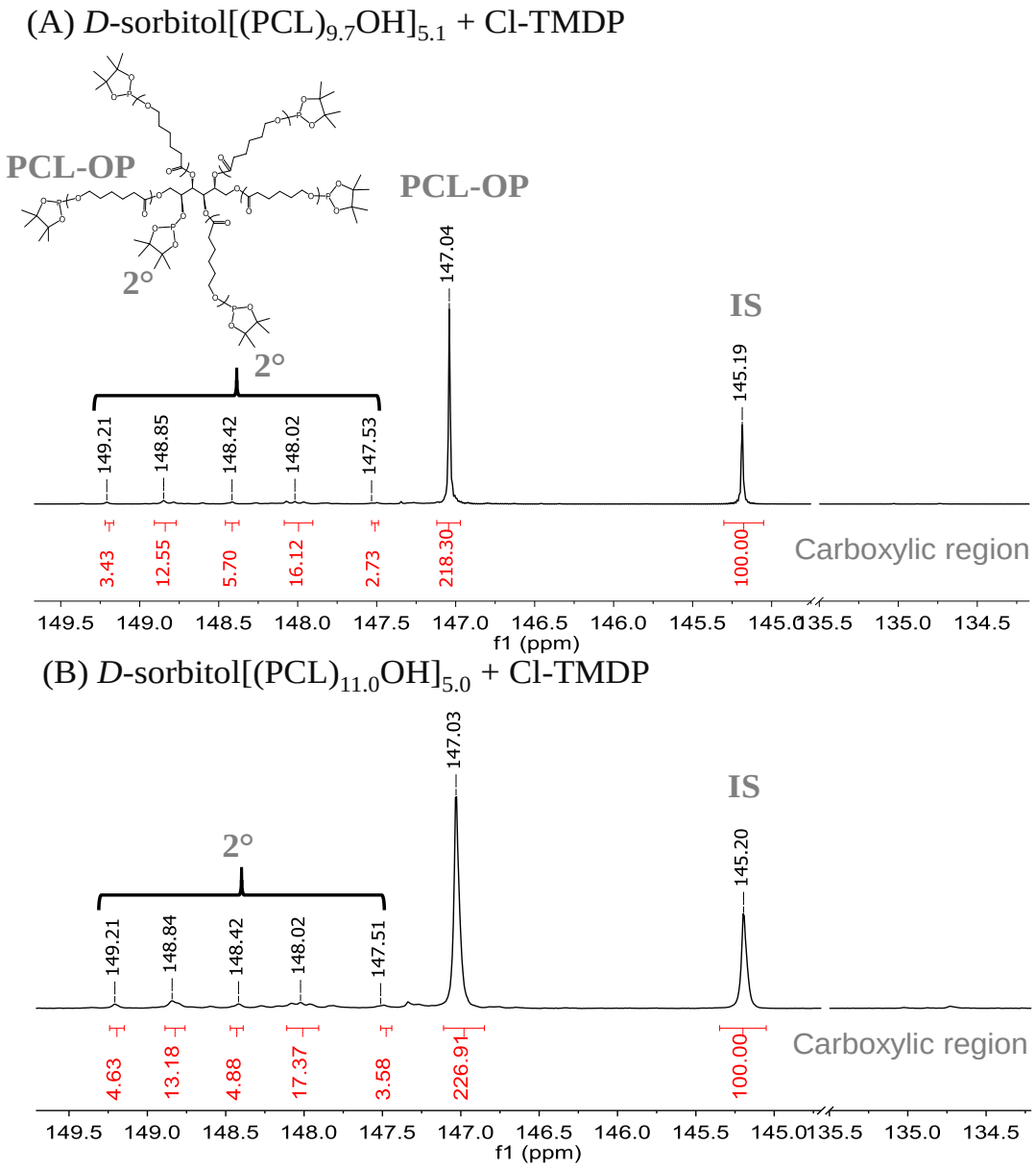



Figure 4.14. Inverse gated decoupled $^{31}P$ NMR spectra of $Sn(Oct)_2$ catalysed star samples after phosphitylation by Cl-TMDP. (A) star *D*-sorbitol$[(PCL)_{9.7}OH]_{5.1}$ synthesised in the bulk (Table 4.4, Entry 3) and (B) star *D*-sorbitol$[(PCL)_{11.0}OH]_{5.0}$ in $scCO_2$ (Table 4.4, Entry 4) using $Sn(Oct)_2$ as the catalyst. IS: internal standard (cyclohexanol).

Table 4.4. Determination of the number of arms and the molecular weight by $^{31}$P NMR for star *D*-sorbitol-PCL synthesised in the presence of $Sn(Oct)_2$.

| $^{31}$P NMR (Phosphitylation) | | | | |
|---|---|---|---|---|
| Sample | $N_{arms}$ ($^{31}$P)[a] | $M_n$ P-NMR [b] (arm) (g mol$^{-1}$) | $M_n$ P-NMR (star polymer) [c] (g mol$^{-1}$) | Notation of samples in Table 1 |
| 1 | 5.0 | 1250 | 6300 | star *D*-sorbitol[$(PCL)_{11.3}OH]_{5.0}$ |
| 2 | 4.8 | 1190 | 5750 | star *D*-sorbitol[$(PCL)_{11.0}OH]_{4.8}$ |
| 3 | 5.1 | 1100 | 5600 | star *D*-sorbitol[$(PCL)_{9.7}OH]_{5.1}$ |
| 4 | 5.0 | 1300 | 6500 | star *D*-sorbitol[$(PCL)_{11.0}OH]_{5.0}$ |

[a] Average number of arms quantified following Eq. 4.5 and the corresponding inverse gated decoupled $^{31}$P NMR spectra (Figure 4.14).
[b] Number average molecular weight of arms determined following Eq. 4.6
[c] Molecular weight of star polymer determined following Eq. 4.7.

**Equations for quantification by the $^{31}$P phosphitylation method**

| | | |
|---|---|---|
| $M_n$ P-NMR (arm) | $= [m_s / n_{PCL\text{-}OP}] \times 1000$ | Eq 4.6 |
| $M_n$ P-NMR (star polymer) | $= M_n$ P-NMR (arm) $\times N_{arms}$ $^{31P}$ | Eq 4.7 |
| %COOH | $= (\int_{PCL\text{-}COOP} / \int_{PCL\text{-}OP}) \times 100$ | Eq 4.8 |
| $n_{PCL\text{-}OP}$ | $= (n_{IS} \times \int_{PCL\text{-}OP}) / \int_{IS}$ | Eq 4.9 |

For the polymerisation using enzyme catalysis, regardless of the reaction medium, the $^{31}$P NMR analysis of the star *D*-sorbitol$[(PCL)_{24\text{-}30}OH]_m$ sample (Table 4.3) shows resonances associated with carboxylic acid groups (singlet,-COO**P,** $\delta$ = 134.74± 0.01 ppm), corresponding to linear PCL (refer to Appendix B). It correlates well with MALDI-TOF analysis of these samples (e.g. Figure 4.12), confirming the presence of low molecular weight linear PCL chains initiated by water. However, the quantity of linear PCL chains present in star *D*-sorbitol-PCL samples synthesised by enzyme catalysis was very low (1.4 -11.3%) (Followed using Eq. 4.10) (Table 4.5 and for detailed analytical data refer to Appendix B).

The $N_{arms}$($^{31}$P) for enzyme catalysed star PCL was evaluated accounting for the water initiated linear PCL chains (**H**OOC-PCL-O**H**) (Eq. 4.10):

$$N_{arms}(^{31}P) = \frac{\int_{PCL-OP} - \int_{PCL-COOP}}{\int_{(1°+2°)} + \int_{PCL-OP} - \int_{PCL-COOP}} \times 6 \qquad \text{Eq. 4.10}$$

Table 4.5. Determination of the number of arms and the molecular weight by $^{31}$P NMR for *D*-sorbitol-PCL synthesised in the presence of Novozym 435.

| $^{31}$P NMR (Phosphitylation) | | | | | |
|---|---|---|---|---|---|
| Sample | $N_{arms}$ ($^{31}$P) [a] | %COOH [b] (linear chains) | $M_n$ P-NMR [c] (arm) (g mol$^{-1}$) | $M_n$ P-NMR [d] (star polymer) (g mol$^{-1}$) | Notation of samples in Table 2 |
| 1 | 3.1 | 1.4 | 2000 | 6200 | star *D*-sorbitol[(PCL)$_{24}$OH]$_{3.1}$ |
| 2 | 3.3 | 5.2 | 3200 | 10600 | star *D*-sorbitol[(PCL)$_{29}$OH]$_{3.3}$ |
| 3 | 3.2 | 5.4 | 3000 | 9600 | star *D*-sorbitol[(PCL)$_{28}$OH]$_{3.2}$ |
| 4 | 2.9 | 11.3 | 2900 | 8400 | star *D*-sorbitol[(PCL)$_{30}$OH]$_{2.9}$ |

[a] Average number of arms quantified following Eq. 4.10 and the corresponding inverse gated decoupled $^{31}$P NMR spectra (refer to Appendix B).
[b] Amount of linear PCL chains quantified following Eq. 4.8
[c] Number average molecular weight of arms determined following Eq. 4.6
[d] Molecular weight of star polymer determined following Eq. 4.7

Following Eq. 4.10 the $N_{arms}$($^{31}$P) for all the star *D*-sorbitol-PCL synthesised using Novozym 435 (Table 4.3, Entries 1-4) was about 3, regardless of the catalyst loading and the reaction medium (Table 4.5). The $N_{arms}$ SEC-MALS/NMR values are slightly lower than the $N_{arms}$ ($^{31}$P) values because SEC-MALS cannot account for the presence of linear PCL in the star polymer samples. In $^{31}$P NMR analysis of the Novozym 435 catalysed star *D*-sorbitol[(PCL)$_{28}$OH]$_m$ sample (Table 4.3, Entry 3, refer to Appendix B, Figure B2 (A)), the resonances corresponding to residual hydroxy groups of *D*-sorbitol core show that 72% of the primary hydroxy groups initiate ROP of ε-CL (1.5 growing arms in average), whereas about 45% of the secondary hydroxy groups initiate ROP of ε-CL (1.8 growing arms on average). This indicates that the Novozym 435 catalyst is preferentially initiating the eROP of ε-CL from the primary hydroxy groups of *D*-sorbitol but Novozym 435 is not completely regioselective towards primary alcohols under the reaction conditions studied. The overall number of arms determined for star *D*-sorbitol[(PCL)$_{28}$OH]$_{3.2}$ sample in this way is 3.2 (Table 4.5, Entry 3).

The $M_n$ P-NMR (arm) determined by $^{31}$P NMR (Table 4.4 and Table 4.5) are in good agreement with the results from $M_n$ H-NMR (arm) analysis (Table 4.2 and Table 4.3). An average number of arms of 5 is determined by both the $^{31}$P and $^{1}$H NMR analyses. In addition to the narrow dispersities observed by SEC-MALS ($Đ$ = 1.03-1.12, Table 4.2) the uniform distribution (uniform Gaussian curve) observed by MALDI-TOF confirms the controlled synthesis of well-defined, regular star polymers in the presence of Sn(Oct)$_2$ in the bulk and in scCO$_2$ (Figure 4.15(A)). When using Novozym 435 as a

catalyst, a lower value of 3 for the average number of arms, higher molecular weights of the arms and slightly higher dispersities ($Đ$ = 1.23-1.36) were observed compared to using $Sn(Oct)_2$. This indicates that a lower number of hydroxy groups of *D*-sorbitol initiate the eROP leading to less regular star architectures (Figure 4.15 (B)). It is important to state that detailed analysis of the phosphitylation process (phospholane ester of *D*-sorbitol, Figure 4.13 (A)) does show that the process is unlikely to be fully quantitative on *D*-sorbitol and that there are some minor impurities arising from other species that are revealed in the 2° peaks. These will, of course, contribute to the $^{31}P$ NMR spectra of the star polymers (Figure 4.13) and introduce some error into our calculations of the $N_{arms}(^{31}P)$ but nevertheless, these data corroborate the differences observed in the products arising from tin catalysis and from the enzyme.

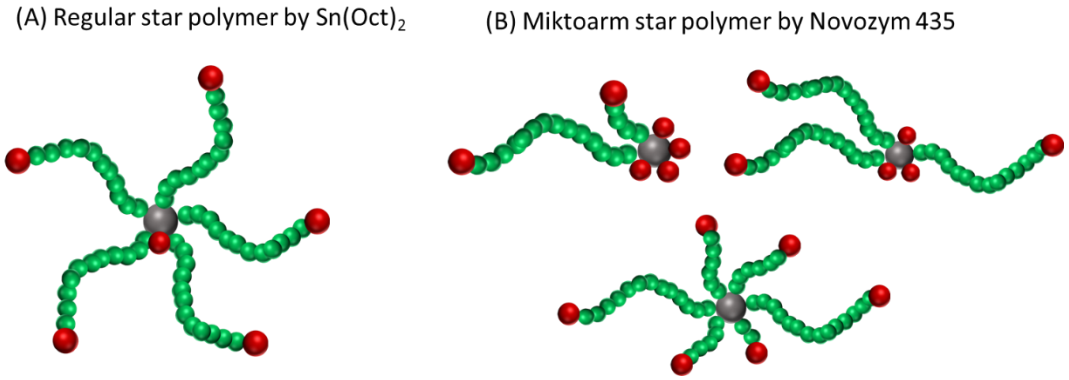



Figure 4.15. Schematic representation of star *D*-sorbitol-PCL synthesised by (A) $Sn(Oct)_2$ giving regular star polymers with 5 arms ($M_n$ = 6000 g $mol^{-1}$)and by (B) Novozym 435 yielding a mixture of miktoarm star polymers. The *D*-sorbitol core (●), PCL arms (●●●) and hydroxy groups (●) are presented.

Furthermore, supplementary methods were investigated for determination of branching of star polymers by SEC approach.

### 4.4.7 Mark-Houwink Plot for Structure of Star-Branched PCL

The structure of the star polymers can be confirmed by SEC analysis with an RI and a viscosity detector using the Mark-Houwink (MH) relationship. The MH slope (α) of the double-logarithmic Mark-Houwink plots, derived for star *D*-sorbitol-PCL from $[\eta] = K \times M^{\alpha}$, where [η] is intrinsic viscosity, M is molecular weight, α and K are the Mark-Houwink constants, is related to the branching of the polymers (Figure 4.16). The MH α value is a polymer conformation parameter that decreases with the compactness of the structure.

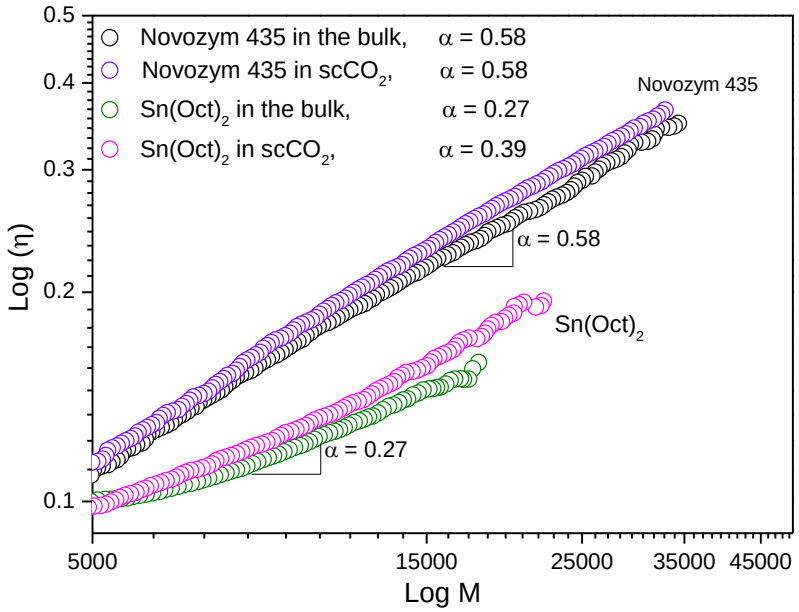



Figure 4.16. Intrinsic viscosity [η] as a function of the molar mass M for star *D*-sorbitol-PCL polymers catalysed by Novozym 435 in the bulk (black symbols) and in $scCO_2$ (blue symbols) and of star *D*-sorbitol-PCL polymers catalysed by $Sn(Oct)_2$ in the bulk (green symbols) and in $scCO_2$ (pink symbols).

An α-value between 0.1 to 0.6 is representative of star polymers and a value from 0.6 to 1 corresponds to linear coil structures.[71–73] Branched polymers have a higher segment density compared to linear polymers of equivalent molecular weight, resulting in a decrease in intrinsic viscosity.[74,75] All the *D*-sorbitol-PCL polymers synthesised by Novozym 435 and $Sn(Oct)_2$ have α-values between 0.27 to 0.58, which is in good accordance with a star-like architecture of the polymers. However, it is worth noting that star *D*-sorbitol-PCL polymers synthesised with $Sn(Oct)_2$ either in the bulk or in $scCO_2$ have a slightly lower intrinsic viscosity in comparison to those obtained with Novozym 435 (Figure 4.16). We hypothesise that this shows a lower number of arms for the star polymers synthesised by enzyme catalysis compared to those synthesised using $Sn(Oct)_2$. The α-values of the *D*-sorbitol-PCL polymers synthesised by Novozym 435 (0.57-0.58; Table 4.3, Entries 1-4) are close to 0.6 indicating structures in between a star-like and a linear-like topology. This observation might suggest structures composed of two main arms with a low amount of shorter arms radiating from the secondary *D*-sorbitol –OH groups. Star *D*-sorbitol polymers synthesised with $Sn(Oct)_2$ either in the bulk or in $scCO_2$ show lower values of α (0.27 – 0.39; Table 4.2) which indicates a more branched structure and thus a larger number of arms. The use of SEC-

UC- MH plots approach was extended for determination of a number of arms from intrinsic viscosity and of the radius of gyration of branched molecules.

### 4.4.8. Determining Arms by SEC-UC-MH Conformation Plots

The SEC Universal Calibration ($SEC^{UC}$) characterisation of the star polymer was further extended for the calculation of branching of star *D*-sorbitol-PCL (refer Chapter 3 Section 3.2.3); for this linear and star polymers falling in the molecular weight (MW) regime (~10000 – 11000 g $mol^{-1}$) were also prepared in the bulk using $Sn(Oct)_2$ catalyst at 140 °C. A slightly higher MW was targeted so that the obtained polymers were comparable to the Novozym 435 catalysed *D*-sorbitol-PCL.

For simplification in the discussion, the samples are named by a prefix corresponding to the initiator and a suffix corresponding to the MW regime as 10K or 6K for 10000 or 6000 g $mol^{-1}$ respectively (Table 4.6). The $SEC^{UC}$ characterisation data of previous discussed $Sn(Oct)_2$ catalysed star *D*-sorbitol-PCL prepared in the bulk and in $scCO_2$ (Table 4.2, Entry 3 and 4) and the star *D*-sorbitol-PCL prepared by using Novozym 435 catalyst in $scCO_2$ (Table 4.3, Entry 4) are included (Table 4.6, Entry 4, 5 and 6 respectively).

The method for determining the number of arms of star-shaped PCL sample is based on two well-known facts:

(1) SEC separates various molecules based on their hydrodynamic volume which is the product of the intrinsic viscosity [$\eta$] and the molecular weight [M], (Benoit 1967)[76]

(2) The intrinsic viscosities of a star polymer and a linear polymer of equal molecular weights differ, and the difference can be approximated by a radius of gyration contraction factor, g [77] (also see Chapter 3).

$$\left(\frac{[\eta]_{\text{star}}}{[\eta]_{\text{linear}}}\right)^{1/\varepsilon} = g = \frac{3f-2}{f^2} \ldots. \qquad \text{Eq 4.11}$$

Where *f* if star functionality i.e., number of arms of a star molecule.

The contraction factor from intrinsic viscosity, g', was calculated by taking a ratio of the intrinsic viscosity of a star polymer and linear analogues, for example; of star *D*-Sorb-PCL-10K and a linear HexD-PCL-10K having same molecular weight.

As proposed by Zimm,[78] the radius of gyration contraction factor g was calculated by $g = (g')^{1/0.5}$. After substituting this number in the Eq. 4.11 and solving the second-degree polynomial equation for each entry, the value of *f* was calculated.

The average of all the *f* values i.e. an average number of arms per star polymer molecule is calculated. The analytical data are summarised for all the samples (Table 4.6 Entries 1-3).

The *f* values, for all the samples, corroborate with our number of arms values determined by phosphitylation and SEC-MALS (Table 4.6, last three columns). It should be noted that a minimum *f* value in this model is 2 thus functionality is 2 for linear polymers.[79]

The analysis of each polymer gives the average $M_w$ and $M_n$ from which the average of number of arms has been calculated. For each sample with MW less than 6000 g mol$^{-1}$, the number of arms begins at 2 (same as for the linear polymer) and increases rapidly with the molecular weight to reach 6 arms when the MW is 6000g mol$^{-1}$ or more (Figure 4.17 and Table 4.6, Entry 3-5). All the *D*-sorb-PCL samples synthesised using $Sn(Oct)_2$ were found to have an average of five or six number of arms by SEC$^{UC}$ MH plot.

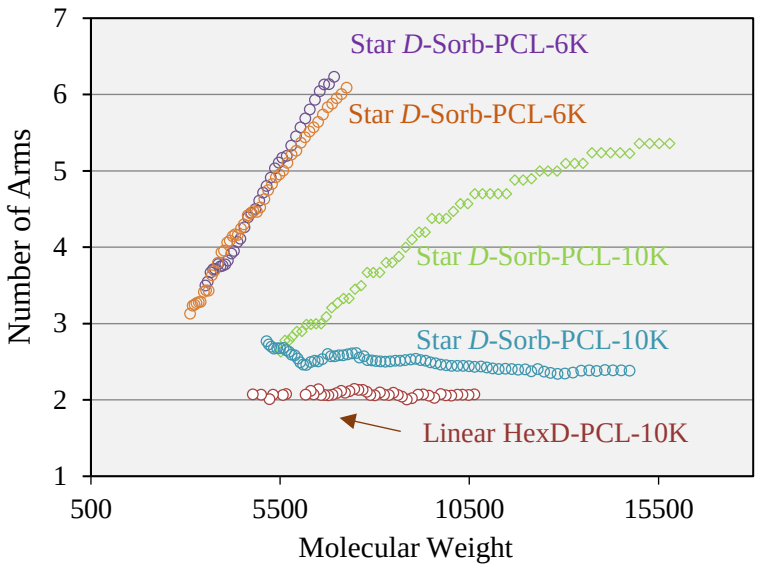



Figure 4.17. Star functionality *f* plot for linear and different star *D*-sorb-PCL polymers (obtained from equation 4.1.4). The lines in the plot are colour coded according to the samples in Table 4.6; where maroon for Entry 2, green for Entry 3, orange for Entry 4, purple for Entry 5 and finally the blue for Entry 6.

The *D*-sorb-PCL prepared using Novozym 435 catalyst has an average number of arms 2.5 which is slightly lower than the expected value of 3 arms (Figure 4.17 and Table 4.6, Entry 6). Interestingly, it showed a flat profile indicating that the number of arms is consistent across the molecular weight distribution. Indeed, this approach to determine the average number of arms of *D*-sorb-PCL samples synthesised using Sn(Oct) or Novozym 435 catalyst are close to those obtained by phosphorus NMR.

Table 4.6. Summary of the molecular weights by SEC-MALS, Phosphitylation-$^{31}$P and SEC-$^{UC}$ data of linear and the star-branched PCL. *R*g, η and Mark-Houwink (MH) conformation slope α of star *D*-sorbitol-PCL polymers prepared using different $Sn(Oct)_2$ and Novozym 435* catalyst.

| Entry | Solv. | Sample Name | SEC-MALS | 31-P NMR | SEC- Universal calibration Mark Houwink | | | | SEC-MALS | 31-P NMR |
|---|---|---|---|---|---|---|---|---|---|---|
| | | | $M_n$ SEC-MALS a (g mol$^{-1}$) | $M_n$ P-NMR b (g mol$^{-1}$) | $M_n$ SEC-UC c (g mol$^{-1}$) | MH K d | MH α d | $N_{arms}$ (SEC-UC) ($f$) e | $N_{arms}$ SEC-MALS/NMR f | $N_{arms}$ ($^{31}$P) g |
| Linear poly(ε-caprolactone) | | | | | | | | | | |
| 1 | Bulk | Bz-PCL-10K | 10000 | 9800 | 9500 | 80 | 0.60 | 2 | 1.0 | 1.0 |
| 2 | | HexD-PCL-10K | 10000 | 10100 | 10200 | 100 | 0.60 | 2 | 2.0 | 2.0 |
| Star poly(ε-caprolactone) | | | | | | | | | | |
| 3 | Bulk | *D*-Sorb-PCL-10K | 9000 | 9500 | 9600 | 520 | 0.37 | 5 | 5.1 | 5.2 |
| 4 | | *D*-Sorb-PCL-6K | 5600 | 5600 | 5000 | 680 | 0.27 | 5 | 5.1 | 5.1 |
| 5 | $scCO_2$ | *D*-Sorb-PCL-6K | 6100 | 6500 | 6800 | 380 | 0.39 | 6 | 4.9 | 5.0 |
| 6 | | *D*-Sorb-PCL-10K* | 10100 | 8400 | 8000 | 70 | 0.58 | 2.5 | 3.0 | 2.9 |

*Novozym 435 employed as a catalyst.
[a] Determined by SEC-MALS.
[b] Determined by phosphitylation $^{31}$P-method discussed in section 4.4.6.
[c] Determined by SEC-Universal Calibration.
[d] From Mark-Houwink (MH) equation: $[\eta] = kM^{\alpha}$
[e] Average number of arms *f* calculated following Eq. 4.12.
[f] Average number of arms estimated by SEC-MALS and $^1$H NMR.
[g] Average number of arms determined by phosphitylation - inverse gated decoupled $^{31}$P NMR spectra.

The conformation plot, in which the contraction factor (g) of the radius of gyration is plotted against molecular weight (Figure 4.18), shows a significant decrease of g with the molecular weight for $Sn(Oct)_2$ catalysed star *D*-sorb-PCL polymers (Figure 4.18, green, orange and purple circles). This indicates a more compact radius of gyration because the density increases with the higher number of arms (Burchard *et al.*[80]), which is 5 or 6 in our study.

For the $Sn(Oct)_2$ catalysed star PCL polymers, the conformation plots (Figure 4.18, green, blue and orange circles) are non-linear in nature, which is typical for branched polymers. The Novozym 435 catalysed star PCL (purple circles) showed a linear-like profile but the contraction factor is in between those of $Sn(Oct)_2$ catalysed stars and the HexD-PCL polymer (red circles), indicating that there are slight differences in branching between linear HexD-PCL and Novozym 435 catalysed stars.

For star *D*-sorb-PCL catalysed by Novozym 435 (Figure 4.18, purple circles), a slight increase in g with values close to 1 indicates that the density varies slightly (lower than the radius of gyration of linear HexD-PCL polymers), which are in agreement with the calculated arm number of 2.5 which is close to those of linear PCL polymers whose value is 2.

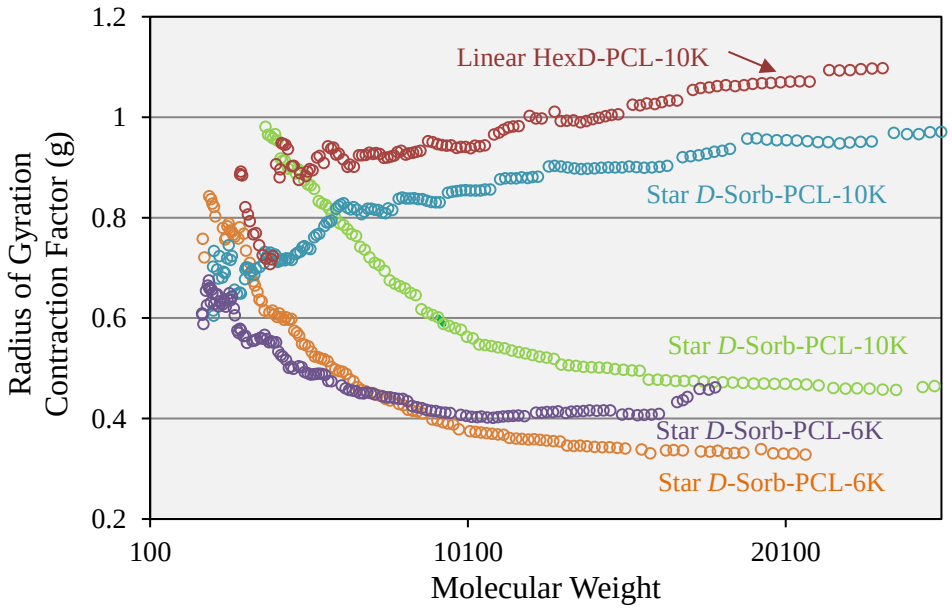



Figure 4.18. The conformation plots of the radius of gyration contraction factor (g) vs. MW for linear and different star *D*-sorbitol-PCL polymers. The lines in the plot are colour coded according to the samples in Table 4.6; where maroon for Entry 2, green for Entry 3, orange for Entry 4, purple for Entry 5 and finally the blue for Entry 6.

### 4.4.9 Thermal Analysis of Star Polyol-PCL by DSC

DSC (in $N_2$) was employed to investigate the thermal properties of polyol-PCL ($M_n$ $^{SEC\text{-}MALS}$ = 6000 g mol$^{-1}$, Table 4.2) synthesised in the presence of $Sn(Oct)_2$ and star *D*-sorbitol-PCL synthesised using Novozym 435 (Table 4.3). As expected, the polymers were semi-crystalline. The melting point of the polyol-PCL decreases with an increasing number of arms (Figure 4.19), which may hinder the formation of crystalline domains in PCL (Figure 4.20). This result is in agreement with a previous report by Endo *et al*.[20] who observed that a four-arm star PCL exhibited the lowest $T_m$ when compared to star PCL of similar molecular weights with three or two arms. The melting temperature ($T_m$) of the regular star *D*-sorbitol-PCL ($N_{arms}(^{31}P) = 5.1$) synthesised in the bulk using $Sn(Oct)_2$, ($T_m$ = 35 °C) is lower compared to the star *D*-sorbitol-PCL made by eROP in $scCO_2$ ($N_{arms}(^{31}P) = 3.2$, $T_m$ = 41 °C). This, in turn, is lower than the $T_m$ of the hexanediol-PCL synthesised in the bulk using $Sn(Oct)_2$ ($N_{arms}(^{31}P) = 2$, $T_m$ = 45 °C) (Table 4.7).

Table 4.7. DSC thermal analysis of star polyol-PCL of a variable number of arms catalysed by $Sn(Oct)_2$ and star *D*-sorbitol-PCL synthesised using Novozym.435.

| Sample [a] | $M_n$ $^{SEC\text{-}MALS}$ (star polymer) [b] (kg mol$^{-1}$) | $N_{arms}$ ($^{31}P$) [c] | $T_m$ (°C) [d] | $T_c$ (°C) [d] | ΔH (J/g) [e] |
|---|---|---|---|---|---|
| Hexanediol-PCL | 5.90 | 2.0 | 45 | 38 | 68 |
| Star Glycerol-PCL | 5.90 | 2.6 | 43 | 33 | 40 |
| Star Pentaerythritol-PCL | 5.80 | 3.0 | 40 | 32 | 72 |
| Star Triglycerol-PCL | 5.60 | 4.5 | 38 | 30 | 68 |
| Star *D*-Sorbitol-PCL | 5.60 | 5.1 | 35 | 24 | 62 |
| Star *D*-Sorbitol-PCL* | 5.65 | 3.1 | 42 | 33 | 72 |
| Star *D*-Sorbitol-PCL* | 8.80 | 3.2 | 41 | 31 | 64 |

[a] Polyol-PCL (polyol = hexanediol, glycerol, pentaerythritol, triglycerol, *D*-sorbitol).
[b] Molecular weight determined by SEC-MALS.
[c] Average number of arms by phosphitylation.
[d] Melting temperature and crystallisation temperature measured by DSC under nitrogen at a heating/cooling rate of 10 °C min$^{-1}$.
[e] Melting enthalpy measured by DSC.
* Star samples prepared using Novozym 435 catalyst.

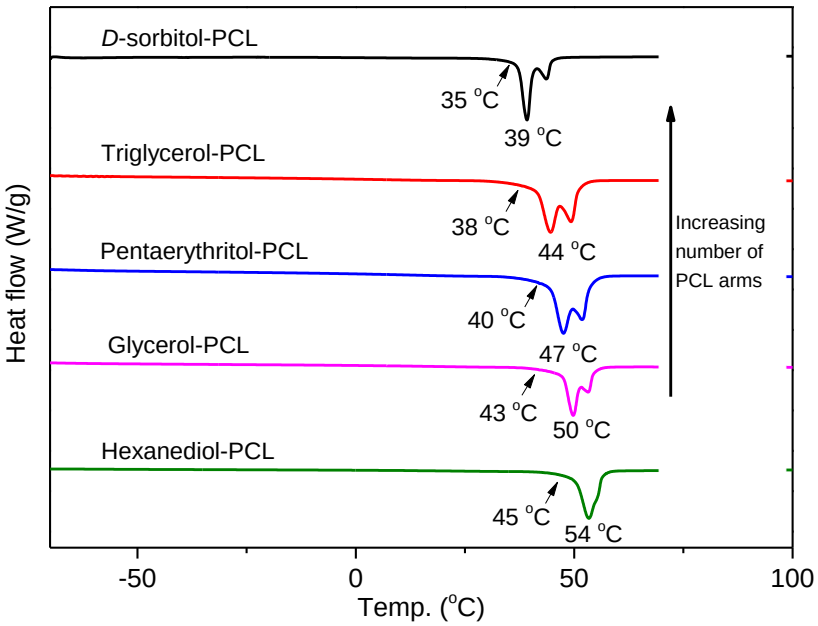



Figure 4.19. Comparison of DSC thermogram of polyol-PCL. The melting temperatures were obtained from the second heating scan.

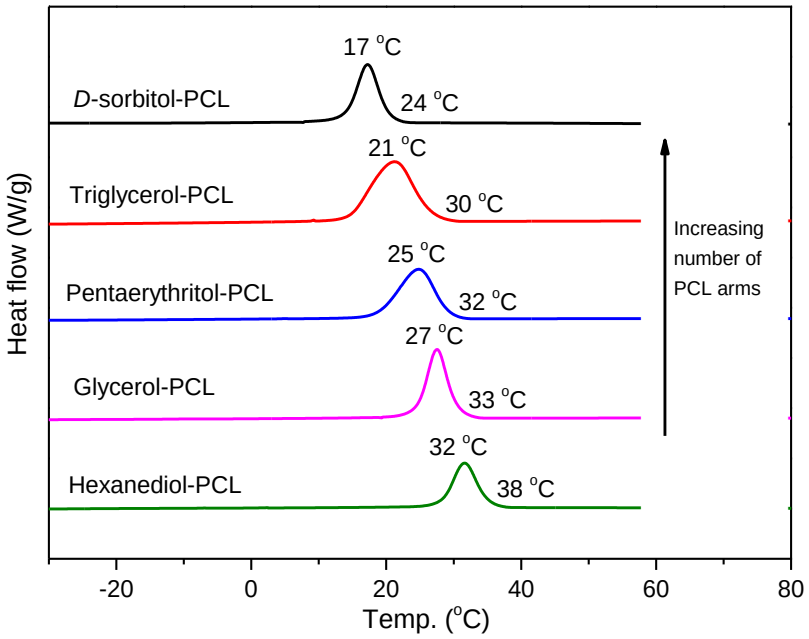



Figure 4.20. Comparison of DSC thermograms of polyol-PCL. The cooling scan from the melt after holding the sample at 120 °C for 10 min is shown.

Multiple melting peaks have also been reported in the literature for both linear poly(L-lactic acid)[81] and also for star-shaped poly(L-lactic) acid.[82] This observation is attributed to the presence of crystalline domains of different size and different perfection.

## 4.5 Conclusions

A sustainable route for star-shaped poly(ε-caprolactone) synthesis was implemented using renewable feedstock in clean solvents or in the absence of solvent ($scCO_2$ and bulk). The effect of the catalytic system ($Sn(Oct)_2$ and Novozym 435) on the architecture of star polymer was investigated in detail by NMR ($^1H$ and $^{31}P$), MALDI-TOF, SEC-MALS and Mark Houwink plot. Depending on the differences in architecture, the star polyol-PCLs show different thermal properties, where the melting temperature and crystallisation temperature decrease with increasing number of arms as evidenced by DSC.

Using $scCO_2$, the star synthesis can be performed at a significantly lower temperature (95 °C) as opposed to bulk synthesis (140 °C) with $Sn(Oct)_2$ catalyst. In addition, a significant reduction of the induction period (<15 h) was observed in $scCO_2$ in comparison to the bulk reaction (75 h) performed at the same temperature (95 °C) while maintaining a regular star architecture. Well-defined, star *D*-sorbitol-PCL with 5 arms, narrow dispersities ($Đ$ = 1.03-1.12) and an excellent agreement between targeted and experimental molecular weight ($M_n^{targ}$ = 6000 g mol$^{-1}$ and $M_n$ $^{SEC\text{-}MALS}$ = 5500 - 6100 g mol$^{-1}$) were achieved in both the bulk and in $scCO_2$.

The synthesis of star *D*-sorbitol-PCL by enzyme whether in the bulk (91% in 7 h at 60 °C) or in $scCO_2$ (96% in 7 h at 60 °C) is much faster even at significantly lower temperatures compared to the $Sn(Oct)_2$ catalyst in the bulk (97% in 10.5 h at 140 °C) and in $scCO_2$ (96% in 56 h at 95 °C).

Novozym 435 with a CaLB loading as low as 0.3 and 1 wt% was employed in $scCO_2$ which successfully resulted in star architectures of *D*-sorbitol-PCL with lower dispersities and higher molecular weight than in the bulk ($Đ$ = 1.23 – 1.24 vs. 1.34 – 1.36 and $M_n^{SEC\text{-}MALS}$ = 10100 – 8800 g mol$^{-1}$ vs. 5650 – 7800 g mol$^{-1}$). These data clearly highlight that a combination of $scCO_2$ and Novozym 435 could provide a fully green route to novel star polymers that completely avoids the use of volatile organic solvents and metal catalysts. The star architectures from eROP show a reduced number of arms ($N_{arms}$ close to 3) but longer individual arms when compared to those obtained from traditional catalyst $Sn(Oct)_2$. Moreover, the eROP route leaves residual unreacted hydroxy groups on the core, something that cannot be achieved by a metal catalyst.

## 4.6 References


1. Galbis, J. A., García-Martín, M. D. G., de Paz, M. V. & Galbis, E. Synthetic Polymers from Sugar-Based Monomers. *Chem. Rev.* **116,** 1600–1636 (2016).
2. Ren, J. M. *et al.* Star Polymers. *Chem. Rev.* **116,** 6743–6836 (2016).
3. Wu, W., Wang, W. & Li, J. Star polymers: Advances in biomedical applications. *Prog. Polym. Sci.* **46,** 55–85 (2014).
4. Aloorkar, N. H., Kulkarni, A. S., Patil, R. A. & Ingale, D. J. Star Polymers: An Overview. *Int. J. Pharm. Sci. Nanotechnol.* **5,** 1675–1684 (2012).
5. Cameron, D. J. A. & Shaver, M. P. Aliphatic polyester polymer stars: synthesis, properties and applications in biomedicine and nanotechnology. *Chem. Soc. Rev.* **40,** 1761–1776 (2011).
6. Higashihara, T., Hayashi, M. & Hirao, A. Synthesis of well-defined star-branched polymers by stepwise iterative methodology using living anionic polymerization. *Prog. Polym. Sci.* **36,** 323–375 (2011).
7. Fetters, L. J., Kiss, A. D., Pearson, D. S., Quack, G. F. & Vitus, F. J. Rheological Behavior of Star-Shaped Polymers. *Macromolecules* **26,** 647–654 (1993).
8. Schaefgen, J. R. & Flory, P. J. Synthesis of Multichain Polymers and Investigation of their Viscosities. *J. Am. Chem. Soc.* **70,** 2709–2718 (1948).
9. The return of a forgotten polymer : Polycaprolactone in the 21st century. (2010).
10. Woodruff, M. A. & Hutmacher, D. W. The return of a forgotten polymer - Polycaprolactone in the 21st century. *Prog. Polym. Sci.* **35,** 1217–1256 (2010).
11. Labet, M. & Thielemans, W. Synthesis of polycaprolactone: a review. *Chem. Soc. Rev.* **38,** 3484–3504 (2009).
12. Mohamed, R. M. & Yusoh, K. A Review on the Recent Research of Polycaprolactone (PCL). *Adv. Mater. Res.* **1134,** 249–255 (2015).
13. Buntara, T. *et al.* Caprolactam from Renewable Resources: Catalytic Conversion of 5-Hydroxymethylfurfural into Caprolactone. *Angew. Chemie Int. Ed.* **50,** 7083–7087 (2011).
14. Caretto, A., Noè, M., Selva, M. & Perosa, A. Upgrading of Biobased Lactones with Dialkylcarbonates. *ACS Sustain. Chem. Eng.* **2,** 2131–2141 (2014).
15. Thomas, S. M., DiCosimo, R. & Nagarajan, V. Biocatalysis: Applications and potentials for the chemical industry. *Trends Biotechnol.* **20,** 238–242 (2002).
16. Irfan, M. *et al.* Synthesis and meticulous molecular, morphological and thermal characterization of linear and star-shaped polycaprolactones. *RSC Adv.* **6,** 98117–98127 (2016).
17. Sobczak, M., Witkowska, E., Olędzka, E. & Kolodziejski, W. Synthesis and structural analysis of polyester prodrugs of norfloxacin. *Molecules* **13,** 96–106 (2008).
18. Huang, S., Xiao, J., Zhu, Y. & Qu, J. Synthesis and properties of spray-applied high solid content two component polyurethane coatings based on polycaprolactone polyols. *Prog. Org. Coatings* **106,** 60–68 (2017).
19. Dong, C.-M., Qiu, K.-Y., Gu, Z.-W. & Feng, X.-D. Synthesis of Star-Shaped Poly(ε-caprolactone)- b -poly( dl -lactic acid- alt -glycolic acid) with Multifunctional Initiator and Stannous Octoate Catalyst. *Macromolecules* **34,** 4691–4696 (2001).
20. Sanda, F., Sanada, H., Shibasaki, Y. & Endo, T. Star polymer synthesis from ε-caprolactone utilizing polyol/protonic acid initiator. *Macromolecules* **35,** 680–683 (2002).
21. Deokar, M. D., Idage, S. B., Idage, B. B. & Sivaram, S. Synthesis and characterization of well-defined random and block copolymers of ε-caprolactone with l -lactide as an additive for toughening polylactide: Influence of the molecular architecture. *J. Appl. Polym. Sci.* **133,** 1–12 (2016).
22. Lu, C. *et al.* Micellization and gelation of aqueous solutions of star-shaped PEG-PCL block copolymers consisting of branched 4-arm poly(ethylene glycol) and polycaprolactone blocks. *Eur. Polym. J.* **43,** 1857–1865 (2007).

23. Jia, Z., Zhou, Y. & Yan, D. Amphiphilic star-block copolymers based on a hyperbranched core: Synthesis and supramolecular self-assembly. *J. Polym. Sci. Part A Polym. Chem.* **43,** 6534–6544 (2005).
24. Marques, C., Tarek, R., Sara, M. & Brar, S. K. Sorbitol Production From Biomass and Its Global Market. *Platf. Chem. Biorefinery* 217–227 (2016). doi:10.1016/B978-0-12-802980-0.00012-2
25. Isikgor, F. H. & Becer, C. R. Lignocellulosic biomass: a sustainable platform for the production of bio-based chemicals and polymers. *Polym. Chem.* **6,** 4497–4559 (2015).
26. Cameron, D. J. A. & Shaver, M. P. Aliphatic polyester polymer stars: synthesis, properties and applications in biomedicine and nanotechnology. *Chem. Soc. Rev.* **40,** 1761–1776 (2011).
27. Goddard, A. R. *et al.* Controlled polymerisation and purification of branched poly(lactic acid) surfactants in supercritical carbon dioxide. *Green Chem.* **18,** 4772–4786 (2016).
28. Albertsson, A.-C. & Srivastava, R. K. Recent developments in enzyme-catalyzed ring-opening polymerization. *Adv. Drug Deliv. Rev.* **60,** 1077–1093 (2008).
29. Yang, Y. *et al.* Lipase/esterase-catalyzed ring-opening polymerization: A green polyester synthesis technique. *Process Biochem.* **46,** 1900–1908 (2011).
30. Uppenberg, J., Hansen, M. T., Patkar, S. & Jones, T. A. The sequence, crystal structure determination and refinement of two crystal forms of lipase B from Candida antarctica. *Structure* **2,** 293–308 (1994).
31. Kumar, A. & Gross, R. A. *Candida a ntartica* Lipase B Catalyzed Polycaprolactone Synthesis: Effects of Organic Media and Temperature. *Biomacromolecules* **1,** 133–138 (2000).
32. Deng, F. & Gross, R. A. Ring-opening bulk polymerization of ε-caprolactone and trimethylene carbonate catalyzed by lipase Novozym 435. *Int. J. Biol. Macromol.* **25,** 153–9 (1999).
33. Poojari, Y. & Clarson, S. J. Thermal stability of Candida antarctica lipase B immobilized on macroporous acrylic resin particles in organic media. *Biocatal. Agric. Biotechnol.* **2,** 7–11 (2013).
34. Comim Rosso, S. R., Bianchin, E., De Oliveira, D., Oliveira, J. V. & Ferreira, S. R. S. Enzymatic synthesis of poly(ε-caprolactone) in supercritical carbon dioxide medium by means of a variable-volume view reactor. *J. Supercrit. Fluids* **79,** 133–141 (2013).
35. Varma, I. K., Albertsson, A.-C., Rajkhowa, R. & Srivastava, R. K. Enzyme catalyzed synthesis of polyesters. *Prog. Polym. Sci.* **30,** 949–981 (2005).
36. Li, C., Tan, T., Zhang, H. & Feng, W. Analysis of the conformational stability and activity of Candida antarctica lipase B in organic solvents: Insight from molecular dynamics and quantum mechanics/simulations. *J. Biol. Chem.* **285,** 28434–28441 (2010).
37. Xue, L., Dai, S. Y. & Li, Z. Synthesis and Characterization of Three-Arm Poly(epsilon-caprolactone)-Based Poly(ester-urethanes) with Shape-Memory Effect at Body Temperature. *Macromolecules* **42,** 964–972 (2009).
38. Arumugasamy, S. K. & Ahmad, Z. Candida antarctica as catalyst for polycaprolactone synthesis: Effect of temperature and solvents. *Asia-Pacific J. Chem. Eng.* **6,** 398–405 (2011).
39. Rodrigues, R. C., Ortiz, C., Berenguer-Murcia, Á., Torres, R. & Fernández-Lafuente, R. Modifying enzyme activity and selectivity by immobilization. *Chem. Soc. Rev.* **42,** 6290–6307 (2013).
40. Cabrera, Z., Fernandez-Lorente, G., Fernandez-Lafuente, R., Palomo, J. M. & Guisan, J. M. Novozym 435 displays very different selectivity compared to lipase from Candida antarctica B adsorbed on other hydrophobic supports. *J. Mol. Catal. B Enzym.* **57,** 171–176 (2009).
41. Zhou, X. & Hong, L. Controlled ring-opening polymerization of cyclic esters with phosphoric acid as catalysts. *Colloid Polym. Sci.* **291,** 2155–2162 (2013).
42. Nalawade, S. P., Picchioni, F. & Janssen, L. P. B. M. Supercritical carbon dioxide as a green solvent for processing polymer melts: Processing aspects and applications. *Prog.*

*Polym. Sci.* **31,** 19–43 (2006).
43. Zhang, X., Heinonen, S. & Levänen, E. Applications of supercritical carbon dioxide in materials processing and synthesis. *RSC Adv.* **4,** 61137–61152 (2014).
44. Kröber, H. & Teipel, U. Microencapsulation of particles using supercritical carbon dioxide. *Chem. Eng. Process. Process Intensif.* **44,** 215–219 (2005).
45. Du, L., Kelly, J. Y., Roberts, G. W. & DeSimone, J. M. Fluoropolymer synthesis in supercritical carbon dioxide. *J. Supercrit. Fluids* **47,** 447–457 (2009).
46. García-Arrazola, R., López-Guerrero, D. A., Gimeno, M. & Bárzana, E. Lipase-catalyzed synthesis of poly-l-lactide using supercritical carbon dioxide. *J. Supercrit. Fluids* **51,** 197–201 (2009).
47. Santos, R. D. *et al.* Lipase-catalyzed synthesis of poly(e-caprolactone) in supercritical carbon dioxide. *Biocatal. Agric. Biotechnol.* **1,** 280–283 (2012).
48. Tsivintzelis, I., Pavlidou, E. & Panayiotou, C. Biodegradable polymer foams prepared with supercritical CO2-ethanol mixtures as blowing agents. *J. Supercrit. Fluids* **42,** 265–272 (2007).
49. Grignard, B., Stassin, F., Calberg, C., Jérôme, R. & Jérôme, C. Synthesis of biodegradable poly-epsilon-caprolactone microspheres by dispersion ring-opening polymerization in supercritical carbon dioxide. *Biomacromolecules* **9,** 3141–9 (2008).
50. Thurecht, K. J. *et al.* Kinetics of enzymatic ring-opening polymerization of ε-caprolactone in supercritical carbon dioxide. *Macromolecules* **39,** 7967–7972 (2006).
51. Loeker, F. C. *et al.* Enzyme-Catalyzed Ring-Opening Polymerization of -Caprolactone in Supercritical Carbon Dioxide. 2450–2453 (2004).
52. Curia, S., Barclay, A. F., Torron, S., Johansson, M. & Howdle, S. M. Green process for green materials: viable low-temperature lipase-catalysed synthesis of renewable telechelics in supercritical CO 2. *Philos. Trans. R. Soc. A Math. Phys. Eng. Sci.* **373,** 20150073 (2015).
53. Curia, S. & Howdle, S. M. Towards sustainable polymeric nano-carriers and surfactants: facile low temperature enzymatic synthesis of bio-based amphiphilic copolymers in scCO 2. *Polym. Chem.* 2130–2142 (2016). doi:10.1039/C6PY00066E
54. Yılmaz, M., Eğri, S., Yıldız, N., Çalımlı, A. & Pişkin, E. Ring-opening copolymerization of L-lactide and ε-caprolactone in supercritical carbon dioxide using triblock oligomers of caprolactone and PEG as stabilizers. *Polym. J.* **43,** 785–791 (2011).
55. Jerome, C. & Lecomte, P. Recent advances in the synthesis of aliphatic polyesters by ring-opening polymerization. *Adv. Drug Deliv. Rev.* **60,** 1056–1076 (2008).
56. Li, J., Spina, A., Moulijn, J. A. & Makkee, M. Sorbitol dehydration into isosorbide in a molten salt hydrate medium. *Catal. Sci. Technol.* **3,** 1540 (2013).
57. Taylor, P., Storey, R. F. & Taylor, A. E. Journal of Macromolecular Science , Part A : Pure and Applied Chemistry Effect of Stannous Octoate on the Composition , Molecular Weight , and Molecular Weight Distribution of Ethylene Glycol-Initiated Poly ( ϵ - Caprolactone ). *J. Macromol. Sci. Part A Pure Appl. Chem.* **35,** 723–750 (1998).
58. Storey, R. F. & Sherman, J. W. Kinetics and Mechanism of the Stannous Octoate-Catalyzed Bulk Polymerization of ε-Caprolactone. *Macromolecules* **35,** 1504–1512 (2002).
59. Bratton, D., Brown, M. & Howdle, S. M. Tin(II) Ethyl Hexanoate Catalyzed Precipitation Polymerization of ε-Caprolactone in Supercritical Carbon Dioxide. *Macromolecules* **38,** 1190–1195 (2005).
60. Goddard, A. R. *et al.* Controlled polymerisation and purification of branched poly(lactic acid) surfactants in supercritical carbon dioxide. *Green Chem.* **18,** 4772–4786 (2016).
61. Kendall, J. L. J. L., Canelas, D. A., Young, J. L. J. L. & DeSimone, J. M. Polymerizations in supercritical carbon dioxide. *Chem. Rev.* **99,** 543–563 (1999).
62. Labet, M. & Thielemans, W. Synthesis of polycaprolactone: a review. *Chem. Soc. Rev.* **38,** 3484 (2009).
63. Mei, Y., Kumar, A. & Gross, R. A. Probing water-temperature relationships for Lipase-catalyzed lactone ring-opening polymerizations. *Macromolecules* **35,** 5444–5448

(2002).
64. Uyama, H., Inada, K. & Kobayashi, S. Regioselectivity control in lipase-catalyzed polymerization of divinyl sebacate and triols. *Macromol. Biosci.* **1,** 40–44 (2001).
65. Kulshrestha, A. S., Gao, W. & Gross, R. A. Glycerol copolyesters: Control of branching and molecular weight using a lipase catalyst. *Macromolecules* **38,** 3193–3204 (2005).
66. Kobayashi, S. Lipase-catalyzed polyester synthesis – A green polymer chemistry. *Proc. Japan Acad. Ser. B* **86,** 338–365 (2010).
67. Uyama, H., Klegraf, E., Wada, S. & Kobayashi, S. Regioselective Polymerization of Sorbitol and Divinyl Sebacate Using Lipase Catalyst. *Chem. Lett.* **174,** 800–801 (2000).
68. Córdova, A., Iversen, T., Hult, K. & Martinelle, M. Lipase-catalysed formation of macrocycles by ring-opening polymerisation of ε-caprolactone. *Polymer (Guildf).* **39,** 6519–6524 (1998).
69. Spyros, A., Argyropoulos, D. & Marchessault, R. A study of poly (hydroxyalkanoate) s by quantitative 31P NMR spectroscopy: Molecular weight and chain cleavage. *Macromolecules* **30,** 327–329 (1997).
70. Ben, H. & Ragauskas, A. J. NMR characterization of pyrolysis oils from kraft lignin. *Energy and Fuels* **25,** 2322–2332 (2011).
71. Weissmuller, M. & Burchard, W. Viscosity of fractions from end-linked polystyrene star macromolecules. *Acta Polym.* **48,** 571–578 (1997).
72. Hu, J., Gao, W., Kulshrestha, A. & Gross, R. A. "Sweet Polyesters": Lipase-Catalyzed Condensation−Polymerizations of Alditols. *Macromolecules* **39,** 6789–6792 (2006).
73. Döring, A., Schneider, M., Wycisk, A. & Kuckling, D. Branching Analysis of Star Polymers by SEC. (2014).
74. Zimm, B. H. & Stockmayer, W. H. The Dimensions of Chain Molecules Containing Branches and Rings. *J. Chem. Phys.* **17,** 1301–1314 (1949).
75. Zimm, B. H. & Kilb, R. W. Dynamics of branched polymer molecules in dilute solution. *J. Polym. Sci.* **37,** 19–42 (1959).
76. Grubisic, Z., Rempp, P. & Benoit, H. A universal calibration for gel permeation chromatography. *J. Polym. Sci. Part B Polym. Lett.* **5,** 753–759 (1967).
77. Liu, J.-M., Chang, C.-S. & Tsiang, R. C.-C. Method of determining the degree of branching from the gel permeation chromatogram for star-shaped SBS thermoplastic block copolymers. *J. Polym. Sci. Part A Polym. Chem.* **35,** 3393–3401 (1997).
78. Zimm, B. H. & Kilb, R. W. Dynamics of branched polymer molecules in dilute solution. *J. Polym. Sci.* **37,** 19–42 (1959).
79. Hadjichristidis, N. *et al.* in *Polymer Science: A Comprehensive Reference, 10 Volume Set* **6,** 29–111 (2012).
80. Burchard, W. in *Light Scattering from Polymers* 1–124 (Springer Berlin Heidelberg, 1983). doi:10.1007/3-540-12030-0_1
81. Yasuniwa, M., Tsubakihara, S., Sugimoto, Y. & Nakafuku, C. Thermal analysis of the double-melting behavior of poly(L-lactic acid). *J. Polym. Sci. Part B Polym. Phys.* **42,** 25–32 (2004).
82. Zhao, Y. *et al.* Synthesis and thermal properties of novel star-shaped poly(l-lactide)s with starburst PAMAM–OH dendrimer macroinitiator. *Polymer (Guildf).* **43,** 5819–5825 (2002).

# Chapter 5
# Poly(ε-Caprolactone) – *Block* – Poly(Ethyl Phosphonate) Copolymers

## 5.1 Abstract

The anionic ring-opening polymerisation of ethyl phosphonate initiated by benzyl alcohol was performed in a solvent-free pathway using an organocatalyst, DBU and afforded a water-soluble poly(phosphoester) with a high control over molecular weight and narrow molecular weight distributions ($Đ$ < 1.12) up to full conversion. This approach was extended to prepare a linear amphiphilic diblock copolymer from a monohydroxy linear hydrophobic poly(ε-caprolactone) (PCL) as a macroinitiator. Subsequently, renewable bio-based PCL macroinitiators (dihydroxy HO-PCL-OH based on 1,6-hexanediol and star *D*-sorbitol-PCL-$OH_6$ based on *D*-sorbitol core) were employed to prepare a comprehensive set of novel amphiphilic poly(ε-caprolactone)-*block*-poly(ethyl phosphonate) block copolymers of variable topology (linear triblock and star diblock copolymers). Copolymers consisted of well-defined architectures, molecular weight, and composition of hydrophobic-hydrophilic blocks as confirmed by SEC, $^{1}$H and $^{31}$P NMR spectroscopies (including after phosphitylation reactions) and MALDI-TOF analyses. The aqueous self-assembly behaviour of the amphiphilic copolymers and their nanoparticle size in water were investigated by DLS and TEM and their surface-active properties were investigated by tensiometry.

Supercritical carbon dioxide ($scCO_2$) was exploited to efficiently extract the residual ethyl phosphonate monomer up to 98-99% from polymer products and to improve the yield of the polymer product compared to other purification techniques. We have shown some preliminary success in the synthesis of poly(phosphonate)s in $scCO_2$ using DBU as a catalyst at mild conditions (40 °C, 100 bar). The polymer products were systematically characterised by SEC, $^{1}$H and $^{31}$P NMR spectroscopies, and high resolution ESI-MS.

## 5.2 Introduction

Amphiphilic copolymers can have a wide variety of applications ranging from detergents, emulsifiers and cosmetics to medicines. Amphiphilic block copolymers are known to spontaneously self-assemble into (discrete) aggregates consisting of a hydrophobic core and hydrophilic shell (corona) in an aqueous medium.[1,2] The self-assembled aggregates induce the formation of advanced morphologies such as micellar or vesicular[2] conformations that have been widely investigated as nano-vehicles in the biomedical-pharmaceutical field.[3,4] The morphology of the aggregates depends on the design and the hydrophilic-lipophilic balance (HLB) of the primary structure (i.e. the composition of blocks, chain length, and sequence).[5] The conventional linear amphiphiles form aggregates (i.e. micelles) above their critical aggregation (micellization) concentration (CAC or CMC) and these aggregates are usually in thermodynamic equilibrium (exchange of individual components between the micelles and/or the solution occurs readily). However, the shape of the nanoaggregates highly depends on the concentration, temperature, solvent, and pH.[6] For instance, high dilution in the bloodstream causes disassembly of the nano-carriers and premature drug release.[6–8]

Branched amphiphilic macromolecules (dendrimers,[8,9] hyperbranched,[8,10,11] star polymers[6,8,10,12,13]) that possess different moieties of contrasting polarity, bound altogether in a covalently tethered three-dimensional core-shell system, are sometimes referred as "unimolecular micelles".[4,14–19] In sharp contrast to these conventional linear block copolymer micelles, these unimolecular micelles cannot de-assemble, thereby leading to the formation of monodisperse and structurally stable spherical macromolecules that are by nature not affected upon high dilution.[9,12,19–21]
Researchers have also reported independently the formation of large micelles (>100 nm) from the solution, self-assembly of dendrimers and hyperbranched polymers.[22] The question arises as to what drives the aggregation of the stable "unimolecular micelle"? Mai *et al.*[10] explained a mechanism for the hyperbranched star-like copolyether consisting of a hydrophobic hyperbranched poly[3-ethyl-3-(hydroxymethyl)oxetane] (HBPO) core and multiple hydrophilic poly(propylene oxide) (PPO) arms (Figure 5.1).

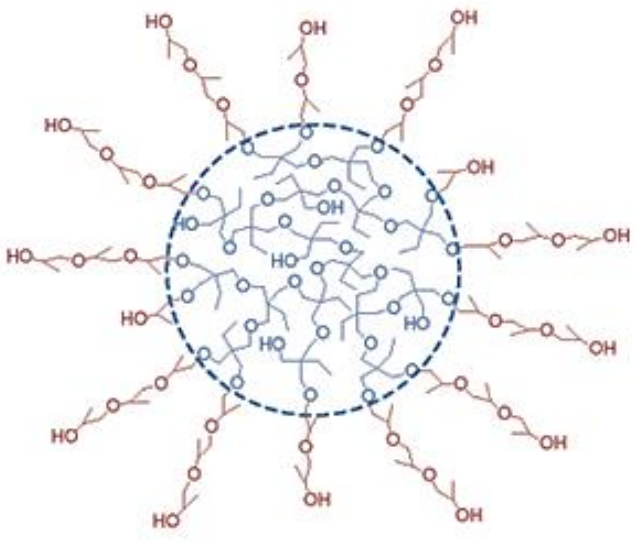



Figure 5.1. Hyperbranched poly[3-ethyl-3-(hydroxymethyl)oxetane]-star-poly(propylene oxide).[10]

The self-assembly behaviour in the HBPO-star-PPO polymer was attributed to two main factors; the hydrophobic interactions of HBPO in polymer due to their amphiphilic nature in water, and to the hydrogen bonds that are created in the structure of the "large micelles" ("unimolecular micelles") that causes such intermicellar interactions.[10] This explanation was supported experimentally by protecting the hydroxy end-groups of PPO with acetyl chloride that faded the colour of the micellar solution, and size of the micelles as measured by dynamic light scattering (DLS) sharply decreased from 225 nm to ~117 nm. This decrease in micelle size was attributed to decreased interaction (H-bonds) between hydroxy groups or between hydroxy groups and ether oxygen atoms in the self-assembly process of HBPO-star-PPO.[10] From this evidence, it was concluded that hydroxy groups play an important role in the self-assembly of dendritic HBPO-star-PPO copolyethers.[10]

Shortly after that, Hong *et al.*[23] proposed that hyperbranched polymers consisting of an HBPO core and many linear poly[2-(dimethylamino)ethyl methacrylate] (PDMAEMA) arms also form unimolecular micelles with size smaller than 10 nm in solution that can self-assemble into multimolecular micelle aggregates from nano to micro size aggregates (Figure 5.2 (a)).[23]. The driving force for the aggregation of the unimolecular micelles was hypothesised to be due to the interchain interaction (entangling, overlapping and crumpling of PDMAEMA arms) and to hydrophobic interactions (such as $–CH_3$ and $–CH_2CH–$) in PDMAEMA backbone during the self-assembly.[22] Thus, by

the multimolecular micelle aggregate mechanism they assumed that below the CMC, HBPO-star-PDMAEMAs exist as unimolecular micelles, and above the CMC they further aggregate together to form large multimolecular micelles driven by the intermolecular interaction among the PDMAEMA arms (Figure 5.2 (b)).[22]

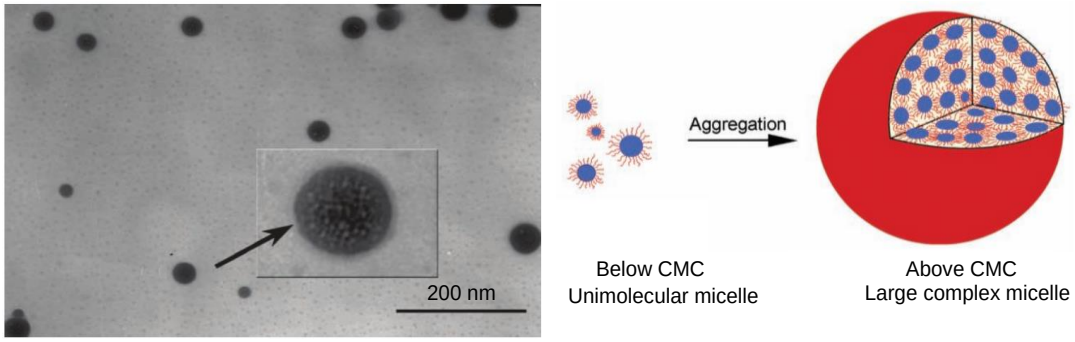



Figure 5.2. A TEM micrograph of large multimolecular micelle from HBPO- star -PDMAEMA (a) and the proposed self-assembly mechanism by the secondary aggregation of unimolecular micelles (b). The hydrophilic arms are in red, and the hydrophobic cores are in blue.[22,23]

In particular, star polymers have attracted significant attention in a wide range of applications due to their similar properties to dendrimers (such as condensed structure, a small hydrodynamic radius, multiple end groups per macromolecule and reduced viscosity).[24–26] One prominent example of star structure polymers is Tetronic (commercialised by BASF) which is a four-arm star poly(ethylene oxide)-*block*-poly(propylene oxide) (star PEO-*b*-PPO) block copolymer widely used in cosmetics, paper industry and petroleum industry.[27]

Amphiphilic star polymers, which integrate moieties of contrasting polarity within the structure, can essentially offer some real benefits over amphiphilic linear polymers, such as reduced CMCs or even the possibility of forming stable unimolecular micelles.[28] The improved micelle stability (e.g. upon dilution) arises from the fact that star polymers are indeed multiple linear polymers covalently connected together so that de-assembly is no longer possible. Broadly, amphiphilic star polymers are classified into three types: layered amphiphilic star block copolymers, segmented amphiphilic miktoarm polymers and star-dendrimer hybrids (Figure 5.3).[8]

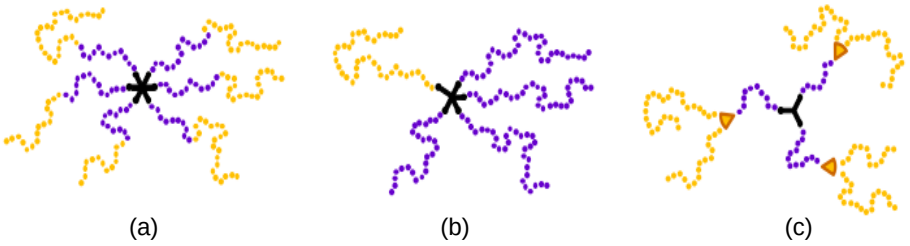



Figure 5.3. Major classification of amphiphilic star polymers: (a) layered amphiphilic star block copolymers, (b) amphiphilic miktoarm star polymer and (c) amphiphilic star-dendrimer hybrid copolymers.[8]

Among all of the star-like polymers, polyesters constitute an attractive class of compounds because they are biodegradable and biocompatible.[29] Indeed, most common FDA approved polyesters that are employed as a hydrophobic segment are poly(lactic acid) (PLA), poly(ε-caprolactone) (PCL), and poly(glycolic acid).[4] However, they possess limited application due to their hydrophobic nature, semi-crystalline properties, and the absence of functionality on the polymer backbone.[30] Thus, a hydrophilic segment is required to promote the applications of these hydrophobic polymers into aqueous dispersed media.

Among the choices of hydrophilic segments, poly(ethylene glycol) (PEG) is today's gold standard in the biomedical field,[31] because it has high water solubility, low toxicity and low immunogenicity. However, PEG is non-biodegradable and it has limitations because there is evidence of accumulation of toxic by-products from uncontrolled and undesirable oxidative degradation. These have raised some serious concerns recently.[32–35] As a consequence, researchers are developing alternative hydrophilic polymers to PEG such as poly(amino acid)s,[36,37] poly(2-oxazoline)s,[38–41] poly(peptoid)s,[42–44] and poly(phosphoester)s[45] (PPE)s.

In this Chapter, focus is placed on cyclic phosphoester monomers. Indeed, the corresponding polymers can be hydrophilic and present numerous opportunities. In the 1970s, Penczek and co-workers were the first to pioneer the synthesis of cyclic six-membered phosphoesters by cationic or anionic ring-opening polymerisation.[46–49] Since then, many researches have demonstrated the high biocompatibility of PPE and shown the enzymatic (e.g. using alkaline phosphatases) or hydrolytic degradation of PPEs under physiological environment.[45,50–55] More importantly, the pentavalency of phosphorous provides flexibility in functionalisation of the side-chain. Consequently, the structurally versatile PPEs can be classified into five important subclasses:

poly(alkylene H-phosphonate)s, poly(phosphate)s, poly(phosphoramidate)s, side-chain poly(phosphonate)s and in-chain poly(phosphonate)s/(phostones)[56] (Figure 5.4).[54–58]

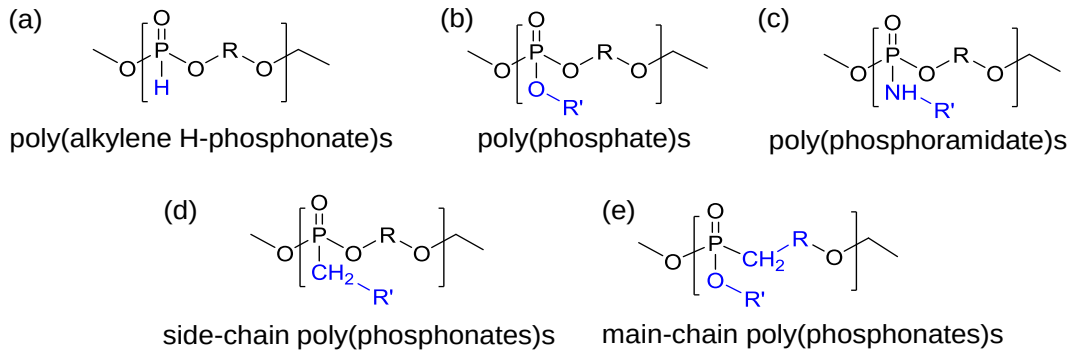



Figure 5.4. The important subgroup of PPEs: (a) poly(alkylene H-phosphonate)s, (b) poly(phosphate)s, (c) poly(phosphoramidate)s, (d) side-chain poly(phosphonate)s and in-chain poly(phosphonate)s.[54–58]

The chemical and mechanical properties of PPEs can be easily modified from amorphous, water-soluble to crystalline and stiff plastics by simply tuning the backbone and side-chain and they found application in a broad range of fields such as flame-retardant, tissue engineering and drug delivery.[45,51,53–55,59–61]

Nonetheless, poly(phosphate)s are known to exhibit rapid degradation. However, remarkable thermal stability and hydrolytic stability are achieved when P–O– in poly(phosphate)s is substituted by P–C– in poly(phosphonate)s.[57,62] The first, well-defined, non-toxic, water-soluble poly(phosphonate) with narrow dispersity was prepared by Wurm and co-workers in 2014 by anionic ring-opening polymerisation (AROP) of a five-membered ring with a methyl side chain and an ethylene in the backbone (Figure 5.5 (a))[62] The length of the pendant alkyl group was varied by Wolf *et al.*[57] and excellent water solubility (up to 25 g $L^{-1}$) of poly(methyl–, ethyl– and iso-propyl phosphonate) without a temperature dependent phase separation and with no toxicity against HeLa cells was demonstrated. The poly(butyl phosphonate), by contrast, exhibits lesser solubility, shows concentration-dependent cloud point (Lower Critical Solution Temperature) and exhibit toxicity against HeLa cells (Figure 5.5).[57]

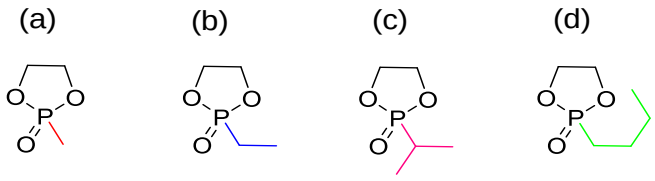



Figure 5.5. Cyclic poly(alkyl phosphonates) where (a-c) are water soluble and non-toxic while (d) is less water-soluble and exhibits toxicity against HeLa cells.[57]

It is worth noting that all the non-toxic polyphosphates above-mentioned are water-soluble but not amphiphilic. Studies have been conducted on amphiphilic polymers of poly(phosphate)s with PCL. These block copolymers have been prepared by ROP of cyclic poly(ethyl ethylene phosphate) (PEEP) from hydrophobic PCL core using $Sn(Oct)_2$ as a catalyst (a well-established method).[30,53,61,63–65] These amphiphilic copolymers demonstrate the formation of spherical nanoparticles or vesicles and have shown potential as a drug delivery systems.[30,53,61,63,64] However, using $Sn(Oct)_2$ as a catalyst limits the control of the polymerisation, and pronounced transesterification reactions occur with poly(phosphate)s because of the presence of potentially cleavable side P–O– bond. The polymer also contains metal derived cytotoxicity.[66,67]

To address these problems, Iwasaki *et al*.[68] was the first to reveal the organocatalysed AROP of phosphates, 2-isopropoxy-2-oxo-1,3,2- dioxaphospholanes, by employing 1,8-diazabicyclo[5.4.0]undec-7-ene (DBU) and 1,5,7-triazabicyclo- [4.4.0]dec-5-ene (TBD).[68] Later, the use of a metal-free organocatalyst and thiourea as a cocatalyst was exploited for poly(phosphate) synthesis to minimise the inter- and intramolecular side-reactions and obtain high MW (up to 70000 g $mol^{-1}$) whilst maintaining low dispersity ($Đ$ = 1.10).[67] However, the major drawback of this system was the use of high quantities of co-catalyst and the problem of removal of both catalysts from the polymer.[62] By contrast, for phosphonates, the major side reactions that broaden dispersity are restricted because the pendant chain in the linear poly(phosphonate)s cannot be exchanged by transesterification reactions as witnessed for polyphosphates.[62,69] To the best of our knowledge, amphiphilic block copolymers containing poly(phosphonate) functional groups and hydrophobic polyesters (PCL or PLA) have not been reported yet.

Additionally, when Iwasaki[68] first performed the AROP of cyclic phosphates using DBU or TBD, the reaction was reported either in the bulk or using a small amount of

toluene. However, the AROP of the cyclic phosphonates has always been reported in dichloromethane (DCM), a volatile organic compound.
To the best of our knowledge, only two publications have reported the organocatalysed ring opening using DBU as a catalyst in $scCO_2$: first by Blakey *et al.*[70] and then by Grignard *et al.*[71] and both were focusing towards the synthesis of hydrophobic PLA. Indeed, the latter research group have employed a dihydroxy poly(phosphate)s as a macroinitiator but only to grow PLA block in $scCO_2$ using DBU and a thiourea as a cocatalyst. But the synthesis of the poly(phosphate)s macroinitiator was performed in toluene[67] and not in $scCO_2$.[71] Thus, no attention has been paid yet towards the AROP of cyclic alkyl phosphonate monomers using $scCO_2$.

A key aim of this Chapter is to determine if such amphiphilic polymers could be formed through a sustainable route and how they might function. To begin with, the first objective of this Chapter is to investigate whether AROP of the ethyl phosphonate (EP) can be performed in a solvent-free pathway using DBU as a catalyst. Could such synthesis yield a well-defined poly(ethyl phosphonate) (PEP) in the bulk system? A part of this Chapter is also dedicated to exploiting the opportunities provided by $scCO_2$. Could the PEP homopolymer be made in $scCO_2$ and could the residual EP be extracted from it using supercritical $CO_2$ fluid extraction (SCFE) technology?

Furthermore, how would the control be when these solvent-free synthesis protocols will be extended to prepare block copolymers? Could this approach synthesise more complex block-copolymer architecture (a star-like topology)? Can the hydrophilicity of the copolymers be tuned? Could these amphiphilic block copolymers be purified utilising SCFE purification method and would it afford any benefit over conventional purification methods?

Finally, could these structures be self-dispersible in water (unimolecular micelles), and would they induce self-assembly in water (aggregates of unimolecular micelles)? Could these novel branched amphiphiles possess some surface–active properties and how would they perform?

## 5.3 Experimental Section

### 5.3.1 Materials

2-Ethyl-2-oxo-1,3,2-dioxaphospholane (EP) was synthesised according to the procedure described by Wurm and coworkers.[72] 1,8-diazabicyclo[5.4.0]undec-7-ene (DBU, 98%) and anhydrous benzyl alcohol (BzOH, 99.8%) were purchased from Sigma-Aldrich. Acetone (ACS grade) was obtained from VWR chemicals and used as received. Synthesis linear benzyl-PCL-OH (Bz-$PCL_{19}OH$), telechelic OH-PCL-OH and star *D*-sorbitol-poly(ε-caprolactone)$_n$$OH_x$ has been discussed in the previous Chapter. These hydrophobes were used as macroinitiator in this Chapter and the analytical results are presented in Table 5.2 and Table 5.3.
Ultrapure water with a resistivity of 18.2 MΩ $cm^{-1}$ was obtained from the Milli-Q system (Merck Millipore®). Regenerated cellulose dialysis membranes with a molecular weight cut-off (MWCO) of 1000 g $mol^{-1}$, Spectra/Por® 7, were purchased from Carl Roth.

### 5.3.2 Synthesis of ethyl phosphonate (EP) monomer

Ethyl phosphonate monomer was synthesised according to the two-step literature procedure.[57]

**Synthesis of ethyl phosphonic dichloride (1).** Briefly, a mixture of *O*, *O*-diethyl ethyl phosphonate (252.8 g, 1.52 mol) and DMF (1.26 mL) was added dropwise to refluxing thionyl chloride (275.9 mL, 3.80 mol). Strong gas evolution of methylene chloride and sulfur dioxide indicated the progress of the reaction. After 24 h the gas evolution declined. Fractionated distillation of the raw product yielded the desired ethyl phosphonic dichloride as a colourless liquid (202.0 g, yield 99.9%, b.p 40-42°C /7 × $10^{-2}$ mbar). $^1$H NMR (300 MHz, $CDCl_3$) $\delta$ (ppm) 2.53 (dq, $^2J_{HP}$ = 15 Hz, $^3J_{HH}$ = 7.5 Hz, 2H), 1.32 (dt, $^3J_{HP}$ = 30 Hz, $^3J_{HP}$ = 7.5 Hz, 3H). $^{31}$P{H} NMR (121 MHz, $CDCl_3$) $\delta$ = 54.72.

**Synthesis of 2-ethyl-2-oxo-1,3,2-dioxaphospholane (2).** A flame-dried three-necked round bottom flask of 2000 mL equipped with a magnetic stirring bar and two dropping funnels was charged with 400 mL of dry THF under an inert atmosphere and cooled to –21 °C in an ice-bath. Ethyl phosphonic dichloride (153.4 g, 1.04 mol) was dissolved

in dry THF (400 mL) and transferred into one dropping funnel *via* a flame-dried stainless-steel capillary. A solution of dry ethylene glycol (64.8 g, 1.04 mol) and dry pyridine (165.1 g, 2.08 mol) in THF (168.5 mL) was transferred into the second dropping funnel *via* a flame-dried stainless-steel capillary. Dropping speed was adjusted to be approximately equal for both mixtures. After complete addition, the solution was stirred for 6 h and stored overnight at –28 °C to facilitate the precipitation of the pyridinium hydrochloride by-product. The precipitate was removed by filtration *via* a flame-dried Schlenk funnel and the solvent was removed at reduced pressure ($10^{-1}$ - $10^{-2}$ mbar). First fractionated distillation yielded the product as a yellow liquid (92.6 g, yield: 70 %, b.p. 67.°C/ $1 \times 10^{-2}$ mbar). Second fractionated distillation yielded the desired product as a colourless liquid (86.3 g, yield 61 %, b.p. 61 °C/ $2.1 \times 10^{-3}$ mbar). The monomer was stored under an inert atmosphere at -20 °C.

**Ethyl phosphonate**. $^{1}$H NMR (300 MHz, $CDCl_3$) $\delta$ (ppm) 4.50 − 4.24 (m, 2H, –P–O–C$H_2$–), 4.19 – 4.00 (m, 2H, –P–O–C$H_2$–), 1.80 (dq, $^{2}J_{HP}$ = 17.8 Hz, $^{3}J_{HH}$ = 7.6 Hz, 2H, –P–C$H_2$–), 1.03 (dt, $^{3}J_{HP}$ = 21.0 Hz, $^{3}J_{HH}$ = 7.7 Hz, 3H, –$CH_3$). $^{13}$P {H} NMR (121 MHz, $CDCl_3$) $\delta$ 52.51.

### 5.3.3 Polymerisation of ethyl phosphonate by AROP using DBU

**Solvent, DCM.** A representative procedure for anionic ring-opening polymerisation (AROP) of phosphonate monomer for $M_n^{targ}$ (PEP block) of 6260 g mol$^{-1}$, EP (182 mg, 1.34 mmol), benzyl alcohol (3.15 mg, $2.9 \times 10^{-2}$ mmol) as an initiator, DBU (4.41 mg, $2.9 \times 10^{-2}$ mmol, 1.0 equivalent with respect to benzyl alcohol) and anhydrous DCM (2.2:1 v/v of solvent: monomer + initiator) were introduced in a flame-dried schlenk tube. The reaction mixture was stirred at 30 °C under argon for 16 h, and the % monomer conversion was 97% monitored by $^{1}$H and $^{31}$P NMR The resulting polymer was purified by precipitation in cold diethyl ether (65 ± 2% gravimetric yield) and dried under reduced pressure.

**Solvent-Free, Bulk.** The bulk AROP of EP ($M_{EP}$ = 136.02 g mol$^{-1}$) for $M_n^{targ}$ of 2720 g mol$^{-1}$was conducted following the same method as described above but without solvent at 40 °C under inert argon atmosphere for 2 hours to reach 95% monomer conversion by $^{1}$H and $^{31}$P NMR. A sample was also withdrawn for SEC analysis.

**Synthesis Using $ScCO_2$.** The AROP of EP in $scCO_2$ was performed in an 8 mL stainless steel base coupled with an octahedral magnetic stirring bar (size 10 mm × 2.5 mm). The autoclave was dried in an oven at 90 °C for 1 h prior use. For molecular weight targeted ($M_n$ $^{targ}$) of 2720 g mol$^{-1}$ (i.e. $DP_n$ $^{targ}$ = 20), EP (150 µL, 190 mg, 1.39 mmol) and BzOH (7.2 µL, 7.5 mg, 6.9 × 10$^{-2}$ mmol) were added to the autoclave and it was immediately sealed after introduction of the catalyst DBU (10.4 µL, 6.9 ×10$^{-2}$ mmol) under argon. The autoclave was heated to 40 °C and pressurised to 100 bar using $scCO_2$. The reaction mixture was kept under these conditions (40 °C, 100 bar) for 16 h, stirring at 300 rpm and stopped by venting $CO_2$ at 16 °C. An aliquot was withdrawn to determine conversion by $^1$H NMR (discussed in section 5.4.2.3).

**Poly(ethyl phosphonate) (PEP).** $^1$H NMR (400 MHz, DMSO-$d_6$) $\delta$ (ppm) 7.48 – 7.31 (m, aromatic proton), 5.02 (dd, $J$ = 8.0, 5.7 Hz, aryl –C$H_2$–), 4.43 – 4.22 (m, backbone, –C$H_2$–C$H_2$–), 3.56 (m, backbone terminal –C$H_2$–), 1.84 – 1.74 (m, side-chain – P– C$H_2$– ), 1.1 – 1.01 (m, side-chain –C$H_3$).

### 5.3.4 Synthesis of PCL-*b*-PEP diblock and triblock copolymer in the bulk

A specific example of the general procedure used to synthesise *initiator*-poly(ε-caprolactone)-*block*-poly(ethyl phosphonate) (*i*-PCL$_n$-*b*-PEP$_m$) diblock copolymers (linear and star) by bulk AROP using DBU is described in the following section (analytical data is in Table 5.2).

A linear Bz-PCL-*b*-PEP diblock copolymer of $M_n^{targ}$ (PEP block) of 6100 g mol$^{-1}$ (i.e. $DP_n$ $^{targ}$ = 45) was synthesised using linear benzyl-PCL-OH (Bz-PCL$_{19}$-OH) as a macroinitiator. Purified and vacuum dried Bz-PCL$_{19}$OH (85.6 mg, 3.72 × 10$^{-2}$ mmol, $M_n^{NMR}$ (macroinitiator) = 2300 g mol$^{-1}$, $Đ$ = 1.02) and EP (227 mg, 1.67 mmol) was charged to a flame-dried Schlenk tube (3 mL), degassed with argon for 30 min while stirring (300 rpm). The Schlenk tube was homogenised at ~55-60 °C for 15-20 min. An aliquot was also withdrawn to ensure there is no initiation at this stage. The catalyst, DBU, (5.6 mg, 3.72 × 10$^{-2}$ mmol, 1.0 equimolar respect to hydroxy on the initiator) was added under inert atmosphere and the polymerisations were conducted for 2 h for linear materials (or more as specified in Table 5.3) to reach monomer conversions of ~88-99% as monitored by $^1$H NMR. In general, polymers were purified either by dialysis to give a gravimetric yield of 67 ± 5% or by SCFE to give a 92 ± 5 % gravimetric yield after purification.

The linear triblock poly(ethyl phosphonate)-*block*-poly(caprolactone)-*block*-poly(ethyl phosphonate) ($PEP_m$-*b*-$PCL_n$-*b*-$PEP_m$) copolymers and star diblock copolymers were synthesised following the same procedure and using the specified molar ratio of feedstock (Table 5.2 and Table 5.3).

**Bz-PCL-*b*-PEP.** $^1$H NMR (400 MHz, DMSO-$d_6$) $\delta$ (ppm) 7.42 – 7.30 (m, aromatic proton), 5.08 (s, aryl –C$H_2$–), 4.86 (t, terminal –O–*H*), 4.43 – 4.22 (m, backbone, –C$H_2$–C$H_2$–), 3.99 (t, methylene ester –C$H_2$OCO– of PCL), 3.95 – 3.90 (m, broad, last methylene ester –C$H_2$OCO– of PCL and methylene in β position of terminal PEP –OP(=O)–C$H_2$–C$H_2$–OH), 3.74 (t, $J$ = 5.2 Hz), 3.56 (m, terminal –C$H_2$–OH), 2.28 (t, methylene in α position to carbonyl group –C$H_2$–CO– of PCL), 1.84 – 1.64 (m, side-chain –P–C$H_2$–), 1.64  1.43 (m,–$COCH_2CH_2CH_2CH_2CH_2O$–), 1.36  1.20 (m, $COCH_2CH_2CH_2CH_2CH_2O$), 1.14 – 0.97 (m, side-chain –C$H_3$).

### 5.3.5 Synthesis of Star PCL-*b*-PEP Diblock Copolymers in DCM

The synthesis of star *D*-sorbitol-PCL with variable length of PCL arm was discussed in Chapter 4. These star PCL were employed as macroinitiators to synthesise star *D*-sorbitol-poly(ε-caprolactone)-*block*-poly(ethyl phosphonate) (star *D*-sorbitol-$PCL_n$-*b*-$PEP_m$) diblock copolymers.

A representative procedure for the synthesis of star PCL-*b*-PEP diblock copolymers with $M_n^{\ targ}$ (PEP block) of 6260 g mol$^{-1}$ (i.e. $DP_n^{\ targ}$ = 46) is as follow. EP (260 mg, 1.91 mmol) monomer and dried star *D*-sorbitol[$PCL_{57}OH_5$]OH as an initiator (278 mg, $4.15 \times 10^{-2}$ mmol, $M_n^{NMR}$ (macroinitiator) = 6700 g mol$^{-1}$, $Đ$ =1.04) were introduced into a flame dried Schlenk tube equipped with a magnetic bar (stirring at 300 rpm) under inert conditions. DBU (38 mg, 0.25 mmol, 1.0 equimolar per hydroxy group of *D*-sorbitol) and anhydrous DCM (~1.2 mL, where the ratio of DCM: monomer + initiator = 2.2:1 wt%) were transferred to the flask under an inert atmosphere. The polymerisations were conducted at 30 °C for 5 h (or reaction times specified in Table 5.3), to reach monomer conversions of ~89-93% as monitored by $^1$H NMR. Excess of DCM was removed under reduced pressure. The reaction mixture was purified by dialysis or by SCFE (refer to section 5.4.4 for protocols). Finally, lyophilisation gave an off-white waxy solid to glue-like colourless sticky paste (Table 5.4) based on the composition of blocks. The gravimetric yield of 60 ± 5%.

**Star *D*-sorbitol-PCL$_n$-*b*-PEP$_m$.** $^1$H NMR (400 MHz, DMSO-$d_6$) $\delta$ (ppm) 4.85 (s, –O*H*), 4.43 4.22- (m, phosphonate backbone –C*H*$_2$C*H*$_2$–), 3.99 (t, methylene ester –C*H*$_2$OCO– of PCL), 3.96 – 3.87 (m, broad, last methylene ester –C*H*$_2$OCO– of PCL and methylene in β position of terminal PEP –OP(=O)–C*H*$_2$–CH$_2$–OH), 3.55 (m,– C*H*$_2$– OH), 2.28 (t, methylene in α position to carbonyl of PCL –C*H*$_2$–CO), 1.84 – 1.64 (m, side-chain –P–C*H*$_2$–), 1.64 1.43 (m,–COCH$_2$C*H*$_2$CH$_2$C*H*$_2$CH$_2$O–), 1.36 1.20 (m, COCH$_2$CH$_2$C*H*$_2$CH$_2$CH$_2$O), 1.14 – 0.97 (m, side-chain –C*H*$_3$).

### 5.3.6 View-Cell Study of Ethyl Phosphonate using scCO$_2$

The effect of $CO_2$ on EP was visualised using a fixed volume view cell (100 mL). In a typical experiment, ~200 mg of the EP monomer was added into a glass vial and placed in the view cell. The windows were sealed and clamped to the body and $CO_2$ was added up to 50 bar. The temperature and $CO_2$ pressure were raised incrementally, as required (up to 80 °C and 260 bar). The autoclave was allowed to cool down to ambient temperature and vented at T<20 °C, P = 50 bar at 3-4 bar min$^{-1}$ (low flow rate).

### 5.3.7 Purification of Polymers

**Supercritical CO$_2$ Fluid Extraction (SCFE) Method.** As a general procedure, typically 1.00 - 3.00 g of crude polymer product was added in a 20 mL or 60 mL autoclave. Extractions were typically conducted at 38 ± 2 °C and 140 ± 5 or 180 ± 5 bar at a constant flow rate under mechanical stirring at 200 rpm. The extraction efficiency of each sample was monitored by taking an aliquot from the base after every 10 min (and the extract was analysed simultaneously after each step).

**Dialysis by a Semi-Permeable Membrane.** The crude product (0.25 – 1.0 g) was dissolved in a mixture of acetone and water (typically 0.5:6 mL v/v) and dialysed against water (200 – 250 mL) for 6 h. Followed by lyophilisation to obtain a dry product.

## 5.4 Results and Discussion

This Chapter has been divided into four key areas:

1) Homopolymer poly(2-ethyl-2-oxo-1,3,2-dioxaphospholane) (PEP) has been first synthesised. To this aim, 2-ethyl-2-oxo-1,3,2-dioxaphospholane (EP) monomer was synthesised according to a two-step procedure described by Wurm and co-workers.[72] Based on the protocol for AROP of EP reported in conventional DCM solvent[72] using DBU, we optimised the AROP polymerisation of EP in solvent-free condition and then an attempt for $scCO_2$ mediated AROP is discussed. The purification of the homopolymer is discussed by conventional methods (precipitation and dialysis) and by alternative greener SCFE approach.

2) Subsequently, the synthesis of linear poly(ε-caprolactone)-*block*-poly(ethyl phosphonate) (PCL-*b*-PEP) diblock and triblock copolymers in the bulk and assessing purification by different routes is discussed.

3) The research then moves towards more different molecular architectures such as star diblock copolymers synthesis, in DCM and in the bulk using DBU catalyst, by employing well-defined renewable star *D*-sorbitol-PCL cores (discussed in Chapter 4). These copolymers consist of PCL as a hydrophobic block (macroinitiator) and PEP as a hydrophilic block.

The preparation and representative structures of all the different copolymer architectures are illustrated in Figure 5.13 and Figure 5.19.

4) Finally, the self-assembly behaviour in aqueous solution of the so-formed amphiphilic copolymers and their morphology assessment by microscopy methods will be discussed.

### 5.4.1 Ethyl Phosphonate (EP) Monomer Synthesis

2-Ethyl-2-oxo-1,3,2-dioxaphospholane was synthesised according to a two-step procedure described by Wurm and coworkers (Figure 5.6).[72]

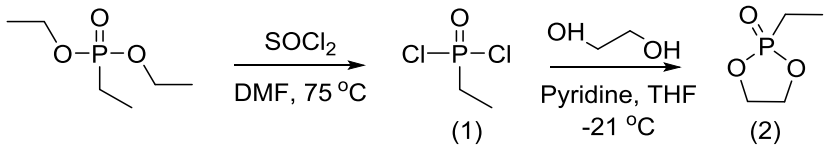



Figure 5.6. Synthesis of monomer 2-ethyl-2-oxo-1,2,3-dioxaphopholane in two-steps. By chlorination of *O, O*-diethyl ethyl phosphonate and subsequent ring closing of (1) with ethylene glycol.

In the first step, the *O, O*-diethyl-ethyl phosphonate was chlorinated with thionyl chloride to give ethyl phosphonic acid dichloride. Because it was a big scale ~202 g, the yield doubled to almost 100 % from 50 % given in the literature.[72] The second step is the ring-closing reaction. Generally, an equal volume of the THF is used in the reaction flask and in both the dropping funnels, which contain an equimolar amount of both reactive (ethylphosphonic acid dichloride (1) and ethylene glycol (EG)) (refer to section 5.3.2). However, when a higher concentration of (1) in THF and EG were taken in the dropping funnel and a low concentration of the THF was present in the reaction flask, yield was better compared to the literature (yield improved to 86.3 g for 61 % vs. 36 % given in the literature).[72].

### 5.4.2 Linear Homo PEP by AROP in DCM, in the Bulk and in $scCO_2$

#### 5.4.2.1 Poly(Ethyl Phosphonate) Synthesis in DCM and in the Bulk

The AROP of EP to yield a linear hydrophilic poly(ethyl phosphonates) (PEP) homopolymer was reported by Wolf *et al* using 2-(benzyloxy)ethanol as an initiator.[72] They performed the reaction at a low temperature (as low as 30 °C) using DBU as an organocatalyst in DCM to give monomer conversions of up to 91% in 16 h. $BzOC_2H_4$-$PEP_m$-OH with number molecular weights ($M_n$ $^{NMR}$) up to 7500 g mol$^{-1}$ and narrow $Đ$ (1.04-1.07) were reported.[72] We utilised the same protocol and as expected, linear Bz-$PEP_{44}$OH with $M_n^{NMR}$ of 6100 g mol$^{-1}$ (i.e. close to the theoretical $M_n^{theo}$ value of 6360 g mol$^{-1}$), low dispersity ($Đ$ = 1.11) and a slightly higher monomer conversion (97%) in 16 h was obtained (Table 5.1, Entry 1).

However, in this work, it was investigated whether the organocatalysed bulk AROP of ethyl phosphonate can be achieved in VOC free conditions (absence of DCM) using DBU. To the best of our knowledge, the bulk AROP of cyclic phosphonate monomers with DBU as an organocatalyst in solvent-free conditions has not been reported elsewhere. Therefore, the reaction conditions for homopolymerisation of EP in the bulk

at a low-temperature range of 30-50 °C was first optimised with an aim to obtain higher monomer conversion (~88-98%). A slightly higher temperature of 40 °C seems necessary in the bulk to reduce the viscosity of the reaction mixture developed at higher conversions. It also ensured to afford a narrow molecular weight distribution. Hence, the AROP of EP was conducted at 40 °C in the bulk using a monohydroxy BzOH as an initiator (Figure 5.7 (a)). To begin with, firstly a degree of polymerisation ($DP^{targ}$) of 20 (i.e. [EP]:[Bz] = 20:1, $M_n^{targ}$ of 2720 g mol$^{-1}$) for a linear Bz-PEP$_{18}$OH homopolymer (.

Table 5.1, Entry 2) was targeted. Clearly, the reaction seems to be much faster (2 h in the bulk at 40 °C vs.16 h in DCM at 30 °C) to reach a similar level of conversion (95 vs. 97%) (Table 5.1, Entry 1 vs. Entry 2).

Table 5.1 Analytical data of linear Bz-PEP$_m$-OH homopolymer synthesised in DCM, in the bulk and in scCO$_2$ with benzyl alcohol initiator

| Ent-ry | Code[a] | $[M]_0$:$[I]_0$:$[C]_0$ (mmol) | Solv. | T (°C) | t (h) | Conv[b] | $DP^{NMR}$ [b] | $M_n^{NMR}$ [b] (g mol$^{-1}$) | $M_n^{SEC}$ [c] (g mol$^{-1}$) | $Đ$ [c] |
|---|---|---|---|---|---|---|---|---|---|---|
| 1 | Bz-PEP$_{44}$OH | 46:1:1 | DCM | 30 | 16 | 97 | 44 | 6100 | 7900 | 1.11 |
| 2 | Bz-PEP$_{18}$OH | 20:1:1 | Bulk | 40 | 2 | 95 | 18 | 2550 | 2000 | 1.12 |
| 3 | Bz-PEP$_{7.5}$OH | 20:1:1 | scCO$_2$ | 40 | 16 | 37 | 7.5[d] | 1100 | 800 | 1.21 |

[a] Sample label, the subscripts represent the $DP^{NMR}$ from $^1$H-NMR.
[b] Determined *via* $^1$H-NMR, where $M_n{}^{NMR} = (DP^{NMR} \times M_{EP}) + M_{BzOH}$
[c] Determined *via* SEC-E in DMF at 40 °C (vs. PMMA standards).
[d] The reaction was conducted in a diluted condition (refer to synthesis protocols) hence a low conversion and low $DP^{NMR}$

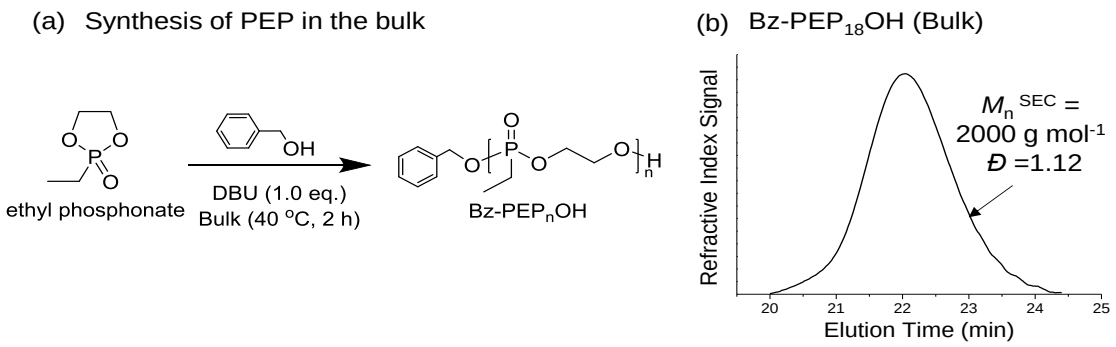



Figure 5.7. (a) Synthesis of Bz-PEP$_{18}$OH by AROP (Table 5.1, Entry 2) using benzyl alcohol as an initiator in the bulk; (b) the corresponding SEC-E traces (DMF eluent, RI detector (PMMA standards)).

From SEC of crude Bz-PEP$_{18}$OH, a monomodal distribution and narrow dispersity of 1.12 was obtained (Figure 5.7, (b)). Moreover, the molecular weight from SEC-E in

DMF (vs. PMMA standards) was lower than those obtained from $^{1}$H NMR ($M_n^{SEC}$ = 2000 g mol$^{-1}$ vs. $M_n^{NMR}$ = 2550 g mol$^{-1}$) due to PMMA SEC calibration standard used for Bz-PEP$_m$-OH.

The $^{1}$H NMR spectra of Bz-PEP$_{44}$OH and Bz-PEP$_{18}$OH (Figure 5.8(a, b)) show the resonance at $\delta$ 7.48 – 7.31 ppm of protons corresponding to the benzyl end-group (–C$_6$*H*$_5$–CH$_2$–OP(=O)–, a) and the chemical shift at $\delta$ 5.02 ppm was ascribed to the methylene protons in the α-position to the first phosphonate in the backbone (–C$_6$H$_5$–C*H*$_2$–OP(=O)–, b). The signal associated to the methylene protons of EP backbone (–O–C*H*$_2$–C*H*$_2$–O–, c) were visible at $\delta$ 4.43 – 4.22 ppm. The signal corresponding to the methylene protons (–OP(=O)–(C*H*$_2$CH$_3$)–, e) of the pendant ethyl group of the phosphonate were visible at $\delta$ 1.84 – 1.74 ppm whereas the methyl groups (–OP(=O)–(CH$_2$C*H*$_3$)–, f) resonate between $\delta$ 1.1 – 1.01 ppm. The signal at $\delta$ 3.89 ppm corresponds to the methylene in β-position to a hydroxy group (–OP(=O)–O–C*H*$_2$–CH$_2$–OH, d) (not integrated into NMR due to poor signal-to-noise ratio). Note the presence of residual DBU ($\delta$ 3.2 – 3.7 ppm) even after several polymer precipitations (Figure 5.8, (a)) and in the crude Bz-PEP$_{18}$OH polymer made in the bulk for comparison. (Figure 5.8, (b)) The signals of DBU were found to be overlapping with terminal methylene (–C*H*$_2$–OH) resonating at $\delta$ 3.56. Reactions were also monitored from $^{31}$P NMR following the change in the chemical shift of cyclic ring (~50 ppm) to the linear phosphonate backbone (~35 ppm) indicating the opening of the five-membered ring. The monomer conversions were calculated based on the integrals of the remaining unreacted monomer: EP at $\delta$ 4.50−4.24 ppm (4H, –P–O–C*H*$_2$C*H*$_2$–, p) to that of corresponding units **c** in the polymer at $\delta$ 4.43 – 4.22 ppm. In addition, the $M_n^{NMR}$ can be estimated by comparing the integral of the methylene protons of the phosphonate backbone **c** with the aromatic protons of the initiator **a,** from Eq. 5.1.

$$M_n^{NMR} = \frac{(\int_c)/4}{(\int_a)/5} \times M_{EP} + M_{BzOH} \qquad \text{Eq. 5.1}$$

Where $\frac{(\int_c)/4}{(\int_a)/5}$ corresponds to the degree of polymerisation ($DP^{NMR}$), $M_{EP}$ to the molar mass of EP ($M_{EP}$ = 136.02 g mol$^{-1}$) and $M_{BzOH}$ to benzyl alcohol ($M_{BzOH}$ = 108.14 g mol$^{-1}$).

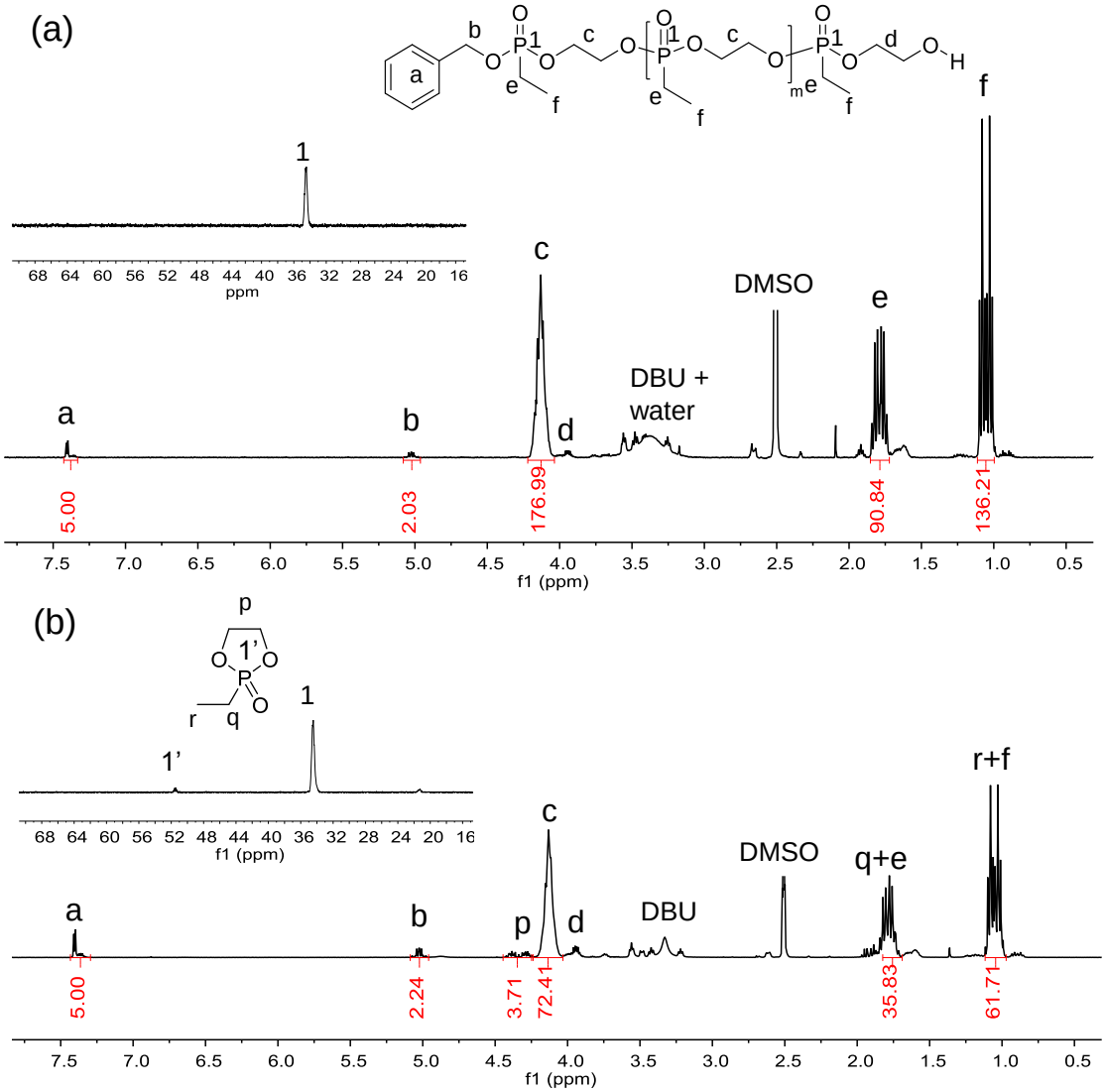



Figure 5.8. $^{1}$H NMR spectra in DMSO-$d_6$ of (a) purified Bz-PEP$_{44}$OH synthesised in DCM and (b) crude Bz-PEP$_{18}$OH homopolymer synthesised in the bulk showing residual monomer. The inset shows the corresponding $^{31}$P NMR spectra of the polymers.

The data demonstrate that Bz-PEP$_m$OH homopolymer can be successfully synthesised by a solvent-free pathway without the need of any toxic organic solvents.

### 5.4.2.2 View-cell to Assess Solubility of Ethyl Phosphonate in scCO$_2$

The phase equilibrium and solubility of ethyl phosphonate monomer in scCO$_2$ were investigated through the fixed volume high-pressure view-cell (Figure 5.9). These view-cell studies clearly showed that ethyl phosphonate monomer is a pale liquid in the presence of CO$_2$ gas (25 °C, 54 bar) (Figure 5.9 (a)). But in the presence of scCO$_2$ (38°C, 190 bar) it appears to bulge as visualised by a slight increase in meniscus

separating the EP from $scCO_2$ phase and by change in the meniscus at the bottom of the EP phase from a flat to curvy and some motion (dynamics) in the bulk of EP phase (Figure 5.9 (b)). This indicates supercritical carbon dioxide might be partly soluble and swelling phosphonate monomer (38 °C and 190 bar, ρ 838.7 kg $m^{-3}$). On raising further the temperature and pressure, the volume of the EP monomer decreased compared to the initial volume (marked in the inset) (Figure 5.9 (c)) showing the partial solubilisation of EP in $scCO_2$ (55 °C, 260 bar, ρ 818.54 kg $m^{-3}$) and the droplets observed in the EP phase was attributed to droplets of $scCO_2$ into the EP phase. Because the boiling of EP at ambient pressure would occur at extremely high temperature, so the presence of EP bubbles is ruled out. Note that the temperature was reduced to ambient condition (T<20 °C, P = 50 bar) at 3-4 bar $min^{-1}$ (low flow rate) and view-cell was slowly depressurised (1 psi/1 sec). Any observed reduction in the mass of EP in $scCO_2$ (100 mL fixed volume view-cell, 55 °C, 260 bar, and at ρ of 818.5 kg $m^{-3}$) can be employed to measure the solubility of EP in $scCO_2$.

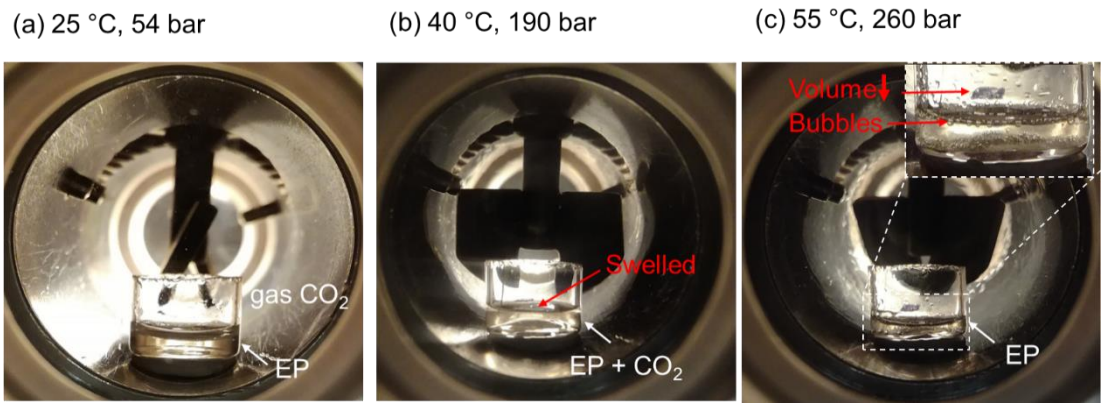



Figure 5.9. Behaviour of EP observed in $CO_2$ using the view cell at increasing temperature and pressure; (a) EP, monomer as a colourless liquid (gas $CO_2$, 25°C, 54 bar); (b) supercritical carbon dioxide was partly soluble in the phosphonate monomer (38 °C, 190 bar) causing swelling of the EP phase; and (c) $scCO_2$ droplets into the EP phase and a reduction in the volume of the monomer phase compared to the initial quantity.

The weight solubility of EP in $scCO_2$ (55 °C, 260 bar, ρ 818.54 kg $m^{-3}$) in our experimental condition measured by Eq. 5.2 was 0.1 wt%.

$$\text{weight solubility (\%)} = m_{EP} / (m_{EP} + m_{scCO_2}) \times 100 \qquad \text{Eq. 5.2}$$

Where $m_{EP}$ corresponds to the mass of EP monomer soluble in $scCO_2$ (0.0815 g) and $m_{scCO_2}$ to the mass of $scCO_2$ (81.8 g).

The view-cell study helped to visualise that $scCO_2$ was miscible in ethyl phosphonate monomer in the low-temperature range (36 - 40 °C) and in the pressure range of 140 - 190 bar (Figure 5.9 (b)). 38 °C, 190 bar shown for clarity). In $scCO_2$ (at 55 °C, 260 bar, ρ 818.54 kg $m^{-3}$), EP seems to have a very small (but not null) solubility. However, we chose to do the extraction of monomer using $scCO_2$ at lower temperature and pressure (to save energy) utilising the high $CO_2$ densities. Thus, SCFE was investigated at 38 °C, 140 bar (ρ 766.36 kg $m^{-3}$) and at 38 °C, 190 bar (ρ 838.76 kg $m^{-3}$).

### 5.4.2.3 Poly(Ethyl Phosphonate) Synthesis in $ScCO_2$

The AROP of ethyl phosphonate using DBU was also explored in $scCO_2$.
To access the polymerisation condition, view-cell studies on the catalyst, DBU, and BzOH initiator were performed. DBU showed partial cloudiness in $CO_2$ (at 25 °C and 70 bar) which made the further phase behaviour visualisation through sapphire windows difficult. Additionally, BzOH seems to be soluble in $scCO_2$ only at a high-temperature range (> 85-95 °C) but the harsh condition is not elegant nor favourable for polymerising of EP using DBU catalyst. Thus, our strategy was to employ milder conditions: low temperature and particularly low pressure (~40 °C, P ~ 100-150 bar) to assure that both monomer and initiator (EP and BzOH) are swollen by $CO_2$. Thus, DBU and EP will partition between the $scCO_2$-rich phase and the EP+BzOH-rich phase. The presence of the catalyst, DBU, in the EP+BzOH-rich phase swollen by $scCO_2$ will promote the polymerisation. For AROP of EP in $scCO_2$, $M_n^{targ}$ of 2720 g $mol^{-1}$ (same as the bulk reaction) was targeted and performed under mild conditions (T = 40 °C, P = 100 bar, 16 h). The reaction was continued for up to 16 h only, to compare it with literature reported reaction time for PEP synthesis in DCM,[72] that yielded a maximum $M_n^{NMR}$ of up to 7500 g $mol^{-1}$ using DBU.

The $^1$H NMR spectrum of the crude Bz-$PEP_m$OH synthesised in $scCO_2$ is shown (Figure 5.10). When employing a conventional formula for monomer conversion ($\int P/\int(P+M) \times 100$), a value of 77% conversion is obtained by $^1$H NMR (Figure 5.10).

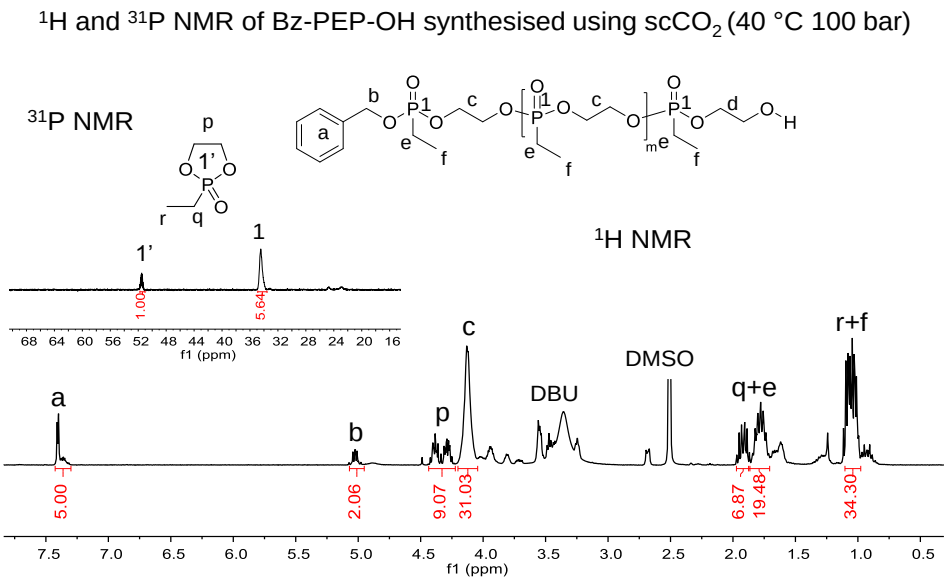



Figure 5.10. The $^{1}$H NMR spectra in DMSO-$d_6$ of crude Bz-PEP$_m$OH homopolymer synthesised in scCO$_2$ showing residual monomer. The inset shows the corresponding $^{31}$P NMR spectrum of the crude polymer.

However, as discussed earlier, $CO_2$ is partially soluble in ethyl phosphonate and viceversa. Any unreacted monomer present in the autoclave may be vented during the depressurisation step. Hence, it is likely that the conventional way to determine the percent of monomer conversion by comparing the ratio of (∫P/∫(P+M)) could be overestimated. As we have slowly depressurised the autoclave and vented (18 °C, 60 bar), from the NMR of the vented material, it was noticed that only EP monomer was removed and signals corresponding to vented BzOH were not present. Considering this, we have compared the polymer to initiator ratio (∫P/∫(Bz)) at time t with the monomer to initiator ratio (∫$M_0$/∫$(Bz)_0$) at time zero. Therefore, percent monomer conversion was estimated following Eq. 5.3.

$$\% \text{ Monomer conversion} = \frac{(\text{polymer/initiator})_{\text{final}}}{(\text{monomer/initiator})_{\text{initial}}} \qquad \text{Eq. 5.3}$$

Again, it should be noted that signals corresponding to unreacted BzOH were not present in the $^{1}$H NMR of the sample obtained from the autoclave and neither observed from the vented material. In this case, it is thought that BzOH is fully reacted (100% initiator efficiency) and thus it is linked to the polymer chains which are most likely not soluble in $CO_2$. Thus, on this basis, a conversion of 37% and a molecular weight $M_n^{PEP}$of 1100 g mol$^{-1}$ was determined by $^{1}$H NMR. The resulting polymer was then analysed by ESI-MS (Figure 5.11, Table 5.1, entry 3) which confirmed the formation

of PEP chains initiated by benzyl alcohol and adduct with sodium ion. The $M_n^{SEC}$ (vs. PMMA standards) of 800 g mol$^{-1}$ was in rather good agreement with NMR and ESI-MS values.

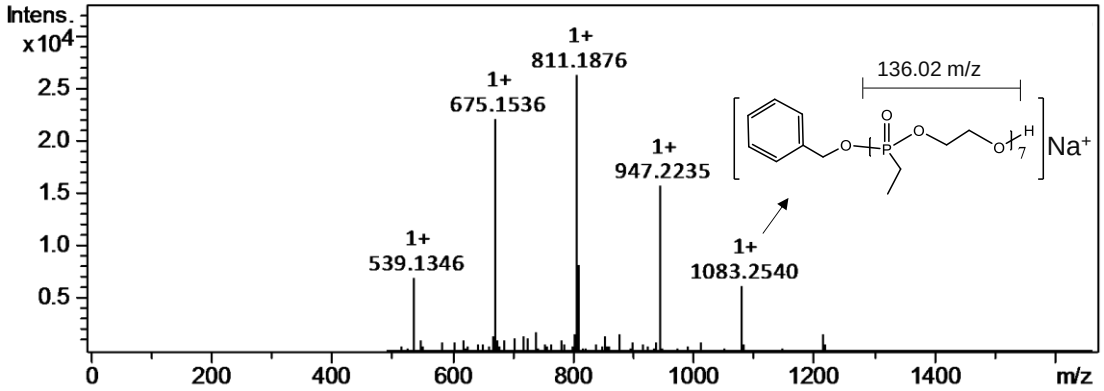



Figure 5.11. ESI-MS (in positive mode) of Bz-PEP$_7$-OH (Table 5.2, Entry 3) homopolymer synthesised in scCO$_2$.

It is important to consider that the reactions in scCO$_2$ were performed using 150 μL of the EP monomer in the autoclave which has a volume capacity of 8 mL (the smallest size reactor available for high-pressure polymerisation in our laboratories). Hence, the very low conversion observed in this case could be the dilution effect. For a controlled experiment, 150 μL in 8 mL DCM (in a Schlenk flask) using the same amount of the catalyst, DBU (1.0 eq), and BzOH was also performed at 40 °C, however, no monomer conversion was noted at all when monitored for 16 h, 20 h, and up to 3 days.

Hence, by using DBU at low-temperature and pressure conditions in scCO$_2$ (40 °C, 100 bar) it was possible to polymerise EP monomer. It is important to note that a much-diluted reaction (0.15 mL monomer in 8 mL capacity autoclave for CO$_2$) may be the reason for incomplete conversion at 16 h. These results were consistent that the diluted system gave a low yield. It is also noticeable from this study that dry DBU was employed for reactions and white precipitate, which is indicative of the bicarbonate salt [DBUH$^+$][HCO$^{3-}$], was not observed. This is always a worry when wet DBU reacts with CO$_2$.[73] Thus showing that our CO$_2$ system can be considered dry (unless [DBUH$^+$][HCO$^{3-}$] would be soluble in the polar EP+BzOH-rich monomer phase).

These data demonstrate that attempts to polymerise ethyl phosphonate in scCO$_2$ using DBU catalyst have shown promising results and a $M_n^{NMR}$ of 1000 g mol$^{-1}$ was achieved using mild conditions (40 °C, 100 bar). Furthermore, it was demonstrated that EP monomer can be extracted in scCO$_2$ just after the synthesis; hence, this opens up

avenues to perform a 'clean one pot' synthesis followed by recovery/recycling of a residual monomer.

As discussed earlier that polymerisation of linear hydrophilic PEP homopolymer was successfully implemented in DCM and in the bulk. In the following sections (5.4.2 and 5.4.3) this system is extended to synthesise amphiphilic diblock and triblock copolymers and star diblock copolymers of various architectures consisting of a hydrophobic PCL and hydrophilic PEP block (Figure 5.13).

#### 5.4.2.4 Purification of PEP Homopolymer using $scCO_2$

The supercritical $CO_2$ fluid extraction (SCFE) is considered as a 'green technology' since a concentration step is most often eliminated after the extraction process and the product obtained at the end is in a dry state. To purify the PEP homopolymer, the crude product (typically 0.5 -1.0 g) and $CO_2$ having ρ 766 kg $m^{-3}$ (38 °C, 140 bar) were introduced to the 20 mL autoclave, followed by mechanical agitation for 15 min to establish a dissolving equilibrium. The efficiency of the extraction process at a constant $CO_2$ flow rate was monitored at regular time intervals by analysing both the extract and the sample in the autoclave *via* $^1$H NMR. From the $^1$H NMR spectra of the aliquots collected after extraction (38 °C, 140 bar), it is clear that all the ethyl phosphonate was completely removed from the sample after 25 min (Figure 5.12 (a) *vs* (c)). Thus, SCFE seems to be a promising method for purification of a poly(ethyl phosphonate)s from residual monomer and any residual DBU catalyst.

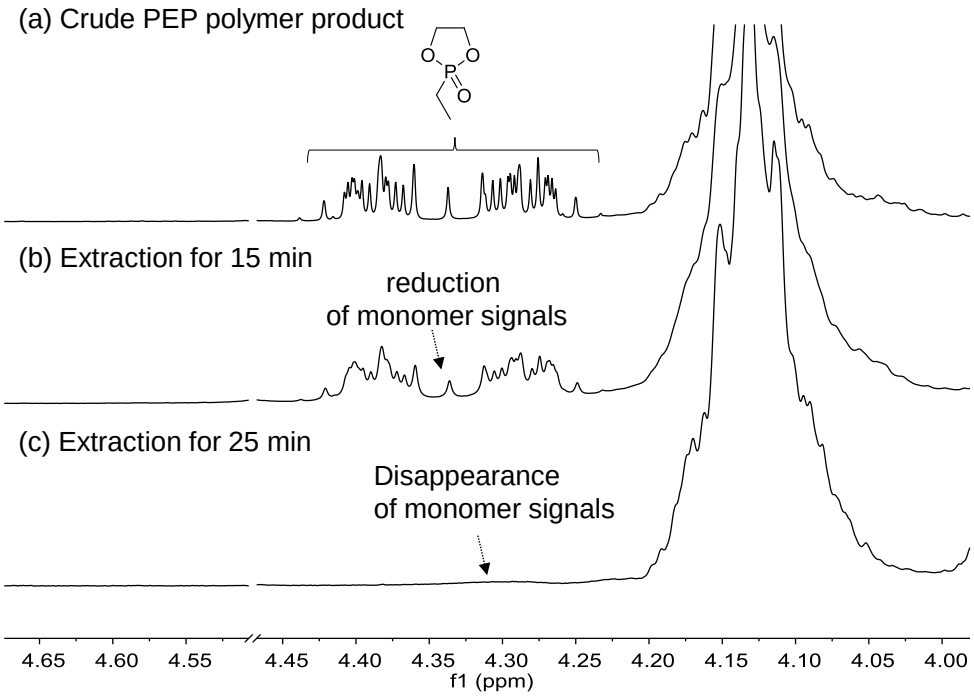



Figure 5.12. $^{1}$H NMR spectra of the Bz-PEP$_{18}$OH synthesised in the bulk at 40 °C (a) crude polymer product before extraction; (b) after extraction for 15 min a decrease in the intensity of ethyl phosphonate signals and (c) after extraction for 25 min showing the complete disappearance of the monomer signals. This indicates that the extraction using sc$CO_2$ (38 ± 2 °C, 140 ± 5 bar) efficiently removes ethyl phosphonate monomer from samples.

### 5.4.3 Linear PCL-*b*-PEP Diblock and PEP-*b*-PCL-*b*-PEP Triblock Copolymers

Three hydrophobic PCL macroinitiators, a monohydroxy Bz-PCL$_{19}$OH and two dihydroxy telechelic HO-PCL$_4$-OH and HO-PCL$_9$-OH, were employed as the starting point to synthesise block copolymers (Table 5.2) (discussed in Chapter 4).

The notation for linear diblock copolymer as Bz-PCL$_n$-*b*-PEP$_m$ and a triblock copolymer as PEP$_{m/2}$-*b*-PCL$_n$-*b*-PEP$_{m2}$ will be used in the following discussion where n and m correspond to the average amount of PCL and PEP present on the polymer, respectively. The polymerisation reaction with notation is schematically represented (Figure 5.13).

Firstly, if the hydroxy group of these PCL macroinitiators could act as the initiating site for AROP of EP monomer using DBU in the bulk was investigated. For this, a temperature range of 40-60 °C was investigated. The temperature of 60 °C seemed to be the most suitable to overcome the developed viscosity and to drive the reaction to high conversion (~88-98%). Thus, all the PCL-*b*-PEP block copolymer syntheses were

performed in the bulk at 60 °C (Table 5.2, all the macroinitiators are in a white rows while the resulting copolymers are in coloured rows) and the products were purified using SCFE method (and by dialysis for comparison).

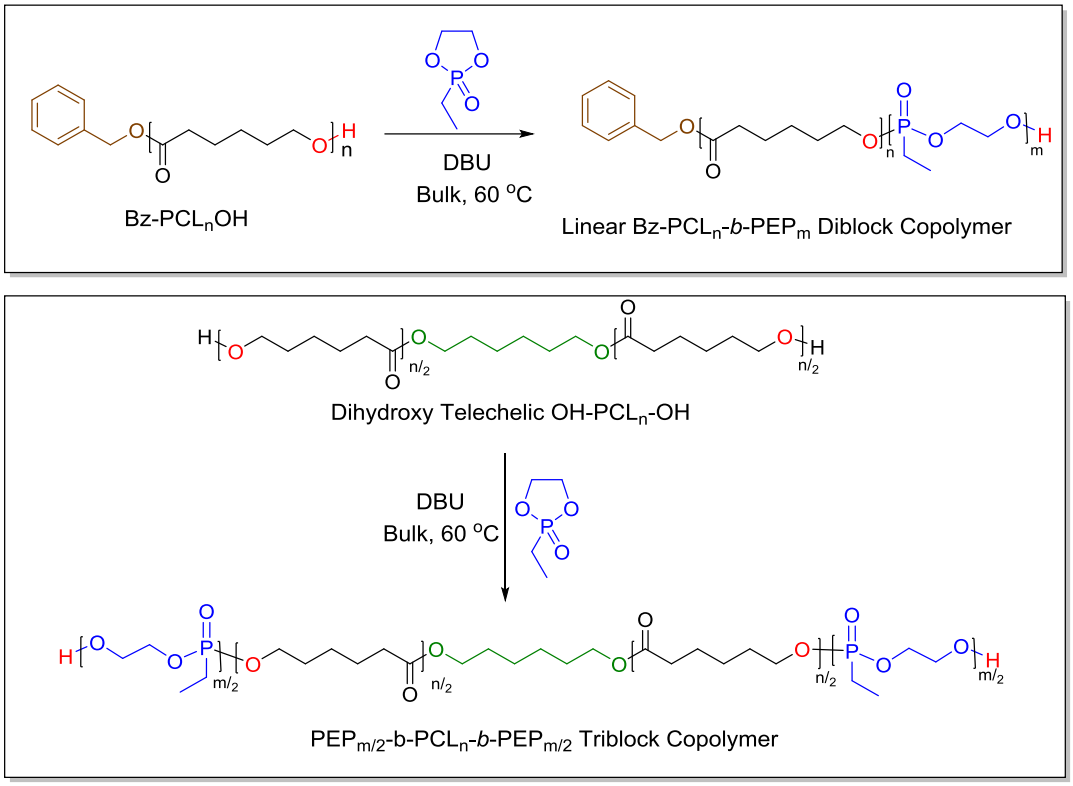



Figure 5.13. Schematic representation of the AROP of ethyl phosphonate using DBU as a catalyst in the bulk by two different architecture of macroinitiators. Linear monohydroxy Bz-PCL$_n$OH and dihydroxy telechelic HO-PCL$_n$-OH to afford linear Bz-PCL$_n$-OH diblock, linear PEP$_{m/2}$-PCL$_n$-PEP$_{m/2}$ triblock copolymers.

Table 5.2. Analytical data and thermal characteristics for linear $PCL_n$-*b*-$PEP_m$ diblock and linear $PEP_{m/2}$-*b*-$PCL_n$-*b*-$PEP_{m/2}$ triblock copolymers synthesised in the bulk (reaction time 2 h).

| | Code [a] | $[M]_0$:$[I]_0$:$[C]_0$ | Conv[e] (%) | $DP^{NMR}$ | $M_n^{NMR\ h}$ (g mol$^{-1}$) (macro-initiator) | $M_n^{NMR\ h}$ (g mol$^{-1}$) (PEP block) | $M_n^{Copoly\ i}$ (g mol$^{-1}$) | $M_n^{SEC\text{-}DMF}$ (g mol$^{-1}$) | $Đ$ | $T_g$ [l] (°C) | $T_m$ [l] (°C) | $\Delta H_m$ [l] (J g$^{-1}$) | $T_c$ [l] (°C) | $\Delta H_{cryst}$ [l] (J g$^{-1}$) |
|---|---|---|---|---|---|---|---|---|---|---|---|---|---|---|
| | $Bz\text{-}PCL_{19}OH$ | 22:1:0.1 [b] | 90 | 19 | 2300 | - | - | 2600 [j] | 1.02 | n/o | 46.5 | 97.3 | 31.9 | 97.3 |
| | Linear $Bz\text{-}PCL_{19}$-*b*-$PEP_{30}$ | 45:1:1 [c] | 92 | 30 [f] | - | 4100 | 6400 | 6400 [j] | 1.04 | -52.3 | 44.4 | 39.4 | 23.1 | 30.2 |
| Triblock | Dihydroxy $HO\text{-}PCL_4\text{-}OH$ | 4.2:1:0.1 [d] | 99 | 4.0 [g] | 600 | - | - | 600 [k] | 1.25 | n/o | 2.4 | 71.6 | -0.8 | 50.8 |
| Triblock | $PEP_{1.6}$- *b*-$PCL_4$- *b*-$PEP_{1.6}$ | 5.3:1:0.5 [c] | 88 | 3.2 [g] | - | 440 | 1040 | 850 [k] | 1.29 | -61.7 | n/o | n/o | n/o | n/o |
| Triblock | $PEP_{3.6}$- *b*-$PCL_4$- *b*-$PEP_{3.6}$ | 9.6:1:0.5 [c] | 94 | 7.3 [g] | - | 1000 | 1600 | 1100 [k] | 1.34 | -60.3 | n/o | n/o | n/o | n/o |
| Triblock | Dihydroxy $HO\text{-}PCL_9\text{-}OH$ | 9:1:0.1 [d] | 99 | 8.8 [g] | 1100 | - | - | 1000 [k] | 1.29 | n/o | 24.6 | 76.4 | 13.8 | 68.4 |
| Triblock | $PEP_{7.2}$- *b*-$PCL_9$- *b*-$PEP_{7.2}$ | 16:1:0.5 [c] | 98 | 14.5 [g] | - | 2000 | 3100 | 1500 [k] | 1.25 | -53.7 | n/o | n/o | n/o | n/o |

[a] Sample label, the subscripts represent the degree of polymerisation of PCL and PEP blocks determined from $^1$H NMR.
[b,c,d] Molar ratio of $[Monomer]_0$:$[Initiator]_0$:$[Catalyst]_0$ based on $DP_n^{targ}$ = [M]/[I]; [b] $[\varepsilon\text{-CL}]_0$:$[BzOH]_0$:$[Sn(Oct)_2]_0$ [c] $[EP]_0$:[macroinitiator]$_0$:$[DBU]_0$ and [d] $[\varepsilon\text{-CL}]_0$:[1,6-hexanediol]$_0$:$[Sn(Oct)_2]_0$.
[e] Determined by $^1$H NMR.
[f,g] Determined from $^1$H NMR after purification; [f] by dialysis using cellulose membrane (MWCO 1000 Da), [g] using SCFE.
[h] $M_n^{NMR}$ (macroinitiator) and $M_n^{NMR}$ (PEP block) determined by $^1$H NMR following Eq. 5.4 and 5.6 respectively.
[i] $M_n^{Copoly}$ is $M_n$ $^{NMR}$ (macroinitiator) + $M_n$ $^{NMR}$ (PEP block) (Eq. 5.7)
[j] Determined by SEC-U in DMF at 45 °C (RI, Double-angle LS) from the dn/dc values of $Bz\text{-}PCL_{19}OH$ (0.04 mL g$^{-1}$) and $Bz\text{-}PCL_{19}$-*b*-$PEP_{30}$ (0.026 mL g$^{-1}$).
[k] Determined *via* SEC-G in DMF at 50 °C (RI, vs. PEG standards).
[l] Determined by differential scanning calorimetry; n/o (not observed).

To begin with, a monohydroxy Bz-PCL$_{19}$OH macroinitiator ($M_n^{NMR}$ of 2300 g mol$^{-1}$, $Đ$ of 1.02) was employed to synthesise a linear Bz-PCL$_{19}$-*b*-PEP$_{30}$OH diblock copolymer in the bulk at 60 °C that yielded 92% conversion in only 2 h using DBU (1.0 eq respect to BzOH).

The structure and the molecular characteristics of the linear Bz-PCL$_{19}$-*b*-PEP$_{30}$ diblock copolymer synthesised in the bulk were confirmed by $^1$H NMR spectroscopy.

All the characteristic resonances corresponding to the Bz-PCL$_{19}$OH and Bz-PCL$_{19}$-*b*-PEP$_{30}$ were annotated in $^1$H NMR spectra (Figure 5.14 (a and b)). In the $^1$H NMR ($CDCl_3$) spectrum of Bz-PCL$_{19}$OH, multiplets at $\delta$ 1.54 and 1.29 ppm were assigned to the methylene protons (–C(=O)CH$_2$C*H*$_2$C*H*$_2$C*H*$_2$CH$_2$O–, **f** and **g**) of the repeating unit of ε-CL. The signal associated to the methylene ester protons in the α-position of the carboxy group (–C*H*$_2$OC(=O)–, **c**) was visible at $\delta$ 3.98 ppm whereas methylene protons in the α-position of the carbonyl group (–OC(=O)C*H*$_2$CH$_2$–, **e**) was visible at $\delta$ 2.27 ppm. The signal between $\delta$ 7.42 – 7.30 was assigned to aromatic benzylic protons (C$_6$*H*$_5$–, **a**) and at $\delta$ 5.02 to aryl protons (C$_6$H$_5$C*H*$_2$–, **b**), respectively (Figure 5.14 (a)). Specifically, the signals at $\delta$ 3.66 ppm are due to the methylene protons (–CH$_2$C*H*$_2$OH, **d**) in α-position to the hydroxy end-groups of linear Bz-PCL$_{19}$OH (Figure 5.14 (a)). It is noteworthy that in $^1$H NMR (DMSO-$d_6$) spectrum of Bz-PCL$_{19}$-*b*-PEP$_{30}$ copolymer, these methylene protons disappear. A new multiplet appears at $\delta$ 3.56 ppm which is attributed to the methylene protons in α-position to the hydroxy group of the phosphoester backbone (–OP(=O)–O–CH$_2$–C*H*$_2$–OH, **i**) (Figure 5.14(b)). This indicates that all the terminal hydroxy signals of PCL chains have initiated the AROP of the EP monomer. All the other signals corresponding to the PEP block in the Bz-PCL$_{19}$-*b*-PEP$_{30}$ diblock copolymer were assigned as discussed previously (section 5.4.2.1). Thus, the successful growth of the PEP block from the Bz-PCL$_{19}$OH macroinitiator was confirmed by $^1$H NMR spectroscopy. The % monomer conversion and the molecular weight of the homopolymer and diblock copolymer were also calculated from $^1$H NMR and will be discussed simultaneously. The monomer conversions were determined by $^1$H NMR analysis based on the resonance intensities of the remaining unreacted monomers to that of the polymer block as discussed previously. The linear Bz-PCL$_{19}$-*b*-PEP$_{30}$ diblock copolymer gave a monomer conversion of 92% in 2 h (Table 5.2). The degree of polymerisation by NMR ($DP^{NMR}$) for Bz-PCL$_{19}$OH macroinitiator was determined from the integral of the ε-CL repeating

unit (**e**) to the methylene protons adjacent to the end group (**d**), to give $DP^{NMR}$ of 19 (~19.5) (Figure 5.14(b)). The number-average molecular weight of the PCL macroinitiator ($M_n^{NMR}$ (macroinitiator)) was calculated to be 2300 g mol$^{-1}$ following Eq. 5.4 (Table 5.2).

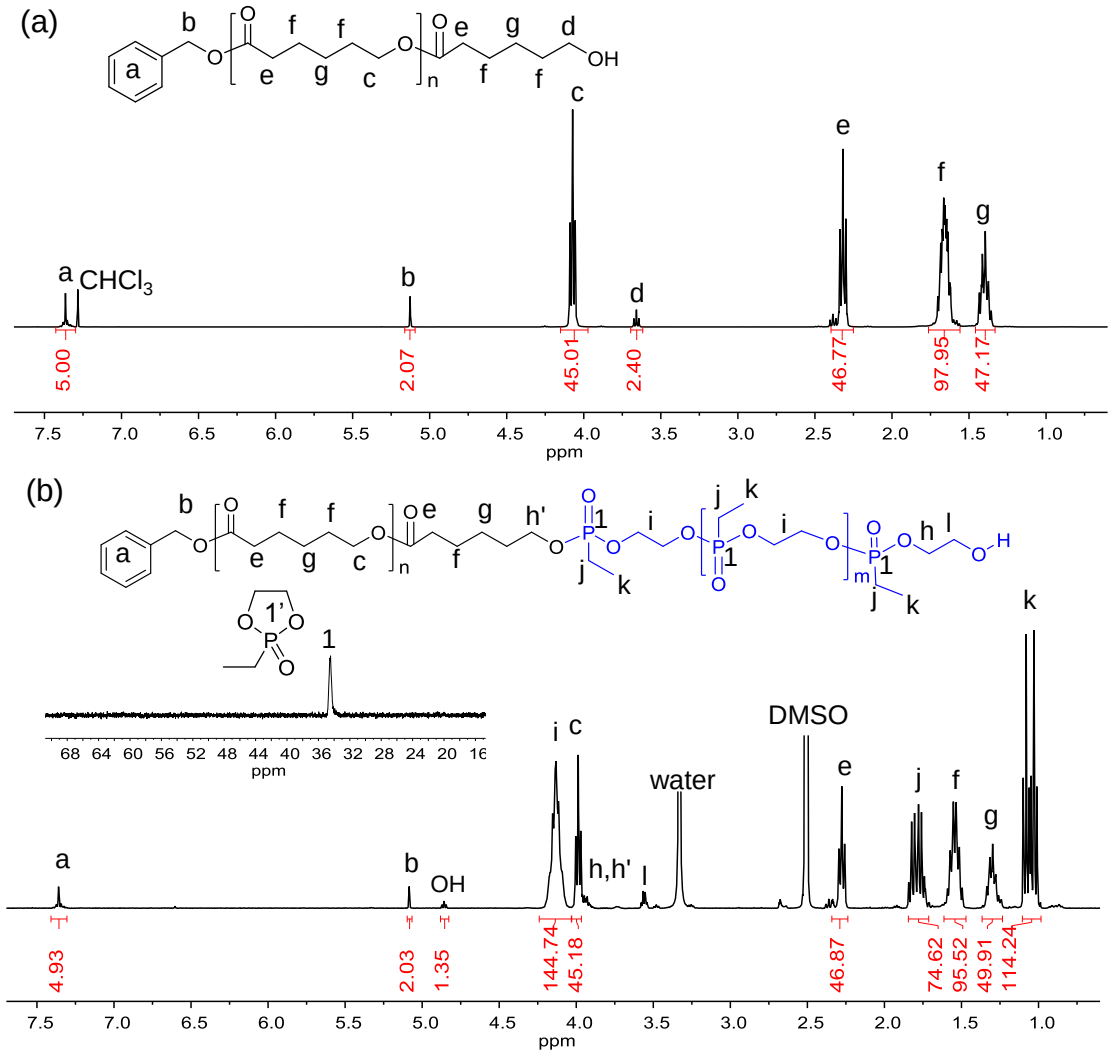



Figure 5.14. The $^{1}$H NMR spectra of purified polymers (a) linear Bz-PCL$_{19}$OH homopolymer ($CDCl_3$) to aid the interpretation for the diblock and (b) linear Bz-PCL$_{19}$-b-PEP$_{30}$ diblock copolymer (DMSO-$d_6$) synthesised in the bulk and the inset shows the corresponding $^{31}$P NMR spectrum. Note the difference solvent employed for NMR analysis is due to the solubility difference between homo- and copolymer.

**Equations.**

| | | |
|---|---|---|
| PCL macroinitiator | $M_n^{NMR}$ (macroinitiator) = ($DP^{NMR} \times M_{\varepsilon\text{-CL}}$) + $M_I$ | Eq. 5.4 |
| PEP block | $DP^{NMR}$ (PEP block) = $\frac{(\frac{\int 4.13}{4})}{(\frac{\int 3.99}{2})} \times DP^{NMR}$ (PCL block) | Eq. 5.5 |
| | $M_n^{NMR}$ (PEP block) = ($DP^{NMR}$ (PEP block) × $M_{EP}$) | Eq. 5.6 |
| Copolymer | $M_n^{Copoly} = M_n^{NMR}$ (PEP block) + $M_n^{NMR}$ (macroinitiator) | Eq. 5.7 |

Where $M_n^{NMR}{}_{macroinitiator}$ corresponds to the molar mass of whole PCL macroinitiator chain. $M_{\varepsilon\text{-CL}}$ to the molar mass of ε-CL (114.14 g mol$^{-1}$) and $M_{EP}$ to ethyl phosphonate (136.02 g mol$^{-1}$), $M_I$ to the benzyl alcohol (108.14 g mol$^{-1}$) for monohydroxy Bz-PCL$_{19}$OH and to 1,6-hexanediol (118.18 g mol$^{-1}$) for dihydroxy HO-PCL$_n$-OH macroinitiators, respectively.

The $DP^{NMR}$ value of the PEP block in the Bz-PCL$_{19}$-*b*-PEP$_{30}$ diblock copolymer was determined by comparing the integrated intensities of the characteristic protons in phosphonate backbone ($\delta$ 4.14 ppm, **i**) with those of the methylene protons in PCL ($\delta$ = 3.99 ppm, **c**). Thus, the $DP^{NMR}$ of 30 (~29.8) and $M_n^{NMR}$ (PEP block) value of 4100 g mol$^{-1}$ were observed following Eq. 5.5 and Eq. 5.6. The $M_n^{Copoly}$ value obtained following Eq. 5.7 was 6400 g mol$^{-1}$.

The success of linear diblock copolymer synthesis in the bulk was also confirmed by SEC analysis. The clear increase in the SEC elution time of the linear Bz-PCL$_{19}$-*b*-PEP$_{30}$ diblock copolymer observed compared to the macroinitiator in the bulk, confirms the growth in molecular weight during copolymerisation (Figure 5.15). The obtained Bz-PCL$_{19}$-*b*-PEP$_{30}$ diblock copolymer has a unimodal shape and narrow $Đ$ of 1.04 (Table 5.2, Figure 5.15). $M_n^{SEC\text{-}DMF}$ (RI, Double-angle LS) values obtained using dn/dc (given in the footnotes of Table 5.2) of the corresponding polymers were in great agreement with those calculated from the $M_n^{NMR}$ values. For the linear Bz-PCL$_{19}$OH macroinitiator ($M_n^{SEC\text{-}DMF}$ = 2600 g mol$^{-1}$ vs. $M_n^{NMR}$ = 2300 g mol$^{-1}$) and for the linear Bz-PCL$_{19}$-*b*-PEP$_{30}$ diblock copolymer ($M_n^{SEC\text{-}DMF}$ = 6400 g mol$^{-1}$ vs. $M_n^{Copoly}$ = 6400 g mol$^{-1}$) were obtained (Table 5.2, Figure 5.15).

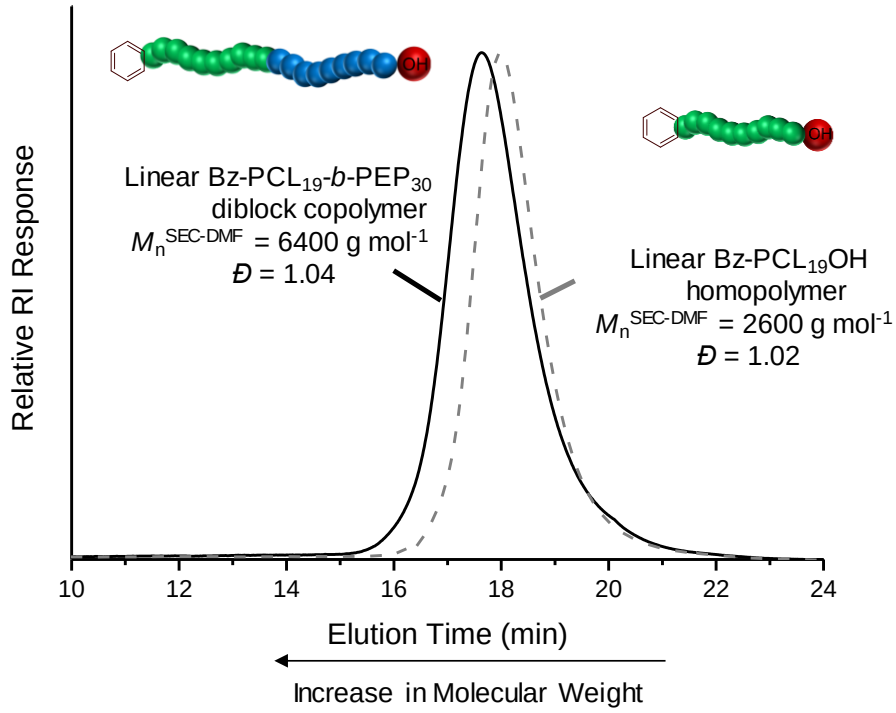



Figure 5.15. SEC (RI+DALS) traces of linear Bz-$PCL_{19}$OH macroinitiator synthesised using $scCO_2$ and the corresponding linear Bz-$PCL_{19}$-*b*-$PEP_{30}$ diblock copolymer synthesised in the bulk and purified using dialysis membrane.

Thus, the $^1$H NMR and SEC (RI + Double-angle LS) analysis confirm that PCL and PEP polymer block are covalently linked. The synthesis of linear Bz-$PCL_{19}$-*b*-$PEP_{30}$ diblock copolymer occurred in the bulk condition with good control over dispersity.

This linear Bz-$PCL_{19}$-*b*-$PEP_{30}$ diblock copolymer with 19 units of water-insoluble (hydrophobic) PCL and 30 units of water-soluble (hydrophilic) PEP block, when directly suspended in water, gave a faintly cloudy solution. The linear Bz-$PCL_{19}$OH hydrophobe on contrary remained insoluble, hence the copolymerisation with PEP certainly made the linear Bz-$PCL_{19}$-*b*-$PEP_{30}$ diblock copolymer amphiphilic but it seems that to ensure the full direct dissolution of the compound in the water, the ratio of PEP:PCL or MW need to be tuned. The solubility of the surfactant in water (primary solvent) is very important as it allows the polymer to travel either to the air-water interface to modulate the interfacial tension or to adsorb at the liquid/water or solid/water interface to stabilise emulsions or suspensions, respectively. Solubility in water is dependent on the length (and structure) of hydrophilic and hydrophobic segments, and these are the crucial parameters to define the properties of surfactants.[74] Thus, a different architecture (triblock, similar to Pluronic$^{TM}$) and particularly a short

central hydrophobic PCL block was employed. Specifically, two $PEP_{m/2}$-*b*-$PCL_n$-*b*-$PEP_{m/2}$ triblock amphiphiles with a fixed length of dihydroxy HO-$PCL_n$-OH hydrophobe ($M_n^{NMR}$ (macroinitiator) of 600 g $mol^{-1}$ for HO-$PCL_4$-OH) and increasing the amount of $PEP_{m/2}$ blocks (for example, $DP_n^{targ}$ ($PCL_n$) = 4 then $DP_n^{targ}$ ($PEP_m$) = ~5.3 and ~9.6) was employed. Additionally, a slightly higher MW of a dihydroxy HO-$PCL_n$-OH hydrophobe ($M_n^{NMR}$ =1100 g $mol^{-1}$ for HO-$PCL_9$-OH) was also employed to make a triblock copolymer with an aim to nearly double both the hydrophilic $PEP_m$ block and hydrophobic $PCL_n$, i.e. to increase the MW but to maintain the same hydrophilicity.

Both dihydroxy macroinitiators were synthesised using $scCO_2$ (discussed in Chapter 4) and all the corresponding triblock copolymers were prepared in the bulk and purified using SCFE method.

### 5.4.3.1 Purification of Triblock Copolymers using SCFE

It is well-known that purification of amphiphilic copolymer or surfactants is not straightforward and often multiple purification steps using volatile organic solvents are involved.[75] In these terms, dialysis of polymer product by semi-permeable membrane against water can be a comparatively benign approach but it is a long process always followed by an energy-intensive freeze-drying process. Besides, in our case, the surfactants/low molecular weight copolymers (~600-3500 g $mol^{-1}$) gave a low yield (67 ± 5%) after dialysis (membrane with MWCO of 1000 g $mol^{-1}$). Thus, it became necessary to investigate whether the alternative sustainable and clean approach of using $scCO_2$ for purification of the amphiphiles could overcome the yield factor.

In order to purify the triblock, the crude product (typically 2.0-2.5 g) and $CO_2$ having ρ of 766 kg $m^{-3}$ (at 38 °C, 140 bar) were introduced to the 20 mL autoclave. Followed by mechanical agitation for 25 min (for homopolymer) to establish a dissolving equilibrium.

After extraction at a constant flow rate in $scCO_2$, about ~11.5 wt% of ethyl phosphonate was extracted from the $PEP_{3.6}$-*b*-$PCL_4$-*b*-$PEP_{3.6}$ triblock amphiphile within 25 min (Figure 5.16 (b)).

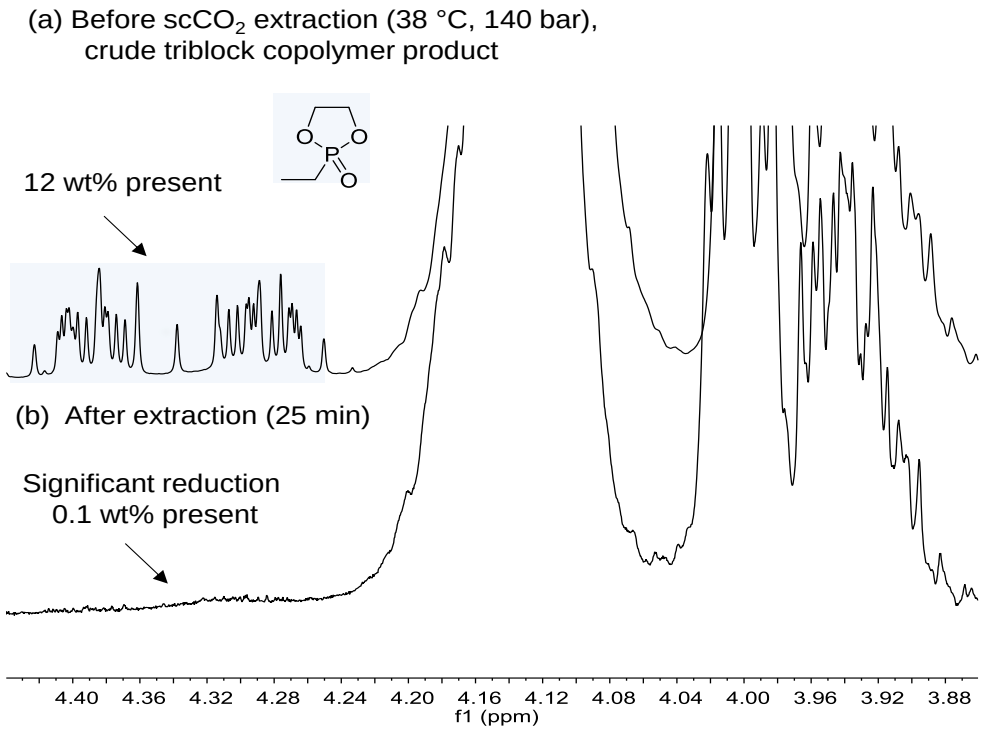



Figure 5.16. $^{1}$H NMR spectra of the $PEP_{3.6}$-*b*-$PCL_{4}$-*b*-$PEP_{3.6}$ triblock copolymer synthesised in the bulk at 60 °C (a) crude triblock product before and (b) after extraction for 25 min showing a significant (~11.5 wt%, ~300 mg) reduction in the intensity of ethyl phosphonate signals when extracting using scCO2 (38 °C, 140 bar).

Moreover, it is important to note that $^{1}$H NMR of extracts showed the cyclic ethyl phosphonate ring remained intact and no hydrolytic degradation of the monomer was observed (given in Appendix, Figure C1). Majority of signals in extract corresponds to the EP and few signals of oligomeric species (up to ~4% relative to monomer) were identified. Recycling of the cyclic phosphonate monomer is not possible when purification is performed by dialysing against water. It is due to the fact that these cyclic phosphonates hydrolyse immediately when comes in contact with the aqueous medium.

Thus, SCFE seems to be a promising method for the purification of $PEP_{m/2}$-*b*-$PCL_{n}$-*b*-$PEP_{m/2}$ triblock amphiphile and recovering monomer. This is highlighting the fact that this process can be employed in the future to recycle and reuse the cyclic phosphonate monomers. These low molecular weight amphiphiles were a clear viscous liquid that made the recovery of the product difficult, but with proper care, a gravimetric yield of ~92 ± 2% was observed.

Similarly, all the other triblock copolymers were purified by SCFE method (ρ of 766 kg $m^{-3}$ at 38 °C, 140 bar). It was discussed earlier (in section 5.4.1) that precipitation

method for purification of the homopolymer Bz-PEP$_m$OH using cold diethyl ether gave a low yield of 65 ± 2% and traces of DBU were present (Figure 5.8). Therefore, the diblock copolymer was purified by dialysis against Milli-Q water. In this way, most of the DBU was removed from samples (Figure 5.14 (a)) and only traces were observed but the yield (60 ± 5%) was more or less similar to those obtained after solvent precipitation. It is important to note that the yield was dramatically improved after purification using scCO$_2$ extraction method (gravimetric yield of ~92 ± 2%).

Also, note that some discrepancy in the theoretical degree of polymerisation ($DP^{theo}$; $DP^{theo} = DP^{targ} \times$ % monomer conversion) and experimental NMR ($DP^{NMR}$) values were noticeable for linear diblock copolymer ($DP^{theo}$ = 41 vs. $DP^{NMR}$ = 30) when purified by dialysis. This could be because purification by dialysis is fractionating polymers. However, after scCO$_2$ purification, calculated $DP^{NMR}$ values were significantly closer to those $DP^{theo}$ for the triblock PEP$_{m/2}$-*b*-PCL$_n$-*b*-PEP$_{m/2}$ copolymers ($DP^{theo}$ = 4.6 vs. $DP^{NMR}$ = 3.2 for PEP$_{1.6}$-*b*-PCL$_4$-*b*-PEP$_{1.6}$, $DP^{theo}$ = 9.0 vs. $DP^{NMR}$ = 7.3 for PEP$_{3.6}$-*b*-PCL$_4$-*b*-PEP$_{3.6}$ and $DP^{theo}$ = 15.7 vs. $DP^{NMR}$ = 14.5 for PEP$_{7.2}$-*b*-PCL$_9$-*b*-PEP$_{7.2}$). These data display the fact that purification of amphiphiles using scCO$_2$ (38 °C, 140 bar) indeed helped to dramatically improve the yield of the low MW triblock products (precipitation/dialysis ~60 ± 5% vs. scCO$_2$ ~92 ± 2% yield).

A representative $^1$H NMR spectrum (DMSO-$d_6$) of linear triblock PEP$_{m/2}$-*b*-PCL$_n$-*b*-PEP$_{m/2}$ amphiphile purified using scCO$_2$ shows all the characteristic peaks of PCL and PEP segments as discussed previously for linear copolymer (Figure 5.17 (b)) and dihydroxy HO-PCL$_4$-OH is also presented to aid interpretation (Figure 5.17 (a)). Significantly reduced monomer signals were observed after SCFE for 15 min (Figure 5.17 (b)). However, a minor trace of DBU close to the resonance of water $\delta$ 3.33 ppm was observed (Figure 5.17 (b)). The analytical data calculated from $^1$H NMR of all the dihydroxy macroinitiators and the corresponding triblock amphiphile are presented (Table 5.2). These purified triblock copolymers were also analysed by SEC and a clear shift toward lower elution time was observed after copolymerisation using dihydroxy HO-PCL$_4$-OH macroinitiator indicating the successful synthesis of linear PEP$_{m/2}$-*b*-PCL$_n$-*b*-PEP$_{m/2}$ triblock copolymers in the bulk at 60 °C (Figure 5.18).

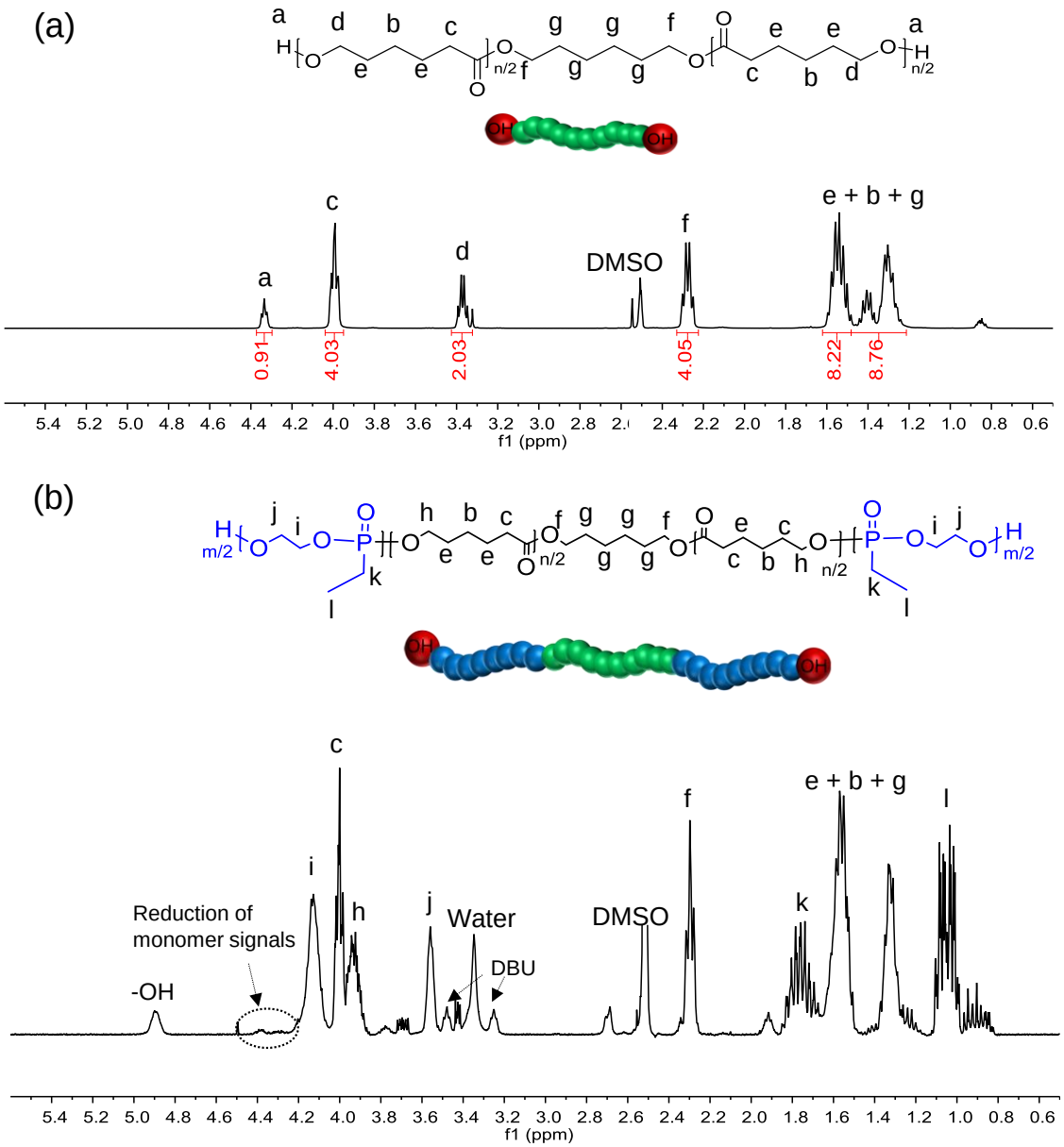



Figure 5.17. $^{1}$H NMR spectra in DMSO-$d_6$ of (a) dihydroxy HO-PCL$_4$-OH macroinitiator synthesised in scCO$_2$ using Sn(Oct)$_2$ and (b) a representative linear PEP$_{m/2}$-*b*-PCL$_n$-*b*-PEP$_{m/2}$ triblock copolymer synthesised in the bulk and purified using a constant flow rate of scCO$_2$ (38 °C, 140 bar) for 15 min.

However, the $M_n^{SEC\text{-}DMF}$ (RI vs. PEG) values were slightly lower than $M_n^{Copoly}$ values estimated by $^{1}$H NMR, such as for PEP$_{1.6}$-*b*-PCL$_4$-*b*-PEP$_{1.6}$ $M_n^{SEC\text{-}DMF}$ = 850 g mol$^{-1}$ vs. $M_n^{Copoly}$ = 1040 g mol$^{-1}$ and for PEP$_{3.6}$-*b*-PCL$_4$-*b*-PEP$_{3.6}$ $M_n^{SEC\text{-}DMF}$ = 1100 g mol$^{-1}$ vs. $M_n^{Copoly}$ of 1600 g mol$^{-1}$. It could be due to the fact that the hydrodynamic volume of these poly(phosphonate)s based materials is different compared to the PEG standards used for SEC calibration. A linear PEP$_{7.2}$-*b*-PCL$_9$-*b*-PEP$_{7.2}$ triblock copolymer ($M_n^{Copoly}$ =3100 g mol$^{-1}$, $Đ$ = 1.25) with the slightly higher molecular weight of hydrophobe but

similar hydrophilicity compared to $PEP_{3.6}$-*b*-$PCL_4$-*b*-$PEP_{3.6}$ was also successfully prepared. However, a slight broadening in dispersities (*Đ* = 1.25 -1.34) was thought to be characteristic for these low molecular weight triblock compounds (Table 5.2).

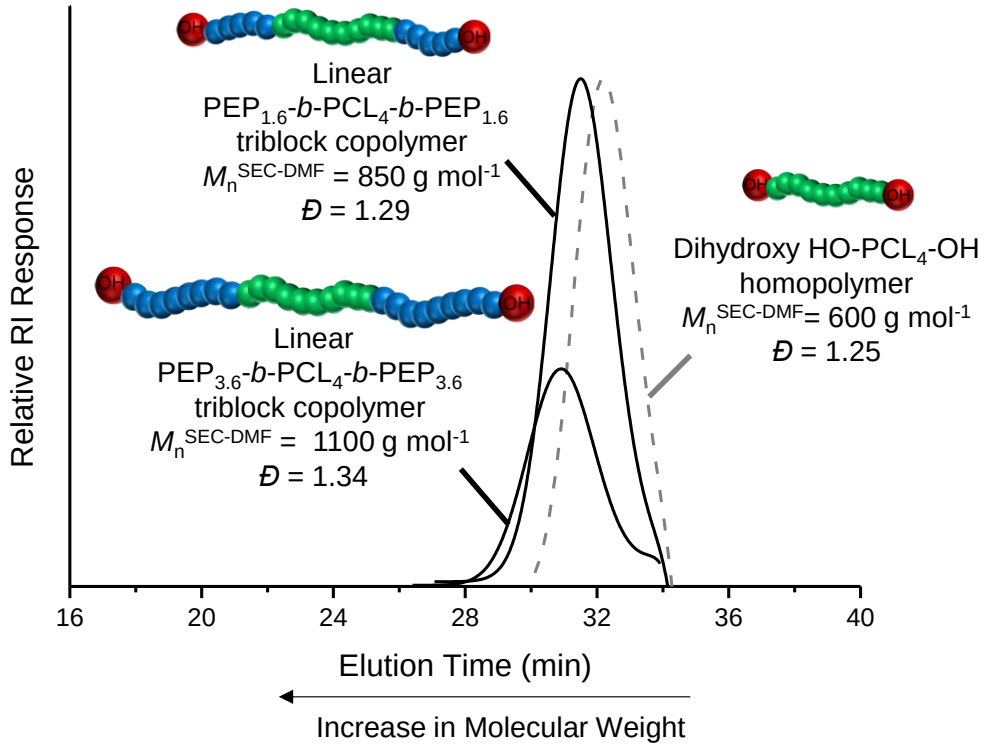



Figure 5.18. SEC-G (vs. PEG) traces of dihydroxy OH-$PCL_4$-OH and the corresponding triblock $PEP_m$-*b*-$PCL_n$-*b*-$PEP_m$ copolymers.

It was shown the clean synthesis of linear diblock and a series of linear triblock copolymers of variable MW in the bulk system using an organocatalyst DBU. These copolymers were successfully purified employing SCFE methods. Now the synthesis of more complex architectures, such as synthesis of star diblock copolymers will be explored.

### 5.4.4 Star-Shaped PCL-*b*-PEP Diblock Copolymer

#### 5.4.4.1 High MW Star PCL-PEP Diblock Copolymer (DCM vs. Bulk)

Practically, the notation for star homopolymer and diblock copolymer (Figure 5.19) can be represented as star *D*-sorbitol[$PCL_nOH_x$]$OH_y$ and star *D*-sorbitol[$PCL_n$-*b*-$PEP_mOH_x$]$OH_y$ respectively; where n, m and x corresponds to the average amount of PCL, PEP and average arms on the PCL and y to residual hydroxy group on *D*-sorbitol (as analysed by $^{31}P$ NMR method). However, an alternative and more appropriate nomenclature for such star diblock materials would be star *D*-sorbitol[$PCL_{n/x}$-*b*-

$PEP_{m/(x+y)}]_x[PEP_{m/(x+y)}]_y[OH]_{6-x-y}$, this was utilised for estimation of arms by phosphitylation-$^{31}$P NMR part (for detailed calculation refer to Appendix C).

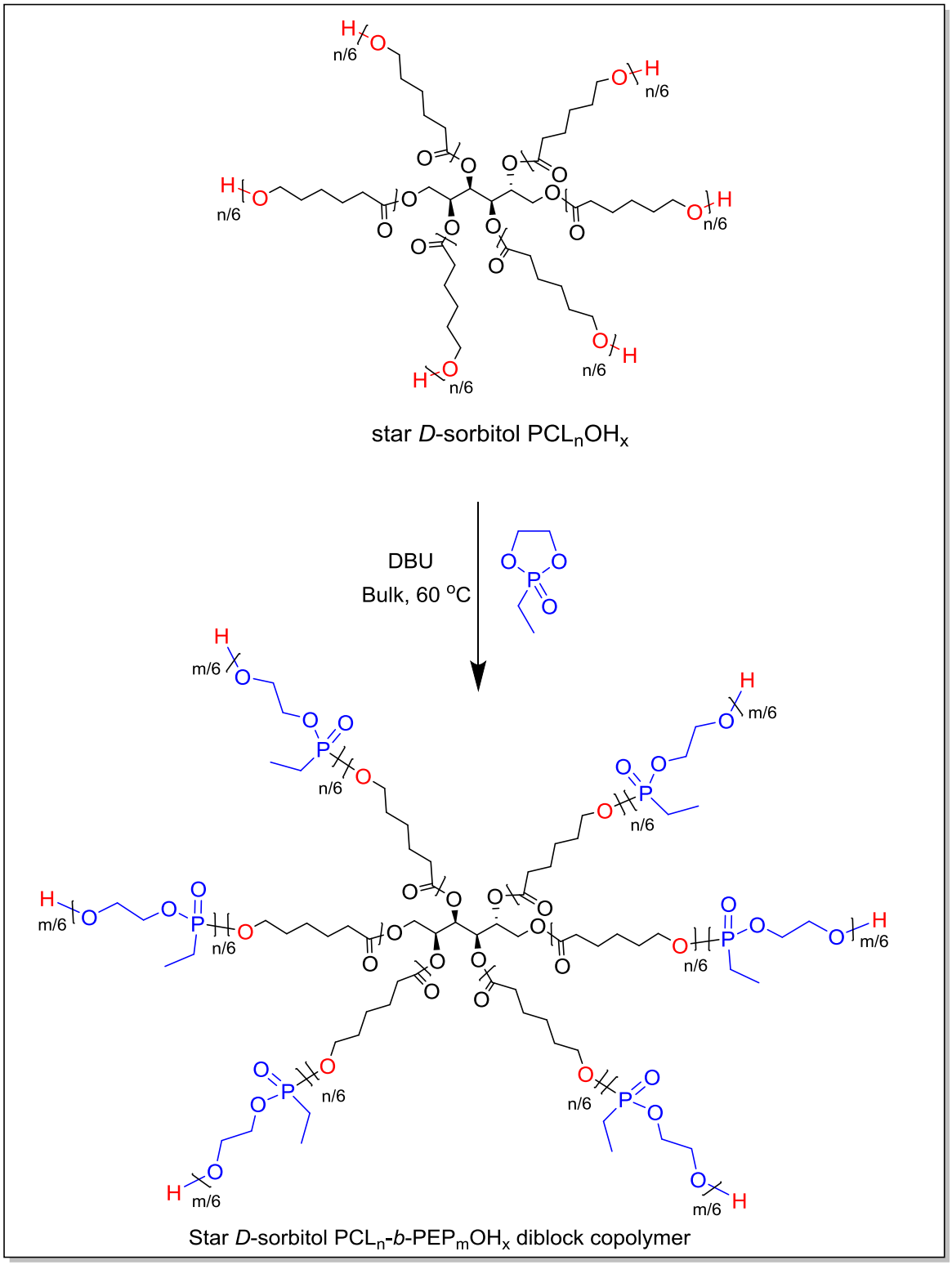



Figure 5.19. Schematic representation of the AROP of ethyl phosphonate using DBU as a catalyst in the bulk to give star architecture *D*-sorbitol[$PCL_{n/x}$-*b*-

$PEP_{m/(x+y)}]_x[PEP_{m/(x+y)}]_y[OH_{m/(x+y)}]_{6-x-y}$ diblock copolymers from star *D*-sorbitol-[$PCL_n$-*b*-$PEP_mOH_x$]$OH_y$ macroinitiator.

A comprehensive set of amphiphilic star *D*-sorbitol-[$PCL_n$-*b*-$PEP_mOH_x$]$OH_y$ copolymers of various molecular weights composed of a different proportion of the PCL hydrophobe and PEP hydrophile were prepared by AROP using DBU catalyst (Table 5.3). Typically, synthesis of these star copolymers was either conducted in DCM at 30 °C or in the bulk at 60 °C. Four hydrophobic star *D*-sorbitol[$PCL_nOH_x$]$OH_y$, having different lengths and number of arms were used as macroinitiators (Table 5.3, star macroinitiators are in white while the resulting star diblock copolymers are blue rows).

As a starting point for the synthesis of star diblock copolymers, a *D*-sorbitol[$PCL_{57}OH_5$]OH (synthesis and characterisation discussed in Chapter 4) possessing an average of five –PCL arms radiating from *D*-sorbitol, and one residual –OH group on *D*-sorbitol (so in total 6 hydroxy groups on macroinitiator) was employed. An EP monomer conversion of 89% was obtained within 5 h as determined by $^1$H NMR for the bulk AROP while only a slightly higher conversion of 92% was yielded in 10 h for AROP using DCM solvent (Table 5.3)

Table 5.3. Analytical data for star *D*-sorbitol-$PCL_n$-*b*-$PEP_m$-$OH_x$ diblock copolymers synthesised in the bulk or in DCM.

| Code [a] | $[M]_0$:$[I]_0$:$[C]_0$ | Sol-vent. | t (h) | T (°C) | Conv[d] (%) | $DP^{NMR}$ [e] | $M_n$ NMR [f] (g mol$^{-1}$) (macroinitiator) | $M_n$ NMR [f] (g mol$^{-1}$) (PEP block) | $M_n$ Copoly [g] (g mol$^{-1}$) | $M_n$ SEC-DMF (g mol$^{-1}$) | *Đ* |
|---|---|---|---|---|---|---|---|---|---|---|---|
| star *D*-sorbitol[$PCL_{57}OH_5$]OH | 57:1:0.1 [b] | Bulk | 11 | 140 | 99 | 57 | 6700 | - | n/a | 8300 [h] | 1.04 |
| star *D*-sorbitol[$PCL_{57}$-*b*-$PEP_{36}OH_6$] | 46:1:6 [c] | Bulk | 5 | 60 | 89 | 36 | - | 4900 | 11600 | 12500 [h] | 1.10 |
| star *D*-sorbitol[$PCL_{57}$-*b*-$PEP_{38}OH_6$] | 46:1:6 [c] | DCM | 10 | 30 | 92 | 38 | - | 5200 | 11900 | 13000 [h] | 1.09 |
| star *D*-sorbitol[$PCL_{57}$-*b*-$PEP_{64}OH_6$] | 76:1:6 [c] | DCM | 10 | 30 | 90 | 64 | - | 8700 | 15000 | 9000 [h] | 1.15 |
| star *D*-sorbitol[$PCL_{34}OH_5$]OH | 35:1:0.1 [b] | Bulk | 8 | 140 | 98 | 34 | 4000 | - | n/a | 3000 [h] | 1.21 |
| star *D*-sorbitol[$PCL_{34}$-*b*-$PEP_{65}OH_6$] | 82:1:6 [c] | DCM | 10 | 30 | 93 | 65 | - | 8800 | 12800 | 8000 [h] | 1.21 |
| star *D*-sorbitol[$PCL_{18}OH_4$]$OH_2$ | 18:1:0.1 [b] | Bulk | 6 | 140 | 98 | 18 | 2200 | - | n/a | 3700 [h] | 1.18 |
| star *D*-sorbitol[$PCL_{18}$-*b*-$PEP_{27}OH_6$] | 38:1:6 [c] | DCM | 10 | 30 | 89 | 27 | - | 3700 | 6000 | 6500 [h] | 1.25 |
| star *D*-sorbitol[$PCL_4OH_3$]$OH_3$ | 4:1:0.1 [b] | Bulk | 2 | 140 | 96 | 4 | 640 | - | n/a | 698 [i] | 1.36 |
| star *D*-sorbitol[$PCL_4$-*b*-$PEP_{2.8}OH_6$] | 5.3:1:0.5 [c] | Bulk | 2.2 | 60 | 99 | 2.8 | - | 380 | 1000 | 605 [i] | 1.42 |
| star *D*-sorbitol[$PCL_4$-*b*-$PEP_{6.4}OH_6$] | 9.9:1:0.5 [c] | Bulk | 2.3 | 60 | 89 | 6.4 | - | 870 | 1500 | 800 [i] | 1.73 |
| star *D*-sorbitol[$PCL_4$-*b*-$PEP_{14}OH_6$] | 15:1:0.5 [c] | Bulk | 2.4 | 60 | 92 | 14 | - | 1900 | 2540 | 1000 [i] | 1.74 |

[a] Sample label, the subscripts represent the overall degree of polymerisation of PCL and PEP blocks determined from $^1$H NMR.
[b,c] Molar ratio of $[Monomer]_0$:$[Initiator]_0$:$[Catalyst]_0$ based on $DP_n^{targ} = [M]/[I]$; [b] $[\varepsilon\text{-CL}]_0$:[*D*-sorbitol]$_0$:$[Sn(Oct)_2]_0$ and
[c] $[EP]_0$:$[macroinitiator]_0$:$[DBU]_0$. [d] Determined by $^1$H NMR. [e] Determined from $^1$H NMR after purification using $scCO_2$ when copolymer made in the bulk and by dialysis using cellulose membrane (MWCO 1000 g mol$^{-1}$) when copolymer synthesised using DCM. [f] $M_n^{NMR}$ (macroinitiator) and $M_n^{NMR}$ (PEP block) determined by $^1$H NMR following Eq. 5.4 and Eq. 5.6, respectively. [g] Summation of $M_n$ NMR (macroinitiator) and $M_n$ NMR (PEP block) (Eq. 5.7).
[h] Determined *via* SEC-N in DMF at 50 °C (RI, vs. PMMA standards), [i] determined *via* SEC-G in DMF at 50 °C (RI, vs. PEG standards). n/a: not applicable.

All the characteristic resonances in the $^{1}$H NMR (DMSO-$d_6$) spectrum of star *D*-sorbitol-[$PCL_{57}$-*b*-$PEP_{36}OH_6$] diblock copolymers are assigned to PCL and PEP blocks as discussed for diblock copolymers except that no benzylic protons signals are present for star copolymers (Figure 5.20). It is important to note that the signal of the end group methylene protons (PCL–C$H_2$OH) at $\delta$ 3.66 ppm disappears in the $^{1}$H NMR ($CDCl_3$) of the star *D*-sorbitol[$PCL_{57}OH_5$]OH macroinitiator (Figure 5.20 (a)), and a new signal appears in the downfield chemical shift. Thus, signals on $^{1}$H NMR (DMSO-$d_6$) spectrum at $\delta$ 3.56 ppm were attributed to the terminal methylene protons of the phosphoester end-group (PEP–OP(=O)–O–$CH_2$–C$H_2$–OH, **h**) in the star diblock copolymer (Figure 5.20 (b)). In the $^{1}$H NMR spectra of star *D*-sorbitol-[$PCL_{57}$-*b*-$PEP_{36}OH_6$] diblock copolymers, the $DP^{NMR}$ (PEP block) was calculated to be 36 (from Eq. 5.5), the $M_n^{NMR}$ (PEP block) was 4900 g mol$^{-1}$ (Eq. 5.6) and the $M_n^{Copoly}$ values was 11600 g mol$^{-1}$ (Eq. 5.7) (Table 5.3 and Figure 5.20). A parallel reaction carried out in DCM, for star *D*-sorbitol-[$PCL_{57}$-*b*-$PEP_{38}OH_6$] diblock copolymers yielded only a slightly higher molecular weight value, $M_n^{NMR}$ (PEP block) of 5200 g mol$^{-1}$ and the $M_n^{Copoly}$ of 11900 g mol$^{-1}$. The signals corresponding to the *D*-sorbitol core were not visible in the $^{1}$H NMR (DMSO-$d_6$) spectrum, which may be due to high MW of the arms in relation to the protons of the *D*-sorbitol. However, SEC-N in DMF at 50 °C (RI, vs. PMMA standard), clearly showed an increase in elution time and monomodal narrow molecular weight distribution ($Đ$ = 1.10) for star *D*-sorbitol[$PCL_{57}$-*b*-$PEP_{36}OH_6$] made in the bulk (Figure 5.21). This confirms that there is a rise in molecular weight from the star *D*-sorbitol[$PCL_{57}OH_5$]OH macroinitiator and that there is no tailing or any residual PCL homopolymer signal present in the SEC trace (Figure 5.21). The SEC data generated using PMMA calibration were slightly overestimated in comparison to $^{1}$H NMR values for star *D*-sorbitol[$PCL_{57}OH_5$]OH synthesised in the bulk ($M_n^{SEC\text{-}DMF}$ 8300 g mol$^{-1}$ vs. $M_n^{Copoly}$ 6700 g mol$^{-1}$) and for star *D*-sorbitol-$PCL_{57}$-*b*-$PEP_{36}$ diblock copolymer in the bulk ($M_n^{SEC\text{-}DMF}$ 12500 g mol$^{-1}$ vs. $M_n^{Copoly}$ 11600 g mol$^{-1}$) (Table 5.3).

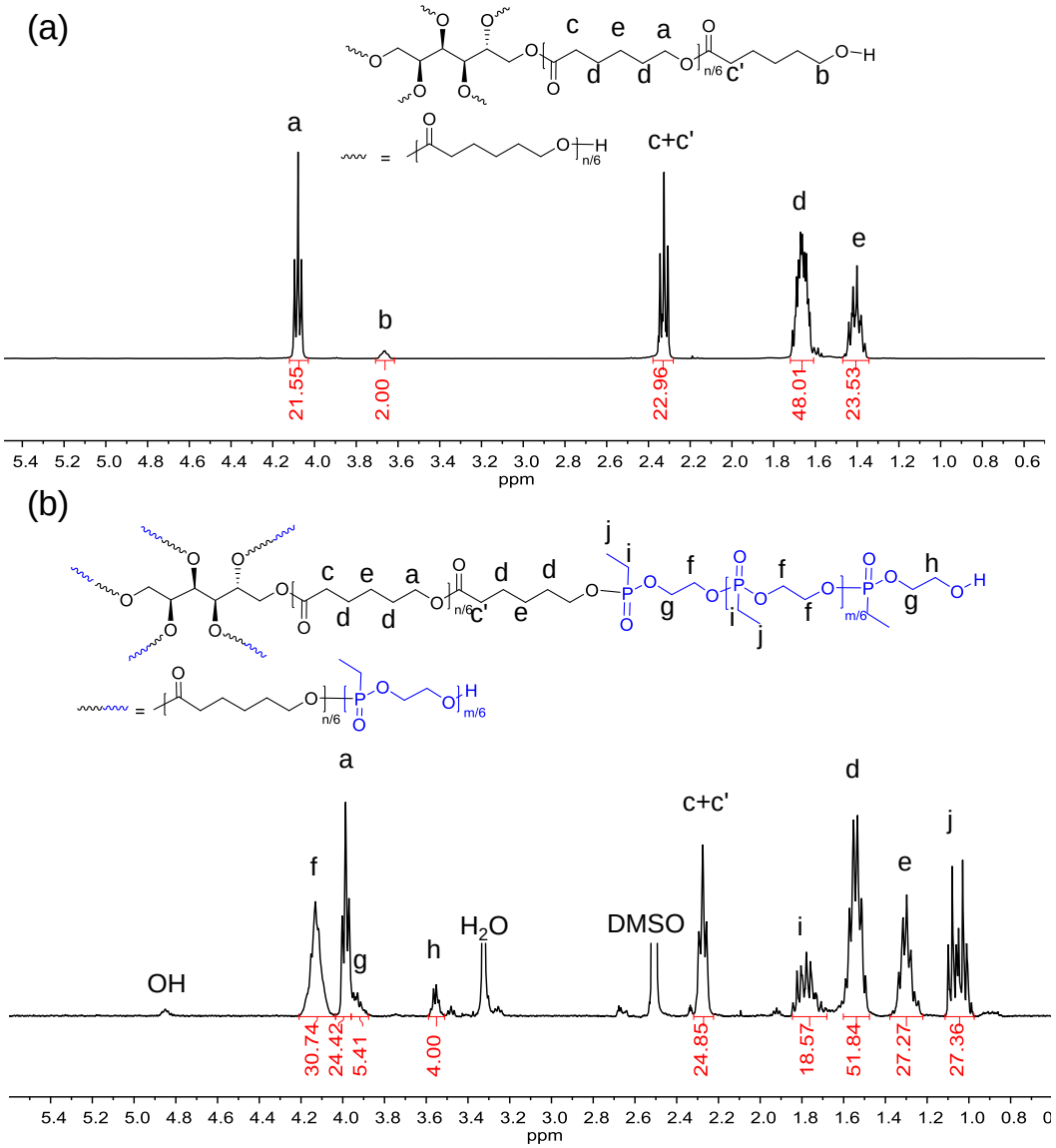



Figure 5.20. $^{1}$H NMR spectra of (a) star *D*-sorbitol-[$PCL_{57}OH_5$]OH macroinitiator (in $CDCl_3$) synthesised in the bulk using $Sn(Oct)_2$ and (b) the star *D*-sorbitol[$PCL_{57}$-*b*-$PEP_{36}OH_6$] diblock copolymer (in DMSO-$d_6$) synthesised in the bulk at 60 °C using DBU and purified using $scCO_2$.

Moreover, it is important to note that, chemical characteristics by $^{1}$H NMR and SEC-DMF for star *D*-sorbitol[$PCL_{57}$-*b*-$PEP_{38}OH_6$] synthesis in DCM at 30 °C were not very different than those obtained in the bulk at 60 °C for star *D*-sorbitol[$PCL_{57}$-*b*-$PEP_{36}OH_6$] diblock copolymer (Table 5.3). This phenomenon highlights the fact that a solvent-free pathway for synthesis of star diblock copolymer using DBU catalyst did not compromise the quality of synthesis and a high molecular weight amphiphilic star copolymer (as high $M_n^{SEC\text{-}DMF}$ as 12500 g mol$^{-1}$) with narrow dispersity ($Đ$ = 1.10) can be effectively prepared in the bulk without the need of any VOCs.

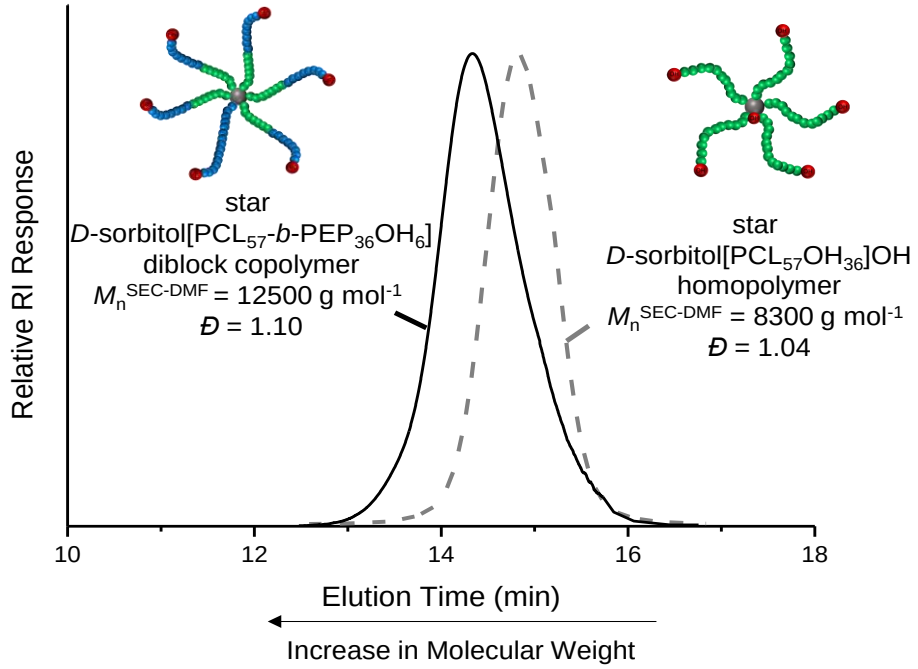



Figure 5.21. SEC (vs. PEG) traces of star *D*-sorbitol[$PCL_{57}OH_5$]OH synthesised in the bulk using $Sn(Oct)_2$ at 140 °C and the corresponding star *D*-sorbitol[$PCL_{57}$-*b*-$PEP_{36}OH_6$] diblock copolymer synthesised in the bulk using DBU at 60 °C.

Before moving further on to the discussion of the other copolymer in star diblock series (Table 5.3), we move our discussion towards what happens to the other unreacted hydroxy group of *D*-sorbitol core. How many numbers of arms does the resulting star copolymers have or even are these all arms amphiphilic?

### 5.4.4.2 Quantifying Number of Arms by a Phosphitylation/$^{31}$P NMR Method

To answer these questions, the quantification-$^{31}$P phosphitylation method (comprehensively exploited in Chapter 4) is applied on star *D*-sorbitol-PCL samples. Indeed, as discussed earlier an appropriate detailed nomenclature of star homopolymer macroinitiator might be star *D*-sorbitol[$PCL_{n/x}OH]_x[OH]_{6-x}$; where n corresponds to PCL repeating unit, x to PCL-OH arms on *D*-sorbitol and 6-x to sorbitol-OH groups on the core. Similarly, a detailed nomenclature of the star diblock copolymer might be *D*-sorbitol[$PCL_{n/x}$-*b*-$PEP_{m/(x+y)}]_x[PEP_{m/(x+y)}]_y[OH]_{6-x-y}$ considering x PCL-OH arms present on the starting macroinitiator, 6-x sorbitol-OH groups on the macroinitiator, y PEP arms initiated by sorbitol-OH, and 6-x-y residual sorbitol-OH groups obtained after EP polymerisation. For a careful assessment of the number of arms, this thorough nomenclature was used but for the sake of simplicity, the simple nomenclature

discussed earlier will be utilised throughout this Thesis. It was previously emphasised in detail (Chapter 4) how powerful this approach is to titrate any residual hydroxy group (or carboxy group in case of PCL homopolymer chain initiated by water) present on the polymer and that aided all the quantification. In this chapter, we have expanded this approach on to the amphiphilic star diblock copolymers to determine any unreacted hydroxy on the *D*-sorbitol core, unreacted PCL arm and the total number of growing arms from *D*-sorbitol or from PCL arms using the detailed nomenclature.

To estimate the number of arms, we begin our discussion with the $^{31}$P {H} NMR spectrum of the star *D*-sorbitol[$PCL_{57}OH_5$]OH macroinitiator (as a reminder) (Figure 5.22 (a)). The signals corresponding to the residual phosphitylated secondary alcohol of *D*-sorbitol (2°, $\delta$ = 145.5-147.0 ppm) and the PCL arms at $\delta$ ~147.02 ppm (1°, triplet, -PCL-O**P**). Thus, $N_{arms}(^{31}P)$ = 5.4 arms were obtained following equation, which corresponds to *D*-sorbitol[$PCL_{n/5.44}OH]_{5.44}[OH]_{0.56}$ by detailed notation or simply to star *D*-sorbitol[$PCL_{57/5}OH]_5OH_{0.56}$ by the simple notation (refer Appendix C for detailed analysis).

$$N_{arms}(^{31}P) = \frac{\int_{PCL-OP}}{\int_{(1^\circ + 2^\circ)} + \int_{PCL-OP}} \times 6 \text{ (equation from Chapter 4).}$$

In regard to $^{31}$P NMR analysis of the amphiphilic star *D*-sorbitol[$PCL_{57}$-*b*-$PEP_{36}OH_6$] diblock copolymers, it showed no resonances at $\delta$ ~147.02 ppm which corresponds to the chain ends of macroinitiator (PCL-O**P**). (Figure 5.22 (b) implying that all the primary hydroxy groups of PCL arms have initiated the ROP of EP monomer. In return, a new signal appears at downfield chemical shift $\delta$ 147.14 ppm that is in correspondence to the primary hydroxy groups on the phosphonate backbone (–P(=O)–O–$CH_2$–$CH_2$–OH) which is expected to observe downfield shift and appear as triplet after phosphitylation with Cl-TMDP (1°, triplet, PEP-O**P**) (Figure 5.22 (b)). Interestingly, the residual signals of *D*-sorbitol present in the star sample decreased and only one 2° signal at $\delta$ 147.9 ppm remained (Figure 5.22 (b)).

The $N_{arms}(^{31}P)$ (star copolymer) can be quantified by comparing the phosphitylated PEP chain ends ($\int_{PEP\text{-}OP}$) and PCL chains end ($\int_{PCL\text{-}OP}$) with the total number of phosphitylated hydroxy on the star copolymer following Eq. 5.8.

$$N_{arms}(^{31}P) = \frac{\int_{PEP-OP} - \int_{PCL-OP}}{\int_{(1^\circ + 2^\circ)} - \int_{PCL-OP} + \int_{PEP-OP}} \times 6 \qquad \text{Eq. 5.8}$$

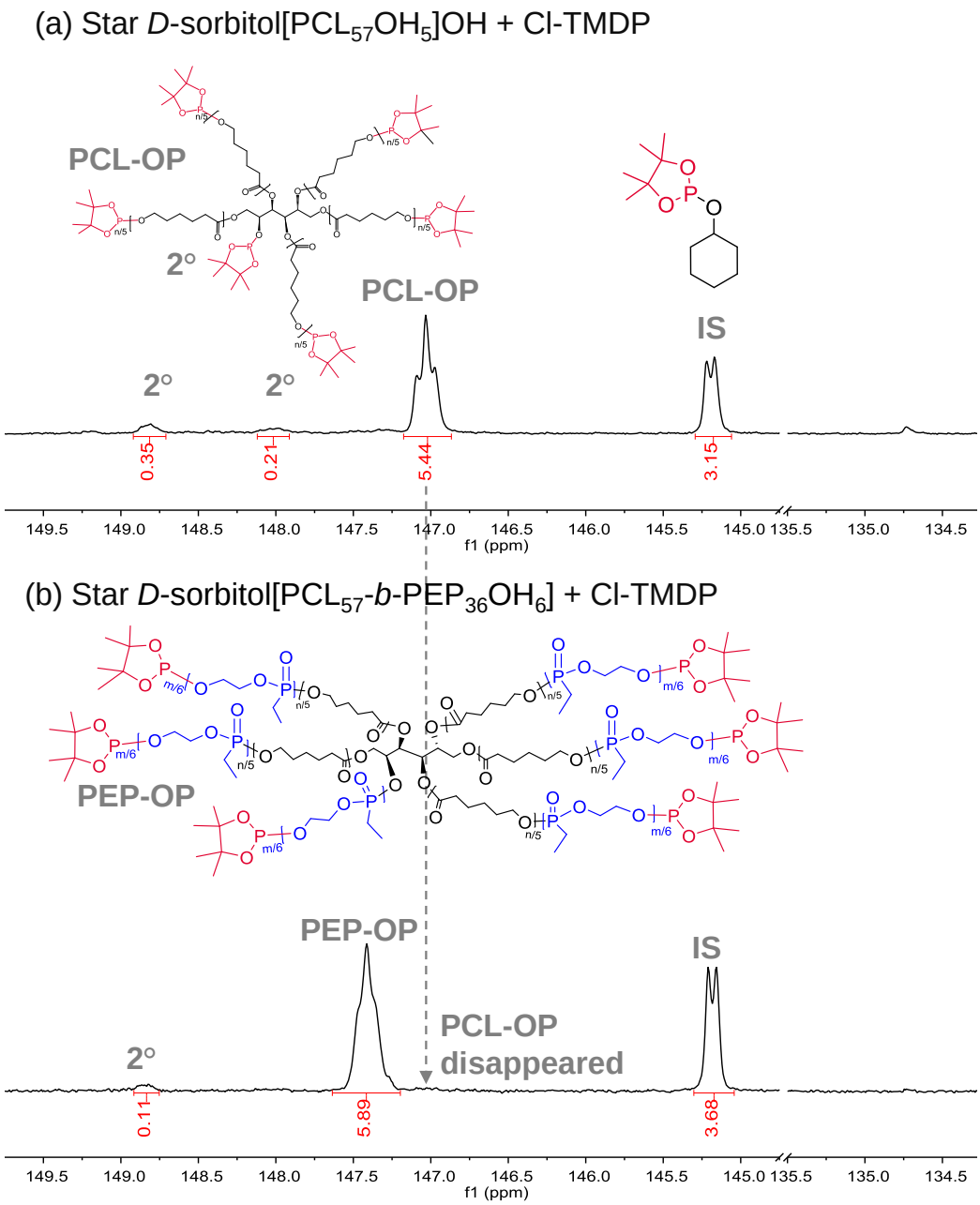



Figure 5.22. $^{31}$P NMR spectra without decoupling of phosphitylated (a) star *D*-sorbitol[$PCL_{57}OH_5$]OH showing residual secondary hydroxy groups on the *D*-sorbitol core and (b) star *D*-sorbitol[$PCL_{57}$-*b*-$PEP_{36}OH_6$] diblock copolymers showing barely any signal from secondary hydroxy groups on *D*-sorbitol and full disappearance of signals originating from the PCL-OH. IS: internal standard (cyclohexanol). The integrals are normalised.

In the $^{31}$P NMR spectrum, the integrals are normalised to six for clear understanding, so each integral in the spectrum denotes the amount present in the copolymer. From this calculation, $N_{arms}(^{31}P)$ (star copolymer) = 5.89 corresponding to star *D*-Sorbitol[$(PCL\text{-}OH)_{0.0}$-*b*-$(PEP\text{-}OH)_{5.89}$]$OH_{0.11}$ was obtained. By a detailed notation, this

also corresponds to *D*- sorbitol[$PCL_{n/(5.44)}$-*b*-$PEP_{m/(5.89)}$]$_{5.44}$[$PEP_{m/(5.89)}$]$_{0.45}$[OH]$_{0.11}$ (refer to Appendix C for a complete and detailed analysis).

Note that this nomenclature assumes that the different PCL arms of the macroinitiator have the same chain length. This is an approximation which is expected to be valid for the feed ratio of [ε-CL]$_0$:[*D*-Sorbitol]$_0$ above [25]:[1] as explained below. Similarly, this nomenclature assumes that the different PEP blocks have the same chain length. Again, this is expected to be valid provided that [PEP]$_0$:[macroinitiator]$_0$ is high enough.

Practically, the star copolymers can be represented as star *D*-sorbitol[$PCL_{57}$-*b*-$PEP_{36}OH_6$], implying the stars possess overall an average of 6 arms whether either growing from PCL chains-ends or from *D*-sorbitol (Figure 5.23 (a) and (c)).

It is noteworthy to mention here that several attempts to estimate the $M_n$ $^{P\text{-}NMR}$ (arm) and the $M_n$ $^{P\text{-}NMR}$ (star copolymer) were performed, however, the values were underestimated by about 2000 – 3000 g mol$^{-1}$. Hence, the estimation of $M_n$ $^{P\text{-}NMR}$ (star copolymer) by $^{31}$P NMR was not pursued further.

### 5.4.4.3 Bulk ROP of Low MW Star PCL and Star PCL-PEP Compounds

As discussed earlier, *D*-sorbitol based star $PCL_nOH_x$ materials may have up to 6 hydrophobic PCL arms radiating from the central sorbitol core. Previous studies on feed ratio of [ε-CL]$_0$:[*D*-sorbitol]$_0$ above [25]:[1] revealed that between 5 to 6 PCL arms were obtained by phosphitylation-$^{31}$P NMR which correlated with SEC-MALS/$^1$H NMR results.

Star PCL compounds were also synthesised using Sn(Oct)$_2$ in the bulk at 140 °C achieving monomer conversions of 96-99% and were purified using $scCO_2$ (refer to Appendix C). These star *D*-sorbitol-PCL samples are promising candidates to investigate the self-assembly and the surface activity of the star polymers (discussed in Chapter 6).

Going to a lower molar ratio of [ε-CL]$_0$:[*D*-sorbitol]$_0$ (i.e. when a lower amount of ε-CL was employed for ROP from *D*-sorbitol), the number of arms were altered. Goddard *et al.*[76] systematically studied the tuning of arms for star *D*-sorbitol-poly(lactic acid) by tuning the feed ratio of *D*-sorbitol and *D, L*-lactide. Similarly, a change to a lower number of arms occurred when decreasing the ratio of [ε-CL]$_0$:[*D*-sorbitol]$_0$ from 57:1 to 35:1, 18:1 and 4:1 resulting in star *D*-sorbitol-$PCL_nOH_x$ with varying numbers of

arms from 5, 5 to 4 and 3 arms, respectively (Table 5.3) as observed by phosphitylation-$^{31}$P NMR and by SEC-MALS/$^{1}$H NMR results.

However, a threshold molecular weight exists, above which the number of arms would remain around ~ 5 regardless of the feed ratio when $Sn(Oct)_2$ was employed as a catalyst for ROP. Say for example targeting a low molecular weight compound of $M_n^{targ}$ = 600 g mol$^{-1}$, if only 4 mol of ε-CL was allowed to react with 1 mol of *D*-sorbitol that has 6 initiating sites so it can not lead to a 'star-like polymer' but it could produce a miktoarm star structure. In our case, any feed ratio of $[\varepsilon\text{-CL}]_0$:$[D\text{-sorbitol}]_0$ above [25]:[1] yielded ~5 arm stars as observed by phosphitylation-$^{31}$P NMR and by SEC-MALS/$^{1}$H NMR data on at least 15 samples of differing MW from star *D*-sorbitol-PCL series.

In regards to star copolymer, as observed by phosphitylation-$^{31}$P NMR, all the –PCL-OH arms have grown PEP blocks and in fact, the *D*-sorbitol hydroxy signals that were pendant on the star *D*-sorbitol-PCL also participated to grow PEP blocks to give a six arm star copolymer (Figure 5.23 (a and c)). Similarly, when employing a star *D*-sorbitol$[PCL_{18}OH_4]OH_2$ (Table 5.3) possessing four –PCL-OH arms and two pendant secondary –OH on the *D*-sorbitol core (Figure 5.23 (b)), all of the hydroxy groups on the star PCL radiated PEP blocks to give a six arm star *D*-sorbitol$[PCL_{18}$-*b*-$PEP_{27}OH_6]$ diblock copolymer with four –PCL-*b*-PEP arms and two –PEP arm (Figure 5.23 (b and d)). As noted in the previous section, for the length of PCL and PEP blocks high enough, we assume the same length of all PCL blocks and for all PEP blocks.

For star *D*-sorbitol$[PCL_{18}OH_4]OH_2$ with ~4 PCL-OH arms, the $^{1}$H NMR analysis yielded a $M_n^{NMR}$ of 2240 g mol$^{-1}$ and its copolymer star *D*-sorbitol$[PCL_{18}$-*b*-$PEP_{27}OH_6]$ with $M_n^{Copoly}$ of 6000 g mol$^{-1}$ was obtained (Table 5.3, second last white row) (Figure 5.23 (b) and (d)).

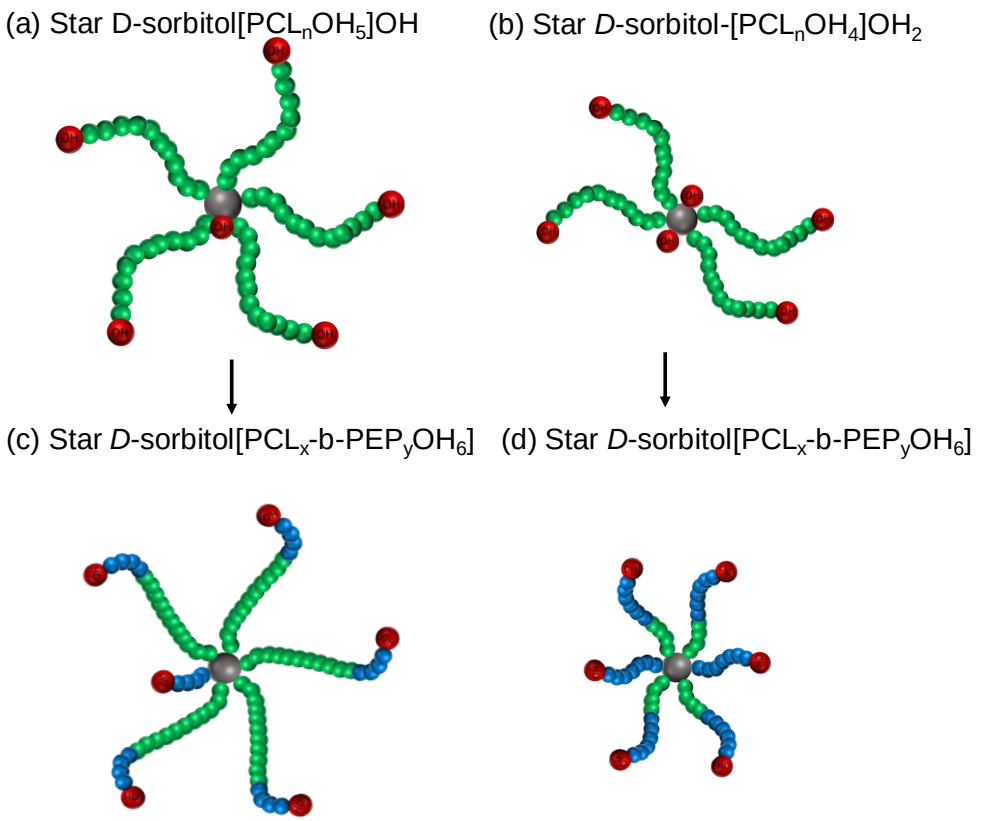



Figure 5.23. Representation of star *D*-sorbitol-PCL synthesised by $Sn(Oct)_2$; (a) having 5 –PCL arm and 1 –OH on *D*-sorbitol ($M_n$ $^{NMR}$ (PCL) = 6700 g mol$^{-1}$); (b) having 4 –PCL arm and 2 –OH on *D*-sorbitol ($M_n$ $^{NMR}$ (PCL) 2240 g mol$^{-1}$). The corresponding star *D*-sorbitol-PCL-*b*-PEP (c) having 5 –PCL-*b*-PEP arm and 1–PEP arm on *D*-sorbitol ($M_n$ $^{Copoly}$ = 11600 g mol$^{-1}$), and (d) having 4 –PCL-*b*-PEP arm and 2 –PEP arm on *D*-sorbitol ($M_n$ $^{Copoly}$ = 6000 g mol$^{-1}$). The *D*-sorbitol core (●), PCL arms (●●●), PEP arms (●●● ) and hydroxy groups (● ) are presented.

The SEC-DMF (vs. PMMA) analysis of the star homopolymer macroinitiator revealed some tailing that may be due to slow initiation relative to propagation of arms. A slightly broader dispersity was also noted in star PCL (*Đ* = 1.10 for 5 arm star and *Đ* = 1.18 for 4 arm star). However, SEC trace on star copolymer clearly showed an increase in MW and the broadening of dispersity to *Đ* = 1.31. Indeed, the absolute MW values for star copolymers consisting of PPEs are not easy to obtain on standard SEC due to not having the commercial availability of right calibration standards.

In our case, low MW star PCL-*b*-PEP compounds were analysed by at least 3-4 different SEC equipment for reliable data (linear polymers were used as calibration standards, refer Chapter 3) but the SEC traces of the samples were always very close to flow marker signal. Besides, some polymers (usually hyperbranched) often exhibit adsorption on SEC columns due to their large number of end groups (OH groups in the

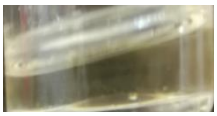
present case). These low MW amphiphiles have small arms vs. a high density of chain ends that might induce high interaction with column and broad dispersities ($Đ$ = 1.42 – 1.74, Table 5.3).

Further moving on to the low MW star compounds using star *D*-sorbitol[$PCL_4OH_3$]$OH_3$ macroinitiator (Table 5.3, last white row) the $M_n^{targ}$ (PEP block) of 720, 1350 and 2000 g $mol^{-1}$ the reaction time was significantly fast (~2.2 - 2.5 h) by bulk AROP at 60 °C using DBU catalyst, with conversion ranging from 89-99%. These low MW amphiphilic compounds (surfactants) were also purified using $scCO_2$ (at 38 °C, 180 bar at ρ of 838.76 kg $m^{-3}$) following the same procedure as described earlier except that here the equilibrium was allowed to establish for slightly longer time (typically ~30-45 min) based on the viscosity of the product. Although these compounds have honey-like stickiness, this made the recovery of samples from the autoclave difficult, but with proper care, the gravimetric yield of ~92 ± 2% was observed after purification. Like what was observed in the case of triblock compounds, the $DP^{NMR}$ values of star compounds obtained after SCFE purification method were very close to the theoretical values (Table 5.3).

To sum up, on star copolymers section, the $DP^{NMR}$ values of all the star *D*-sorbitol-$PCL_nOH_x$ macroinitiators correlate very well with the theoretical values ($DP^{theo}$ vs. $DP^{NMR}$ = 57 vs. 57, 35 vs. 34, 18 vs. 18 and 3.8 vs. 3.8). The corresponding $M_n^{NMR}$ (macroinitiator) values for star *D*-sorbitol-$PCL_nOH_x$ were 6700, 4000, 2240 and 620 g $mol^{-1}$, respectively (Table 5.3). A well characterised (SEC-MALS/$^1$H NMR, phosphitylation-$^{31}$P NMR, MALDI-TOF) star PCL macroinitiator with excellent control of MW was employed for the star copolymer synthesis. A family of star *D*-sorbitol-[$PCL_n$-*b*-$PEP_mOH_6$] diblock copolymers differing in their average molecular weights and composition of PCL and PEP block was successfully synthesised and purified using SCFE or dialysis method. Clear advantages in the yield of products were observed when the $scCO_2$ extraction method was chosen for purifications (Table 5.3).

Depending on the composition of the copolymers (PCL and PEP chain lengths, and PEP/PCL ratio), the physical form and aesthetics of homo and copolymers varied (Table 5.4).

Table 5.4. The appearance of star homo- and copolymers.

| Sample code | Physical form | Aesthetics |
|---|---|---|
| star *D*-sorbitol[$PCL_{57}OH_5$]OH homopolymer | White solid powder |  |
| star *D*-sorbitol-$PCL_{57}$-*b*-$PEP_{36}$ copolymer | Off-white waxy solid |  |
| star *D*-sorbitol-$PCL_{57}$-*b*-$PEP_{64}$ | Colourless sticky paste |  |
| star *D*-sorbitol-$PCL_{18}$-*b*-PEP $_{27}$ | Hazy off-white liquid |  |
| star *D*-sorbitol[$PCL_{3.8}OH_3$]$OH_3$ | Clear, colourless viscous liquid |  |
| star *D*-sorbitol-$PCL_{3.8}$-*b*-PEP $_{2.8}$<br>star *D*-sorbitol-$PCL_{3.8}$-*b*-PEP $_{6.4}$<br>star *D*-sorbitol-$PCL_{3.8}$-*b*-PEP $_{14.1}$ | Clear, amber-like Sticky liquid |  |
| Triblock $PEP_{1.6}$- *b*-$PCL_4$- *b*-$PEP_{1.6}$<br>Triblock $PEP_{3.6}$- *b*-$PCL_4$- *b*-$PEP_{3.6}$<br>Triblock $PEP_{7.2}$- *b*-$PCL_9$- *b*-$PEP_{7.2}$ | Clear, pale-yellow liquid |  |

### 5.4.5 MALDI-TOF of PEP-*b*-PCL-*b*-PEP Triblock Copolymer

To gain an understanding of the structure of the copolymers formed in the bulk, MALDI-TOF-MS was performed. The MALDI-TOF spectrum of a representative $PEP_{7.2}$-$PCL_9$-$PEP_{7.2}$ triblock copolymer displays a monomodal Gaussian distribution (Figure 5.24). It shows that only one series of peaks were present which was assigned to triblock copolymers and no residual HO-PCL-OH was detected in the spectrum, confirming that a copolymer is efficiently formed. To have an insight about the composition of the blocks in the copolymer, chain-ends and initiator, the region corresponding to the strongest peak (1675 – 1900 m/z) was analysed in detail (Figure 5.25 and Table 5.5).

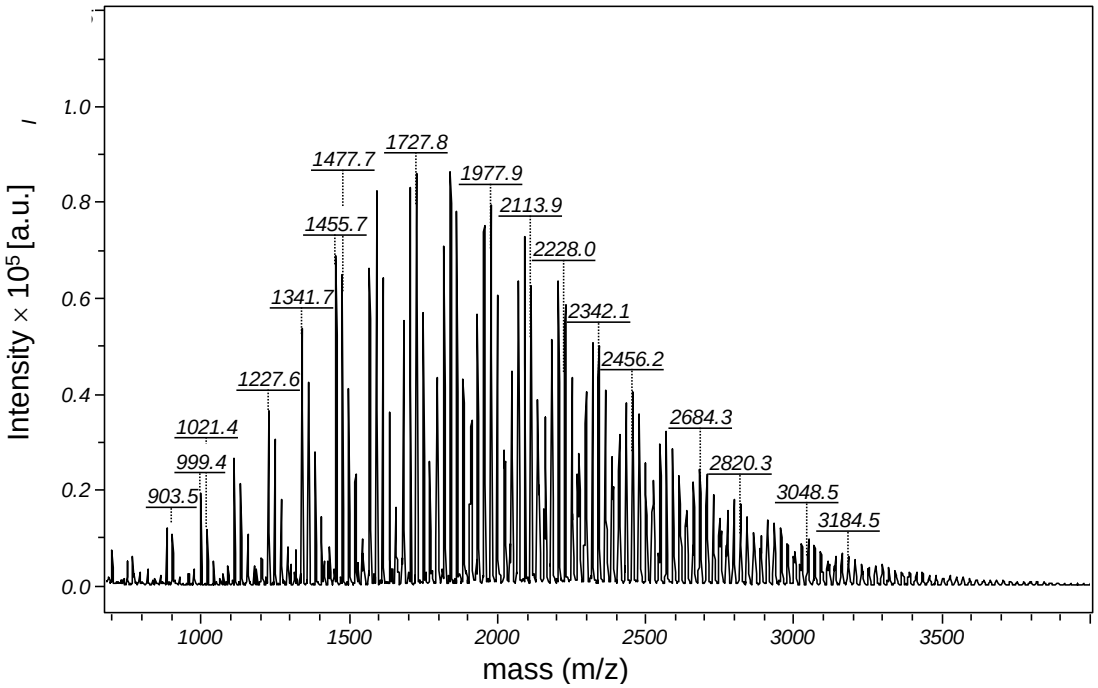



Figure 5.24. Full MALDI-TOF mass spectrum (reflection mode).of a $PEP_{7.2}$-$PCL_9$-$PEP_{7.2}$ triblock copolymer synthesised in the bulk in the presence of DBU. The MALDI-TOF spectrum was acquired in reflection mode.

Each peak of the triblock copolymer consisted of one 1,6-hexanediol group, a few units of ε-caprolactone, and a few units of ethyl phosphonate. Additionally, during ionisation, one potassium cation becomes attached to form the molecular ion of the triblock copolymer. Therefore, it enables to determine the number of repeating unit of ε-CL (n) and EP (m) present in the copolymer by comparing the experimental mass/charge ($(m/z)_{expt}$) values with the calculated monoisotopic mass/charge ($(m/z)_{calc}$) values (Eq. 5.9):

$$(m/z)_{calc} = n_{\varepsilon\text{-CL}} M_{\varepsilon\text{-CL}} + m_{EP} M_{EP} + M_{1,6\text{-hexanediol}} + M_K \quad \text{Eq. 5.9}$$

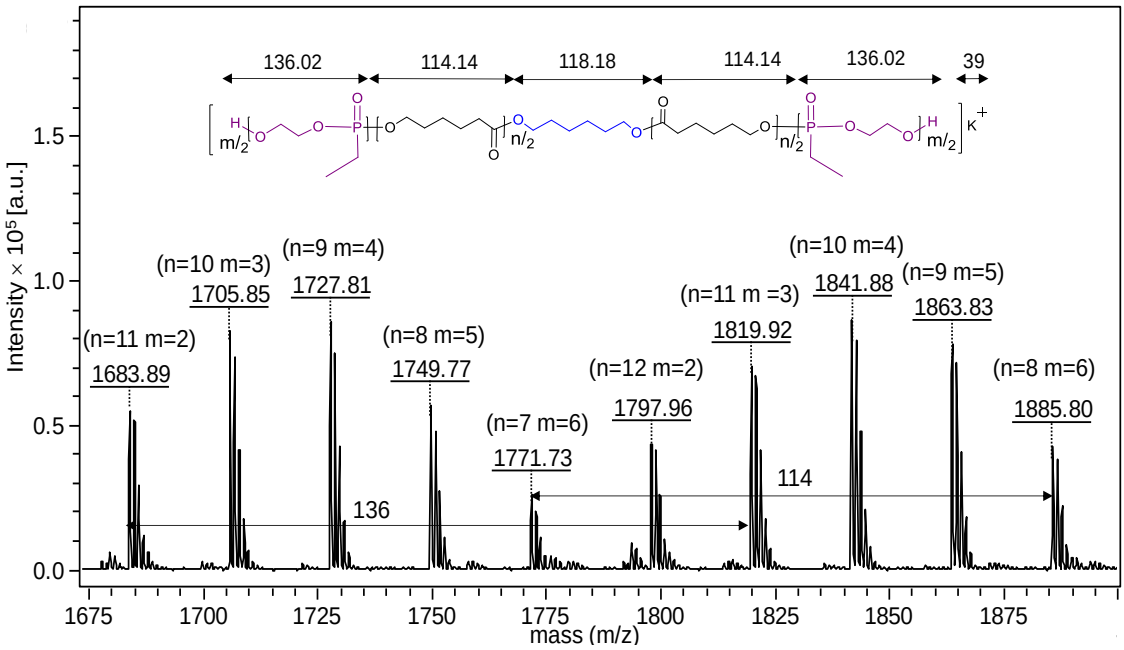



Figure 5.25. Enlarged MALDI-TOF mass spectrum (reflection mode).of a $PEP_{7.2}$-$PCL_9$-$PEP_{7.2}$ triblock copolymer synthesised in the bulk in the presence of DBU. The structure and the masses of the triblock copolymer are presented for interpretation.

Table 5.5. Assignments of the peaks in $PEP_{7.2}$-$PCL_9$-$PEP_{7.2}$ triblock copolymers, with n ε-CL units and m EP units.

| $(m/z)_{expt}$ | n | m | $(m/z)_{calc}$[a] | $\Delta = (m/z)_{calc} - (m/z)_{expt}$ |
|---|---|---|---|---|
| 1683.89 | 11 | 2 | 1683.8692 | -0.0208 |
| 1705.85 | 10 | 3 | 1705.8301 | -0.0199 |
| 1727.81 | 9 | 4 | 1727.7910 | -0.019 |
| 1749.77 | 8 | 5 | 1749.7518 | -0.0182 |
| 1771.73 | 7 | 6 | 1771.7126 | -0.0174 |
| 1793.69 | 6 | 7 | 1793.6735 | -0.0165 |
| 1797.96 | 12 | 2 | 1797.9373 | -0.0227 |
| 1815.61 | 5 | 6 | 1815.6343 | 0.0243 |
| 1819.92 | 11 | 3 | 1819.8982 | -0.0218 |
| 1841.88 | 10 | 4 | 1841.8591 | -0.0209 |
| 1863.83 | 9 | 5 | 1863.8199 | -0.0101 |
| 1885.79 | 8 | 6 | 1885.7807 | -0.0093 |

[a] Calculated from the monoisotopic mass.

The MALDI-TOF spectrum of the copolymer appears in the form of groups of peaks, where the successive differences in the $(m/z)_{expt}$ values between the peaks of previous groups and in the neighbouring groups were about 136.03 ($m_{EP}$ = 136.02) (e.g. 1683.39 and 1819.92, 1705.85 and 1841.88 etc.), or 114.07 ($n_{\varepsilon\text{-CL}}$ = 114.14) (e.g. 1771.73 and 1885.80, 1797.96 and 1911.99 etc). All the $(m/z)_{expt}$ values for these series of peaks were in good correlation with the calculated $(m/z)_{calc}$ values (Table 5.5). Hence, the

MALDI-TOF spectrum confirms the formation of the copolymer $PEP_m$-$PCL_n$-$PEP_m$ synthesised in the bulk using DBU as a catalyst.

### 5.4.6 Self-Assembly of PCL-*b*-PEP Amphiphilic Block Copolymers

The self-assembly behaviour in aqueous solution of all the amphiphilic PCL-*b*-PEP block copolymers was investigated by dynamic light scattering (DLS).

A range of amphiphilic copolymers with differing architectures (linear diblock, linear triblock and star diblock), compositions and hydrophilicity were successfully synthesised as discussed earlier. To simplify the self-assembly discussion, in the next sections these copolymers are grouped based on molecular weight (MW) as low, intermediate (Int.) and high MW copolymer (Table 5.6). For example, the low MW linear triblock amphiphile is referred to as per its architecture Triblock 1, Triblock 2 and Triblock 3 (in blue rows) and star as Star 1 and Star 2 (in the purple rows), and so on.

Table 5.6. The hydrophilic-lipophilic balance of amphiphilic linear and star $PCL_n$-*b*-$PEP_m$ diblock and linear $PEP_m$-*b*-$PCL_n$-*b*-$PEP_m$ triblock copolymer.

| | Code[a] | Amphiphilic copolymers | Hydrophilicity[b] |
|---|---|---|---|
| Low MW linear triblock | Triblock 1 | Triblock $PEP_{1.6}$-$PCL_4$-$PEP_{1.6}$ | 8.5 |
| | Triblock 2 | Triblock $PEP_{3.6}$-$PCL_4$-$PEP_{3.6}$ | 12.5 |
| | Triblock 3 | Triblock $PEP_{7.2}$-$PCL_9$-$PEP_{7.2}$ | 12.9 |
| Low MW star diblock | Star 1 | star *D*-sorbitol[$PCL_4$-*b*-$PEP_{2.8}OH_6$] | 7.6 |
| | Star 2 | star *D*-sorbitol[$PCL_4$-*b*-$PEP_{6.4}OH_6$] | 11.6 |
| Int. MW star diblock | Star PCL:PEP 2200:3700 Da | star *D*-sorbitol[$PCL_{18}$-*b*-$PEP_{27}OH_6$] | 12.3 |
| Int. MW linear diblock | Linear diblock PCL: PEP 2300:4100 Da | Linear diblock Bz- $PCL_{19}$-$PEP_{30}$ | 12.8 |
| High MW star diblock | Star 1 | star *D*-sorbitol[$PCL_{57}$-*b*-$PEP_{36}OH_6$] | 8.4 |
| | Star 2 | star *D*-sorbitol[$PCL_{57}$-*b*-$PEP_{64}OH_6$] | 11.6 |
| | Star 3 | star *D*-sorbitol[$PCL_{34}$-*b*-$PEP_{65}OH_6$] | 13.7 |

[a] Abbreviation, amphiphilic copolymers.

[b] Calculated, hydrophilicity = 20 × [$M_n^{NMR}$ (PEP block)/$M_n^{Copoly}$], adapting Griffin's formula of HLB on scale of 0 to 20 where 0 is fully lipophilic and 20 is fully hydrophilic. Da = Dalton.

When surfactant (amphiphilic) molecules are dissolved in water, above a certain concentration, they form aggregates or micelles and this point is referred to as critical aggregation concentration (CAC).

The CAC graphs of two samples is discussed simultaneously with DLS study.

### 5.4.6.1 Low MW Triblock and Star Compounds: Direct Dissolution Method

#### 5.4.6.1.1 Critical Aggregation Concentration of Triblock Amphiphile

At first, the CAC of the triblock $PEP_{7.2}$-$PCL_9$-$PEP_7$ (triblock 3) was determined by measuring the surface tension at a range of concentrations using the Wilhelmy plate method. When more triblock surfactant molecule is added, the surface tension of the solution rapidly decreases since more and more surfactant molecules will be at the air/water interface. When the interface becomes saturated, the addition of more surfactant molecules will lead to the formation of micelles. Indeed, for triblock copolymers, a sharp change in the slope occurs, and this point corresponds to CAC. The concentration at which two regression lines intersect was determined to be at 47.9 μM (0.014 wt%) (Figure 5.26). Above the CAC, the surface tension is nearly constant at about 34 $mN.m^{-1}$.

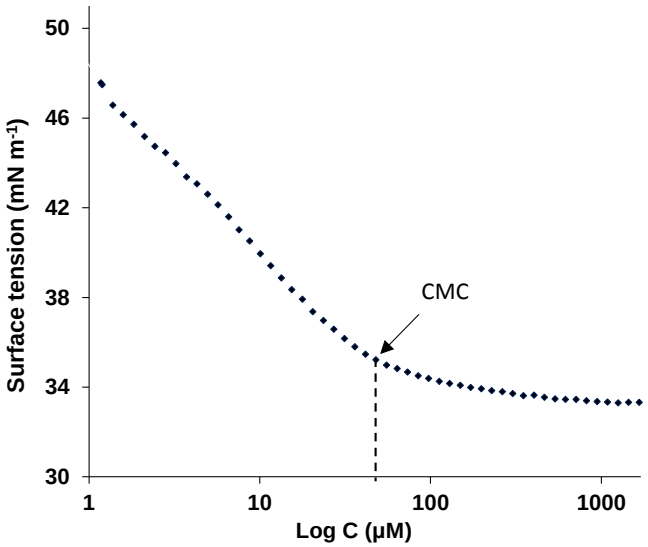



Figure 5.26. Surface tension (γ) plotted vs. log C (linear triblock $PEP_{7.2}$-$PCL_9$-$PEP_{7.2}$). Determination of CMC of the linear $PEP_{7.2}$-$PCL_9$-$PEP_{7.2}$ triblock copolymer (1000:1100:1000 g $mol^{-1}$) following the Wilhelmy plate method. The CMC value is calculated at the intersection between the two linear portions of the curve.

Thus, in this study the self-assembly by DLS at two different concentrations, 0.1 wt% and 0.5 wt% which is above the CAC, and to have consistency all amphiphiles were investigated at these two concentration.

#### 5.4.6.1.2 Low MW Triblock Amphiphile Size Investigation by DLS

To brgin with, the results obtained by direct dissolution of the copolymers in water, which is a good solvent for PEP and antisolvent for PCL is discussed. The self-assembly behaviour of the low MW triblock and low MW star-shaped diblock amphiphile was studied (at 0.1 wt% and 0.5 wt%).

The auto-correlation functions of the low MW triblock amphiphilic copolymers were measured at an angle of 173° resulting in up to 2 or 3 distinct size populations by intensity-weighted distributions (CONTIN analysis) (Figure 5.27, top). Despite two to three nanoparticle populations, we have studied the self-assembly without using filters to have full information about the particle sizes in their natural state.

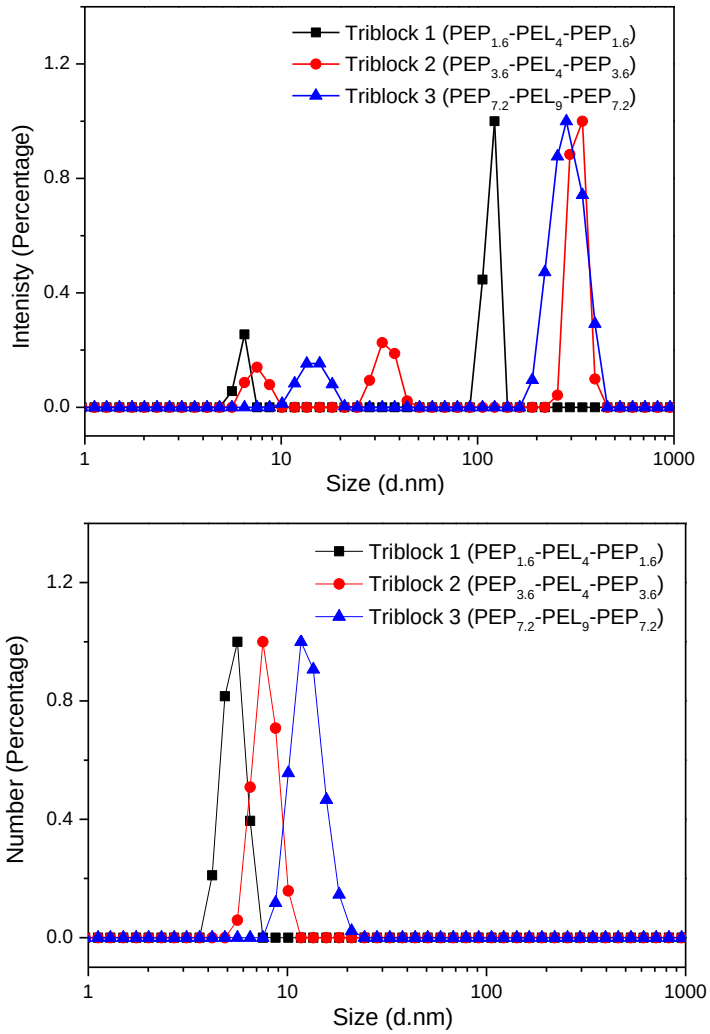



Figure 5.27. Intensity-weighted (top) and Number-weighted (bottom) size distributions of low MW $PEP_m$-*b*-$PCL_n$-*b*-$PEP_m$ triblock amphiphiles directly dissolved in water at 0.1 wt% concentration obtained by DLS measurements according to the CONTIN analysis.

The number-weighted distributions gave only 1 population (Figure 5.27, bottom). By number-weighted distributions, the hydrodynamic diameter ($D_H$) increases from Triblock 1 to Triblock 2 (same DP of PCL core and increasing DP of PEP shell) and was found to be $D_{H,\,DLS}$ = 5.6 nm and 7.4 nm, respectively in water (at 0.1 wt%). $D_{H,\,DLS}$ also increases from Triblock 2 to Triblock 3 (similar hydrophilicity but an increase of both DP of PLC core and PEP shell) and $D_{H,\,DLS}$ for Triblock 3 was 14.5 nm. This most likely corresponds to micelles since the theoretical evaluation of the size of a triblock ($PEP_7$-*b*-$PCL_9$-*b*-$PEP_7$) unimer gives a size of 3.5 nm considering a condensed $PCL_9$ chain linked to two $PEP_7$ chains in a mushroom conformation, in comparison with $D_{H,\,DLS}$ = 14.5 nm (thus a $14.5^3/3.5^3$ =71-fold excess of volume compared to unimer) (Figure 5.27, bottom).

In intensity-weighted distribution, secondary and tertiary bigger populations, having $D_H$ values from 35 nm to 100-283 nm, also coexisted for triblock amphiphile (Figure 5.28, low MW triblock) and these nanoparticles may correspond to the stabilisation of water-insoluble PCL-rich copolymers by adsorbed water-soluble triblock surfactants.

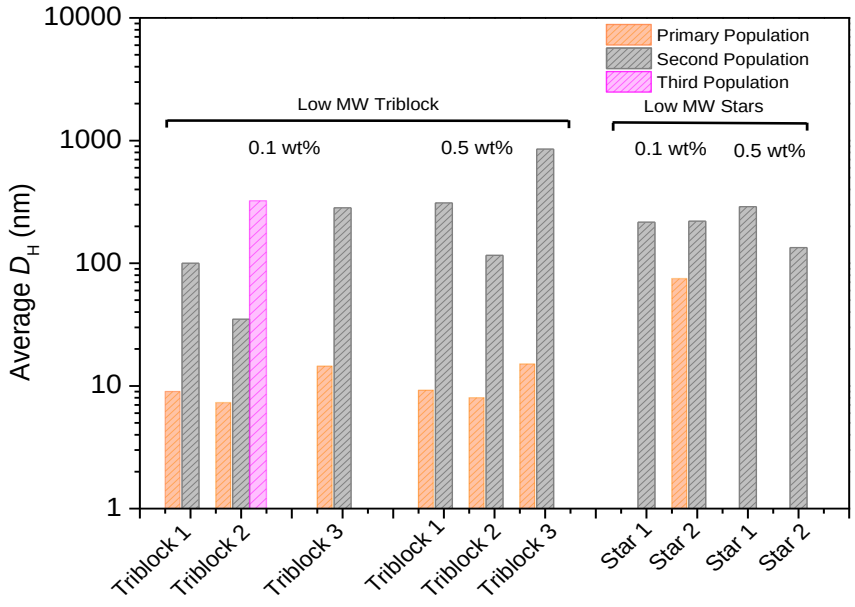



Figure 5.28. Hydrodynamic diameter by DLS ($D_{H,\,DLS}$) of low MW triblock $PEP_m$-*b*-$PCL_n$-*b*-$PEP_m$ amphiphile by intensity-weighted distribution and low MW star $PCL_n$-*b*-$PEP_m$ analogues determined by direct dissolution in water at 0.1 wt% and 0.5 wt% concentration.

However, it is important to consider the fact that the surface area of the size distribution peaks corresponding to the bigger objects (i.e. right-hand side peaks) is higher than that of the smaller objects (i.e. left-hand size peak) does not mean that bigger nanoparticles

are more numerous than the smaller ones (Figure 5.27, top vs. bottom). DLS measurements are much more sensitive to the bigger objects than small ones,[78] thus, these bigger objects appearing in the intensity-weighted distribution were null in terms of number-weighted distribution (Figure 5.27, top vs. bottom).

The bigger objects might correspond to the formation of intermicellar aggregation due to interactions such as hydrogen bonds between the hydroxy groups of the PEP of different nano-objects.[10] Alternatively, the bigger objects may suggest the coexistence of different morphologies for a single amphiphilic copolymer (Figure 5.28). Indeed, not only spheres but also cylinders and vesicles have been frequently observed for poly(ethylene oxide) based block copolymers.[79] More likely, the bigger objects might correspond to water-insoluble PCL-rich nanoparticles stabilised by water-soluble PEP-rich surfactants.

A similar trend is noticeable in the $D_H$ size distribution of various population at a higher concentration of triblock in water (0.5 wt%) (Figure 5.28).

Before discussion of the size-distribution of low MW star amphiphiles (Figure 5.28 (right)) in water, the question is could a star polymer form micelles or aggregates?

#### 5.4.6.1.3 Critical Aggregation Concentration of Star Amphiphile

For conventional linear surfactants, the surface tension decreases with an increase in amphiphile concentration up to a certain point (CAC) and then becomes nearly constant. Above the CAC, amphiphile has populated at all the interfaces so it will begin to aggregate in solution.

To investigate if a star amphiphile would show the same shape of the curve as the conventional linear amphiphile, the change in surface tension was measured for the star diblock PCL: PEP (2200:3700) g $mol^{-1}$ in water. Addition of more star amphiphile in water decreases the surface tension gradually (Figure 5.29 and Figure 5.30 (step 1)). Notably, in contrast to the former case with the linear triblock copolymer, the surface tension was not plateauing at high concentration. Indeed, the surface tension did not become constant and it still decreased from 49 mN $m^{-1}$ (at 0.012 wt%) to 46.9 mN $m^{-1}$ (at 0.5 wt%) (Figure 5.29). However, two regimes were observed, and by extrapolating the graph at the intersection between two regimes, a critical point might be estimated to be 21.2 μM (0.012 wt%). The surface tension is not plateauing; thus this critical point cannot be unambiguously assigned to a CAC.

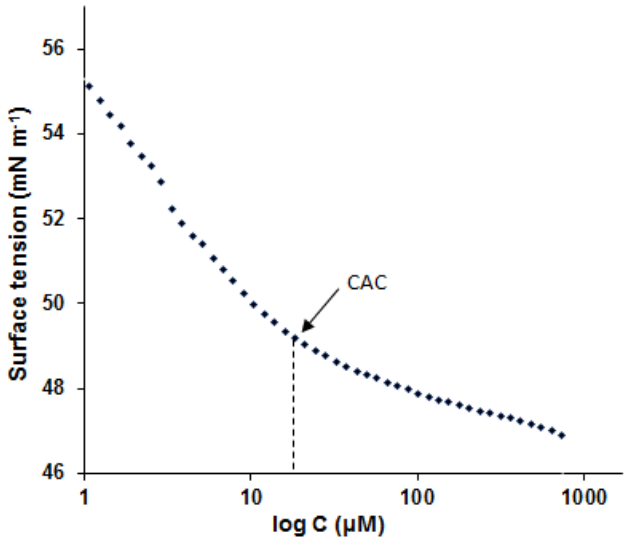



Figure 5.29. Surface tension (γ) plotted vs. log C (star copolymer concentration). Determination of CAC of star $PCL_{18}$-*b*-$PEP_{27}$ (2200:3700) g $mol^{-1}$ diblock copolymer following the Wilhelmy plate method. The critical point (CAC) might be estimated at the intersection between the two different linear regimes linear portions of the curve.

It is thought that star polymers may exist as mixtures of unimers (single star molecule) and micelles (aggregates of several star molecules) above the critical point (CAC) (Figure 5.30). The star amphiphilic copolymer can be visualised to have two conformations, a starfish-like conformation (Figure 5.31, top left) or a triangular-like conformation (Figure 5.31, top right). It is expected that the starfish-like conformer is colloidally stable in water provided that the hydrophilic PEP shell offers enough steric stabilisation (steric barrier) to the hydrophobic PCL moieties located in the inner part of the nanoparticles (PCL core) (Figure 5.31, middle). These objects are sometimes called 'unimolecular micelles' in the literature.[80] Actually, the term 'unimolecular + micelle' is misleading because 'micelle' is an association of multiple loose chains while 'unimolecular' contradict the meaning of micelles. A more appropriate term 'star unimers' will be, therefore, used for this study.

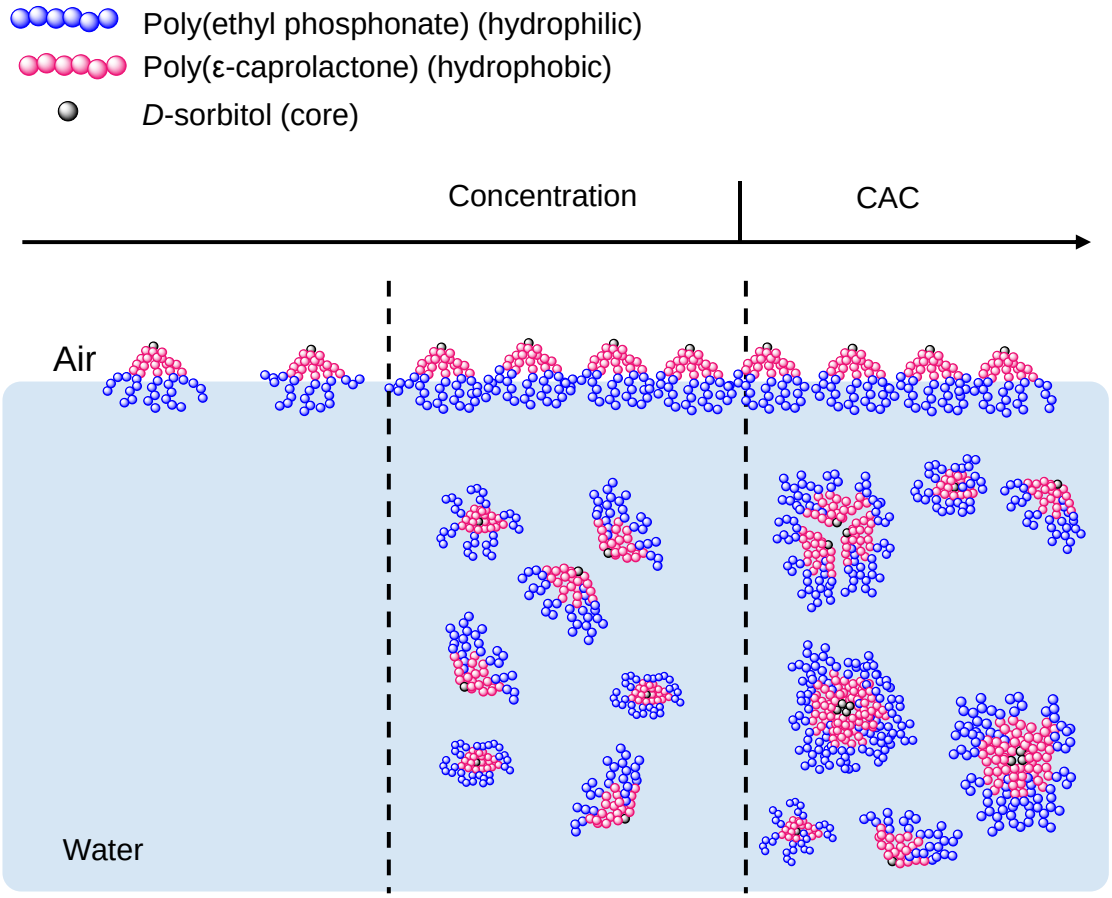



Figure 5.30. Representation of critical aggregation concentration of star diblock copolymer in water.

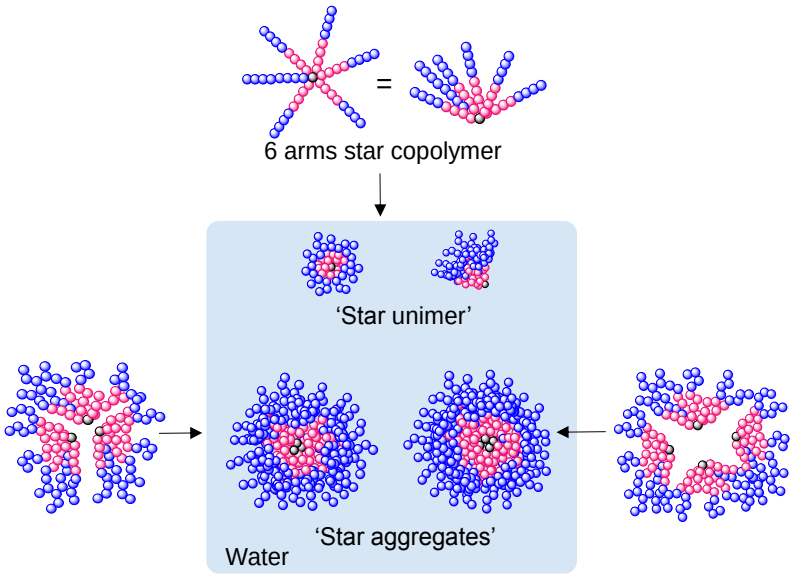



Figure 5.31. Proposed schematic diagram of the self-assembly of star copolymers: from star unimers (starfish-like conformation, and triangular-like conformation, top) to star aggregates (representation of 3 to 4 triangular-like star aggregates, bottom) in water.

The hydrogen bonds may drive the aggregation of starfish-like star micelles; however, as discussed earlier, such effects are more common in dendrimers or hyperbranched amphiphiles where a vast amount of hydroxy group is present on the shell of unimers.[10] More likely, aggregation of the star diblock copolymers can be expected to occur due to hydrophobic interaction prevailing between the hydrophobic PCL moieties in the triangular-like conformers as depicted for aggregation numbers of 3 – 4 (in Figure 5.31, bottom). Indeed, such aggregation would decrease the total surface developed by the objects dispersed in water, thus making them energetically more stable. This kind of aggregation behaviour for star amphiphiles is sometimes called 'multi-micellar aggregation' in the literature,[23] and it will be referred as "star aggregates" in this Thesis.

#### 5.4.6.1.4 Low MW Star Diblock Amphiphile Size Investigation by DLS

The self-assembly of star samples, that are directly dissolved in water at 0.1 wt% and 0.5% concentration, was investigated by DLS-size-distribution. It should be noted that the low MW star diblock amphiphile had a hydrophilicity from 7.6 to 11.6 (i.e. slightly lower than that of low MW linear triblock where hydrophilicity was from 8.5 to 12.5) (Figure 5.28). In contrast to triblock, the intensity-weighted size distribution of star amphiphile was mostly monomodal (bi-modal in one case) and, the absence of small nanoobjects was noted. Thus, a $D_{H,\,DLS}$ of 216 nm was observed for Star 1. As the hydrophilicity increased from Star1 to Star 2 (at fixed DP of PCL core), the smallest population appears at $D_{H,\,DLS}$ of 75 nm together with a bigger one at $D_{H,\,DLS}$ of 220 nm. The presence of smaller objects with $D_H$ of 75 nm may imply that the presence of more hydrophilic PEP block was stabilising the PCL core to give small objects, however, the size of the bigger object did not change. These big particle sizes may represent the star aggregates. Aggregation leads to a smaller total surface area developed by the nanoparticles, which is energetically more favoured. The big objects can also correspond to water-insoluble PCL-rich nanoparticles stabilised by adsorbed water-soluble PEP-rich surfactants. Additionally, for a more concentrated solution (0.5 wt%), these amphiphiles tend to further aggregate to give monomodal distribution ($D_{H,\,DLS}$ = 289 nm for star 1 and 134 nm for star 2). It is worth noting that, as expected, the more hydrophilic star copolymers give the smallest nano-objects in water.

### 5.4.6.2 Intermediate MW Linear vs. Star Size Investigation: Direct Dissolution Method

Intermediate MW star diblock amphiphile and its linear diblock counterpart of similar molecular weight [i.e. the composition star PCL: PEP (2200:3700 g $mol^{-1}$) having hydrophilicity = 12.3 and linear PCL: PEP (2300:4100 g $mol^{-1}$) having hydrophilicity =12.8] were introduced in the previous sections (Table 5.6).

To understand if there was any influence of the architecture on the self-assembly, a star diblock PCL: PEP (2200:3700g $mol^{-1}$) and its linear diblock PCL: PEP (2300:4100 g $mol^{-1}$) copolymer counterpart was investigated by DLS. For the linear amphiphile, the high concentration (0.5 wt%) in water gave a turbid solution; thus only 0.1 wt% was studied. For linear diblock PCL:PEP (2300:4100 g $mol^{-1}$), broad monomodal distribution with $D_{H,\,DLS}$ of 145 nm was observed in an aqueous medium at 0.1 wt% (Figure 5.32). In contrast, the star diblock copolymer was fully soluble in water at 0.5 wt%, which displays the first indication that the topology of the amphiphile is having an influence on the self-assembly in water. Interestingly, star diblock at 0.5 wt% gave bimodal size distribution and the primary objects were small nanoparticles with $D_{H,\,DLS}$ of 7 nm which coexisted with bigger aggregates of $D_{H,\,DLS}$ of 111 nm (Figure 5.32, top). More importantly, for the star diblock copolymer, the size distribution of the objects remains unchanged for a lower concentration ($D_{H,\,DLS}$ of 6.3 nm and bigger particles having $D_{H,\,DLS}$ of 107 nm). Moreover, the theoretical average size of star *D*-sorbitol[$PCL_{18}$-*b*-$PEP_{27}OH_6$] diblock amphiphile should be about ~5 nm, assuming the fully extended chain conformation of $PEP_{4.5}$ corona chains surrounding a condensed $PCL_{18}$ core. Since DLS was performed at 0.1 and 0.5 wt% (above CMC = 0.012 wt% for this star diblock copolymer) and water is a good solvent only for the hydrophilic PEP block (hydrophobic PCL block shrinking), it is reasonable to conclude that the measured diameter ($D_H$ value = ~7 nm) is that of star unimers (Figure 5.32).

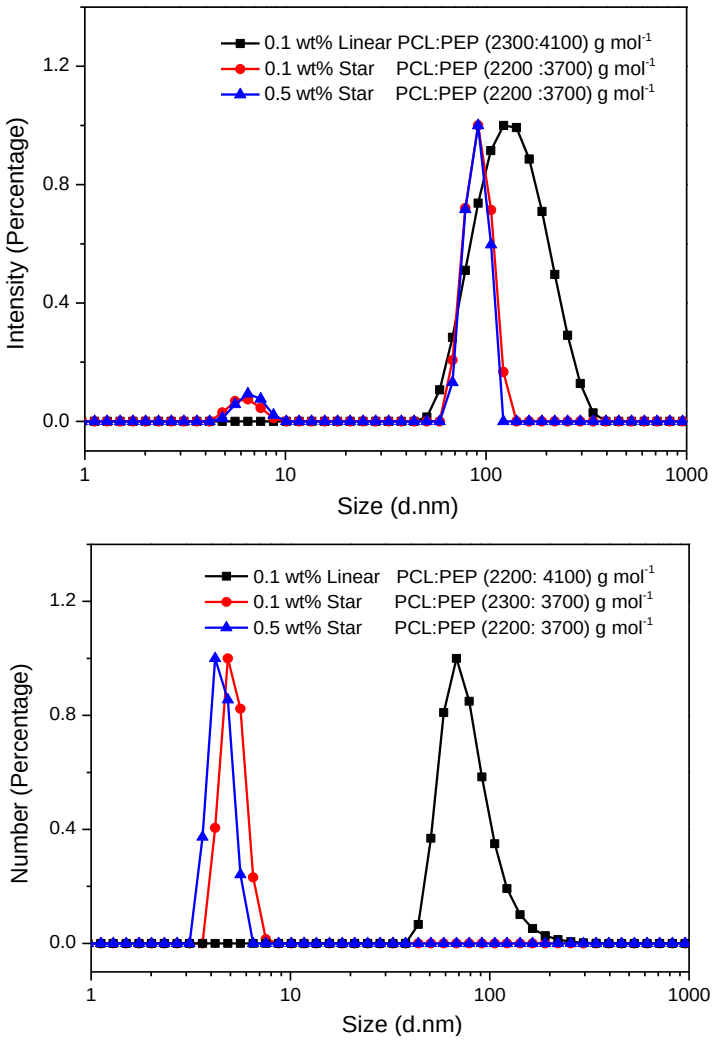



Figure 5.32. Intensity-weighted (top) and Number-weighted (bottom) size distributions DLS results obtained for star *D*-sorbitol[$PCL_{18}$-*b*-$PEP_{27}OH_6$] (2200:3700 g $mol^{-1}$) amphiphile and its linear analogues, linear diblock Bz-$PCL_{19}$-$PEP_{30}$ (2300:4100 g $mol^{-1}$) directly dissolved in water at 0.1 wt% concentration.

The bigger $D_H$-values may be observed by intensity-weighted distribution present an aggregation of a few star unimers (Figure 5.32, top). They might also correspond to water-insoluble PCL-rich nanoparticles stabilised by adsorbed water-soluble PEP-rich surfactants. It is worthy to note that these big particles observed in star diblock PCL: PEP were only observed by intensity-weighted distribution, meaning that they are in the minority. The number-weighted distributions only showed one population (monomodal) (Figure 5.32, bottom).

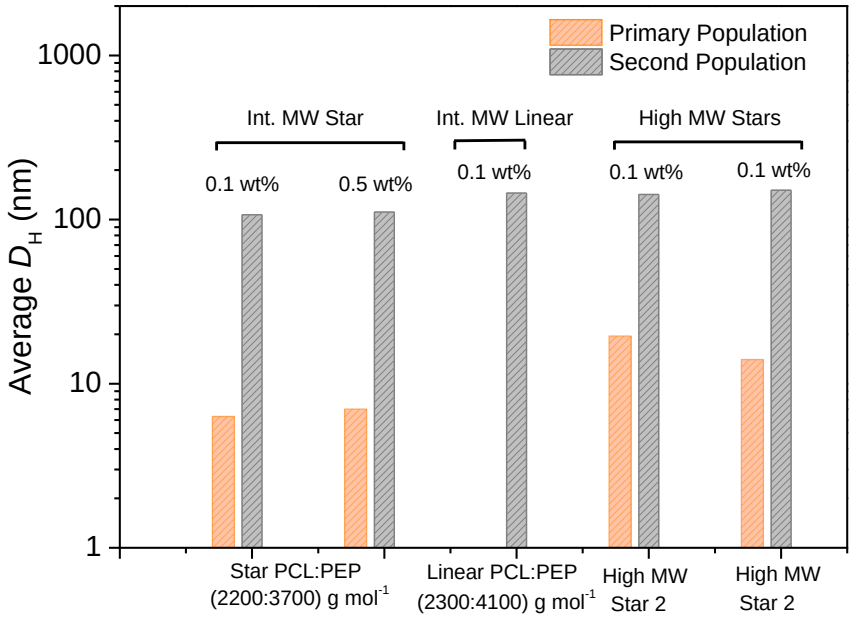



Figure 5.33. Hydrodynamic diameter ($D_H$) of high MW star $PCL_n$-*b*-$PEP_m$, Int. MW star by intensity-weighted distribution and analogue Int. MW linear diblock determined by direct dissolution in water at 0.1 wt% and 0.5 wt% by intensity distribution.

As a reminder, in star *D*-sorbitol[$PCL_{18}$-*b*-$PEP_{27}OH_6$] diblock copolymer, the 18 PCL units would be distributed on 4 arm-segments (roughly ~4-5 PCL per arm). This would decrease the overall hydrophobicity of the individual arms when compared to the linearly distributed 19 PCL units in linear Bz-$PCL_{19}$-*b*-$PEP_{30}$ diblock copolymers. This characteristic may be responsible for the lower solubility of the linear copolymer in water and bigger objects being observed (Figure 5.32 and Figure 5.33). Furthermore, (from $^{31}P$ analysis) the 27 PEP units are also distributed over 6 hydroxy groups of sorbitol, giving ~4 amphiphilic PCL-*b*-PEP arms and ~2 hydrophilic PEP arms. It indicates that overall shorter $PCL_n$-*b*-$PEP_m$ arms tethered from the sorbitol core along with some hydrophilic arm segments could explain the colloidal stability of star unimers (star unimers, $D_{H,\ DLS}$ ~7 nm). Contrary, the linear orientation of 19 PCL and 30 PEP units in the Bz-$PCL_{19}$-*b*-$PEP_{30}$ diblock copolymer may be responsible for the very low solubility of unimers in water, thus leading to self-assembly into bigger objects ($D_{H,\ DLS}$ of 145 nm) when suspended in water directly. Besides, it is known that the topology and proportion of hydrophilic and hydrophobic blocks are some of the important parameters that modulate self-assembly features.[81] Thus, the population of big particles in the case of the linear diblock copolymers more likely corresponds to water-insoluble PCL-rich nanoparticles stabilised by adsorbed water-soluble PEP-rich surfactants.

### 5.4.6.3 High MW Star PCL-*b*-PEP Copolymers: Direct Dissolution Method

Due to the medium-to-high hydrophilicity of the high MW star copolymers (hydrophilicity = 8.4 to 13.7), their self-assembly was investigated by direct dissolution in an aqueous medium (Figure 5.33). High MW star diblock copolymers (Star 1 and Star 2, with $PCL_{57}$ core) exhibit a slight cloudiness even at 0.1 wt% concentration; hence, the use of higher concentration (0.5 wt%) was not relevant. DLS results by intensity-weight distribution revealed that up to two populations coexisted for high MW stars in water ($D_{H,\,DLS}$ = 142 nm and 151 nm for bigger objects Star 1 and Star 2, respectively), but these bigger populations were negligible in number-weighed distribution. The self-assembly of high MW star diblock is discussed in detail next section.

A slight increase in the hydrophilicity between Star 3 vs. 2 (11.6 vs. 13.7) leads to a decrease in $D_{H,\,DLS}$ of smaller objects (star *D*-sorbitol-$PCL_{34}$-*b*-$PEP_{65}$ $D_{H,\,DLS}$ = 14 nm vs. star *D*-sorbitol-$PCL_{57}$-*b*-$PEP_{64}$ $D_{H,\,DLS}$ = 19.5 nm). Complementary to what was observed in the case of low MW star amphiphiles, these results indicate that the size of the nanoparticles decreases slightly when the size of the PCL core of the star unimers decreases (34 vs. 57 CL units) at a constant size of the PEP shell (64-65 EP units) (Figure 5.33). The number-weight distribution for high MW Star 3 (hydrophilicity =13.7), showed only monomodal distribution and smaller objects with $D_{H,\,DLS}$ = 7.5 nm corresponding to unimer. Due to the poor solubility of the high MW star copolymers in water by direct dissolution in water, the nanoprecipitation method was subsequently explored.

### 5.4.6.4 High MW Star PCL-*b*-PEP Diblock Copolymers: Nanoprecipitation Method

To understand whether the particle size of the high MW star diblock copolymers can be tuned towards smaller nanoparticles in aqueous solution the nanoprecipitation method was explored in which the copolymers were suspended in water through a favourable solvent (refer Chapter 3 for preparation method).

The obtained amphiphilic star *D*-sorbitol-$PCL_n$-*b*-$PEP_m$ block copolymers were first dissolved in acetone: a favourable solvent for both PCL and PEP. The self-assembly in water, a selective good solvent for PEP only, was induced by gradually adding this star

copolymer/acetone solution into Milli-Q water followed by vacuum removal of acetone. As a control experiment, the self-assembly behaviour of the hydrophobic star *D*-sorbitol[$PCL_nOH_x$]OH macroinitiators (at 0.1 wt%) was studied in parallel. The dispersion of star *D*-sorbitol[$PCL_nOH_x$]OH macroinitiators in water gave a turbid solution. The DLS measurement showed monomodal particle sizes with $D_{H,\,DLS}$ of 70 and 69 nm for star *D*-sorbitol[$PCL_{57}OH_5$]OH and star *D*-sorbitol[$PCL_{34}OH_5$]OH, respectively. These large $D_H$ particle sizes obtained for the hydrophobic star-PCL homopolymer indicate that larger aggregates were formed. The particles detected by DLS are thought to be a minor part of the polymer while the major part of the polymer was not colloidally stable in water (settling at the bottom of the flask). The length of the PCL arms does not seem to have a pronounced influence on the size of the aggregates in water. It is not surprising that the 6 hydroxy group present on the star *D*-sorbitol[$PCL_nOH_6$] homopolymer were insufficient to provide a steric stabilisation to the objects in water even when dispersed by the nanoprecipitation method.

In contrast, irrespective of the molecular weight and composition of the arms, DLS measurements of the amphiphilic high MW star copolymers (star *D*-sorbitol-$PCL_m$-*b*-$PEP_nOH_6$) show that two populations of particles are visible in the water (Figure 5.34). Contrary to what was observed with the star PCL hydrophobe, the length of the hydrophobic PCL block on the star amphiphile seems to have an influence on the aggregation behaviour of the nanoparticles. For the star copolymer systems having a PCL block of the same length, the $D_H$-values are similar for the smaller population ($D_{H,\,DLS}$ = 18 nm for high MW Star 1, 57 CL units and 36 EP units, hydrophilicity = 8.4 vs. $D_{H,\,DLS}$ 19 nm for high MW star 2, 57 CL units and 64 EP units, hydrophilicity = 11.6) (Figure 5.34). On the other hand, as already observed in the direct dissolution method, a decrease of the hydrodynamic diameter from 19 to 15 nm was observed for high MW Star 3 vs. Star 2. This is to say that when the length of the hydrophobic block decreases from 57 to 34 repeating CL units in the core while keeping 64-65 EP units in the shells) (Figure 5.34).

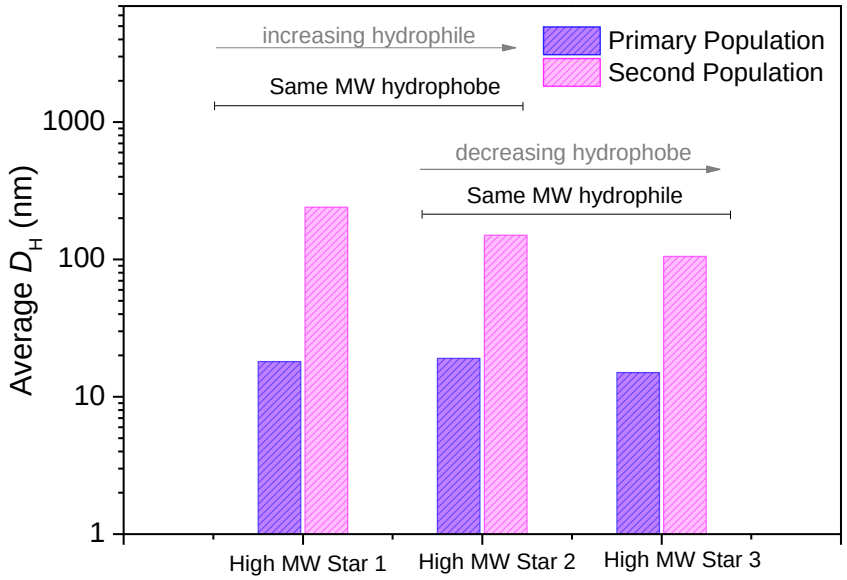



Figure 5.34. Hydrodynamic diameter ($D_H$) of high MW star $PCL_n$-*b*-$PEP_m$ in an aqueous medium at 1 mg $mL^{-1}$ concentration by nanoprecipitation method. The $D_H$- values of intensity-weighted size-distribution obtained by DLS are presented.

It is worth noting that, in the direct dissolution method, a bimodal particle size distribution was observed in both the intensity-weighted distribution and the number-averaged distribution for Star 1 and Star 2. In contrast, in the nanoprecipitation method, a bimodal particle size distribution was only observed from the intensity-weighted distribution (Figure 5.34). As the bigger objects diffuse more compared to smaller ones, the DLS measurements become much more sensitive to bigger objects. The size by intensity distribution of the bigger objects $D_{H,\,DLS}$ is 240 nm, 150 nm and 105 nm, for Star 1, Star 2 and Star 3, respectively. Indeed, the actual number of these larger particles by number-weighted distributions do not show the presence of bigger aggregates, implying that the number of larger aggregates for all stars is negligible in the system. The intensity- and number-weight distributions for Star 1 and the auto-correlation function is represented in Figure 5.35 (top) and (bottom) respectively.

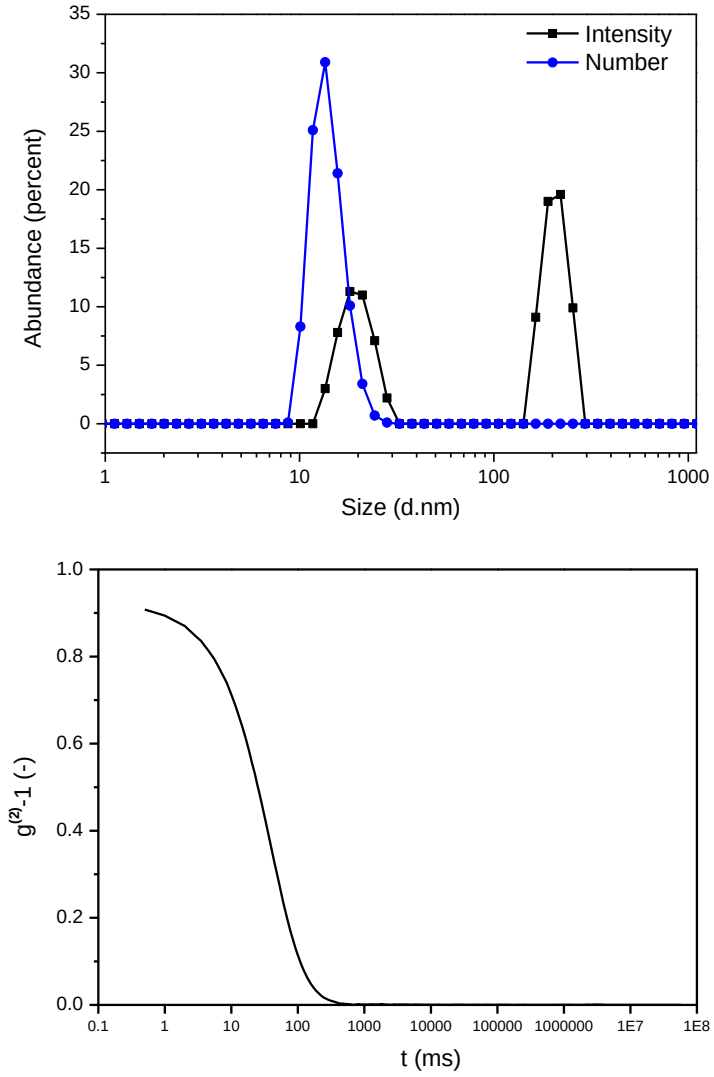



Figure 5.35. Intensity-weighted and number-weighted size distribution of star *D*-sorbitol[$PCL_{57}$-*b*-$PEP_{36}OH_6$] in an aqueous medium (0.1 wt%) (top) and autocorrelation function (bottom) obtained by nanoprecipitation method as analysed by DLS.

Moreover, the size of the small nanoparticles remains constant at several concentrations ranging from 0.0125 to 1 mg $mL^{-1}$ both in number-weight (Figure 5.36 (top)) and intensity-weight size distribution (Figure 5.36 (bottom)).

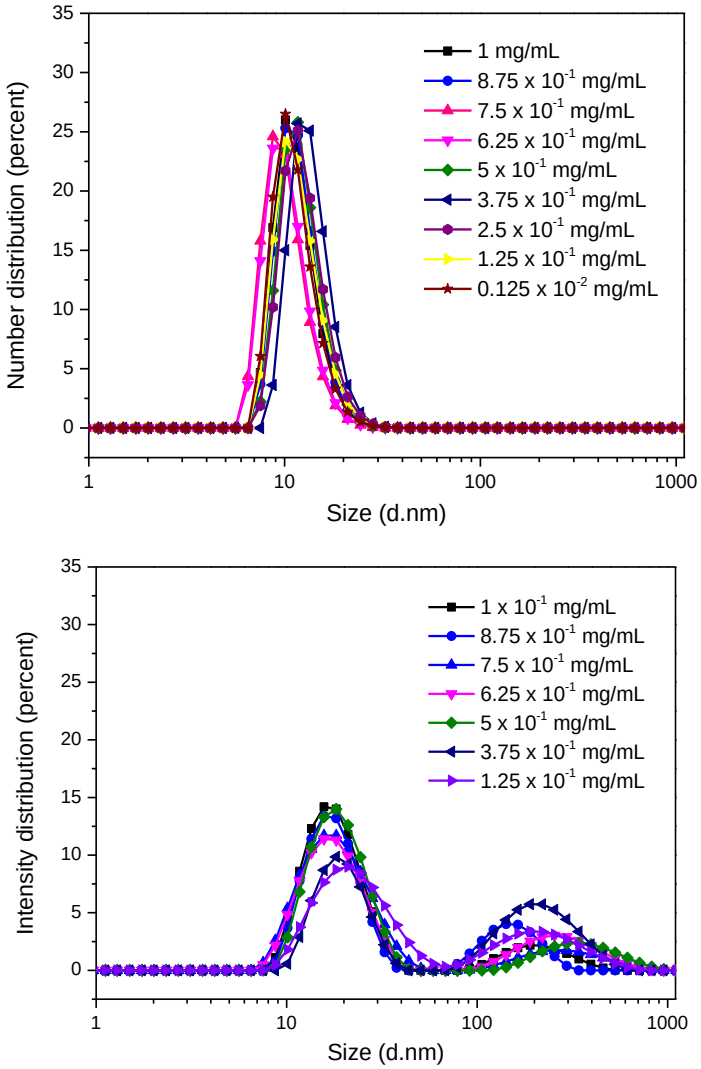



Figure 5.36. Number-weighted (top) and intensity-weighted (bottom) distribution of star *D*-sorbitol[$PCL_{57}$-*b*-$PEP_{36}OH_6$] in an aqueous medium at several concentrations obtained by nanoprecipitation method as analysed by DLS.

The theoretical average size of this star sample (*D*-value = 7 nm, considering a condensed PCL core surrounded by a fully extended PEP corona) being close to the smaller object obtained by number-weight distribution DLS ($D_{H,\ DLS}$ = ~13.6 nm), we can assign this population to 'star unimers'. The bigger objects most likely correspond to either star aggregates and/or water-insoluble PCL-rich nanoparticles stabilised by adsorbed water-soluble PEP-rich surfactants.

### 5.4.6.5 TEM and Cryo-TEM of Star *D*-sorbitol[PCL-*b*-PEP] Copolymer

Morphology of star *D*-sorbitol[$PCL_{57}$-*b*-$PEP_{36}OH_6$] diblock copolymers formed in an aqueous medium (prepared by nanoprecipitation method) was investigated by transmission electron microscopy. TEM images show the uniform size dark sphere of star diblock copolymer (Figure 5.37). The average particle size (diameter) observed from TEM analyses was smaller than the hydrodynamic diameter value found by DLS ($D_{TEM}$ = 14.3 nm and $D_{H,\ DLS\ (IWD)}$ = 18 nm by intensity-weighted distribution) (size by number-weighted distribution $D_{H,\ DLS\ (NWD)}$ is 13.6 nm) (Figure 5.37, histogram and Figure 5.35). Indeed, $D_{TEM}$ of spherical nanoparticles observed in the TEM pictures is always slightly smaller than the $D_H$-values (DLS) since TEM represent the size of the dry aggregates (particles shrink in a vacuum) while DLS measured the size of hydrated particles (solvated/swelled PEP shell). The quite low difference between the TEM diameter and the $D_H$-value found by DLS ($D_{H,\ DLS\ (IWD)} = 1.2 \times D_{TEM}$) suggests that the shrinking upon drying of the smallest objects is relatively limited. The absence of bigger aggregates on TEM images is not surprising considering that according to DLS number measurements, the absolute number of big particles approaches zero (Figure 5.35 and Figure 5.37).

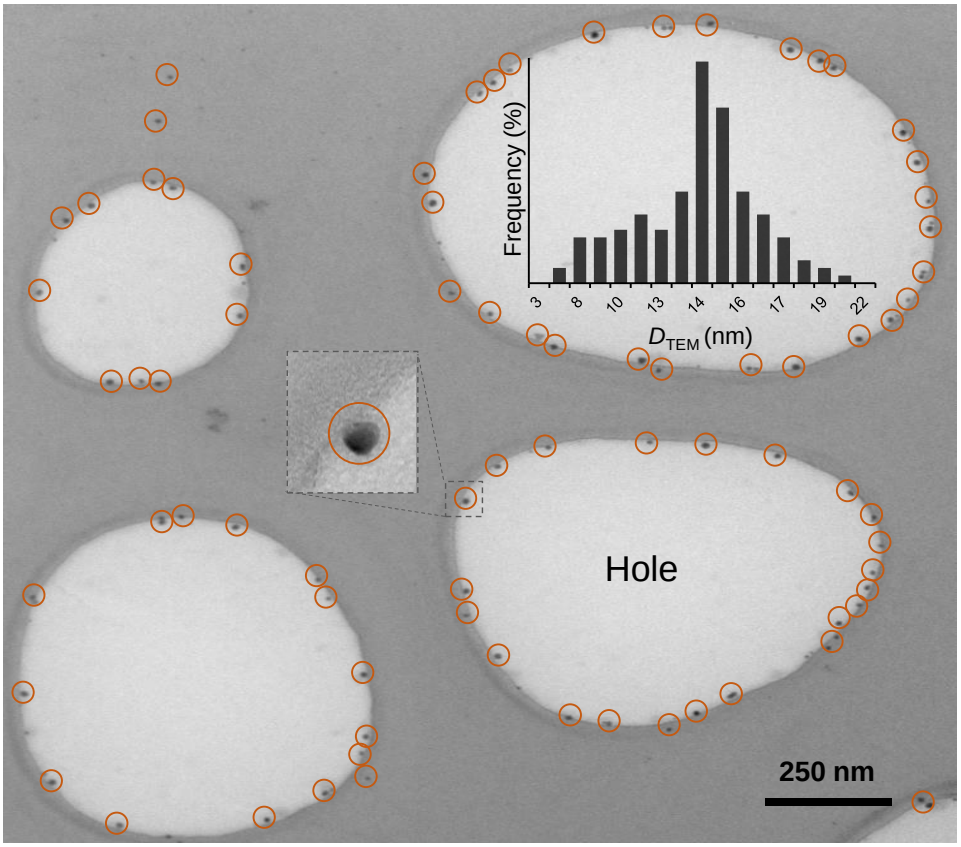



Figure 5.37. TEM images and size distribution histogram (analysed by ImageJ software) of a star *D*-sorbitol[$PCL_{57}$-*b*-$PEP_{36}OH_6$] in an aqueous solution (0.1 wt%) prepared by nanoprecipitation method on a graphene oxide-coated holey carbon copper grid. Uniformly sized spherical nanoparticles were pushed toward the edge of the hole in the carbon-polymer layer. Images acquired without staining. Scale bar 250 nm.

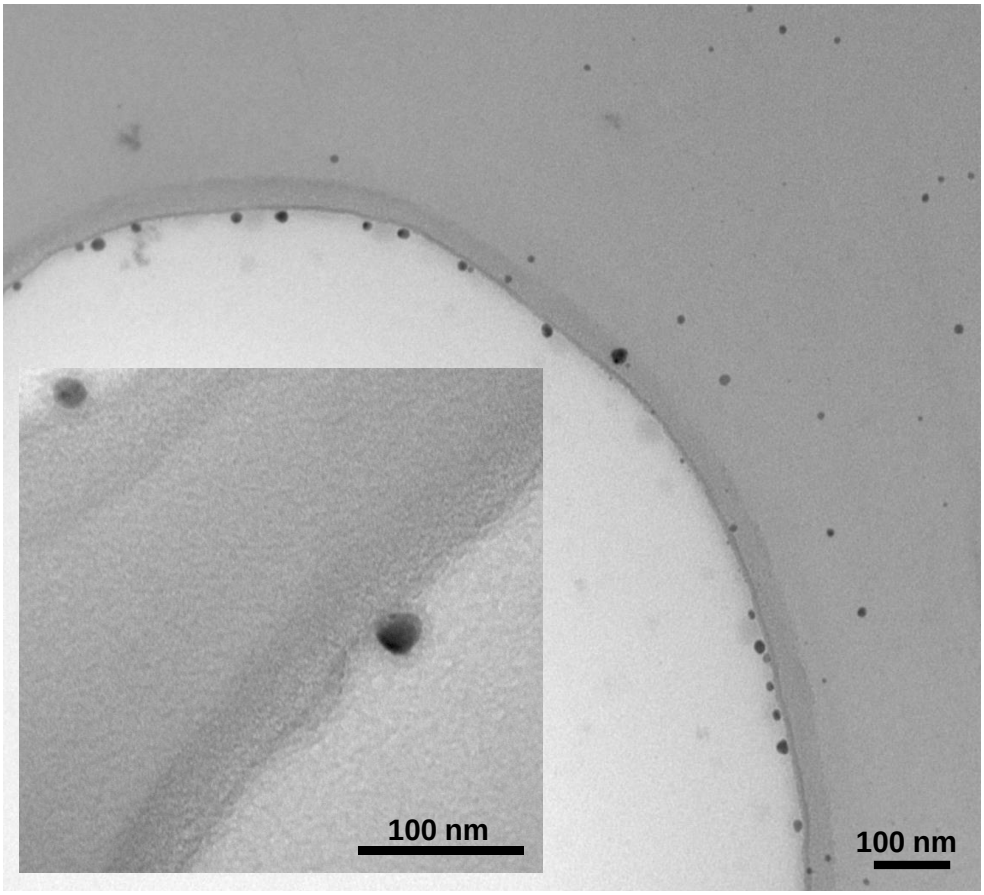



Figure 5.38. TEM images of star *D*-sorbitol[$PCL_{57}$-*b*-$PEP_{36}OH_6$] in an aqueous solution (1 mg $mL^{-1}$) by nanoprecipitation method on a graphene oxide-coated holey carbon copper grid. Images acquired without staining at magnification × 60 000 and inset at a higher magnificent × 220 000 for clarity. Scale bar 100 nm for both.

In TEM, at higher magnification, these particles appeared as spheres, but no strict pattern was visualised.

To observe the samples into its native state, Cryo-TEM was performed. For this, a very thin slide of the sample (in water) was rapidly plunged into a liquid ethane bath. It is essential to plunge the sample into the cooling liquid quickly so that the solvent water around the specimen is frozen in place thus cryogenically preserving and protecting the sample. Thus, the sample was investigated in frozen (frozen-hydrated) state. Indeed, in cryo-TEM, water is an amorphous solid, not a crystalline solid due to the quick temperature drop.

The Cryo-TEM images performed on star *D*-sorbitol[$PCL_{57}$-*b*-$PEP_{36}OH_6$] (Figure 5.39) show scattered spherical particles with a diameter $D_{cryo\text{-}TEM}$ of 17.7 nm. The structures

and size are in very good accordance with the DLS measurements ($D_{H,\ DLS\ (IWD)}$ = 18 nm).

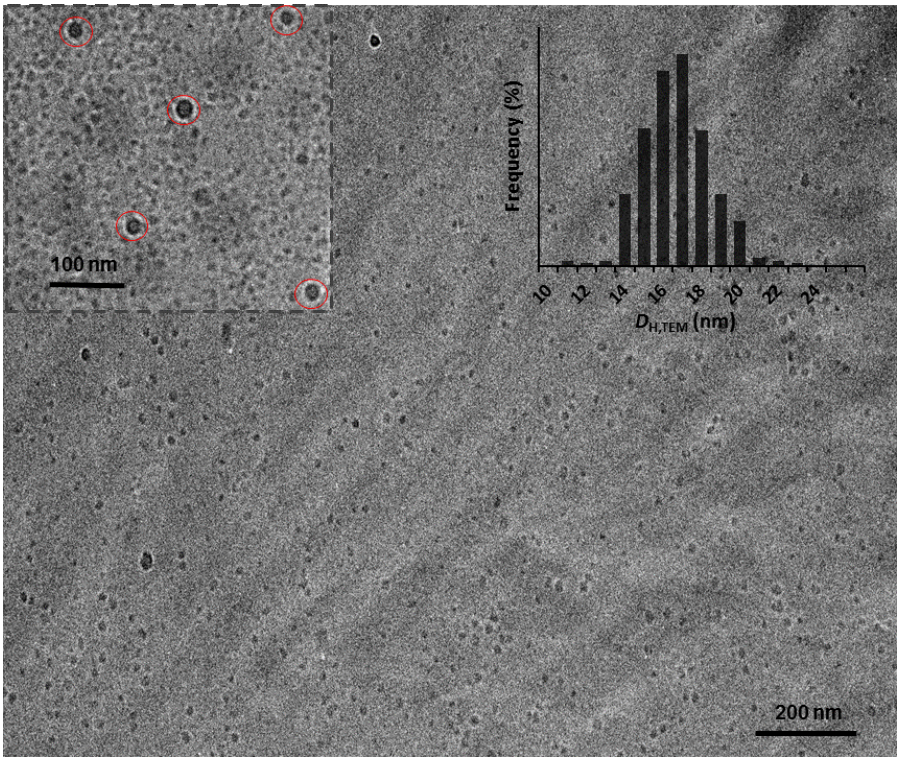



Figure 5.39. Cryo-TEM micrograph and size distribution histogram (analysed using ImageJ software) of spherical nanoparticles formed by star *D*-sorbitol[$PCL_{57}$-*b*-$PEP_{36}OH_6$] diblock copolymer in aqueous solution (0.1 wt%) prepared by the nanoprecipitation method. The scale bar is 200 nm. Images obtained without staining.

Such spherical morphologies have been frequently reported for star unimers from star-like and dendrimers structures. [6,15,18,20] In the inset of Figure 5.39, the dark black ring at the interface might be the PEP segment between two blocks (i.e. interface between the PCL core and the PEP corona), where the water concentration is low (i.e. a high concentration of phosphorus). The light grey (white-like ring) covering the dark black ring might be the PEP in the corona diluted by water. The grey core might be the condensed PCL core (very little or not swollen by water) whereas the PEP coils (possibly highly stretched) in the corona might be highly swollen by water (diluted by water) (Figure 5.31, top, star unimer in starfish-like conformation).

## 5.5 Conclusions

We have demonstrated that organocatalysed AROP of poly(ethyl phosphonate)s can be achieved in sustainable pathways (in the bulk or in $scCO_2$) without the need for conventional volatile organic compounds. Bz-$PEP_{18}$OH ($M_n$ $^{NMR}$ = 2550 g mol$^{-1}$, $Đ$ = 1.12) was obtained in bulk polymerisation, with a full conversion of ~97% being reached within a short time (up to 2 h). For the Bz-$PEP_{7.5}$OH ($M_n$ $^{NMR}$ = 1100 g mol$^{-1}$) prepared by polymerisation in $scCO_2$, the ESI-HR-MS analysis confirmed that the PEP chains were growing from the benzyl alcohol initiator. To our knowledge, this study represents the first example of poly(phosphonate)s synthesis in the bulk and in $scCO_2$.

Renewable building-blocks, '1,6-hexanediol' and '*D*-sorbitol' sugar core, utilised to prepare multifunctional PCL macroinitiators by ROP using $Sn(Oct)_2$ catalyst in the bulk and/or in $scCO_2$ (discussed in Chapter 4), were successfully employed to grow PEP blocks. Thus, DBU mediated AROP of the EP from the PCL monofunctional macroinitiator (Bz-PCL-OH) and from PCL multifunctional macroinitiators (OH-PCL-OH and *D*-sorbitol-PCL-$OH_6$) yielded linear diblock, linear triblock and star diblock copolymers of variable molecular weights and compositions in the bulk system or in the DCM. The well-controlled nature of the bulk-AROP made possible to produce amphiphilic copolymers with a low dispersity ($Đ$ = 1.04 – 1.34) and $M_n^{NMR}$-values for all the samples was corroborating well with the $M_n^{theo}$-values. Moreover, when SEC coupled with double-angle light scattering (SEC-DALS) was employed to measure $M_n^{SEC\text{-}DMF}$ of diblock copolymer using the dn/dc of copolymers measured in DMF, these molecular weights values by NMR were in close agreement with SEC-DMF results (for Bz-$PCL_{19}$OH homopolymer $M_n^{NMR}$ = 2300 g mol$^{-1}$, $M_n^{SEC\text{-}DMF}$ = 2600 g mol$^{-1}$ and for Bz-$PCL_{19}$-*b*-$PEP_{30}$ diblock copolymer $M_n^{Copoly}$ = 6400 g mol$^{-1}$ and $M_n^{SEC\text{-}DMF}$ = 6400 g mol$^{-1}$).

The ability to purify these copolymers by using low-energy $scCO_2$ extraction process achieving complete removal of the residual ethyl phosphonate in only 25 min, at low temperature (T 38 °C) and pressure (P 140 bar to 180 bar), eliminating the need for energy-intensive multi-step purification methods, toxic organic solvents and energy consuming vacuum drying steps was demonstrated. Besides, the copolymers were obtained in a remarkably high yield when purified using $scCO_2$ (~92% using $scCO_2$ vs. ~60-65% using solvent-precipitation or dialysis methods).

The successful initiation from the PCL macroinitiator (a representative case of a triblock $PEP_m$-$PCL_n$-$PEP_m$ copolymer was discussed) was confirmed by MALDI-TOF analysis in reflection mode.

The self-assembly behaviour of a series of copolymers with variable MW, composition, architecture and hydrophilicity was studied. To summarise,

Low MW linear triblock:

- Three distinct populations by intensity but only one by number-weighted distribution. Smaller population 7-15 nm corresponds to micelles (i.e. the only population visible by number distribution). Bigger objects 35-280 nm corresponds to water-insoluble PCL-rich nanoparticles stabilised by adsorbed water-soluble PEP-rich surfactants (or aggregates of micelles by hydrogen bonding, or different morphologies such as cylinders and vesicles).

Intermediate MW linear $PEP_{7.2}$-$PCL_9$-$PEP_{7.2}$ (1000:1100:1000 g $mol^{-1}$) triblock:

- By tensiometry, CAC with a clear breakpoint and nearly constant surface tension (about 34 mN $m^{-1}$) above the CAC.

Intermediate MW star $PCL_{18}$-*b*-$PEP_{27}$ (2200:3700 g $mol^{-1}$) diblock copolymer:

- By tensiometry, two regimes with a break point but the surface tension still decreases after the breakpoint thus CAC is not unambiguously defined. The surface tension stays quite high: about 47 mN $m^{-1}$ at 0.5 wt%.

Low MW star amphiphile: direct dissolution method:

- No small objects, only big objects are observed by DLS (75 nm + 220 nm), assigned to star aggregates (the star unimers are not colloidally stable enough, they aggregate in bigger objects to decrease the total surface area, which is energetically more favourable) and/or water-insoluble PCL-rich nanoparticles stabilised by adsorbed water-soluble PEP-rich surfactants.

Intermediate MW linear diblock PCL-*b*-PEP: direct dissolution method:

- The sample gives a turbid solution. One broad population of 145 nm corresponds to water-insoluble PCL-rich nanoparticles stabilised by adsorbed water-soluble PEP-rich surfactants.

Intermediate MW star diblock PCL-*b*-PEP: direct dissolution method:

- The sample is readily dispersible in water. One population at 7 nm corresponds to star unimers and another population at 111 nm corresponds to star aggregates and/or water-insoluble PCL-rich nanoparticles stabilised by adsorbed water-

soluble PEP-rich surfactants. The population of big particles is negligible in number distribution.

High MW star PCL-*b*-PEP diblock copolymers:

- ❖ Direct dissolution method: High MW star copolymers exhibit a slight cloudiness even at 0.1 wt% concentration. One population at 14-19 nm corresponds to star unimers and another population at about 150 nm corresponds to star aggregates and/or water-insoluble PCL-rich nanoparticles stabilised by adsorbed water-soluble PEP-rich surfactants.
- ❖ Nanoprecipitation method: One population at 15-19 nm corresponds to star unimers and another population in the range 100-200 nm corresponds to star aggregates and/or water-insoluble PCL-rich nanoparticles stabilised by adsorbed water-soluble PEP-rich surfactants. The actual number of the larger particles by number-weighted distributions does not show the presence of bigger aggregates, implying that the number of larger aggregates is negligible in the system.

The hydrodynamic diameter analyses in an aqueous medium of the amphiphilic star and linear copolymer analogous having similar hydrophilicity revealed that the self-assembly features were significantly affected by the block arrangements and branched architecture of the amphiphilic copolymers. The star-shaped diblock amphiphilic copolymer behaves as star unimers in water whereas the analogous linear diblock and triblock copolymers tend to self-assemble in bigger micellar aggregates.

The TEM and cryo-TEM performed on a star *D*-sorbitol-[$PCL_{57}$-*b*-$PEP_{36}OH_6$] dispersed in water (by nanoprecipitation method) confirmed the presence of uniform size spherical nanoparticles. The size of the smaller population determined by DLS intensity-weighted distribution was in good agreement with the number histogram obtained by cryo-TEM ($D_{H,\ DLS}$ = 18 nm vs. $D_{,cryo\text{-}TEM}$ = 17.7 nm), and close to the size determined by TEM ($D$ = 14.3 nm). Finally, the potential applications of such $PCL_n$-*b*-$PEP_m$ block copolymers is investigated in the next Chapter.

## 5.6 References


1. Zhang, L. & Eisenberg, A. Multiple Morphologies of 'Crew-Cut' Aggregates of Polystyrene-b-poly(acrylic acid) Block Copolymers. *Science (80-. ).* **268,** 1728–1731 (1995).
2. Discher, D. E. & Eisenberg, A. Polymer Vesicles. *Science (80-. ).* **297,** 967–973 (2002).
3. Kataoka, K., Harada, A. & Nagasaki, Y. Block copolymer micelles for drug delivery: Design, characterization and biological significance. *Adv. Drug Deliv. Rev.* **47,** 113–131 (2001).
4. Gaucher, G. *et al.* Block copolymer micelles: Preparation, characterization and application in drug delivery. *J. Control. Release* **109,** 169–188 (2005).
5. Shibata, M. *et al.* Intramolecular Folding or Intermolecular Self-Assembly of Amphiphilic Random Copolymers: On-Demand Control by Pendant Design. *Macromolecules* **51,** 3738–3745 (2018).
6. Pang, X., Zhao, L., Akinc, M., Kim, J. K. & Lin, Z. Novel amphiphilic multi-arm, star-like block copolymers as unimolecular micelles. *Macromolecules* **44,** 3746–3752 (2011).
7. Alexandridis, P. Amphiphilic copolymers and their applications. *Curr. Opin. Colloid Interface Sci.* **1,** 490–501 (1996).
8. Wang, Y. & Grayson, S. M. Approaches for the preparation of non-linear amphiphilic polymers and their applications to drug delivery. *Adv. Drug Deliv. Rev.* **64,** 852–865 (2012).
9. Bosman, A. W., Janssen, H. M. & Meijer, E. W. About Dendrimers: Structure, Physical Properties, and Applications. *Chem. Rev.* **99,** 1665–1688 (1999).
10. Mai, Y., Zhou, Y. & Yan, D. Synthesis and size-controllable self-assembly of a novel amphiphilic hyperbranched multiarm copolyether. *Macromolecules* **38,** 8679–8686 (2005).
11. Gao, C. & Yan, D. Hyperbranched polymers: from synthesis to applications. *Prog. Polym. Sci.* **29,** 183–275 (2004).
12. Heise, A., Hedrick, J. L., Frank, C. W. & Miller, R. D. Starlike Block Copolymers with Amphiphilic Arms as Models for Unimolecular Micelles. *J. Am. Chem. Soc.* **121,** 8647–8648 (1999).
13. Jin, X., Sun, P., Tong, G. & Zhu, X. Star polymer-based unimolecular micelles and their application in bio-imaging and diagnosis. *Biomaterials* 1–13 (2018). doi:10.1016/j.biomaterials.2018.01.051
14. Sisson, A. L., Ekinci, D. & Lendlein, A. The contemporary role of ε-caprolactone chemistry to create advanced polymer architectures. *Polym. (United Kingdom)* **54,** 4333–4350 (2013).
15. Jia, Z., Zhou, Y. & Yan, D. Amphiphilic star-block copolymers based on a hyperbranched core: Synthesis and supramolecular self-assembly. *J. Polym. Sci. Part A Polym. Chem.* **43,** 6534–6544 (2005).
16. Chmielarz, P. Synthesis of α- d -glucose-based star polymers through simplified electrochemically mediated ATRP. *Polymer (Guildf).* **102,** 192–198 (2016).
17. Higashihara, T., Hayashi, M. & Hirao, A. Synthesis of well-defined star-branched polymers by stepwise iterative methodology using living anionic polymerization. *Prog. Polym. Sci.* **36,** 323–375 (2011).
18. Wang, Y., Qi, G. & He, J. Unimolecular Micelles from Layered Amphiphilic Dendrimer-Like Block Copolymers. *ACS Macro Lett.* **5,** 547–551 (2016).
19. Fan, X., Li, Z. & Loh, X. J. Recent development of unimolecular micelles as functional materials and applications. *Polym. Chem.* **7,** 5898–5919 (2016).
20. Yang, X., Grailer, J. J., Pilla, S., Steeber, D. a & Gong, S. Tumor-Targeting, pH-Responsive, Stable Unimolecular Micelle as Drug Nanocarrier for Targeted Cancer Therapy. *Bioconjug. Chem.* **21,** 496–504 (2010).
21. Lin, W. *et al.* Controlled construction of gold nanoparticles in situ from β-cyclodextrin

based unimolecular micelles for in vitro computed tomography imaging. *J. Colloid Interface Sci.* **528,** 135–144 (2018).
22. Hong, H., Mai, Y., Zhou, Y., Yan, D. & Cui, J. Self-assembly of large multimolecular micelles from hyperbranched star copolymers. *Macromol. Rapid Commun.* **28,** 591–596 (2007).
23. Zhou, Y., Huang, W., Liu, J., Zhu, X. & Yan, D. Self-assembly of hyperbranched polymers and its biomedical applications. *Adv. Mater.* **22,** 4567–4590 (2010).
24. Grossen, P., Witzigmann, D., Sieber, S. & Huwyler, J. PEG-PCL-based nanomedicines: A biodegradable drug delivery system and its application. *Journal of Controlled Release* **260,** 46–60 (2017).
25. Kono, K. *et al.* Preparation and cytotoxic activity of poly(ethylene glycol)-modified poly(amidoamine) dendrimers bearing adriamycin. *Biomaterials* **29,** 1664–1675 (2008).
26. Chen, S., Zhang, X.-Z., Cheng, S.-X., Zhuo, R.-X. & Gu, Z.-W. Functionalized Amphiphilic Hyperbranched Polymers for Targeted Drug Delivery. *Biomacromolecules* **9,** 2578–2585 (2008).
27. Moeller, Martin & Matyjaszewsk, K. *Polymer Science: A Comprehensive Reference*. **6,** (Elsevier Science, 2012).
28. Dong, R. *et al.* Functional supramolecular polymers for biomedical applications. *Adv. Mater.* **27,** 498–526 (2015).
29. Claesson, H., Malmström, E., Johansson, M. & Hult, A. Synthesis and characterisation of star branched polyesters with dendritic cores and the effect of structural variations on zero shear rate viscosity. *Polymer (Guildf).* **43,** 3511–3518 (2002).
30. Song, W.-J. *et al.* Functionalized Diblock Copolymer of Poly (ε-caprolactone) and Polyphosphoester Bearing Hydroxyl Pendant Groups : Synthesis ,. *Macro* **41,** 6935–6941 (2008).
31. Kim, K. H. *et al.* Synthesis and micellization of star-shaped poly(ethylene glycol)-block-poly(ε-caprolactone). *Macromol. Chem. Phys.* **205,** 1684–1692 (2004).
32. Ulbricht, J., Jordan, R. & Luxenhofer, R. On the biodegradability of polyethylene glycol, polypeptoids and poly(2-oxazoline)s. *Biomaterials* **35,** 4848–4861 (2014).
33. Hamad, I., Hunter, A. C., Szebeni, J. & Moghimi, S. M. Poly(ethylene glycol)s generate complement activation products in human serum through increased alternative pathway turnover and a MASP-2-dependent process. *Mol. Immunol.* **46,** 225–232 (2008).
34. Knop, K., Hoogenboom, R., Fischer, D. & Schubert, U. S. Poly(ethylene glycol) in Drug Delivery: Pros and Cons as Well as Potential Alternatives. *Angew. Chemie Int. Ed.* **49,** 6288–6308 (2010).
35. Herold, D. A., Keil, K. & Bruns, D. E. Oxidation of polyethylene glycols by alcohol dehydrogenase. *Biochem. Pharmacol.* **38,** 73–76 (1989).
36. Romberg, B. *et al.* Poly(amino acid)s: Promising enzymatically degradable stealth coatings for liposomes. *Int. J. Pharm.* **331,** 186–189 (2007).
37. Li, C. & Wallace, S. Polymer-drug conjugates: Recent development in clinical oncology. *Adv. Drug Deliv. Rev.* **60,** 886–898 (2008).
38. de Macedo, C. V., da Silva, M. S., Casimiro, T., Cabrita, E. J. & Aguiar-Ricardo, A. Boron trifluoride catalyzed polymerisation of 2-substituted-2-oxazolines in supercritical carbon dioxide. *Green Chem.* **9,** 948–953 (2007).
39. Luxenhofer, R. *et al.* Poly(2-oxazoline)s as polymer therapeutics. *Macromol. Rapid Commun.* **33,** 1613–1631 (2012).
40. Verbraeken, B., Monnery, B. D., Lava, K. & Hoogenboom, R. The chemistry of poly(2-oxazoline)s. *Eur. Polym. J.* **88,** 451–469 (2017).
41. Luxenhofer, R. *et al.* Doubly amphiphilic poly(2-oxazoline)s as high-capacity delivery systems for hydrophobic drugs. *Biomaterials* **31,** 4972–4979 (2010).
42. Fetsch, C. & Luxenhofer, R. Thermal Properties of Aliphatic Polypeptoids. *Polymers (Basel).* **5,** 112–127 (2013).
43. Fetsch, C. & Luxenhofer, R. Highly defined multiblock copolypeptoids: pushing the limits of living nucleophilic ring-opening polymerization. *Macromol. Rapid Commun.* **33,** 1708–1713 (2012).

44. Luxenhofer, R., Fetsch, C. & Grossmann, A. Polypeptoids: A perfect match for molecular definition and macromolecular engineering? *J. Polym. Sci. Part A Polym. Chem.* **51,** 2731–2752 (2013).
45. Steinbach, T. & Wurm, F. R. Poly(phosphoester)s: A New Platform for Degradable Polymers. *Angew. Chemie - Int. Ed.* **54,** 6098–6108 (2015).
46. Sosnowski, S., Libkzowski, J., Stomkowski, S. & Penczek, S. Thermodynamics of. **244,** 239–244 (1984).
47. Jlapienis, G. & Penczek, S. Kinetics and Thermodynamics of Anionic Polymerization of 2-Methoxy-2-oxo-1,3,2- dioxaphosphorinane. *J. Polym. Sci. Part A Polym. Chem.* **15,** 371–382 (1977).
48. Lapienis, G., Penczek, S. & Pretula, J. Poly (dialkylphosphates) based on deoxyribose. *Macromolecules* **16,** 153–158 (1983).
49. Lapienis, G. & Penczek, S. Cationic Polymerization of 2-Alkoxy-2-oxo- 1,3,2-dioxaphosphorinanes (1,3-Propylene Alkyl Phosphates). *Macrololecules* **10,** 1301–1306 (1977).
50. Wang, F., Wang, Y.-C., Yan, L.-F. & Wang, J. Biodegradable vesicular nanocarriers based on poly(ε-caprolactone)-block-poly(ethyl ethylene phosphate) for drug delivery. *Polymer (Guildf).* **50,** 5048–5054 (2009).
51. Wen, J., Kim, G. J. A. & Leong, K. W. Poly(D,Llactide-co-ethyl ethylene phosphate)s as new drug carriers. *J. Control. Release* **92,** 39–48 (2003).
52. Xiong, M. H. *et al.* Lipase-sensitive polymeric triple-layered nanogel for 'on-demand' drug delivery. *J. Am. Chem. Soc.* **134,** 4355–4362 (2012).
53. Wang, Y. C., Liu, X. Q., Sun, T. M., Xiong, M. H. & Wang, J. Functionalized micelles from block copolymer of polyphosphoester and poly(e{open}-caprolactone) for receptor-mediated drug delivery. *J. Control. Release* **128,** 32–40 (2008).
54. Bauer, K. N., Tee, H. T., Velencoso, M. M. & Wurm, F. R. Main-chain poly(phosphoester)s: History, syntheses, degradation, bio-and flame-retardant applications. *Prog. Polym. Sci.* **73,** 61–122 (2017).
55. Zhao, Z., Wang, J., Mao, H.-Q. & Leong, K. W. Polyphosphoesters in drug and gene delivery. *Adv. Drug Deliv. Rev.* **55,** 483–499 (2003).
56. Bauer, K. N. *et al.* Polymerizing Phostones: A Fast Way to In-Chain Poly(phosphonate)s with Adjustable Hydrophilicity. *Macromolecules* **51,** 1272–1279 (2018).
57. Wolf, T., Steinbach, T. & Wurm, F. R. A Library of Well-Defined and Water-Soluble Poly(alkyl phosphonate)s with Adjustable Hydrolysis. *Macromolecules* **48,** 3853–3863 (2015).
58. Henke, H., Brüggemann, O. & Teasdale, I. Branched Macromolecular Architectures for Degradable, Multifunctional Phosphorus-Based Polymers. *Macromol. Rapid Commun.* **38,** 1600644 (2017).
59. Guo, C., Zhou, L. & Lv, J. Effects of expandable graphite and modified ammonium polyphosphate on the flame-retardant and mechanical properties of wood flour-polypropylene composites. *Polym. Polym. Compos.* **21,** 449–456 (2013).
60. Chen, L. & Wang, Y. Z. Aryl polyphosphonates: Useful halogen-free flame retardants for polymers. *Materials (Basel).* **3,** 4746–4760 (2010).
61. Wang, Y.-C. *et al.* Self-Assembled Micelles of Biodegradable Triblock Copolymers Based on Poly(ethyl ethylene phosphate) and Poly(ϵ-caprolactone) as Drug Carriers. *Biomacromolecules* **9,** 388–395 (2008).
62. Steinbach, T., Ritz, S. & Wurm, F. R. Water-soluble poly(phosphonate)s via living ring-opening polymerization. *ACS Macro Lett.* **3,** 244–248 (2014).
63. Sun, T. M., Du, J. Z., Yan, L. F., Mao, H. Q. & Wang, J. Self-assembled biodegradable micellar nanoparticles of amphiphilic and cationic block copolymer for siRNA delivery. *Biomaterials* **29,** 4348–4355 (2008).
64. Cuong, N.-V., Hsieh, M.-F., Chen, Y.-T. & Liau, I. Doxorubicin-Loaded Nanosized Micelles of a Star-Shaped Poly(ε-Caprolactone)-Polyphosphoester Block Co-polymer for Treatment of Human Breast Cancer. *J. Biomater. Sci. Polym. Ed.* **22,** 1409–1426

(2011).
65. Zhang, Y. & Zhuo, R. X. Synthesis and in vitro drug release behavior of amphiphilic triblock copolymer nanoparticles based on poly (ethylene glycol) and polycaprolactone. *Biomaterials* **26,** 6736–6742 (2005).
66. Xiao, C. S., Wang, Y. C., Du, J. Z., Chen, X. S. & Wang, J. Kinetics and mechanism of 2-ethoxy-2-oxo-1,3,2-dioxaphospholane polymerization initiated by stannous octoate. *Macromolecules* **39,** 6825–6831 (2006).
67. Clément, B., Grignard, B., Koole, L., Jéroîme, C. & Lecomte, P. Metal-free strategies for the synthesis of functional and well-defined polyphosphoesters. *Macromolecules* **45,** 4476–4486 (2012).
68. Iwasaki, Y. & Yamaguchi, E. Synthesis of well-defined thermoresponsive polyphosphoester macroinitiators using organocatalysts. *Macromolecules* **43,** 2664–2666 (2010).
69. Macdonald, E. K. & Shaver, M. P. An expanded range of catalysts for synthesising biodegradable polyphosphonates. *Green Mater.* **4,** 81–88 (2016).
70. Blakey, I., Yu, A., Howdle, S. M., Whittaker, A. K. & Thurecht, K. J. Controlled polymerisation of lactide using an organo-catalyst in supercritical carbon dioxide. *Green Chem.* **13,** 2032 (2011).
71. Grignard, B. *et al.* Merging supercritical carbon dioxide and organocatalysis for the precision and green synthesis of poly(lactide)-based (co)polymers. *Eur. Polym. J.* **95,** 635–649 (2017).
72. Wolf, T., Steinbach, T. & Wurm, F. R. A Library of Well-Defined and Water-Soluble Poly(alkyl phosphonate)s with Adjustable Hydrolysis. *Macromolecules* **48,** 3853–3863 (2015).
73. Heldebrant, D. J., Jessop, P. G., Thomas, C. A., Eckert, C. A. & Liotta, C. L. The reaction of 1,8-diazabicyclo[5.4.0]undec-7-ene (DBU) with carbon dioxide. *J. Org. Chem.* **70,** 5335–5338 (2005).
74. Kumar, N. & Tyagi, R. Industrial Applications of Dimeric Surfactants: A Review. *J. Dispers. Sci. Technol.* **35,** 205–214 (2014).
75. Rayeroux, D., Lapinte, V. & Lacroix-Desmazes, P. One-pot synthesis of amphiphilic diblock copolymers of poly(styrene) and poly(2-methyl-2-oxazoline) by the direct combination of reverse iodine transfer polymerization (RITP) and cationic ring-opening polymerization (CROP) processes. *J. Polym. Sci. Part A Polym. Chem.* **50,** 4589–4593 (2012).
76. Goddard, A. R. *et al.* Controlled polymerisation and purification of branched poly(lactic acid) surfactants in supercritical carbon dioxide. *Green Chem.* **18,** 4772–4786 (2016).
77. Woodruff, M. A. & Hutmacher, D. W. The return of a forgotten polymer - Polycaprolactone in the 21st century. *Prog. Polym. Sci.* **35,** 1217–1256 (2010).
78. Loos, K. *et al.* Micellar aggregates of amylose-block-polystyrene rod-coil block copolymers in water and THF. *Macromolecules* **38,** 873–879 (2005).
79. Won, Y. Y., Brannan, A. K., Davis, H. T. & Bates, F. S. Cryogenic transmission electron microscopy (cryo-TEM) of micelles and vesicles formed in water by poly(ethylene oxide)-based block copolymers. *J. Phys. Chem. B* **106,** 3354–3364 (2002).
80. Newkome, G. R., Moorefield, C. N., Baker, G. R., Saunders, M. J. & Grossman, S. H. Unimolecular Micelles. *Angew. Chemie Int. Ed. English* **30,** 1178–1180 (1991).
81. Satoh, Y. *et al.* Synthesis of Well-Defined Amphiphilic Star-Block and Miktoarm Star Copolyethers via t-Bu-P4-Catalyzed Ring-Opening Polymerization of Glycidyl Ethers. *Macromolecules* **49,** 499–509 (2016).

# Chapter 6
# Applications of Star Polymers

## 6.1 Abstract

The focus of this Chapter is to explore some applications of the star materials synthesised in this thesis. Thus, this Chapter has been divided into two main areas: surfactants and coatings.

In the first part, the surface activity of some of the PCL:PEP based compounds (discussed in Chapter 5) is investigated. The polymers are evaluated as surfactants that might have utility in the delivery of fragrances and as emulsifiers as required in personal care products.

In a second part, star PCL-based samples prepared in Chapter 4 were derivatised (maleate) and utilised to prepare UV-curable films for coatings.

**Surfactants**

Static and dynamic surface tension of the novel star PCL:PEP and triblock PCL:PEP were investigated by using a Wilhelmy plate and bubble pressure tensiometer. The surface activity of the surfactants was compared with some commercial petroleum-based surfactant such as Tweens and Pluronics. The triblock $PEP_{7.2}$-$PCL_{9}$-$PEP_{7.2}$ of 1000:1100:1000 g $mol^{-1}$ copolymer has out-performed the commercial Pluronic L35 and L64 surfactants in reducing the surface tension of water. Surfactants are needed to incorporate essential oils and fragrances in personal care products, cosmetics, and perfumes due to their diverse properties and pleasant odour. Some preliminary evaluation of the synthesised surfactants as a solubiliser of fragrances and as an emulsifier of oils as required in personal care products were investigated. Star-shaped PCL:PEP diblock compounds of 2200:3700 g $mol^{-1}$ have shown good performance in solubilising bisabolol up to 9.8: 1 wt %.

On the other hand, the biobased hydrophobic star *D*-sorbitol-PCL were end-capped with hemi-ester of maleic acid in order to improve their dispersibility in water. The corresponding neutralised stars with triethylamine were found to be fully water-soluble and surface active. It is worth noting that the anionic biobased star PCL (~3100 g $mol^{-1}$) functionalised with hemi-ester of maleic acid triethylammonium salt and the nonionic star PCL:PEP surfactants have shown similar surface activity to reduce the surface tension down to ~ 42 mN $m^{-1}$.

**Coatings**

Star-shaped poly(ε-caprolactone)s (S-PCL) were functionalised with polymerisable maleate terminal groups. The star S-PCL precursors of 3100 g $mol^{-1}$ were prepared by Novozym 435 catalysed eROP in the presence of *D*-sorbitol as an initiator (discussed in Chapter 4). The functionalised S-PCL maleates were employed to synthesise crosslinked polymer coatings by photo-induced radical copolymerisation with 10 wt% of tri(ethylene glycol) divinyl ether in the presence of Darocur 1173 as a photoinitiator. The kinetics of the UV-polymerisation was monitored by real-time Fourier-Transform Infrared (FTIR) spectroscopy, which revealed that the star S-PCL maleate/divinyl ether system was not scavenged by molecular oxygen (donor/acceptor polymerisation). The UV-crosslinking reaction was fast (~10 s) to reach near quantitative conversions. The S-PCL / divinyl ether liquid formulation cast on glass substrates successfully gave polymer coatings upon UV-crosslinking. The thermal properties and degradation behaviour of the polymer films and its precursor polymers were characterised by DSC and TGA while the characterisation of the surface properties of these films is the perspective of this preliminary work.

## 6.2 Introduction

Water-soluble surface-active block copolymers have a great potential as alternatives or additives to traditional small-molecule surfactants. They have shown great promise for actual or potential application in various fields (including medicines, detergents, cosmetics ingredients, wetting agents, lubricants, viscosity modifiers, agriculture, paints, textile goods) as emulsifiers, solubilisers, and as dispersants.[1,2]

An emulsifier is a third component that is required to disperse two immiscible liquids together (typically oil and water), i.e. to make an emulsion of two immiscible liquids and the process of mixing them is called emulsification.[3] The liquid droplets (the dispersed phase) are dispersed in a liquid medium (the continuous phase). Several classes may be distinguished: oil-in-water (O/W), water-in-oil (W/O), oil-in-oil (O/O), multiple emulsions (e.g. water-in-oil-in-water W/O/W), and mixed emulsion consisting of two different dispersed droplets that do not mix in a continuous medium (e.g. O1/W + O2/W).

According to the size of their droplets, emulsions are distinguished as (a) macroemulsions (O/W or W/O typically with a size range of 0.1–5 μm), (b) nanoemulsions or miniemulsions (usually size range ~100 nm, they only exhibit kinetic stability), (c) micellar emulsions or microemulsions (5-50 nm, they are usually thermodynamically stable).[3] This Thesis only deals with macroemulsions.

Emulsion stability is a critical parameter, which refers to the colloid stability of an emulsion to keep its properties unchanged over a certain period (typically on storage for up to 2 years) under different conditions such as temperature changes and during transportation. Emulsions are, however, thermodynamically unstable thus changes of emulsion properties will occur; the more slowly the properties change the more stable the emulsion is.[3] Although the emulsions exist in a thermodynamically unstable state, some remain kinetically stable for months or years.

Several breakdown processes may occur on storage depending on droplet size distribution and density difference between the dispersed phase and the continuous medium. The phenomena responsible for thermodynamic instability that can alter emulsion properties are coalescence, flocculation, creaming, sedimentation, phase inversion and Ostwald ripening (Figure 6.1).[4] Indeed, colloidal droplets in a dispersion medium are constantly moving due to Brownian motion. When gravitational or

centrifugal forces exceed the thermal motion of the droplets (Brownian motion), a concentration gradient builds up in the system so that the larger droplets tend to move up or down through the continuous phase. If the droplet density is lower than that of the medium then they tend to move up and form a layer of emulsion on the top. This phenomenon is called creaming (Figure 6.1, (a)). In contrast, when the droplets have a higher density than that of the medium they tend to move down to form a layer at the bottom of the emulsion. This phenomenon is known as sedimentation (Figure 6.1, (b)).[4] Usually, the density of oil is lower than that of water, thus droplets of O/W emulsions tend to cream, while those of W/O emulsions tend to sediment.

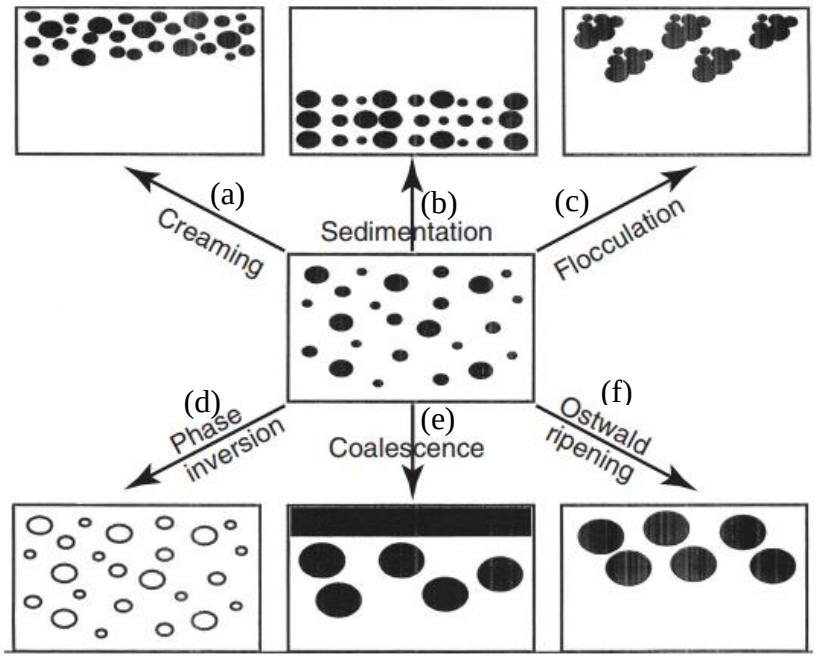



Figure 6.1. Schematic representation of the various breakdown processes in emulsions.[3]

Because they are constantly moving, by gravity or mechanical agitation, emulsion droplets frequently collide with each other and can move either apart or aggregate. There are two main types of aggregation: flocculation and coalescence (Figure 6.1, (c) and (e)). Flocculation is the aggregation of droplets that preserve their physical properties while coalescence is the aggregation of droplets that merges. Flocculation may be reversible (weak flocculation) or irreversible (strong flocculation) while coalescence is irreversible.[3,4]

As discussed above, atoms or molecules always attract each other at short distances of separation. Similarly, interactions also exist between dispersed colloidal droplets.

Three main types of interactions exist between dispersed droplets when they are approaching each other: [5]

(i) Attractive interactions due to Van der Waals forces (it tends to destabilise emulsions),

(ii) Repulsive interactions due to the presence of charges on the surface of the droplets (Coulombic forces) (generally impart stability: electrostatic stabilisation) and

(iii) Attractive or repulsive interactions due to the presence of uncharged adsorbed layers (nonionic surfactants) (possible steric stabilisation).

**There are three different possible origins for Van der Waals forces**: permanent dipole-dipole interaction (Keesom) forces, the permanent dipole-induced dipole interactions (Debye) and London dispersion force. The London dispersion forces are the most important and display longer range attractions between colloidal droplets since it occurs for polar and nonpolar molecules. It arises from fluctuations in the electron density distribution and range of the van der Waals-London (VDWL) attraction is between 5 and 10 nm.[5] To achieve the stability of the emulsion, it is essential to create an effective repulsion mechanism in order to overcome the ever-present Van der Waals attraction between the droplets. The stabilisation of emulsion relies on electrostatic stabilisation, steric stabilisation, or electrosteric stabilisation.

**Electrostatic Stabilisation.** Generally, two types of repulsion (Coulombic repulsion) mechanisms counterbalance the VDWL attraction exhibited between colloidal droplets in polar liquids: Electrostatic repulsion is produced by creating an electrical double layer around the droplets because of charge separation. In charge stabilisation, it is the mutual repulsion of these double layers surrounding the droplets that create strong repulsion which can overcome the van der Waals attraction (Figure 6.2).[6] Electrostatic stabilisation can be achieved by using ionic emulsifiers (ionic surfactants).

**Steric Stabilisation.** Stabilisation *via* a steric barrier is also known as steric stabilisation. Steric stabilisation is achieved by attaching (chemisorption in the case of droplets) macromolecules to the surface of the droplets. The adsorbed non-ionic surfactants or polymer layers produce steric repulsion of droplets upon overlapping their steric barrier. For example, triblock surfactants such as a PEO-*b*-PPO-*b*-PEO (Pluronics), can be utilised to provide steric stabilisation. The hydrophobic PPO chain resides at the hydrophobic surface, leaving the two PEO chains dangling in aqueous

solution.[7] Hydrocolloids such as xanthate gum, Arabic gum, guar gum etc can also be utilised as steric stabilisers.

**Electrosteric Stabilisation.** The combination of electrostatic repulsion and steric repulsion is referred as electrosteric stabilisation (Figure 6.2). This is, for instance, the case when using a mixture of ionic and nonionic stabilisers.[6,8] In fact, it is considered that mixtures of nonionic surfactants can be more effective than a single surfactant system for emulsification and stabilisation of the emulsion.[3]

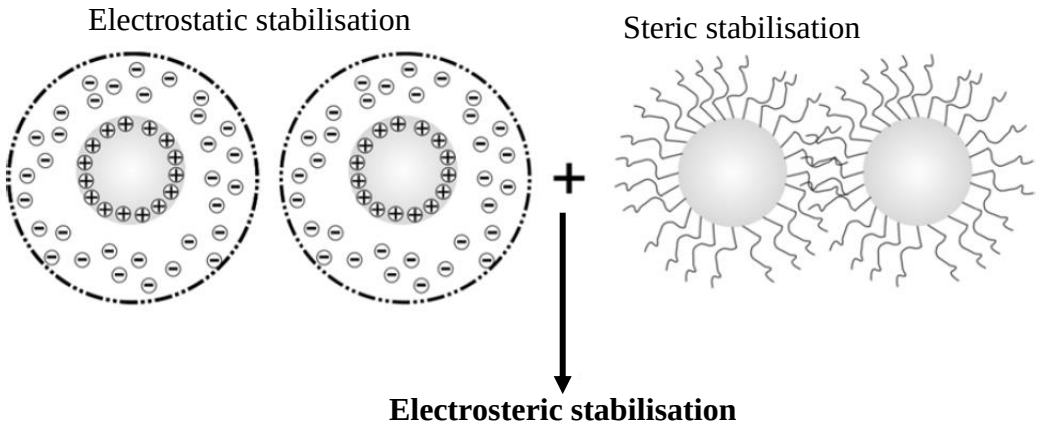



Figure 6.2. Schematic of electrostatic, steric and electrosteric stabilisation.[8]

Block copolymer surfactants offer several advantages over small-molecule surfactants, for example, a longer range of repulsion (steric and/or electrosteric) between surfaces covered by amphiphilic molecules or a better anchoring of the stabilisers on the surfaces.[9]

Macromolecular amphiphilic polymers are commonly referred as polymeric surfactants that contain both hydrophilic and hydrophobic parts in their structure. For example, water-soluble triblock copolymers consisting of poly(ethylene oxide) PEO and poly(propylene oxide) (PPO), (i.e. $PEO_m$-$PPO_n$-$PEO_m$, $E_mP_nE_m$) represent an important class of the commercially available macromolecular surfactants that find industrial applications in the field including but not limited to pharmaceuticals, emulsification, lubrication, and cosmetic formulations.[10] These PEO/PPO block copolymers, also called Poloxamers, are commercialised as Synperonic (when manufactured by Croda) or as Pluronics (when manufactured by BASF).[10,11]

In recent years, advanced macromolecular architectures that possess various chemical functionalities have been designed and thus the properties are efficiently tailored

without any limitations.[12] Polymeric surfactants can be broadly divided into two types: 'polysoaps'[2,12,13] (macromolecules constituted by repeating units of intrinsically amphiphilic monomers or oligomers) and 'macrosurfactants' (polymers in which there is a neat separation between the two parts).[14]

Polymeric surfactants display interesting association phenomena in selective solvents, peculiar rheological behaviour and result in self-assembled structures. At sufficiently low concentrations in water, 'polysoaps' give intra-molecular hydrophobic association (Figure 6.3, left), forming unimeric micelles or begin to undergo intermolecular aggregation at higher concentrations. [2,12,13]

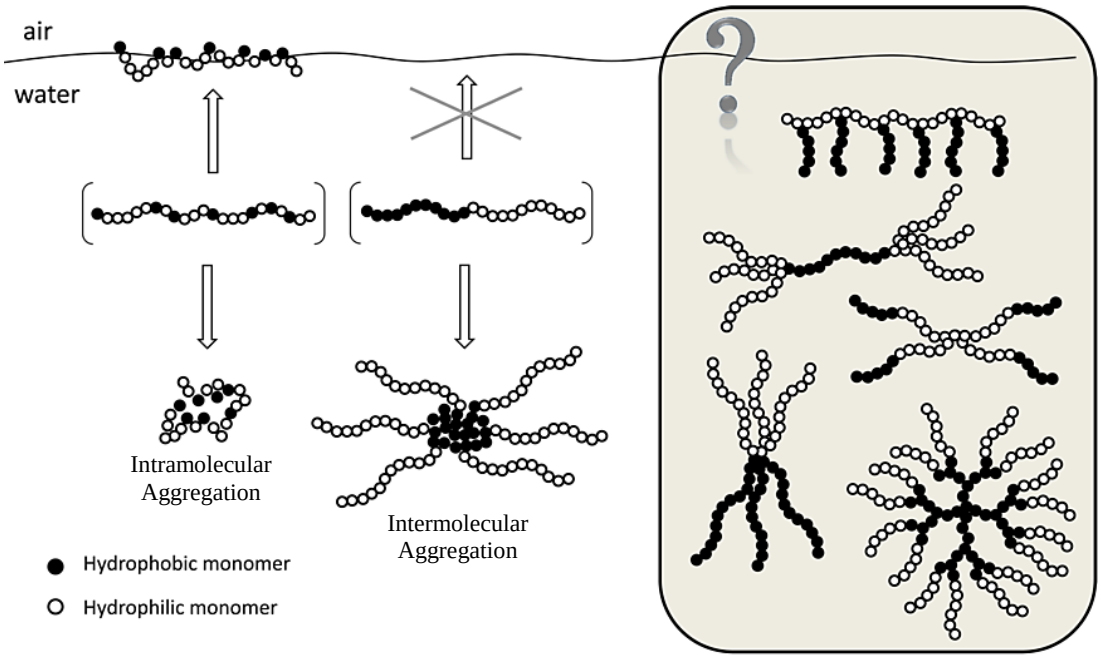



Figure 6.3. Representation of the different behaviours exhibited by polymer surfactants of different architectures at the air/water interface and in the bulk. The polysoaps (left) and macrosurfactants (centre). Limited data are available about complex branched architectures (right).[12]

A completely different associative behaviour is displayed by diblock copolymers (i.e. macrosurfactants) which seem to exclusively give intermolecular aggregation in water solutions, even in conditions of extreme dilution (Figure 6.3, middle).[2,15]

Concrete information is available to understand the surface properties and self-assembly behaviour of short-chain amphiphiles. In return, from an applicative perspective and from the fundamental standpoint, little is known about the structural−properties relationship of structurally-complex macromolecules (comb,[16] stars,[17,18] etc.) in aqueous solution (Figure 6.3, right).[12] Only recently (2018), Fan *et*

*al*.[19] gave a detailed summary and listed peculiar surfactant properties of star-shaped (ionic, non-ionic and zwitterionic) oligomeric surfactants in comparison with other architectures (such as Gemini, linear) (Figure 6.4). For example, with detailed studies on the critical aggregation concentration of star-surfactants, they showed that it is rather a normal phenomenon for the star-shaped oligomeric surfactants to show a continuous decrease in the surface tension even after reaching a CAC, suggesting that the self-assembly is changing.[19]

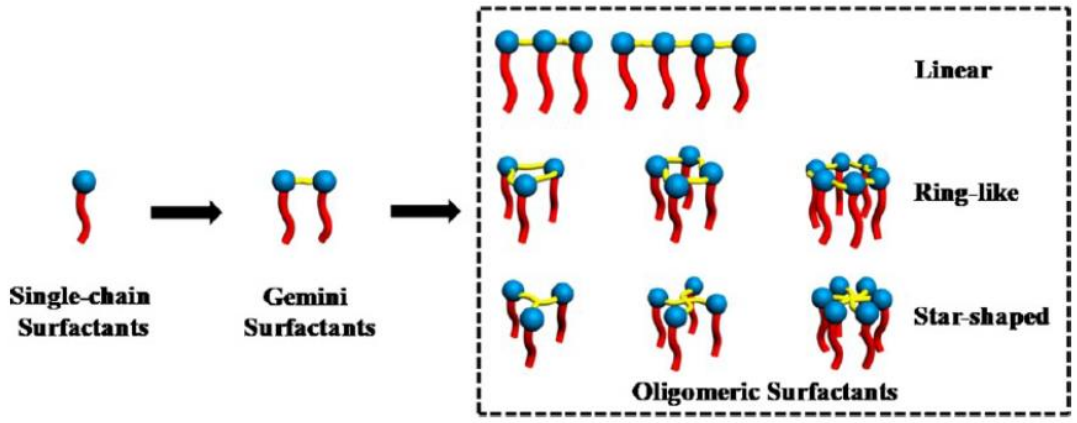



Figure 6.4. Diverse architectures of oligomeric surfactants with two molecular variables: degree of oligomerisation and topological structures. The covalent link between head-group (spacer) is represented in yellow.[19]

Branched macromolecular surfactants are, in general, synthesised by controlled radical polymerisation methods (such as catalytic chain transfer polymerisation, radical addition−fragmentation polymerisation methods and atom-transfer radical polymerisation).[1,12] Thus, the most common hydrophobic blocks employed using these methods are polystyrene, polyacrylates, polyolefin, or non-water-soluble polyethers.[12] The hydrophilic blocks are vinylic or acrylic monomers bearing sulfonated, carboxylic, or amino groups, or neutral blocks, which are essentially PEO moieties or water-soluble acrylates such as 2-hydroxyethyl methacrylate (HEMA) or PEGylated acrylic monomers.[12] In fact, the combination of ROP/controlled/living polymerisation methods to combine the properties of hydrophobic biodegradable polyesters and the above hydrophilic moieties has been reported frequently, in particular, PCL-*graft*-PEO.[20]

Research on branched surfactants has suggested that the differences in molecular structure affect surface tension, interfacial tension, CAC, film stability, and orientation and density of molecular packing at air/water interface in water, solid surface hydrophobicity at air/water, oil/water and water/solid interfaces.[17,19] Indeed, the surface

tension values at the CAC, dynamic surface tension, the surfactant surface excess concentration ($\Gamma_{max}$), and the surface area occupied by a surfactant molecule ($A_{min}$) are the most basic information on surfactant self-assembly at the air/water interface.

Generally, it is envisaged that CAC reduces exponentially with the increase of the length of the hydrophobic group (or block), while the dependence upon the hydrophilic block length is much less noticeable.[12] A similar effect was observed by Gong *et al.*[18] for the 7-arm star-like surfactant consisting of tetraethylenepentamine initiator and PPO-*b*-PEO-*b*-PPO arms. The effect of the length of the amphiphilic block on the surface activity of dendritic macro surfactant was investigated by Zhang *et al.*[21] for dendrimers consisting of poly(amidoamine) (PAMAM) dendrimer as a core and PPO-*b*-PEO as arms (Figure 6.5).

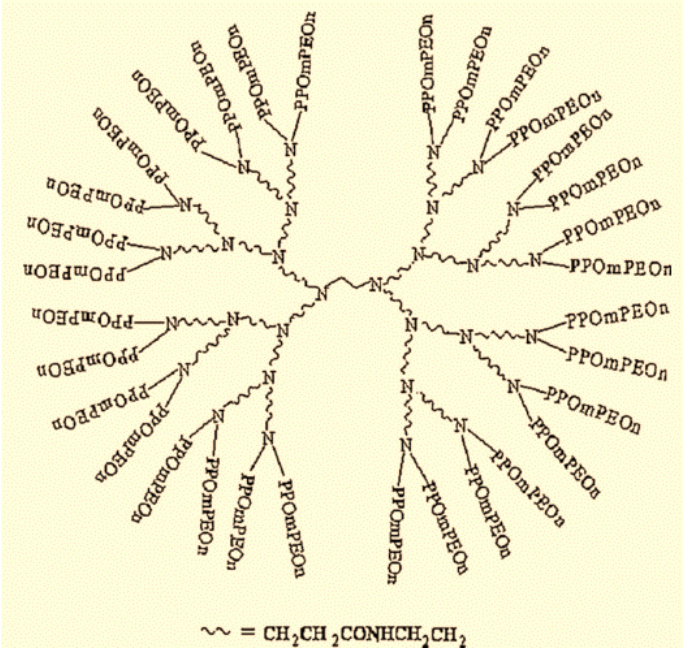



Figure 6.5. The dendritic copolymers composed of poly(amidoamine) (PAMAM) as the core and PPO-*b*-PEO as the amphiphilic blocks.[21]

Zhang *et al.*[21] reported that as the length of the amphiphilic PPO-*b*-PEO branch increases, both the surface tension and the CAC decrease gradually. This displays that they are surface active by increasing the branch length. The phenomenon is mainly attributed to the contribution from the longer hydrophobicity of PPO segments, resulting in lower CAC values of the copolymer with longer branches (Figure 6.6).[21] Although these investigations show the advantage of branched structures (i.e. lower CAC values), it is not very clear how the number of the hydrophilic-hydrophobic

groups, the composition or the architecture influence the physicochemical properties in water solution.

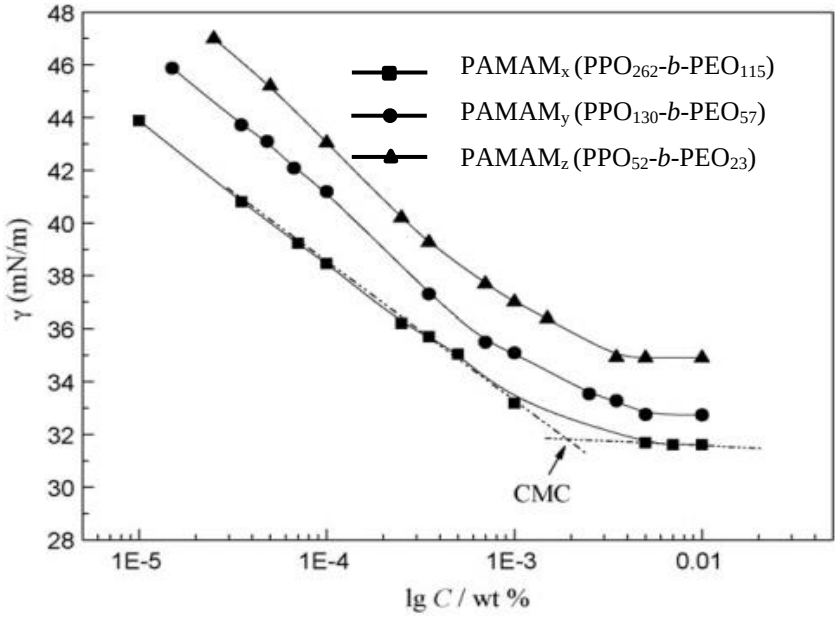



Figure 6.6. The surface tension vs. copolymer concentration plot (where x,y,z = 0.5, 1.0 and 2.5 wt% respectively).[21]

In this Chapter, we investigate the surface-active properties (equilibrium and dynamic surface tension) of a series of water-soluble PCL$_n$-*b*-PEP$_m$ copolymer structures (star and triblock) (synthesised in Chapter 5). We also present some preliminary data on the solubilisation of fragrances in aqueous solutions containing star-like surfactants and examine the colloidal stability of the emulsions prepared with star PCL-*b*-PEP by varying the temperature and salt concentration.

The shape of the surfactants (such as branching or unsaturation) also has a strong influence on the physicochemical properties. For example, according to Bhadani *et al*.[22], the surface-activity measurement on oleic acid, in comparison to stearic acid, based cationic surfactants having imidazolium head group and two-ester functional groups in fatty ester tail, i.e. Oleic Surf and Stearic Surf (Figure 6.7) respectively, showed that the Oleic Surf containing one unsaturated double bond displayed; (i) more favourable adsorption ($A_{min}$) and random orientation at the air-water interface; (ii) greater propensity to reduce surface tension (γ) of aqueous solution; (iii) but takes a longer time to attain equilibrium γ value and (iv) also showed lower $\gamma_{CAC}$ value.

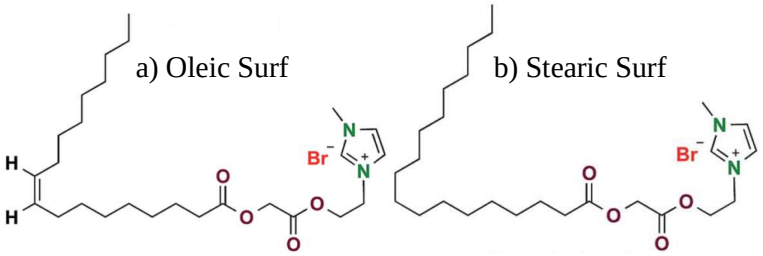



Figure 6.7. Structure of the oleic and stearic acid based cationic surfactants referred as Oleic Surf and Stearic Surf respectively.[22]

These properties were mainly attributed to the intermolecular forces (cation–π interaction) between the positively charged imidazolium head groups and the carbon-carbon double bond (– CH=CH–) of oleyl hydrocarbon tail. Such cation–π interaction interferes with the other interaction (dipole-dipole, ion-dipole, electrostatic repulsion and hydrophobic interaction) as it compensates the positive charge on the imidazolium and in turn result into a closely associated network of the head group and double bond both at the air-water interface and in the bulk. This also results in smaller aggregates in the bulk water solution (Figure 6.8).

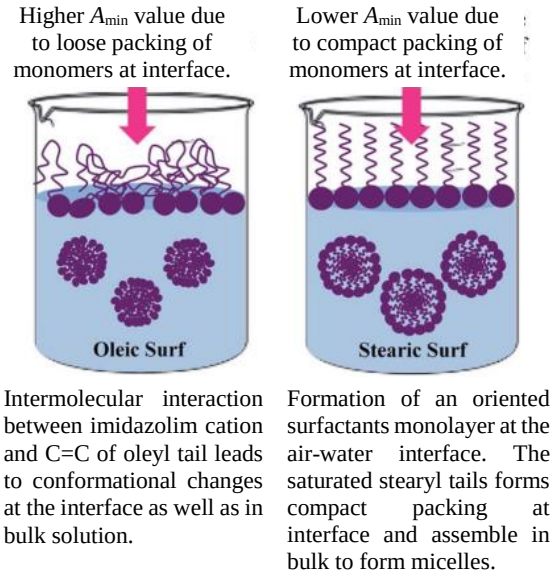



Figure 6.8. Representation of the molecular arrangement of Oleic Surf and Stearic Surf surfactant monomers at the air-water interfaces and in bulk aqueous solution.[22]

Star polymers also present an opportunity to create new coatings. The use of photopolymerisation to create new surface materials is explored in this Chapter.

Photopolymerisation is emerging as a green technology characterised by low energy requirements, low-temperature processing and the absence of volatile organic

compounds (solvent-free systems).[23,24] The advantages of photocuring over a thermally induced process include shortened cure times, reduced environmental pollution, low-solvent or solvent-free resinous formulations and energy savings.[25]

Photopolymerisation is polymerisation that takes place when a light of suitable wavelength is irradiates on the monomer/oligomers. Photopolymerisation (photoinduced curing) is an irreversible process converting a liquid polymerisable formulation into a solid polymer using radiation energy such as UV/visible light.[24] Typically, a UV-radiation curing system includes a small-molecule photoinitiator (upon absorption of that converts photon energy into chemical energy and produce radicals, cations and in some cases anions)[26] capable of initiating chain-growth photoinitiated-polymerisation of unsaturated multi-functional monomers that are converted into a 3D (crosslinked) polymer network (Figure 6.9).[27,28]

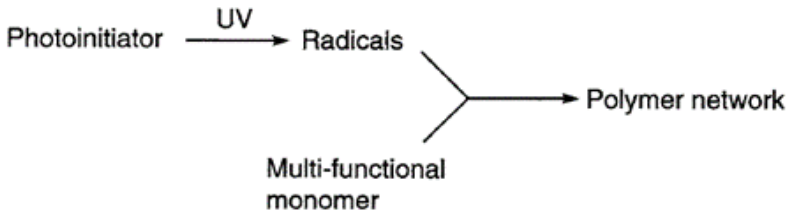



Figure 6.9. A general representation of a UV-induced curing in presence of a photoinitiator and typically a multi-functional monomer resulting in a polymer network.[27]

Hyperbranched star-like polymers are gaining attention due to a lower melt viscosity in relation to their molecular weight, and to their compact structure that minimises chain entanglements, while in the same time, the large number of functional end-groups enables efficient cross-linking compared to linear analogues.[29,30] The peculiar physical and chemical properties of hyperbranched polymers have shown wide potential in various fields such as biomaterials, nanocomposites, coatings, cross-linkers, adhesives, rheology modifiers and functional additives.[29]

The most widely investigated hyperbranched core in the field of coatings are the two commercially available Boltorn™ (hyperbranched aliphatic polyesters)[30–32] and Hybrane™ (hyperbranched polyester amides)[33]. These cores are functionalised to make them responsive to photochemical initiated curing, generally by end-capping with acrylates or, less commonly, methacrylates.[30,31]

The approach to the use of star polymers in this work has been inspired by the recent patent literature[34] on hyperbranched star polymer coating that has fast UV-curing capacity and biodegradability. It also improves the coating levelling, curing rate, hardness, adhesion and resistance and is expected to be applicable in the automotive and medical fields.[34] This hyperbranched polymer was synthesised by ROP of ε-CL from a hydroxy-functional hyperbranched polyester Boltron $H_{40}$ (average 64 –OH end-group per molecule) using $Sn(Oct)_2$ as a catalyst, and the polymer is claimed to have ~15-25 PCL-OH (Figure 6.10). The PCL chain-ends were capped with methacrylic anhydride where the functionalisation proceeded using triethylamine and 4-dimethylaminopyridine catalysts in dichloromethane solvent.[34]

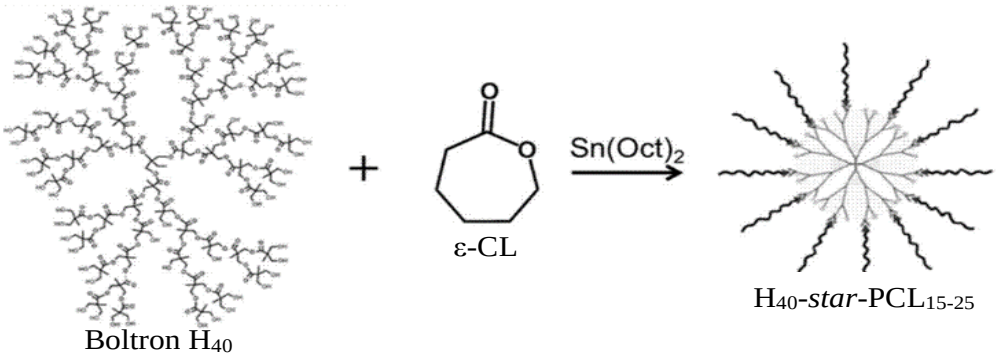



Figure 6.10. Schematic of hyperbranched polyester where the PCL arms are radiating from the Boltron $H_{40}$ core.[34]

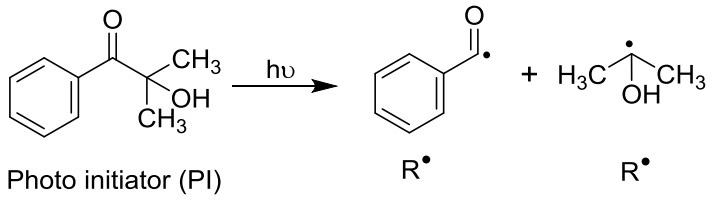
From the industrial application point-of-view, the fast kinetics of acrylate makes them highly desirable, but the drawback is the sensitivity of their radical polymerisation to molecular $O_2$ inhibition resulting in an incomplete cure. This can result in poor quality tacky upper surfaces or in the worse cases a complete failure to cure.[25] Since open-air curing is the easiest method for industrial processing, $O_2$ inhibition is a rather common issue and is essentially universal to free radical photocuring applications.[25]

An alternative is to use maleate as an acceptor monomer (A) for UV-curing in combination with donor (D) monomers, such as a divinyl ether.[33] This kind of A-D copolymerisation is fast and less sensitive to $O_2$ than acrylate polymerisation.[35] Besides, it is known that vinyl ether double bonds do not homopolymerise in the presence of free radicals which is the case with acrylates.[36]

The photoinitiator (PI), for example, Darocur 1173 produces reactive benzoyl radical (R*) by homolytic scission in the initiation step (Figure 6.11 (a)) and in the propagation

step the vinyl ether/maleate systems follow a donor-acceptor free radical mechanism to give an alternating copolymer PI radicals (Figure 6.11 (b)).[36]

(a) Homolytic scission of photoinitiator, Darocur 1173




(a) Donor-Acceptor Mechanism of vinyl ether – Maleates [VE-MA]

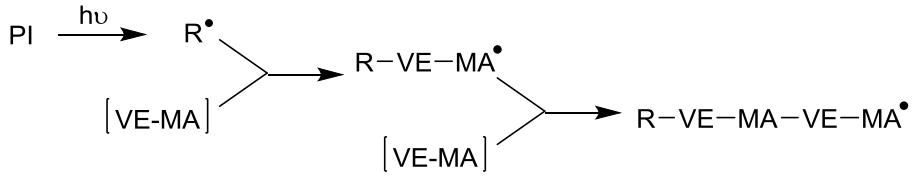



Figure 6.11. Schematic showing (a) the radical generation by photoinitiator and (b) a general donor-acceptor radial polymerisation mechanism between vinyl ethers and maleates.[36]

The design of a branched/star macromolecule is actually ideal for film forming applications. Indeed, as emphasised earlier the viscosity is lower, but the large number of functional end-groups enables efficient cross-linking.[33]

In this work, a functionalised biobased star PCL as introduced in Chapter 4 using Novozym 435 catalyst and *D*-sorbitol as an initiator is targeted. The star PCL with polymerisable maleate groups are then functionalised. The UV-cured films of star PCL maleate were prepared using tri(ethylene glycol) divinyl ether in presence of Darocur 1173 as a photoinitiator. The photo-polymerisation kinetics was monitored by using real-time fourier transform infrared spectroscopy. The PCL networks were characterised by differential scanning calorimetric (DSC) and thermogravimetric analysis (TGA) while the characterisation of the surface properties of these films is the perspective of this preliminary work.

## 6.3 Experimental (Surfactants)

### 6.3.1 Materials and Methods

Amphiphilic linear $PEP_m$-$PCL_n$-$PEP_m$ triblock and star *D*-sorbitol[$PCL_n$-*b*-$PEP_mOH_6$] diblock copolymers (preparation discussed in Chapter 5) and enzymatic ROP (eROP) mediated star $PCL_nOH_x$ (preparation disclosed in Chapter 4) will be used in this Chapter.

The commercial surfactants Tween$^{TM}$ 20 ($PEG_{20}$-sorbitan laurate, ~1230 g mol$^{-1}$), Tween$^{TM}$ 80 ($PEG_{20}$-sorbitan oleate, ~1310 g mol$^{-1}$) and oils Crodamol$^{TM}$ SFX (PPG-3 benzyl ether ethylhexanoate), Crodamol$^{TM}$ IPM (isopropyl myristate) and Crodamol$^{TM}$ TN (isotridecyl isononanoate), Carbomer (poly(acrylic acid)) and Keltrol CG SFT (Xanthate Gum) were supplied by Croda Europe Ltd. (UK). Pluronic$^{TM}$ L35 ($PEG_{11}$-$PPG_{13}$-$PEG_{11}$, 1900 Da) and Pluronic$^{TM}$ L64 ($PEG_{13}$-$PPG_{30}$-$PEG_{13}$, 2900 Da) were purchased from Sigma Aldrich (UK) and used as received.

Triethylamine (TEA, $Et_3N$, 99%) and maleic anhydride (MAH, 99%) were purchased from Sigma Aldrich (France).

### 6.3.2 Surface Active Properties and Applications

#### 6.3.2.1 Solubilisation of Fragrance

The protocols for solubilisation of fragrances was adapted from Tokuoka *et al*. [37] In a 3 ml glass vials, 20 parts of a given star PCL:PEP surfactant was mixed with 1 part of fragrance (bisabolol, citronellol, and limonene) followed by addition of water to give a concentration of 20 wt% solution. The mixtures were stirred by vortexing and the clarity of the formulation was accessed.

**Qualitative Determination of the Maximum Additive Concentration**. If the above solution remains clear, then 1 part of fragrance was further added, and the process is repeated until the formulation becomes cloudy. If the formulation appears cloudy, it is allowed to stand for 24 h and reassessed. The turbidity and maximum additive concentration of the formulation were visually inspected.

#### 6.3.2.2 Emulsion Studies

Simple O/W emulsion was formulated utilising Crodamol SFX, Crodamol IPM and Crodamol TN oils, water and star polymeric surfactants (discussed in section 6.4.1.5). Emulsions consisted of 20:75 wt% ratio of oil in water and the surfactant concentration was fixed at 5 wt% relative to total formulation (i.e. surfactant:oil:water = 5:20:75 wt% ratio). The ingredients were heated to 80 °C. The oil was added slowly to the aqueous surfactant solution while stirring using a high-speed stirrer (Ultra-Turrax) at 5000 rpm for 2 min (per 100 g). The emulsion formulation was allowed to cool down to room temperature after which formulations were divided into parts and salt stability at ambient/room temperature and at 40 °C was assessed after 1 day.

1 wt% of Carbomer (polyacrylic acid) solution (15 wt% in water) was also utilised as a viscosity modifier keeping the amount of oil and surfactant constant.

### 6.3.3 Biobased Star *D*-sorbitol-PCL$_n$OH$_x$ Functionalisation with Maleic Anhydride (Surfactants and Coatings)

The protocol for end-functionalisation of star *D*-sorbitol-PCL$_n$OH$_x$ polymers (star polymers synthesised by using Novozym 435 as a catalyst) was adapted from the procedure by Lacroix-Desmazes *et al*.[38]

A general procedure for the synthesis of star *D*-sorbitol-poly(caprolactone)$_n$-hemi ester of maleic acid (*D*-sorbitol[PCL$_n$-MAc$_x$]) is as followed. Purified star *D*-sorbitol-PCL$_n$OH$_x$ (2.01 g, 0.65 mmol) ($M_n$ $^{NMR}$ = 1170 g mol$^{-1}$; $M_n$ $^{SEC\text{-}MALS}$ = 3100 g mol$^{-1}$ so $M_n$ $^{SEC\text{-}MALS}/^{1H\ NMR}$ = ~3 and $Đ$ = 1.34; $M_n$ $^{P\text{-}NMR}$ = 3200 g mol$^{-1}$; $N_{arms}$ ($^{31}$P) = ~3) and MAH (1.27 g, 98.06 g/mol, 13 mmol) were added to a round bottom flask (RBF) at 1:20 molar ratio (i.e. 3.3 excess vs. the six hydroxy groups of the star polymer). The mixture was placed under argon for 30 min before immersing the RBF to a preheated oil bath set at 80 °C. The mixture was allowed to react at 80 °C under an argon atmosphere, typically for 2 h, until 99.9% end-functionalisation was monitored by $^1$H NMR (discussed in Section 6.4.2.1). Depending on the molecular weight of the starting star *D*-sorbitol[PCL$_n$OH$_x$] and its solubility, the star *D*-sorbitol[PCL$_n$-MAc$_x$] was purified either by (a) using conventional precipitation method of solvent : antisolvent (DCM: cold diethyl ether) with a ratio of 1:20 v/v or ; (b) adding excess of cold diethyl ether where the precipitates were allowed to settle at 4 $^o$C overnight. The excess of

supernatant (with MAH) was decanted and repeated several time. The precipitates were vacuum dried at 25 °C overnight.

**Star *D*-sorbitol[$PCL_n$-$MAc_x$].** $^1$H NMR (400 MHz, DMSO-$d_6$, ppm) $\delta$ 6.38 (d, $^3J_{H\text{-}H}$ = 12.0 Hz, =C*H*), 6.34 (d, $^3J_{H\text{-}H}$ = 12.0 Hz, =C*H*), 4.08 (t,–C$H_2$–OC(=O)CH=CH–COOH), 4.00 (t, methylene ester –C$H_2$OCO–), 2.28 (t, methylene in α position to carbonyl group –C$H_2$–CO–), 1.55 (m,–$COCH_2CH_2CH_2CH_2CH_2O$–), 1.31 (m, – $COCH_2CH_2CH_2CH_2CH_2O$–). Isomerisation of the double bond into the fumaric derivative (typical $^3J_{H\text{-}H}$ values = 15.6-16Hz) was not observed.

## 6.4 Result and Discussion (Surfactants)

The synthesis of amphiphilic $PCL_n$-*b*-$PEP_m$ based star and triblock compounds was discussed in Chapter 5. The first part focuses on the surfactant propertie assessment (static, equilibrium, and dynamic surface tension) of these amphiphiles. Comparisons have been made with some commercial petrochemical and biobased surfactants. The preliminary evaluations for the applicability of this novel branched water-soluble amphiphiles to form an oil in water (O/W) emulsion, for the solubilisation of fragrances and its foaming capabilities is discussed.

In addition, the biobased hydrophobic star *D*-sorbitol-$PCL_nOH_x$ (synthesised using Novozym 435 as a catalyst, discussed in Chapter 4) were end-functionalised with an unsaturated anhydride (maleic anhydride) to prepare a hemi-ester of maleic acid star *D*-sorbitol-$PCL_n$-MA-$COOH_x$. These functionalised star materials were exploited in two ways.

a) the protocols to disperse the biobased hydrophobic star *D*-sorbitol-$PCL_n$-MA-$COOH_x$ in water by creating some ionic-charges and the subsequent surface tension values will be discussed.

b) they are also utilised in preparing films discussed in Coatings in section 6.6 of this Chapter.

### 6.4.1 Surface Activity of $PCL_n$-$PEP_m$ Block Copolymers

The equilibrium (Krüss Tensiometer) surface tension of the low, intermediate and high MW star *D*-sorbitol-[$PCL_n$-*b*-$PEP_mOH_6$] diblock and low MW $PEP_m$-*b*-$PCL_n$-*b*-$PEP_m$

triblock copolymers were determined. Measurements were typically performed at 0.5 wt% in an aqueous solution at 25 ± 0.5 °C when using the Wilhelmy plate method. Measurements were made in duplicate and the commercial surfactants Pluronic™ L35 (Figure 6.12), Pluronic™ L64 (Figure 6.12), Tween™ 20 (Figure 6.13, top) and Tween™ 80 (Figure 6.13, bottom) were assessed as a comparison.

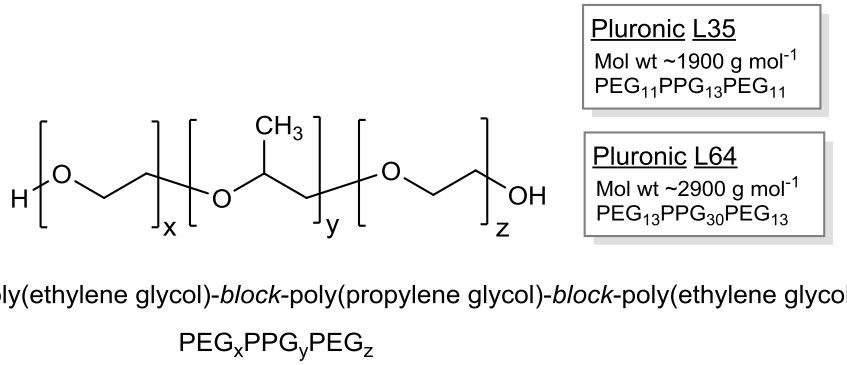



Figure 6.12. Structural representation, chemical composition and molecular weight of Pluronic™ L35 and Pluronic™ L64.

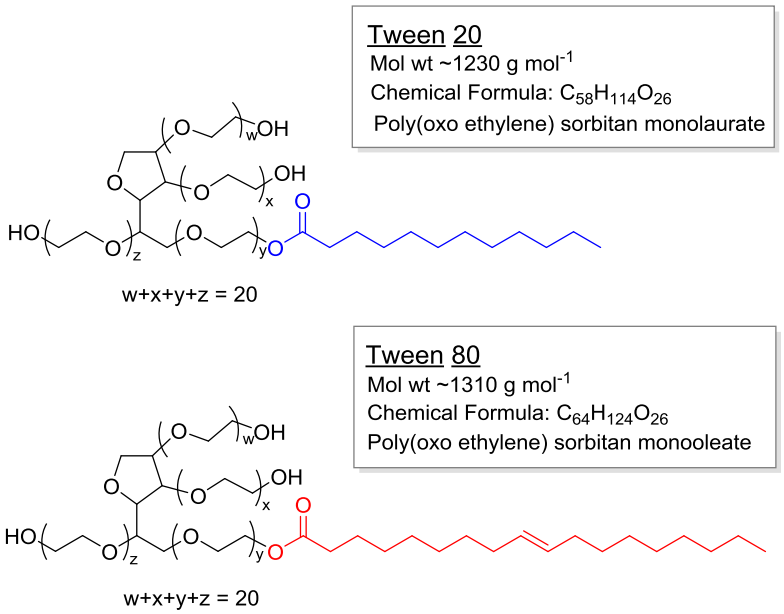



Figure 6.13. Structural representation, chemical formula, composition and molecular weight of Tween™ 20 and Tween™ 80.

Goddard *et al.*[39] investigated the surface active properties of three *D*-sorbitol[poly(*D*, *L*-Lactide)$OH_6$] (S-PLA-$OH_6$) based compounds of varying MW and possessing 6 hydroxy groups on the star compounds (800 g $mol^{-1}$(2 arms), 1800 g $mol^{-1}$ (4 arms) and 6800 g $mol^{-1}$ (6 arms)). As the weight fraction of hydrophobic PLA arms increased whereas the number of hydrophilic hydroxy groups remains constant (i.e. decreasing hydrophilicity) in the above series, the surface-active properties decreased. The surface-

active properties were clearly better for low MW compound, the 800 g $mol^{-1}$ (2 arms of S-PLA-$OH_6$) and 1800 g $mol^{-1}$ (4 arms of S-PLA-$OH_6$) reduce surface tension to 42 mN $m^{-1}$ and 54 mN $m^{-1}$ above their CAC, respectively, whereas the 6800 g $mol^{-1}$ sample displayed a high surface tension of 65 mN $m^{-1}$.

Having that in mind, the surface-active properties of star *D*-sorbitol[$PCL_n$-*b*-$PEP_mOH_6$] diblock amphiphiles (referred as star PCL: PEP) of variable MW and composition (given in Table 6.1) will be investigated. Simultaneously, a linear $PEP_m$-*b*-$PCL_n$-*b*-$PEP_m$ triblock amphiphile counterpart (referred to as triblock PCL: PEP) was also investigated. The hydrophilicity (or hydrophobicity) of the block copolymeric surfactants was tuned by changing the chain length of the hydrophobe and the hydrophile (Table 6.1).

Table 6.1. Amphiphilic water-soluble star PCL:PEP copolymers and triblock copolymers of the variable $M_n^{NMR}$, composition and hydrophilicity.

| | Amphiphilic copolymers | $M_n$ $^{NMR}$ (Macroinitiator: PEP block) [a] (g $mol^{-1}$) | Hydrophilicity[b] |
|---|---|---|---|
| Low MW linear | Triblock $PEP_{1.6}$-$PCL_4$-$PEP_{1.6}$ | 220: 600: 220 | 8.5 |
| | Triblock $PEP_{3.6}$-$PCL_4$-$PEP_{3.6}$ | 500: 600: 500 | 12.5 |
| | Triblock $PEP_{7.2}$-$PCL_9$-$PEP_{7.2}$ | 1000: 1100: 1000 | 12.9 |
| Low MW | star *D*-sorbitol[$PCL_4$-*b*-$PEP_{2.8}OH_6$] | 640: 380 | 7.6 |
| | star *D*-sorbitol[$PCL_4$-*b*-$PEP_{6.4}OH_6$] | 640: 870 | 11.6 |
| | star *D*-sorbitol[$PCL_4$-*b*-$PEP_{14}OH_6$] | 640: 1900 | 14.9 |
| Int. MW | star *D*-sorbitol[$PCL_{18}$-*b*-$PEP_{27}OH_6$] | 2200: 3700 | 12.3 |
| High MW | star *D*-sorbitol[$PCL_{34}$-*b*-$PEP_{65}OH_6$] | 4000: 8800 | 13.7 |

[a] Ratio of macroinitiator and the PEP block determined by $^1$H NMR (discussed in Chapter 5).
[b] Calculated, hydrophilicity = 20 × [$M_n^{NMR}$ (PEP block)/$M_n^{Copoly}$], adapting Griffin's formula of HLB on scale of 0 to 20 where 0 is fully lipophilic and 20 is fully hydrophilic. Da = Dalton.

Table 6.2. Commercial low MW petrochemical (PEG-based) water-soluble surfactants of variable molecular weight composition and HLB.

| Commercial Surfactants | | Chemical Formula | Mol. wt. (g $mol^{-1}$) | HLB [a] |
|---|---|---|---|---|
| Triblock | Tween™ 20 | $PEG_{20}$-sorbitan laurate | ~1230 | 16.7 |
| | Tween™ 80 | $PEG_{20}$-sorbitan oleate | ~1310 | 15.0 |
| | Pluronic™ L35 | $PEG_{11}$-$PPG_{16}$-$PEG_{11}$ | ~1900 | 10.0 |
| | Pluronic™ L64 | $PEG_{13}$-$PPG_{30}$-$PEG_{13}$ | ~2900 | 8.0 |

[a] Calculated, hydrophilic-lipophilic balance using Griffin's formula where a range of HLB is from 0 to 20, 0 fully lipophilic and 20 is fully hydrophilic.

### 6.4.1.1 Surface Tension: Static and Equilibrium

Surface tension (γ) is measured in terms of force (Newton) per metre of the surface of the liquid (mN $m^{-1}$). Water has a γ of 72 mN $m^{-1}$ at 25° C and any compound which can reduce this tension has been classed as a surfactant (typically γ ≤ 60 mN $m^{-1}$)[40] in this Thesis. Adsorption at the air/water interface for all the water-soluble star and triblock copolymer samples was determined using surface tensiometry. A representative structure of all the star PCL-*b*-PEP copolymers are represented (Figure 6.14) and the molecular weights are colour coded according to their corresponding surface tension bar graph. *D*-sorbitol (core) and ethyl phosphonate (monomer) were not surface active (Figure 6.15). However, it is clear that all the star diblock copolymers reduce the surface tension to ~ 40-45 $mNm^{-1}$.

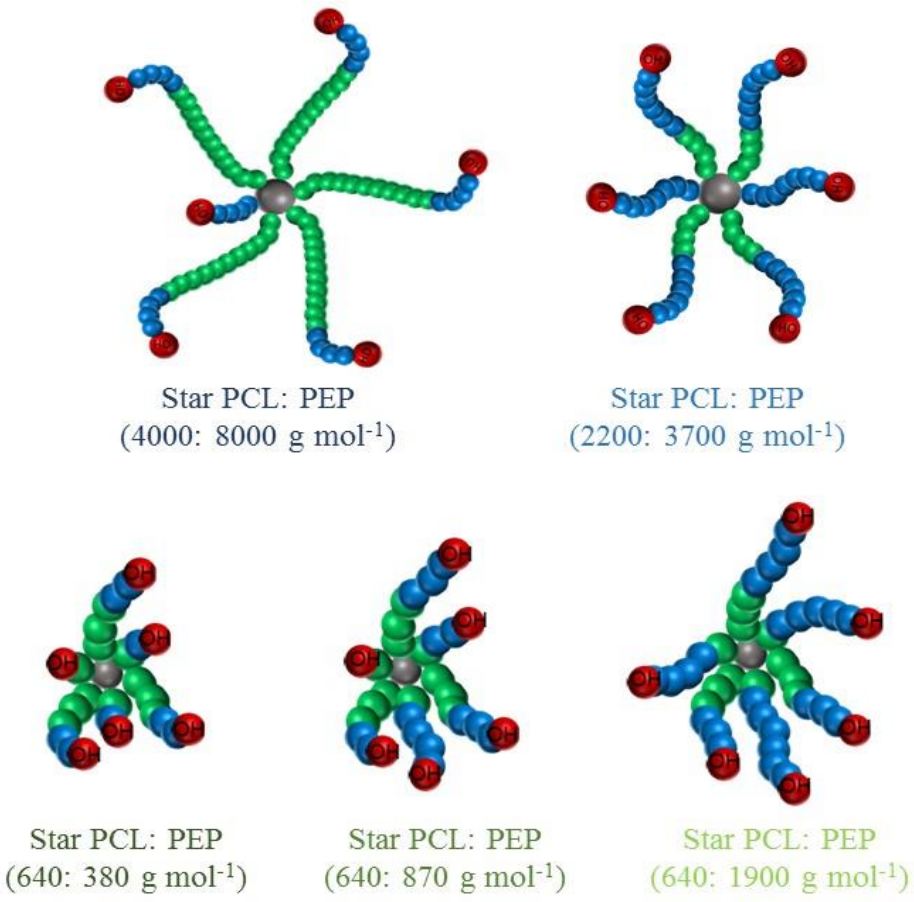



Figure 6.14. Representation of star $PCL_n$-*b*-$PEP_m$ compounds with its different molecular weight and composition. The *D*-sorbitol core (●), PCL arms (●●●), PEP arms (●●●) and hydroxy groups (●) are presented with its molecular weight. Nomenclature and MW are colour coded according to their corresponding surface tension bar graph (Figure 6.15).

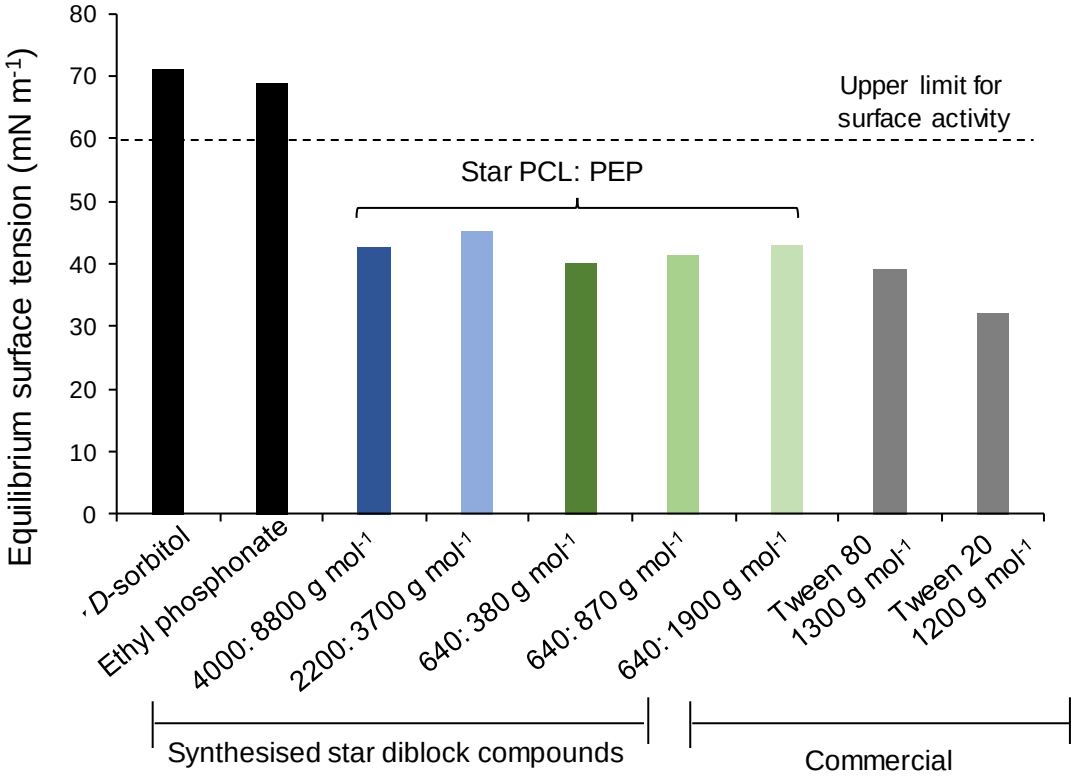



Figure 6.15. Equilibrium surface tension values of the *D*-sorbitol and ethyl phosphonate building blocks (black bars) and synthesised star PCLn-*b*-PEPm diblock copolymers of variable molecular weights and compositions (blue bars) measured against some commercial standard surfactants (grey bars). Compounds below the dashed line are considered surface-active agents.

A significant difference of about 8-10 mN $m^{-1}$ was noted between the compounds of S-PLA-$OH_6$ series of Goddard *et al*.[39] (800, 1600 and 6800 g $mol^{-1}$ had γ of 42 mN $m^{-1}$, 54 mN $m^{-1}$and 65 mN $m^{-1}$). In contrast, our star $PCL_n$-$PEP_m$ diblock copolymers presented here display a very different behaviour since even our highest MW star (4000: 8800 g $mol^{-1}$) has an equilibrium γ of 42 mN $m^{-1}$.

In opposition to the S-PLA-$OH_6$ series, no substantial reduction in surface tension values were observed for lowest MW star $PCL_n$-$PEP_m$ diblock series (600: 400, 600: 900 and 600: 2000 g $mol^{-1}$ has γ of ~40-43 mN $m^{-1}$) compared to highest MW star copolymer (4000: 8800 g $mol^{-1}$ has γ of 42.6 mN $m^{-1}$) (Figure 6.15). However, only a small change was observed for the amphiphile consisting of the same type of hydrophobe (640 g $mol^{-1}$ PCL series): the smaller the PEP hydrophilic block, the higher the surfactant adsorbs at the interface and the lower the surface tension. Indeed, the surface tension values increase successively by ~1-1.5 mN $m^{-1}$ between ~40 – 43 mN $m^{-1}$ for S-PCL: PEP in this 640 g $mol^{-1}$ PCL series. A similar trend was noted in the literature example of poly(ethylene oxide)$_m$-*block*-poly(butylene oxide)$_n$ ($E_mB_n$).[41]

These results show that the novel star amphiphile has surface-activity at air/water interface, but no significant difference in γ values were noted for stars of variable molecular weights (in the range of molecular weights and composition studied herein) although they display different hydrophilicity values (ranging from 7.6 to 14.9). These results are, however, very promising when tested against commercial petrochemical surfactants (Table 6.2) where the γ values range from 35-42 mN $m^{-1}$ (Figure 6.15).

To investigate if the structure has any influence on the surface activity, three linear $PEP_m$-$PCL_n$-$PEP_m$ triblock amphiphiles (Figure 6.16) with two commercial triblock surfactants (Pluronic$^{TM}$) (Figure 6.12) were studied.

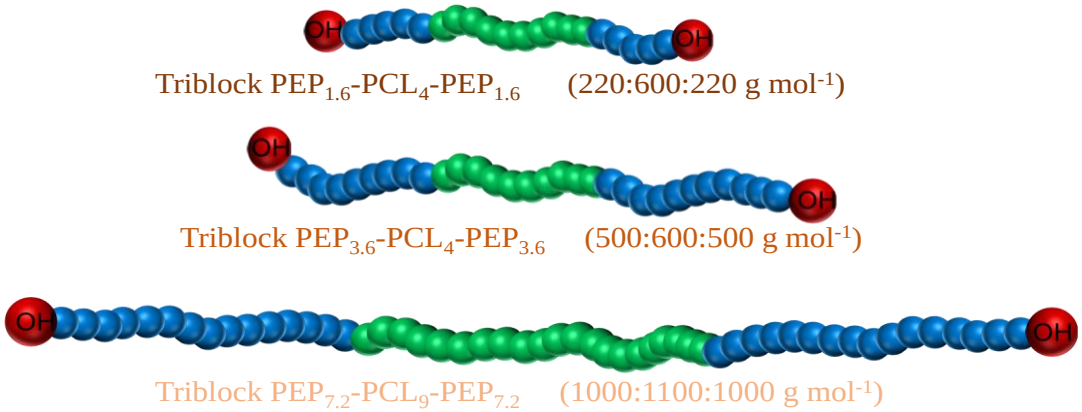



Figure 6.16. Representation of linear triblock $PEP_m$-$PCL_n$-$PEP_m$ compounds with its different molecular weight and composition. The PCL arms (●●●), PEP arms (●●●) and hydroxy groups (●) are presented. Nomenclature and MW are colour coded according to their corresponding surface tension bar graph (Figure 6.17).

The surface tension data suggest that all the linear triblock copolymers were also surface active (Figure 6.17). Triblock amphiphile had only a slightly lower surface tension when compared to star counterpart, such as for PCL: PEP ratio of 220:600:220 g $mol^{-1}$: the γ value of the star amphiphile is 40.1 mN $m^{-1}$ and triblock amphiphile is 38.1 mN $m^{-1}$. A maximum reduction in surface tension was observed for linear $PEP_{7.2}$-$PCL_9$-$PEP_{7.2}$ triblock copolymer (PEP:PCL:PEP block ratio of 1000:1100: 1000 g $mol^{-1}$): γ value of 31.7 mN $m^{-1}$, which was much lower when compared to the commercial Pluronics $^{TM}$ (where the γ values range from 40-49 mN $m^{-1}$) (Figure 6.17).

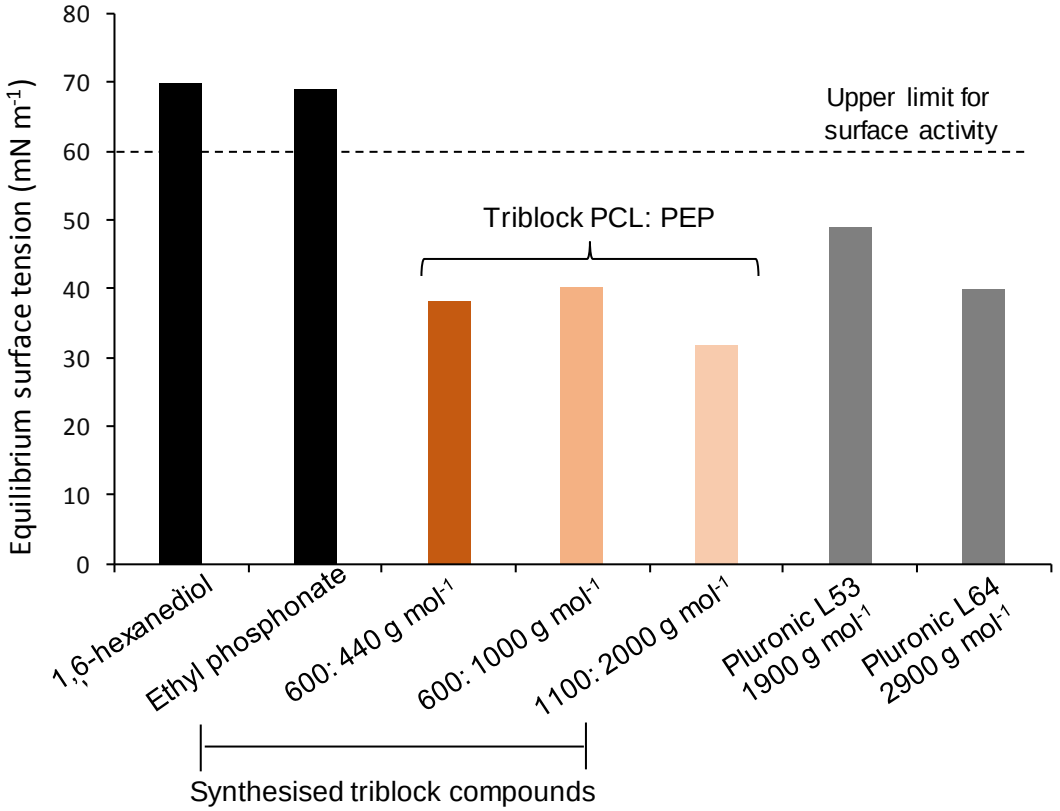



Figure 6.17. Equilibrium surface tension values of 1,6 hexanediol and ethyl phosphonate building blocks (black bars) and synthesised triblock $PEP_m$-*b*-$PCL_n$-*b*-$PEP_m$ copolymers of variable MW and compositions (brown bars) measured against commercial triblock surfactants, Pluronic.

### 6.4.1.2 Dynamic Surface Tension

The dynamic surface tension of the synthesised $PCL_n$-*b*-$PEP_m$ copolymers was determined using bubble pressure tensiometry. Bubble profile analysis tensiometer allows measuring the time trajectory of the surface tension of a surfactant solutions.[42]

In this method, air bubbles are created at an increasing rate through the end of the capillary tube that is immersed in a liquid sample (Figure 6.18).[44] The pressure inside the air bubble changes continuously with its radius ($r_B$). When the radius of the tip of the capillary ($r_{cap}$) becomes equal to the radius of curvature of the bubble ($r_B$), the maximum pressure is developed (Figure 6.18, (b)). The pressure decreases quickly as the bubble expands further (Figure 6.18, (c)) at this point surface tension is measured. This method of measuring surface tension is based on the determination of the pressure difference inside and outside an air bubble at the moment when the bubble is detached from the end of a capillary.[43]

Thus, surface tension (γ) is calculated from the difference between the maximum and minimum pressure following Eq. 6.1.

$$\gamma = k\,(P_{max} - P_{min}) \qquad \text{Eq. 6.1}$$

Where k (m) is a calibration factor measured automatically taking the radius of the capillary into account, $P_{max}$ and $P_{min}$ (N $m^{-2}$) are pressure maximum and pressure minimum respectively.

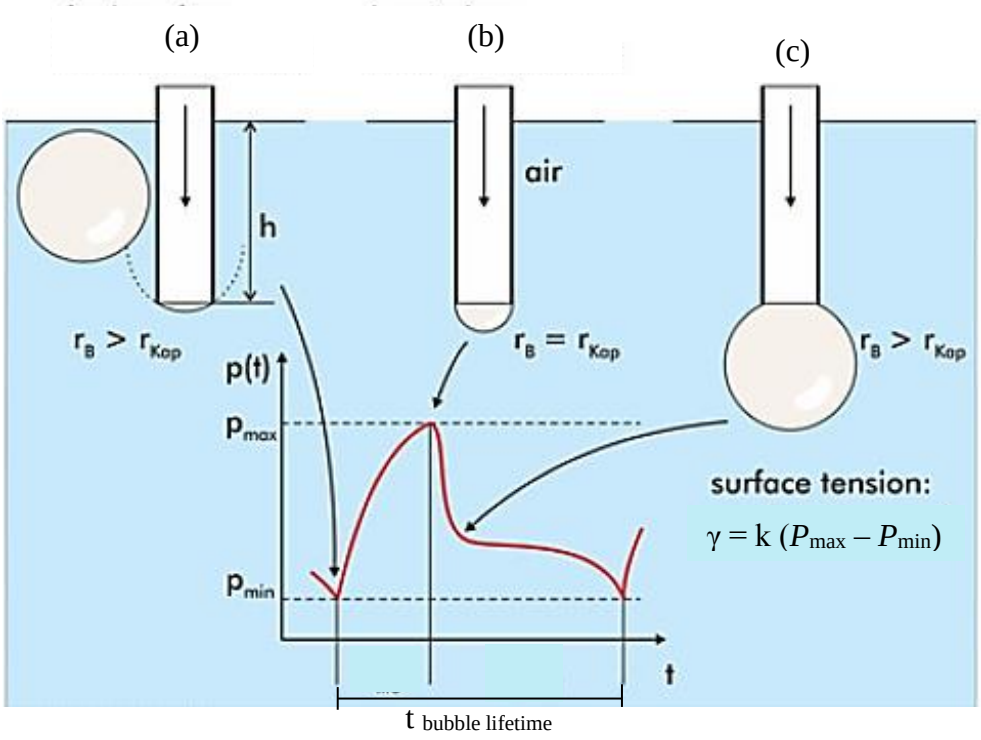



Figure 6.18. Changes observed in the air-bubble pressure during dynamic surface tension measurements; rB: is the radius of the bubble, rcap is the radius of the capillary, and t bubble lifetime represents the lifetime of the bubble (in milliseconds (msec)) (figure adapted from SITA).[44]

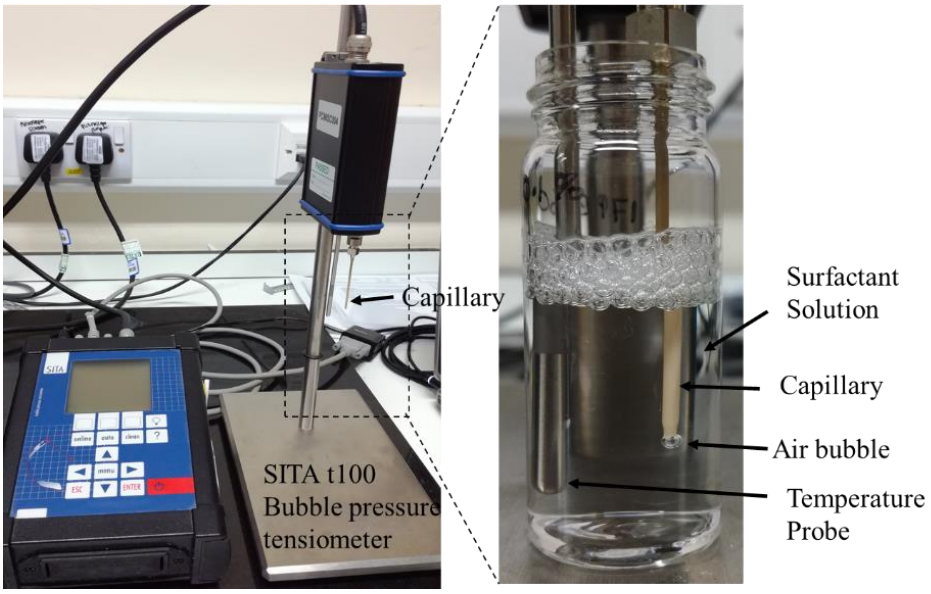
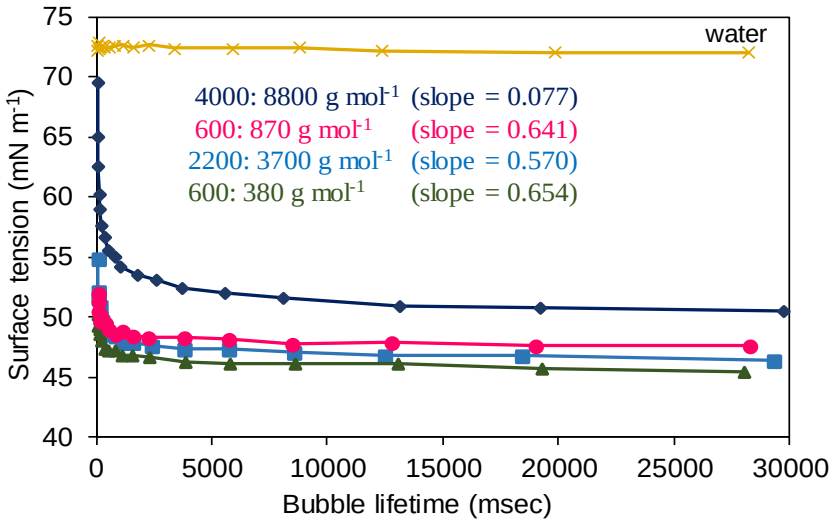



Figure 6.19. Image showing the SITA t100 Bubble Pressure tensiometer (left) and a representation of surface tension measurement using surfactant solution (right).

In other words, dynamic surface tension also signifies how fast the amphiphile migrates to the water-air bubble interface at a specific concentration and within a given frame of time.

The surface tension of water is 72 mN $m^{-1}$ (at 25 °C) (yellow line as a reference in Figure 6.20). The dynamic surface tension results show that all the star $PCL_n$-*b*-$PEP_m$ diblock and triblock copolymers reduced the surface tension of water down to ~55-45 mN $m^{-1}$ and 47-42 mN $m^{-1}$ (Figure 6.20, top and bottom), respectively, when measured dynamically between 0-30000 msec. In particular, a faster drop in surface tension was observed by almost all the star and triblock copolymers at the origin when the bubble lifetime was between 0-30 m sec (slope = 0.570 - 0.823), while only the high MW star PCL:PEP (4000: 8800) g $mol^{-1}$ (slope = 0.07) migrated slowly to the bubble-water interface (Figure 6.20, top and bottom). Such a speedy drop in the γ value is indicative of the faster rate of surfactant transfer to the newly formed bubble-water interface. Slow diffusion profile shown by the highest MW star PCL:PEP (4000:8800 g $mol^{-1}$) could be attributed to the bulky size of the copolymer (Figure 6.20, top). Overall, the lowest MW triblock showed significantly faster migration behaviour at the initial stage (bubble lifetime of 0-30 millisecond; slope = 0.82) and was also able to reduce the water surface tension down to 42.2 mN $m^{-1}$ within only 30 sec (Figure 6.20).

(A) Star PCL-*b*-PEP Diblock Copolymer




(B) Linear PEP-*b*-PCL-*b*-PEP Triblock Copolymer

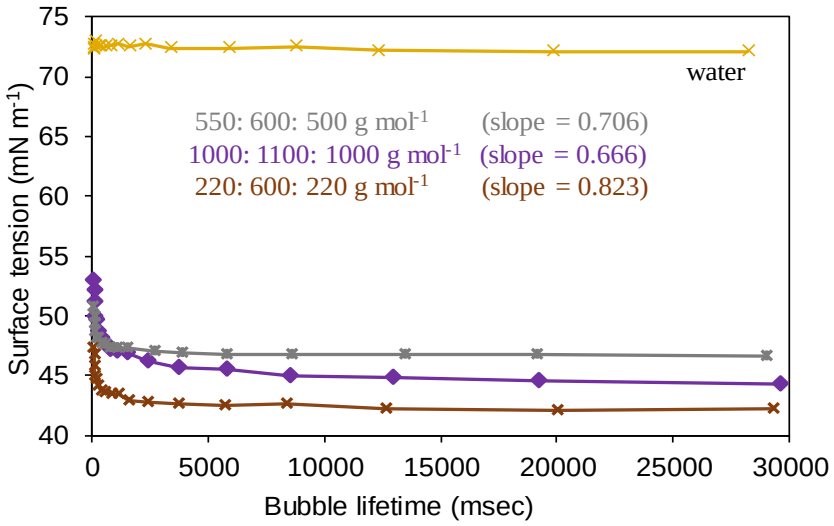



Figure 6.20. Dynamic surface tension at increasing bubble lifetimes for (a) star PCL-b-PEP diblock and (b) linear PEP-b-PCL-b-PEP triblock copolymers (0.5 wt%). The method shows how fast the amphiphile migrate towards the surface of the expanding bubble (bubble-water interface). Surface tension as a function of time between 0 to 30 m sec (i.e. the slope at the origin in N $m^{-1}$ $sec^{-1}$) is also indicated.

### 6.4.1.3 Solubilisation of Fragrances

Essential oils and their fragrance compounds are the key components of the perfume and cosmetic industry as they can serve as natural or natural-like chemical preservatives and, at the same time, offer various benefits for skin and body. Furthermore, these chemicals improve the value of cosmetic products due to their pleasant odour.[45] However, lipophilic substances such as fragrances, actives, oils, anti-oxidants etc. require a surfactant to solubilise them into an aqueous system. The ability of our

surfactants to transport insoluble perfume oils (such as citronellol, bisabolol and (+)-limonene, Figure 6.21) into an aqueous phase was inspected visually (refer to Section 6.3.2.1).

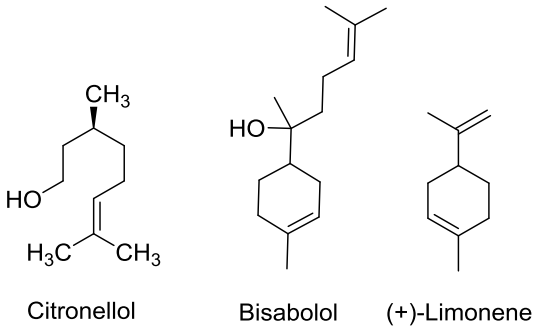



Figure 6.21. Chemical Structure of the fragrances employed to investigate the solubilisation capacity of star PCL: PEP and triblock amphiphiles.

Two-star PCL: PEP amphiphiles, 2200: 3700 g $mol^{-1}$ and 4000: 8800 g $mol^{-1}$, and a triblock PCL: PEP, 1000: 1100: 1000 g $mol^{-1}$, as well as a commercial Tween 20 surfactant were tested to solubilise citronellol, bisabolol and limonene in water. As a control experiment, the solubilisation of oil was performed in parallel in the absence of surfactants (i.e. only in water).

In a typical solubilisation test, at first, a low level of fragrance (5 wt% with respect to surfactant, i.e. 20:1 surfactant:fragrance ratio) was mixed with surfactant (star PCL: PEP amphiphile and a commercial Tween 20) to which water was added to form a 20 wt% surfactant solution. When a clear solution was observed, then the amount of fragrance in the surfactant solution was increased systematically until the medium became cloudy.

Bisabolol is a clear, pale yellow liquid that possesses anti-inflammatory, healing, soothing and antimicrobial properties. Due to its pleasant sweet floral odour, it is used as a component in personal care and cosmetics such as moisturisers and sun creams.[45]

All the tested star and triblock amphiphiles were able to solubilise the three tested fragrances (Figure 6.21) up to 15:1 ratio. For representation, results with bisabolol and star PCL: PEP (2200: 3700 g $mol^{-1}$) are shown (Figure 6.22). It is clear, that the bisabolol is insoluble in water (Figure 6.22, a). The star surfactant was able to solubilise bisabolol up to 10:1 ratio (10.0 wt% relative to surfactant) but slight turbidity was noticed above 9.8: 1 ratio (10.2 wt% relative to surfactant). Such turbidity was also prevalent in Tween 20 solution above a surfactant/fragrance ratio of 8:1 (12.5 wt%

relative to surfactant). For representation, the solubilised bisabolol in star amphiphile solution (Figure 6.22, b) and in Tween 20 surfactant solution are presented (Figure 6.22, c). The cloudiness in the 20 wt% star surfactants solution was also observed in the absence of fragrances; this may be due to the fact that the surfactants may not be homogeneously dispersed at a molecular level into the water phase at very high surfactant concentration (Figure 6.22, b).

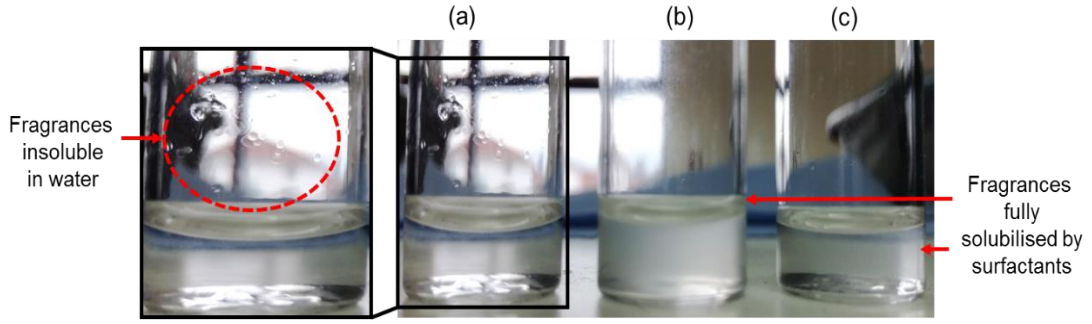



Figure 6.22. Representation of the solubilisation of bisabolol in water with and without surfactant, (a) in absence of surfactants the oil droplets clearly do not mix with water and remain insoluble; (b) up to 10.2 wt% of fragrance relative to surfactant (9.8:1 surfactant: fragrance ratio) was solubilised by star PCL: PEP (2200: 3700 g $mol^{-1}$) and (c) up to 12.5 wt% of fragrance relative to surfactant (8: 1 surfactant: fragrance ratio) was solubilised by Tween 20.

The maximum additive concentration is defined as the highest concentration of a lipophilic compound that could be incorporated into a micellar surfactant solution at a given surfactant concentration.[46] These preliminary results have shown that the maximum solubilised concentration of bisabolol in a 20 wt% aqueous solution of star PCL: PEP (2200: 3700 g $mol^{-1}$) surfactant is 10.2 wt%.

It is important to note that if a surfactant can solubilise oil up to a weight ratio of 3:1 (33 wt% of fragrance relative to surfactant) then it is considered by CRODA to be an excellent solubiliser.

Preliminary evaluation of the solubilisation of fragrance by star PCL:PEP have shown some premising results. The use of the star block copolymer for emulsification of oil is explored.

#### 6.4.1.4 Emulsion Studies using Star *D*-sorbitol[PCL-*b*-PEP]

Initially, three oils (Crodamol SFX, Crodamol IPM and Crodamol TN) with different polarities were tested (Figure 6.23). The required HLB (for definition refer to Appendix D) of surfactants by these oils is 14, 10 and 10, respectively.

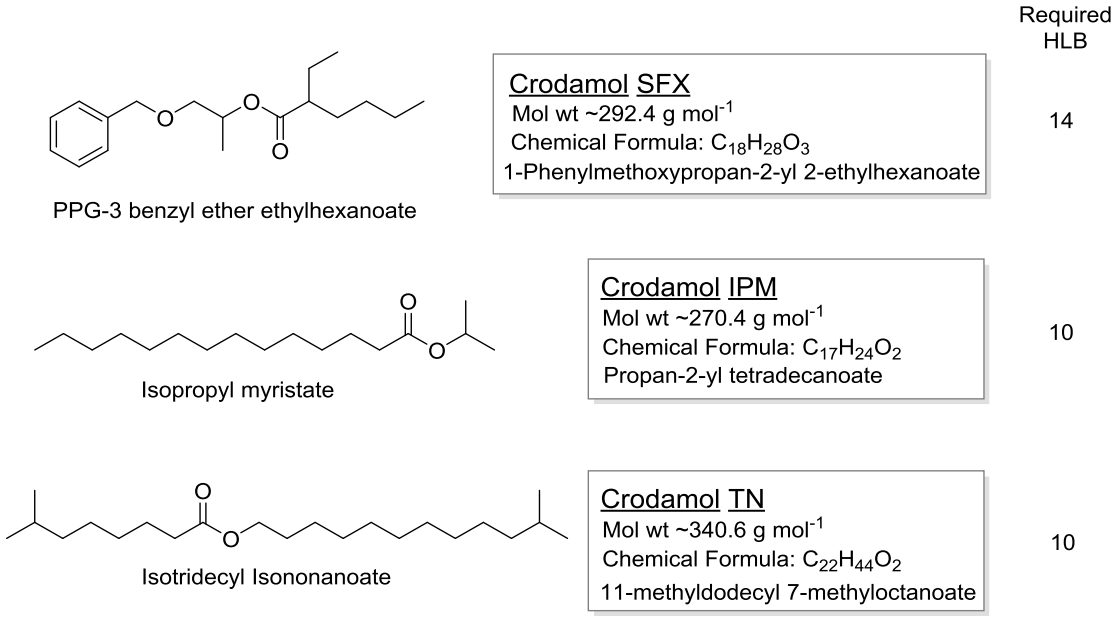



Figure 6.23. Structural representation, chemical composition and molecular weight of oils (Crodamol SFX, Crodamol IPM and Crodamol TN) employed to form O/W emulsion.

A star *D*-sorbitol[$PCL_4$-*b*-$PEP_{14}OH_6$] with MW of 640:1900 g $mol^{-1}$ and hydrophilicity of ~15 was utilised to test its ability to form an emulsion. When oils: water at 20: 75 wt% ratio were formulated with 5 wt% star surfactants relative to water, indeed star surfactants were shown to be capable of emulsifing all the tested oils where the upper phase represents the milky O-in-W emulsion (Figure 6.24, left). The bottom phase displays a water-rich phase on the same day and splitting phenomenon becomes more apparent after 1 day (Figure 6.24, right).

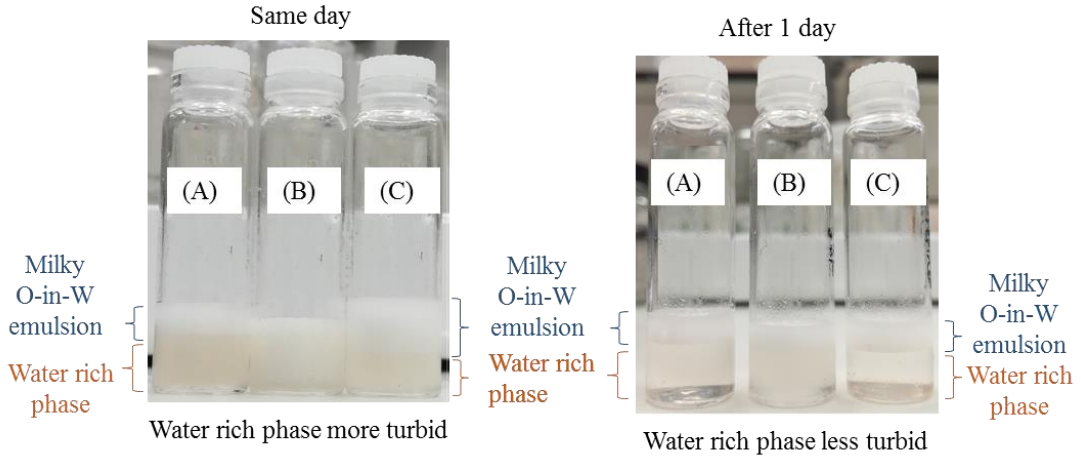



Figure 6.24. Emulsification of 25 wt% of Crodamol IPM (A), Crodamol TN (B) and Crodamol SFX (C) using 5 wt% of star *D*-sorbitol[$PCL_4$-*b*-$PEP_{14}OH_6$] surfactant in water.

Indeed, the solubility of the hydrophobic block seems to be an important parameter to influence the emulsification process. PCL $(-C_6H_{10}O_2-)_n$, is a hydrophobic polymer but evidently it is not soluble in commonly used oils under ambient conditions.[47] Similarly, a simple solubility test of some linear PCL and star PCL of few different MW (below 2000 g $mol^{-1}$) showed that PCL had good solubility in aromatic oils (such as toluene, naphthalene, Crodamol TN which is also PPG-3 benzyl ether ethylhexanoate) while it is poorly soluble in the other two oils (Crodamol SFX, Crodamol IPM).

Crodamol IPM is one of the most common ester oils applicable in various personal care formulations thus emulsification of this oil was further inspected. Firstly, salt stability was tested. The emulsions prepared with star surfactant seem to cream or split fully with or without any addition of NaCl salt, in just one day. This displays that star surfactant might not impart to the emulsion kinetic stability, not even at room temperature (RT, usually lab temperature). Indeed, salt was added deliberately to test the stability of the emulsion at higher ionic strength. The salt accelerated the splitting process. In addition, the thermal stability of the emulsion was also explored, showing a decrease of the stability at higher T (40 °C) (Figure 6.25). The emulsion at 40°C was splitting faster than at room temperature.

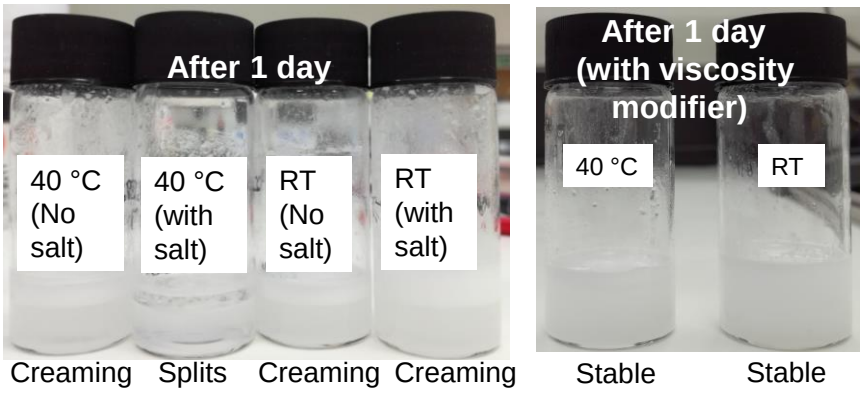



Figure 6.25. Oil-in-water emulsion using star *D*-sorbitol[$PCL_4$-*b*-$PEP_{14}OH_6$] observed after 1 day at 40 °C and at room temperature, without and with NaCl salt (left), and showing the use of Carbomer (1 wt%) viscosity modifier enabling a more stable formulation event at 40°C.

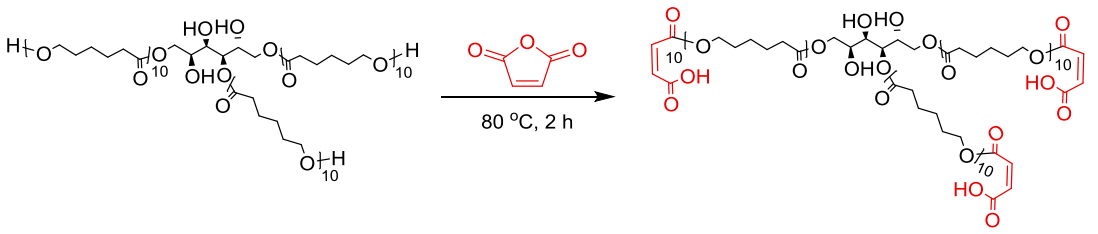
A thickener such as Carbomer or Xanthate gum are commonly employed to increase the viscosity (thus slowing down the creaming and splitting process) and to provide steric stabilisation by adsorption at the interface. Carbomer Solution (15 wt%) in water was thus prepared and 1 wt% was employed in the formulation relative to the total composition during the emulsification process. It indeed improved the stability of the emulsion for up to 1 day (Figure 6.25, right). These preliminary tests are evident that

star surfactants in combination with a viscosity modifier might have applicability in high viscosity formulations.

### 6.4.2 Biobased Star PCL Surfactants

#### 6.4.2.1 Star *D*-Sorbitol[$PCL_nOH_x$] Functionalisation (Surfactants and Coatings)

The enzymatic ROP of ε-CL from the *D*-sorbitol core to create star *D*-sorbitol[$(PCL)_nOH_x$] possessing terminal hydroxy groups was discussed in Chapter 4. Star PCL of two different $M_n$ $^{SEC\text{-}MALS}$ (~5700 g $mol^{-1}$ and ~3100 g $mol^{-1}$) were investigated to determine the efficiency of end-functionalisation with maleic anhydride (MAH) (Figure 6.26). As a reminder, the star *D*-sorbitol[$(PCL)_{49}OH_3$]$OH_3$ (S-PCL5700) has an average of 3 PCL arms, 3 pendant hydroxy groups on the *D*-sorbitol core and has $M_n$ $^{SEC\text{-}MALS}$ = 5650 g $mol^{-1}$, $Đ$ = 1.34 and $M_n$ $^{P\text{-}NMR}$ of 6100 g $mol^{-1}$. A star *D*-sorbitol[$(PCL)_{27}OH_3$]$OH_3$ (S-PCL3100) having the same number of arms but a slightly lower molecular weight ($M_n$ $^{SEC\text{-}MALS}$ = 3100 g $mol^{-1}$, $Đ$ = 1.39, $M_n$ $^{P\text{-}NMR}$ = 3200 g $mol^{-1}$) was also employed for functionalisation (Figure 6.26).




star *D*-sorbitol[$(PCL)_{30}OH_3$]$OH_3$ star *D*-sorbitol[$(PCL)_{30}$MA-$COOH_3$]$OH_3$

Figure 6.26. A representative schematic showing end-functionalisation of biobased star *D*-sorbitol-PCL (3100 g $mol^{-1}$) with maleic anhydride.

The derivatisation of the hydroxy groups (either at the chain-ends of PCL arms or on the sorbitol core) into hemi ester of maleic acid proceeded in the melt in the absence of a catalyst and at moderate temperature (80 °C). A quantitative conversion was reached within 2 h. The functionalisation was monitored using $^1$H NMR by measuring the reduction in methylene end-group resonances **y** compared to the methylene **c** in the PCL backbone (Figure 6.27, a). The pre- and post-functionalised S-PCL3100 is represented in $^1$H NMR spectra (Figure 6.27, a and b).

The degree of substitution in the functionalisation was nearly 100% because the hydroxymethylene protons resonance **y** at $\delta$ 3.63 ppm (Figure 6.27, a) completely

disappeared at the end of the post-functionalisation reaction (Figure 6.27, b). In addition, there was no trace of residual MAH at $\delta$ 7.46 ppm (–C*H*=C*H*–COO–) after purification (Figure 6.27, b). It was further observed that new peaks appeared at $\delta$ 4.08 ppm corresponding to the methylene protons **b** in α-position of the maleate group (–C$H_2$–O-(C=O)CH=CH–) and at $\delta$ 6.34 ppm corresponding to the methine groups of the alkene (–C$H_2$–C*H*=C*H*–, **a**, **a'**). These confirm that the derivatisation of star *D*-sorbitol[$(PCL)_nOH_x$] into star *D*-sorbitol-PCL-hemi ester of maleic acid (*D*-sorbitol[$PCL_n$-$MAc_x$]) was successful.

Additionally, the $DP^{NMR}$ calculated from the ratio of methylene signals **c** in the PCL backbone to the protons in α-position of the maleate group **b** was found to be ~10. This gives an average of ~10 PCL units per arm, similar to the value before functionalisation, which suggests that only the primary hydroxy chain-ends of PCL-arms were derivatised into hemi ester of maleic acid functions. If the 3 pendant secondary hydroxy groups of the *D*-sorbitol core have been functionalised, an increase in the ratio of methine protons (**a**, **a'**) over methylene function **b** would have been observed. This is not the case, as identified by $^1$H NMR analysis (Figure 6.27, b). Thus, it suggests that a star *D*-sorbitol[$(PCL)_{27}COOH_3$]$OH_3$ with an average of ~3 PCL hemi ester of maleic acid functionalities and ~3 (secondary) pendant OH groups were synthesised under the conditions employed (80 °C, ~2 h, the absence of catalyst). The non-reaction of the three remaining secondary hydroxy groups of the sorbitol core with the three-fold excess of MAH is rather surprising. It might be because the reaction proceeded in the melt without a catalyst for a short period.

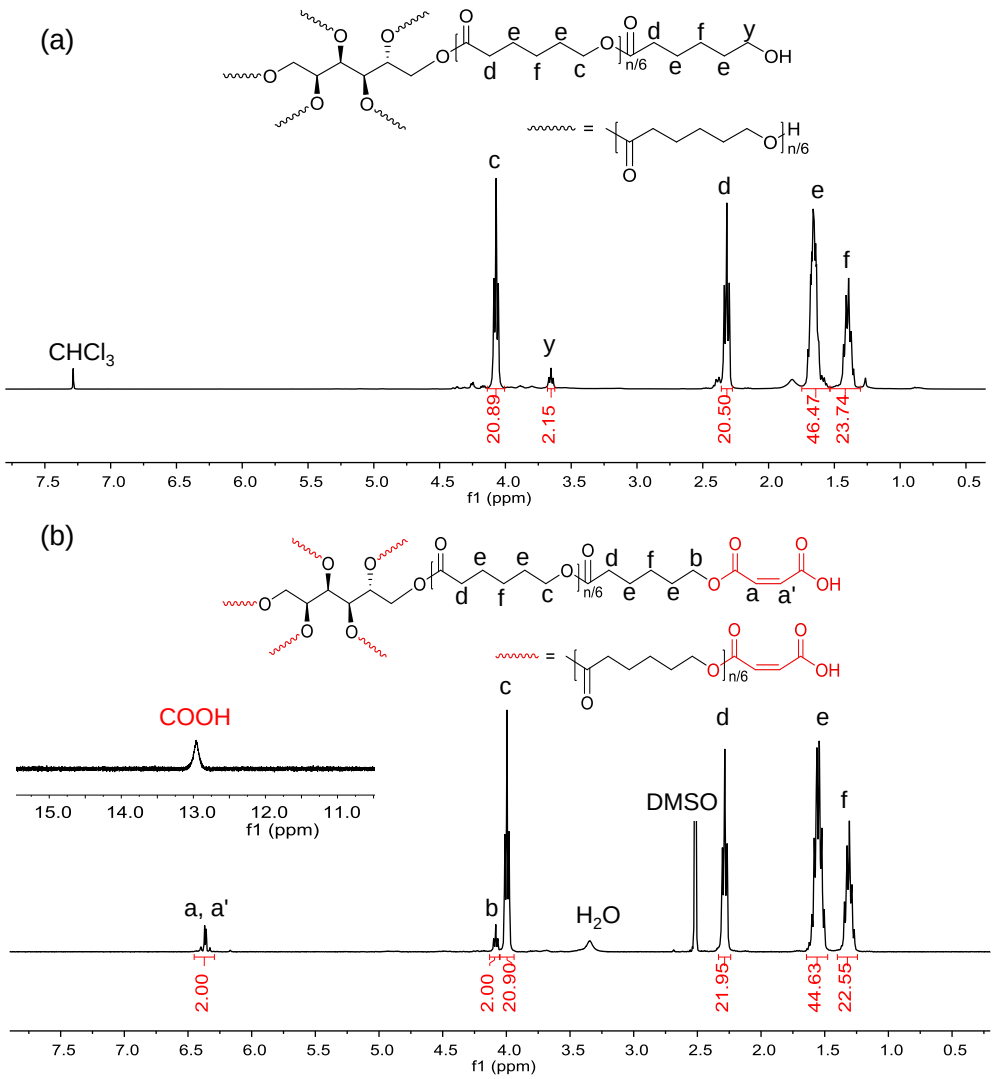



Figure 6.27. The $^{1}$H NMR spectra (400 MHz) of purified (a) precursor star *D*-sorbitol[$(PCL)_{27}OH_3$]$OH_3$ in $CDCl_3$ and (b) a PCL hemi ester of maleic acid functionalised star *D* sorbitol[$(PCL)_{27}COOH_3$]$OH_3$ in DMSO-$d_6$. Inset in the (b) shows the signal corresponding to terminal COOH.

Side reactions that may occur during functionalisation include *cis-trans* isomerisation of maleic acid to fumaric acid and consumption of double bond induced by oxygen (oxidation) or hydroxy group *via* electrophilic addition (predominant at temp. >160 °C).[48] However, no chemical shift was found for oxidised or hydroxylated MA at $\delta = 2.8–3.1$ ppm[49] nor for the isomerisation of MA into fumaric acid at $\delta$ 6.83 ppm[49] (Figure 6.27, b). Isomerisation to fumaric acid would decrease the reactivity of our functionalised star in the A/D polymerisation with vinyl ethers.[50] Such isomerisation is not observed in our case.

For the sake of consistency, this hemi-ester of maleic acid functionalised star *D*- sorbitol[$(PCL)_{27}COOH_3$]$OH_3$ will be referred as S-PCL-MAc3100 (where 3100 is

the $M_n^{SEC\text{-}MALS}$ of S-PCL3100). Similarly, the star *D*-sorbitol[$(PCL)_{49}COOH_3$]$OH_3$ will be denoted as star S-PCL-MAc5700 from the precursor star S-PCL5700.

For comparative study, the $Sn(Oct)_2$ catalysed star PCL ($M_n^{SEC\text{-}MALS}$ = ~2500 g $mol^{-1}$, $Đ$= 1.10) was also successfully functionalised with maleic anhydride. However, due to the waxy physical state of low MW star made using $Sn(Oct)_2$ as a catalyst, the removal of the excess of MAH from the final mixture was challenging by solvent purification method. In sharp contrast, the handling of biobased star PCL samples (that was synthesised using Novozym 435 as a catalyst) was much easier due to the soft-powdery physical state of the pre- and post-functionalised samples. Thus, Novozym 435 catalysed samples S-PCL-MAc5700 and S-PCL-MAc3100 were efficiently purified from any residual MAH and were investigated further.

#### 6.4.2.2 Dispersion of Star *D*-sorbitol[$PCL_n$-MA-$COOH_{3x}$]$OH_3$ in Water (Surfactants)

The stars S-PCL-MAc5700 and S-PCL-MAc3100, were dissolved in a favourable solvent (300 mg in 2 ml acetone) and the carboxy end-groups were neutralised by trimethylamine (TEA) (1 equimolar TEA to MAc in 0.5 ml acetone). A nanoprecipitation method was employed to disperse the S-$PCL_n$-MA-$COONEt_{3x}OH_3$ in water (Figure 6.28).

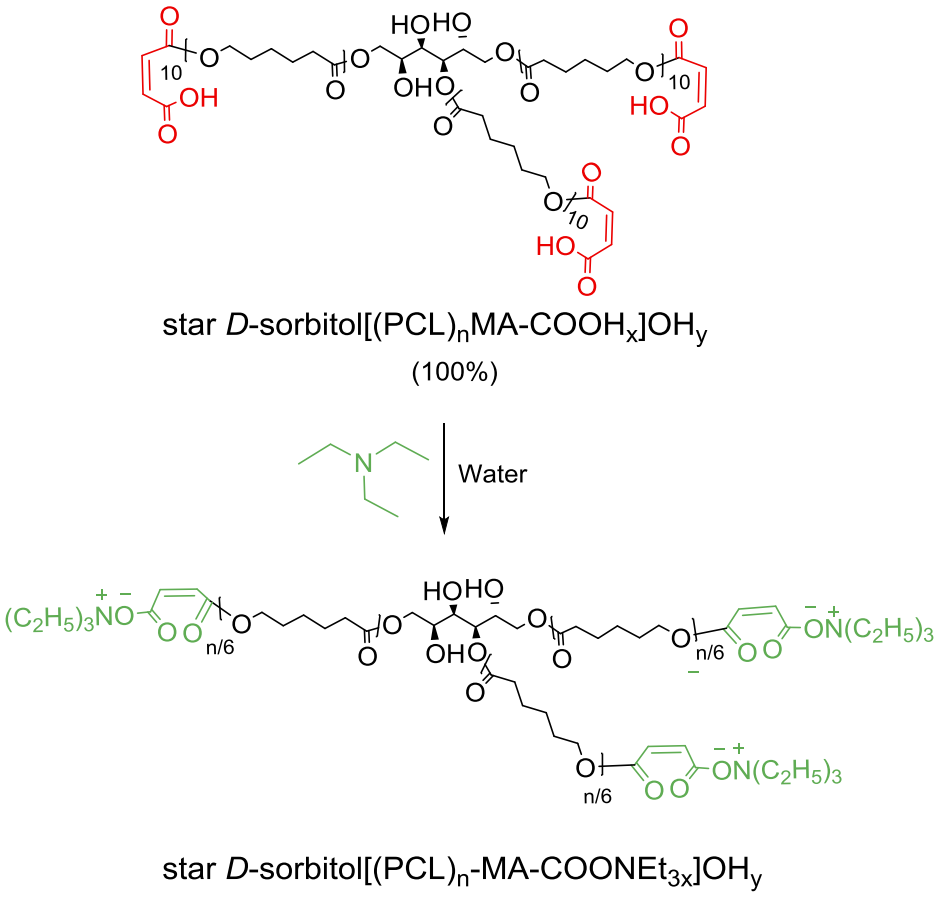



Figure 6.28. General schematic showing functionalisation of star *D*-sorbitol[(PCL)$_n$OH$_x$] polymer with MAH to give star *D*-sorbitol[(PCL)$_n$-MAc$_x$] followed by neutralisation with TEA and subsequent dispersion in aqueous media.

It was noticed that the sequence by which dispersion was created (i.e. mixing favourable and poor solvent during neutralisation of S-PCL-MA-COOH sample) was also affecting the surface activity. To investigate this effect, the neutralisation was performed in two ways. The star *D*-sorbitol-PCL$_n$-MA-COONEt$_{3x}$ was divided into two equal parts (to give 150 mg mL$^{-1}$ in acetone). One part of the neutralised star (in acetone) was dropwise added into water (30 mL, stirring at 500 rpm) by means of a syringe positioned with the needle directly in the dispersion medium[51] (30 mL). For the second part, water was added to the neutralised star (present in acetone) following exactly the same procedure. In both cases, acetone was removed under reduced pressure and the surface tension was measured using the Wilhelmy plate method.[51] For the control test, a suspension of star PCL-OH$_x$ (Figure 6.29, a) and star S-PCL-MA-COOH$_x$OH$_x$ obtained by the nanoprecipitation method in water was attempted (Figure 6.29, b).

(a) S-PCL5700 (b) S-PCL-MAc5700 (c) S-PCL-MA-$COONEt_3$5700

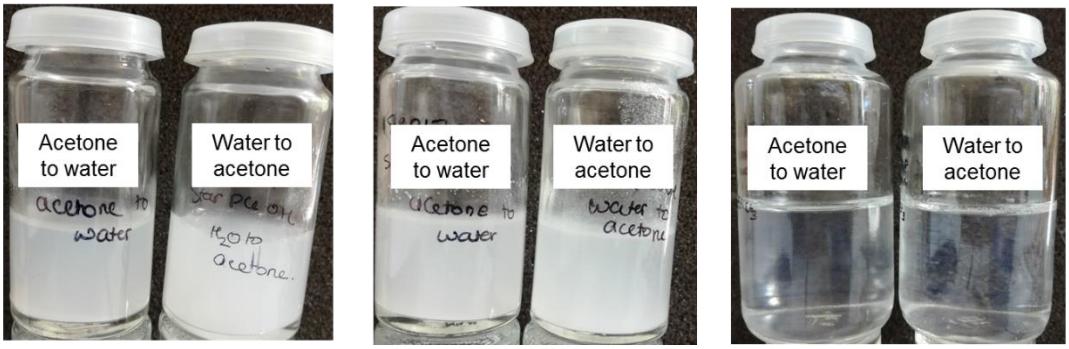



Figure 6.29. Transition in the nanoprecipitation of star *D*-sorbitol[$(PCL)_{49}OH_3$]$OH_3$ polymer in water by acetone (a) before end-functionalisation (b) star *D*-sorbitol[$(PCL)_{49}COOH_3$]$OH_3$ after end-functionalisation and (c) star *D*-sorbitol[$(PCL)_{49}$OH-MA-$COONEt_3$]$OH_3$ after neutralisation with TEA. Pictures were taken before evaporation of acetone.

It is apparent that regardless of the sequence of dispersion, the star *D*-sorbitol-PCL samples possessing hydroxy (Figure 6.29, a) or carboxy chain-ends (Figure 6.29, b) pre- and post-functionalisation, respectively, did not disperse in water at all. Furthermore, precipitates were observed when left overnight at room temperature. In sharp contrast, neutralisation with TEA leads to a clear suspension of samples (Figure 6.29, c). On closer inspection, a slight opaqueness in the dispersion was, however, noticeable for star PCL-MA-$COONEt_3$ (5700 g $mol^{-1}$) even after acetone removal. By contrast, a lower MW star PCL-MA-$COONEt_3$ (3100 g $mol^{-1}$, Figure 6.30 (a)) gave a clear solution and led to foaming in water (Figure 6.30 (b)).

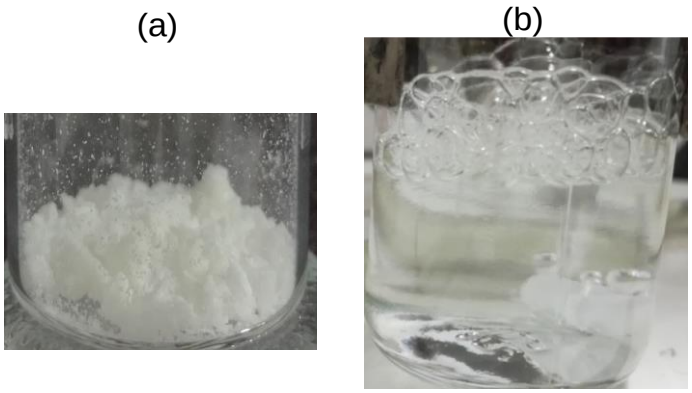



Figure 6.30. The bio-based star *D*-sorbitol[$(PCL)_n$-Maleic $acid_x$] showing (a) white soft-powder compound obtained after purification and (b) star *D*-sorbitol[$(PCL)_{27}$-MA-$COONEt_3$]$OH_3$ dispersed in water by nanoprecipitation (acetone in water) method after acetone evaporation.

### 6.4.2.3 Surface Tension of Functionalised S-PCL-MA-COONEt$_3$OH$_3$

Static and equilibrium surface tension was measured for the stars S-PCL-MA-COONEt$_3$OH$_3$ dispersed in water. The water to acetone dispersion did not reduce the surface tension significantly ($\gamma$ is 60 mN m$^{-1}$ (static) and 57.6 mN m$^{-1}$ (equilibrium)) for a star with higher MW of 5700 g mol$^{-1}$ (Figure 6.31). The acetone to water nanoprecipitation method showed a slight reduction in surface tension ($\gamma$ is 56.3 mN m$^{-1}$ (static) and 55.4 mN m$^{-1}$ (equilibrium)). These results are promising as they support the fact that end-functionalisation of star PCL with maleate-carboxy acid and subsequent neutralisation of acid to create ionic charges on star PCL certainly enabled to improve its surface activity (Figure 6.31).

The acetone to water nanoprecipitation method served better to create a dispersion.

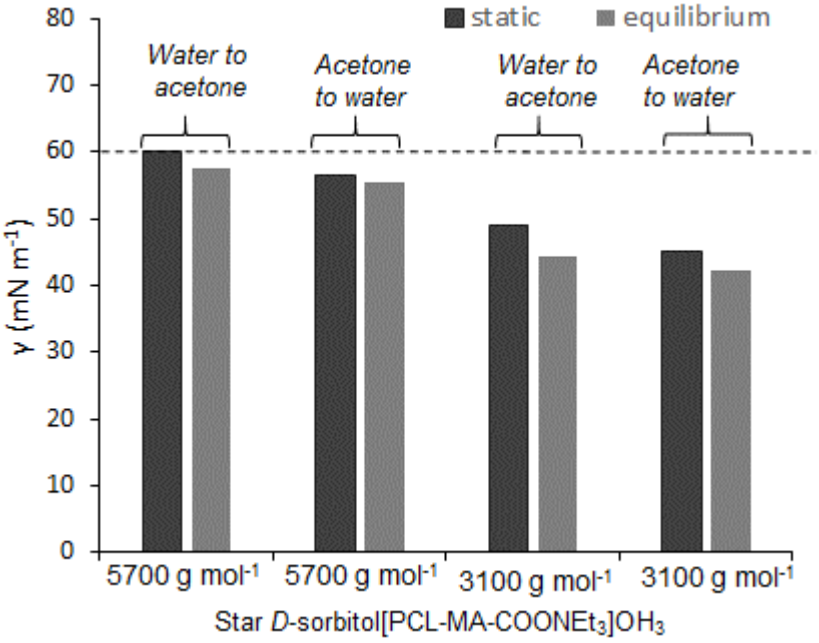



Figure 6.31. Static and equilibrium surface tension values of star *D*-sorbitol-[PCL$_n$-MA-COOEt$_3$]OH$_3$ (5700 g mol$^{-1}$ and 3200 g mol$^{-1}$) dispersed in water by the nanoprecipitation method. Compounds below the dashed line are considered surface active agents.

A significant reduction in surface tension values, down to about 42.2 mN m$^{-1}$ (equilibrium) was noticed when the MW of hydrophobic PCL was decreased to ~3100 g mol$^{-1}$. Indeed, the overall ionic charges and the terminal hydroxy group between stars (5700 g mol$^{-1}$ 3100 g mol$^{-1}$) are constant and only the hydrophobic length is decreased (i.e. hydrphilicity is increased). These results are consistent with previous data obtained[39] where the high MW S-PLA-OH$_6$ (6800 g mol$^{-1}$) was insufficient to lower

the surface tension while 1800 g $mol^{-1}$ decreased the tension to 54 mN $m^{-1}$. These results are promising and show that by tuning the length of the hydrophobic star PCL and by the introduction of ionic-charges to the end-functionalised star PCL-MA-COOH enables a lowering of the surface tension of water.

Comparing these results with the directly water soluble star PCL (made by $Sn(Oct)_2$ catalyst) that have PEP as a hydrophilic block (PCL:PEP ratio = 4000:8800 g $mol^{-1}$), it is evident that also star *D*-sorbitol[PCL-MA-$COOEt_3$]$OH_3$ (PCL core 3100 g $mol^{-1}$) showed similar performance to reduce the surface tension (for both $\gamma \sim 42$ mN $m^{-1}$).

The results highlight that fact the biobased star PCL can reduce the surface tension following a quick, simple and sustainable process by the post-functionalisation method.

## 6.5 Conclusions (Surfactants)

All the star diblock and linear triblock PCL: PEP copolymers were able to reduce the surface tension down to ~45 mN $m^{-1}$. A triblock $PEP_{7.2}$-$PCL_9$-$PEP_{7.2}$ (PCL: PEP = 1000: 1100: 1000 g $mol^{-1}$) showed an excellent reduction of water surface tension down to 31.7 mN $m^{-1}$. These results are even superior when compared to commercial Pluronic L35 and L64 where the $\gamma$ values range from 40-49 mN $m^{-1}$. In addition, the star *D*-sorbitol[$PCL_{18}$-*b*-$PEP_{27}OH_6$] (PCL: PEP = 2200: 3700 g $mol^{-1}$) surfactant has shown promising results to solubilise bisabolol fragrance up to 9.8: 1 ratio.

Two biobased star *D*-sorbitol-PCL (Novozym 435 catalysed) were successfully functionalised with a terminal maleate carboxy groups. The surface activity measurement on S-PCL neutralised by triethylamine was investigated; it confirms that these new biobased star S-PCL of 3100 g $mol^{-1}$ reduces the surface activity to a similar value when compared to star PCL: PEP surfactants (42.2 mN $m^{-1}$).

To sum up, the green synthesis pathways described in Chapter 4 to prepare novel biobased telechelic PCL and star PCL, and their corresponding triblock and star diblock compounds in Chapter 5 they might be interesting candidates as surfactants in personal care products. Further analyses to investigate in-depth their biodegradability is needed to evaluate their real potential in formulations.

Biobased hydrophobic star *D*-sorbitol-$PCL_nOH_x$ possessing unsaturation with hemi ester of maleic acid (star *D*-sorbitol-$PCL_n$-MA-$COOH_x$) were tested as a surfactant in previous sections.

Diverting slightly from surfactant-applications and these maleate-functionalised star materials were also exploited to prepare biobased films and are discussed below.

## 6.6 Experimental (Coatings)

### 6.6.1 Materials and Methods

Enzymatic ROP (eROP) mediated star $PCL_nOH_x$ (preparation disclosed in Chapter 4) were used in this Chapter. The 2-hydroxy-2-methyl propiophenone (Darocur 1173, 100%) was a from Sigma, polypropylene films (thickness: 6 μm) were purchased from Goodfellow and tri(ethylene glycol) divinyl ether (DVE) was purchased from Sigma (98% purity).

### 6.6.2 Biobased Star PCL (Coatings)

#### 6.6.2.1 Functionalisation of Star *D*-sorbitol-$PCL_nOH_x$ (Surfactants and Coatings)

Refer to section 6.3.3.

#### 6.6.2.2 Photo-curable Formulation of Star *D*-Sorbitol[$PCL_n$-$MAc_x$]

The trifunctional star *D*-sorbitol[$(PCL)_{27}$-MA-$COOH_3$]$OH_3$ (103 mg, 33 μM, $M_n$ $^{SEC\text{-}MALS}$ = 3100 g $mol^{-1}$) as an acceptor (A) was mixed with bifunctional tri(ethylene glycol) divinyl ether ($H_2C{=}CH(OCH_2CH_2)_3OCH{=}CH_2$,10.3 mg, 202.25 g $mol^{-1}$, 50.9 μM, DVE) as a donor (D) in a 2:3 A/D molar ratio; that is to say a stoichiometric ratio between hemiester of maleic acid on star PCL and vinyl ether functions of DVE. Darocur 1173 (4.5 mg, 4 wt% respect to monomer feedstock) as a photoinitiator along with a minimal amount of acetone (~150 μL, 117.6 mg) was added to the mixture followed by intensive mixing (vortexing ~3-5 min) at ambient condition up to the formation of a clear, homogeneous viscous liquid.

#### 6.6.2.3 Films of Star *D*-Sorbitol[$PCL_n$-$MAc_x$] and UV-curing Procedure

The above stoichiometric solution was cast onto glass slides at a thickness of about 25 μm using a film applicator bar coater (Sheen 1117/100 mm, UK). The glass slides

were immediately placed on the conveyor under a UV production-curing unit (Fusion UV, LC6B Benchtop Conveyor) equipped with a UV vapour mercury lamp (type H, Fusion F300S, 120 W.cm$^{-2}$, 200-600 nm). A film after evaporation of the acetone under ambient condition was prepared for curing similarly. Finally, the glass slides were passed repeatedly under the UV lamp at a speed of 1 m min $^{-1}$.

## 6.7 Results and Discussion (Coatings)

### 6.7.1 Functionalisation of Biobased Star *D*-Sorbitol[$PCL_nOH_x$]

Discussed in section 6.4.2.1.

### 6.7.2 Star PCL Film Preparation and Characterisation.

The synthesis of hemi ester of maleic acid functionalised S-PCL-MAc3100 from the precursors S-PCL3100 and its characterisation by $^1$H NMR spectroscopy was discussed in section 6.4.2.1.

FTIR analyses, in principle, should enable to detect a change in the sample before- and after functionalisation. The hydroxy absorption band (3510 cm$^{-1}$) of the S-PCL-MAc3100 should decrease and the carboxy absorption band (3200 cm$^{-1}$) should increase. In addition, the incorporation of the carbon-carbon double bond in the polymer should have an absorption band at ~1640/1645 cm$^{-1}$. Surprisingly, no significant spectral differences were noticed in the FTIR of star *D*-sorbitol[$(PCL)_{27}OH_3$]$OH_3$ pre- and post-functionalised with maleate group (Figure 6.32).

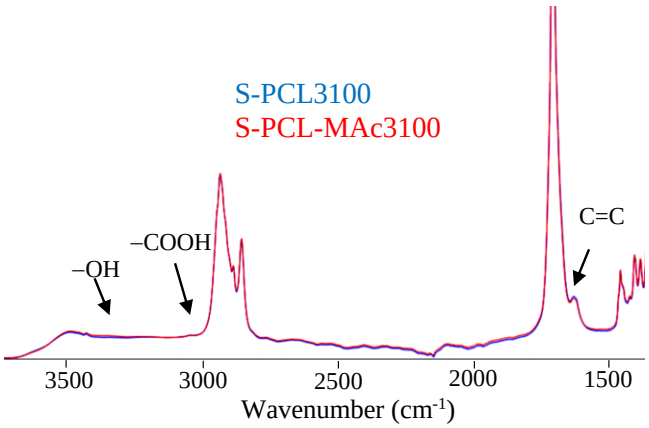



Figure 6.32. The stacked FTIR spectra of star *D*-sorbitol[$(PCL)_{27}OH_3$]$OH_3$ (blue line) and star *D*-sorbitol[$(PCL)_{27}$MA-$COOH_3$]$OH_3$ (red line) shows no spectral differences.

Despite that, $^{1}$H NMR analysis clearly confirmed the complete substitution of the terminal primary hydroxy of PCL arms (Figure 6.27 a vs. b, section 6.4.2.1), i.e. the functionalised S-PCLMAc3100 has ~3 terminal hemi ester of maleic acid, implying that ~3 pendant secondary hydroxy groups remained on *D*-sorbitol core (refer to section 6.4.2.1). Since an excess of maleic anhydride was used (feed ratio of the star: MAH =1:20 ratios, thus (20 MAH)/(1-star × 6 hydroxy groups) = 3-fold excess of MAH), so as we expected, the $^{1}$H NMR analyses of crude samples detected unreacted MAH. However, the purified sample showed the absence of MAH signals (Figure 6.27, b). This data demonstrates that the hemi ester of maleic acid is indeed covalently linked to PCL arms and a quantitative functionalisation of PCL-OH arms into PCL-hemi ester of maleic acid has occurred.

The acceptor/donor (A/D) molar ratio is an important parameter to consider when monitoring the photo-induced polymerisation or crosslinking.[52] Among the choice of the donor, we selected tri(ethylene glycol) divinyl ether (DVE) because of its polar nature, to favour its miscibility with the functionalised star PCL. Indeed, a quick test of dissolution of S-PCL-MAc3100 in DVE as a solvent at 10 wt% ratio has proven its excellent compatibility in DVE. Nonetheless, the formulation of a starting trifunctional star *D*-Sorbitol-[PCL-MAc] and bifunctional DVE should have a stoichiometric proportion of A/D (i.e. 2:3 trifunctional A / difunctional D molar ratio).[52] When choosing this proportion, the content of solid S-PCL-MAc3100 in the A/D formulation is ~91 wt% (refer section 6.6.2.2). Hence, a favourable common solvent (acetone) at an optimised concentration (~50 wt% respect to total feed) was necessary to obtain a homogeneous solution of the functionalised PCL star and DVE. It gave a clear and transparent mixture. After which the photoinitiator (Darocur 1173, 4 wt% respect to monomers) was added. This formulation was employed to study the kinetics of polymerisation by Real Time-FTIR and for UV-curing.

### 6.7.3 Kinetic Analysis of Star *D*-Sorbitol [PCL-MAc$_x$] Polymerisation with DVE

The light-induced polymerisation between maleate group and DVE was recorded by Real Time-FTIR spectroscopy, under UV-irradiation at the intensity of 10 mW cm$^{-2}$ under air (Figure 6.33, left) and in its absence by protecting with a PP film (Figure 6.33, right).

The conversion was continuously monitored *in situ* for 300 s following the decay of the IR band at 1615 $cm^{-1}$ and 1635 $cm^{-1}$ characteristic of the tri(ethylene glycol) divinyl ether double bond (refer to Appendix D, Figure D2). The DVE consumption was very fast whether the polymerisation was performed in the absence of air or in contact with air. The reaction seems to be slightly faster in absence of air upon irradiation for 2 s (green line, Figure 6.33, right).

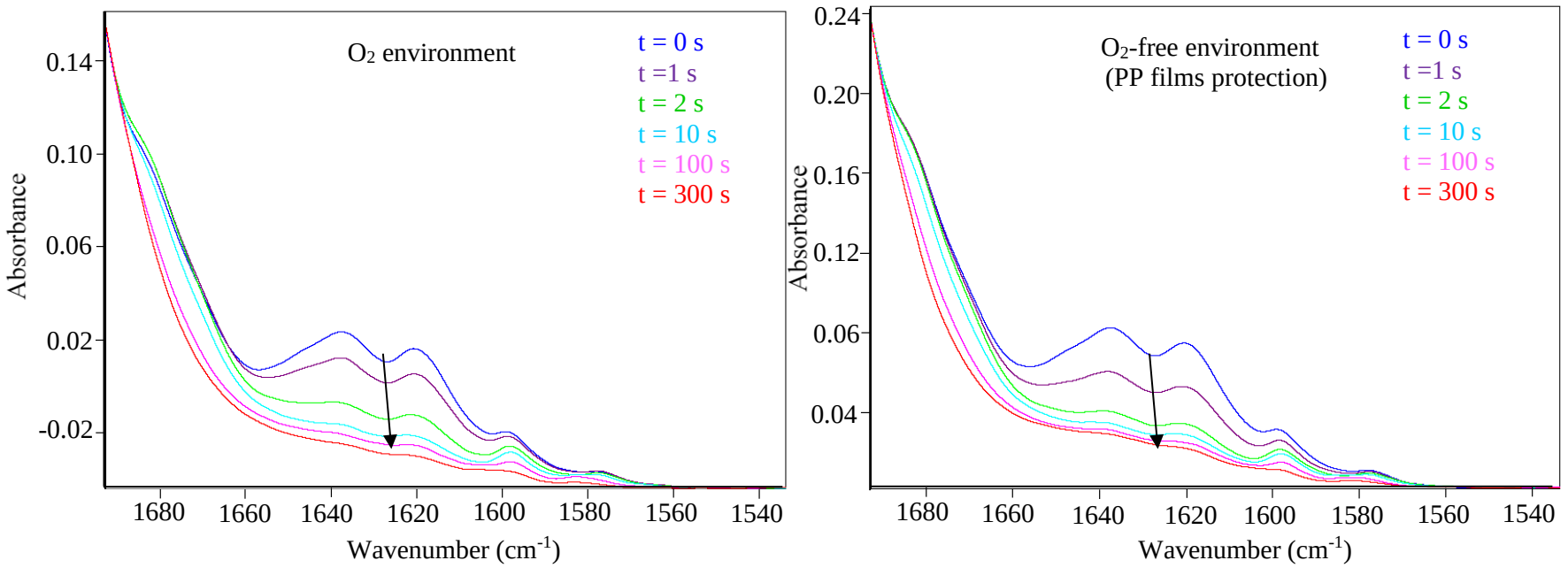



Figure 6.33. The stacked plot of RT/FTIR spectra shows the kinetics of the UV-polymerisation of star *D*-Sorbitol[PCL-MA$c_x$] with tri(ethylene glycol) divinyl ether over a reaction time period of 300 s. The degree of decline in the absorption peaks between 1660-1580 $cm^{-1}$ peak and in particular, at 1615 $cm^{-1}$ and 1635 $cm^{-1}$ as a function of time represents the rate of the consumption of the unsaturated double bonds of maleate and DVE.

A significant change is however not evidenced in the kinetic profiles (Figure 6.33, left and right) suggesting that the system is not sensitive to oxygen inhibition, which is an advantage over acrylate systems. Full DVE conversion may be estimated from such profiles because the full decay of unsaturated groups is noticeable (Figure 6.33). Yet, the quantitative conversion of maleate was not possible to evaluate by FTIR due to overlapping between C=C stretch band peaks of maleate and DVE. Nevertheless, knowing that the vinyl ether cannot homopolymerise (it was checked using the same experimental conditions), and given the stoichiometric ratio maleate/vinyl ether used in the experiment, the full conversion of DVE implies a full conversion of the maleate.

### 6.7.4 UV-Cured Network of Star Poly[CL-Maleate-*alt*-Vinyl Ether] Films

An important factor in making a high-performance UV-curable adhesive is to ensure an excellent adhesion onto the various types of supports (glass, plastics, metals or paper).[27] Thus, the two films were prepared. Using the above liquid formulation of hemi ester of maleic acid functional star *D*-sorbitol[$(PCL)_{27}MA\text{-}COOH_3$]$OH_3$ (abbreviated as star *D*-sorbitol[$(PCL)_nMAc_x$] for simplicity), DVE, photo-initiator (Darocur 1173) alongwith acetone were successfully coated on the two glass substrates (refer to section 6.6.2.2 and 6.2.2.3). A coated film was cured in the presence of acetone and another in its absence in order to fabricate the star *D*-Sorbitol[$PCL_n\text{-}MAc_x\text{-}C\text{-}DVE_y$] crosslinked network films *via* the UV-curing process (Figure 6.34)

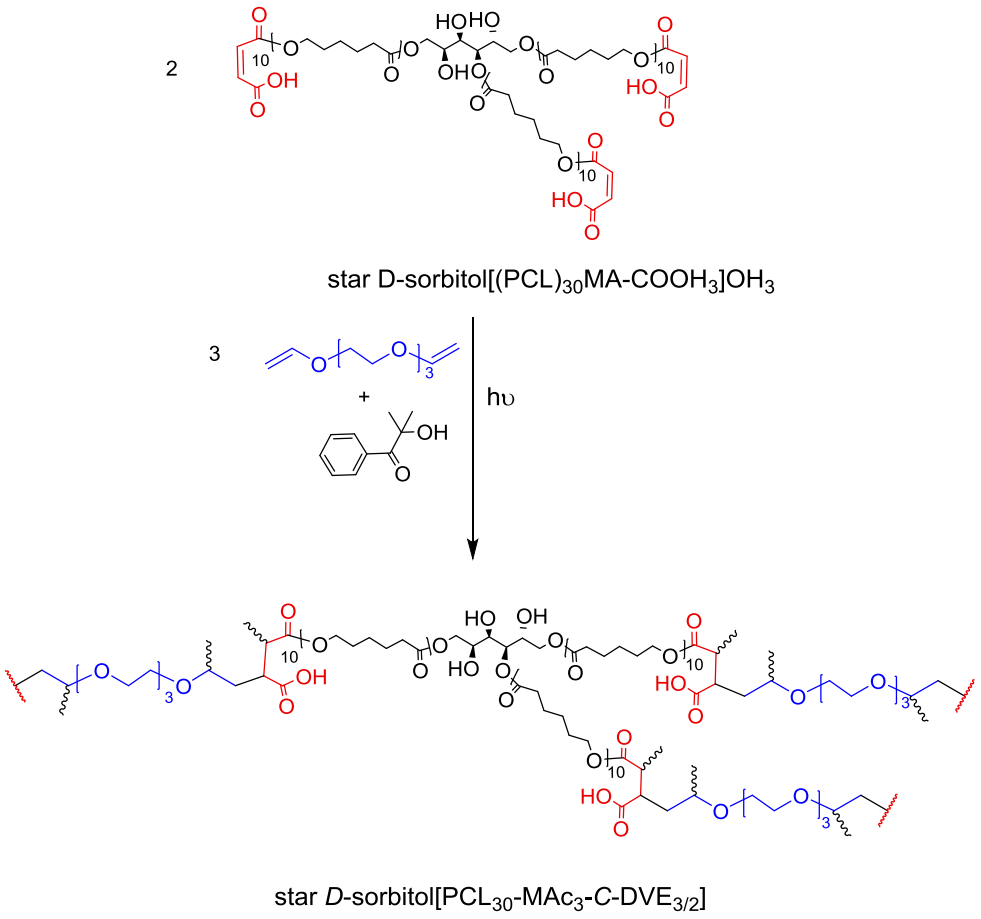



Figure 6.34. Schematic representation of the UV-crosslinking of maleate groups of star *D*-sorbitol-$PCL_n$-$MAc_x$ (acceptor) (3 maleates per star polymer) with tri(ethylene glycol) divinyl ether (donor) in the presence of Darocur 1173 as a photoinitiator.

The films in which the acetone was evaporated during the UV-curing cycles (acetone-borne films) appeared transparent (Figure 6.35, a). In contrast, when acetone was evaporated before the UV-curing process, this left an opacity in the film both before and after the UV-crosslinking process (Figure 6.35, b). It appeared after the UV-curing process that these network films adhere to the glass substrate strongly.

(a) Transparent film of star PCL-MAc-*C*-DVE for acetone-borne UV-curing

(b) Opaque film of star PCL-MAc-*C*-DVE for UV-curing without acetone

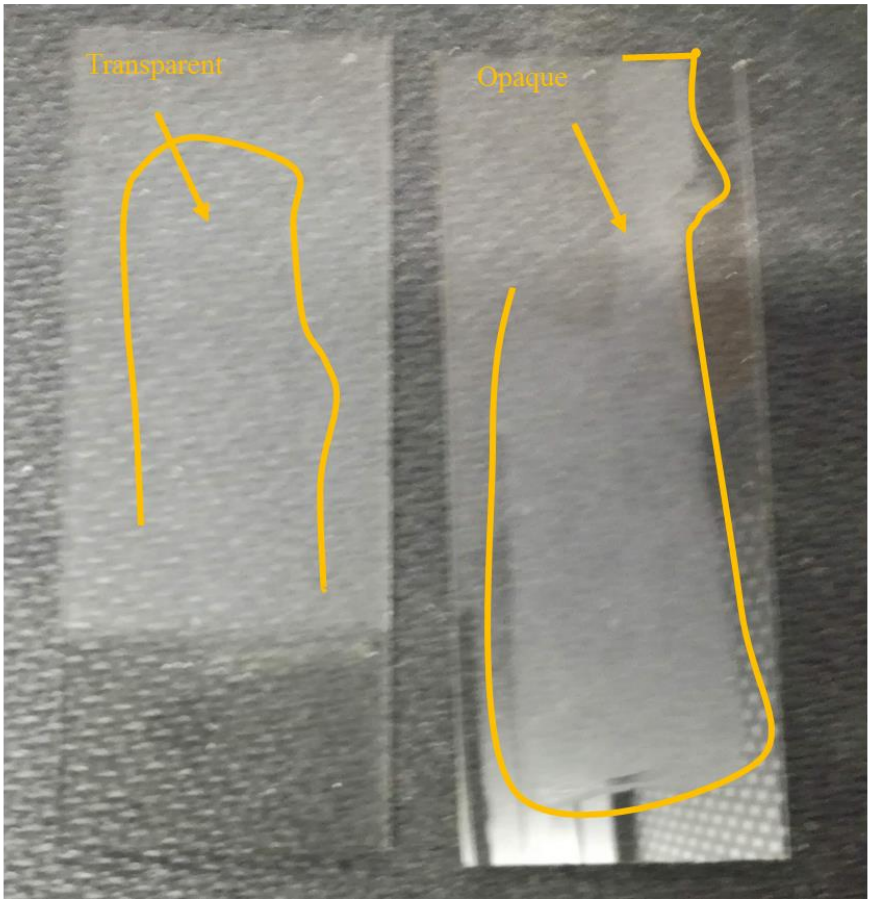



Figure 6.35. The UV-cured films of the star *D*-Sorbitol[PCLn-MAc$_x$-*C*-DVE$_y$] coatings where (a) acetone-borne curing gave a transparent film and (b) acetone-absence films gave an opaque film. Both the films were coated to a thickness of about 25 µm and were irradiated with a 120 W cm-2 polychromatic UV-light source (200-600 nm, Hg lamp).

The efficiency of UV-curing of the acetone-borne and acetone-evaporated films in air, was determined using Real Time-FTIR spectroscopy by comparing the intensity of the DVE band at 1615 and 1635 cm$^{-1}$ (Figure 6.36, top black line), which almost completely disappeared upon UV-curing, to that of the carbonyl peak at 1720 cm$^{-1}$ which do not change upon curing (Figure 6.36). Indeed, no spectral differences were noted between the liquid formulated acetone-borne and the acetone-absent UV-cured films (Figure 6.36, red and blue line).

Additionally, it is also evident from FTIR spectra that the UV-light-induced homopolymerisation of the starting tri(ethylene glycol) divinyl ether in presence of Darocur 1173 (at 2.3 wt% ratio of DVE and Darocur 1173; i.e. the same ratio as those

used for film formulations, refer section 6.6.2.2) into PDVE does not occur (Figure 6.36) and its schematic (Figure 6.38, top).

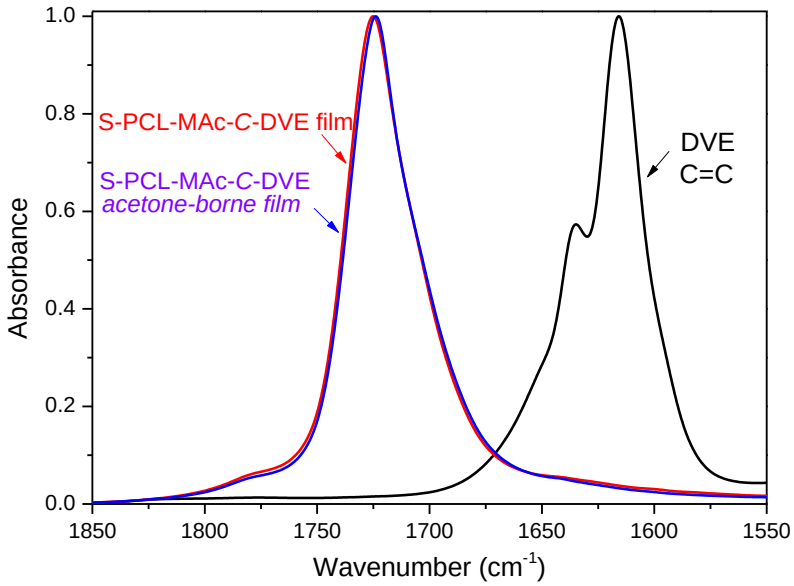



Figure 6.36. The stacked FTIR spectra of the DVE monomer (black line) and the star *D*-sorbitol[$PCL_n$-$MAc_x$-*C*-$DVE_y$] films; acetone-borne UV-cured film (red line) and film curved after acetone evaporation (blue line).

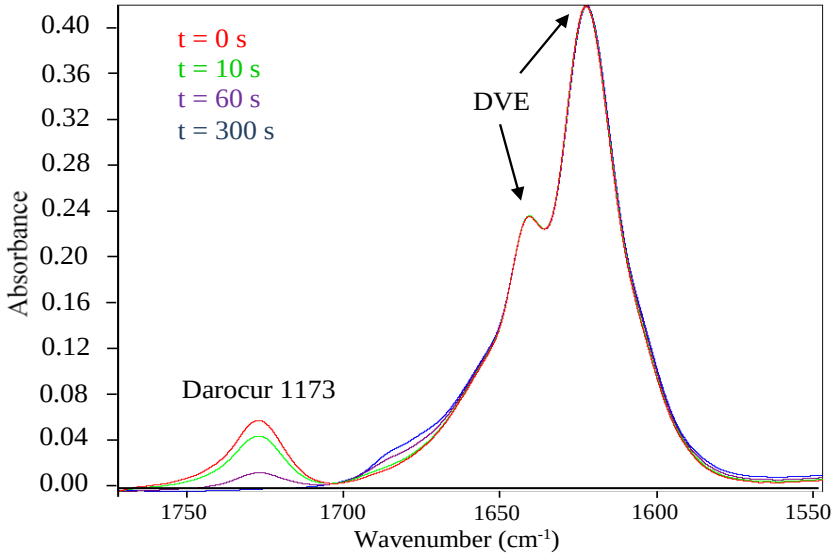



Figure 6.37. The FTIR spectra for the UV-photopolymerisation reaction of a mixture of DVE monomer and Darocur 1173 at 2.3 wt%.

The process and curing by UV of the star *D*-sorbitol[$PCL_n$-$MA_x$-*C*-$DVE_y$] to create cross-linked polymer thin films are illustrated (Figure 6.38).

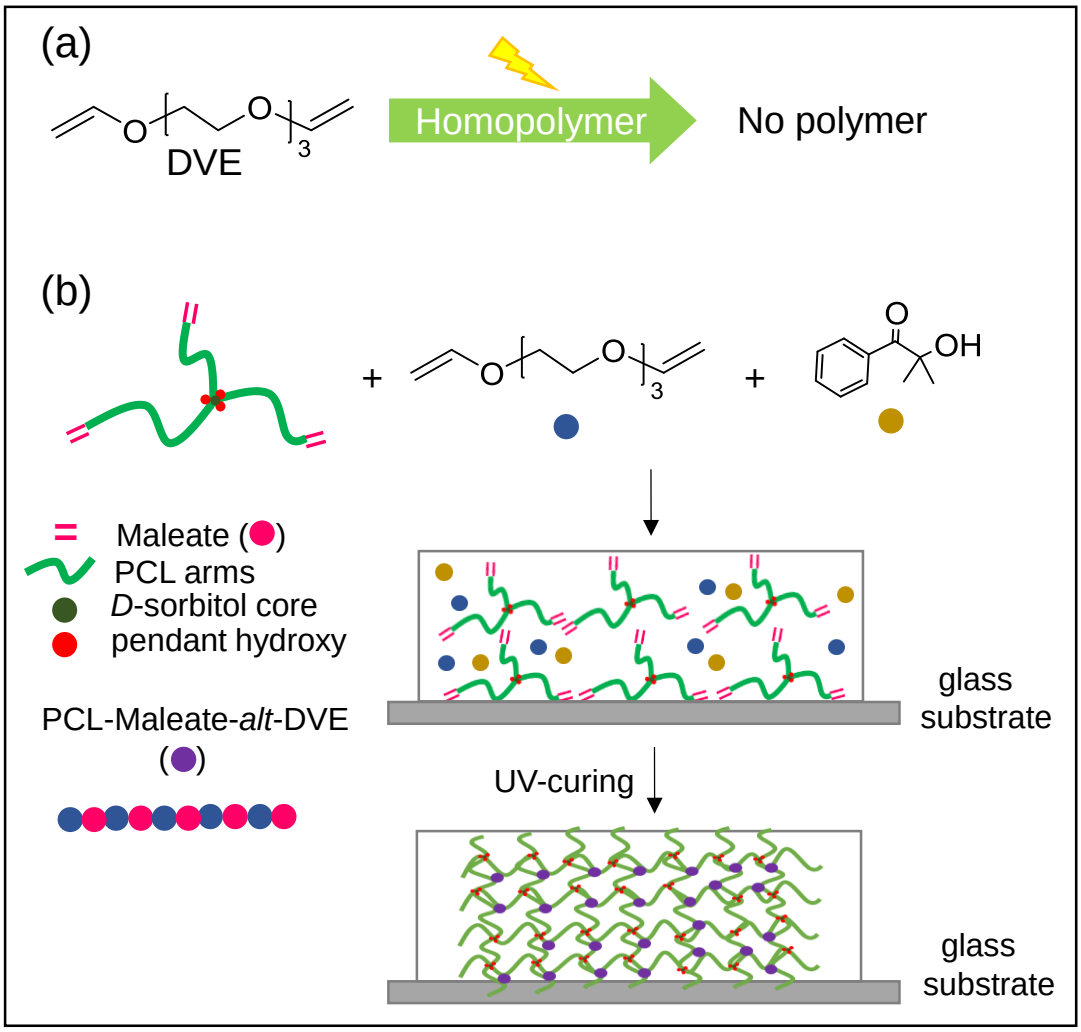



Figure 6.38. Representation of (a) the UV-induced DVE polymerisation reaction and (b) schematic showing UV-curing process for coating.

### 6.7.5 DSC Studies

DSC thermograms show that the precursor S-PCL3100 and the functionalised S-PCL-MAc3100 are both semi-crystalline (black and red in exotherm, Figure 6.39). The substitution of the terminal primary hydroxy groups on the star PCL with hemi ester of maleic acid only slightly increased the crystallisation temperature (from $T_c$ = 27.2 °C to $T_c$ = 29.8 °C) and the melting temperature (from $T_m$ = 34.3 °C to $T_m$ = 37.6 °C). Both S-PCL3100 and PCL-MAc3100 exhibited two melting endotherms. The double melting behaviour is more pronounced after end-group functionalisation. Such multiple melting endotherms are rather a common phenomenon with branched polymers but often explained ambiguously.[53–55] Analysis of the S-PCL-MAc-*C*-DVE film revealed the amorphous nature of the network in both heating and cooling runs because the crosslinking process completely suppresses the crystallisation. Indeed, the crosslinking

density of the network suppressed the mobility of molecular chain, hence remarkably restricting the PCL crystal formation after the photocrosslinking reaction.

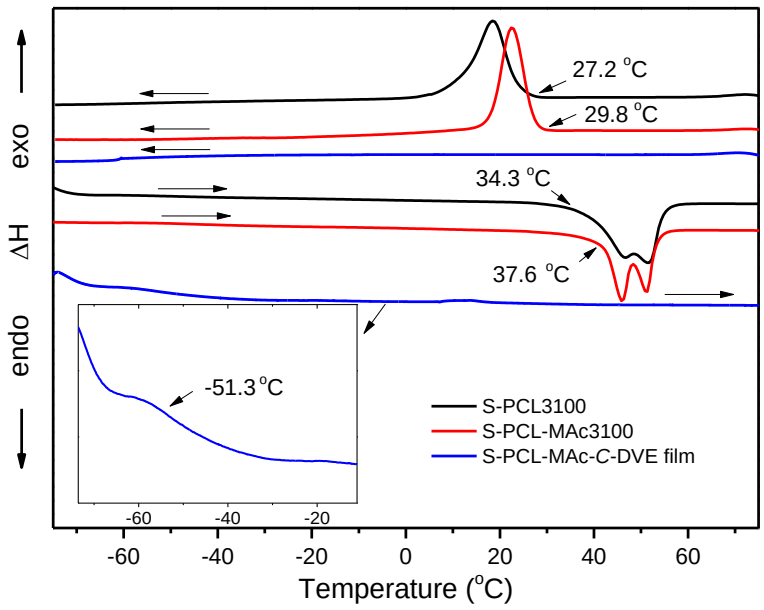



Figure 6.39. DSC curves of S-PCL3100 prepolymer (black line), hemi ester of maleic acid functionalised S-PCL-MAc3100 (red line) and the S-PCL-MAc-*C*-DVE crosslinked networks (blue line). The inset shows the enlarged endotherm network for clarity of $T_g$ in the case of the crosslinked film.

Such an effect has been observed previously, for example, in the case of the PCL crosslinking with poly(urethanes),[56] PCL fumarate[57] and PCL acrylate.[58] The glass transition temperature ($T_g$ = –51.3 °C) was identified after photocrosslinking reaction (blue line, Figure 6.39) because of the motion restriction imposed by the cross-links.

### 6.7.6 TGA Studies

TGA has been performed to determine the thermal stability of both S-PCL3100, uncrosslinked S-PCL-MAc3100 and crosslinked S-PCL-MAc-*C*-DVE in an air environment. All samples show one single degradation step (Figure 6.40). The onset thermal degradation temperature ($T_d$) decreases slightly after crosslinking. $T_{d,10\%}$ for S-PCL3100, S-PCL-MAc3100 and crosslinked S-PCL-MAc-*C*-DVE in this study is 286, 296 and 288 °C respectively corresponding to the total weight of the sample. The triethylene glycol of DVE is thought to be prone to thermal degradation below 350°C under air (like oligo-ethylene glycol). Yet, despite the presence of about 9 wt% DVE in its composition, the crosslinked S-PCL-MAc-*C*-DVE polymer film kept a thermal stability as good as its parent S-PCL-MAc3100 functionalised star polymer. Although

no significant change was observed in the decomposition profile of the starting S-PCL3100 and the crosslinked film. The final decomposition temperature corresponding to 90 wt% weight loss ($T_{d,90\%}$) for S-PCL-MAc-*C*-DVE was 443 °C that which is very close to parent S-PCL3100 at 433 °C and its functionalised S-PCL-MAc3100 at 437 °C.

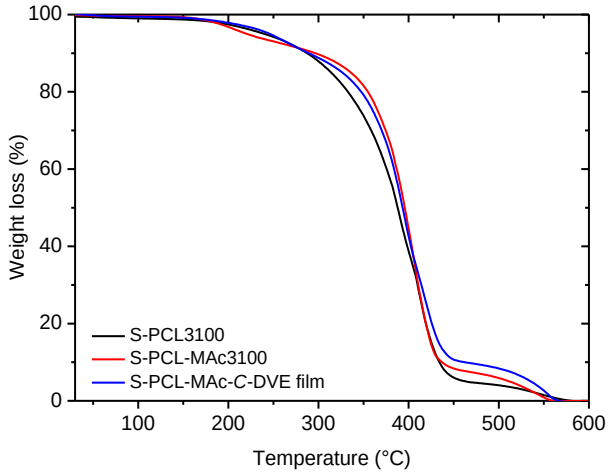



Figure 6.40. TGA thermograms under an air of S-PCL3100, S-PCL-MAc3100 and crosslinked S-PCL-MAc-*C*-DVE network. The inset shows the enlarged thermal degradation curves.

## 6.8 Conclusions (Coatings)

The UV-cured films of the functionalised S-PCL-MAc star polymer (3100 g mol$^{-1}$) bearing three-hemi esters of maleic acid were successfully prepared by using a small amount of DVE and in the presence of Darocur 1173 as a radical photoinitiator. This amount of DVE is only ~9 wt% relative to the star polymer, corresponding to 3:2 molar ratio of star polymer to DVE (i.e. a stoichiometric ratio of maleate acceptor to vinyl ether donor). The films could be prepared with the quantitative conversion of the maleate and vinyl ether functions. It was found that some transparent films could be obtained when acetone was used during UV-irradiation. The UV-curing was not very sensitive to inhibition by oxygen, in contrast to systems based on acrylates. Finally, the thermal properties of the crosslinked films have been studied. After crosslinking, the S-PCL maleate network loses the crystallinity completely and the films were amorphous. The thermal stability of the crosslinked S-PCL-MAc-*C*-DVE polymer film was as good as its parent S-PCL-MAc3100 functionalised star polymer. The crosslinked films showed good adhesion on a glass substrate. Future prospects include the study of the surface energy of the crosslinked films by measurements of contact angles with various liquids.

## 6.9 References


1. Alexandridis, P. Amphiphilic copolymers and their applications. *Curr. Opin. Colloid Interface Sci.* **1,** 490–501 (1996).
2. Laschewsky, A. in *Polysoaps/Stabilizers/Nitrogen-15 NMR* 1–86 (Springer-Verlag, 1995). doi:10.1007/BFb0025228
3. Tadros, T. F. Emulsion Formation,Stability, and Rheology. *Emuls. Form. Stab.* 1–76 (2013).
4. McClements, D. J. *Food Emulsion Principle,Practices, and Techniques*. (CRC Press, 2004).
5. Hiemenz, P. C. & Rajagopalan, R. *Principles of Colloid and Surface Chemistry*. *Principles of Colloid and Surface Chemistry* (CRC Press, 1997).
6. Heijman, S. G. J. & Stein, H. N. Electrostatic and steric stabilization of TiO2 dispersions. *Langmuir* **11,** 422–427 (1995).
7. Tadros, T. F., Vandamme, A., Levecke, B., Booten, K. & Stevens, C. V. Stabilization of emulsions using polymeric surfactants based on inulin. *Adv. Colloid Interface Sci.* **108–109,** 207–226 (2004).
8. Sehlleier, Y. H., Abdali, A., Schnurre, S. M., Wiggers, H. & Schulz, C. Surface functionalization of microwave plasma-synthesized silica nanoparticles for enhancing the stability of dispersions. *J. Nanoparticle Res.* **16,** (2014).
9. Jacquin, M. *et al.* Chemical analysis and aqueous solution properties of charged amphiphilic block copolymers PBA-b-PAA synthesized by MADIX®. *J. Colloid Interface Sci.* **316,** 897–911 (2007).
10. Alexandridis, P. & Alan Hatton, T. Poly(ethylene oxide)poly(propylene oxide)poly(ethylene oxide) block copolymer surfactants in aqueous solutions and at interfaces: thermodynamics, structure, dynamics, and modeling. *Colloids Surfaces A Physicochem. Eng. Asp.* **96,** 1–46 (1995).
11. Brown, W., Schillén, K., Almgren, M., Hvidt, S. & Bahadur, P. Micelle and gel formation in a poly(ethylene oxide)/poly(propylene oxide)/ poly(ethylene oxide) triblock copolymer in water solution. Dynamic and static light scattering and oscillatory shear measurements. *J. Phys. Chem.* **95,** 1850–1858 (1991).
12. Raffa, P., Wever, D. A. Z., Picchioni, F. & Broekhuis, A. A. Polymeric Surfactants: Synthesis, Properties, and Links to Applications. *Chem. Rev.* **115,** 8504–8563 (2015).
13. Borisov, O. V. & Halperin, A. Self-assembly of polysoaps. *Curr. Opin. Colloid Interface Sci.* **3,** 415–421 (1998).
14. Raffa, P., Broekhuis, A. A. & Picchioni, F. Polymeric surfactants for enhanced oil recovery: A review. *J. Pet. Sci. Eng.* **145,** 723–733 (2016).
15. Riess, G. Micellization of block copolymers. *Prog. Polym. Sci.* **28,** 1107–1170 (2003).
16. Raduan, N. H., Horozov, T. S. & Georgiou, T. K. 'Comb-Like' Non-Ionic Polymeric Macrosurfactants. *Soft Matter* **6,** 2321–2329 (2010).
17. Khristov, K. *et al.* Foam, emulsion and wetting films stabilized by polyoxyalkylated diethylenetriamine (DETA) polymeric surfactants. *Adv. Colloid Interface Sci.* **168,** 105–113 (2011).
18. Gong, H., Xu, G., Ding, H., Shi, X. & Tan, Y. Aggregation behavior of block polyethers with branched structure at air/water surface. *Eur. Polym. J.* **45,** 2540–2548 (2009).
19. Fan, Y. & Wang, Y. Self-Assembly and Functions of Star-Shaped Oligomeric Surfactants. *Langmuir* **34,** 11220–11241 (2018).
20. Rieger, J., Dubois, P., Jérôme, R. & Jérôme, C. Controlled synthesis and interface properties of new amphiphilic PCL-g-PEO copolymers. *Langmuir* **22,** 7471–7479 (2006).
21. Zhang, W. *et al.* Synthesis, surface and aggregation properties of a series of amphiphilic dendritic copolymers. *Colloids Surfaces A Physicochem. Eng. Asp.* **348,** 45–48 (2009).
22. Bhadani, A. *et al.* Sustainable oleic and stearic acid based biodegradable surfactants. *RSC Adv.* **7,** 10433–10442 (2017).
23. Tehfe, M., Louradour, F., Lalevée, J. & Fouassier, J.-P. Photopolymerization Reactions:

On the Way to a Green and Sustainable Chemistry. *Appl. Sci.* **3,** 490–514 (2013).
24. Yang, D. B. Kinetic studies of photopolymerization using real time FT-IR spectroscopy. *J. Polym. Sci. Part A Polym. Chem.* **31,** 199–208 (1993).
25. Ligon, S. C., Husár, B., Wutzel, H., Holman, R. & Liska, R. Strategies to reduce oxygen inhibition in photoinduced polymerization. *Chem. Rev.* **114,** 577–589 (2014).
26. Yagci, Y., Jockusch, S. & Turro, N. J. Photoinitiated Polymerization : Advances , Challenges , and Opportunities. 6245–6260 (2010). doi:10.1021/ma1007545
27. Decker, C. UV-radiation curing of adhesives. *Handb. Adhes. Surf. Prep.* **2,** 221–243 (2011).
28. Hoyle, C. E., Clark, S. C., Jonsson, S. & Shimose, M. Photopolymerization using maleimides as photoinitiators. *Polymer (Guildf).* **38,** 5695–5697 (1997).
29. Gao, C. & Yan, D. Hyperbranched polymers: from synthesis to applications. *Prog. Polym. Sci.* **29,** 183–275 (2004).
30. Claesson, H. *et al.* Rheological behaviour during UV-curing of a star-branched polyester. *Prog. Org. Coatings* **44,** 63–67 (2002).
31. Johansson, M., Malmstrom, E., Jansson, A. & Hult, A. Novel Concept for Low Temperature Curing Powder Coatings Based on Hyperbranched Polyesters. *J. Coat. Technol.* **72,** 49–54 (2000).
32. Lange, J., Stenroos, E., Johansson, M. & Malmström, E. Barrier coatings for flexible packaging based on hyperbranched resins. *Polymer (Guildf).* **42,** 7403–7410 (2001).
33. van Benthem, R. A. T. . Novel hyperbranched resins for coating applications. *Prog. Org. Coatings* **40,** 203–214 (2000).
34. Chen, Yuying; Zhu, Yunji; Wang, Nan; Jin, Xin; Tong, G. Ultraviolet curable hyperbranched star polymer, its preparation method and application in ultraviolet curing coating preparation (Patent). (2017).
35. Haraldsson, T., Johansson, M. & Hult, A. The effects of abstractable hydrogen in radical photopolymerization of maleate/vinyl ether monomers studied with EPR and photo-RTIR. *J. Polym. Sci. Part A Polym. Chem.* **48,** 2810–2816 (2010).
36. Decker, C. & Decker, D. Photoinitiated radical polymerization of vinyl ether-maleate systems. *Polymer (Guildf).* **38,** 2229–2237 (1997).
37. Tokuoka, Y., Uchiyama, H., Abe, M. & Ogino, K. Solubilization of synthetic perfumes by nonionic surfactants. *J. Colloid Interface Sci.* **152,** 402–409 (1992).
38. Lacroix-Desmazes, P. & Guyot, A. Reactive Surfactants in Heterophase Polymerization. 2. Maleate Based Poly(ethylene oxide) Macromonomers as Steric Stabilizer Precursors in the Dispersion Polymerization of Styrene in Ethanol−Water Media. *Macromolecules* **29,** 4508–4515 (1996).
39. Goddard, A. R. *et al.* Controlled polymerisation and purification of branched poly(lactic acid) surfactants in supercritical carbon dioxide. *Green Chem.* **18,** 4772–4786 (2016).
40. Goddard, A. R. Sustainable Synthesis of Renewable Surfactants. *Thesis* (2016).
41. Ullah, F., Khan, A., Akil, H. M. & Siddiq, M. Effect of Hydrophilic/Hydrophobic Block Ratio and Temperature on the Surface and Associative Properties of Oxyethylene and Oxybutylene Diblock Copolymers in Aqueous Media. *J. Dispers. Sci. Technol.* **36,** 1777–1785 (2015).
42. Christov, N. C., Danov, K. D., Kralchevsky, P. A., Ananthapadmanabhan, K. P. & Lips, A. Maximum bubble pressure method: Universal surface age and transport mechanisms in surfactant solutions. *Langmuir* **22,** 7528–7542 (2006).
43. Benedetto, F. E., Zolotucho, H. & Prado, M. O. Critical Assessment of the Surface Tension determined by the Maximum Pressure Bubble Method. *Mater. Res.* **18,** 9–14 (2015).
44. Solutions, S. P. Bubble pressure method for measuring the dynamic surface tension. Available at: https://www.sita-process.com/information-service/process-parameter-surface-tension/overview/. (Accessed: 28th September 2018)
45. Sarkic, A. & Stappen, I. Essential Oils and Their Single Compounds in Cosmetics—A Critical Review. *Cosmetics* **5,** 11 (2018).
46. Abe, M., Kubota, T., Uchiyama, H. & Ogino, K. Solubilization of oleyl alcohol by pure

and mixtures of surfactants. *Colloid Polym. Sci.* **267,** 365–370 (1989).
47. Nam, Y. S., Kim, J. W., Shim, J., Hoon Han, S. & Kon Kim, H. Silicone oil emulsions stabilized by semi-solid nanostructures entrapped at the interface. *J. Colloid Interface Sci.* **351,** 102–107 (2010).
48. Paatero, E. *et al.* Kinetic model for main and side reactions in the polyesterification of dicarboxylic acids with diols. *Chem. Eng. Sci.* **49,** 3601–3616 (1994).
49. Kharas, G. B. *et al.* Synthesis and characterization of fumarate-based polyesters for use in bioresorbable bone cement composites. *J. Appl. Polym. Sci.* **66,** 1123–1137 (1997).
50. Crivello, J. V. & McGrath, T. M. Photoinitiated alternating copolymerization of dialkyl maleates and fumarates with vinyl ethers. *J. Polym. Sci. Part A Polym. Chem.* **48,** 4726–4736 (2010).
51. Bilati, U., Allémann, E. & Doelker, E. Development of a nanoprecipitation method intended for the entrapment of hydrophilic drugs into nanoparticles. *Eur. J. Pharm. Sci.* **24,** 67–75 (2005).
52. Morel, F., Decker, C., Jönsson, S., Clark, S. C. & Hoyle, C. E. Kinetic study of the photo-induced copolymerization of N-substituted maleimides with electron donor monomers. *Polymer (Guildf).* **40,** 2447–2454 (1999).
53. Li, Y. & Kissel, T. Synthesis, characteristics and in vitro degradation of star-block copolymers consisting of L-lactide, glycolide and branched multi-arm poly(ethylene oxide). *Polymer (Guildf).* **39,** 4421–4427 (1998).
54. Tasaka, F., Miyazaki, H., Ohya, Y. & Ouchi, T. Synthesis of comb-type biodegradable polylactide through depsipeptide-lactide copolymer containing serine residues. *Macromolecules* **32,** 6386–6389 (1999).
55. Turunen, M. P. K., Korhonen, H., Tuominen, J. & Seppälä, J. V. Synthesis, characterization and crosslinking of functional star-shaped poly(ε -caprolactone). *Polym. Int.* **51,** 92–100 (2002).
56. Mi, H.-Y. *et al.* In situ synthesis of polyurethane scaffolds with tunable properties by controlled crosslinking of tri-block copolymer and polycaprolactone triol for tissue regeneration. *Chem. Eng. J.* **348,** 786–798 (2018).
57. Wang, S., Yaszemski, M. J., Gruetzmacher, J. A. & Lu, L. Photo-crosslinked poly(ε-caprolactone fumarate) networks: Roles of crystallinity and crosslinking density in determining mechanical properties. *Polymer (Guildf).* **49,** 5692–5699 (2008).
58. Kweon, H. Y. *et al.* A novel degradable polycaprolactone networks for tissue engineering. *Biomaterials* **24,** 801–808 (2003).

# Chapter 7
# Conclusions and Future Work

Through this Thesis, a sustainable approach and precise characterisation of well-defined, controlled star-shaped PCL synthesised using both metal catalyst and biocatalyst in the bulk and in $scCO_2$ is presented. These PCL-based architectures were used as macroinitiators for the AROP of the ethyl phosphonate (EP) monomer to form amphiphilic copolymers. Together with their aggregation behaviour in water, the potential of the copolymers as surfactants and as a coating material was discussed.
The main conclusions, as well as some prospects of future research for the continuation of this work, are given below.

## 7.1 Conclusions

The development of a novel clean approach towards synthesis and precise characterisation of star PCL polymers based on renewable building blocks; sugars (i.e. *D*-sorbitol, triglycerol, glycerol, 1-6-hexanediol) and biobased ε-CL (**Chapter 4**) is presented.
A clean route and green catalyst for synthesis of well-defined star *D*-sorbitol-PCL polymers have been exploited for the first time using FDA approved $Sn(Oct)_2$ or by using an enzyme (commercial immobilised lipase Novozym 435) in supercritical $CO_2$ (Figure 7.1). Initially, reactions using $Sn(Oct)_2$ catalyst were carried out at a rather low temperature (T = 95°C) without organic solvents (bulk) but this needed a long reaction time (~150 h) to reach a MW of 6000 g $mol^{-1}$. Such long reactions are economically non-viable, and it is for this reason industry normally uses high temperatures (~180 °C) to overcome the high melting point of building blocks and to overcome high viscosity during polymerisation. A higher temperature (T = 140 °C) solvent-free approach reduced the reaction time to 11 h for the preparation of *D*-sorbitol-PCL (MW ~6000 g $mol^{-1}$) and indeed well-defined star *D*-sorbitol-PCL with low dispersity ($Đ$ = 1.03 by SEC-MALS) were obtained. In terms of sustainability, such energy consumption at elevated temperature is not favourable on an industrial scale: colouration due to side-product formation from dehydration of sorbitol could arise. The use of $scCO_2$ (P = 240 bar) not only significantly reduced the reaction temperature (95 °C in $scCO_2$ vs. 140 °C in bulk) but also the reaction time (~56 h in $scCO_2$ vs. 150 h in bulk, at T = 95 °C). In high-pressure $CO_2$ affords an added value for completely removing any residual ε-CL

and reducing the amount of metal catalyst from the product thus highlighting the possibility of the one-pot energy-saving route. A well-defined controlled 5-arms star PCL was thus yielded using $Sn(Oct)_2$ catalyst (Figure 7.1, left).

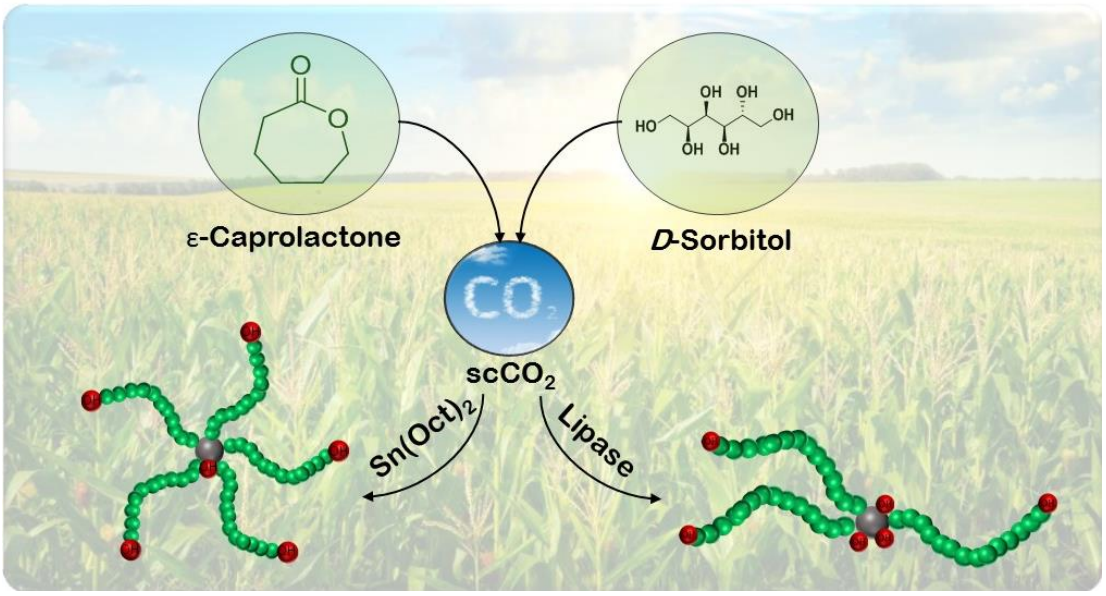



Figure 7.1. The eco-friendly route for the green synthesis of biobased star *D*-sorbitol-poly(ε-caprolactone) using $Sn(Oct)_2$ or enzymes as catalysts.

The results are supported by a range of characterisation techniques. MALDI-TOF analyses showed no side-reactions for $Sn(Oct)_2$ catalysed samples both by bulk polymerisation in anhydrous conditions and in $scCO_2$. Furthermore, the characterisation of the arms was achieved through meticulous investigation by SEC-MALS/$^1$H NMR, which corroborated strongly with our phosphitylation approach for distinguishing primary vs. secondary hydroxy groups in addition to the quantification of the average number of arms ($N_{arms}$ ($^{31}$P)), length of arms (average MW of arms) and MW of star polymers. Supplementary analysis for estimation of average $N_{arms}$ (SEC-UC) by SEC-Universal Calibration approach was also presented.

A novel enzymatic catalysis approach was described by using lower temperature $scCO_2$-assisted processes (T = 60 °C, P = 217 bar) for the preparation of biobased star-type *D*-sorbitol-PCL (MW ~6000-10000 g mol$^{-1}$, $Đ$ = 1.23-1.24). These resulted in unique miktoarm 3-arms star PCL polymers that possess on average three hydroxy functional groups on arms and three remaining hydroxy on the sorbitol core. The formation of three arms was obtained due to the specific selectivity of the enzyme for primary rather than for secondary hydroxy groups. It is noteworthy that the use of $CO_2$ was essential to enable the reaction at milder conditions because the enzymatic bulk

polymerisation (at T = 60 °C) of such samples requires a homogenising step at a higher temperature (95 °C). In addition, despite the mixing step, the bulk polymerisation at 60 °C resulted in incomplete monomer conversions (% Conv. = 87% in bulk vs. 97% in $scCO_2$). The detailed analysis and careful characterisation of these new mikto-arm PCL star structures showed that only a small amount of by-products was formed (free water initiated PCL chains and macro cycles of PCL) during the enzyme-catalysed reaction.

This fully green approach (organic solvent free, low-temperature route in $scCO_2$) for the synthesis of well-defined star architecture PCL from a biobased initiator has been our starting point for the design of surface-active branched materials, as explored in the subsequent Chapters.

Cyclic hydrophilic ethyl phosphonate (EP) monomer offers great potential as a novel, water-soluble, biodegradable and biocompatible monomer in the surfactant design **(Chapter 5).** The unique properties of $scCO_2$ to replace the VOCs for synthesis and purification to demonstrate a more sustainable route for organocatalysed AROP of poly(ethyl phosphonate)s (PEP)s was adopted. To the best of the author's knowledge, polymerisation of hydrophilic ethyl phosphonate monomer in $scCO_2$ and extraction of EP for purification of the polymer have never been reported in the literature. A linear Bz-$PEP_{7.5}$OH of low MW ($M_n$ $^{NMR}$ of 1100 g $mol^{-1}$ and $M_n$ $^{SEC}$of 800 g $mol^{-1}$) for $M_n^{targ}$ of 2720 g $mol^{-1}$ in $scCO_2$ was synthesised. Good correlation between the NMR, SEC and ESI-HR-MS analyses was observed.

Complete removal of the ethyl phosphonate monomer was achieved in just 25 min in the final product using $scCO_2$ extraction (T = 38 ± 2 °C, P = 140 ± 5 bar) and the extracted EP monomer appeared to not undergo hydrolysis under these $scCO_2$ conditions. If the synthesis and purification could be performed in one pot with the further opportunity of recycling the unused monomer, this would open up avenues of sustainable 'energy-saving pathways' to minimise or completely avoid the use of conventional organic solvents for designing new synthetic routes for green materials (Figure 7.2).

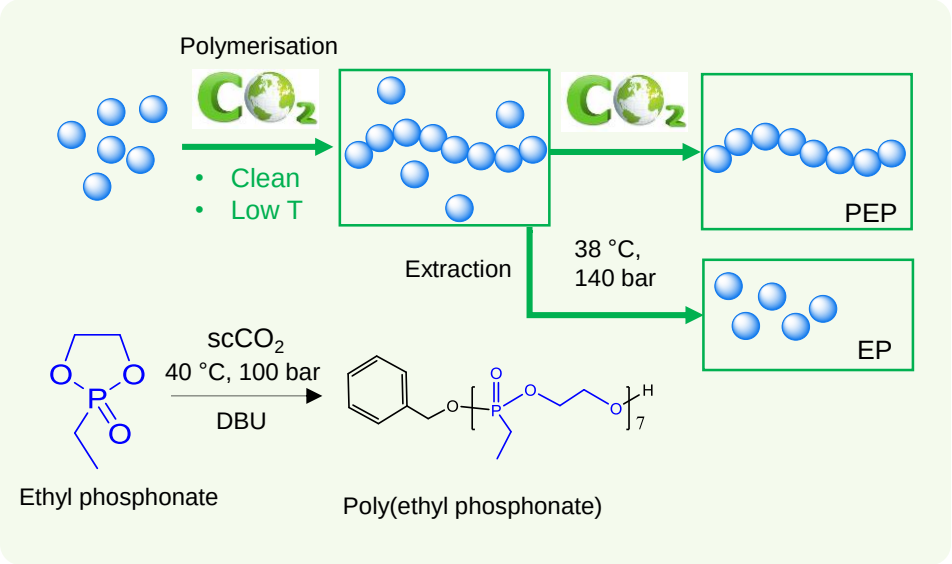



Figure 7.2. Synthesis and purification of poly(ethyl phosphonate) using novel green supercritical $CO_2$ approach.

A library of amphiphilic poly(ε-caprolactone)-*block*-poly(ethyl phosphonate) block copolymers was then created. These copolymers of various architectures (linear diblock, linear triblock, and star diblock copolymers) and molecular weights were successfully synthesised by a clean solvent-free approach in the bulk (at T = 60 °C) (Figure 7.3). The AROP of ethyl phosphonate was carried out in the presence of the PCL macro-initiators previously described (refer to Chapter 4) and using eco-friendly organocatalyst, DBU. Polymerisations were fast in the bulk process and proceeded in a controlled manner (analysed by SEC and NMR). Structural analysis for the number of arms of star copolymers was assessed by $^{31}P$ NMR phosphitylation and suggested the formation of the 6-arm star PCL-*b*-PEP copolymer (Figure 7.3, right and Figure 7.4, (A)). Structural analysis of linear $PEP_{7.2}$-$PCL_9$-$PEP_{7.2}$ triblock copolymer (Figure 7.3, bottom left) by MALDI-TOF confirmed the formation of a monomodal Gaussian distribution and no residual telechelic dihydroxy HO-PCL-OH was detected. SEC coupled with double-angle light scattering (SEC-MALS) determined the absolute molecular weight of the linear diblock copolymer (Figure 7.3, top left) and its homopolymer. Additionally, these MW values were close to those observed by NMR.

.

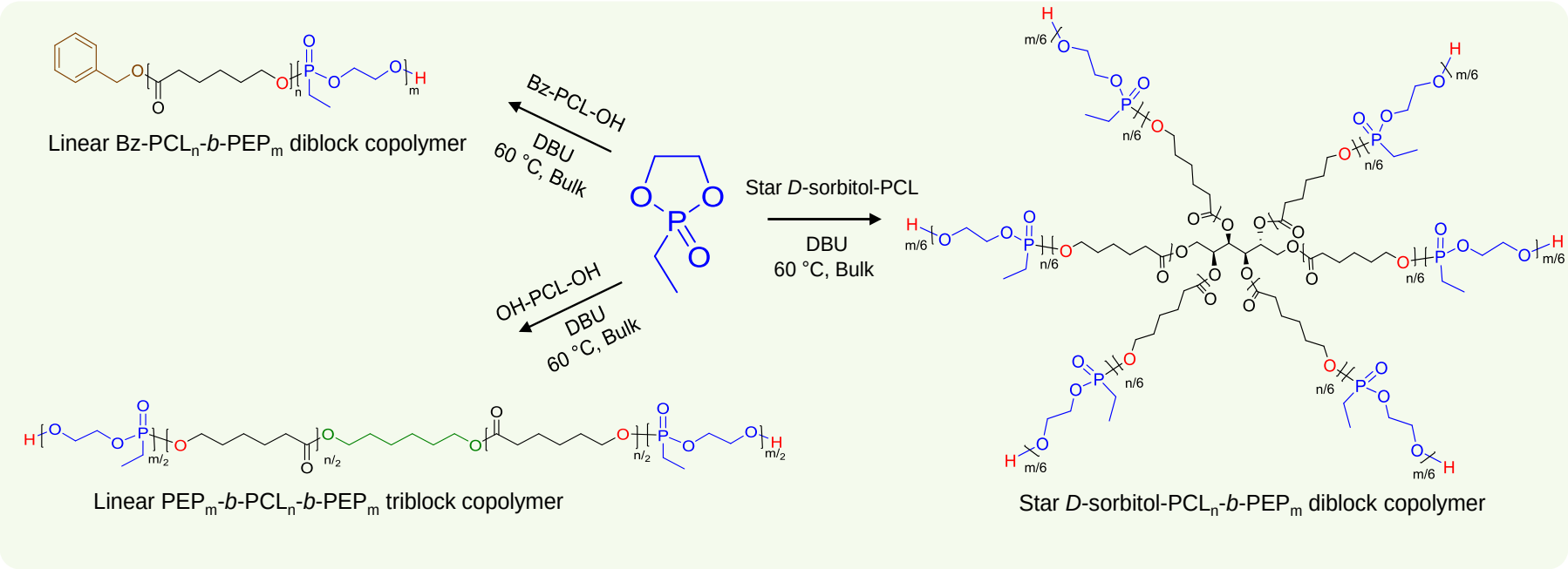



Figure 7.3. Schematic representation of the amphiphilic block copolymer of various architecture (linear Bz-PCL$_n$-OH diblock, linear PEP$_{m/2}$-PCL$_n$-PEP$_{m/2}$ triblock and star *D*-sorbitol-PCL$_n$-*b*-PEP$_m$OH$_6$ diblock copolymers) prepared in this Thesis.

The ability to purify these copolymers by using clean and low-energy supercritical $CO_2$ extraction technology was demonstrated. A complete removal of the residual EP was achieved from the samples in ~25 min (at low temperature (T=38 °C) and pressure (P= 140 bar to 180 bar). Clear advantages in the yield of polymers were obtained using extraction by $scCO_2$ compared to traditional methods (gravimetric yield = ~92% using $scCO_2$ vs. ~60-65% using solvent-precipitation or dialysis methods). This confirms the versatility of $CO_2$-assisted processes and highlights once again a cost-saving 'green process' that eliminates the need of energy-intensive multi-step purification methods, toxic VOCs and energy consuming vacuum drying steps.

Furthermore, the self-assembly behaviour of these materials was accessed through light scattering and electron microscopy methodology and comparisons were made between various structures and compositions which suggests the formation of micelles for the triblock copolymers and star unimers for star diblock copolymers in water. For the star *D*-sorbitol[$PCL_{57}$-*b*-$PEP_{36}OH_6$] having a theoretical average size *D*-value of 7 nm (considering PCL as condensed core surrounded by a fully extended PEP corona), $D_{TEM}$ of 14.3 nm was in good correlation with the size of DLS by number-weighted distribution i.e. $D_{H,\ DLS\ (NWD)}$ of 13.6 nm (Figure 7.4, (C)). In the DLS intensity-weighted distribution, the size of smaller population $D_{H,\ DLS\ (IWD)}$ of 18 nm correlated well with the mean diameter, $D_{cryo\text{-}TEM}$ of 17.7 nm.

The usefulness of the prepared star and triblock copolymers composed of PCL and PEP were studied by surface tension method (Chapter 6) which confirmed that all samples were surface active (Figure 7.4, (B)). The potential use of these star surfactants as emulsifiers or solubilising agents of fragrances was tested and suggest a potential use of these materials in personal care products.

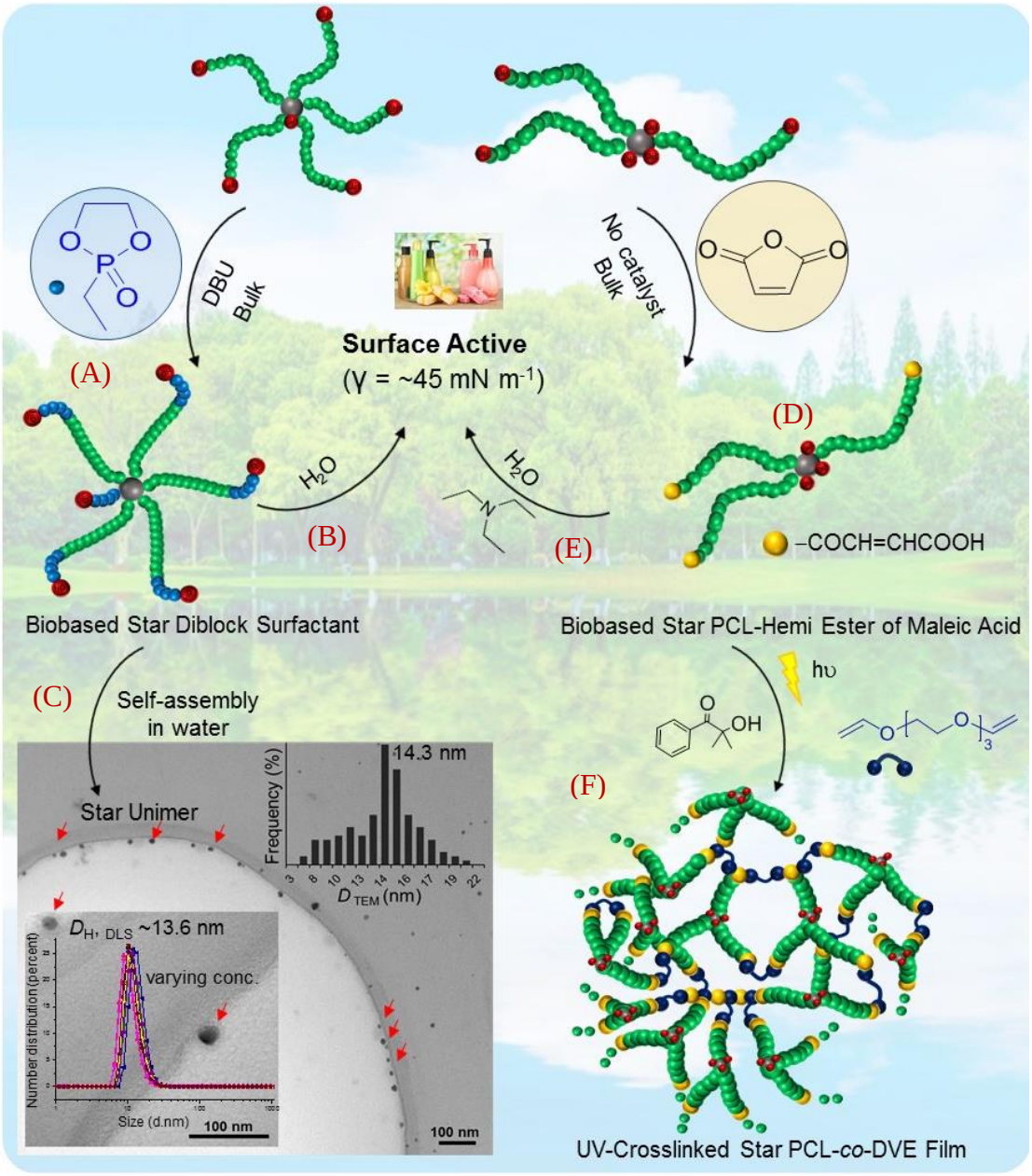



Figure 7.4. Clean synthesis of 6 arm amphiphilic star PCL-*b*-PEP diblock copolymer (A) which are surface active (B) and forms star unimer in water (C), preparation of biobased star PCL terminated by hemi ester of maleic acid (D), which reduces surface tension when carboxy group are neutralised in water (E). Alternatively, the unsaturated maleic terminal groups were photopolymerised with a small amount of DVE (~9 wt%) that gave UV-cured network of star PCL-*co*-DVE on a glass substrate (F).

In particular, linear $PEP_{7.2}$-$PCL_9$-$PEP_{7.2}$ triblock copolymer showed very good surface activity ($\gamma$ = 31 mN $m^{-1}$), comparing well with some commercial triblock surfactants (for example Pluronic L35 and L64 surfactants) in reducing the surface tension of water.

Respecting the green chemistry principles, biobased star-shaped PCL (MW = ~3000 g mol$^{-1}$ and ~6000 g mol$^{-1}$, $N_{arms}$ = ~3) prepared by enzymatic Novozym 435 catalysis were functionalised with the lignocellulosic biomass precursor, maleic anhydride,[1] to give a ionogenic carboxylic acid terminal group ((Figure 7.4, (D)). These PCL-$OH_x$ functionalised with hemi ester of maleic acid (star *D*-sorbitol[(PCL)-MA-$COOH_3$]$OH_3$) were then neutralised with triethylamine in water. The resulting star PCL carboxylate ammonium salts were water dispersible and showed surface activity (Figure 7.4, (E)).

The use of this biobased star type PCL structure offers a green and economically viable alternative highlighting the great potential to design environmentally promising alternative novel materials with unique properties. The potentialities of these unsaturated groups on PCL chain-ends derived from anhydride molecule maleic anhydride as an acceptor and tri(ethylene glycol) divinyl ether (DVE) as a donor by using photopolymerisation methodology (Figure 7.4, (F)) was explored. Films of star PCL-*co*-DVE were fabricated on glass substrate during UV-curing. Such films showed qualitatively good adhesive properties on the glass. Kinetics of photopolymerisation together with thermal (DSC) and degradation behaviour (TGA) of these samples have shown promising results for future utilisation of these biobased crosslinked films.

## 7.2 Future Work

The investigation of star PCL preparation by using the popular commercial Novozym 435 as a biocatalyst has shown great potential for creating these novel star type PCL with low side-products and narrow dispersity. This was made using a complete green pathway; nonetheless, there are still a number of areas where there is room for improvements that have not been fully addressed here, nor in the available literature. A lower number of arms by the enzyme catalysed star-PCL polymer did not offer the same thermal properties as $Sn(Oct)_2$ catalyst star does (shown by DSC investigation in Chapter 4).

The investigation could be done to improve the degree of branching: (1) Other lipases (porcine pancreatic lipase, (PPL) or *Pseudomonas fluorescens* (PF), *Pseudomonas species* lipase (PS) are commercial and have been utilised for polyesterification and are less selective catalysts than Novozym 435. Or some non-commercial enzymes, such as Lactonases, could be exploited. Nevertheless, their compatibility with $scCO_2$ would need to be assessed. The use of CALA, which is commercially immobilised and considered less selective catalyst with a high enzyme loading, could be considered. (2) Use of a polyol with more number of primary hydroxy group (for example, dipentaerythritol) preferably a biobased alternative could be considered.

Poly(phosphonates) represent a new class of polymers emerging with a bright future in drug delivery. Literature studies have already proven their water solubility, biocompatibility, tuneable biodegradability, although, the literature lacks the use of biocatalyst for polymerisation which would be a significant step forward in this field. Some very specific non-commercial enzymes which are thought to cleave P-O bond *in vivo* such as EcoRV and Myosin (hydrolase enzyme)[2] and phosphatase (EC 3.1.8.1) or Lactonases could be exploited to test their substrate compatibility with phosphonate.

The low-temperature $CO_2$-assisted extraction of ethyl phosphonate monomer during purification of polymers and copolymers showed no hydrolytic degradation of EP by $CO_2$. Reuse of this extracted monomer could open up an exciting cost-effective process that follows atom economy. Moreover, the polymerisation of phosphonate in $scCO_2$ has been exploited but only on a small scale, further studies need to be done to optimise the process and test its large-scale viability.

Amphiphilic copolymers of various architectures (diblock, triblock and star diblock) have been described in Chapter 5. These displayed interesting self-assembly and surface-active properties, however, a detailed investigation should be carried out to test their drug loading/release properties. Furthermore, their biocompatibility must be assessed to consider their real applicability for medical applications or as a surfactant.

Production capacity of biomaterials (including biopolymers), is projected to hit 1.7 million metric tons in 2020 in Europe,[3] and due to its high demand and consumption the PCL market alone is forecast to generate revenue worth of about USD 670,000 million by 2026.[4] Another reason behind the adoption of PCL as a raw material is because it offers exceptional properties (such as hydrophobic characteristics, wear and chemical resistance, UV-resistance, resistance to oil & grease, glossy, adhesion and low-temperature flexibility).[4]

Preliminary studies have been carried out to create star PCL films from photocrosslinkable biobased star polymers that were prepared by Novozym 435 catalyst; however, one small improvement that can be done in the formulations step is the removal or reduction of the amount of acetone used for film formulation (~50% by wt of acetone). Although literature research on such PCL based formulation reports the use of harsh dioxane as a cosolvent,[5] the tuning of arms or targeted MW could help. For example, the lower MW star PCL (3000 g $mol^{-1}$ instead of 6000 g $mol^{-1}$) showed efficient solubility in the polar tri(ethylene glycol) divinyl ether.

Nonetheless, more comprehensive mechanical and application investigations need to be carried out to examine their real usefulness as coatings and cross-linked materials on large scale (e.g. adhesion, gel content, surface properties/contact angle, scratch and impact resistance *etc*.).

Such biobased star-type PCL material offers a possibility to fabricate biocompatible 3D structures.[5,6]

To summarise, this Thesis demonstrates excellent potential for future investigation of biobased star PCL and copolymers with phosphonates for a wide range of possible applications in coatings and as surfactants.

## 7.4 References

1. Isikgor, F. H. & Becer, C. R. Lignocellulosic biomass: a sustainable platform for the production of bio-based chemicals and polymers. *Polym. Chem.* **6,** 4497–4559 (2015).
2. Gade, Lutz H. & Hofmann, P. *Molecular Catalysts: Structure and Functional Design*. *Applied Organometallic Chemistry* **30,** (Wiley-VCH Verlag GmbH & Co. KGaA, 2014).
3. Alex Scott. Biobased chemical start-ups seek niche in Europe. *Chemical & Engineering News* 25–26 (2016).
4. Persistence Market Research. Global market Study On Polycaprolactone. 215 (2018). Available at: https://www.persistencemarketresearch.com/market-research/polycaprolactone-market.asp. (Accessed: 20th September 2018)
5. Green, B. J. *et al.* Effect of Molecular Weight and Functionality on Acrylated Poly(caprolactone) for Stereolithography and Biomedical Applications. *Biomacromolecules* (2018).
6. Yagci, Y., Jockusch, S. & Turro, N. J. Photoinitiated polymerization: Advances, challenges, and opportunities. *Macromolecules* **43,** 6245–6260 (2010).

# Appendix A (Related to Chapter 3)

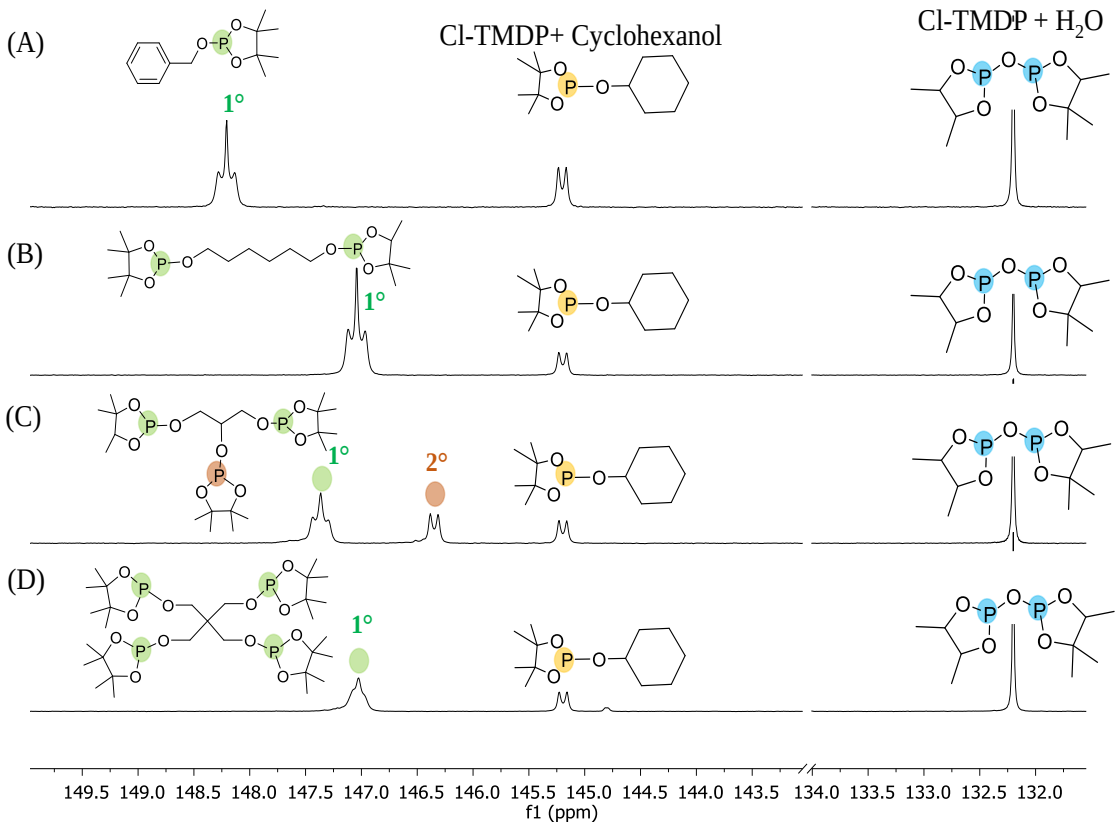



Figure A1. Coupled $^{31}P$ NMR spectra of alcohols derivatised by 2-chloro-4,4,5,5-tetramethyl-1,3,2-dioxaphospholane. (A) benzyl alcohol, (B) 1,6-hexanediol, (C) glycerol, and (D) pentaerythritol where the phospholane ester of the primary (1°) and secondary (2°) hydroxy groups show triplet (●) and doublet (●) resonances, respectively.

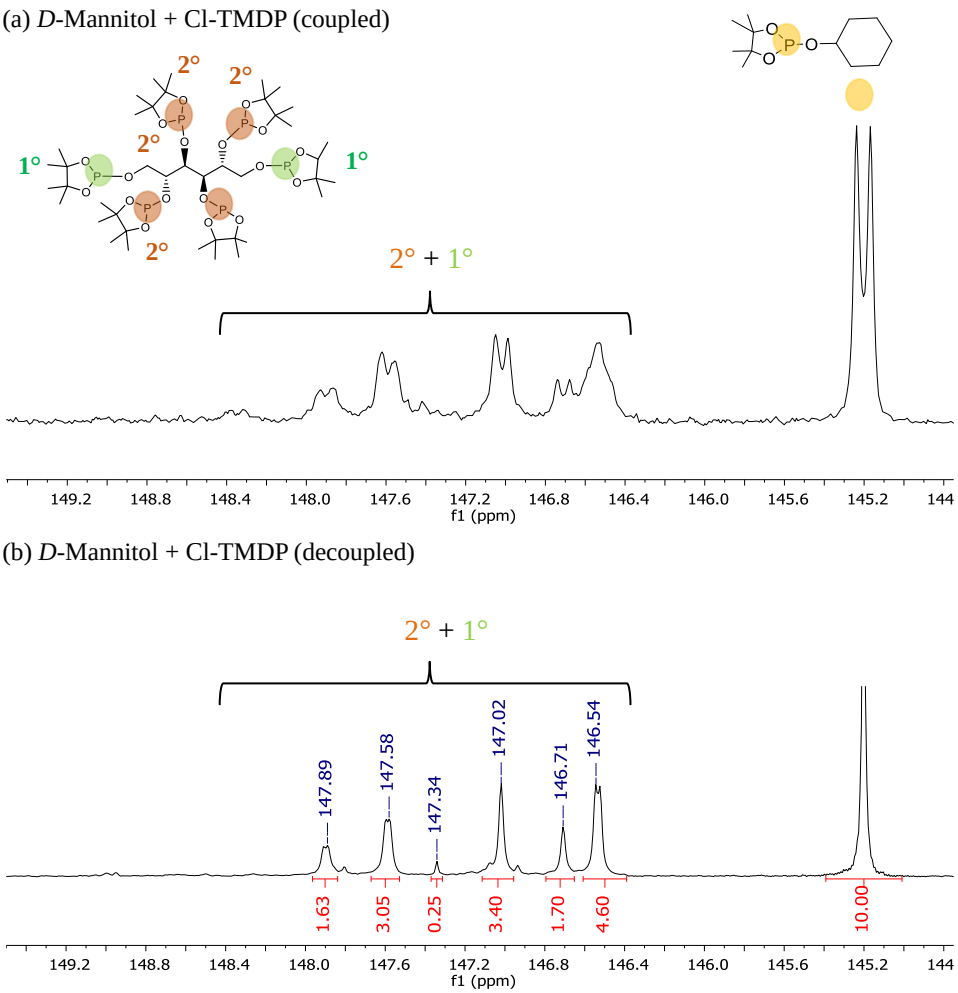



Figure A2. $^{31}$P NMR spectra of *D*-mannitol derivatised by 2-chloro-4,4,5,5-tetramethyl-1,3,2-dioxaphospholane. (a) $^{31}$P NMR spectrum without decoupling, where the phospholane ester of the primary (1°) and secondary (2°) hydroxy groups show triplet ( ) and doublet ( ) resonances, respectively. (b) The corresponding inverse gated decoupled $^{31}$P NMR spectrum used for quantification. IS: Internal standard (cyclohexanol, ).

# Appendix B (Related to Chapter 4)

Table B1. Analytical results from $^{31}$P NMR analysis of star *D*-sorbitol-PCL synthesised using Novozym 435 as the catalyst (Table 4 Entries 1-4).

| Sample (S) | Each Sample | $^{31}$P NMR spectrum | | | $^{31}$P NMR calculation | | $\int_{COOP}$ [f] | %COOH (linear chains) [g] | $N_{arms}$ ($^{31}$P) [h] | $M_n^{P\text{-}NMR}$ (star polymer) [i] |
|---|---|---|---|---|---|---|---|---|---|---|
| | $n_{IS}$ (μmol) | $m_s$ [a] (mg) | $\int_{IS}$ [b] | $\int_{PCL\text{-}OP}$ [c] | $n_{PCL\text{-}OP}$ [d] (μmol) | $M_n^{P\text{-}NMR}$ (arm) [e] ($g mol^{-1}$) | | | | ($g mol^{-1}$) |
| 1 | 10.6 | 25.7 | 100 | 121.2 | 12.8 | 2000 | 1.73 | 1.4 | 3.1 | 6200 |
| 2 | 10.7 | 25.5 | 100 | 73.68 | 7.88 | 3200 | 3.86 | 5.2 | 3.3 | 10600 |
| 3 | 10.8 | 26.3 | 100 | 81.39 | 8.79 | 3000 | 4.42 | 5.4 | 3.2 | 9600 |
| 4 | 10.4 | 26.0 | 100 | 86.39 | 8.98 | 2900 | 9.74 | 11.3 | 2.9 | 8400 |

[a] Mass of the sample ($m_s$) used for derivatisation with Cl-TMDP and subsequent NMR analysis. [b] Integral corresponding to the resonance of internal standard ($\delta$ = 147.04 ppm). [c] Integral of star sample relative to the IS. [d] Moles of hydroxy groups. [e] Number average molecular weight of arms. [f] Integrals corresponding to COOH in the sample. [g] Amount of linear PCL chains. [h] Average number of arms. [i] Molecular weight of star polymer.

**Equations for quantification by the $^{31}$P phosphitylation method**.

| | | |
|---|---|---|
| $M_n^{P\text{-}NMR}$ (arm) | $= [m_s / n_{PCL\text{-}OP}] \times 1000$ | Eq 4.6 |
| $M_n^{P\text{-}NMR}$ (star polymer) | $= M_n^{P\text{-}NMR}$ (arm) $\times N_{arms}^{31P}$ | Eq 4.7 |
| %COOH | $= (\int_{PCL\text{-}COOP} / \int_{PCL\text{-}OP}) \times 100$ | Eq 4.8 |
| $n_{PCL\text{-}OP}$ | $= (n_{IS} \times \int_{PCL\text{-}OP}) / \int_{IS}$ | Eq 4.9 |

$$N_{arms}(^{31}P) = \frac{\int_{PCL-OP} - \int_{PCL-COOP}}{\int_{(1°+2°)} + \int_{PCL-OP} - \int_{PCL-COOP}} \times 6 \qquad \text{Eq. 4.10}$$

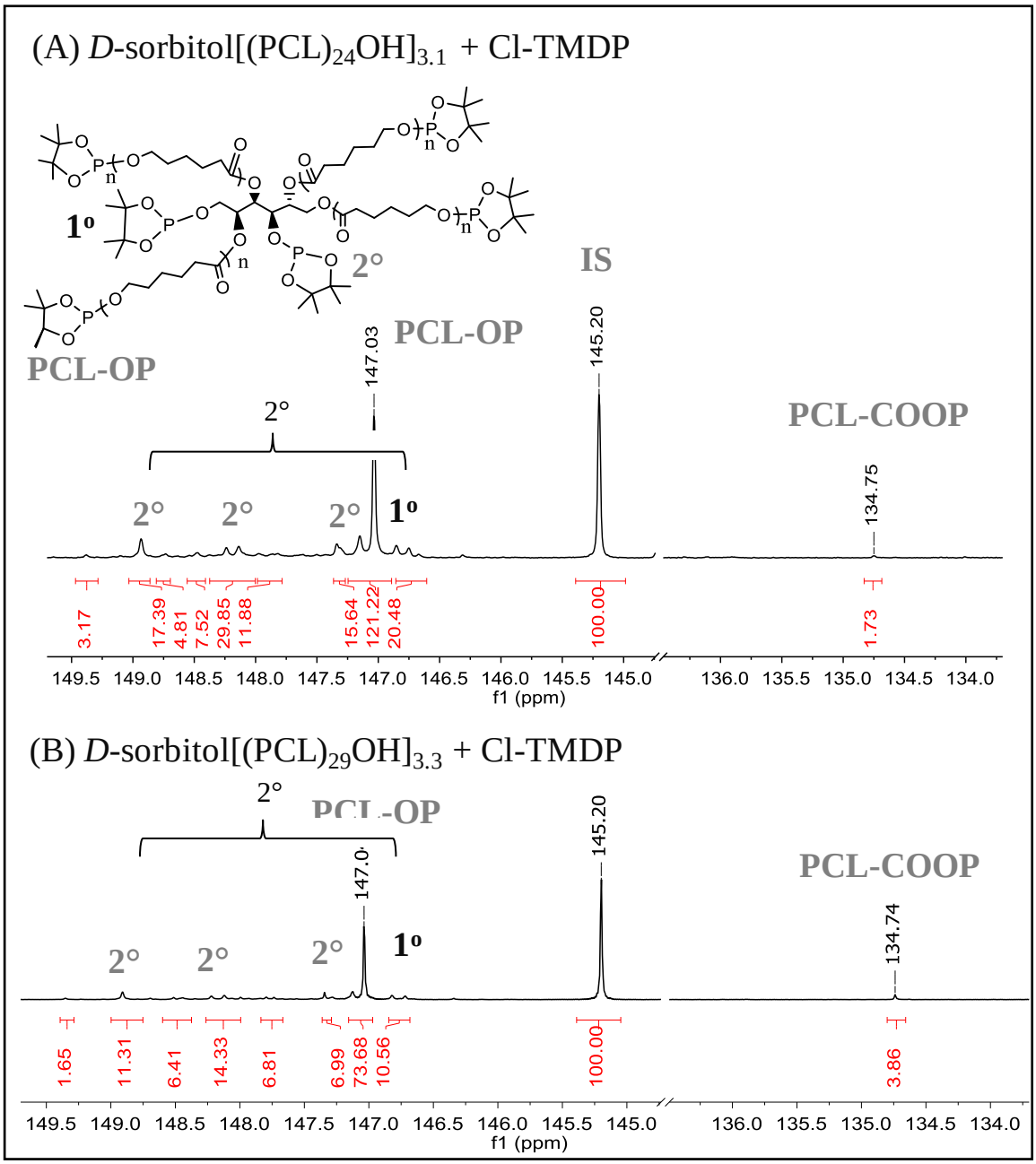



Figure B1. Inverse gated proton-decoupled $^{31}P$ NMR spectra after phosphitylation by Cl-TMDP. (A) star *D*-sorbitol[$(PCL)_{24}OH]_{3.1}$ synthesised in the bulk using Novozym 435 (3 wt%) as the catalyst (Table 4.5 Entry 1 and Table B1 Entry 1) and (B) star *D*-sorbitol[$(PCL)_{28}OH]_{3.3}$ synthesised in the bulk using Novozym 435 (10 wt%) as the catalyst (Table 4.5 Entry 2 and Table B1 Entry 2). IS: internal standard (cyclohexanol).

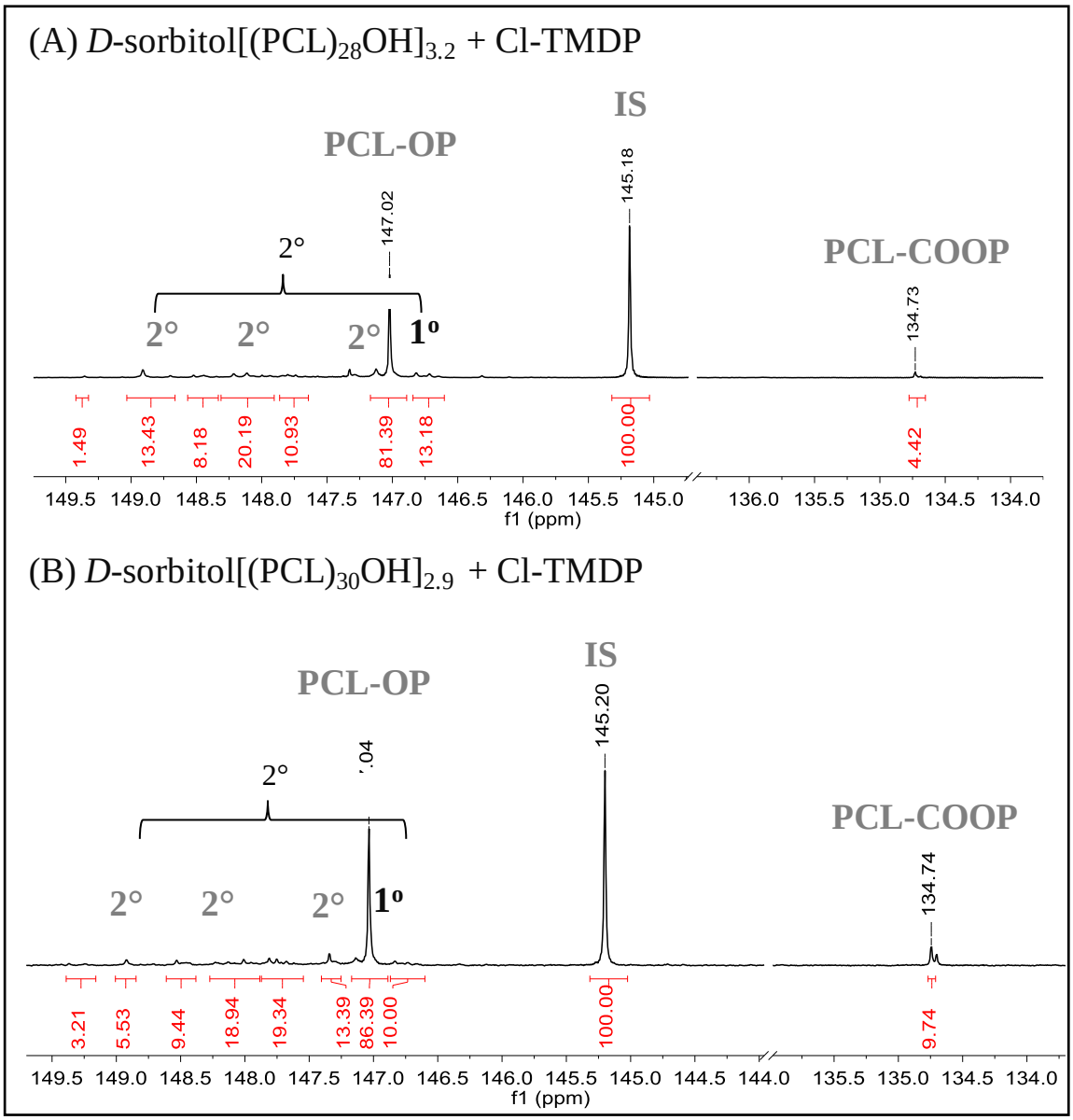



Figure B2. Inverse gated proton-decoupled $^{31}P$ NMR spectrum after phosphitylation by Cl-TMDP. (A) star *D*-sorbitol[$(PCL)_{28}OH]_{3.2}$ synthesised in $scCO_2$ using Novozym 435 (3 wt%) (Table 4.5 Entry 3 and Table B1 Entry 3) and (B) star *D*-sorbitol[$(PCL)_{30}OH]_{2.9}$ synthesised in $scCO_2$ using Novozym 435 (10 wt%). (Table 4.5 Entry 4 and Table B1 Entry 4). IS: internal standard (cyclohexanol).

**View-Cell Study of *D*-sorbitol with ε-CL using $scCO_2$**

The effect of $CO_2$ on *D*-sorbitol was visualised using a fixed volume view cell (100 mL). In a typical experiment, the amount of ε-CL and *D*-sorbitol (500: 15 mg respectively) (i.e. the feed ratio of monomer: initiator same as the polymerisation condition) was added into a glass vial and placed in the view cell. The windows were sealed and clamped to the body. The temperature and $CO_2$ pressure were raised incrementally as required (up to 60 or 95 °C and 250 bar). The autoclave was allowed to cool down to ambient temperature and vented at T< 20 °C, P = 50 bar (at ~3- 4 bar $min^{-1}$) (low flow rate).

**View-Cell Studies: Mixture of *D*-sorbitol and ε-CL in $scCO_2$ (95 °C)**

Solubility tests of individual components in $scCO_2$ were carried out in a high-pressure fixed volume view cell before investigating the phase behaviour of the entire reactive system (ε-CL+*D*-sorbitol) similar to experiments performed by Bratton *et al.*[1]. Stassin *et al.*[2] already reported that $scCO_2$ readily solubilises ε-CL at variable temperature and pressure for example at 35, 40, 50, 55 and 60 °C and at 90, 101, 132, 148 and 165 bar, respectively.

Considering all this, our view-cell study seeks to test whether $scCO_2$ has an effect on the solubility of *D*-sorbitol when it is combined with the $CO_2$ soluble monomer (ε-CL). The transition observed in the mixture of ε-CL and *D*-sorbitol at a constant concentration ([CL]:[*D*-Sorb] = 43.8 mM: 823 μM) was assessed by view-cell studies. The ε-CL is colourless liquid and *D*-sorbitol is a white solid at ambient temperature and pressure (Figure B3). Upon increasing the temperature and pressure, $scCO_2$ solubilised ε-CL as observed by a decrease in volume of the ε-CL phase. This mixture plasticises *D*-sorbitol, thus leading to a biphasic regime where the monomer is present in both the $scCO_2$ rich phase and the *D*-sorbitol rich liquid/semi-solid phase (Figure B3, b). In addition, some condensed droplets are noticeable above the *D*-sorbitol rich phase that may correspond to the mixture of liquefied *D*-sorbitol mixed with ε-CL.

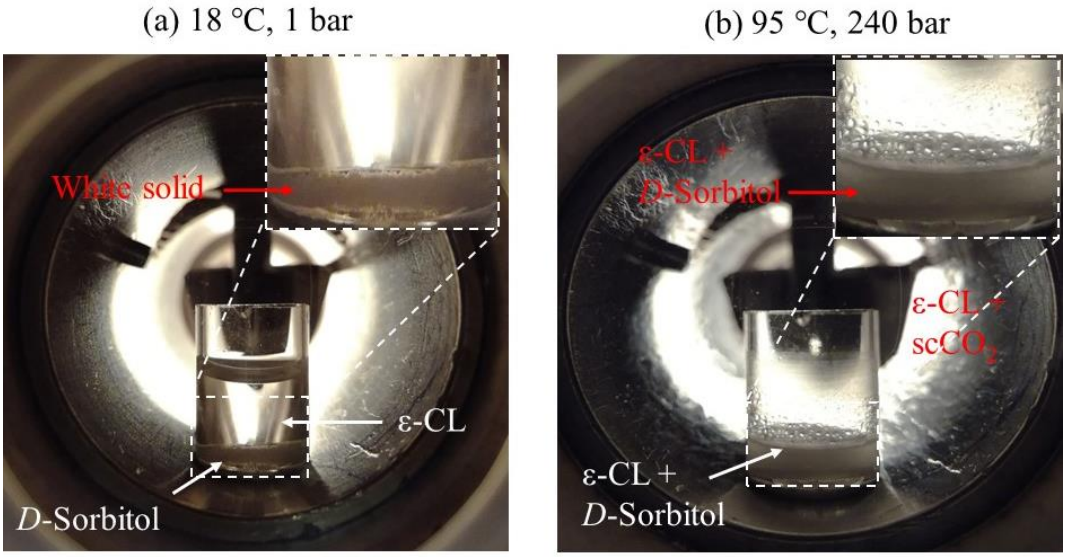



Figure B3. Phase equilibria for a mixture of ε-CL and *D*-sorbitol (33:1 ratio) in a high-pressure fixed volume view cell at increasing temperatures and pressure; (a) the ε-CL monomer is liquid while *D*-sorbitol is a white solid powder (at ambient conditions); (b) a biphasic regime is observed. A part of the monomer is solubilised by $scCO_2$ as the volume in the vial has decreased and the resulting mixture plasticises *D*-sorbitol thus giving a cloudy mixture (at 95 °C and 240 bar). The inset shows the enlarged region of the vial for clarity. Although the mechanical stirrer is visible, the content of the autoclave was not stirred during the experiments

**View-cell Studies: Mixture of *D*-sorbitol and ε-CL in $scCO_2$ (60 °C)**

View-cell studies on the mixture of *D*-sorbitol and ε-CL at 60 °C and 250 bar showed an opaque phase in the glass vials and on the sapphire windows (Figure B4, (c)) when compared to the initial state (Figure B4, (a)). Such opaqueness in *D*-sorbitol is also visible at a lower pressure (Figure B4, (b)). A clear swelling of ε-CL by $scCO_2$ is evidenced by the slight rise in volume above the marked area (a black mark on the right side of the vial in Figure B4, (a) and (b)). It becomes more clear from the change of the curvature of the interface in Figure B4, (b). Such opaqueness in the *D*-sorbitol might be attributed to some degree of swelling by a mixture of ε-CL and $CO_2$. Upon depressurisation some cloudiness remained on the *D*-sorbitol suggesting very little (but not zero) solubility of *D*-sorbitol in the $scCO_2$+ε-CL rich phase (Figure B4 (c)). Our starting hypothesis is that if indeed some degree of solubility/swelling of D-sorbitol occurs in $scCO_2$+ε-CL supercritical rich phase and it would be plasticised by the $scCO_2$: thus, a melt is formed which acts as a co-solvent for the remaining *D*-sorbitol.

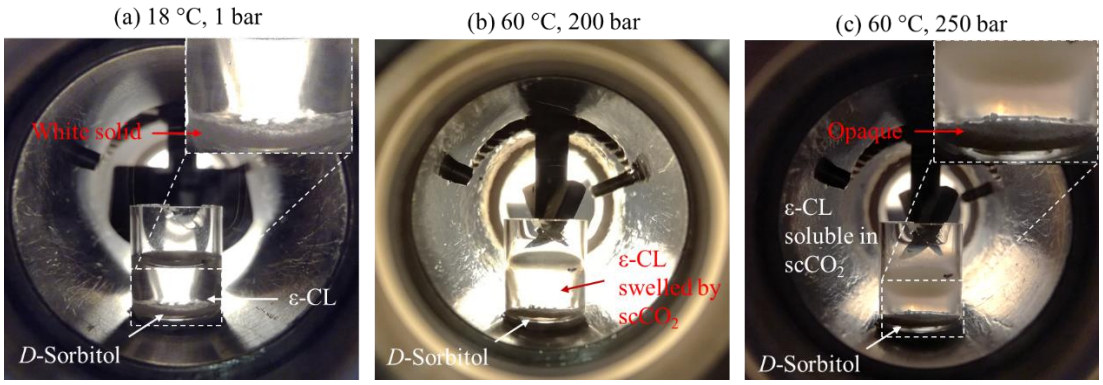



Figure B4. Visual inspection of a mixture of ε-CL and *D*-sorbitol (33:1 ratio) (a) under the ambient condition the ε-CL monomer is liquid while *D*-sorbitol is a white solid powder (b) $scCO_2$ (at 60 °C, 200 bar) swells the ε-CL monomer while *D*-sorbitol remains as solid. (c) Upon increasing pressure to 250 bar, the ε-CL monomer is fully miscible in the $scCO_2$ rich phase. Darkening of *D*-sorbitol and upon venting a quasi-foamed structure of *D*-sorbitol occurred. Although the mechanical stirrer is visible, the content of the autoclave was not stirred during the experiments.

# Appendix C (Related to Chapter 5)

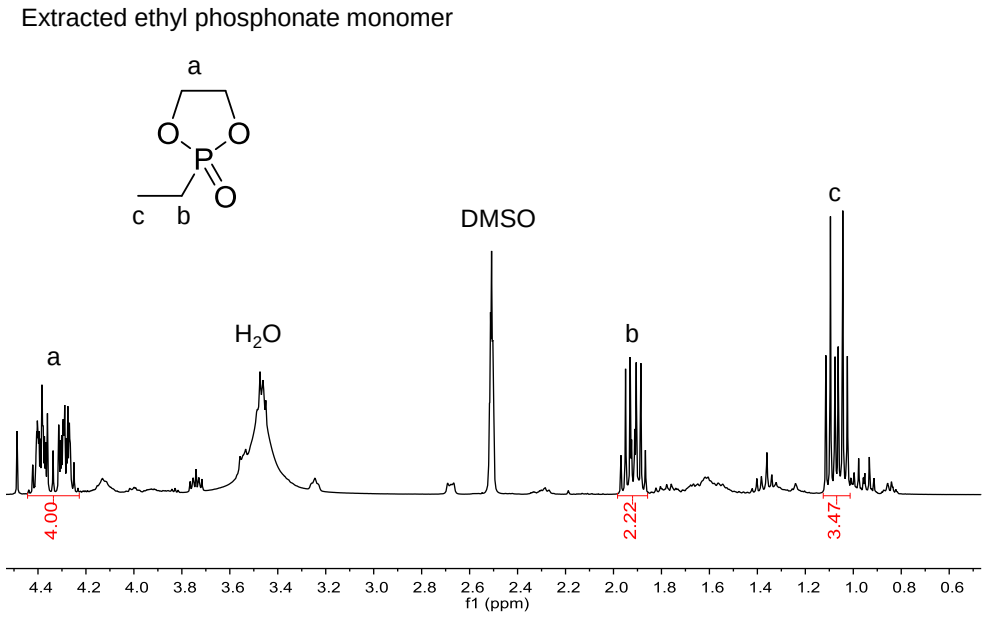



Figure C1. Representative $^{1}$H NMR spectra of the extracted ethyl phosphonate monomer during purification of shows no hydrolytic degradation a triblock $PEP_{3.6}$-*b*-$PCL_4$-*b*-$PEP_{3.6}$ copolymers.

**Extracting Sn(Oct)$_2$ and ε-CL Using ScCO$_2$: Purification Of Star *D*-Sorbitol-PCL**

A representative $^{1}$H-NMR spectrum of a star *D*-sorbitol-$PCL_nOH_x$ polymer of low MW is shown (Figure C2). It is known that the complete extraction of tin catalyst impurities from PCL by pure $CO_2$ is challenging because the tin species are thought to be coordinated by the chain-ends of the ester carbonyl groups.

Our aim was to completely remove the ε-CL from the low molecular weight (MW) star *D*-sorbitol-PCL samples and to reduce the amount of residual tin species as much as possible.

In our case, purification using a co-solvent (ethanol) was attempted but for low MW star *D*-sorbitol-$PCL_nOH_x$ compounds (~600 g mol$^{-1}$) also solubilised and removed oligomeric species resulting in reduced yields of star PCL and increasing MWs.

A representative $^{1}$H-NMR spectrum of low MW *D*-sorbitol-$PCL_nOH_x$ (~600 g mol$^{-1}$) containing 15 wt% of ε-CL in the crude sample (Figure C2 (a)) is shown below. A clear reduction in the resonances of both ε-CL and Sn(Oct)$_2$ (Figure C2 (b)) after extraction for only 15 min was observed. About 99.9% of the residual ε-CL (~15 wt%) was extracted using scCO$_2$ (40 °C, 150 bar) after 35 min (Figure C2 (c)) which is below the detection limits of this method.

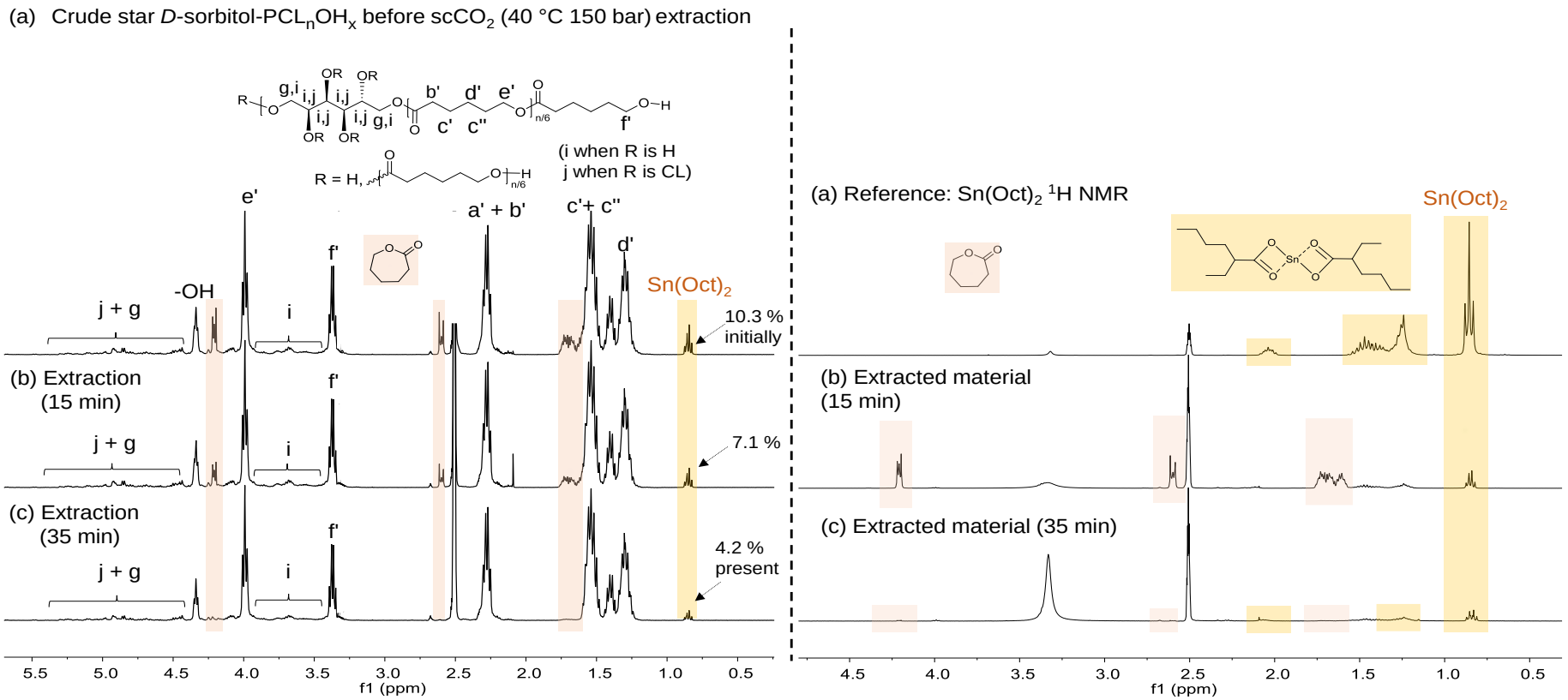



Figure C2. $^1$H-NMR spectra of star *D*-sorbitol-[PCL$_{3.8}$OH$_3$]OH$_3$ ($M_n^{NMR}$ of 600 g mol$^{-1}$) synthesised at 140 °C for 2 h (a) crude sample before, (b) after purification with scCO$_2$ for 15 min and (c) disappearance and reduction in peaks corresponding to ε-CL (pink bar) and Sn(Oct)$_2$ (orange bar), respectively after 35 min.

**Quantifying Number of Arms by Phosphitylation/$^{31}$P NMR**

According to our detailed nomenclature for the star *D*-sorbitol[$PCL_{n/X}OH]_X[OH]_{6-X}$ macroinitiator, we have:

$$X = 6 \times \text{PCL-OP} / (1° + 2° + \text{PCL-OP}) \qquad \text{Eq. C.1}$$

When applying Eq. 5.8 to the $^{31}$P NMR (Figure 5.22 (a)), it gives: x = 5.44 which corresponds to *D*-sorbitol[$PCL_{n/5.44}OH]_{5.44}[OH]_{0.56}$ by detailed notation or to star *D*-sorbitol[$PCL_{n/5}OH]_5OH_{0.56}$ by simple notation.

When applying these equations to $^{31}$ P NMR Figure C3 below:

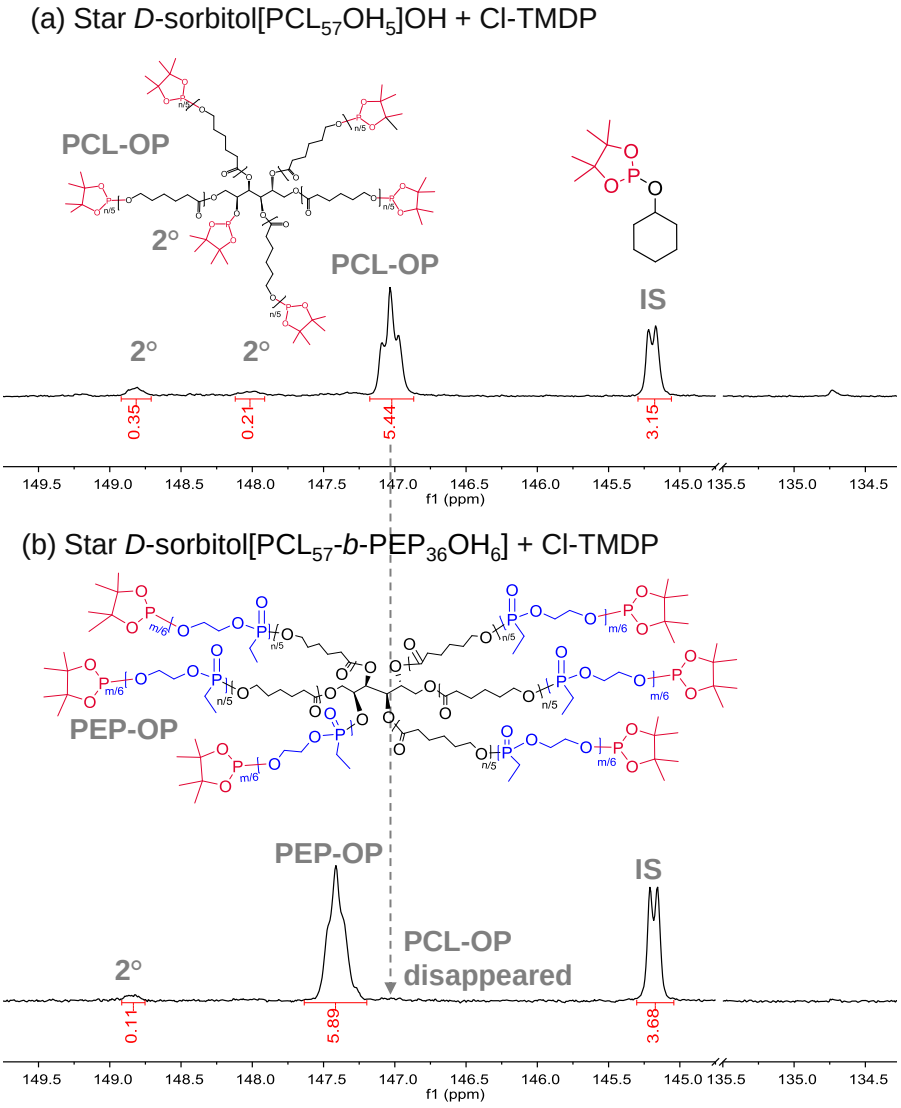



Figure C3. $^{31}$P NMR spectra without decoupling of phosphitylated (a) star *D*-sorbitol[$PCL_{57}OH_5$]OH showing residual secondary hydroxy groups on the *D*-sorbitol core and (b) star *D*-sorbitol[$PCL_{57}$-*b*-$PEP_{36}OH_6$] diblock copolymers showing barely any signal from secondary hydroxy groups on *D*-sorbitol and full disappearance of signals originating from the PCL-OH. IS: internal standard (cyclohexanol). The integrals are normalised.

It gives, X = 5.44, thus it corresponds to *D*-sorbitol[$PCL_{n/5.44}OH]_{5.44}[OH]_{0.56}$.

According to the nomenclature *D*-sorbitol[$PCL_{n/(x+x')}]_{x'}$[$PCL_{n/(x+x')}$-*b*-$PEP_{m/(x+y)}]_x[PEP_{m/(x+y)}]_y[OH]_{6-x-x'-y}$, we have:

| | |
|---|---|
| $x' = 6 \times$ PCL-OP/(1°+2°+PCL-OP+PEP-OP) | Eq. C.2 |
| $z = 6 \times (1°+2°)/(1°+2°+PCL\text{-}OP+PEP\text{-}OP)$ | Eq. C.3 |
| $x = X - x'$ | Eq. C.4 |
| $y = 6 \times PEP\text{-}OP/(1°+2°+PCL\text{-}OP+PEP\text{-}OP) - x$ | Eq. C.5 |

On applying these equations to $^{31}$P NMR (Figure C3, (b)), it gives:

$x' = 0$; $z=0.11$; $x= 5.44 - 0 = 5.44$; $y=5.89 - 5.44 = 0.45$

Thus, it corresponds to *D*-sorbitol[$PCL_{n/(5.44)}$-*b*-$PEP_{m/(5.89)}]_{5.44}[PEP_{m/(5.89)}]_{0.45}[OH]_{0.11}$.

In addition, since n/X=11.75 (according to $^1$H NMR of Figure C4, (a)),

It leads to $n=11.75\times5.44=63.9$, corresponding to *D*-sorbitol[$PCL_{63.9/5.44}OH]_{5.44}[OH]_{0.56}$.

And since m/n=((f+g+h)/4)/(d/4)=(30.74+5.41+4)/51.84)= about 0.7745 (according to $^1$H NMR of Figure C4, (b)),it leads to $m=63.9\times0.6973=49.49$

Finally, the complete nomenclature of the star polymer is *D*-sorbitol[$PCL_{63.9/(5.44)}$-*b*-$PEP_{44.5/(5.89)}]_{5.44}[PEP_{44.5/(5.89)}]_{0.45}[OH]_{0.11}$.

Practically, *D*-sorbitol[$PCL_{63.9/(5.44)}$-*b*-$PEP_{44.5/(5.89)}]_{5.44}[PEP_{44.5/(5.89)}]_{0.45}[OH]_{0.11}$ can be represented as star *D*-sorbitol[$PCL_{63.9}$-*b*-$PEP_{44.5}OH_6$].

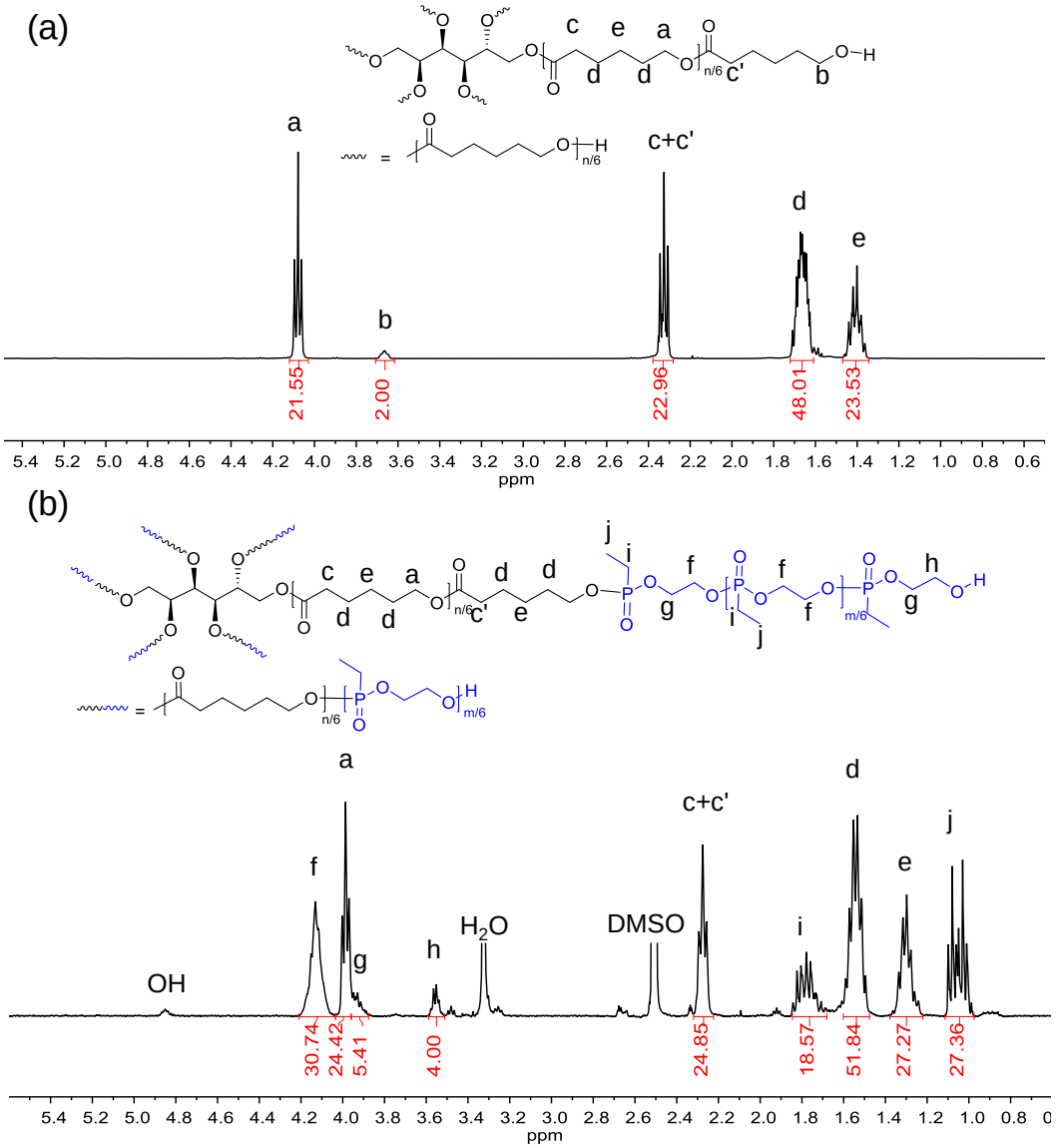



Figure C4. $^{1}$H NMR spectra of (a) star *D*-sorbitol-[$PCL_{57}OH_5$]OH macroinitiator (in $CDCl_3$) synthesised in the bulk using $Sn(Oct)_2$ and (b) the star *D*-sorbitol[$PCL_{57}$-*b*-$PEP_{36}OH_6$] diblock copolymer (in DMSO-$d_6$) synthesised in the bulk at 60 °C using DBU and purified using $scCO_2$.

Table C1. Thermal characteristic properties of star polymers.

| Code [a] | $T_g$[f] (°C) | $T_m$[e] (°C) | $\Delta H_m$ (J g$^{-1}$) | $T_m$[e] (°C) | $\Delta H_m$ (J g$^{-1}$) | $T_c$[e] (°C) | $\Delta H_{cryst}$ (J g$^{-1}$) |
|---|---|---|---|---|---|---|---|
| star *D*-sorbitol[$PCL_{57}OH_5$]OH | n/o | 35 | 39.4 | n/o | n/o | 24 | 39.4 |
| star *D*-sorbitol[$PCL_{57}$-*b*-$PEP_{36}OH_6$] | n/o | 30.8 | 25.5 | n/o | n/o | -1.1 | 32.5 |
| star *D*-sorbitol[$PCL_{57}$-*b*-$PEP_{64}OH_6$] | n/o | 28.5 | 22.4 | n/o | n/o | 3.0 | 10.6 |
| star *D*-sorbitol[$PCL_{18}OH_4$]$OH_2$ | -58 | 8.6 | 16.3 | 20.3 | 16.3 | -1.7 | 42.8 |
| star *D*-sorbitol[$PCL_{18}$-*b*-$PEP_{27}OH_6$] | -51 | n/o | n/o | n/o | n/o | n/o | n/o |
| star *D*-sorbitol[$PCL_4OH_3$]$OH_3$ | -48 | n/o | n/o | n/o | n/o | n/o | n/o |
| star *D*-sorbitol[$PCL_4$-*b*-$PEP_{2.8}OH_6$] | -60 | n/o | n/o | n/o | n/o | n/o | n/o |
| star *D*-sorbitol[$PCL_4$-*b*-$PEP_{6.4}OH_6$] | -47 | n/o | n/o | n/o | n/o | n/o | n/o |
| star *D*-sorbitol[$PCL_4$-*b*-$PEP_{14}OH_6$] | -52 | n/o | n/o | n/o | n/o | n/o | n/o |

[g] Determined by differential scanning calorimetry.

# Appendix D (Related to Chapter 6)

## Critical Aggregation Concentration

The ability of amphiphile (surfactant) to self-assemble in an aqueous medium depends on its concentration. This is followed by some structural transition of the block copolymer at the interface resulting in compaction, which accounts for the change in the slope of the surface tension curve (CAC graphs are discussed in Chapter 5).

The micellization of block copolymers (which depends strongly on their composition) is inherently more complex than that of conventional, low molecular weight surfactants.[43] Firstly, the CAC of star $PCL_{18}$-*b*-$PEP_{27}$ copolymer (from surface tension method at air/water interface) was found to be 0.012 wt%.

The CAC values of Tween™ 20 and Tween™ 80 indicates that these petrochemical surfactants are efficient below 60 μM. It is clear that both star $PCL_{18}$-*b*-$PEP_{27}$ diblock and linear $PEP_{7.2}$-$PCL_9$-$PEP_{7.2}$ triblock copolymer were also equally efficient at much lower concentrations (< 60 μM). A very low concentration typically 10 order of magnitude lower $PEP_{7.2}$-$PCL_9$-$PEP_{7.2}$ triblock copolymer is required to reach the CAC value comparable to those shown by Pluronic L64. This effect was even more predominant when compared to Pluronic™ L35, which exhibit a very high CAC values.

Table D1. Comparing CAC values of triblock and star compounds with commercial surfactants.

| Entry | Amphiphile | $M_n$ (g mol$^{-1}$) | CAC (μM) | CAC (wt%) | Ref. |
|---|---|---|---|---|---|
| 1 | Star $PCL_{18}$-*b*-$PEP_{27}$ diblock | 5900 | 21.2 [b] | 0.012% | - |
| 2 | Tween™ 20 | 1200 | 59 | 0.007% | [44] |
| 3 | Tween™ 80 | 1300 | 12 | 0.002% | [44] |
| 4 | Linear $PEP_{7.2}$-$PCL_9$-$PEP_{7.2}$ | 3100 | 48 [b] | 0.014% | - |
| 5 | Pluronic™ L35 | 1900 | 5300[a] | 1.00% [a] | [45] |
| 6 | Pluronic™ L64 | 2900 | 480[a] | 0.139% [a] | [45] |

[a] Literature values determined by fluorescence spectroscopy at 25 °C. [b] Automated measurements using a Wilhelmy plate, CAC graphs (discussed in Chapter 5).

The dynamic surface tension profile of the synthesised star and triblock copolymers was also compared to commercial surfactants Tween 20. It is evident that Tween 20 is faster to reduce the γ of water very quickly at the initial stage from 72 mN m$^{-1}$ to 57

mN $m^{-1}$ and moves with the speedy pace to reduce γ further to 41 mN $m^{-1}$ for bubble lifetime between 30-30600 millisecond.

Interestingly, at the beginning the triblock PEP: PCL: PEP (1000:1100:1000 g $mol^{-1}$) copolymer was the fastest to migrate to the interface (γ = 52.9 mN $m^{-1}$ for bubble lifetime 0 -32 milli second) but it subsequently reduces the surface tension in a more linear fashion. The star PCL:PEP (4000:8800 $gmol^{-1}$) copolymers by contrast has a slower migration rate at the beginning and it appeared to migrate at a constant slow pace subsequently (Figure D1). Crowding at the interface of the bubble might be a reason for it slow behaviour. This is to say that when surfactants has already reached to interface and lower surface tension but as bubble is more crowded, it becomes harder for other surfactants to migrate to interface, hence a slow pace subsequently.

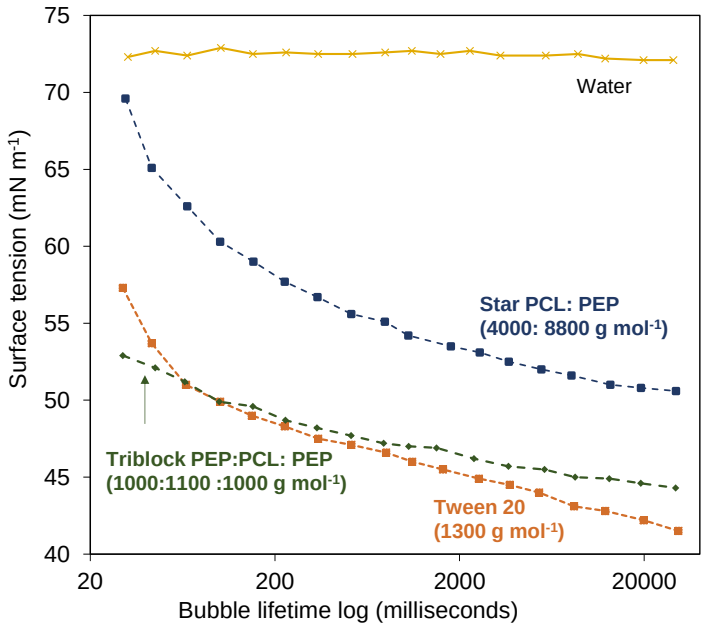



Figure D1. Dynamic surface tension at increasing bubble lifetimes (log) for the star and triblock copolymers (0.5 wt%) in comparison to commercial petrochemical Tweens.

**Required HLB:** To form a stable emulsion with surfactants of known HLB, the HLB of the mixture of surfactants to prepare such stable emulsion is the so called required HLB.

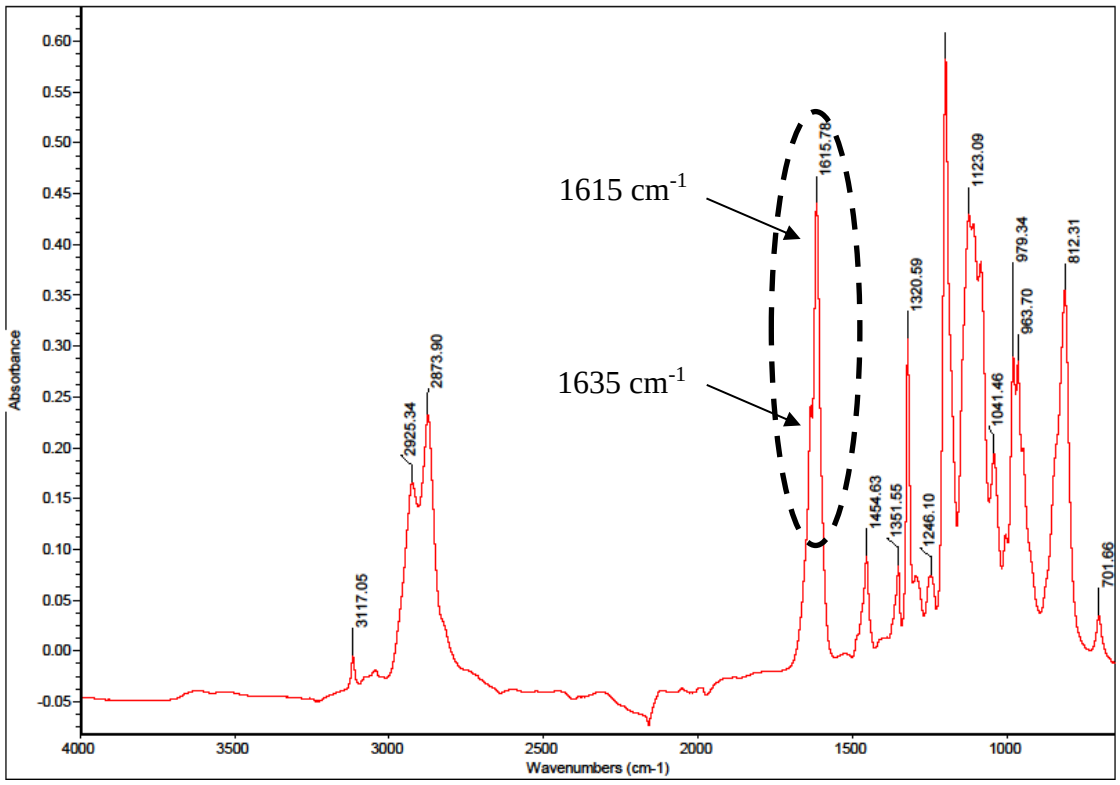



Figure D2. The FTIR spectra of tri(ethylene glycol) divinyl ether showing vinyl group C=C absorption bands at 1615 and 1635cm$^{-1}$.

# Appendix E (Résumé Étendu)

A travers ce travail de thèse, nous avons étudié la synthèse et la caractérisation précise d'étoiles de PCL d'architecture contrôlée obtenues par une approche durable basée sur l'utilisation d'un catalyseur métallique ou d'un biocatalyseur en milieu $CO_2$ supercritique ou en masse. Ces PCL ont ensuite été utilisées comme macro-amorceurs pour l'AROP d'un monomère cyclique de type phosphonate d'éthyle. Le comportement d'auto-assemblage en solution aqueuse des copolymères obtenus, ainsi que leur potentiel à être utilisés comme tensio-actifs et comme précurseurs de matériaux de revêtement ont été discutés.

Les principales conclusions et quelques pistes sur l'orientation future à donner à ce travail sont exposées ci-dessous.

## Conclusions

Nous avons mis en place une nouvelle approche « propre » pour la synthèse de polymères en étoile de type PCL constitués de synthons renouvelables tels que les sucres (i.e. *D*-sorbitol, triglycerol, glycerol, 1-6-hexanediol) et d'ε-CL bio-sourcée (chapitre 4). Cette approche s'appuie sur l'utilisation de $Sn(Oct)_2$ (qui est un catalyseur métallique approuvé par la FDA) ou d'enzyme (la lipase commerciale supportée Novozyme 435) pour la synthèse de polymères en étoile bien définis de type *D*-sorbitol-PCL en milieu $CO_2$sc (Figure E1).

Les réactions faisant appel au $Sn(Oct)_2$ ont été initialement réalisées à température assez basse (T = 95°C) en l'absence de solvant organique (en masse) et nécessitaient des temps de réactions très longs (~ 150 h) pour atteindre des masses molaires de 6000 g mol$^{-1}$. Des temps de réaction si longs rendent la synthèse non-viable économiquement. Le milieu industriel travaille donc à beaucoup plus haute température (~180 °C) en raison de la température de fusion élevée des monomères et pour contrebalancer l'augmentation de viscosité qui se produit au cours de la polymérisation. Une approche à haute température (T = 140°C) sans solvant nous a permis de réduire le temps de réaction à 11 h pour la synthèse d'étoile de *D*-sorbitol-PCL ($M_n$ ~6000 g mol$^{-1}$) d'architecture définie et de faible dispersité ($Đ$ = 1.03 par SEC-MALS). Cependant, en terme de développement durable, une telle température est énergivore et donc inappropriée. Par ailleurs, à l'échelle industrielle, de telles températures peuvent provoquer une coloration du matériau en raison de la formation de sous-produits due à

la déshydratation du sorbitol. L'utilisation de $CO_2$sc (P = 240 bars) n'a pas pour seul avantage de réduire la température de réaction (95°C dans le $CO_2$sc *vs* 140°C en masse). Cela permet également de diminuer de manière significative les temps de réaction (~56 h dans le $CO_2$sc *vs* 150 h en masse à T = 95°C). De plus, le $CO_2$ supercritique présente l'intérêt supplémentaire de permettre l'élimination complète des traces résiduelles d'ε-CL mais également de réduire la quantité de catalyseur métallique « piégé » dans l'échantillon polymère. Une approche « one-pot » économe en énergie devient alors envisageable. Des étoiles de PCL bien définies à 5 bras ont ainsi été obtenues en présence de $Sn(Oct)_2$ comme catalyseur (Figure E1, gauche).

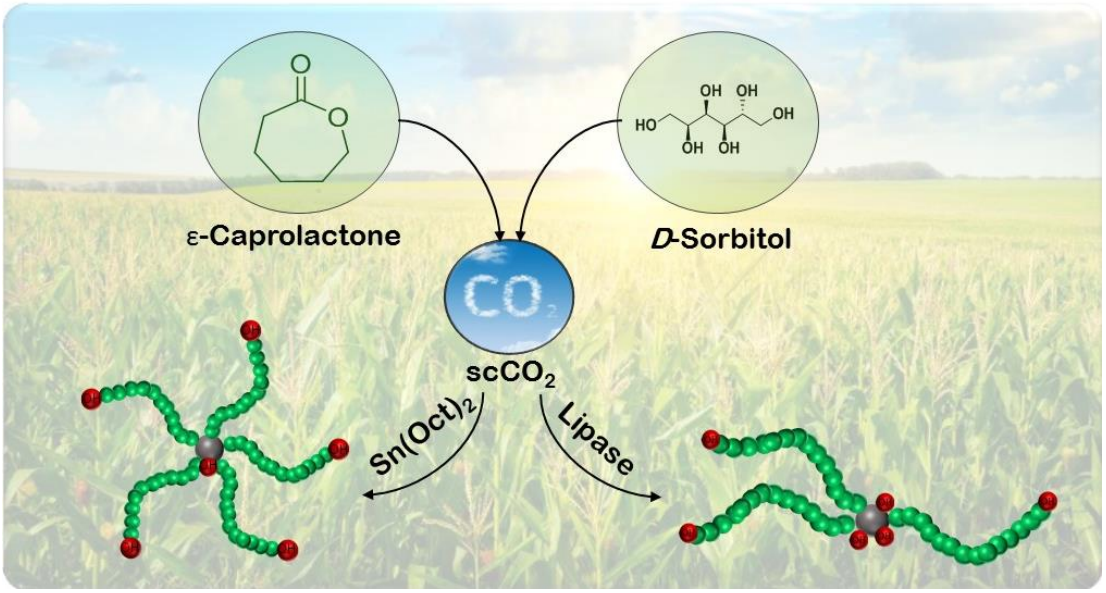



Figure E1. Approche de chimie durable pour la synthèse de polymère en étoile biosourcé *D*-sorbitol-poly(ε-caprolactone) avec $Sn(Oct)_2$ ou une enzyme comme catalyseurs.

Les échantillons synthétisés ont été analysés par plusieurs techniques de caractérisation qui confirment toutes nos résultats. Les analyses MALDI-TOF ont montré l'absence de réactions secondaires dans le cas des polymérisations catalysées par le $Sn(Oct)_2$ que ce soit en masse en conditions anhydres ou en milieu $CO_2$sc. Par ailleurs, les bras des étoiles ont été méticuleusement caractérisés par différentes techniques incluant les analyses SEC-MALS et RMN $^1$H. Les résultats sont en très bon accord avec l'approche par phosphitylation que nous avons développée et qui permet de distinguer les groupement hydroxyle primaires et secondaires et de quantifier le nombre moyen de bras ($N_{arms}$ ($^{31}$P)), la longueur des bras (masse molaire moyenne des bras) et la masse molaire des étoiles. Des analyses supplémentaires permettant d'estimer le $N_{arms}$ par SEC par calibration universelle (SEC-UC) sont aussi présentées.

Nous avons aussi décrit une nouvelle approche basée sur la catalyse enzymatique utilisant des températures plus faibles en milieu $CO_2$sc (T = 60°C, P = 217 bar) pour la préparation d'étoiles *D*-sorbitol-PCL bio-sourcées. (masse molaire ~6000-10000 g mol$^{-1}$, $Đ$ = 1.23-1.24). Des polymères en étoiles de PCL d'architecture unique de type miktoarm à 3 bras possédant trois fonctions hydroxyle aux extrémités de chaque bras de PCL et trois fonctions hydroxyle au niveau du cœur sorbitol ont ainsi été obtenus. La présence de seulement 3 bras est liée à la sélectivité spécifique de l'enzyme pour les alcools primaires par rapport aux secondaires. Notons également l'importance de l'utilisation du $CO_2$ supercritique dans cette synthèse. En effet, ce dernier permet de travailler intégralement dans des conditions douces (T=60°C) alors que l'approche en masse nécessite une étape préalable d'homogénéisation des réactifs à plus haute température (95°C). De plus, outre cette étape d'homogénéisation, la polymérisation en masse à 60°C ne permet pas d'atteindre une conversion totale du monomère (% conv = 87% en masse *vs* 97% en milieu $CO_2$sc). L'analyse détaillée et la caractérisation précise de ces nouvelles étoiles de PCL de structure miktoarm synthétisées par catalyse enzymatique ont montré la présence d'une faible quantité de réactions secondaires (en particulier la formation de chaines de PCL linéaires amorcées par l'eau et la présence de macrocycles de PCL). Cette approche totalement « verte » (absence de solvant organique, faible température de réaction dans le $CO_2$sc) pour la synthèse de PCL d'architecture en étoile bien définie à partir d'amorceurs de polymérisation bio-sourcés nous a servi de point de départ pour le design de tensio-actifs de structures branchées. Ces nouveaux systèmes sont détaillés dans les chapitres suivants.

En étant biodégradable et biocompatible, le monomère cyclique hydrophile phosphonate d'éthyle (EP) est un très bon candidat pour le design de tensio-actifs (chapitre 5). Une fois de plus, le recours au $CO_2$sc en remplacement des VOC offre une voie plus « verte » pour la synthèse et la purification de poly(ethyl phosphonate)s (PEP)s par AROP en présence d'un organo-catalyseur. A notre connaissance, la polymérisation du monomère hydrophile phosphonate d'éthyle et la purification du polymère afférent par extraction du monomère EP résiduel en milieu $CO_2$sc n'ont jamais été reportés dans la littérature.

Dans un premier temps, un polymère linéaire Bz-PEP$_{7.5}$OH de faible masse molaire ($M_n$ $^{NMR}$ = 1100 g mol$^{-1}$ et $M_n$ $^{SEC}$ = 800 g mol$^{-1}$) pour $M_n$ $^{targ}$ = 2720 g mol$^{-1}$ a été synthétisé dans le $CO_2$sc. Une bonne cohérence entre les analyses RMN, SEC et ESI-

HR-MS a été observée. L'élimination totale du monomère résiduel phosphonate d'éthyle du produit final a été réalisée en seulement 25 min en utilisant l'extraction par le $CO_2$sc (T = 38 ± 2 °C, P = 140 ± 5 bar). De plus, aucune trace d'hydrolyse du monomère EP ainsi extrait n'est visible à la suite de cette méthode de purification. Une stratégie offrant à la fois une synthèse et une purification de matériaux bio-sourcés « one-pot » ainsi que la possibilité d'isoler et de recycler les monomères résiduels serait d'un intérêt considérable à la fois pour développer des procédés durables économes en énergie et pour s'affranchir complètement de l'utilisation de composés organiques volatils (Figure E2).

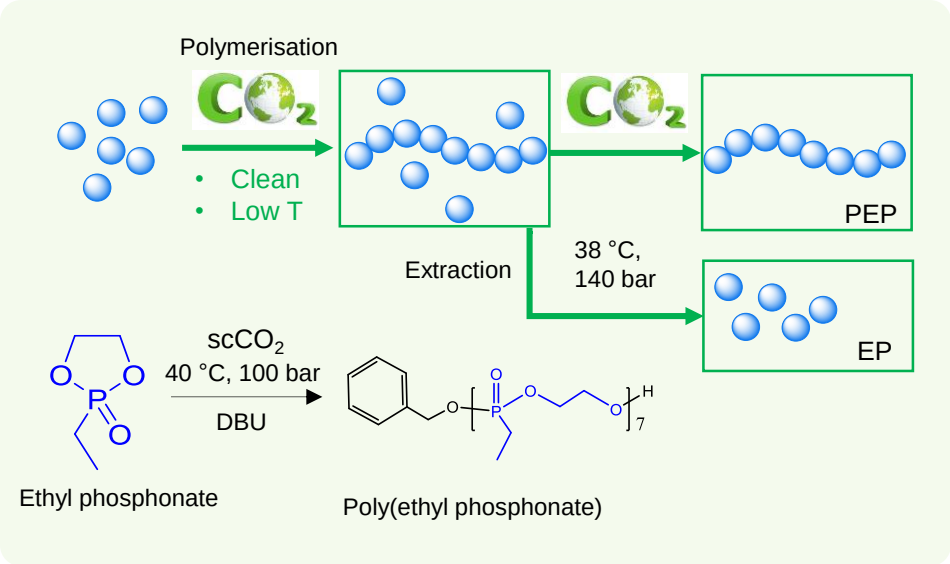



Figure E2. Synthèse et purification de poly(ethylphosphonate) utilisant une nouvelle approche durable dans le $CO_2$ supercritique.

Dans un second temps, nous avons confectionné une large gamme de copolymères à blocs amphiphiles poly(ε-caprolactone)-*bloc*-poly(ethyl phosphonate) de masses molaires et d'architectures variées (copolymères diblocs et triblocs linéaires, copolymères en étoile avec des bras du type diblocs) selon une approche sans solvant (en masse) (à T = 60°C) (Figure E3). Pour se faire, les PCL décrits précédemment (chapitre 4) ont été utilisés comme macro-amorceurs pour l'AROP du monomère phosphonate d'éthyle en présence d'un organocatalyseur bénin pour l'environnement, à savoir la base DBU. Des polymérisations relativement rapides et contrôlées ont été réalisées (analyses par SEC et RMN). Le nombre de bras PCL-*b*-PEP des copolymères en étoiles a été estimé égal à 6 pour par RMN $^{31}$P selon le procédé de phosphitylation (Figure E3, droite et Figure E4 (A)). L'analyse des copolymères triblocs linéaires $PEP_{7.2}$-$PCL_9$-$PEP_{7.2}$ (Figure E3, en bas à gauche) par MALDI-TOF montre bien la

présence d'une distribution Gaussienne monomodale et l'absence d'homopolymères téléchéliques dihydroxy HO-PCL-OH résiduels. Des analyses SEC couplées à un détecteur de diffusion de la lumière (SEC-MALS) ont permis de déterminer la masse molaire absolue des copolymères diblocs linéaires (Figure E3, en haut à gauche) et de l'homopolymère afférent. De plus, notons que les valeurs de ces masses molaires sont proches de celles déterminées par RMN.

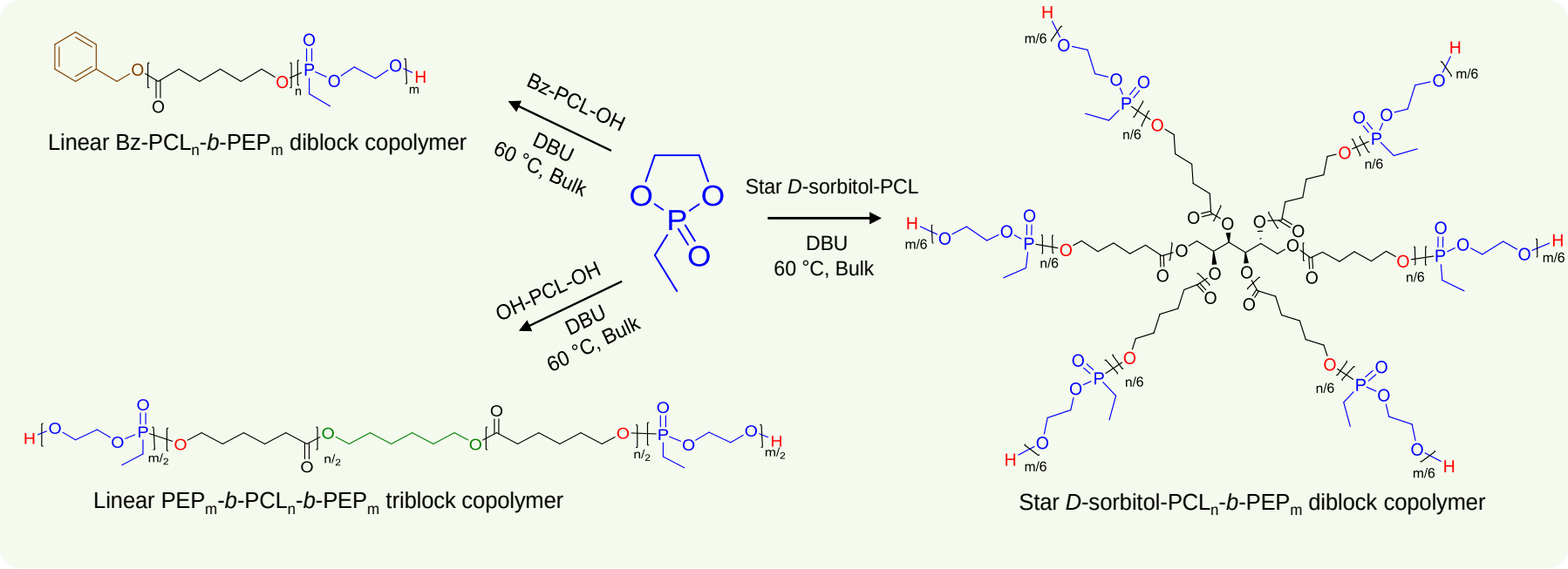



Figure E3. Représentation schématique de copolymères à blocs amphiphiles d'architectures variées (diblocs linéaire Bz-PCL$_n$-OH, triblocs linéaire PEP$_{m/2}$-PCL$_n$-PEP$_{m/2}$ et copolymères en étoile avec bras diblocs *D*-sorbitol-PCL$_n$-*b*-PEP$_m$OH$_6$ ) préparés durant cette Thèse.

Nous avons également démontré qu'il était possible de purifier ces copolymères en utilisant le procédé d'extraction en milieu $CO_2$ supercritique qui est propre et peu demandeur en énergie. Comme précédemment, l'élimination complète du monomère EP résiduel de chaque échantillon a été réalisée en 25 min (à faible température (T=38 °C) et pression (P=140 à 180 bar). Cette méthode de purification apporte un avantage indéniable en terme de rendement en polymère final en comparaison aux méthodes traditionnelles (rendement gravimétrique = ~92% en utilisant le $CO_2$sc *vs* ~60-65% en utilisant la méthode de précipitation en milieu solvant ou la dialyse). Ces données confirment la versatilité des procédés à base de $CO_2$ supercritique et soulignent une nouvelle fois leur aspect « vert » et économe en énergie en permettant de s'affranchir de multiples étapes de purifications faisant appel à des VOCs toxiques et à des étapes de séchage sous vide énergivores.

Par ailleurs, le comportement d'auto-assemblage en solution de ces systèmes a été étudié par diffusion dynamique de la lumière et par microscopie électronique à transmission. La formation de micelles a ainsi été observée en solution aqueuse dans le cas des copolymères triblocs alors que des unimères sont observés pour les étoiles de copolymères. Pour les étoiles *D*-sorbitol[$PCL_{57}$-*b*-$PEP_{36}OH_6$] ayant un diamètre moyen théorique de 7 nm (en considérant un cœur de PCL condensé et entouré par une couronne de PEP étirée), une bonne corrélation est observée entre le $D_{TEM}$ de 14.3 nm et le $D_H$ de 13.6 nm mesuré par DLS selon la distribution en nombre (Figure E.4 (C)). De plus, le $D_H$ obtenu par la mesure DLS en intensité ($D_{H,\ DLS\ (IWD)}$) de la plus petite population est égal à 18 nm et est tout à fait cohérent avec le diamètre moyen mesuré par cryo-TEM ($D_{cryo\text{-}TEM}$ of 17.7 nm).

La capacité des copolymères à base de PCL et de PEP d'architecture triblocs et en étoile à avoir des propriétés tensio-actives a également été étudiée et s'est avérée positive dans tous les cas (Figure E4, (B)). L'utilisation potentielle des tensio-actifs en étoile comme émulsifiants ou agents de solubilisation de parfums a également été testée en vue d'une application de ces copolymères dans le marché des produits de soin.

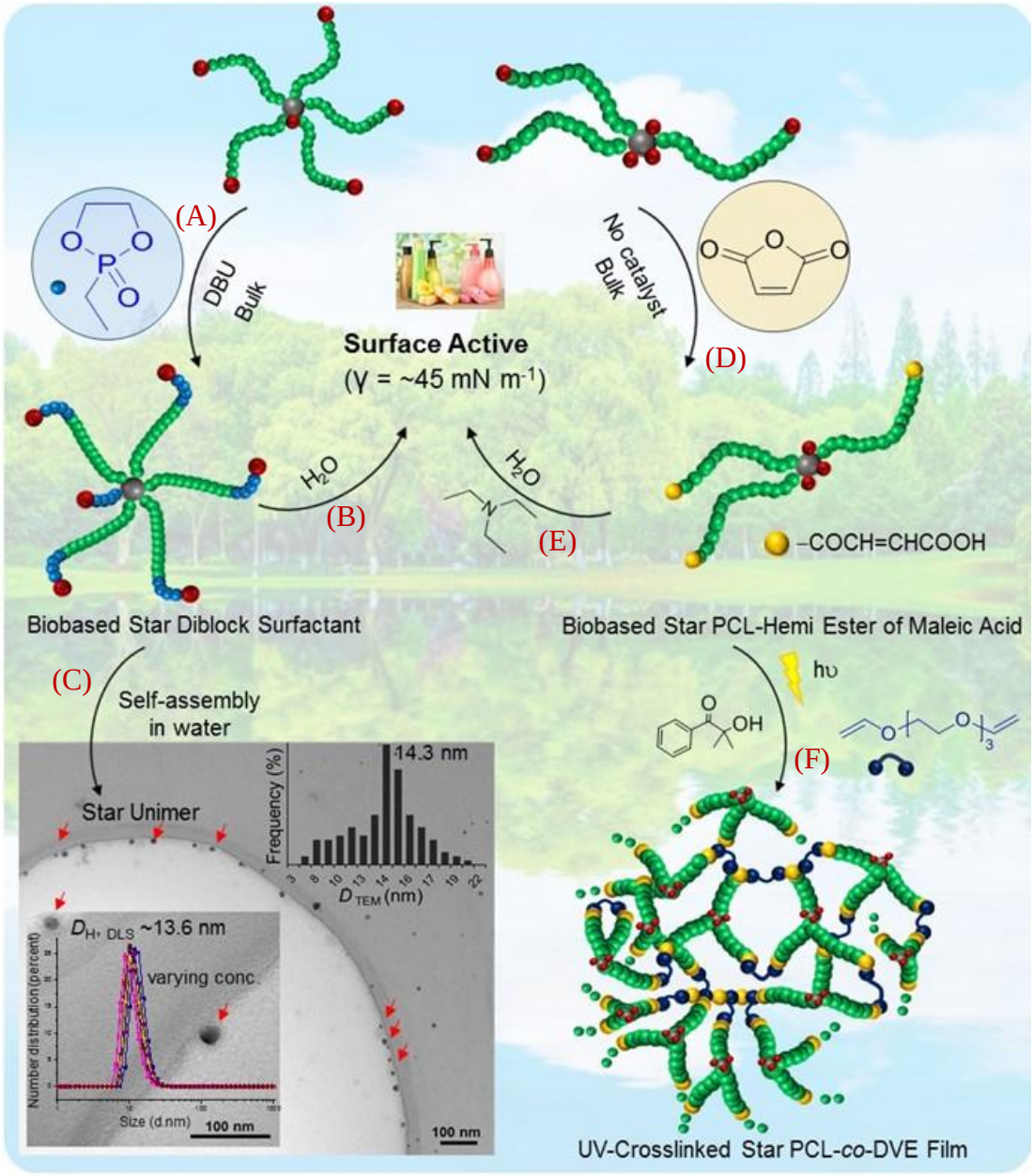



Figure E4. Synthèse "propre" d'un copolymère en étoile avec 6 bras diblocs amphiphiles PCL-*b*-PEP (A) qui est tensioactif (B) et qui forme des unimères étoile dans l'eau (C), préparation de PCL étoile terminé par un hémiester de l'acide maléique (D), qui réduit la tension de surface de l'eau après neutralisation du groupe acide carboxylique par la triéthylamine (E). D'autre part, les groupes insaturés terminaux ont été photopolymérisés avec une petite quantité de divinyl ether DVE (~9 % massique), conduisant à un matériau photoréticulé de type PCL étoile-*co*-DVE sur un substrat en verre (F).

Notons en particulier que le copolymère triblocs linéaire $PEP_{7.2}$-$PCL_{9}$-$PEP_{7.2}$ montre une très bonne activité de surface ($\gamma$ = 31 mN $m^{-1}$), ce qui le rend compétitif avec les tensio-actifs triblocs commerciaux (par exemple les Pluronic L35 et L64).

Selon les principes de la chimie verte, le polymère en étoile à base de PCL ($M_n$ = ~3000 g mol$^{-1}$ et ~6000 g mol$^{-1}$, $N_{arms}$ = ~3) synthétisé par voie enzymatique en présence de Novozyme 435 a été fonctionnalisé par réaction avec l'anhydride maléique afin d'obtenir des groupements acide carboxylique ionogénique aux extrémités des bras (Figure E4, (D)). Ces PCL-$OH_x$ fonctionnalisés par des hémi ester d'acide maléique (star *D*-sorbitol[(PCL)-MA-$COOH_3$]$OH_3$) ont été ensuite neutralisés par ajout de triéthylamine dans l'eau. Les étoiles de PCL portant des groupements de sels d'ammonium carboxylate correspondantes sont dispersibles dans l'eau et présentent des propriétés tensio-actives (Figure E4, (E)).

L'utilisation de cette structure PCL de type étoile biosourcée offre une alternative verte et économiquement viable mettant en évidence le grand potentiel de conception de matériaux innovants alternatifs, prometteurs sur le plan environnemental et aux propriétés uniques. Nous avons exploré les potentialités de ces groupes insaturés maléate sur les extrémités de la chaîne PCL, en tant qu'accepteur, et le tri (éthylène glycol) divinyl éther (DVE), en tant que donneur, en utilisant la méthodologie de photopolymérisation (Figure E4). (F)). Des films de PCL étoile-*co*-DVE ont été fabriqués sur un substrat en verre par photoréticulation sous irradiation UV. De tels films ont montré de bonnes propriétés adhésives sur le verre. La cinétique de la photopolymérisation ainsi que le comportement thermique (DSC) et de dégradation (TGA) de ces échantillons ont montré des résultats prometteurs pour l'utilisation future de ces films réticulés biosourcés.

**Perspective Générale**

L'étude de la préparation de PCL en étoile en utilisant le produit commercial Novozym 435 en tant que biocatalyseur a montré un grand potentiel pour la production de cette nouvelle PCL de type étoile avec peu de produits secondaires et une dispersité étroite. Cela a été fait en utilisant une voie verte; néanmoins, il y a encore un certain nombre de domaines dans lesquels des améliorations sont encore possibles, et qui n'ont pas été abordés dans la littérature. Un nombre plus faible de bras pour le polymère étoile-PCL préparé avec l'enzyme a conduit à des propriétés thermiques différentes de l'étoile préparée avec le catalyseur $Sn(Oct)_2$ (comme indiqué dans l'étude DSC au chapitre 4).

L'étude pourrait ainsi être complétée pour améliorer le degré de ramification: (1) d'autres lipases (lipase porcine pancréatique (PPL) ou Pseudomonas fluorescens (PF), Pseudomonas species lipase (PS)) sont commerciales et ont été utilisées pour la polyestérification et sont moins sélectives que Novozym 435. On pourrait exploiter certaines enzymes non commerciales telles que les lactonases, bien que leur compatibilité avec le $CO_2$sc soit à considérer. Une utilisation de l'enzyme CALA qui est considérée comme moins sélective avec une charge enzymatique élevée pourrait être envisagée. (2) L'utilisation d'un polyol avec un plus grand nombre de groupes hydroxy primaires (par exemple, le dipentaérythritol) pourrait de préférence être envisagée.

Les poly(phosphonates) représentent une nouvelle classe de polymères émergeant avec un avenir prometteur dans les produits pharmaceutiques. Des études de littérature ont déjà prouvé leur solubilité dans l'eau, leur biocompatibilité et leur biodégradabilité ajustable. Cependant, la littérature ne reporte pas de biocatalyseur pour la polymérisation des phosphonates cycliques, ce qui constituerait une avancée significative dans ce domaine. Certaines enzymes non commerciales très spécifiques, supposées cliver la liaison P-O in vivo, telles que EcoRV et Myosine (enzyme hydrolase)[1] et phosphatase (EC 3.1.8.1) ou Lactonases, pourraient être utilisées pour tester leur compatibilité avec le phosphonate.

L'extraction assistée par $CO_2$sc à basse température du monomère de phosphonate d'éthyle lors de la purification de polymères et de copolymères ne montre aucune dégradation hydrolytique de EP. La réutilisation de ce monomère extrait pourrait ouvrir

la voie à un processus rentable en accord avec le principe d'économie d'atome. De plus, la polymérisation du phosphonate dans le $CO_2$sc a été explorée mais à petite échelle ; des études supplémentaires pourraient être menées pour optimiser le processus et tester sa viabilité à plus grande échelle.

Les copolymères amphiphiles de diverses architectures (diblocs, triblocs et étoiles) ont été décrits au chapitre 5 et présentent des propriétés d'auto-assemblage et tensioactives intéressantes. Toutefois, une étude plus approfondie pourrait être menée afin de tester leurs capacités d'encapsulation et de délivrance. En outre, leur biocompatibilité pourrait être évaluée afin de déterminer leur applicabilité réelle dans des applications médicales ou en tant que tensioactifs.

La capacité de production de biomatériaux (biopolymères compris) devrait atteindre 1,7 million de tonnes en 2020 en Europe[2] et, en raison de sa forte demande et de sa consommation, le seul marché PCL devrait générer environ 670 milliards de dollars d'ici à 2026.[3] L'adoption de la PCL en tant que matière première s'explique par ses propriétés exceptionnelles (caractéristiques hydrophobes, résistance à l'usure et aux produits chimiques, résistance aux UV, résistance à l'huile et à la graisse, souplesse, adhérence et flexibilité à basse température).[3]

Des études préliminaires ont été effectuées pour créer des films PCL réticulés à partir de polymère étoile biosourcé photoréticulable préparé avec le catalyseur Novozym 435; cependant, une amélioration pourrait être faite dans l'étape de formulation en supprimant ou en réduisant la quantité d'acétone utilisée pour la formulation du film (~ 50% en poids d'acétone). Bien que des études de la littérature sur une telle formulation à base de PCL rapportent l'utilisation du dioxane comme cosolvant,[4] l'ajustement du nombre de bras et de leurs masses molaires pourrait être bénéfique. Par exemple, l'étoile PCL de masse molaire plus faible (3000 g $mol^{-1}$ au lieu de 6000 g $mol^{-1}$) a montré une bonne solubilité dans l'éther divinylique de tri (éthylène glycol) qui est polaire.

Néanmoins, des recherches plus approfondies sur les applications doivent être effectuées pour examiner l'utilité réelle des films PCL étoile en tant que revêtements et matériaux réticulés (par exemple adhérence, taux de gel, propriétés de surface / angle de contact, résistance aux rayures et aux chocs, etc.).

Un tel matériau PCL de type étoile biosourcé offre la possibilité de fabriquer des structures 3D biocompatibles. [4,5]

En bref, cette thèse démontre un excellent potentiel pour des recherches futures sur les PCL en étoile biosourcées et leurs copolymères avec des phosphonates pour une large gamme d'applications possibles dans les revêtements et en tant que tensioactifs

**Références (Relatif à l'Annexe E).**

1. Gade, Lutz H. & Hofmann, P. *Molecular Catalysts: Structure and Functional Design*. *Applied Organometallic Chemistry* **30,** (Wiley-VCH Verlag GmbH & Co. KGaA, 2014).
2. Alex Scott. Biobased chemical start-ups seek niche in Europe. *Chemical & Engineering News* 25–26 (2016).
3. Persistence Market Research. Global market Study On Polycaprolactone. 215 (2018). Available at: https://www.persistencemarketresearch.com/market-research/polycaprolactone-market.asp. (Accessed: 20th September 2018)
4. Green, B. J. *et al.* Effect of Molecular Weight and Functionality on Acrylated Poly(caprolactone) for Stereolithography and Biomedical Applications. *Biomacromolecules* (2018). doi:10.1021/acs.biomac.8b00784
5. Yagci, Y., Jockusch, S. & Turro, N. J. Photoinitiated polymerization: Advances, challenges, and opportunities. *Macromolecules* **43,** 6245–6260 (2010).
1. Gade, Lutz H. & Hofmann, P. *Molecular Catalysts: Structure and Functional Design*. *Applied Organometallic Chemistry* **30,** (Wiley-VCH Verlag GmbH & Co. KGaA, 2014).
2. Alex Scott. Biobased chemical start-ups seek niche in Europe. *Chemical & Engineering News* 25–26 (2016).
3. Persistence Market Research. Global market Study On Polycaprolactone. 215 (2018). Available at: https://www.persistencemarketresearch.com/market-research/polycaprolactone-market.asp. (Accessed: 20th September 2018)
4. Green, B. J. *et al.* Effect of Molecular Weight and Functionality on Acrylated Poly(caprolactone) for Stereolithography and Biomedical Applications. *Biomacromolecules* (2018). doi:10.1021/acs.biomac.8b00784
5. Yagci, Y., Jockusch, S. & Turro, N. J. Photoinitiated polymerization: Advances, challenges, and opportunities. *Macromolecules* **43,** 6245–6260 (2010).

## ABSTRACT

Star polymers have attracted considerable attention because of their unique thermal and mechanical properties. At the same time, as sustainable chemistry field is growing in impact at an unprecedented rate, we propose in this work to implement a greener pathway for the synthesis of star *D*-sorbitol-poly(ε-caprolactone) (star PCL-$OH_x$) using clean solvents (polymerisation in the bulk or in supercritical $CO_2$) and either FDA-approved $Sn(Oct)_2$ catalyst or enzyme catalyst (Novozym® 435). The influence of these parameters on the star architecture (number of arms, MW of arms etc.) was rigorously analysed and corroborated with various analytical techniques ($^1$H NMR, SEC-MALS, SEC-UC, phosphitylation quantitative $^{31}$P NMR approach). Linear monohydroxy PCL-OH and dihydroxy telechelic OH-PCL-OH samples were also prepared. The PCL materials obtained were used as hydrophobic macroinitiators for the polymerisation of cyclic hydrophilic ethylene ethyl phosphonate monomer for the synthesis of a range of different amphiphilic materials (i.e. star diblock, linear diblock and triblock copolymers). Self-assembly behaviour in aqueous solution of these copolymers was investigated by DLS, TEM and cryo-TEM. Triblock and star amphiphilic copolymers were revealed to be able to reduce the surface tension (γ) of water down to 45 mN $m^{-1}$. Finally, enzyme catalysed star PCL-$OH_x$ polymers were functionalised with carboxylic end-groups using maleic anhydride. Water-dispersible surface-active ionic star polymers were then obtained. These maleate-functionalised star polymers were then photopolymerised with a small amount of tri(ethylene glycol) divinyl ether (~9wt% of total composition). The UV-cured crosslinked star PCL films produced were then analysed by FTIR, DSC and TGA.

**Key words:** star polymer, PCL, cyclic phosphonate, enzyme, $scCO_2$, surfactants

## RESUME

Les polymères en étoile connaissent un intérêt accru en raison de leurs propriétés thermiques et mécaniques inimitables. Partant du constat qu'en parallèle la chimie durable se développe à un rythme sans précédent, nous proposons dans cette thèse de développer une stratégie plus « verte » pour la synthèse de polymères en étoile de type *D*-sorbitol-poly(ε-caprolactone) (star PCL-$OH_x$). Ces derniers seront synthétisés sans solvant (en masse) ou dans des solvants « propres » ($CO_2$ supercritique) et en présence du catalyseur métallique $Sn(Oct)_2$ (qui a été approuvé par la FDA) ou d'un catalyseur enzymatique (Novozym® 435). L'influence de ces paramètres sur l'architecture des étoiles (nombre de bras, masse molaire des bras…) a été rigoureusement analysée et confirmée par différentes techniques d'analyse (RMN $^1$H, SEC-MALS, SEC-UC, analyse RMN $^{31}$P quantitative *via* la méthode de phosphitylation). Des polymères linéaires monohydroxy (PCL-OH) et téléchéliques dihydroxy (OH-PCL-OH) ont également été synthétisés en parallèle. Ces différentes PCL ont été utilisées comme macro-amorceurs hydrophobes pour la polymérisation du monomère cyclique hydrophile éthylphosphonate d'éthylène. Une large gamme de copolymères amphiphiles a ainsi pu être développée (i.e. des copolymères diblocs en étoile ou des copolymères diblocs et triblocs linéaires). Le comportement d'auto-assemblage en solution de ces copolymères a été étudié par DLS ainsi que par TEM et cryo-TEM. Nous avons également montré que les copolymères amphiphiles triblocs et en étoile sont capables de diminuer la tension de surface (γ) de l'eau en dessous de 45 mN $m^{-1}$. Enfin, les étoiles PCL-$OH_x$ synthétisées en présence d'enzyme ont été fonctionnalisées par réaction avec l'anhydride maléique. Des polymères en étoile, ioniques, tensio-actifs et directement dispersables dans l'eau ont ainsi pu être obtenus. Dans un second temps, ces mêmes polymères ont été photopolymérisés en présence d'une faible quantité de tri(éthylène glycol) divinyl éther (~ 9% par rapport à la masse totale). Les films afférents à ces copolymères en étoile réticulés sous UV ont été analysés par IRTF, DSC et ATG.

**Mots clés** : polymère en étoile, PCL, phosphonate cyclique, enzyme, $CO_2$sc, tensio-actifs